NASA
Reference
Publication
1314

September 1993

NASA Handbook for Nickel-Hydrogen Batteries

James D. Dunlop
Gopalakrishna M. Rao
Thomas Y. Yi

NASA Reference Publication 1314

1993

NASA Handbook for Nickel-Hydrogen Batteries

James D. Dunlop
Consultant
Gaithersburg, Maryland

Gopalakrishna M. Rao and
Thomas Y. Yi
Goddard Space Flight Center
Greenbelt, Maryland

National Aeronautics and Space Administration

Scientific and Technical Information Branch

PREFACE

Nickel-hydrogen batteries are finding more and more applications in the spectrum of aerospace energy storage requirements. Starting with the INTELSAT V Flight 6 spacecraft launched in 1983, nickel-hydrogen batteries have become the primary energy storage system used for geosynchronous-orbit communication satellites. The first NASA application for nickel-hydrogen batteries was the low-earth-orbit Hubble Space Telescope satellite launched April 24, 1990.

The handbook was prepared as a reference book to aid in the application of this technology. That is, to aid in the cell design, battery design, procurement, testing, and handling of nickel-hydrogen batteries. This "Battery System Task" as part of the Code Q battery program was created by the need to establish a program that would deal not only with the cell and battery technology, but also take into consideration the integration of the battery into the power system [Schulze and O. D. Gonzalez-Sanabria, "NASA Aerospace Flight Battery System Program—Issues and Actions," 1988 IECEC, Vol. 2, p. 3]. Preparation of this handbook was initially carried out under the direction of Thomas Yi and then finished under the direction of Gopalakrishna M. Rao at NASA Goddard Space Flight Center.

The design of individual pressure vessel nickel-hydrogen cells is covered in Chapter 1. Low-earth-orbit (LEO) and geosynchronous orbit (GEO) applications and their requirements are discussed in Chapter 2. The design of nickel-hydrogen batteries for both GEO and LEO applications is discussed in Chapter 3. Advanced design concepts such as the common pressure vessel and bipolar nickel-hydrogen batteries are described in Chapter 4. Performance data are presented in Chapter 5. Storage and handling of the nickel-hydrogen cells and batteries are discussed in Chapter 6. Standard test procedures, both at the cell level and the battery level, are presented in Chapter 7. Cell procurement and battery procurement are discussed in Chapter 8, along with mandatory inspection points both at the cell level and the battery level. The mandatory inspection points are designated for quality control of the manufacturing processes. Finally, safety procedures are discussed in Chapter 9.

The author would like to specifically thank Michelle A. Manzo at NASA Lewis Research Center and D. W. Maurer from AT&T Bell Laboratories for reviewing the text and providing many beneficial technical inputs as well as providing recommendations on the organization and structure of the contents. They were both a great help to me in the preparation of this handbook. A special debt of gratitude goes to Martin Earl and his staff at COMSAT Laboratories for providing inputs on INTELSAT cell designs, battery designs, performance data on cell characteristics, and SEM data. I would also like to thank Andrew Dunnet and Dennis Cooper for their inputs on the INTELSAT cell and battery designs and for the in-orbit performance data. In addition, the author would like to acknowledge inputs and comments from the following: Fred Betz at the Naval Research Laboratory; Lee Miller at Eagle-Picher, Inc.; H. Vaidyanathan and Todd Burke at COMSAT Laboratories; David W. Wong, Howard H. Rogers, and H. S. Lim at Hughes Aircraft Company; Arnold M. Hall at Yardney Technical Products, Inc.; Robert Patterson at TRW; C. W. Koehler and A. Z. Applewhite at Space Systems/Loral; David E. Nawrocki and John Armantrout at Lockheed Missiles and Space Company, Inc.; Steve Schiffer at GE Astro Space Division; Joseph Stockel at the Office of Research and Development; William Billerbeck at MRS; and Lawrence

A. Tinker at Gates Energy Products. A special thank you also goes to David E. Nawrocki, William Billerbeck, Michelle Manzo, and Steve Schiffer, who each reviewed the final draft and provided many useful comments, which have been incorporated into the final manuscript.

The author would also like to express his appreciation to Theresa Cunningham Burke for her contributions as technical editor of this handbook.

LIST OF ACRONYMS AND ABBREVIATIONS

Aq	Aqueous
Ah	Ampere hour
Al	Alcohol
AT&T	American Telephone and Telegraph
C	Rated capacity (nameplate capacity)
C_{meas}	Measured capacity
c	Ampere hours returned on charge
cm	centimeter
COMSAT	Communications Satellite Corporation
CPV	Common pressure vessel nickel-hydrogen battery
d	Ampere hours removed on discharge
DOD	Depth of discharge based on rated capacity
DPA	Destructive Physical Analysis
EB	Electron beam welding
EI	Electrochemical impregnation
EOC	End of charge
EOCP	End-of-charge pressure
EOD	End of discharge
EODP	End-of-discharge pressure
EP (CS)	Eagle-Picher (Colorado Springs)
EP (Joplin)	Eagle-Picher (Joplin)
EPI	Eagle-Picher Industries
EUTELSAT	European Telecommunications Satellite Corporation
FACC	Ford Aerospace and Communications Corporation
F-6	Flight Six spacecraft
g	grams
GEO	Geosynchronous earth orbit
GEP	Gates Energy Products
GSFC	Goddard Space Flight Center
GSTAR	GTE Satellite Program
H_2	Hydrogen gas
HAC	Hughes Aircraft Company
HST	Hubble Space Telescope
INCO	International Nickel Limited
INTELSAT	International Telecommunications Satellite Organization
IPV	Individual pressure vessel nickel-hydrogen cell
JSC	Johnson Spaceflight Center
K_2CO_3	Potassium carbonate
KOH	Potassium hydroxide
L	liter
LEO	Low earth orbit
LeRC	Lewis Research Center
LMSC	Lockheed Missile and Space Company
MANTECH	Manufacturing Technology
MCD	Manufacturing Control Document
mg	milligrams

MIP	Mandatory Inspection Point
m m	millimeters
MSFC	Marshall Space Flight Center
$N_2 + H_2$	forming gas
NASA	National Aeronautical and Space Administration
NHB	NASA Handbook
$Ni(OH)_2$	Nickel hydroxide
Ni(OOH)	Nickel oxyhydroxide
Ni-Cd	Nickel cadmium cell
$Ni-H_2$	Nickel hydrogen cell
NTS-2	Navigational Technology Satellite 2
ORU	Orbital replacement unit
OSR	Optical solar reflectors
ΔP	pressure difference
$\Delta P/Ah$	pressure difference/amphere-hour (Pressure Constant)
psi	pounds per square inch
P_c	Pressure constant (ΔP/A-hr)
Pt	Platinum
QA	Quality assurance
QC	Quality control
SSF	Space Station Freedom
SSL	Space Systems Loral
T	temperature
t	time
TIG	Tungsten inert gas welding
V	volts
V-T	Voltage vs temperature charge control limits
W h	Watt hours
Wh/cm^3	Watt hours/centimeters cubed (energy density)
Wh/kg	Watt hours/kilogram (specific energy)
Wh/L	Watt hours/liter (energy density)
YEC	Yardney Electric Corporation (Yardney Technical Products)
ZrO	Zirconium oxide separator
ZYK	Knit Zircar cloth material
ZYW	Woven Zircar cloth material
°C	degrees centigrade

TABLE OF CONTENTS

LIST OF FIGURES

LIST OF TABLES

CHAPTER 1
NICKEL-HYDROGEN CELL DESIGN

A sealed nickel-hydrogen ($Ni-H_2$) secondary cell is a hybrid, combining battery and fuel-cell technologies [1-1]. The nickel positive electrode comes from the nickel-cadmium cell, and the negative platinum fuel-cell electrode from the hydrogen-oxygen fuel cell. Salient features of this hybrid $Ni-H_2$ battery are a long cycle lifetime that exceeds any other maintenance-free secondary battery system; high specific energy (gravimetric energy density); high power density (pulse or peak power capability); and a tolerance to overcharge and reversal. It is these features that make the $Ni-H_2$ battery system the prime candidate for the energy storage subsystem in many aerospace applications, such as geosynchronous-earth-orbit (GEO) commercial communications satellites, and low-earth-orbit (LEO) satellites like the Hubble Space Telescope.

Major advantages and disadvantages of the $Ni-H_2$ cell are the following:

Advantages	Disadvantages
High Specific Energy (60 Wh/kg)	High initial cost
Long cycle life (40,000 cycles at 40% DOD for LEO applications)	Self-discharge proportional to H_2 pressure
Long lifetime in orbit (over 15 years for GEO applications0	Low Volumetric Energy Density 50 to 95 Wh/L (IPV cell) 20 to 40 Wh/L (battery)
Cell can tolerate overcharge and reversal	
H_2 pressure gives an indication of state-of-charge	

This chapter describes the 8.89-cm (3.5-in.) diameter individual pressure vessel (IPV) $Ni-H_2$ cell technology. Presented is a description of the electrode stack components, electrode stack design, the electrochemical reactions of an $Ni-H_2$ cell on charge and discharge, the COMSAT and Air Force cell designs (cells used in the 1980s), advanced designs (cells for the 1990s), and a summary of the different $Ni-H_2$ cell manufacturers' design features. NASA R&D programs for IPV $Ni-H_2$ cells are presented at the end of this chapter.

1.1.0 BACKGROUND

In 1970, COMSAT Laboratories, together with Tyco Laboratories, first started the development of the hermetically sealed individual pressure vessel (IPV) $Ni-H_2$ cell [1-2]. This research and development effort was sponsored by the International Telecommunications Satellite Organization (INTELSAT). The objective was to develop a new technology (the $Ni-H_2$ battery technology) to replace the nickel-cadmium (Ni-Cd) batteries that were then being used on the INTELSAT commercial communication satellites in geosynchronous orbit (GEO). Back in the 1970s, these

Ni-Cd batteries were limiting the operational lifetime of the satellites to about seven years in orbit.

In parallel with the COMSAT/INTELSAT development effort, Hughes Aircraft Company (HAC) started the development of a Ni-H_2 cell for low-earth-orbit (LEO) applications [1-3]. This work was sponsored by Wright Patterson Air Force Base.

The first flight demonstrations of these new Ni-H_2 batteries were aboard the Navy's Navigation Technology Satellite NTS-2 and the Air Force's Nickel-Hydrogen Flight Experiment, both launched in June 1977. These flight experiments demonstrated that hermetically sealed IPV Ni-H_2 cells could operate successfully in a zero-gravity space environment for long periods of time (over four years).

In 1983, Ni-H_2 batteries replaced Ni-Cd batteries as the energy storage subsystem aboard the INTELSAT V commercial communication satellites. Since then, IPV Ni-H_2 batteries have become the baseline energy storage system for commercial communication satellites [1-4].

NASA is interested in the use of Ni-H_2 batteries for LEO applications such as the Hubble Space Telescope and the Space Station Freedom Program. These applications require cyclic lifetimes of up to 50,000 cycles. For Space Station Freedom, NASA would like to achieve 35 to 40 percent depths-of-discharge (DOD) to save weight. NASA-Lewis has supported and continues to support a number of both in-house and outside-contract R&D investigations to extend the cyclic lifetime of IPV Ni-H_2 cells. These investigations have focused on the design and fabrication of the positive electrodes, the concentration of the electrolyte, and the development of new and different types of separator materials. Results of the NASA-Lewis work are discussed in this text.

Ni-H_2 battery technology is gaining acceptance throughout the world for use in space applications because of its reliability and long cycle life expectancy at deep DOD. At the same time, the technology is still relatively new and advancing. This chapter concentrates on the IPV cell components and design features that have been developed and used in flight programs. IPV Ni-H_2 cell technology has advanced to the point where there are fairly well established design preferences from which to choose, but one must still look for the design features that favor his specific application. This chapter will help identify the advantages and disadvantages of these different design features. Advanced technology developments for IPV cells are discussed at the end of this chapter.

1.2.0 ELECTRODE STACK COMPONENTS

This section describes the electrode stack components currently being used for the fabrication of aerospace individual pressure vessel (IPV) Ni-H_2 cells. Figure 1-1

presents the truncated disk electrode stack components used in the COMSAT back-to-back design, and Figure 1-2 presents the pineapple-slice components used in the Air Force recirculating design.

1.2.1 Positive Electrode (Sintered)

The sintered positive electrode consists of a sintered porous-nickel plaque that is impregnated with nickel-hydroxide active material. Two procedures are used to make sintered plaque: one is the wet slurry process and the other is the dry powder (loose powder) process.

Active material is impregnated into the sintered plaque by an electrochemical impregnation process. There are two electrochemical impregnation processes used: the aqueous electrochemical impregnation process and the alcoholic electrochemical impregnation process.

Sintered Plaque

The porous sintered plaque serves to retain the active nickel hydroxide material within its pores and to conduct the electric current to and from the active material. Essential features of the sintered plaque are high porosity, large surface area, and electrical conductivity in combination with good mechanical strength [1-5].

Two different methods are used to fabricate the sintered plaque:

1. Dry powder (loose powder process)
2. Wet slurry process.

Sintering is defined as a thermal process through which a loose mass of nickel particles is transformed into a coherent body without reaching a melting point [1-5].

Carbonyl-derived nickel powders obtained from International Nickel Company Limited (INCO) are used to make the sintered plaque. Powder type 287, with a high apparent density of 0.8 to 1.0 g/cm^3, is used for the dry powder plaque, and powder type 255, with a low apparent density of 0.45 to 0.6 g/cm^3, is used to make the wet slurry plaque.

Dry Powder Plaque. The dry powder (loose powder) plaque is made by passing the INCO 287 loose powder through a screen into a mold. During the process of filling the mold with loose powder, a pure nickel wire mesh screen is placed either in the center of the loose powder or close to the bottom side of the mold. After the nickel powder is added, a cover plate is normally put on top of the mold. There are many variations to this process for adding the loose powder into the molds [1-5].

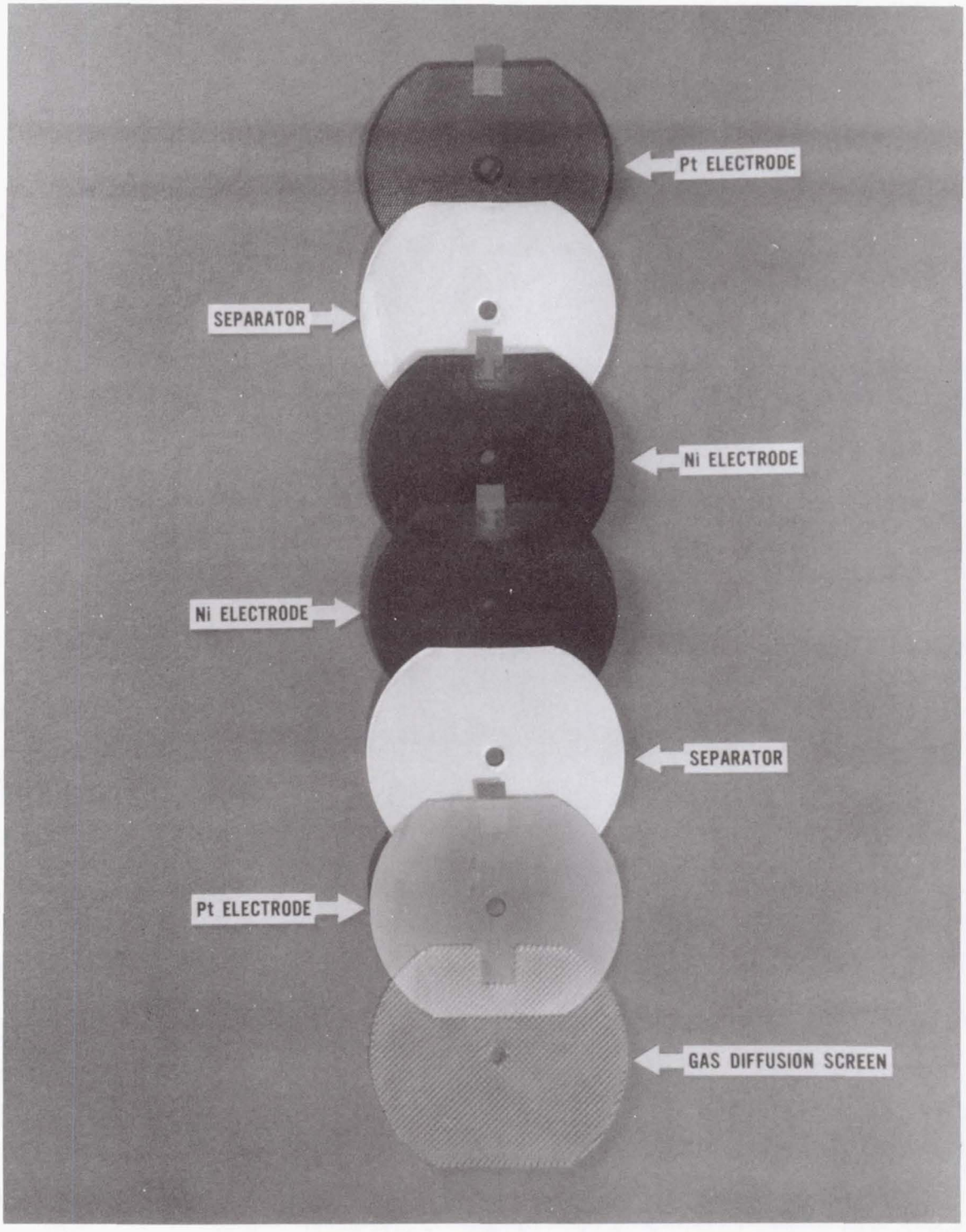

Figure 1-1. COMSAT electrode stack components (bus bar configuration).

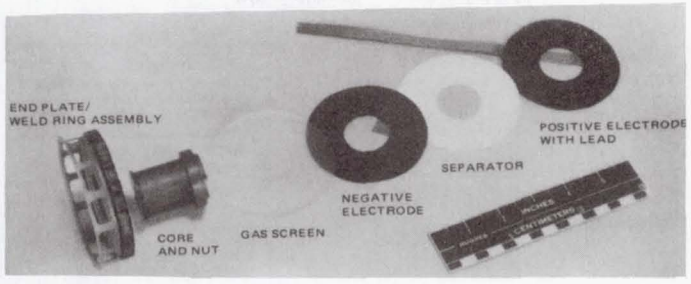

a

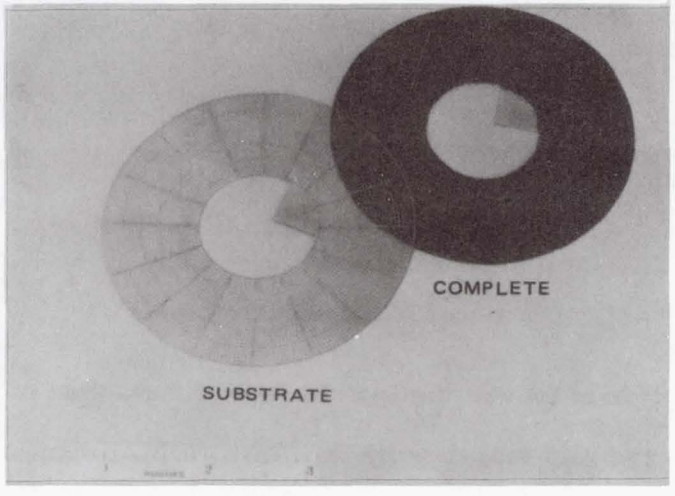

b

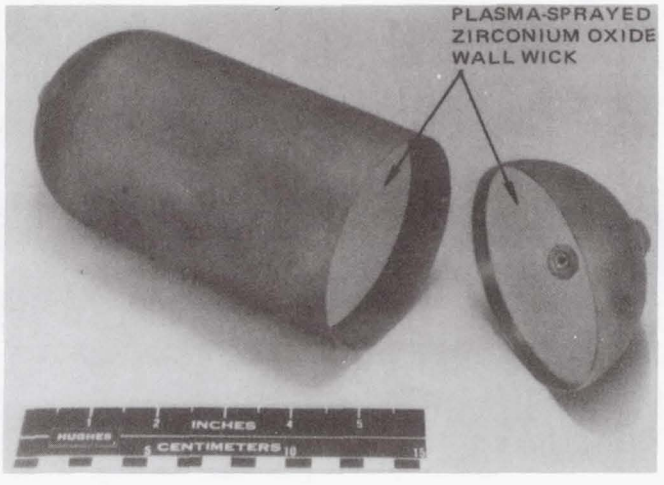

c

Figure 1-2. Air Force electrode stack components (pineapple-slice configuration).

The molds are transferred to the sintering furnace. A continuous mesh-belt type of furnace is used. The temperature in the sintering zone is 800 to 1,000°C. A reducing atmosphere is used in the sintering furnace; the atmosphere is normally either 100 percent hydrogen gas, forming gas ($N_2 + H_2$), or cracked natural gas.

Wet Slurry Plaque. The continuous wet slurry plaque is made as follows: a nickel slurry is prepared by mixing low-density INCO 255 carbonyl-derived nickel powder with a viscous aqueous solution of a binder, typically carboxy methyl cellulose. A nickel grid is continuously carried through a container filled with the slurry. The grid takes up a certain amount of slurry on both sides, which is adjusted to the desired thickness with doctor blades. The strip is passed through a vertical drying zone to evaporate the water and then through a sintering furnace at 800 to 1000°C with a reducing atmosphere. The binder is decomposed in the sintering furnace.

Wet Slurry vs Dry Powder Plaque. Both of these sintering processes have been around for many years, and there have been many investigations of their sintered properties. These investigations include studies of the bend strength, porosity, pore size distribution, mean pore diameter, resistance to corrosion, etc. No clear advantage exists for one type of plaque over the other based on these studies. Both types of plaque are currently being used for aerospace nickel hydrogen electrodes and the choice is dependent on the preference of the manufacturer or user.

One of the major differences in their physical properties is porosity.

	Porosity of Sintered Nickel
Dry Powder (INCO 287)	83 ± 2 percent
Wet Slurry (INCO 287)	83 ± 2 percent
Wet Slurry (INCO 255)	81 ± 2 percent

The above percentages are the porosity of the sintered nickel plaque without the substrate. The porosity of the plaque including the sintered nickel and the substrate, is 2 to 3 percent lower than the porosity of the sintered nickel alone.

The dry powder process involves more manual labor (is more labor intensive). The wet slurry process, being a continuous process, is better suited to large-scale production.

Porosity values and the porosity range specified of ±2 percent are typical values for sintered nickel plaque presently used for aerospace Ni-H_2 cells. Plaques with higher and lower porosities have been used in past programs and probably will be used in the future.

Both wet slurry and dry powder plaques are used with the Bell Laboratories aqueous impregnation process for the fabrication of positive nickel-hydroxide

electrodes. The plaque must be wet oxidized to avoid corrosion in the aqueous impregnation bath [1-6].

Dry powder plaque with INCO 287 is used with the Air Force/HAC alcoholic impregnation process for the production of positive nickel electrodes. This plaque is not wet oxidized. With the lower boiling point of the alcoholic impregnation bath, there is less concern about corrosion during impregnation.

Both the wet slurry and dry powder plaque use pure nickel wire mesh screen for the grid structure. A perforated foil substrate is more desirable from a strength standpoint; however, it is less desirable in terms of voltage performance. During high rates of discharge there is significantly higher polarization (voltage loss) observed for positive electrodes made using plaque with the perforated foil, compared to with the wire mesh screen [1-7].

The sintered plaque is coined at the periphery of the electrode (both on the outside edge and inside edge) and in the tab region. After impregnation, a tab is spot welded to the coined tab region. Coining is defined as the procedure for compressing the nickel sinter around the edge of the periphery and the center hole of the plaque and in the tab region. The coined region is compressed under high pressure. Coining is used to prevent any flaking or loss of material around the edge of the electrode. Coining in the tab region is done so that a tab can be spot welded in the coined region, making a good electrical contact to the nickel sinter.

Chemical Impregnation

The process by which the porous sintered plaques are filled with active material is called impregnation. The plaques are submerged into an aqueous or alcoholic solution of nickel nitrate and then subjected to a chemical or electrochemical process to precipitate nickel hydroxide into the pore structure.

Chemical impregnation is accomplished by means of four steps carried out in sequence; namely, soaking or vacuum impregnating the plaques in a nickel nitrate solution, drying, soaking in a sodium hydroxide solution to precipitate out the $Ni(OH)_2$, and then washing and drying. This four-step chemical impregnation process is repeated until the desired weight gain is obtained. It usually requires six or more impregnation cycles to obtain the desired weight gain [1-5].

Cobalt nitrate is added to the impregnation bath, with the cobalt content being 4 to 11 percent of the nickel content. The cobalt addition is used to maintain capacity during cycling [1-5].

The sintered nickel plaque is attacked by the nitrate solution during chemical impregnation. Twenty-five percent or more of the sintered material is typically corroded away during impregnation, even though the sintered plaques were wet oxidized prior to impregnation.

Chemically impregnated aerospace nickel-oxide electrodes are loaded to between 1.9 and 2.4 grams of active material/cm^3 of void volume and the loading tends to be concentrated toward the surface of the electrode by the nature of the process. With cycling, the active material within the positive electrode migrates toward the surface of the electrode, increasing the micropore structure (concentration of the active material) in the region near the surface of the electrode facing the separator [1-8]. As this active material expands and contracts with cycling within the pores of the sinter structure, it fractures the sintered structure, causing the electrode to expand. As the positive electrode expands and changes its composition, electrolyte is drawn by capillary attraction from the separator into the micropore structure of the positive electrode drying out the region at the separator-electrode interface. The internal impedance of the Ni-Cd cell increases, causing a voltage loss and, eventually, cell failure.

Electrochemical Impregnation.

All of the aerospace Ni-H_2 cells use electrochemically impregnated positive electrodes. The sintered nickel plaques are placed in a polarization tank where they are cathodically polarized in an alcoholic or aqueous based nickel nitrate solution. During electrolysis, the pH value of the solution within the pores increases as a result of the reduction of nitrate ions, which is related to the consumption of hydrogen ions. Nickel hydroxide thus precipitates within the pores. The solution outside the plates is maintained at a constant pH value, which does not permit precipitation of the nickel hydroxide.

Aqueous Impregnation Process (Bell Laboratories Process). This impregnation process uses an aqueous-based nickel nitrate solution for the impregnation bath. During electrochemical impregnation, the bath is maintained at its boiling temperature of approximately 100°C. The Bell Laboratories aqueous electrochemical impregnation (EI) process is described in Reference 1-9. Cobalt nitrate is added to the nickel nitrate bath to give approximately 5 percent by weight of cobalt hydroxide in the active material of the finished electrode (approximately 7 percent cobalt in the bath).

Alcoholic Impregnation Process (Air Force Process). This impregnation process uses an alcohol-based nickel nitrate solution for the impregnation bath. During electrochemical impregnation, the bath is maintained at its boiling point of approximately 70°C. The major advantage of the lower temperature is to reduce corrosion during the impregnation. Cobalt nitrate is added to the nickel nitrate bath to give approximately 9 percent by weight of cobalt hydroxide in the active material of the finished electrode (11.2 percent cobalt in the bath). Parameters for production of positive electrodes by the alcoholic impregnation process [1-10] are the following:

Nickel nitrate concentration	1.6–1.7 molar
Cobalt nitrate concentration	0.16–0.18 molar

Ethanol concentration	46% by volume
Impregnation time	90 minutes
pH	2.5–3.0
Solution temperature	61°C to 72°C

Advantages of Electrochemical Impregnation. Both the aqueous and the alcoholic impregnation processes provide the following advantages over chemical impregnation:

1. Loading of Active Material. Electrochemical impregnation gives very uniform loading of the active material within the pores of the nickel sinter.

2. Loading Level. The loading level of active material can be accurately controlled by the EI process. Typical loading values are the following:

1.67 ± 0.1 g/cm^3 void volume	geosynchronous applications
1.55 ± 0.1 g/cm^3 void volume	low-earth-orbit applications*

   Chemically impregnated electrodes are loaded to between 1.9 and 2.4 grams of active material per cubic centimeter of void volume.

3. Corrosion. During electrochemical impregnation, the sintered plaques are cathodically polarized, which reduces corrosion of the plaque during impregnation. For the aqueous process, if the plaques are properly passivated (wet oxidized), very little or no corrosion will occur during impregnation [1-6]. Without proper wet oxidation, significant corrosion can occur during the aqueous electrochemical impregnation at the 100°C boiling point of the impregnation solution. For the alcoholic impregnation process, the plaques are not passivated (wet oxidized). The plaques are partially oxidized in air when they come out of the sintering furnace. Even without wet oxidation, very little corrosion of the plaque occurs during impregnation with the alcoholic process because of the lower boiling point. For both the alcoholic and aqueous impregnation process, the corrosion of the plaque is normally small, less than 2 percent, which is quite low compared to the 25 percent corrosion of the sintered plaque observed during chemical impregnation [1-8].

4. Utilization. Higher utilization of the active material is achieved with the electrochemically impregnated positive electrodes compared to chemically

---

* An exception is the Ni-H_2 cells used for the Hubble Space Telescope (HST) satellite. The HST is orbiting in a low-earth orbit, and the loading level of active material is 1.67 g/cm^3. Ni-H_2 batteries/cells on board the HST are expected to last for 20,000 to 40,000 cycles because HST batteries/cells are being operated at very low depths-of-discharge (between 6 to 8 percent DOD). The HST is an exception in this regard; normally, Ni-H_2 batteries used for LEO applications are operated at 20 to 40 percent DOD. At these higher DODs, the loading should be reduced to 1.55 g/cm^3. For a more detailed discussion of LEO and GEO applications, refer to Chapter 2.

impregnated positive electrodes. Typical utilization values are 120 percent for electrochemically impregnated electrodes and 80 percent for chemically impregnated electrodes. The higher utilization for electrochemically impregnated electrodes results from the more uniform loading of the active material within the pore structure and lower loading levels.

5. Expansion. The rate of expansion with cycling was four times greater for chemically impregnated nickel hydroxide electrodes than for electrochemically impregnated nickel-hydroxide electrodes [1-11]. The reduction in the rate of expansion results from the reduction in loading and less corrosion of plaque during impregnation.

Aerospace Ni-H_2 cells with the electrochemically impregnated positive electrodes are expected to have at least four times the cyclic life and/or lifetime in orbit as compared to Ni-Cd cells with the standard aerospace chemically impregnated positive electrodes. Since the nickel electrode is the lifetime-limiting component for Ni-H_2 cells, the use of electrochemically impregnated positive electrodes was an obvious choice.

Cobalt Hydroxide Additive in Positive Nickel-Hydroxide Electrodes

Increasing the amount of cobalt hydroxide in the nickel hydroxide active material of electrochemically impregnated positive electrodes results in an active material deposit of decreased mechanical rigidity [1-56]. Decreasing rigidity results in less mechanical strain of the nickel sinter and thus a reduced rate of nickel electrode capacity loss due to mechanical fatigue. The reduced electrode strain results in improved cycle life.

Experimental investigations were conducted with increasing levels of $Co(NO_3)_2$ concentration from 0 to 12 percent, expressed as a percentage of total solution molarity in the impregnation solution [1-56]. The electrochemically coprecipitated cobalt hydroxide correspondingly increased from 0 to 10 percent of the active material in the nickel hydroxide electrode. The reduction in mechanical strain with increasing cobalt levels is striking from these experimental results. At least a three order-of-magnitude difference (reduction) in strain exists between the 0 and 12 percent cobalt level data.

1.2.2 Negative Electrode

The negative electrode, typically referred to as the hydrogen electrode, consists of a Teflon-bonded platinum black catalyst supported with a fine mesh nickel screen with Teflon backing.

The sintered Teflon-bonded platinum electrodes were originally developed at Tyco Laboratories [1-12] for the fuel cell industry. For Ni-H_2 cells, a hydrophobic Teflon backing was added to these platinum electrodes to stop water or electrolyte

loss from the back side of the negative platinum electrode during charge and overcharge while readily allowing diffusion of hydrogen and oxygen gas. The use of Gortex as the microporous Teflon membrane came from EIC under a development contract to HAC [1-7], [1-13].

The physical properties of this hydrogen electrode provide the right interface for the electrochemical reactions to occur without flooding or drying out the electrode at the separator interface.

Substrate

Originally, a fine-mesh nickel screen or an expanded nickel screen was used. An improved photo-etched substrate was developed by HAC [1-14]. This photo-etched substrate eliminates cut edges of the electrodes that caused shorts during cell stack assembly and also provides a solid tab for lead attachment. These photo-etched substrates are now being used by all U.S. manufacturers.

Teflon Membrane

The back of the photo-etched nickel substrate is sprayed with a Teflon 30 emulsion, and the "Gortex" Teflon membrane is pressed onto the back side of the substrate. The Teflon 30 is sprayed on to improve final bonding of the membrane.

Platinum Mix

The platinum mix consists of a Methocel solution, fuel-cell-grade platinum black powder, and a Teflon 30 solution. A fixed amount of this mixture is screened onto the front face of the substrate with the Teflon backing. The entire assembly is dried and then pressed. The platinum content is normally specified as 7.0 mg $\pm$ 1.0 mg/cm^2.

Sintering

The electrodes are sintered following a time-temperature sequence designed to remove the binders and provide Teflon bonding of the platinum powder and bonding of the Teflon membrane to the back of the substrate.

Cleaning

A special cleaning treatment is used in the manufacturing of negative electrodes for Air Force Ni-H_2 cells.

Analysis results by HAC showed the presence of wettable Triton X-100 residues, a material used as a wetting and suspension agent during negative electrode manufacturing. A proprietary cleaning process [1-15], using a mixture of trichloroethylene and ethanol, was developed. This process completely removes

the wettable residues from the negative electrode and enhances its hydrophobic characteristics.

1.2.3 Separator Materials

Two types of separator materials are presently being used for aerospace Ni-H_2 cells:

1. Asbestos, fuel-cell-grade asbestos paper
2. Zircar, untreated knit ZYK-15 Zircar cloth.

Asbestos

The fuel-cell-grade asbestos is a nonwoven fabric with a thickness of 10 to 15 mils. The asbestos fibers are made into a long roll of nonwoven cloth by a paper making process. As an added precaution, the asbestos can be reconstituted in a blender and then reformed into a cloth to avoid any nonuniformity in the original structure that would allow oxygen to bubble through. The fuel-cell-grade asbestos has a high bubble pressure for oxygen gas; a pressure difference of more than 25 psi is required across the wet separator cloth (10 mils thick) to force oxygen bubbles through the material.

The asbestos separator serves the following functions:

1. Acts as an electrical insulator between the positive and negative electrodes.

2. Serves as a reservoir of KOH electrolyte and remains stable in the electrolyte to allow long-term storage and/or cycling.

3. Serves as a medium for charge and discharge current through the separator via ionic conduction of $(OH)^-$ ions in the KOH electrolyte.

4. Provides a barrier to the transfer of oxygen gas. Oxygen gas is forced off the backside of the positive electrode during overcharge because of the high bubble through pressure of the asbestos separator material. The oxygen cannot channel or bubble through the separator to cause rapid recombination at the negative electrode.

5. Asbestos has a dual distribution of pore diameters which tends to prevent separator dryout due to capillary attraction of electrolyte to the micropore structure in the positive electrodes [1-52].

Zircar Separator

Zircar fibrous ceramic separators are available in textile product forms. These textiles are composed of Zirconia fibers stabilized with Yttria. These materials offer

the extreme temperature and chemical resistance of the ceramic Zirconia. The materials are constructed of essentially continuous individual filaments fabricated in flexible textile forms. The ZYK-15 knit cloth type is the material used for Ni-H_2 cells.

Product Forms. Zircar Zirconia textiles are currently available in three woven or knitted cloth types. The series of products offers a variety of thicknesses, cloth weaves, and bulk densities. All cloths are white in color.

General Properties of Zirconia Textiles*

Product Type	ZYW-15	ZYK-15	ZYW-30A
Thickness (mils, nominal)	15	15	30
Fabrication Form	Woven	Knit	Woven
Fabrication Type	Square	Tricot	Satin
Bulk Density (lb/ft^3)	48	56	63
Weight (oz/yd^2)	8	10	22
Breaking Strength (lb/in width)	1.0	1.0	4.0
Porosity (%)	87	85	83

*Zircar Products, Inc. Technical Data
Bulletin No. ZPI-204
November 1, 1978

Properties of Zirconia Fibers in the Cloth Products*

Diameter	microns	4–6
Density	gm/cm^3	5.6–5.9 (92–97% of theoretical)
Surface Area (N_2-BET Method)	m^2/gm	1.0 max.
Y_2O_3 Stabilizer Content	wt. %	8
Crystal Phases		cubic + tetragonal
Composition ($ZrO_2 + HfO_2 + Y_2O_3$)	%	99+
Melting Point	°F	4700
Recommended maximum temperature of application	°F	3300–4000 (depending on application conditions)
Volatile content (1000°C)	%	0

*Zircar Products, Inc. Technical Data
Bulletin No. ZPI-204
November 1, 1978

The inherently brittle nature of a ceramic material such as Zirconia, while partially offset by the fibrous structure, makes them fragile and susceptible to breaking. They must be handled with care.

A 15-mil-thick separator of untreated knit ZYK-15 Zircar cloth is used for Ni-H_2 cells. Either one or two layers of this separator material can be used. The second ZYK-15 layer is normally used as a backup to prevent oxygen channeling in

the event of assembly damage to the first layer [1-16]. As mentioned above, the Zircar cloth is fragile and must be handled with care.

The knit Zircar cloth has a very low oxygen bubble-through pressure and, during charge and overcharge, oxygen gas readily permeates through the separator to recombine at the hydrogen platinum electrode to form water.

The Zircar separator serves the following functions:

1. Acts as an electrical insulator between the positive and negative electrodes.
2. Serves as a reservoir of KOH electrolyte and remains stable in the electrolyte, allowing long-term storage and/or cycling.
3. Serves as a medium for charge and discharge current through the separator via ionic conduction of $(OH)^-$ ions in the electrolyte.
4. Allows oxygen gas to permeate through the separator to recombine at the platinum catalyst in the hydrogen electrode during overcharge.

Asbestos with Zircar

A dual separator combination uses one layer of asbestos and one layer of Zircar. The asbestos is placed adjacent to the positive electrode to act as a barrier, forcing the oxygen gas generated during overcharge off the back of the positive electrode. The Zircar acts as a reservoir to store electrolyte.

Electrolyte Quantity Asbestos vs Zircar

Cells with one layer of Zircar contain slightly more electrolyte than cells with one layer of asbestos (see Table 1-5, Section 1.9.2, "EPI MANTECH Cell Design"). The ZYK Zircar separator has a nominal thickness of 15 mils. Asbestos separator thickness (fuel-cell-grade asbestos) is 12 to 15 mils thick. During cell assembly, the asbestos separator is compressed to approximately 10 mils. The Zircar tends to retain its thickness under compression because of the Zirconia fibers.

Electrolyte retention of asbestos and Zircar are the following [1-57].

	Asbestos	Zircar
Density	11.69 g/in.^{3}	9.65 g/in.^{3}
Retention Electrolyte (g KOH/g separator)	135 %	150%
KOH/unit vol	15.78 g/in.^{3}	14.47 g/in.^{3}
KOH/unit vol in cell	12.62 g/in.^{3}	14.47 g/in.^{3}

The asbestos contains more electrolyte per unit volume of separator. However, under compression in a cell the asbestos contains less electrolyte, at least for the EPI MANTECH cell as shown in Table 5-1.*

Zircar has a lower resistivity than asbestos because of the higher quantity of electrolyte and teh less tortuous path for ionic conduction. Cells with Zircar separators have lower impedance and better discharge voltage performance.

1.2.4 Gas Screen

A polypropylene gas diffusion screen is placed behind the hydrogen electrode to allow hydrogen gas and oxygen gas to diffuse to the back side of the negative electrode with the Teflon backing.

1.3.0 NICKEL-HYDROGEN CELL DESIGNS

1.3.1 Electrode Stack Designs

Two basic types of electrode stack designs are used for aerospace Ni-H_2 cells. These are the back-to-back design (COMSAT) and the recirculating design (Air Force).

Back-to-Back Design (COMSAT Design)

Figure 1-3 shows the basic arrangement of the electrode stack components for the COMSAT back-to-back design. Two positive nickel oxide electrodes are positioned back-to-back. A separator is placed on either side of the pair of positive electrodes. The negative platinum electrodes are placed with the platinum black surface next to the separator material. A plastic gas diffusion screen is placed on the back side of each negative electrode to facilitate gas diffusion from the perimeter of the cell stack into the stack via the back side of the platinum (hydrogen) electrode. These components constitute one module of the electrode stack. The entire electrode stack comprises a number of such modules (see Figure 1-4). The stack is contained within a pressure vessel and surrounded by pressurized hydrogen gas. A more detailed description of the electrode stack components and design features are presented in References 1-17, 1-18, and 1-19.

Oxygen Management. For the back-to-back cell with asbestos separators, during charge and overcharge oxygen gas that evolves at the nickel-oxide electrodes is forced out between the back-to-back positive electrodes (see Figure 1-3). The oxygen diffuses into the gas space between the electrode stack and the pressure vessel wall, into the region of the gas diffusion screens on the back of the negative electrode,

* The asbestos separator is compressed to approximately 80 percent of its original volume (thickness) in a cell.

through the porous backing of the negative electrode, where it combines with hydrogen to form water [1-7]. The partial pressure of oxygen within the cell is dependent on this diffusion process. The limiting step is the oxygen diffusion in the gas phase pores of the Teflon-bonded electrode, not in the Teflon backing [1-7]. The fraction of oxygen was less than 0.5 percent in the surrounding hydrogen gas when the cell is continuously overcharged at the C/2 rate [1-17].

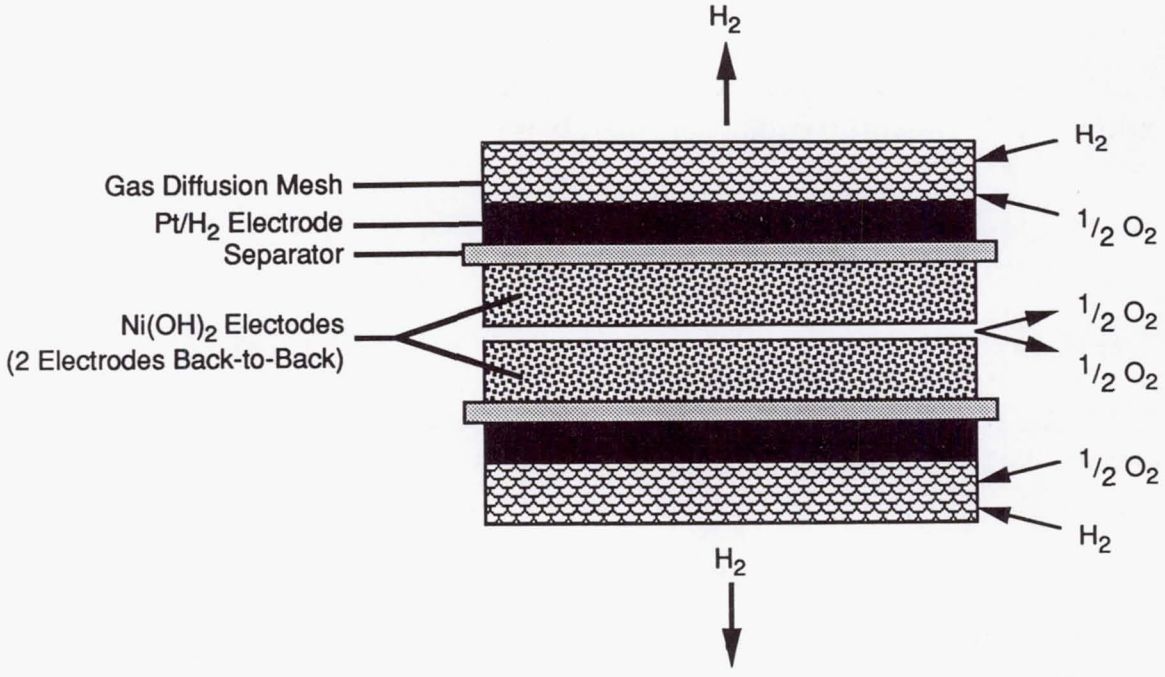

Figure 1-3. COMSAT back-to-back Ni-H_2 cell design.

For the back-to back cell with Zircar separators, the oxygen gas evolved during overcharge at the positive electrode permeates through the knit ZYK-15 Zircar cloth and is recombined at the front surface of the platinum negative electrode. Very little, if any, oxygen diffuses into the gas space surrounding the electrode stack. The fraction of oxygen in the surrounding hydrogen gas is negligible.

Electrolyte Management. An investigation of electrolyte loss mechanisms was performed for the back-to-back cell design [1-20]. This study showed no measurable long-term electrolyte loss—even after 3,000 charge/discharge cycles at 80 percent

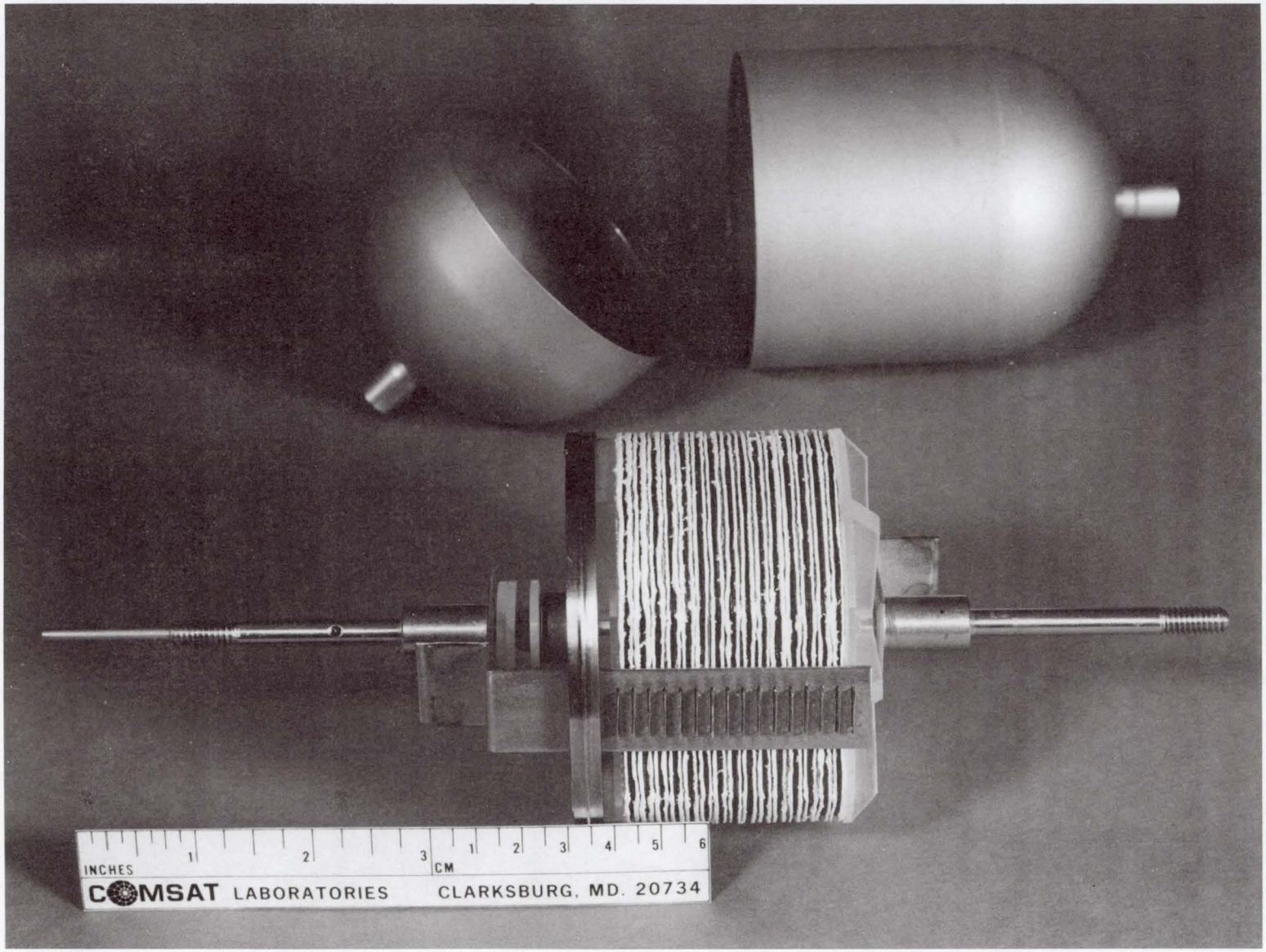

Figure 1-4. COMSAT electrode stack assembly (NTS-2 cell).

depth of discharge (DOD). Based on these results, no wall wick was used for the COMSAT cell design.

Water Loss. Water loss from the electrode stack can occur by evaporation from the electrode stack and condensation at the pressure vessel wall [1-53]. The vapor phase transfer of water is driven by the difference in temperature between the cell stack and the vessel wall; actually, the driving mechanism is the difference in vapor pressure that results from the difference in temperature. Water vapor pressure data for KOH concentrations of interest and for pure water are presented in Figure 1-5. Water condensation occurs when the pressure of the water vapor arriving at the surface is higher than the saturated water vapor pressure that corresponds to the surface temperature. For evaporation condensation to occur from the electrode stack to the pressure vessel wall, the temperature difference must be equal to or greater than the ΔT at the equivalent vapor pressure of water and of the KOH concentration of electrolyte in the electrode stack. The temperature difference ΔT between the stack and cell wall for water to condense on the wall at various KOH concentrations of electrolyte in the stack is presented in Figure 1-6. The ΔT values were calculated using the vapor pressure data at the various KOH concentrations presented in Figure 1-5.

From Figure 1-6 one can observe that the ΔT increases slightly with temperature, but more importantly, that the ΔT is strongly dependent on the KOH concentration. For example, cells with low concentrations of 23 percent KOH require a ΔT of only 4 to 5°C for water to condense, where cells with 36 percent KOH require a ΔT of 10 to 12°C for water to condense. This is a significant consideration for cell designs proposing to use low KOH concentrations [1-54].

In-orbit experience with the INTELSAT V batteries has shown water loss occurring during trickle charge storage of the batteries/cells between eclipse seasons. This water loss mechanism is discussed in more detail in Chapter 5, Section 5.2.2, "Voltage Performance In Orbit" for INTELSAT V batteries.

Because of this potential for water loss, a wall wick is now recommended for use with all cell designs.

Wall Wick. HAC developed a plasma-sprayed zirconium oxide wall wick as shown in Figure 1-2; the yttrium-stabilized zirconium oxide is plasma sprayed onto the inside walls of the INCONEL pressure vessel [1-21].

The separators (asbestos or ZrO_2) extend to the pressure vessel wall. Both the separator and the wall wick combined serve as a reservoir for electrolyte with the pore size structure being such that electrolyte or water will be wicked from the plasma-sprayed wall wick into the separator. Any electrolyte loss or water loss from the cell stack will be returned to the cell stack by way of this wall wick/separator combination.

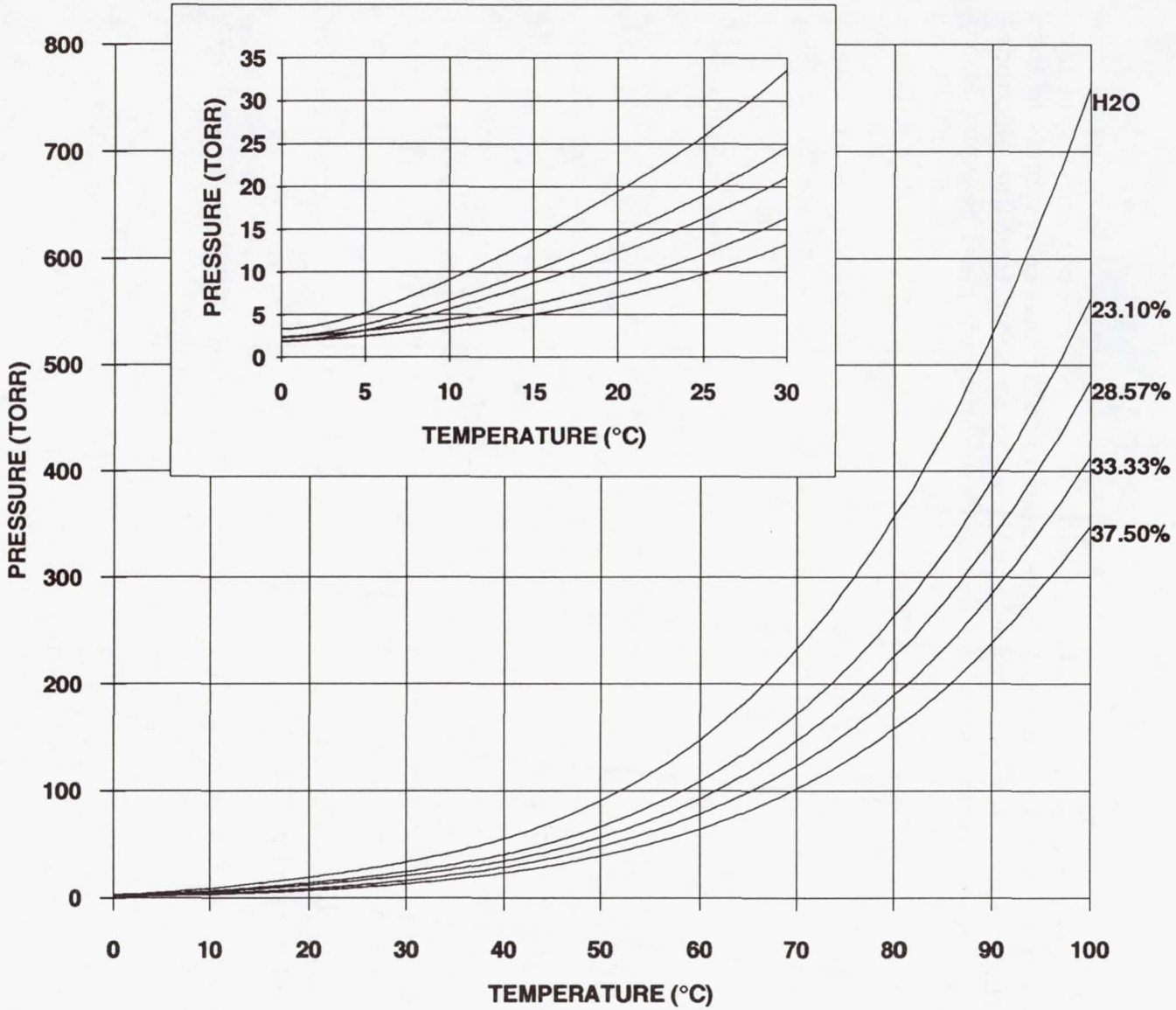

Figure 1-5. Vapor pressure of various KOH concentrations.

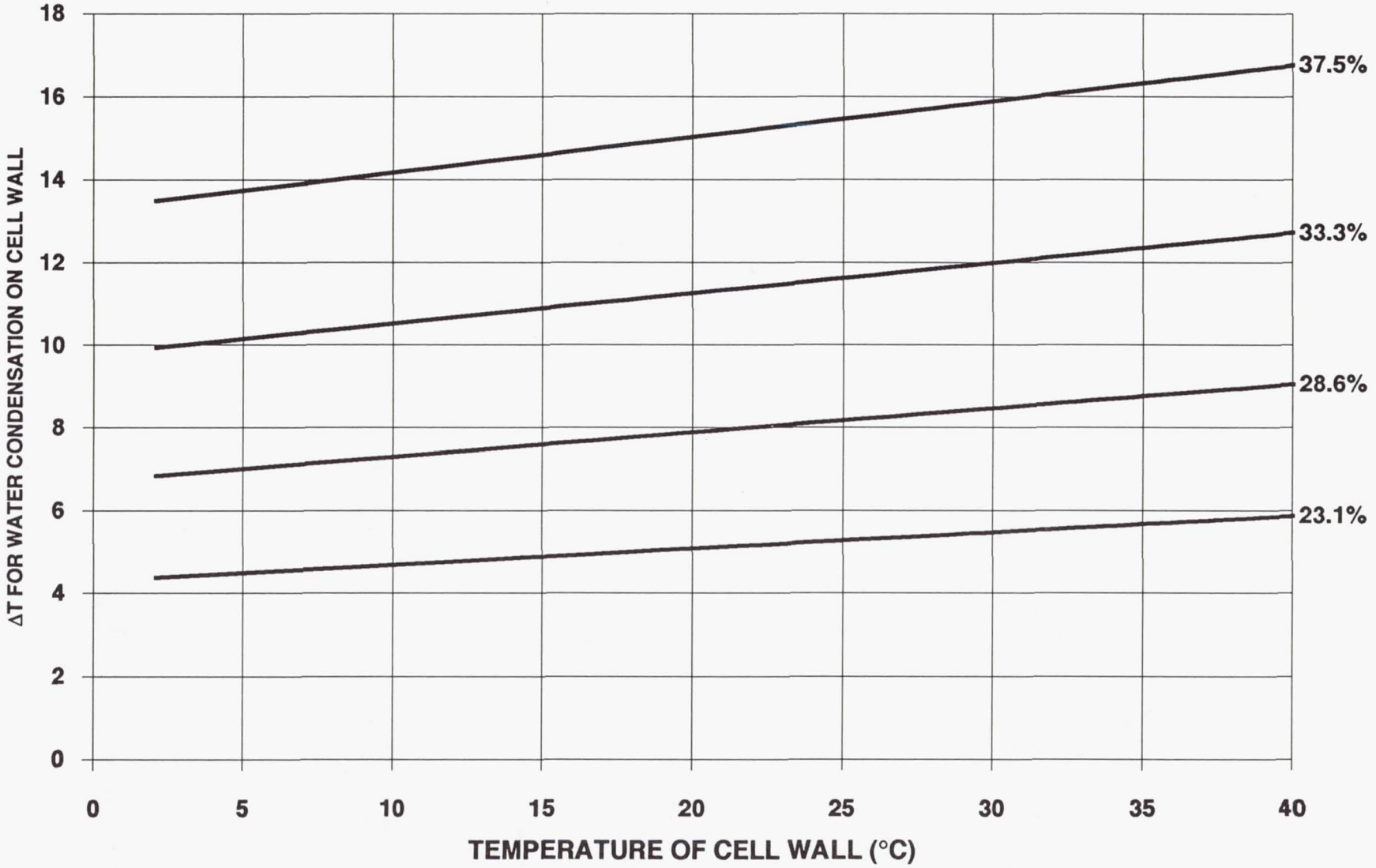

Figure 1-6. Temperature difference between stack and cell wall for water to condense at various KOH concentrations.

Recirculating Design (HAC/Air Force Design)

The Air Force baseline cell uses the recirculating electrode stack design [1-22]. This design was originally referred to as the single positive electrode design; however, it is better known as the Air Force cell design. A sketch of the recirculating design is shown in Figure 1-7 and 1-8a. One module consists of a gas screen, H_2 electrode, separator, and Ni electrode; the last stage consists of a H_2 electrode and separator, as shown in the recirculating stacking sequence in Figure 1-8a. A wall wick returns the electrolyte to the cell stack via separators that extend to the cell wall. The wall wick and separator serve as the reservoir for the electrolyte. The electrode stack components for the Air Force advanced cell design are shown in Figure 1-2.

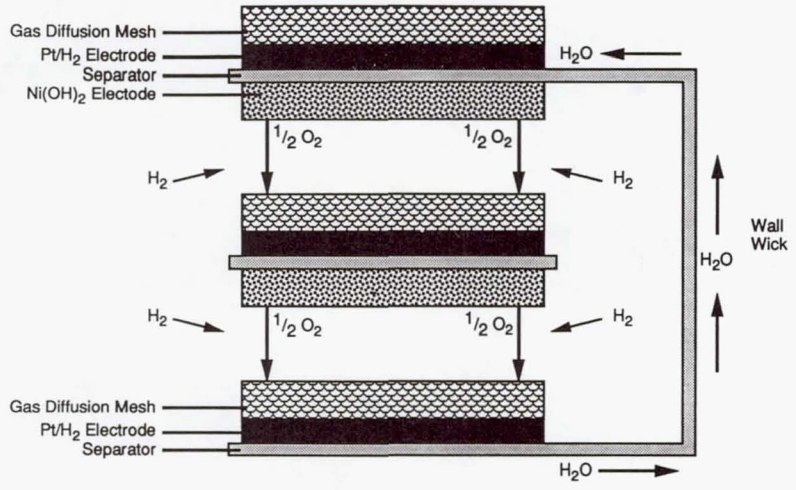

Figure 1-7. Air Force recirculating Ni-H_2 cell design.

Oxygen Management. Either asbestos or Zircar, or a combination of the two, can be used as the separator materials for the recirculating cells.

With the asbestos only or a combination of asbestos and Zircar, all oxygen gas generated on overcharge emerges off the back of the nickel electrode. The diffusion path is very short; the oxygen gas simply travels through the gas screen to recombine at the next hydrogen electrode (Figure 1-7). Oxygen comes off the back side of the positive electrode of one module and recombines to form water at the next module down. During overcharge, this transfer of water to the next module down occurs throughout the electrode stack. The last module in the stack is simply a negative electrode and separator reservoir. The water formed at this electrode separator combination goes to the wall wick and is recirculated back to the first module in the stack (hence the name recirculating design). With this recirculating

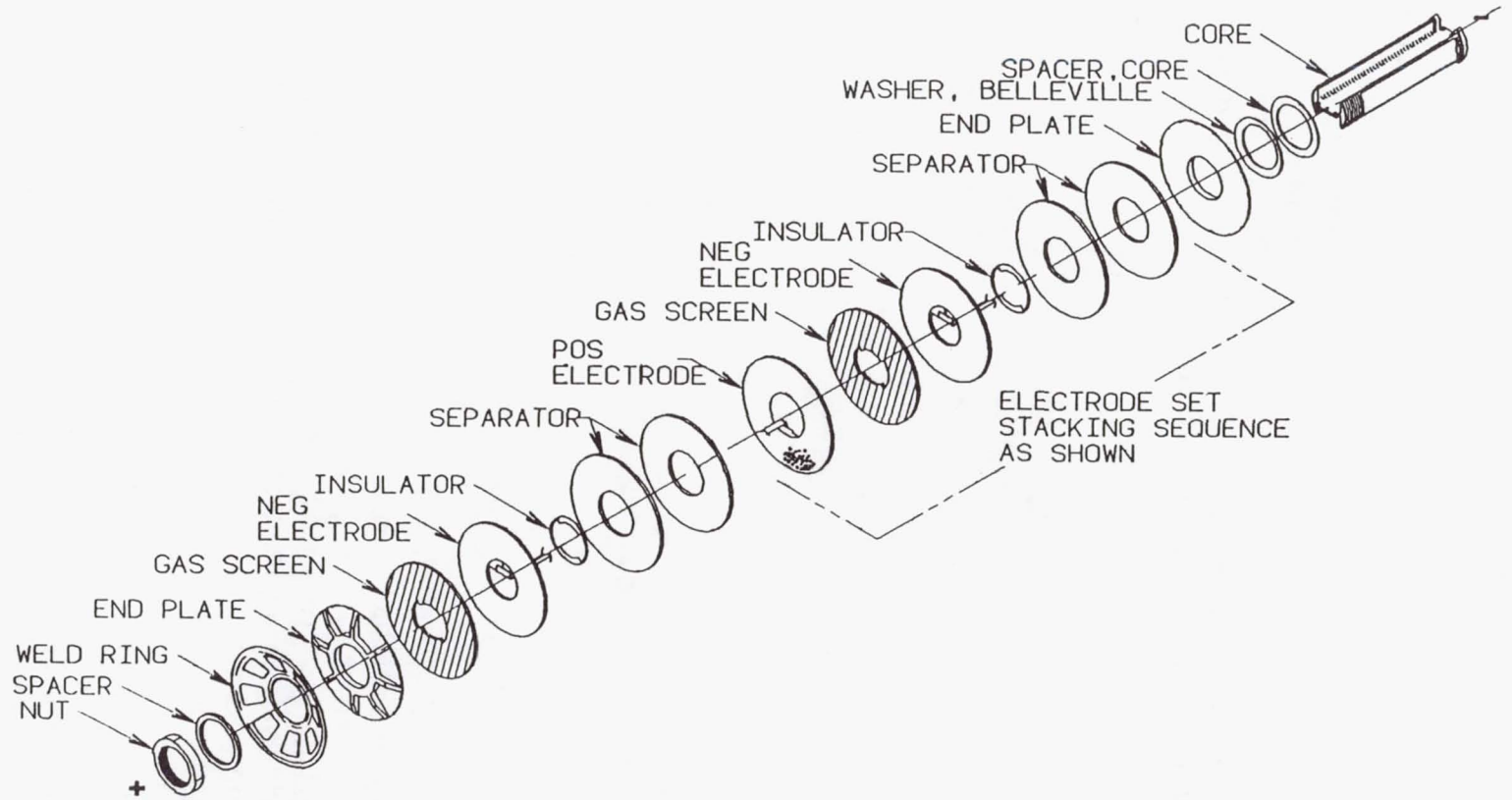

Figure 1-8a. Air Force recirculating stacking sequence.

design, the oxygen concentration is kept very low (below 0.2 percent in the surrounding hydrogen gas) during continuous overcharge at the C rate [1-13].

With the ZYK-15 Zircar only, the separators extend to the wall wick. The Zircar contains large enough pores for oxygen gas generated on overcharge to permeate through the pores of this separator to the platinum electrode, where it recombines to form water. Oxygen can, of course, also emerge off the back side of the nickel electrode and diffuse through the gas screens as before. However, most of the oxygen permeates through the separator and there is little or no recirculation of water in cells with the Zircar separators. For this design, the concentration of oxygen in the surrounding hydrogen gas is negligible.

Electrolyte Management. There are three mechanisms for the loss of the electrolyte from the electrode stack: (1) by entrainment in the hydrogen and oxygen gases evolved during charge and overcharge (2) by weeping of the negative electrode and (3) by electrolyte displacement, that is, the electrolyte being pressed out of the positive electrodes in the cell stack by oxygen gas evolved during charge and overcharge.

Electrolyte loss by both entrainment and weeping of the negative electrode was determined to be negligible for negative electrodes with Gortex backing for both back-to-back and recirculating electrode stack configurations. The major electrolyte loss mechanism is by displacement. When electrolyte is added to the cell, the void volume of the positive electrode is completely saturated with electrolyte. During activation, approximately 25 percent of the electrolyte in the positive electrodes is displaced by oxygen gas during charge and overcharge of the cell [1-7]. It was found that electrolyte loss by displacement occurred during initial cycling (activation) but eventually decreased to zero, leaving enough electrolyte to operate the cell efficiently [1-22].

Once cells are activated, electrolyte loss has not been observed to be a problem for Ni-H_2 cells. No loss of electrolyte has been observed from the electrode stack of the cell during cycling in life tests.

Water Loss/Wall Wick. As previously mentioned, water loss from the electrode stack can result from evaporation and condensation of water vapor from the cell stack to the pressure vessel wall, when a large enough temperature difference exists between the stack and the wall. Cells operating in LEO applications must dissipate more heat because of the high-rate duty cycle. Temperatures between the stack and wall may well exceed the ΔT at the equivalent vapor pressure that would allow water transfer to the wall. Especially since LEO applications use low KOH concentration of electrolyte so that the ΔT needs only to exceed 5 to 7° C for water transfer (see Figure 1-6). HAC developed the ZrO_2 wall wick and the ZrO_2 separators for the Air Force recirculating design for these LEO applications [1-22]. The plasma-sprayed zirconium-oxide wall wick shown in Figure 1-2 provides a return path for any water or electrolyte lost from the cell stack independent of the mechanism [1-21].

Yttrium-stabilized zirconium oxide is plasma sprayed on the inside of the pressure vessel wall throughout the cell except for the terminals and weld area. The weld area is bridged with a metallic wick. The separators are made large enough to contact the cell wall and provide a return path for the electrolyte.

1.3.2 Electrode Configurations

Two electrode configurations are used to fabricate Ni-H_2 cells. One configuration has the bus bars located on the outside of the electrode stack (COMSAT design). The second configuration has the electrodes in the shape of a pineapple slice (Air Force design) with the tabs going through the center slice of the electrode stack.

Bus Bar Configuration

For the bus bar truncated disk configuration, the electrode stack components are fabricated with two sections, located opposite each other, removed from the circumference of the cylindrical electrodes. A tab is located in the center of one of the cut-off sections (see Figure 1-1). When the electrode stack is assembled, the positive electrode tabs come off one side and these tabs are welded to slots in the positive bus bar; the negative electrode tabs come off the opposite side of the electrode stack and these negative tabs are welded to the negative bus bar (see Figure 1-4). The electrode stack components are assembled onto the center rod for alignment; note the hole in the center of the electrode stack components, as shown in Figure 1-1.

Pineapple Slice Configuration

For the pineapple slice configuration, the electrode stack components are shaped like a pineapple slice (see Figure 1-2) with a large center hole for the tabs. These electrode stack components are assembled onto a polysulfone central core (see Figure 1-8a and 1-8b). The electrode tabs are brought out through this center core, the positive electrodes in one direction and the negative electrodes in the opposite direction. This center core serves to align the electrode stack components, provide a conduit for the positive and negative tabs, and insulate the positive and negative tabs from each other and from the electrode stack components.

Heat transfer is better with the pineapple slice configuration than with the bus bar truncated disk configuration. Heat is transferred uniformly from the entire circumference of the pineapple slice electrodes, whereas sections are removed from the circumference of the truncated disk electrodes.

Electrode stack components with the pineapple configuration are now being used in both recirculating and back-to-back electrode stack designs for aerospace Ni-H_2 cells.

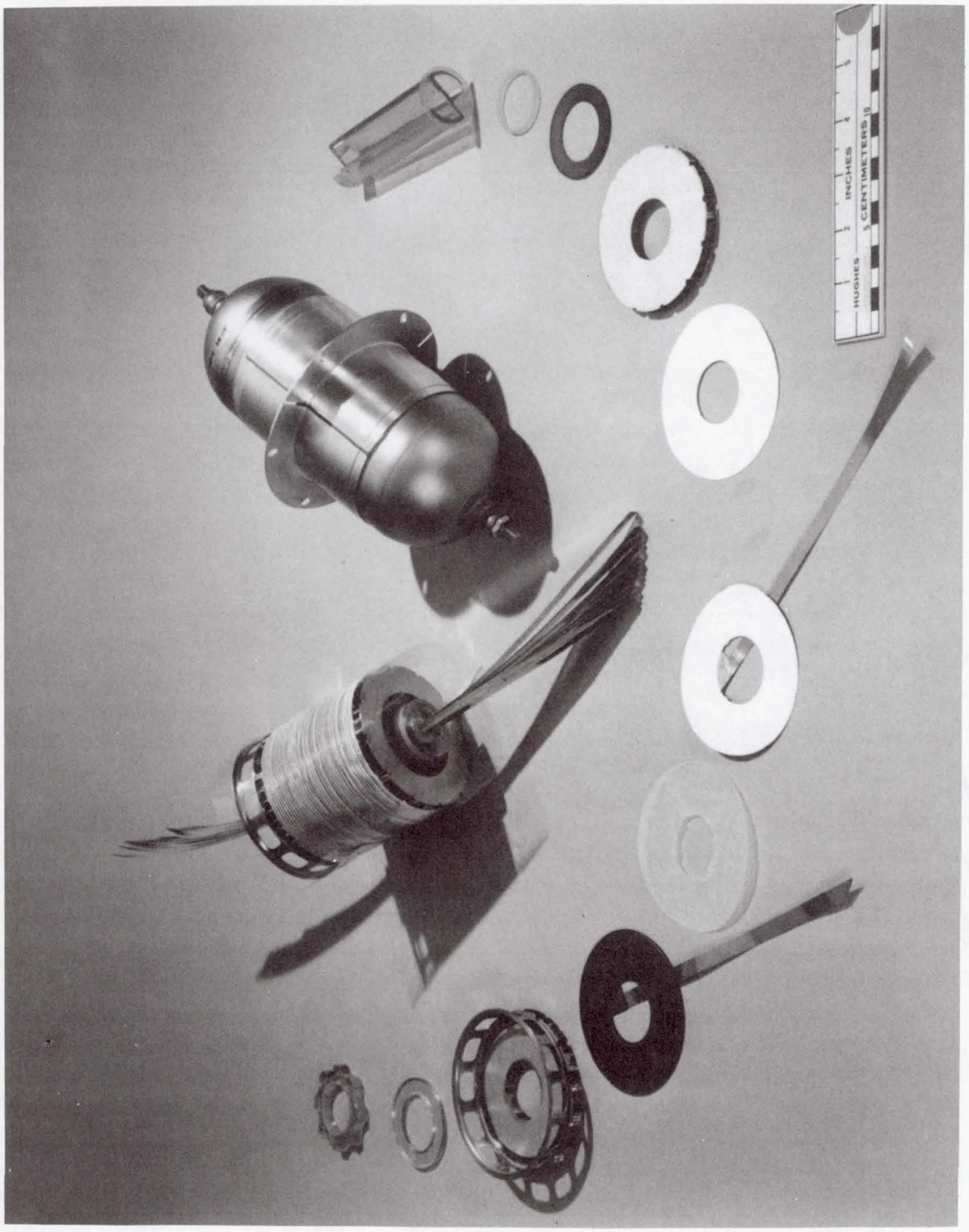

Figure 1-8b. Air Force electrode stack assembly ("advanced cell design").

1.3.3 Activation

Activation for both COMSAT and Air Force type cells includes the following:

- Adding electrolyte and adjusting the electrolyte concentration.
- Initial cycling to create gas passages and force out excess electrolyte from the electrode stack.
- Adjusting the precharge and sealing the pressure vessel.

Most of the different manufacturers classify their respective activation procedures as proprietary. A general discussion of each task is presented without disclosing proprietary procedures.

Electrolyte

The dry cells are initially flooded, back filled with KOH electrolyte under vacuum, and allowed to stand for approximately 24 hours.

The electrolyte concentration can be set with the cell either in the charged or discharged state. It is important to specify the state of charge of the cell when the electrolyte concentration is set, because once the cell completes activation and the excess electrolyte is removed from the cell, the electrolyte concentration will vary from 5 to 7 percent between the charged and discharged states. For example:

Electrolyte Concentration in Cell

Charged	Discharged	Change*
31%	38%	7%
26%	31%	5%
21%	26%	5%

*The change in concentration could vary for different cell designs depending on the quantity of electrolyte per ampere hour of capacity in the cell.

Initial Cycling

The cells should initially be charged vented to create gas passages and force excess electrolyte out of the cell stack. It is recommended that the cells be initially drained and then put on a vented charge and discharge regime for a few cycles to create gas passages. The excess electrolyte should be drained. The cells are normally cycled for an additional 5 to 10 cycles with valves closed to check capacity, pressure range, and to displace excess electrolyte from the positive electrode. As mentioned above, approximately 25 percent of the electrolyte in the positive electrode is displaced during initial cycling. Excess electrolyte should be drained from the cells.

Final Adjustment and Sealing

The cells are discharged and the hydrogen pressure is adjusted to obtain the desired precharge.

If hydrogen gas pressure remains when the cell is fully discharged and sealed, i.e., the positive electrode is fully discharged, this is a negative precharge or hydrogen-precharged cell. Typical values for hydrogen precharge range from 15 to 100 psia of hydrogen gas pressure, with the cell discharged to 0.0 volts.

If the hydrogen pressure drops to zero (a vacuum) before the positive electrode is fully discharged, this is a positive precharged cell. The positive precharge uses the positive electrode capacity below one volt. The amount of positive precharge is approximately 15 percent of the usable capacity to 0.0 volts. The precharge capacity would show up on discharge as capacity in the second plateau below 1.0 volts for hydrogen precharge cells. With a positive precharge cell, the objective is to obtain as much positive precharge as possible without affecting the cell capacity to 1.0 volts on discharge, while at the same time allowing the cell to be discharged to 0 psi absolute at 0.0 volts. But when a positive precharge cell is discharged to 0.0 volts, there is a very steep voltage drop from 1.0 volts to 0.0 volts.

Positive precharge is used to allow for long-term storage of the cells in the fully discharged condition with no hydrogen gas present in the cell. The objective is to eliminate any capacity fading that could result from the presence of hydrogen gas within the cell. This subject of precharge and capacity fading is discussed in Chapter 6, Section 6.8.0, "Effects of Cell Design Variables on Capacity Fading."

1.3.4 Popping

Popping is a term used to define any damage to the electrode stack that results from combustion of oxygen and hydrogen gas. Two different levels of damage have been observed.

Asbestos Separators. Popping only rarely occurs in cells fabricated with asbestos separators. Once the cell is activated, the oxygen gas is forced off the back side of the positive electrode to the periphery of the electrode stack where it diffuses into the hydrogen gas and then to the back surface of the negative electrodes via the gas diffusion screens. The oxygen gas recombines to form water, and small explosions (combustion) are not observed. The percentage of oxygen gas is less than 0.5 percent oxygen (over 99.5 percent hydrogen gas), which is well below the combustion limit (see Table 1-1).

When popping does occur for asbestos cells, the damage is usually extensive. Massive damage was observed in Lot 6 of the INTELSAT V cell program when the cells were not properly activated. It appears that a number of cells were charged sealed without adequately removing excess electrolyte from the cell. Massive

damage occurred within the center of the electrode stack (trapped oxygen bubbles produce one or more large explosions). Plates were warped, the separators pushed out of the electrode stack, and large areas of damage were seen on the negative electrodes.

Asbestos cells with proper activation show no signs of popping damage, even after long-term cycling, based on destructive physical analysis (DPA) analysis of INTELSAT V Ni-H_2 cells on life test for over 10 years.

Zirconium-Oxide Separators. Popping always occurs for cells with zirconium oxide during activation. Small burnt holes are observed in the separator and at the adjacent negative electrode. All of the popping damage seems to occur during the initial activation cycling when the gas channels are being created, and excess electrolyte and trapped oxygen bubbles are being forced out of the cell stack. Popping damage shows up as small mini explosions (combustion) of oxygen and hydrogen at the negative electrode. Once the cell is activated and excess electrolyte is removed from the cell, the combustion damage seems to stop. Again, the popping damage for cells with ZrO seems to be restricted to small localized combustion of pockets of hydrogen and oxygen gas, causing a small amount of localized damage which does not seem to affect the cell performance. It is common to see small burnt holes in the zirconium-oxide separators and negative electrodes after activation.

Pressure Effects on Popping. Pressure range and the end-of-charge pressure (EOCP) are design variables. Early Ni-H_2 cell designs (cells designed in the 1970s) typically had a pressure range of 500 to 600 psi. For these early designs, the emphasis focused on achieving a high pressure vessel safety factor of 4 to 1. With the advanced designs, the emphasis has turned to improving the energy density (Wh/cm^3). For the advanced designs, the pressure range has increased to between 800 and 1000 psi. The size of the trapped oxygen bubbles probably does not change, but, at the higher pressure, the amount of oxygen gas contained within the bubbles increases proportionally to the pressure. The popping damage also increases proportionally when these higher-pressure oxygen bubbles combine catalytically with the hydrogen gas. Damage to the Zircar separators and negative electrodes is more serious for the cells with the higher EOC pressure. The exact extent of the damage to the cycle life of these cells has not been determined.

1.3.5 Electrolyte Concentration

Flooded Plate Capacity Measurements

Flooded plate measurements were carried out using HAC positive plates from the INTELSAT VI program [1-32]. These electrodes were manufactured using dry powder plaque, alcoholic electrochemical impregnation process (see Section 1.8.3).

The positive plates were cut in half and each section was placed in a double-walled beaker filled with electrolyte. One of the beakers always contained 30 weight percent (W/%) KOH electrolyte, and the other beakers contained electrolyte at different W/% concentrations of KOH. Plate capacity was measured at 15, 20, 25, 35, 40, and 45 W/% KOH electrolyte concentrations and compared to the plate capacity measured at 30 W/% KOH concentration. Capacity measurements were taken at 10°C and 20°C. Plate sections were charged at a C/10 rate for 16 hours and discharged at a C/2 rate to 1.0 volts with respect to a Cd reference electrode.

At least five data points were recorded for each concentration, and the standard deviation and mean values were calculated [1-32]. At 20°C the plate capacity reaches a maximum at around 40 W/% KOH concentration, while at 10°C the plate capacity reaches a maximum at around 35 W/% KOH concentration. Plate capacity rapidly decreases below 30 W/% KOH concentration at both 20°C and 10°C (see Figure 1-16 in Section 1.8.3).

The effects of KOH concentration on nickel-hydrogen cell performance are presented in Section 1.8.3, "Capacity as a Function of Electrolyte Concentration for Air Force 50-Ah Cells."

Properties of KOH Solutions

A detailed description of the properties of potassium hydroxide solutions is presented in Falk and Salkind's "Alkine Storage Batteries" [1-5]. Solution properties discussed include: density of KOH solutions as a function of temperature, freezing point diagram (phase diagram) of KOH solutions, effects of lithium hydroxide and potassium carbonate additives to the freezing point of KOH solutions, and the specific conductance of KOH solutions vs. temperature. It is generally accepted that the freezing point decreases with increasing KOH concentration to a eutectic point at -66°C at 31 W/% KOH. At 20 W/% KOH the freezing point increases to about -25°C. Normally, it is not recommended to operate Ni-H_2 batteries below -10°C to avoid any possible chance of freezing the electrolyte.

1.3.6 LEO vs GEO Designs

Low-earth-orbit (LEO) applications require cyclic lifetimes of 40,000 to 50,000 cycles or more at 40 percent depth-of-discharge. Geosynchronous-earth-orbit (GEO) applications require extended lifetime in orbit, 15 to 25 years in orbit with 90 cycles per year at 70 to 80 percent depth-of-discharge.

The requirements for GEO and LEO applications are described in more detail in Chapter 2. The purpose here is to point out that the requirements are quite different. Even so, the cell design features for aerospace Ni-H_2 cells for both applications are becoming quite similar.

Separator. The trend is to use two layers of knit ZYK-15 Zircar cloth separator material to make Ni-H_2 cells for both LEO and GEO applications because of the better voltage performance as compared to cells made with asbestos. In some designs, one layer of ZYK-15 Zircar cloth is used to save weight.

Asbestos is still being used for both LEO and GEO applications, and cells made using asbestos are performing well in space (see Chapter 5 for more information). Concerns with asbestos are the environmental hazards and the long-term availability of fuel-cell-grade asbestos material.

Stack Design. With the back-to-back design, the negative electrodes share one gas diffusion screen, reducing the parts count for gas screens by half for the electrode stack as compared to the recirculating design. The trend is to use the back-to-back design with two layers of Zircar separator for GEO applications. Both back-to-back and recirculating designs are being used for LEO applications. The HST cells have the back-to-back design and the Space Station Freedom is proposing to use the recirculating design with one layer of ZYK-15 Zircar cloth separator.

Electrode Configuration. The trend is to use the pineapple slice configuration for both GEO and LEO applications. The pineapple slice configuration with tabs is easier to assemble into an electrode stack than the bus bar configuration. In addition, the heat transfer is better for the pineapple slice design.

Electrolyte Concentration. A major difference is electrolyte concentration:

31 to 38 percent KOH concentration fully discharged for GEO applications
26 to 31 percent KOH concentration fully discharged for LEO applications

The lower concentration extends the cyclic lifetime but decreases capacity. See Section 1.11.2, "KOH Concentration Effects on the Cycle Life of Ni-H_2 Cells." The higher concentration improves initial capacity and specific energy. See Section 1.8.3, Table 1-3.

Loading of Active Material. The other major difference is the loading of active material in the positive electrode.

1.67 ± 0.1 g/cm^3 void volume for GEO applications
1.55 ± 0.1 g/cm^3 void volume for LEO applications

The lower loading of active material reduces the nickel-hydrogen expansion with cycling (see Section 1.11.3, "Electrode Expansion"). Higher loading of active material increases capacity and specific energy but reduces the cycle lifetime.

1.4.0 ELECTROCHEMICAL REACTIONS FOR Ni-H_2 CELLS

The electrochemical reactions of the Ni-H_2 cell are presented in Table 1-1 for the normal charge and discharge, overcharge, and reversal modes of operation.

Table 1-1. Electrochemical Reactions

Normal operation

(1) Nickel electrode: $NiOOH + H_2O + e^- \underset{\text{charge}}{\overset{\text{discharge}}{\rightleftarrows}} Ni(OH)_2 + OH^-$

(2) Hydrogen electrode: $1/2\ H_2 + OH^- \underset{\text{charge}}{\overset{\text{discharge}}{\rightleftarrows}} H_2O + e^-$

(3) Net reaction: $1/2\ H_2 + NiOOH \underset{\text{charge}}{\overset{\text{discharge}}{\rightleftarrows}} Ni(OH)_2$

Overcharge

(4) Nickel electrode: $2\ OH^- \rightarrow 2e^- + 1/2\ O_2 + H_2O$

(5) Hydrogen electrode: $1/2\ O_2 + H_2O + 2\ e^- \rightarrow 2\ OH^-$

Net reaction of (4) and (5): No net change.
Or:

(6) Hydrogen electrode: $H_2O + e^- \rightarrow OH^- + 1/2\ H_2$

(7) Chemical recombination of O_2: $1/2\ O_2 + H_2 \rightarrow H_2O$

Net reaction of (4) + (6) + (7): No net change.

*Chemical recombination (7) can cause popping if the localized mixture of oxygen and hydrogen is in the combustible range.

Reversal—Hydrogen Precharge

(8) Nickel electrode: $H_2O + e^- \rightarrow OH^- + 1/2H_2$

(9) Hydrogen electrode: $1/2H_2 + OH^- \rightarrow H_2O + e^-$

Net reaction: No change

Reversal—Positive Precharge

(10) Nickel electrode: $2\ NiOOH + 2\ H_2O + 2e^- \rightarrow 2Ni(OH)_2 + 2(OH)^-$

(11) Hydrogen electrode: $2(OH)^- \rightarrow 2e^- + 1/2O_2 + H_2O$

Net reaction: $2NiOOH + H_2O \rightarrow 2Ni(OH)_2 + 1/2\ O_2$

Build up of oxygen pressure and discharge of the nickel oxide electrode

When all of the positive precharge is used (10), then H_2 gas is formed at the positive electrode [same as (8)] and consumed at the hydrogen electrode [same as (9)].

*The limits of inflammability (combustible limits) of hydrogen gas in oxygen are 4.65 for a lower limit and 93.9 for an upper limit [1-55]. The limits of inflammability were determined at atmospheric pressure and room temperature. Values are on a percentage-by-volume basis.

1.4.1 Normal Operation

Electrochemically, the ideal half-cell reactions (1) at the positive nickel-oxide electrode are similar to those occurring in the Ni-Cd system. At the negative electrode, hydrogen gas is oxidized to water during discharge and reformed to gas during charge (2). The net reaction (3) shows hydrogen reduction of nickel oxyhydroxide (NiOOH) to nickel hydroxide ($Ni(OH)_2$) on discharge with no net change in KOH concentration or the amount of water within the cell. Actually, the reactions are more complex than those shown above, with water in the lattice structure of both the nickelic- and nickelous-hydroxide forms of the positive electrode. In addition, the nickel oxide is oxidized to a valence greater than three, with incorporation of potassium ions in the lattice structure of the higher oxide. These more complex reactions result in a net increase in the KOH concentration during discharge of the cell [1-24].

At the positive electrode, $Ni(OH)_2$ is charged to NiOOH up to the onset of oxygen gas evolution (equation 1 to equation 4). As the positive electrode approaches a fully charged state, the positive electrode potential approaches the oxygen evolution potential. Part of the charging current goes into oxygen evolution. The overall charge efficiency, ampere-hour efficiency, is reduced by the percentage of current going into oxygen evolution. Oxygen evolution and overall charge efficiency are discussed in more detail in Chapter 5, Section 5.1.0, Performance Characteristics of Ni-H_2 Cells.

1.4.2 Overcharge

During overcharge, oxygen is generated at the positive electrode (4). The most probable method for oxygen recombination is electrochemical recombination at the catalytic platinum negative electrode in accordance with reaction (5). For these reactions, there is no net change in KOH concentration or the amount of water in

the cell with continuous overcharge. The oxygen recombination rate at the negative platinum electrode is very rapid; the cell is quite capable of sustaining very high rates of continuous overcharge, provided that there is adequate heat transfer away from the cell to avoid thermal runaway. This is one of the operational advantages of the Ni-H_2 cell.

Oxygen gas is generated at the positive electrode on charge when the cell is approaching the fully charged condition and the hydrogen gas pressure is high, approaching the EOC pressure. For cells with asbestos separators, the oxygen generated at the positive electrodes is forced off the back side of the electrode into the surrounding hydrogen gas, where it diffuses to the back side of the catalytic negative electrode and is recombined either chemically (7) or electrochemically (5). The partial pressure of oxygen is a small fraction (less than 0.5 percent) of the surrounding hydrogen pressure. This mixture by diffusion of oxygen gas with hydrogen gas is homogeneous and well below the explosive mixture.

For cells with zirconium separators, excess electrolyte (about 25 percent of the electrolyte) is forced out of the electrode stack during activation to create gas passages for the oxygen gas. The oxygen gas bubbles trapped in the electrolyte can react chemically (7) with hydrogen gas at the catalytic negative electrode to form mini explosions, creating small burn holes. Once the cell is activated, gas passages have been created, the damage to the separators and negative electrodes stops.

1.4.3 Reversal

Negative Precharge Cells

When a hydrogen precharge cell is fully discharged to 0 volts, the positive electrode will be fully discharged. If the cell is forced into cell reversal, hydrogen is generated at the positive electrode (8) and consumed at the negative electrode at the same rate (9). The cell can be continuously operated in the cell reversal mode without pressure buildup or a net change in the electrolyte concentration. This is another of the operational advantages of Ni-H_2 cells with hydrogen precharge.

Positive Precharge Cells

When a positive precharge cell [1-25] is fully discharged to 0 volts, all of the hydrogen gas will be consumed. If this cell is forced into reversal, oxygen gas will be generated at the hydrogen electrode (11) until the positive nickel-oxide electrode is fully discharged (10). This oxygen gas will be consumed when the cell is recharged. It is possible that the hydrogen and oxygen gas mixture would be in the combustible range for this mode of operation and that a rapid recombination could occur.

In addition, it is not recommended to drive a positive precharge cell into reversal because the liberated oxygen can cause another problem. In the alkaline

solution, oxygen can readily dissolve platinum metal from the negative electrode (12).

$$(12)\quad 2Pt^{o} + O_2 + 4(OH)^{-} + 2H_2O \rightarrow 2Pt(OH)_4^{2-}$$

The platinum becomes a soluble material which can diffuse throughout the cell. See Appendix A for a more detailed discussion.

1.4.4 Depth-of-Discharge and Capacity

The terms depth of discharge (DOD), measured capacity, rated capacity, specific energy, and energy density are used throughout this text to describe nickel-hydrogen cells and batteries and their performance. Following is a definition for each of these terms as they are used in this text.

Measured Capacity (Standard Capacity)

The measured capacity (C_{meas}) is the ampere hour capacity measured to 1.0 volts at C*/2 rate discharge with the temperature of the cell pressure vessel maintained at 10°C. See Chapter 7, Section 7.1.0, "Cell Acceptance Tests."

Prior to measuring capacity, the cell is reconditioned and then recharged at a C/10 rate for 16 hours at 10°C. The 16-hour recharge is used to ensure that the cell is fully charged.

One fact to remember is that the measured capacity can and will change as the cell ages, under different storage conditions, operating conditions, etc.

Rated Capacity

The rated capacity (C) is an arbitrary capacity value that is decided on or fixed at the discretion of the cell manufacturer. The rated capacity is less than the measured capacity, again at the discretion of the cell manufacturer. Typically, $C < C_{meas}$ by 5 to 25 percent of the measured capacity. The manufacturer rates the cells lower so that they will pass acceptance testing.

The rated capacity does not change over the lifetime of the cell.

---

* C is rated capacity, C_{meas} is measured capacity

Depth of Discharge

The depth of discharge (DOD) is the ampere-hours removed on discharge expressed as a percentage of the rated capacity. The rated capacity is always used to calculate DOD and charge rates: C/2 rate, C/10 rate, etc.

The advantages of using rated capacity is that it is fixed for the lifetime of the cell, so if one specifies a 40 percent DOD, the ampere-hours removed on discharge at the beginning of life are the same as the ampere-hours removed on discharge at the end of life.

Specific Energy

The specific energy is measured capacity multiplied by the average discharge voltage divided by the cell mass:

$$\text{Specific Energy} = \frac{C_{meas} \times V_{avg}}{\text{Weight of Cell}} \left(\frac{W\,h}{kg}\right)$$

Use the measured capacity to calculate specific energy. The specific energy is used to compare one cell design to another and it should not be biased by an arbitrary rating.

Energy Density

The energy density is the measured capacity multiplied by the average discharge voltage divided by the cell volume:

$$\text{Energy Density} = \frac{C_{meas} \times V_{avg}}{\text{Volume of Cell}} \left(\frac{W\,h}{L}\right)$$

Again, use the measured capacity to calculate energy density. The energy density is used to compare one cell design to another.

1.5.0 HISTORIC OVERVIEW FOR FIRST-GENERATION Ni-H_2 CELLS

A historic overview of the major events and milestones in the development of Ni-H_2 cell technology from 1970 to 1979 is presented in the table below [1-26], which identifies the major R&D programs from the initial exploratory efforts to the flight-qualified status of Ni-H_2 cells for COMSAT/INTELSAT and HAC/Air Force, programs.

A description of the COMSAT cell design and the Air Force cell design follow the historic overview. These two different cell designs have come to represent and identify the first generation of Ni-H_2 cells.

Table 1-2. Historical Overview Summary

1970	INTELSAT (COMSAT and Tyco Laboratories) initiated the first aerospace Ni-H_2 cell development effort for GEO applications.
1972	The Air Force began in-house Ni-H_2 cell development for LEO applications.
1972	INTELSAT awarded a contract for the design and fabrication of a lightweight Ni-H_2 cell to Tyco Laboratories. COMSAT Laboratories performed this work when Tyco dropped out of the battery business.
1973	The Air Force awarded the Nickel-Hydrogen Satellite Energy Storage Program to Hughes Aircraft Company. Subsequently, subcontracts were awarded to Eagle-Picher, ERC, and Tyco Laboratories. Boilerplate cells were constructed for basic system studies.
1973	INTELSAT awarded dual contracts to Eagle-Picher and Energy Research Corp. (ERC) to produce lightweight flight configuration Ni-H_2 cells. Eagle-Picher used the COMSAT pressure vessel and electrode stack designs. ERC used its own designs [1-27].
1974	Under contract to the Western Electric Company, Eagle-Picher established a production facility for electrochemically impregnated (EI) nickel electrodes (the Bell Laboratories aqueous process).
1975	INTELSAT awarded a fundamental Ni-H_2 system study program to Marcoussis Laboratories in France. Electrolyte management, oxygen gas recombination, and positive and negative electrode stack components were investigated.
1975	INTELSAT awarded a mechanical and thermal design study of Ni-H_2 batteries to TRW.
1975	The Air Force awarded the Nickel-Hydrogen Failure Mechanism Program to HAC. A subcontract was subsequently awarded to EIC Corporation for the development of an improved catalytic negative electrode. Limitations associated with electrolyte management and oxygen recombination were studied and design solutions were developed.

1975 COMSAT/INTELSAT and the Naval Research Laboratory agreed to use a Ni-H_2 battery as the primary energy storage system on the NTS-2 satellite. Eagle-Picher (Joplin) manufactured the Ni-H_2 cells for this program under a licensing agreement with INTELSAT. The positive electrodes were made by Eagle-Picher using the Bell Laboratories aqueous electrochemical impregnation process. The INCONEL 718 pressure vessel used for these cells was developed by COMSAT Laboratories, and the technology was transferred to Eagle-Picher . The battery was subjected to a full space qualification program. This satellite was launched in June 1977, and the battery performed its mission successfully, operating for five years in a polar 12-hour orbit at 40 to 60 percent DOD.

1975 The Air Force awarded the Nickel-Hydrogen Flight Experiment Program to Eagle-Picher (Joplin). Lockheed Missiles and Space Company (LMSC) served as the system integration contractor, and a 21-cell, 50-Ah battery was manufactured. EI positive electrodes were used (aqueous process). The battery was qualified for launch on a classified Air Force LEO mission, and the satellite was launched in June 1977. Approximately 2,000 cycles were accumulated over eight months of both shallow and deep DOD. The integration battery was life-cycle tested at LMSC and completed 13,000 real-time LEO cycles at 50 percent DOD.

1976 The Air Force awarded the Electrochemical Deposition Nickel and Cadmium Electrode Manufacturing Technology Program to Eagle-Picher (Colorado Springs) for establishing a production facility to manufacture EI- electrodes (Air Force alcohol process).

1976 The Air Force awarded the Nickel-Hydrogen Advanced Development Program to HAC to develop and qualify a design and establish manufacturing sources for a Ni-H_2 system suitable for both LEO and GEO space missions. Subcontracts were awarded to Yardney Technical Products, Inc., and Eagle-Picher, Joplin, for cell manufacturing. A separate contract was awarded to Eagle-Picher, Colorado Springs, for improvement of EI positive electrodes (alcohol process). HAC and Eagle-Picher, Joplin, were the two manufacturing sources selected. The Eagle-Picher, Colorado Springs, facility supplied EI positive electrodes to both sources. Testing of these cells included cell-level space qualification and real-time LEO cycling that approached 12,000 cycles at 80 percent DOD.

1977 INTELSAT awarded a cell design (electrolyte management study) program to EIC. Approximately 4,000 cycles at 80 percent DOD were accumulated, and advanced design information relative to electrolyte management requirements evolved from this program.

1979 INTELSAT awarded a high-pressure, high-energy-density Ni-H_2 battery development program to Yardney Technical Products. The operation of Ni-H_2 cells at higher pressures was evaluated to improve volumetric and specific energy density. INTELSAT licensed its IPV Ni-H_2 cell technology to Yardney Technical Products.

1979 Ford Aerospace (with INTELSAT's approval) agreed to replace the Ni-Cd batteries with Ni-H_2 batteries on INTELSAT V satellites. Flight 6, launched in 1983, was the first commercial communication satellite to use Ni-H_2 batteries. A total of eight INTELSAT V satellites were launched and are now in operation with Ni-H_2 batteries: flights F6, F7, F8, F10, F11, F12, F13, and F15. FACC fabricated these 30-Ah batteries and integrated them into the INTELSAT V spacecraft. The Ni-H_2 cells were manufactured by Eagle-Picher using EI positive electrodes (aqueous batch process at Joplin).

1979 The Air Force gave HAC approval to prepare for replacement of the Ni-Cd battery with a Ni-H_2 system on the Air Force Satellite Data System Program. HAC designed an 18-cell, 25-Ah battery to support the long-term LEO mission with an early 80s launch date. The Ni-H_2 cells (advanced development design) were manufactured by HAC using Eagle-Picher EI positive electrodes (alcoholic process at Colorado Springs).

1.6.0 COMSAT/INTELSAT DESIGN

The COMSAT/INTELSAT Ni-H_2 cell and battery technology was developed from 1970 to 1975, starting with the basic concept for a sealed Ni-H_2 cell as described in the patent [1-1]. This effort culminated in the NTS-2 and INTELSAT V Ni-H_2 flight battery programs. This technology was developed for use as the energy storage system for commercial communications satellites (INTELSAT) in geosynchronous orbit.

1.6.1 Experimental Cells

The initial development work at COMSAT Laboratories used heavy-walled experimental cells to evaluate different combinations of commercially available aerospace nickel-oxide electrodes and separator materials. Results of this work are reported in Reference 1-28. The back-to-back positive electrode stack design was used for these experimental cells.

1.6.2 NTS-2 Cell Design Features

Electrode Stack. The components for one module of the electrode stack are shown in Figure 1-1. These components were fabricated to the bus bar configuration. The positive electrodes were made with passivated wet slurry plaque and impregnated using the aqueous EI process (Bell Laboratories process) to a loading level of 1.67 ± 0.1 g/cc void volume. The hydrogen electrodes consisted of the sintered Teflon-bonded platinum black catalyst supported with a fine mesh nickel screen with the Gortex Teflon backing (platinum loading of 7 ± 1 mg/cm^2). The separator material used was reconstituted fuel cell–grade asbestos.

One module consists of two positive electrodes back-to-back, two separators, two negative electrodes, and two gas diffusion screens. Fifteen of these modules are stacked on a center rod and held under compression by two endplates (see Figure 1-4). The styrene acrylonitrite endplates were fabricated by an injection molding process. The center rod and end plates position the electrode stack components during assembly.

The electrode stack with rigid endplates was attached to the INCONEL 718 weld ring. A single circumferential electron beam girth weld simultaneously joins the two pressure vessel shells at the weld ring while at the same time anchoring the cell stack assembly into the pressure vessel.

1.6.3 Pressure Vessel

The INCONEL 718 pressure vessel shells were manufactured to a uniform thickness using a hydroforming process and then cut to length; the thickness was 0.508 mm. The pressure shells were "age hardened" using a standard heat treatment process. The barrels for the compression seals were machined from INCONEL 718 material. Nylon plastic was injection-molded into the barrel. After injection molding, the barrels were electron-beam welded into the domes of the pressure vessel shells. The INCONEL 718 weld ring was manufactured using an investment casting process and then machined to final dimensions. The outside diameter of the weld ring was machined as a "T" section to position the pressure shells on the weld ring and to provide a back up support for the electron beam girth weld.

When the electrode stack is assembled into the pressure vessel, the terminals at either end of the stack are pushed up through a slightly oversized hole in the nylon seal. After electron-beam welding the pressure vessel shells to the weld ring assembly, the "Ziegler" compression seal [1-29] is made by crimping the barrels. The girth weld and crimped terminal are shown in a photograph of a cell (see Figure 1-9).

The electrolyte fill tube is part of the negative terminal. A hollow stainless steel tube was brazed into the center hole of the negative terminal. After the electrolyte was added and the cell had completed activation, this fill tube was

pinched off and welded. A cross-sectional view of the NTS-2 cell, Figure 1-10, shows the positioning of the electrode stack within the cell, the endplates, the positive and negative bus bars, and the positive and negative terminals with the fill port in the negative terminal.

The diameter chosen for the pressure vessel was 8.89 cm. This diameter was selected as an engineering compromise between maximum gravimetric energy density and number of modules in the electrode stack. Selecting a smaller diameter of 7.62 cm would have provided a higher gravimetric energy density, as shown in Figure 1-11), but it would also have required more modules, resulting in increased complexity in the assembly of the cell. The data presented in Figure 1-11 are based on the results of a computer optimization study [1-30]. The actual gravimetric energy densities for the NTS-2 and INTELSAT V cells approached the theoretical energy density predicted from the computer model, as shown in Figure 1-12.

The maximum operation pressure for the NTS-2 cells was 600 psi, and the burst pressure was 2,400 psi, providing a 4:1 safety factor.

1.6.4 NTS-2 Cell Design Summary

1. Back-to-back electrode stack design.

2. Bus-bar electrode configuration.

3. INCONEL 718 pressure vessel (0.508 mm thick) with nylon Ziegler compression seals. Electron-beam girth welding of the pressure shells to an INCONEL 718 weld ring.

4. Positive electrodes—wet slurry plaque, aqueous EI process (Bell process).

5. Separator material—single layer of fuel-cell-grade reconstituted asbestos separator, 10 to 12 mils thick.

6. Negative electrodes—platinum black negative electrode with Teflon backing (Gortex). Wire screen grid.

7. KOH electrolyte concentration—31 percent KOH discharged.

8. Hydrogen precharge (14.7 psia).

9. Thirty positive electrodes (15 modules/cell) for the 35-Ah rated NTS-2 cell.

10. Cell dimensions: 8.89-cm diameter and 23.7-cm end to end of terminals; 16.6 cm dome to dome; terminals and seals add about 3.5 cm on each end.

Figure 1-9. EPI nickel-hydrogen cell showing girth weld.

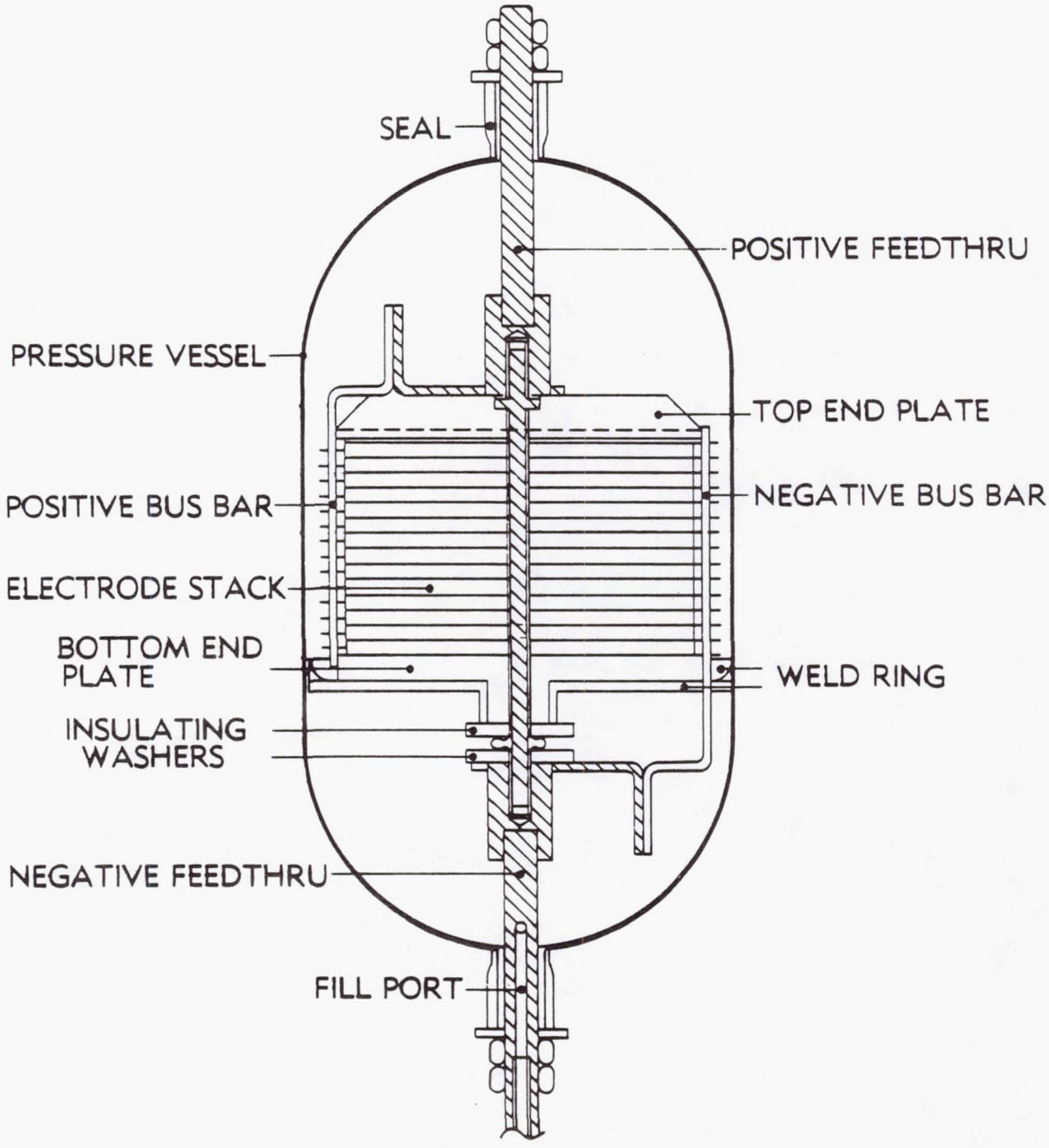

Figure 1-10. COMSAT/EPI NTS-2 cell (cross-sectional view).

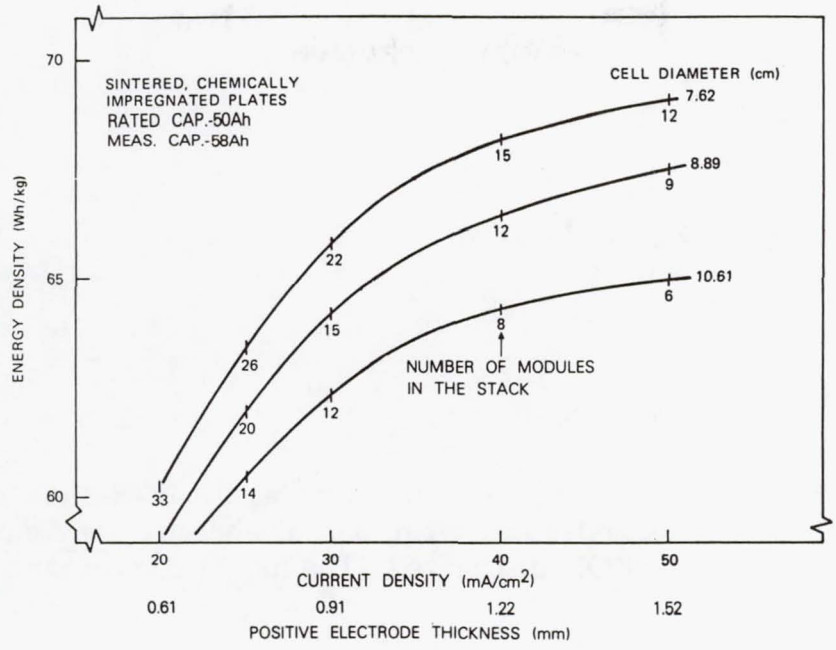

Figure 1-11. Gravimetric energy density vs design variables (50-Ah cell).

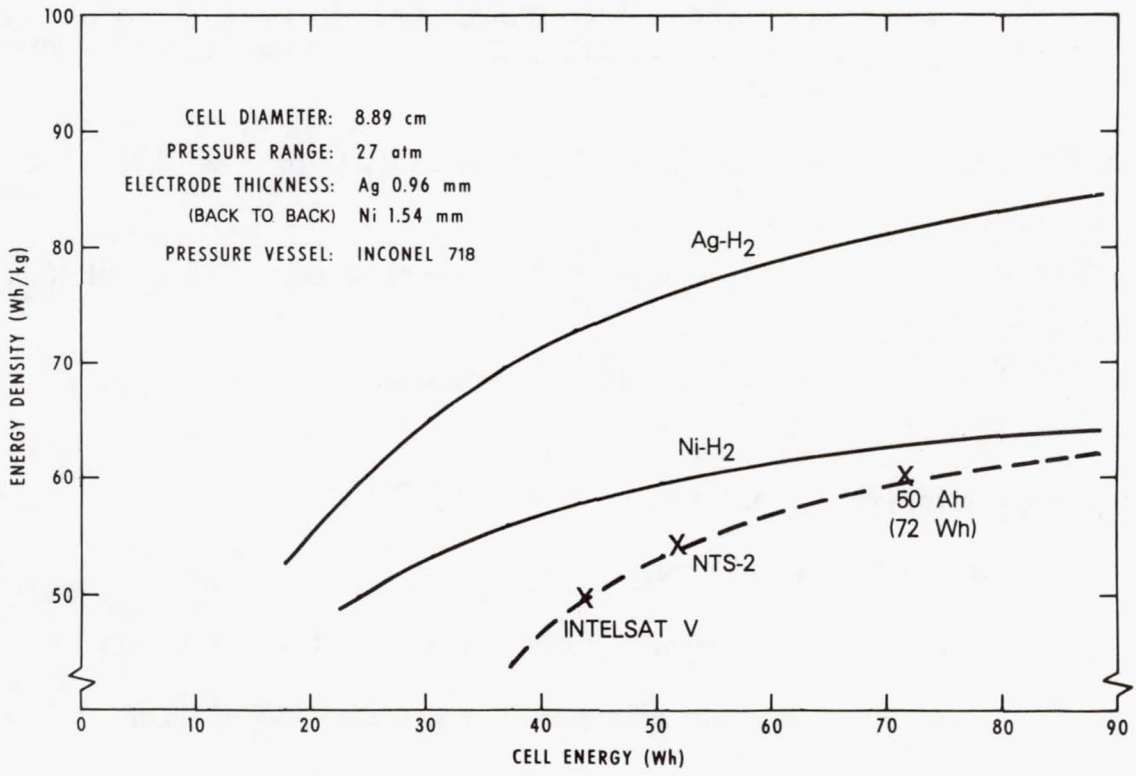

Figure 1-12. Gravimetric energy density of Ni-H_2 cells vs theoretical energy density.

11. The weight of each cell—1.028 kg.

12. Measured capacity at 10°C—43 Ah.

13. Specific energy (10°C)—52.2 Wh/kg.

1.7.0 INTELSAT V CELL DESIGN

The INTELSAT V cell design was the same as the NTS-2 cell design, except there were 24 positive electrodes instead of 30. The electrolyte concentration was also changed to 38 percent KOH discharged. The higher concentration was used to increase capacity.

1. Back-to-back electrode stack design.

2. Bus bar electrode configuration

3. INCONEL 718 pressure vessel (0.508 mm thick) with nylon Ziegler compression seals. Electron beam girth welding of the pressure shells to an INCONEL 718 weld ring.

4. Positive electrodes—wet slurry plaque, aqueous EI process (Bell Laboratories process).

5. Separator material—single layer of fuel-cell-grade reconstituted asbestos, 10 to 12 mils thick.

6. Negative electrodes—Teflon bonded platinum black with Teflon backing (Gortex); wire screen grid.

7. KOH electrolyte concentration—38 percent KOH discharged.

8. Hydrogen precharge (14.7 psia).

9. Twenty-four positive electrodes for 30-Ah rated INTELSAT V cell.

10. Cell dimensions: 8.89 cm diameter, 21 cm end-to-end of terminals, 13.9 cm dome-to dome.

11. The weight of each cell—890 g.

12. Measured capacity at 10°C—36 Ah.

13. Specific energy (10°C)—50.6 Wh/kg.

1.7.1 High-Rate Discharge and Internal Impedance for INTELSAT V Cells

Ni-H_2 cells are capable of very high rates of discharge. To demonstrate this, a 30-Ah INTELSAT V cell was discharged at a 200-A rate (12-minute discharge). The discharge voltage vs time is presented in Figure 1-13. The discharge profile is almost flat at 0.6 V. The potential drop is due to the internal impedance of the cell (3 mΩ). This impedance accounts for the voltage drop of 0.6 V at the 200 A rate. Most of this impedance is in the bus bars and nickel terminals of the cell. These nickel terminals are rather long in the IPV cells, as shown in the cross-sectional view in Figure 1-10.

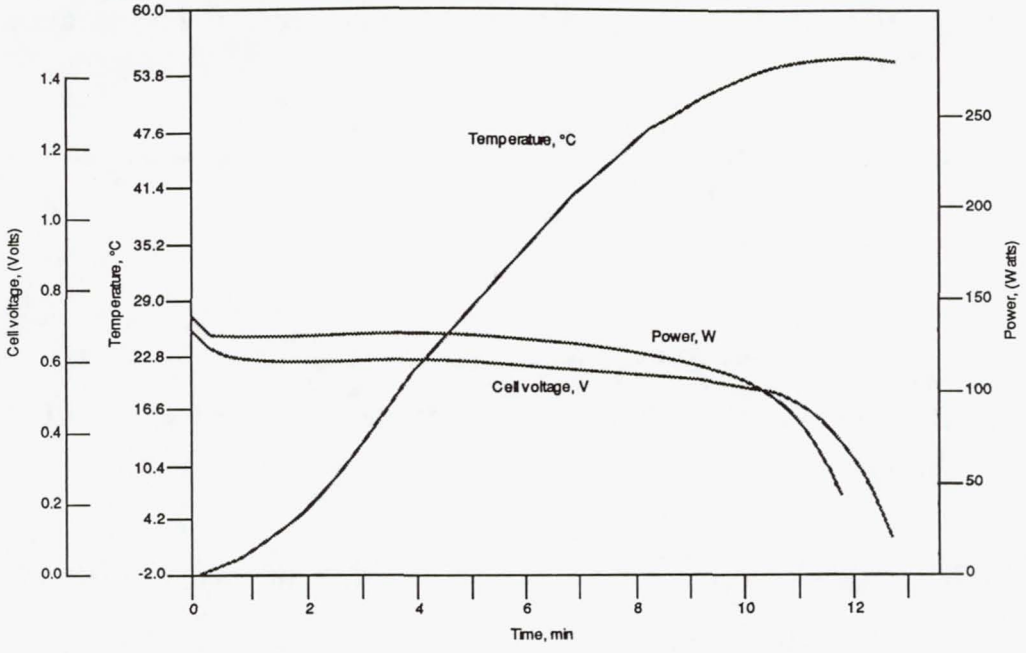

Figure 1-13. High-rate (200-A) discharge of 30-Ah cell.

1.7.2 Specific Energy as a Function of Rate of Discharge for INTELSAT V Cells

The aerospace INTELSAT V Ni-H_2 cells were not optimized for high-rate discharge. Rather, they are optimized for maximum specific energy at discharge rates between C/2 and 2C [1-30]. At rates greater that the C rate of discharge, the specific energy starts to drop off rapidly, as shown in Figure 1-14. This drop off is because of the 3-mΩ terminal impedance of the INTELSAT V cell, as seen for the 200-A rate of discharge above.

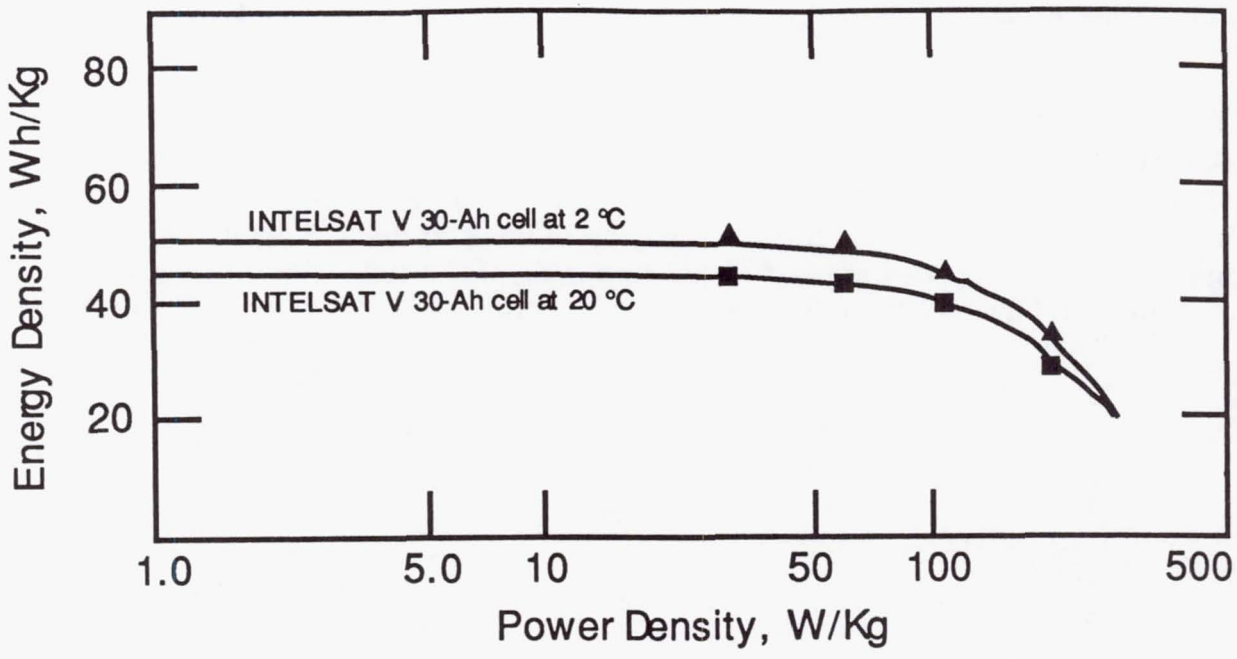

Figure 1-14. Gravimetric energy density vs rate of discharge for INTELSAT V cells.

1.8.0 AIR FORCE NI-H_2 CELL DESIGN

The Air Force cell development program was initially directed toward the more stressful LEO operating mode with high rates of charge and discharge (approximately 1.4C* rate discharge and 1C rate on charge and overcharge).

Problems were identified with oxygen management and water management for the COMSAT back-to-back positive electrode design under these high stress operating conditions [1-7], [1-13]. The "recirculating design" was conceived to resolve these problems.

An R&D effort called the "Advanced Development Program" was carried out to design and develop the electrode stack components and cell technology needed to put the recirculating design concept into practice. Cell design features are described in Reference 1-22 and include the pineapple slice shaped electrode stack components, a recirculating design with a wall wick on the inside of the pressure

* C is the rated capacity of the cell. If the cell is rated at 50 Ah, a C rate discharge is a 50 A rate.

vessel shell, and a zirconium-oxide cloth gas permeable separator, knit ZYK-15 Zircar [1-16].

Air Force-sponsored programs conducted over a ten-year period from 1973 to 1983 brought the HAC/Air Force Ni-H_2 battery technology to the state of readiness for operational spacecraft missions [1-3]. This work culminated with the Air Force baseline 50-Ah Ni-H_2 cell design (see Figure 1-15).

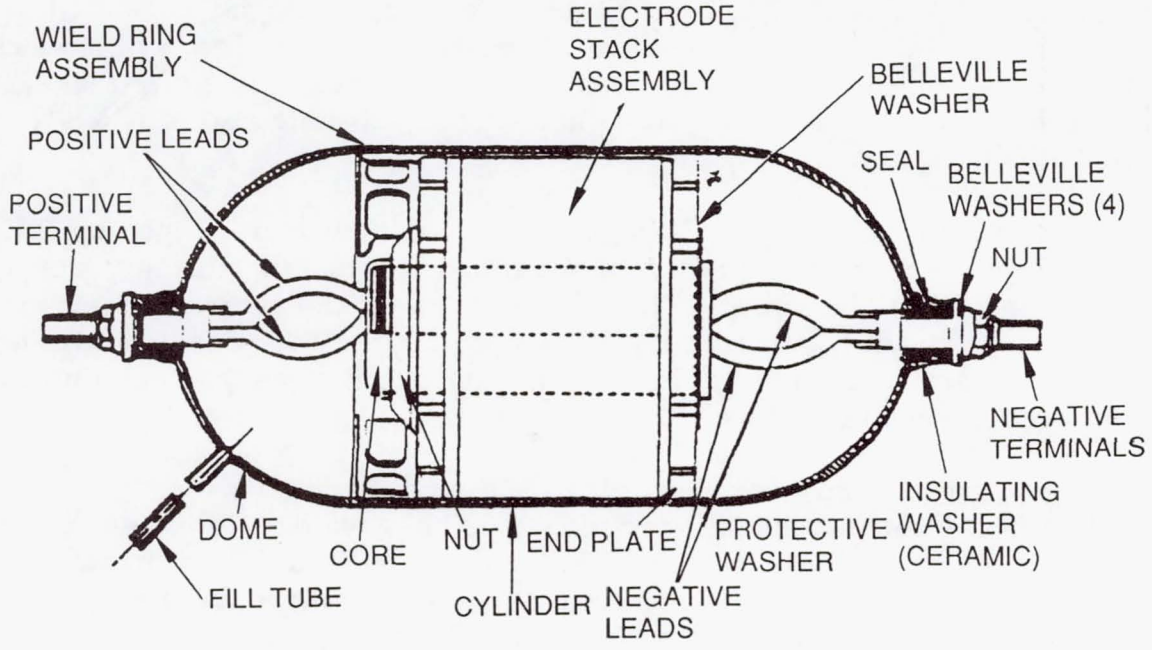

Figure 1-15. Air Force/HAC baseline 50-Ah cell (cross-sectional view).

1.8.1 Air Force Baseline Cell Electrode Stack Components

The baseline cell design electrode stack components are made in a pineapple slice configuration (see Figure 1-2) with the electrode tabs brought out through a large center hole. The purpose of this design is to reduce the thermal resistance between the cell stack and the pressure vessel wall compared to the COMSAT design with the bus bar on the outside of the cell stack.

Zircar Separators. The initial separator selected in the Advanced Development Program for the baseline cell design was the ZYW-15 Zircar cloth, yttrium-stabilized zirconium oxide using polysulfone to reinforce the Zircar. The Zircar cloth was reinforced with polysulfone because of its marginal handling strength [1-23]. However, tests at HAC showed that cells with ZYW-15 polysulfone-reinforced Zircar separators and wall wicks exhibited popping while cells with untreated knit ZYK-15

Zircar separators showed virtually no evidence of rapid oxygen recombination (popping). Based on these results, two layers of the untreated knit ZYK-15 Zircar material were selected for the Air Force baseline cell design. The second ZYK-15 layer was added as a backup to prevent oxygen channeling in the event of assembly caused damage to the first layer [1-16].

Negative Platinum Electrodes. The negative electrode with the gas screen is shown in Figure 1-2. The electrode, as originally developed, used an expanded mesh substrate. HAC improved the negative electrode by changing to a photo-etched substrate [1-14], which eliminates cut edges of the expanded mesh wires that caused shorts during cell stack assembly. The photo-etched substrate also provides a solid tab for lead attachment.

A negative electrode with Gortex (Teflon) backing was developed by EIC for HAC [1-7], [1-13]. The use of Gortex simplified the manufacturing process for fabricating negative electrodes. The EIC electrode with Gortex backing allows hydrogen and oxygen gas to readily diffuse through the back of the electrode for recombination during overcharge, but it completely stops electrolyte entrainment in the hydrogen gas evolved off the back during charge and overcharge.

Positive Electrodes. Positive electrodes were manufactured using the alcoholic electrochemical impregnation (EI) process, sometimes referred to as the Air Force process. Electrodes for HAC were manufactured at the Eagle-Picher manufacturing facility at Colorado Springs. The positive electrodes were made using the dry sinter plaque with 85 percent porosity. Active material loading was 1.67 g/cm^3 of void volume for GEO designs and 1.55 g/cm^3 of void volume for LEO designs. The active material contained 7 to 11 percent by weight cobalt hydroxide [1-10]. Nickel screen was used as the substrate for the nickel sintered plaque.

Electrode Stack. An electrode stack assembly is shown in Figures 1-8a and 1-8b. The electrode stack components are the cylindrical pineapple slice configuration. These components are stacked between rigid endplates preloaded to a specific contact pressure within the cell stack by compressing the assembled stack in a fixture and tightening the nut on the end of the core. Belleville washers provide a constant preload on the electrode stack. Figure 1-15 is a cross-sectional view of the Air Force baseline 50-Ah cell. This figure shows the center core, electrode stack, endplates, nuts, Belleville washers, terminals, seals, and fill tube.

The electrode stack components are assembled onto the polysulfone central core attached to the INCONEL 718 skip ribbon panel endplate. This polysulfone core provides electrode alignment during assembly, position and alignment of the cell stack within the pressure vessel, structural support, and conduits for the positive and negative terminals.

The central core assembly with the rigid endplates is attached to an INCONEL weld ring. A single circumferential tungsten inert gas (TIG) weld simultaneously joins the two pressure vessel shells at the weld ring while anchoring the cell assembly into the pressure vessel (Figure 1-15).

Pressure Vessel. The hydroformed INCONEL 718 cylindrical pressure vessel is 8.89 cm in diameter, with spherical ends. The dome/cylinders are hydroformed to a thickness of 0.078 cm. This thickness of 0.078 cm is maintained in the closure weld and terminal seal areas. The remainder of the cylindrical area is reduced to a thickness of 0.056 cm by chemical milling, and the remainder of the cylindrical dome area is reduced to a thickness of 0.038 cm by chemical milling. The wall thickness and cylindrical dome thickness are reduced for weight reduction of the pressure vessel. The 0.078 cm thickness in the girth weld area is needed to compensate for the strength reduction of the INCONEL 718 material in the heat-affected zone of the TIG weld. The pressure shells are heat treated (age hardened) and chemically milled to their final thickness prior to TIG welding.

The terminal seal bosses are hydroformed as an integral part of the dome/cylinder, with one terminal at either end of the pressure vessel. The terminal seals are hydraulic cold flow Teflon seals [1-31]. An electrolyte fill tube is welded at a 45 degree radial on the dome of the pressure vessel.

The inside walls of the pressure vessel and domes are plasma sprayed with zirconium oxide to form a wall wick.

The maximum operating pressure is 800 psi, and the burst pressure is 2,400 psi, giving a 3:1 safety factor.

1.8.2 Air Force Baseline 50-Ah Cell Design Summary

1. Recirculating electrode stack design.

2. Pineapple slice electrode configuration.

3. INCONEL 718 pressure vessel with Teflon hydraulic compression seals, TIG welding, and zirconium-oxide wall wick plasma sprayed on inside of pressure vessel walls. Chem-milled to final dimensions.

4. Positive electrodes—dry powder plaque, alcohol EI process (Air Force process).

5. Separator material—double-layer knit ZYK-15 Zircar separators, 12 to 15 mils thick each.

6. Negative electrodes—platinum black negative electrodes with Teflon backing (Gortex). Photochemically etched grid.

7. KOH electrolyte concentration—31 percent KOH discharged.

8. Positive precharge.

9. Forty positive electrodes for the 50-Ah rated baseline cell.

10. Cell dimensions—8.89-cm diameter, 28.4 cm end to end of terminals, and 20.7 cm dome to dome.

11. Cell average weight—1.4806 kg.

12. Measured capacity at 10°C—58 Ah.

13. Specific energy (10°C)—48.97 Wh/kg.

1.8.3 Capacity as a Function of Electrolyte Concentration for Air Force 50-Ah Cells

The effects of electrolyte concentration on capacity were determined experimentally. Air Force positive electrodes and HAC/Air Force 50-Ah Ni-H_2 cells from the INTELSAT VI program were used for this investigation. The Air Force positive electrodes were impregnated with active material by the alcohol electrochemical impregnation process. The plaque was manufactured using the dry powder process.

Flooded Plate Capacity. The Air Force positive electrode plate capacity was measured at 15, 20, 25, 30, 35, 40, and 40 weight percent concentrations of electrolyte [1-32].

Figure 1-16 shows the effects of electrolyte concentration on plate capacity at 10°C and 20°C. There was some spread in the data, but a definite trend was established. At 10°C the maximum capacity occurs at a 40 weight percent concentration. At 20°C the maximum capacity occurs at a 35 weight percent concentration. Below 30 weight percent concentration, the capacity decreases rapidly at both 20°C and 30°C.

Standard Air Force 50-Ah Cell. For the HAC/Air Force standard 50-Ah Ni-H_2 cell, the electrolyte concentration was determined to be 26 percent KOH in the charged state and 31 percent KOH in the discharged state. The measured concentration of 31 percent in the discharged state corresponds to the electrolyte concentration added by HAC to the cell during activation. This correlation verifies the accuracy of the analysis procedure used.

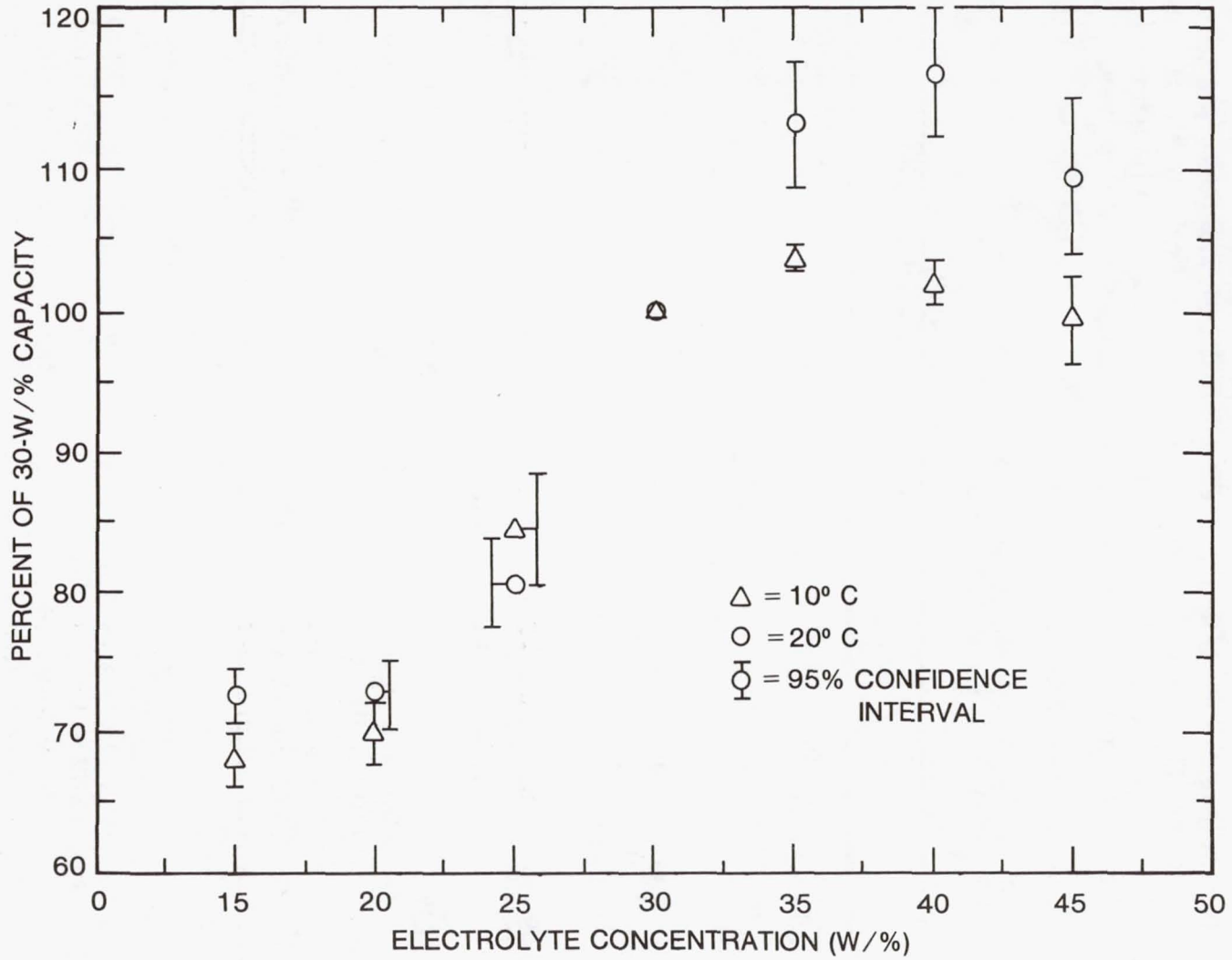

Figure 1-16. Effects of electrolyte concentration on capacity.

Cells with Different Electrolyte Concentrations. Electrolyte concentration significantly affects the performance of Ni-H_2 cells. It affects the cell capacity (specific energy and energy density of the cells). It also affects the cycle life in LEO as reported by HAC [1-33]. The effects of electrolyte concentration on the capacity of HAC/Air Force 50-Ah cells (INTELSAT VI cells) were investigated [1-32]. Cells were activated with three different levels of electrolyte concentration: 25, 31, and 38 weight percent concentration of KOH. The electrolyte concentration in these cells was determined by analyses in both the charged and discharged condition. Table 1-3 [Reference 1-32] presents cell capacity, electrolyte concentration, and average discharge voltage.

Table 1-3. Cell Measured Capacity and Voltage vs Electrolyte Concentration at 10°C

Parameter	Electrolyte Concentration (Discharged)		
	38%	31%	25%
Cell Measured Capacity (Ah)	64	56	43
Number of Positive Plates	40	40	40
Capacity/Plate (Ah)	1.60	1.40	1.08
Electrolyte Concentration:			
Charged w/% KOH	32*	26	21*
Discharged w/% KOH	38	31	25
Average Discharge Voltage (V)	1.247	1.268	1.290

*Estimated

Specific Energy. The cell measured capacity and discharge voltage are a function of the electrolyte concentration as shown above. Specific energy is also affected by the electrolyte concentration as shown in Table 1-4 [Reference 1-32].

Table 1-4. Specific Energy vs Electrolyte Concentration at 10°C

Parameter	Electrolyte Concentration (Discharged)		
	38%	31%	25%
Cell Mass (kg)	1.422	1.410	1.400
Average Discharge Voltage (V)	1.247	1.268	1.290
Measured Capacity to 1.0 V (Ah)	64	56	43
Energy to 1.0 V (Wh)	79.81	71.0	55.5
Specific Energy (Wh/kg)	56.1	50.4	39.6

Summary. The standard HAC/Air Force 50-Ah cells are activated with 31 percent KOH in the fully discharged condition. In the fully charged condition the concentration is 26 percent KOH.

Studies sponsored by NASA LeRC at HAC have shown that cycle life is greater at lower electrolyte concentrations (26 percent KOH) [1-33].

For GEO applications the higher concentration of KOH is used to achieve higher specific energy. The cycle life requirements are only 100 cycles per year, or 1,500 cycles for 15 years, so it is reasonable to select a design that gives 10 to 20 percent more energy per unit weight. In Table 1-4, the cells with 38 percent KOH gave 56.1 Wh/kg, compared to the cells with 31 percent KOH which gave 50.4 Wh/kg (a difference of 11 percent), and the cells with 25 percent KOH gave only 39.6 Wh/kg (a difference of 42 percent).

For LEO applications, the lower concentration of KOH is used to achieve a longer life. The cycle life is expected to be 4 to 10 times greater at the lower electrolyte concentrations. The studies on life expectancy and DOD under LEO cycling conditions are being investigated as described in Sections 1.11.2 and 1.11.3. Cells with concentrations of both 31 percent KOH and 26 percent KOH are included in these studies. For the cells with 26 percent KOH concentration, there is a significant reduction in capacity as shown in Table 1-4 above. The tradeoff between electrolyte concentration capacity and cycle life needs to be determined for individual applications.

1.9.0 Ni-H_2 CELLS FOR THE 1990s (SECOND GENERATION)

Described in this section are the second generation of Ni-H_2 cells, IPV cells for the 1990s. These cell designs incorporate a combination of the design features from the COMSAT and Air Force designs as described in the last section. They also include a number of new features:

- dual electrode stack design
- higher maximum operating pressure, higher pressure range
- modified pressure vessel design to increase burst pressure
- dual weld ring supported single-stack design with floating core
- ceramic to metal terminal seals.

Examples of Ni-H_2 cells that are representative of this next generation of cells are presented in this section.

1.9.1 USAF MANTECH Ni-H_2 Cell

In 1981, the Air Force awarded Yardney Technical Products the Nickel-Hydrogen Cell Manufacturing Technology (MANTECH) Program. The purpose of this program was to develop lower-cost design and manufacturing methods for the production of the baseline Air Force 50-Ah Ni-H_2 cell [1-34]. Changes to the baseline manufacturing processes are described in detail in Reference 1-35. A brief description of the major process changes is presented in the text below.

The Yardney Technical Products MANTECH cell design combines both COMSAT and Air Force design and manufacturing methods along with Yardney's own contributions to the manufacturing methods.

Pressure Vessel Components

The Air Force 50-Ah Ni-H_2 cell design is referred to as the baseline design in the following text (see Figure 1-15).

Dome/Cylinder. The baseline dome/cylinder was hydroformed from INCONEL 718 to a 0.078 cm thickness and then chem-milled to reduce the thickness described in 1.8.0, "Air Force Ni-H_2 Cell Design."

Manufacturing Process Changes:

1.* The Yardney MANTECH dome/cylinder was hydroformed to a uniform thickness of 0.053 cm, +0.005/-0.000 cm.

2. Chem-milling was eliminated.

Terminal Seal Boss. The baseline terminal seal boss was hydroformed as an integral part of the dome/cylinder. A high rejection rate was associated with the hydroforming process. The major cause for this high rejection rate was distortion in the area of the integral terminal seal boss (a thinning occurred in the neck of terminal seal boss where it met the hemisphere).

Manufacturing Process Changes:

1.* A separately machined boss was used.

2.* The boss was EB welded to the dome of the pressure vessel. The EB welding was performed using automated, programmable equipment to produce very repeatable results.

---

* An asterisk indicates COMSAT pressure vessel technology was used.

These pressure vessel manufacturing process changes resulted in significant cost reductions by eliminating the high cost of the chemical milling operation and the high rejection rate associated with hydroforming the domes and cylinders.

Girth Weld. Yardney had accumulated extensive experience in girth welding INCONEL 718 pressure vessels by the electron beam process* using the COMSAT pressure vessel girth weld design, which incorporated a T-section weld ring with cylindrical back-up flanges onto which the pressure vessel parts fitted. This design provided automatic alignment and preventing "blow-through" into the cell interior during welding. The use of the baseline weld ring caused some concern because the T-section with the back-up flange feature was not present. Experimental investigations showed that EB girth welds were acceptable when made with the baseline weld rings.

Manufacturing Process Changes:

1. * EB welding was used for the girth weld rather than TIG welding to significantly reduce the heat-affected zone area.

2. The baseline weld ring design was not changed, but the manufacturing process used to fabricate the weld ring was changed by Yardney [1-35].

Fill Tube. In the baseline design a 0.317-cm stainless steel tube was used as the fill tube. It extended from the dome at an angle of approximately 45 degrees as shown in Figure 1-15. This tube was welded to an area of the dome not chemically milled to provide a thicker pad for welding the fill tube in place. The dome was drilled and slightly flared. The fill tube was then TIG welded into place. This fill tube weld region was an additional risk point for a hydrogen gas leak.

Manufacturing Process Changes:

1.* The fill tube was made into an integral part of the terminal as shown in Figure 1-17.

2.* The stainless steel fill tube was brazed into the terminal.

Terminal Seal. The baseline cell terminal seals are shown in Figure 1-15. The seal is a compression seal with a formed Teflon bushing compressed between the dome-cylinder seal area and the terminal boss by ceramic washers. The washers are loaded by nuts outside the pressure envelope, and Belleville washers maintain a uniform loading on the seal throughout its life to compensate for any cold flow of the Teflon.

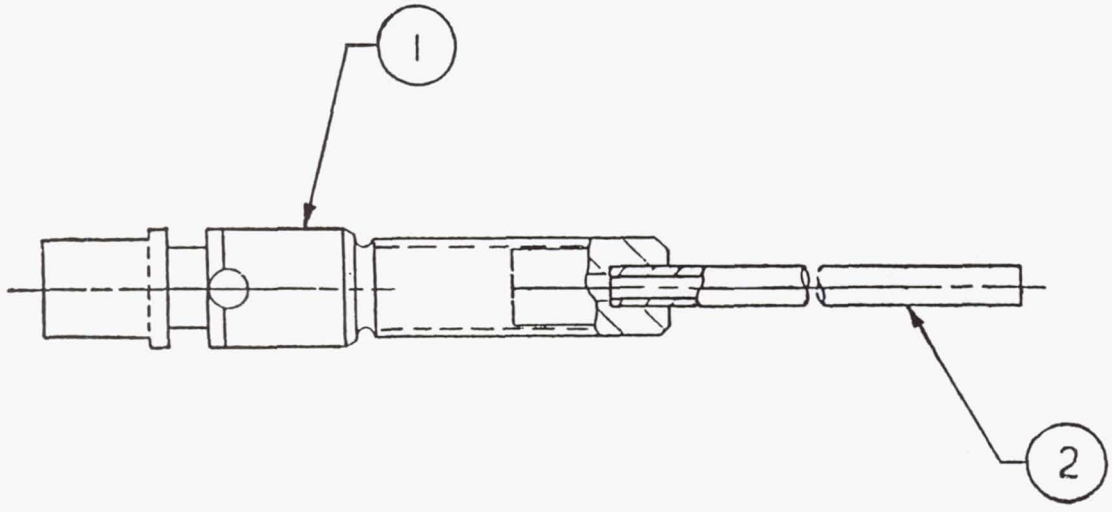

Figure 1-17. Integral fill tube with terminal.

A disadvantage of the baseline seal design was the difficulty in forming the terminal seal boss with enough precision to meet the tolerance needed to match the contour of the Teflon bushing and make a leakproof seal. This problem was the major cause for in-process rejection of the pressure vessel components and represented a major factor in the dome-cylinder final cost.

Manufacturing Process Changes:

1.* The boss was machined separately and then electron-beam welded into the pressure dome, as previously described above. The internal configuration was precisely machined to mate readily with the Teflon bushing and provide a secure, pressure-tight seal.

2. The Teflon bushings were also machined to their final dimensions as described in Reference 1-35.

A major difference between the Yardney MANTECH pressure vessel design and the COMSAT pressure vessel design is the compression seals. With the COMSAT design, nylon is used for the compression seal. The terminal boss is crimped to compress the nylon and form the seal. The nylon material does not cold flow like the Teflon, so there is no requirement for Belleville washers to maintain uniform loading.

Electrode Stack Components

Manufacturing process changes of the electrode stack mechanical components also resulted in substantial cost reductions. Figure 1-18 is a cross sectional view of the Yardney MANTECH 50-Ah cell, showing the redesigned mechanical components.

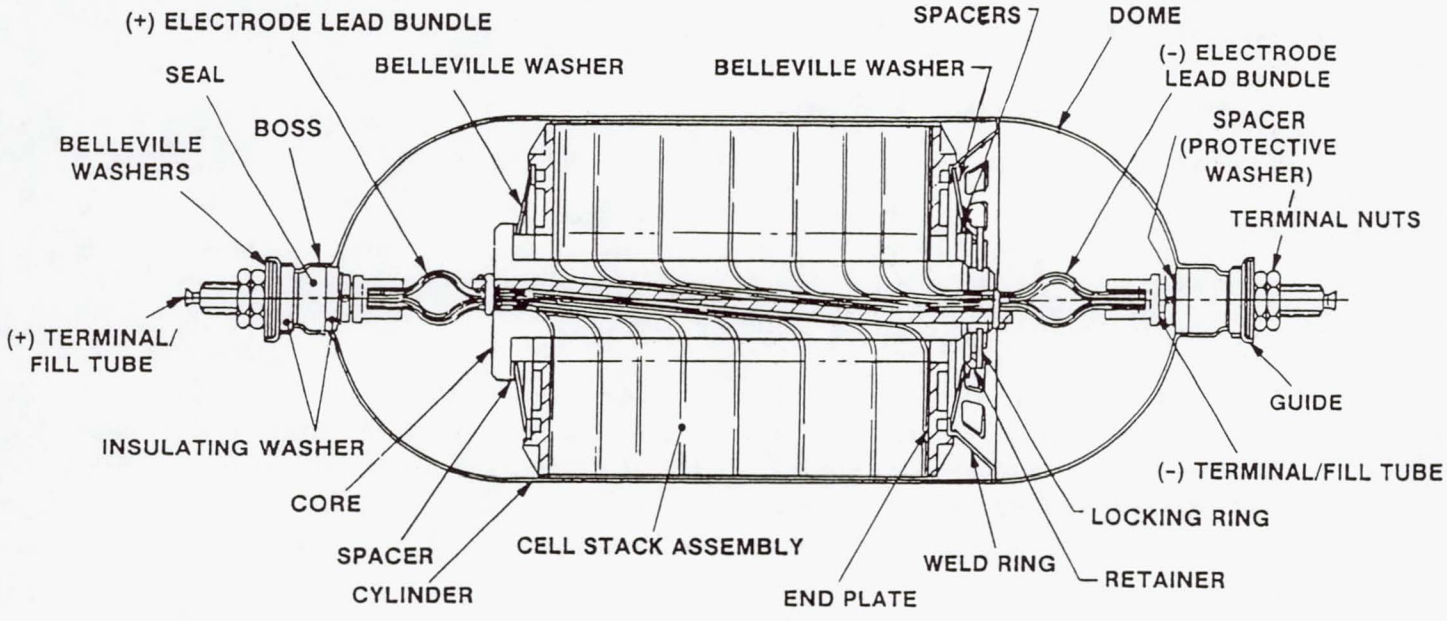

Figure 1-18. Yardney MANTECH 50-Ah cell (cross-sectional view).

Endplates. The baseline endplates were fabricated from INCONEL 718 skip ribbon panels; the unit cost was high.

Manufacturing Process Changes:

1. * Polysulfone endplates, fabricated by machining to final dimensions, were used to replace the skip ribbon panels. For volume production, Yardney recommended manufacturing by injection molding. The final design is shown in Figure 1-19.

2. The weld ring was reconfigured so that identical endplates could be used at either end of the core. This redesign does not require rigid fastening of the weld ring to the endplate.

Core. The baseline core, with its S-shaped cross section, was machined from polysulfone. One end mated with an endplate while the other was threaded to mate with a polysulfone nut. Lead channels were located off the centerline in both axes. The leads (tabs) come out of the core above and to the right of the centerline, requiring compound bends to align the leads with the axial terminals and to provide stress relief between the core and the terminal. This S-shape design limits the width of the leads (tabs) that can be used.

Manufacturing Process Changes:

1. The polysulfone core was redesigned to an H-shape and fabricated by injection molding. This redesign provided for open central lead channels that eased assembly and permitted the use of wider, thinner leads, which are easier to weld, handle, bend, and assemble. The leads exit the core approximately on the centerline of both axes.

2. The core central web was tilted from one end to the other. This facilitated assembly of the electrode stack. During assembly, the tab bundle thickness increased as electrodes were added to the electrode stack. With this new core design, the core cross section area increased to accommodate the increase in thickness as the tabs were fed through the core.

3. Dual Belleville Spring/"Floating Core." The core was suspended in the axial direction between Belleville spring washers which contain the weld ring and stack elements in a compression preload condition. This dual spring configuration provides for possible significant positive electrode growth to be evenly spread over the core length without threat of structural damage.

The endplates and polysulfone core assembly are shown in Figure 1-19.

Separator. A dual separator combination was selected, with one layer of asbestos and one layer of Zircar. The asbestos separator was placed adjacent to the positive electrode to act as a barrier, forcing all of the oxygen gas generated during overcharge off the back of the positive electrode. This eliminates the potential for popping. The Zircar acts as a reservoir to store electrolyte.

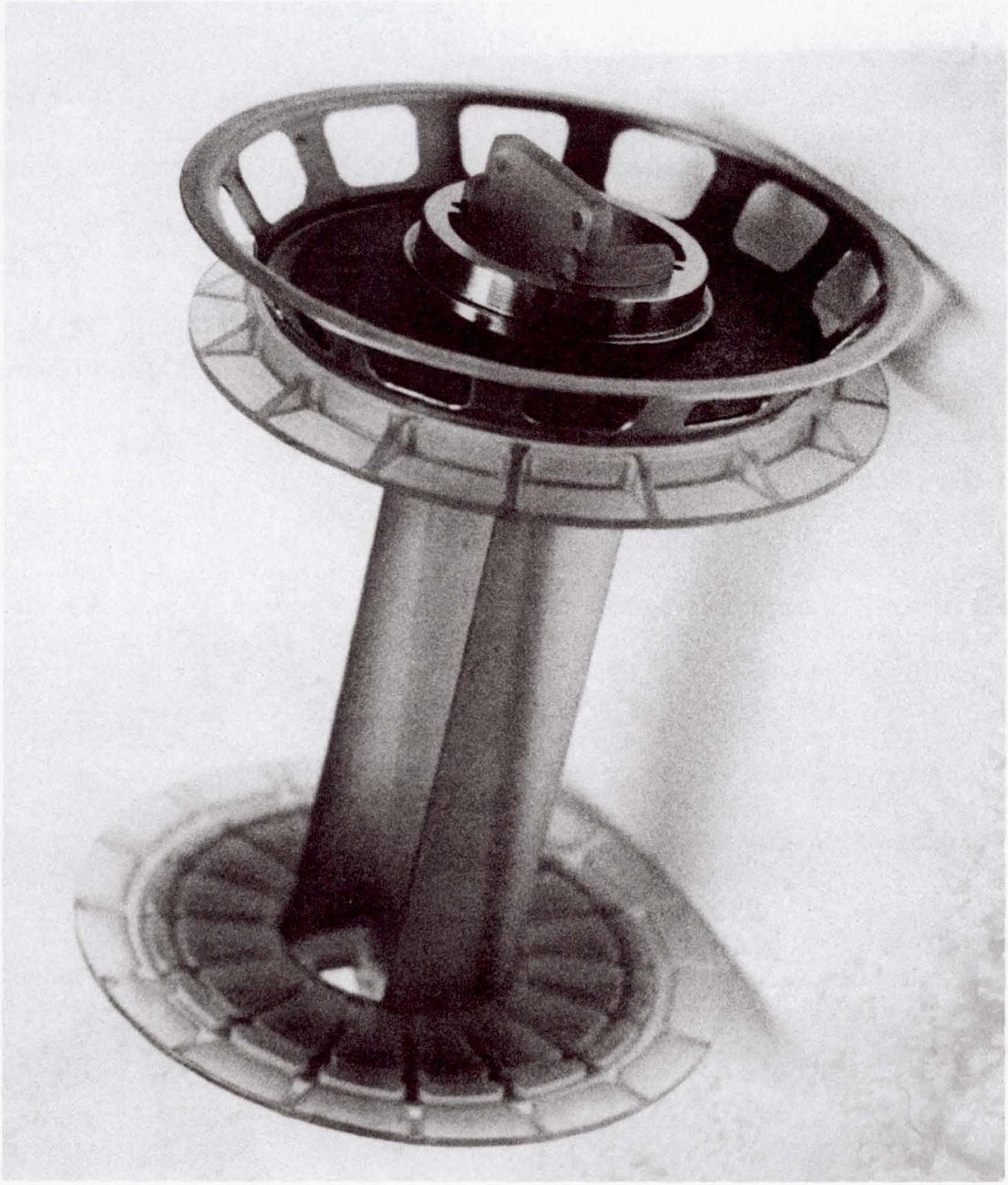

Figure 1-19. Unit stack integral structure (polysulfone endplates and core).

Yardney/MANTECH Cell Design Summary

1. Recirculating electrode stack design.

2. Pineapple slice electrode configuration.

3. INCONEL 718 pressure vessel with Teflon hydraulic compression seals, EB welding, plasma-sprayed zirconium-oxide wall wick.

4. Positive electrodes—dry powder plaque, alcoholic EI process.

5. Separator material—one layer of asbestos separator and one layer of ZYK-15 Zircar.

6. Negative electrode—platinum black negative electrodes with Teflon backing (Gortex) and photochemically etched grid.

7. KOH concentration—31 percent discharged.

8. Positive precharge.

9. Forty positive electrodes for the 50-Ah rated baseline cell.

10. Cell dimensions—8.89-cm diameter, 28.4-cm end to end of terminals, and 20.7 cm dome to dome.

11. Cell average weight—1.486 kg.

12. Measured Capacity at 10°C—55 Ah.

13. Specific Energy (1.25 V)—46.26 Wh/kg.

Yardney Technical Products accomplished its objective of lowering manufacturing costs and reducing rejection rates for the production of Air Force Ni-H_2 cells.

1.9.2 EPI MANTECH Cell Design

Eagle-Picher Industries (EPI) developed its own version of the MANTECH cell design. The EPI MANTECH design is their second-generation design combining manufacturing technology from the COMSAT design and Air Force design, with EPI's own contributions to the technology.

Shown in Figure 1-20 is a cross-sectional view of the EPI MANTECH Ni-H_2 cell design [1-36]. This design is intended for use in either LEO or GEO satellites.

Dual Stack

With the dual-stack design, one electrode stack is mounted on either side of the weld ring, as shown in Figure 1-20. The pressure vessel length was sized so that the two electrode stacks fill up most of the cylindrical portion of the pressure vessel, and most of the hydrogen gas is stored in the domes of the pressure vessel. With this configuration, the pressure range is 750 to 850 psi as compared to the single stack design, where the operating pressure range is typically 500 to 600 psi. The energy density is higher for the dual electrode stack design. Described below is the EPI MANTECH 80-Ah cell. This design is a good example of the next generation of Ni-H_2 cells. Dual-electrode stacks are used for higher capacity IPV cells, capacities of 50 to 100 Ah for 8.89-cm diameter cells.

EPI MANTECH 80-Ah Cell Design

1. Back-to-back electrode stack design, dual electrode stacks (one on each side of the weld ring).

2. Pineapple-slice electrode configuration.

3. INCONEL 718 pressure vessel with nylon Ziegler compression seals. Electron-beam welding of the pressure vessel shells to an INCONEL 718 weld ring. Plasma-sprayed zirconium-oxide wall wick on the inside of the pressure vessel walls.

4. Positive electrodes—wet slurry plaque, aqueous EI process (Bell process).

5. Separator material—optional (see next section).

6. Negative electrode—platinum black negative electrode with Teflon backing, Gortex, photochemically etched substrate.

7. KOH electrolyte concentration—38 percent KOH discharged for GEO; 31 percent KOH discharged for LEO.

8. Hydrogen precharge (optional positive precharge).

9. Cell diameter—8.89 cm, 31.2 cm length terminal to terminal, and 23.2 cm dome to dome.

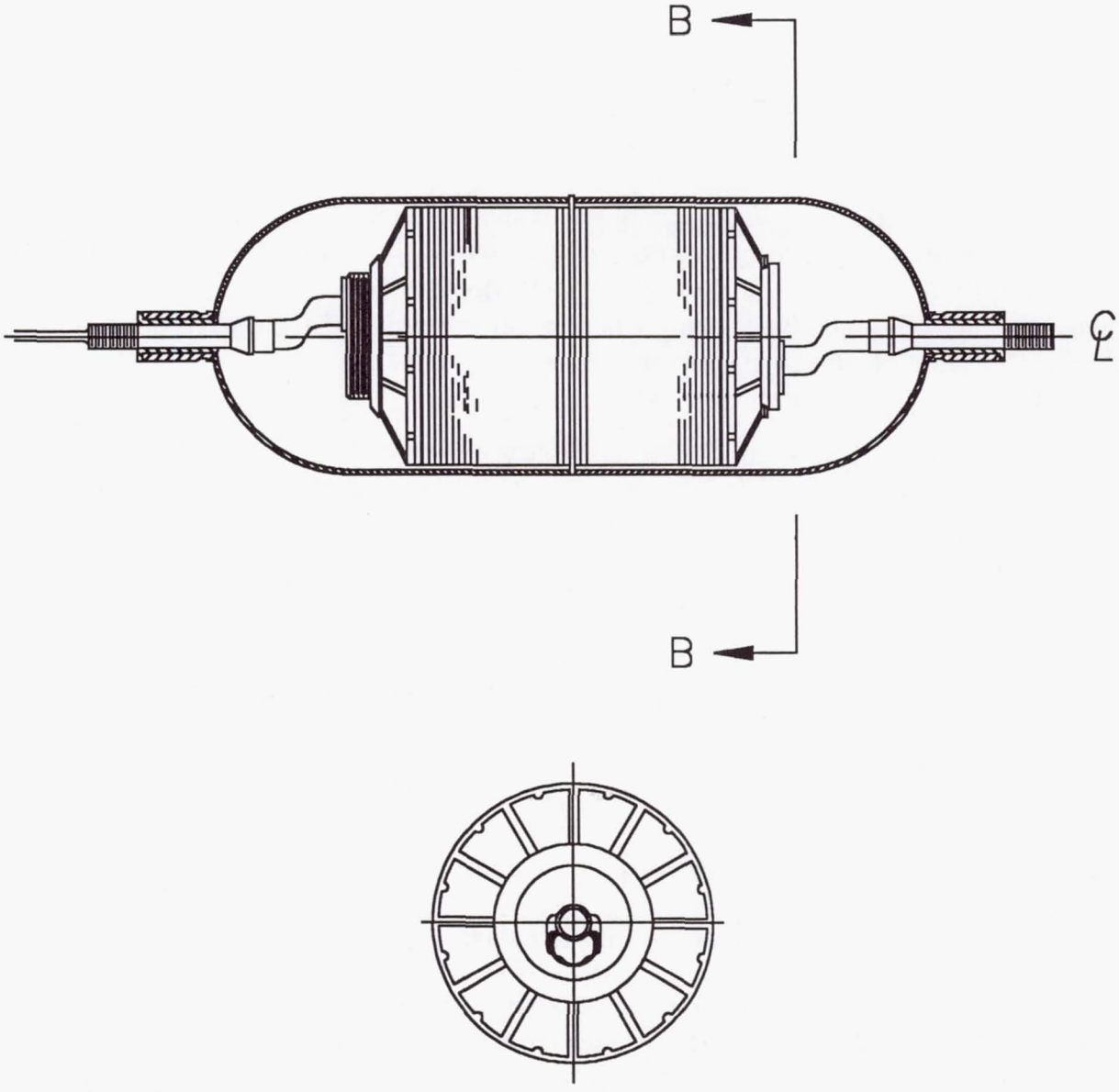

Figure 1-20. EPI MANTECH Ni-H_2 cell design (cross -sectional view).

Separator Options for the 80-Ah Cell Design

There are four options for separator materials.

Baseline. Two layers of Zircar (ZYK-15). This design offers the best end-of-discharge voltage performance.

Option 1. One layer of asbestos and one layer of Zircar (ZYK-15). (The asbestos stops any popping, or oxygen channeling through the separator, and the Zircar serves as a reservoir for the electrolyte.)

Option 2. One layer of asbestos.

Option 3. One layer of Zircar (ZYK-15). This design has the highest specific energy density. However, Zircar is a fragile material and some concern exists with the mechanical integrity of only one layer and its ability to insulate the positive from the negative electrodes.

Cell Mass, Measured Capacity, and Specific Energy for Separator Options

Table 1-5 presents computer projections for the an 80-Ah cell design with the four separator options, comparing the cell mass and specific energy [1-36].

Table 1-5. Specific Energy as a Function of Separator Choice

Separator Choice	Cell Mass	Measured Capacity	Specific Energy	Electrolyte Weight
Two layers of Zircar	1,991 g	88.4 Ah	55.5 Wh/kg	340 g
Asbestos/Zircar	1,947 g	88.4 Ah	56.7 Wh/kg	310 g
*One layer of Asbestos	1,858 g	88.4 Ah	59.6 Wh/kg	223 g
One layer of Zircar	1,803 g	88.4 Ah	61.3 Wh/kg	245 g

*The cell with asbestos has two more positive electrodes than the other three cells. The two positive electrodes were added to overcome the higher impedance of the asbestos cell (Reference private communication with Lee E. Miller).

The specific energy shown in Table 1-5 is a computer projection; the average voltage value used of 1.25/cell was the same for each separator choice. In actuality, the average voltage would be slightly different for each separator choice.

The choice of separator material has a significant effect on the cell mass and quantity of electrolyte within the cell. From Table 1-5 above, note that:

- The cell with two layers of Zircar has the highest mass and also the highest quantity of electrolyte.

- The cell with one layer of Asbestos has the lowest quantity of electrolyte, even with the two additional positive plates.

- The cell with one layer of Zircar has the lightest weight (highest specific energy).

1.9.3 Hubble Space Telescope Ni-H_2 Cell

The Hubble Space Telescope (HST) is the first reported NASA program to use Ni-H_2 batteries in an LEO application. A description of the cell and battery designs is presented in Reference 1-37. Figure 1-21 shows a cross section view of the HST Ni-H_2 cell.

The cells were manufactured by Eagle-Picher to LMSC specifications. The cells are similar in design to the EPI 80-Ah cells described above. A major difference is the pressure vessel design. The INCONEL 718 pressure vessel wall thickness was doubled to 40 mils, and the burst pressure for this vessel is now greater than 4,800 psi.

HST Cell Design Summary

1. Back-to-back positive electrode design, dual electrode stack.

2. Pineapple slice electrode configuration with polysulfone core.

3. INCONEL 718 pressure vessel (40 mils thick) with nylon Ziegler compression seals. Both the positive and negative terminals are at one end of the vessel, rabbit-ear design. The burst pressure for this vessel is over 4,800 psi, with a safety factor of 4 to 1 for a maximum cell operating pressure of 1,200 psi. Electron beam welding of the girth weld and the terminals (barrels).

4. Electrochemically impregnated positive electrodes (using the aqueous process). Dry powder plaque, 35 mils thick. Loading of 1.67 ± 0.1 g/cc void volume.

5. Zircar separator—2 layers (ZYK-15).

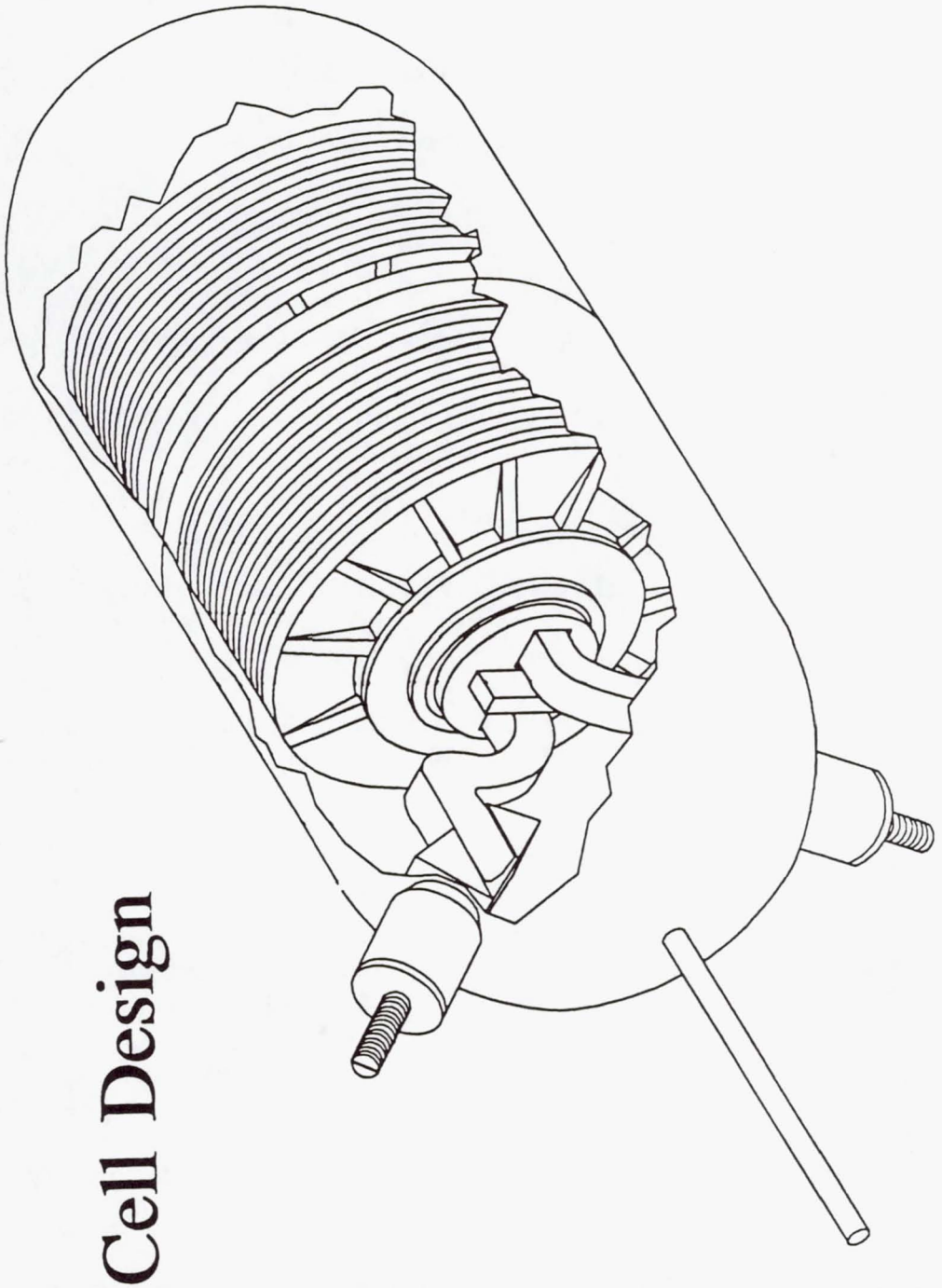

Figure 1-21. HST Ni-H_2 cell (cross-sectional view).

6. Platinum black negative electrode with Teflon backing (Gortex). Photochemically etched grid.

7. KOH electrolyte concentration—31 percent KOH discharged, 27 percent KOH charged.

8. Plasma-sprayed zirconium-oxide wall wick.

9. Hydrogen precharge, one atmosphere (14.7 psi).

10. The weight of each cell—2.100 kg.

11. Measured capacity at 10° C— 96 Ah.

12. Specific energy (10° C)—57.14 Wh/kg.

13. Cell dimensions: 9.03-cm diameter and 24.66 cm bottom dome to end of top terminals, 23.62 cm dome-to-dome, rabbit-ear design terminals.

Terminals (Ziegler Compression Seals)

Normally the bosses (INCONEL 718 barrels) are welded at the axial center of the domes on either end of the pressure vessel to keep the heat dissipation (IR loss at the terminals) symmetrical at either end of the cell.

However, for the HST both terminals are at the same end of the cell and extend diagonally; this is called the "rabbit ear" design (Figure 1-21). It was necessary to locate the terminals at the same end to reduce the length of the cell.

HST Pressure Vessel

The HST pressure vessel is hydroformed to a wall thickness of 1.016 mm (40 mils). Burst pressure for this vessel is over 4,800 psi. The cell maximum operating pressure is designed for 1,200 psi, providing a 4 to 1 safety factor.

This 4:1 safety factor was required for the HST mission because these Ni-H_2 batteries are to be replaced after about 5 years in orbit. The battery orbital replacement unit will be handled by the astronauts, so it is essential that the batteries maintain an adequate safety margin for handling after 5 years of operation.

1.9.4 Superbird and INTELSAT VII 83-Ah Ni-H_2 Cell for GEO Applications

A 27-cell, 83-Ah Ni-H_2 battery was designed, assembled, and qualified by Space Systems/Loral for a GEO communication satellite known as Superbird [1-38]. The cells used for these flight batteries were supplied by Gates Energy Products (GEP). A

cross-sectional view of the cell is shown in Figure 1-22a. This same cell is used for the INTELSAT VII satellite program.

The major differences in this design as compared to the other advanced cell designs are the incorporation of a three-piece pressure vessel with a dual weld ring supported single stack and ceramic terminal seals.

Pressure Vessel. The pressure vessel comprises three INCONEL 718 sections, two hydroformed domes, and one seam-welded cylindrical section, all of uniform thickness. TIG welding is used at the two girth welds joining the pressure vessel and weld rings (see Figure 1-22b and 1-23).

Dual Weld Ring Supported Single-Stack Design. This design contains a single electrode stack supported between fixed endplates and weld rings. The dual weld rings support the single electrode stack in a floating core, as described in Reference 1-39. A Belleville washer system allows for electrode expansion while maintaining uniform stack compression. The dual weld ring support system acts to deload the core and maintain the stack between the fixed endplates.

Ceramic Seals. The ceramic-to-metal seals are similar to the seals used for the Gates Aerospace Ni-Cd cells [1-40]. The terminals are inverted with the seals on the inside (Figure 1-22a). Inverting the seals reduces the length of the cell.

Endplates. INCONEL 718 endplates are used instead of the plastic injection-molded polysulfone endplates [1-41].

INTELSAT VII Cell Design Summary

1. Back-to-back electrode stack design, dual weld ring supported, single-electrode stack with floating core.

2. Pineapple slice configuration with center core design.

3. INCONEL 718 pressure vessel with terminals located at either end in the center of the domes. The terminals are inverted with the seals on the inside. Ceramic seals, TIG welding, plasma-sprayed zirconium-oxide wall wick.

4. Positive electrodes—dry powder plaque, aqueous electrochemical impregnation process.

5. Separator material—two layers of ZYK-15 knit Zircar.

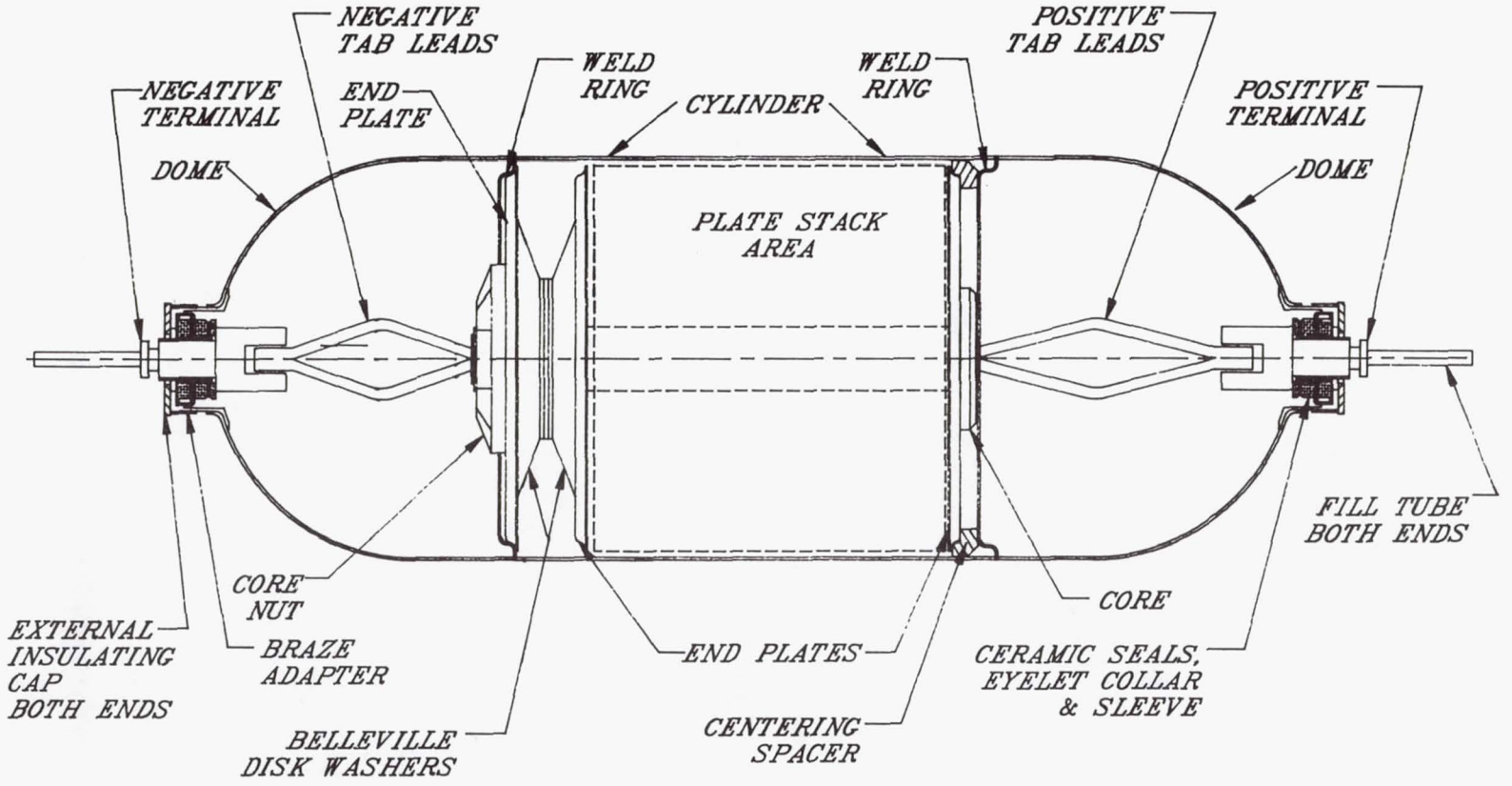

Figure 1-22a. Superbird 83-Ah nickel-hydrogen cell (cross-sectional view).

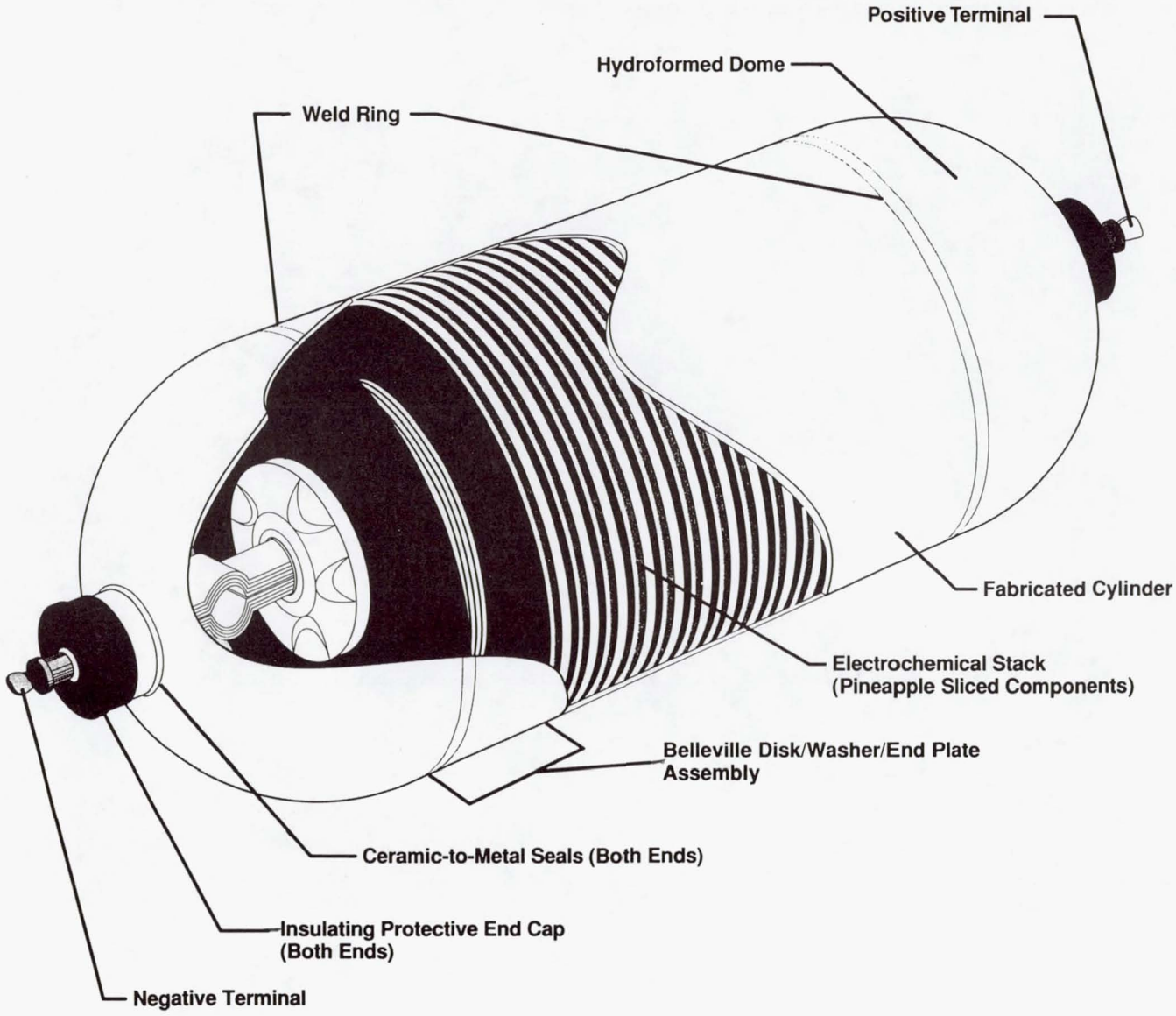

Figure 1-22b. Superbird 83-Ah nickel-hydrogen cell (cut- away view).

Figure 1-23. Gates Energy Products nickel-hydrogen cells (30-Ah cell and 89-Ah cell).

6. Negative electrodes—platinum black negative electrodes with Teflon backing (Gortex) with photochemically etched grid.

7. KOH electrolyte concentration: 31 percent KOH discharged.

8. Positive precharge.

9. Cell dimensions—8.89 cm diameter, 29.67 cm end to end of terminals, 23.67 cm end to end of domes.

10. Weight of each cell—1.867 kg.

11. Measured capacity at 10°C—91.5 Ah.

12. Specific energy (10°C)—61.26 Wh/kg.

1.9.5 Summary of Second-Generation Ni-H_2 Cells

This section presents a summary of the cell design features for the second generation of Ni-H_2 IPV cells for the 1990s.

Pineapple Slice Electrode Configuration. The pineapple slice electrode configuration is used with either the back-to-back or recirculating electrode stack design for both LEO and GEO applications. The advantages of the pineapple slice electrode configuration are that it improves heat transfer from the electrode stack to the pressure vessel wall, and it is easier to fabricate than the bus bar configuration.

Back-to-Back Design. The back-to-back electrode stack design with the pineapple slice electrode configuration and two layers of Zircar ZYK-15 separators has become the design of choice for GEO applications in the 1990s.

Recirculating Design. The recirculating electrode stack design with the pineapple slice electrode configuration and two layers of Zircar ZYK-15 separator material has been selected for the Space Station Freedom program.

Wall Wick. A wall wick with the separator material extended to and in contact with the wall wick is recommended for all IPV Ni-H_2 cells, both recirculating and back-to-back designs. The wall wick separator combination ensures a return path for any electrolyte or water loss mechanism. The wall wick is recommended for use in both LEO and GEO applications.

Positive Electrodes. The positive electrodes for Ni-H_2 cells are manufactured (impregnated) by one of two electrochemical impregnation process, either the

aqueous or alcoholic process using both wet slurry and dry powder plaque. The preference or trend is toward dry powder plaque with aqueous impregnation.

Negative Electrodes. The hydrogen electrodes consist of Teflon-bonded platinum black supported with a photo-etched nickel substrate with Teflon (Gortex) backing.

Separator Materials

Zircar (ZYK-15) separator has become the separator material of choice for most aerospace Ni-H_2 cell designs.

Fuel-cell-grade asbestos remains a strong contender.

A combination of asbestos and Zircar is also an option that is still being evaluated by NASA.

Electrolyte

The effects of KOH concentration on cyclic life are discussed in the next section, 1.8.0. The cyclic lifetime improves at 26-percent KOH concentration. For LEO applications, the lower concentration of 26 percent is recommended by NASA. There is, however, a capacity/weight trade-off because capacity is 25 to 30 percent lower with 26 percent KOH than with 31 percent KOH.

For the Space Station Freedom cell design, 31 percent KOH concentration fully discharged was selected. However, NASA is still investigating experimental cells with 26 percent KOH concentration fully discharged under test at NWSC, Crane, Indiana.

For GEO application cells with both 31 percent KOH concentration fully discharged and 38 percent KOH concentration fully discharged are being used. The user/supplier can decide which concentration to use.

LEO applications	26 to 31% KOH fully discharged
GEO applications	31 to 38% KOH fully discharged

Specific Energy and Energy Density

Table 1-6 is a summary of the specific energies and energy densities for the different cell designs described in this chapter.

Table 1-6.
Summary of Specific Energies and Energy Desities for the Different Cell Designs (8.89-cm diameter pressure vessel)

Cell Design	Capacity* 10°C	Volume Cell	Energy 1.25 V avg	Pressure Range	Weight	Specific Energy	Energy Density
	(Ah)	(L)	(Wh)	(psi)	(kg)	(Wh/kg)	(Wh/L)
COMSAT Design							
INTELSAT V 30-Ah cell	36	.762	45.0	500	0.890	50.6	59.1
NTS-2 35-Ah cell	43.0	.841	53.7	550	1.028	52.3	63.8
Air Force Design 50-Ah cell	58.0	1.119	72.5	580	1.480	48.9	64.7
Yardney MANTECH Design 50-Ah cell	55.0	1.119	68.7	550	1.486	46.2	61.4
HST	96.0	1.256	120	1000	2.100	57.14	95.5
EPI 80-Ah cell MANTECH Design							
2 layers of Zircar	88.4	1.256	110.5	800	1.991	55.5	87.5
Asbestos/Zircar	88.4	1.256	110.5	800	1.947	56.7	87.5
1 layer of asbestos	88.4	1.256	110.5	800	1.858	59.6	87.5
1 layer of Zircar	88.4	1.256	110.5	800	1.803	61.3	87.5
GEP GEO Design (INTELSAT VII) 83-Ah cell	91.5	1.245	114.4	850	1.867	61.26	91.9

*Capacity is the measured capacity to 1.0 volts at 10°C. Charge for 16 hours at C/10 rate discharge at C/2 rate to 1.0 volts.

Specific Energy (Wh/kg)

1. The specific energy increases as the capacity increases but tends to taper off above 50 Ah and approaches an upper limit of about 63 Wh/kg for the 8.89-cm diameter pressure vessel.

2. The choice of separator affects both the weight (quantity of electrolyte) and the discharge voltage, and thus the specific energy of the cell.

Energy Density Wh/L

1. The energy density is primarily a function of the pressure range, or free volume in the cell. The cells used in the 1980s, the COMSAT design, and the Air Force design cells had a pressure range of 500 to 580 psi. The cells in the

1990s, the higher-capacity cells in Table 1-6 (EPI 80-Ah cell and GEP 83-Ah cell), operate with a higher pressure range—800 to 850 psi. For these designs, the EPI dual-stack design and the GEP dual-weld-ring design, the electrode stack(s) fill the entire cylindrical portion of the pressure vessel. The hydrogen gas is stored in the domes. These high-pressure cells have significantly higher energy densities (about 1.6 times the energy density of the INTELSAT V cells).

However, there is a concern with these high pressure cells. The higher the pressure the greater the amount of damage that occurs to the ZYK-15 Zircar separator material and negative electrodes during activation.

1.10.0 Ni-H_2 CELL MANUFACTURERS

Presented below are specific cell design features for the five Ni-H_2 cell manufacturers in the United States.

1.10.1 Hughes Aircraft (HAC)

1. Recirculating electrode stack design.
2. Pineapple slice configuration with polysulfone center core.
3. INCONEL 718 pressure vessel, hydroformed and then chem-milled to final dimensions; TIG welding of girth weld.
4. Teflon hydraulic compression seals.
5. Positive electrodes—dry powder sinter plaque, alcoholic electrochemical impregnation.
6. Separator material—ZYK-15 Zircar cloth.
7. Negative electrodes—Teflon-bonded platinum black with Gortex backing and photochemically etched grid. HAC cleaning process.
8. Endplates—INCONEL 718 skip ribbon panels.
9. Positive precharge.

1.10.2 Eagle-Picher Industries (EPI) Joplin

1. Recirculating and back-to-back electrode stack designs. Dual-stack or single-stack designs.

2. Bus bar and pineapple slice configurations for electrode stack components.

3. INCONEL 718 pressure vessel, hydroformed to uniform thickness. EB welding with INCONEL 718 weld ring at girth weld.

4. Nylon "Ziegler" compression seal.

5. Positive electrodes—plaque made at Colorado Springs either wet slurry or dry powder plaque. Aqueous impregnation process at Joplin.

6. Separator materials— ZYK-15 Zircar cloth and asbestos.

7. Negative electrodes—Teflon-bonded platinum black with Gortex backing and photochemically etched grid.

8. Polysulfone plastic endplates.

9. Positive or negative precharge.

1.10.3 Eagle-Picher Industries (EPI) Colorado Springs

1. Positive electrodes—both wet slurry and dry powder plaque made at Colorado Springs.

2. Alcoholic impregnation process at Colorado Springs.

3. Same as EPI Joplin above for other specifics.

1.10.4 Yardney Technical Products Division

1. Recirculating and back-to-back electrode stack designs.

2. Bus bar and pineapple slice configuration for electrode stack components. Tapered polysulfone center core with pineapple slice design.

3. INCONEL 718 pressure vessel, hydroformed to uniform thickness. EB welding of girth weld.

4. Teflon hydraulic compression seals and nylon "Ziegler" compression seals.

5. Positive electrodes—wet slurry plaque, aqueous impregnation process.

6. Separator material—one layer of ZYK-15 Zircar and one layer of asbestos.

7. Negative electrodes—Teflon-bonded platinum black with Gortex backing and photochemically etched grids.

8. Polysulfone plastic endplates.

9. Positive or negative precharge.

1.10.5 Gates Energy Products

1. Back-to-back or recirculating electrode single-stack design.

2. Pineapple slice configuration with polysulfone core.

3. INCONEL 718 pressure vessel, hydroformed domes with seam-welded cylinder of uniform thickness. TIG welding at two girth welds of pressure vessel.

4. Dual weld ring supported, single electrode stack in floating core.

5. Ceramic to metal seals, similar to the seals used for aerospace Ni-Cd cells.

6. Positive electrodes—dry powder plaque, aqueous impregnation process.

7. Separator material—two layers of ZYK-15 Zircar cloth.

8. Negative electrodes—Teflon bonded platinum black with photochemically etched grids.

9. INCONEL 718 endplates.

Table 1-7. Manufacturers' Cell Design Features

Design Features	Ni-H_2 Cell Manufacturer				
	Hughes	EP Joplin	EP CS	YEC	Gates
Stack Design					
Recirculating	x	x	x	x	x
Back to Back	x	x	x	x	x
Single Stack	x	x	x	x	x
Dual Stack		x	x		
Plate Configuration					
Bus Bar		x			
Pineapple Slice	x	x	x	x	x

Table 1-7. Manufacturers' Cell Design Features (Continued)

Design Features	Ni-H_2 Cell Manufacturer				
	Hughes	EP Joplin	EP CS	YEC	Gates
Vessel					
Chem Milled	x				
Uniform Thickness		x	x	x	x
Weld					
TIG Weld	x/girth				x/2-girth
EB Weld		x/girth	x/girth	x/girth	
Seal					
Teflon	x			x	
Ziegler		x	x	x	
Ceramic to Metal					x
Separator					
Asbestos		x	x		
Zircar	x	x	x		x
Asbestos/Zircar		x	x	x	
Zircar/Zircar	x	x	x		x
Positive Electrode					
Plaque					
Slurry		x	x	x	
Dry Powder	x	x	x		x
Impregnation					
Alcohol	x		x		
Aqueous		x		x	x
Negative Electrode					
Photochemically etched grid	x	x	x	x	x
Teflon/platinum mix	x	x	x	x	x
Gortex Teflon backing	x	x	x	x	x
End Plates					
Skip Ribbon	x				
Polysulfone		x	x	x	
INCONEL 718					x
Precharge					
Positive	x	x	x	x	x
Negative		x	x	x	x

1.11.0 NASA R&D PROGRAMS

1.11.1 Advanced Designs for IPV Nickel-Hydrogen Cells

In 1983, the NASA Lewis Research Center initiated an in-house and contract technology program to improve nickel-hydrogen cycle life and performance to meet NASA LEO mission requirements (30,000 cycles) at deep depths-of-discharge (DOD). The following summarizes the technological contributions of the Lewis Research Center Program.

- NASA Lewis conceived of a number of advanced concepts for IPV Ni-H_2 cells to improve cycle life at deep DOD [1-42]. The proposed design concepts were added to eliminate failure modes commonly found in Ni-H_2 cells. An advanced cell was designed, developed, and tested. The proposed design concepts included a) the use of alternative methods for recombination (i.e., the catalyzed wall wick), b) the use of serrated-edge separators to facilitate the movement of gas within the stack while maintaining physical contact with the cell wall, and c) the incorporation of Belleville washers to yield an expandable stack capable of accommodating some of the nickel electrode expansion that is known to occur with cycling.

- The Lewis Research Center Advanced Development Program also includes the development of alternative separators to replace asbestos and the development of lightweight nickel electrodes to improve cell specific energy [1-43], [1-44], [1-45], [1-46], [1-47].

Oxygen Recombination

The concept proposed for oxygen recombination is to use a catalyzed wall wick. For the back-to-back nickel electrodes design with an asbestos separator, the oxygen generated on overcharge is forced off between the positive electrodes (the back of the positive electrodes opposite the separator). This oxygen is directed toward the catalyzed wall wick where it recombines with hydrogen to form water. The water is then wicked back into the electrode stack. The heat of recombination is generated at the wall of the pressure vessel rather than internally within the cell stack. This design is intended to eliminate popping and excessive heat generation within the cell stack [1-48].

Serrated Separator

The edges of the separator are serrated to facilitate gas movement inside the cell. The outside edge of the serrated separator extends to the zirconium oxide wall wick to facilitate recirculation of electrolyte.

The proposed separators are made of beater-treated asbestos (BTA) rather than conventional fuel-cell-grade asbestos. BTA is reconstituted fuel cell grade asbestos that has 5 percent butyl latex binder by weight added. The sheet is formed in one ply and is approximately 7 mils thick. The properties of BTA are comparable to those of fuel-cell-grade asbestos (resistivity, electrolyte retention, porosity, pore size, bubble pressure), but the BTA is more uniform and stronger. The edges of the separator are serrated to facilitate gas movement inside the cell.

Expandable Electrode Stack

To accommodate the nickel electrode expansion and improve cycle life, an expandable stack was proposed. One method is to use INCONEL 718 Belleville disc springs at each end of the stack between the endplates and the tie rod nuts. The spring will maintain stack compression throughout the life of the cell.

Another method is to share the expansion with the separator. The spring constant can be selected so that some of the electrode expansion is absorbed by the asbestos separator. A standard 10-mil separator can be compressed to about 5 mils without any degradation in performance. NASA has an in-house effort ongoing to investigate the effects of separator compression on resistance and electrolyte content.

1.11.2 KOH Concentration Effect on the Cycle Life of Ni-H_2 Cells

The effects of KOH concentration on the cycle life of Ni-H_2 cells were investigated by Hughes Research Center under contract to NASA Lewis [1-49]. A breakthrough in the LEO cycle life of individual pressure vessel cells was reported [1-50]. Cell cycle life was improved by greater than a factor of 10 when KOH concentration was reduced from 31 percent to 26 percent in full discharge state (Figure 1-24). Boilerplate cells containing 26 percent KOH discharged were cycled for 40,000 accelerated LEO cycles at 80 Percent DOD compared to 3,500 cycles for boilerplate cells containing 31 percent KOH discharged. The accelerated LEO cycle regime consisted of 45-minute cycles run at 80 percent DOD, 27.5-minute charge followed by a 17.5-minute discharge. Temperatures were maintained at 23°C.

The accelerated boilerplate cell test results are in the process of being validated using flight cells and a real-time LEO cycle regime. Cells from various manufacturers containing 26 percent and 31 percent KOH are being cycled at 60 and 80 percent DOD. Six 48-Ah Hughes flight cells were LEO tested at 80 percent at the Naval Weapons Support Center, Crane, Indiana [1-50]. Three of these cells contain 26 percent KOH and three contain 31 percent KOH. The test results are summarized in Figure 1-25. The cells with 31 percent KOH failed at 3,729; 4,165; and 11,355 cycles. The cells with 26 percent KOH failed at 15,314; 19,500; and 23,700 cycles. The superior cycle life of cells containing 26 percent KOH over cells containing 31 percent KOH was validated in this experiment. The following table summarizes the current validation testing of 26 percent KOH sponsored by NASA. To date, the cells have accumulated 2,500 to 5,500 LEO cycles. For all manufacturers, the cells with the 26

percent KOH have a higher end-of-discharge voltage than the cells with 31 percent KOH.

Table 1-8. NASA-Sponsored Validation Testing of 26% KOH

Cell Vendor	Cell Capacity	No. of Cells	Test Conditions	Comments
Eagle Picher	65 Ah	3 – 26% KOH 3 – 31% KOH	60% DOD 10°C	Aqueous Impregnation
Eagle Picher	65 Ah	3 – 26% KOH 3 – 31% KOH	60% DOD 10°C	Alcoholic Impregnation
Gates	65 Ah	3 – 26% KOH 3 – 31% KOH	60% DOD 10°C	Aqueous Impregnation
Yardney	65 Ah	3 – 26% KOH 3 – 31% KOH	60% DOD 10°C	Aqueous Impregnation

1.11.3 Electrode Expansion

Gradual irreversible expansion of nickel electrodes during charge-discharge cycling is believed to be the major failure mechanism for Ni-H_2 cells. Electrode expansion creates voids and increases the micropore volume within the electrode [1-51]. Electrolyte from the separator is drawn into the added pore volume of the electrode, causing the separator to dry out and the impedance of the cell to increase.

The expansion of nickel electrodes with cycling was studied quantitatively using an electrode bending technique, and the findings are summarized as follows [1-51]:

1. Experimental data showed that the rate of the irreversible electrode bending is directly proportional to the rate of electrode expansion. Thus, the electrode bending technique provides a speedy and convenient method of studying electrode expansion.

2. The irreversible rate of electrode expansion with cycling (k) is quantitatively related to the depth-of-discharge (DOD) of cycling by the following equation.

$$k = A\,(DOD)^s$$

where A and s are constants. The value of s is 2.2 in 5.6 molarity of KOH (23.7% KOH) and 2.5 in 8.0 molarity of KOH (31% KOH) electrolyte, respectively.

The irreversibility is dependent on both the KOH concentration and the depth-of-discharge.

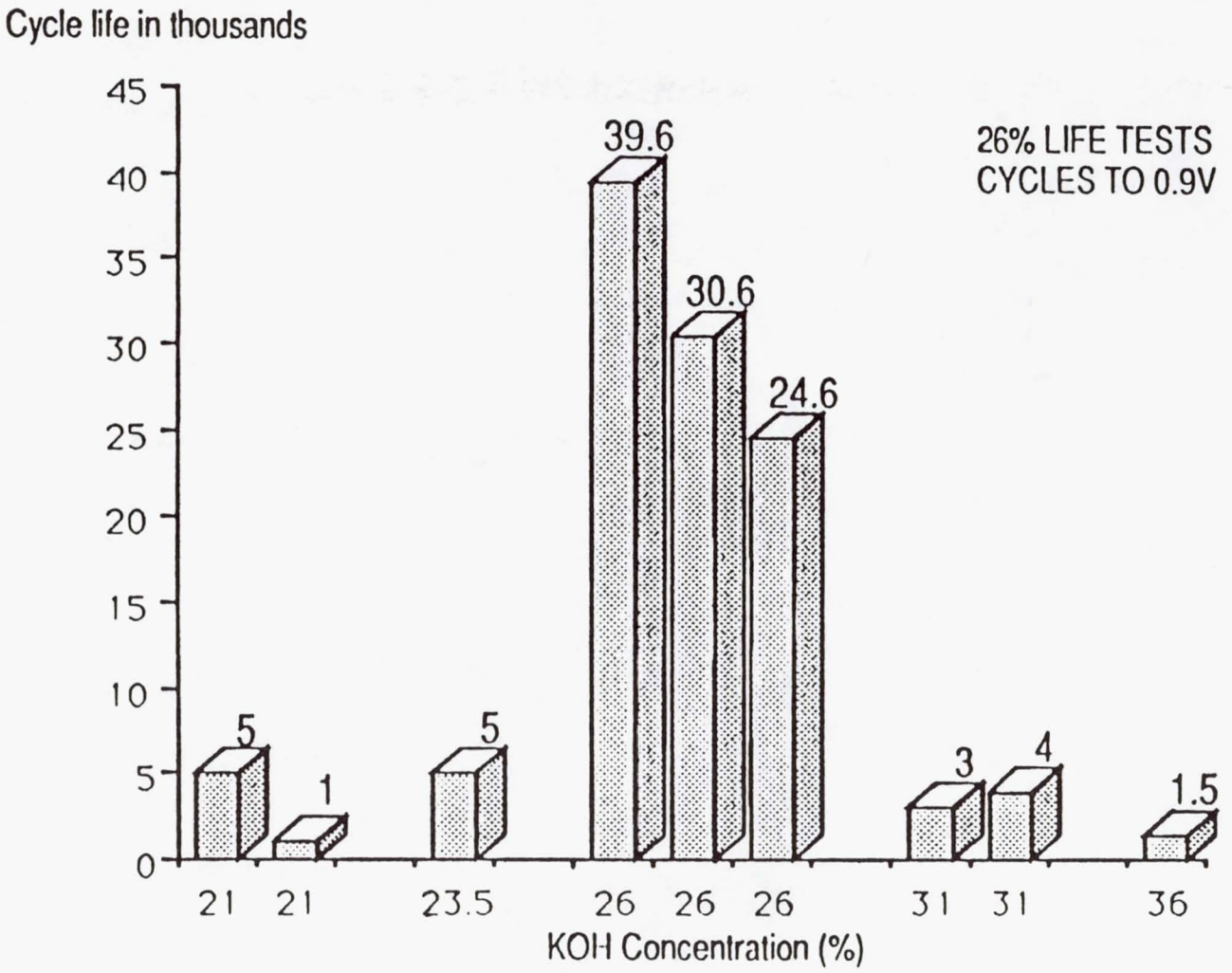

Figure 1-24. Effects of KOH electrolyte concentration on cycle life.

C-2

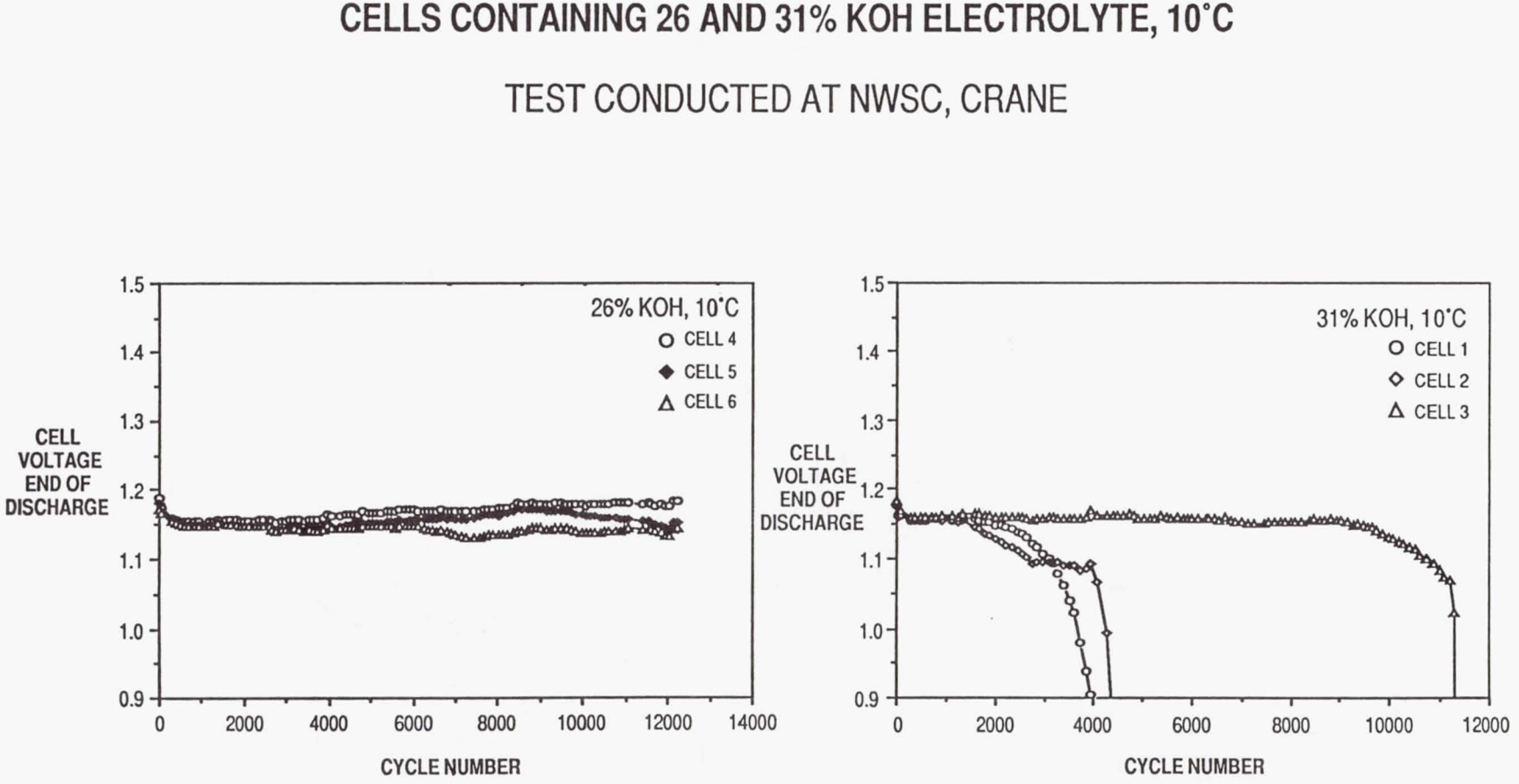

Figure 1-25. Test results at NWSC, Crane, Indiana.

3. A small amount of LiOH in the electrolyte greatly reduces both the irreversible expansion with cycling and the amplitude of the reversible expansion and contraction during cycling.

1.11.4 Summary of NASA R&D Programs

Oxygen Recombination. For LEO applications, the best overall watt-hour efficiency one can achieve for a Ni-H_2 battery is 83 to 85 percent of the usable energy to the spacecraft. The remaining 15 to 17 percent of the energy is dissipated as heat.

Heat dissipation within the IPV cells will increase with the following:

1. Increased depth-of-discharge—usable energy
2. Larger capacity cells—81-Ah cells for Space Station Program
3. Larger diameter cells—220-Ah cells, 4.5-in. diameter.

The catalyzed wall wick concept is the best new design concept being investigated to meet these increased heat dissipation demands for the IPV cells.

Expandable Electrode Stack. A number of the second generation of IPV cells for the 1990s are using a floating core concept, specifically the GEP cell design for the Space Station Freedom.

KOH Concentration. A major breakthrough in LEO cycle life with 26 percent KOH was reported by NASA for boilerplate cells tested at HAC. These results are in the process of being validated by flight cells in real-time LEO cycle regime.

One of the questions for flight cells is what KOH concentration should be used. The KOH concentration changes between the charged and discharged state of the cell. Most LEO aerospace cell designs use 31 percent KOH discharged, which is equivalent to 26 percent KOH charged. Another option would be to use 26 percent discharged, which would provide 21 percent charged. The problem is a significant tradeoff between KOH concentration and capacity. A number of the GEO aerospace cell designs use 38 percent KOH discharged, which is equivalent to 31 percent KOH charged.

1.12.0 REFERENCES

[1-1] J. Dunlop, J. Giner, G. van Ommering, and J. Stockel, 1975, "Nickel-Hydrogen Cell," U.S. Patent 3,867,199.

[1-2] J. Stockel, G. van Ommering, L. Swette and L. Gaines, "A Nickel-Hydrogen Secondary Cell For Synchronous Satellite Applications," *Proc.*, 7th IECEC September 25–29, 1972, San Diego, California, pp. 87–94.

[1-3] E. Levy Jr., "Nickel-Hydrogen Battery Technology—A Tenth Anniversary Review," *Proc.*, 18th IECEC, 1983, Orlando, Florida. p. 1530.

[1-4] L. Miller, "The Ni-H_2 Battery System: A Space Flight Application Summary," *Proc.*, 23 IECEC, 1988, Denver, Colorado. pp. 489-492.

[1-5] Falk and Salkind, *Alkaline Storage Batteries*, copyright 1969 by John Wiley & Son, Inc., Section 2.5.

[1-6] R. L. Beauchamp, D. W. Maurer, and T. D. O'Sullivan, U.S. Patent 4032697, June 28, 1977.

[1-7] G. Holleck, "Failure Mechanisms in Nickel-Hydrogen Cells," *The 1976 Goddard Space Flight Center Battery Workshop*, pp. 297–315.

[1-8] J. Dunlop, G. van Ommering, and M. W. Earl, "Ni-H_2 Battery Flight Experiment," 10th International Symposium on Power Sources, *Power Sources 6* (edited by D. H. Collins) New York: Academic Press, 1977, pp. 231–247.

[1-9] R. L. Beauchamp, "Positive Electrodes for Use in Nickel Cadmium Cells and the Method for Producing Same and Products Utilizing Same," U.S. Patent 3,653,967, April 4, 1972.

[1-10] D. F. Pickett, H. H. Rogers, L. A. Tinker, C. Bleser, J. M. Hill, and J. Meador, "Establishment of Parameters for Production of Long Life Nickel Oxide Electrodes for Nickel-Hydrogen Cells," *Proc.*, IECEC, 1980, Seattle, Washington, p. 1918.

[1-11] M. Bernhardt and D. Maurer, "Results of a Study on the Rate of Thickening of Nickel Electrodes," *Proc.*, 29th Power Sources Conference, June 1980, p. 219–221.

[1-12] L. W. Niedrach and H. R. Alford, *Journal Electrochemical Society*, Vol. 112, 1965, pp. 117–124.

[1-13] H. Rogers, E. Levy and S. J. Stadnick, "Failure Mechanisms In Nickel/Hydrogen Batteries," AFAPL-TR-77-90, Final Report, August 1977.

[1-14] P. S. Du Pont and H. H. Rogers, U.S. Patent 4,250,235 February 10, 1981.

[1-15] H. . Rogers and S. J. Stadnick, U.S. Patent 4,369,212, January 18, 1983.

[1-16] E. Adler, S. Stadnick, and H. Rogers, "Nickel-Hydrogen Battery Advanced Development Program Status Report," *Proc.*, 15th IECEC, Seattle, Washington, 1980, p. 189.

[1-17] J. Dunlop, J. Stockel, G. van Ommering, "Sealed Metal Oxide-Hydrogen Secondary Cells," 9th International Symposium on Power Sources, 1974, *Power Sources 5* (edited by D. H. Collins) New York: Academic Press, 1975, pp. 315–329.

[1-18] G. van Ommering and J. F. Stockel, "Characteristics of Nickel-Hydrogen Flight Cells," *Proc.*, 27th Power Sources Conference, June 1976.

[1-19] J. Dunlop, Chapter 22, "Nickel-Hydrogen Batteries," *Handbook Of Batteries & Fuel Cells*, (edited by David Linden) McGraw-Hill, 1984.

[1-20] G. L. Holleck, M. J. Turchan and D. DeBiccari, "Improvement And Cycle Testing of Ni/H_2 Cells," 28th Power Sources Symposium, 12–15 June 1978, pp. 139–141.

[1-21] H. H. Rogers, U.S. Patent 4,177,325, December 4, 1979.

[1-22] H. H. Rogers, S. J. Krause, and E. Levy Jr., "Design of Long Life Nickel-Hydrogen Cells," *Proc.*, 28th Power Sources Conference, June 1978.

[1-23] H. H. Rogers, U.S. Patent 4,262,016, April 14, 1981.

[1-24] D.M. McArthur, *Journal Electrochemical Society*, 1970, Vol. 117, pp. 422–426.

[1-25] S. J. Stadnick and H. H. Rogers, July 1987, U.S. Patent 4,683,178.

[1-26] L. Miller, "The Nickel-Hydrogen Battery System An Historic Overview" *Proc.*, 16 IECEC 1981 Atlanta, Georgia, pp. 220–223.

[1-27] M. Klein and M. George, "Nickel Hydrogen Secondary Batteries," 26th Power Sources Symposium, 1974, pp.18–20.

[1-28] J. Giner and J. Dunlop, "The Sealed Nickel-Hydrogen Secondary Cell," *Journal of the Electrochemical Society*, Vol. 122, No. 1, January 1975, p. 4–11.

[1-29] E. McHenry and P. Hubbauer, "Hermetic Compression Seals for Alkaline Batteries," *Journal of the Electrochemical Society*, Vol. 119, No. 5, May 1972, pp 564–568.

[1-30] J. D. Dunlop and J. F. Stockel, "Status of COMSAT/Intelsat Nickel-Hydrogen Battery Technology," 15th IECEC Seattle, Washington, 18–22 August 1980, pp. 1878–1884.

[1-31] S. J. Stadnick, U.S. Patent 4,224,388, September 23, 1980.

[1-32] J. F. Stockel, "Self-Discharge Performance and Effects of Electrolyte Concentration on Capacity of Nickel-Hydrogen (Ni/H_2) Cells," 20th Intersociety Energy Conversion Engineering Conference, August 25–29, 1986. Volume 1, p. 1.171.

[1-33] H. S. Lim and S. A. Verzwyvelt, "KOH Concentration Effect on the Cycle Life of Nickel-Hydrogen Cells," 20th Intersociety Energy Conversion Engineering Conference, August 25–29, 1986. Volume 1 p. 1.165.

[1-34] N. Puester, "Phase 1 Value Engineering Study Resulting in Increased Producibility of Air Force Design Ni-H_2 Cells," *Proc.*, 17th IECEC, Los Angeles, California, 1982, p. 786.

[1-35] J. G Bentley and P. J. Denoncourt, "Manufacturing Technology For Nickel/Hydrogen Cells," AFWAL-TR-87-4051, October 1987.

[1-36] L. Miller, J. Brill, and G. Dodson, "Multi-Mission Ni-H_2 Battery Cells For the 1990s," *Proc.*, 24 IECEC, Washington, D.C., 1989, p. 1387.

[1-37] D. E. Nawrocki, J. D. Armantrout, "The Hubble Space Telescope Nickel-Hydrogen Battery Design," *Proc.*, 25 IECEC, Reno, Nevada, 1990.

[1-38] T. M. Yang, C. W. Koehler, A. Z. Applewhite, "An 83-Ah Ni-H_2 Battery For Geosynchronous Satellite Applications," *Proc.*, 24th IECEC, Washington D.C., 1989 p.1375.

[1-39] GEP U.S. Patent 4,950,564.

[1-40] GEP U.S. Patent 4,904,551.

[1-41] GEP U.S. Patent 5,002,842.

[1-42] J. J. Smithrick, M. A. Manzo, and O. Gonzalez-Sanabria, "Advanced Designs for IPV Nickel-Hydrogen Cells," *Proc.*, 19 IECEC, San Francisco, California, 1984, p. 631.

[1-43] D. L. Britton, "Lightweight Nickel Electrode for Nickel-Hydrogen Cells and Batteries, *Proc.*, 32rd International Power Sources Symposium, Cherry Hill, NJ, June 9–12, 1986.

[1-44] D. L. Britton, "Performance of Lightweight Nickel Electrodes," *Proc.*, 33rd International Power Sources Symposium, Cherry Hill, NJ, June 13–16, 1988.

[1-45] D. L. Britton, "Lightweight Fibrous Nickel Electrodes for Nickel-Hydrogen Batteries," *Proc.*, 4th Annual Battery Conference on Applications and Advances, Long Beach, CA, January 17–19, 1989.

[1-46] D. L. Britton, "Characterization and Cycle Tests of Lightweight Nickel Electrodes," *Proc.*, Symposium on Nickel Electrodes, D. Corrigan and A. Zimmerman (eds.) The Electrochemical Society, Inc., 1990. Presented in the ECS Fall meeting, Hollywood, FL, October 16–20, 1989.

[1-47] D. L. Britton, "Electrochemical Impregnation and Cycle Life of Lightweight Nickel Electrodes for Nickel-Hydrogen Cells," *Proc.*, 34th International Power Sources Symposium, Cherry Hill, NJ, June 25–28, 1990.

[1-48] J. Smithrick, U.S. Patent 4,584,249.

[1-49] J. Smithrick, S. Hall, "Effect of KOH Concentration of LEO Cycle Life of IPV Nickel-Hydrogen Fight Battery Cells," *Proc.*, 25th IECEC, Reno, NV, August 12–17, 1990.

[1-50] J. Smithrick, S. Hall, "Effects of KOH Concentration of LEO Cycle Life of IPV Nickel-Hydrogen Flight Cells—An Update," *Proc.*, 26th IECEC 1991, p. 276–281.

[1-51] H. S. Lim and S. A. Verzwyvelt, "Nickel-Electrode Expansion and the Effects of LiOH Additive," *Proc.*, 19th IECEC, Miami Beach, Florida, 1985, p. 1.104.

[1-52] L. H. Thaller, M. A. Manzo, and O. Gonzalez-Sanabria, "Design Principles for Nickel-Hydrogen Cells and Batteries," *Proc.*, 20th IECEC, Miami Beach, Florida, 1985, p. 1.145.

[1-53] M. Earl, T. Burke, and A. Dunnet, "Method for Rejuvination of Ni-H_2 Battery Cells," 27th IECEC, San Diego, California, August 1992.

[1-54] J. J. Smithric and S.W. Hall, "Effects of KOH Concentration on LEO Cyle Life of IPV Nickel-Hydrogen Flight Cells—An Update," 26th IECEC, 1991, p.276.

[1-55] Handbook of Chemistry and Physics, 45th Edition, "Limits of Inflammability," D-55.

[1-56] D. H. Fritts, "The Mechanics of Electrochemically Coprecipitated Cobalt Hydroxide in Nickel Hydroxide Electrodes," *J. Electrochemical Society*, January 1982, Vol. 129, p. 118.

[1-57] M. A. Manzo, private communications, NASA Lewis Research Center.

CHAPTER 2
AEROSPACE APPLICATIONS OF NICKEL-HYDROGEN BATTERIES

Aerospace applications of Ni-H_2 batteries can be divided into two different categories: low-earth-orbit (LEO) applications and geosynchronous-earth-orbit (GEO) applications. While Ni-H_2 batteries can and will be used on other types of aerospace applications, their major use now is for these two types of satellite applications.

These two applications have different requirements for the batteries. The LEO applications stress number of charge/discharge cycles: 20,000 to 40,000 cycles. LEO lifetime in-orbit requirements are typically 3 to 7 years, at approximately 6,000 cycles per year for a total of 18,000 to 42,000 cycles. The GEO applications stress lifetime in orbit, 15 to 20 years in orbit. The batteries are cycled about 100 times per year for a total of 1,500 to 2,000 cycles.

Presented in this chapter are battery system design requirements and constraints for both LEO and GEO applications, including battery requirements, charge control methods, and thermal management requirements. These system design requirements and constraints are presented as a prelude to Chapter 3, "Nickel-Hydrogen Battery Design."

2.1.0 LEO APPLICATIONS

2.1.1 Battery Requirements

A 96-minute orbit is typically used to characterize LEO satellite applications. Ninety-six minutes is the time it takes for a satellite to orbit the earth at 300 nautical miles. The satellite orbits the earth 15 times in one day. The orbital duration remains fixed, but the sunlight and eclipse periods vary with each orbit. To show how the eclipse duration varies with time, data are presented for an LEO satellite orbiting 300 nautical miles above the earth at an inclination of 28.3°. The sunlight duration and eclipse duration for one cycle of each day in December 1991 are presented in Table 2-1. Note that the orbital period is constant at 96 minutes. The eclipse durations vary from a maximum of 35.58 minutes on December 1 to a minimum of 26.97 minutes on December 30. The eclipse durations for all of 1991 are presented in Figure 2-1.

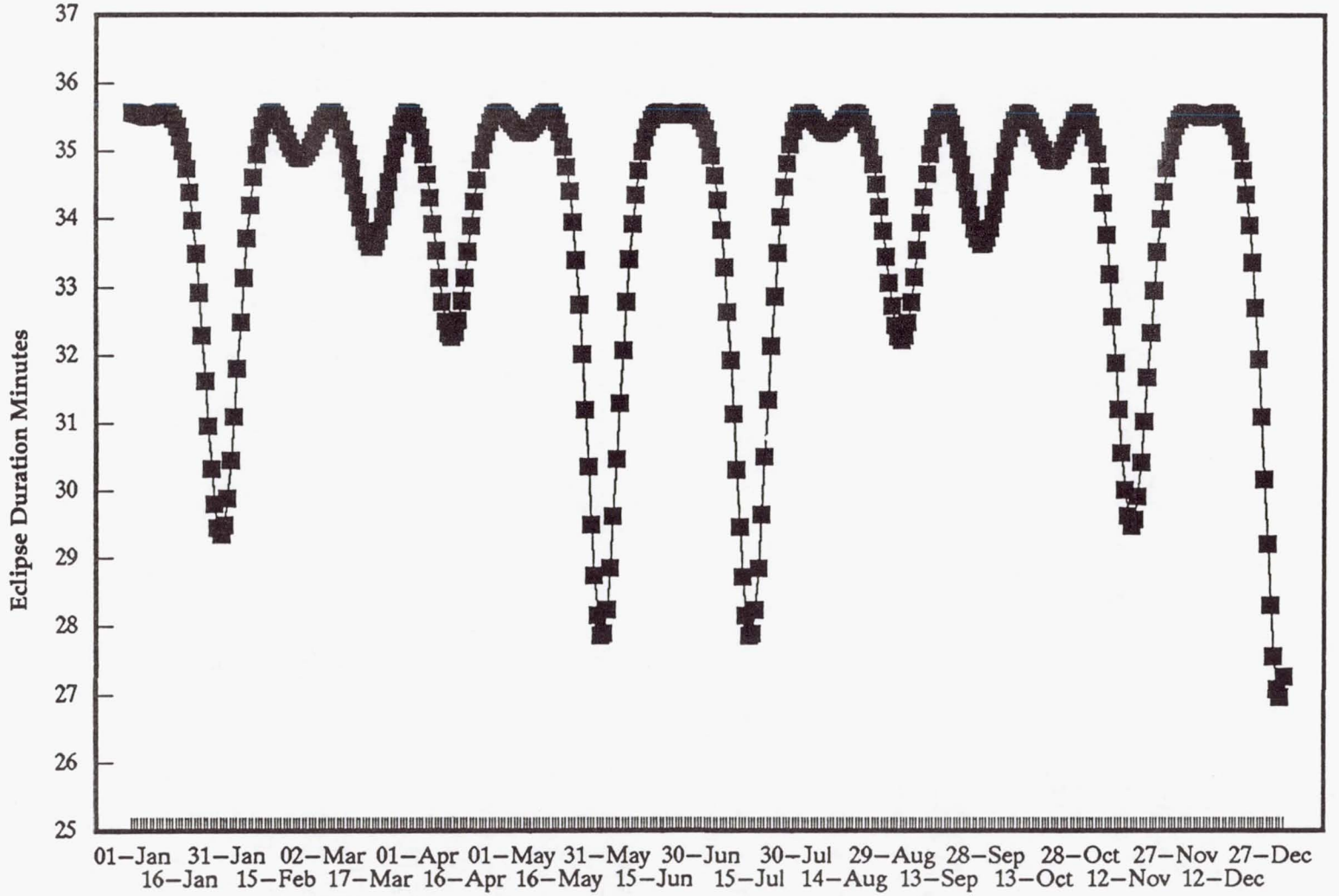

Figure 2-1. Eclipse durations for 1991.

Table 2-1. Eclispe Duration for December 1991

Date	Eclipse Duration	Sunlight Duration	Date	Eclipse Duration	Sunlight Duration
Dec. 1	35.58	60.42	Dec. 16	35.23	60.77
Dec. 2	35.57	60.43	Dec. 17	35.01	60.99
Dec. 3	35.55	60.45	Dec. 18	34.72	61.28
Dec. 4	35.53	60.47	Dec. 19	34.36	61.64
Dec. 5	35.51	60.49	Dec. 20	33.91	62.09
Dec. 6	35.51	60.49	Dec. 21	33.36	62.64
Dec. 7	35.51	60.49	Dec. 22	32.71	63.29
Dec. 8	35.53	60.47	Dec. 23	31.95	64.05
Dec. 9	35.54	60.46	Dec. 24	31.10	64.90
Dec. 10	35.56	60.44	Dec. 25	30.17	65.83
Dec. 11	35.58	60.42	Dec. 26	29.21	66.79
Dec. 12	35.57	60.43	Dec. 27	28.30	67.70
Dec. 13	35.55	60.45	Dec. 28	27.55	68.45
Dec. 14	35.48	60.52	Dec. 29	27.08	68.92
Dec. 15	35.38	60.62	Dec. 30	26.97	69.03
			Dec. 31	27.26	68.74

The battery is charged during the sunlight period and is discharged during the eclipse period. With this high duty cycle, it is essential to minimize overcharge (heat dissipation) and maximize overall watt-hour efficiency for the battery.

A charge method is needed to compensate for the variation in DOD (variation in eclipse duration) and to minimize overcharge.

Cyclic Lifetime

The number of cycles is the most demanding feature of the mission requirements for LEO applications. Typical missions, such as the Hubble Space Telescope and Space Station Freedom, require 5 to 7 years of in-orbit operation:

15	cycles/day
5,475	cycles/year
27,375	cycles/5 years
38,325	cycles/7 years

Depth-Of-Discharge

Depth-of-discharge is defined as the percentage of ampere-hours removed from the battery on discharge divided by the rated capacity of the battery in ampere-hours:

$$\% \text{ DOD} = \frac{\text{Ampere-hours removed on discharge}}{\text{rated capacity of battery}} \times 100\%$$

The goal for Ni-H_2 batteries is to achieve 40,000 cycles at 35 percent depth-of-discharge (DOD) for the Space Station Freedom LEO application [2-1].

2.1.2 Charge Control

Batteries are charged or recharged during cycling by returning on charge the ampere-hours removed on discharge. The ampere-hours returned on charge (c) slightly exceeds the ampere-hours removed on discharge (d) to account for any losses or self-discharge in the process.

Charge control is the control method for recharging the batteries. For LEO applications, the major requirement is to adequately recharge the batteries while at the same time avoiding excessive overcharge to minimize heat dissipation. If the battery can be maintained at a low temperature on charge, between 0 and 10°C, the ampere-hour charge efficiency approaches 100 percent, and the watt-hour efficiency approaches 85 percent. Typical values for the c/d ratio are 1.01 to 1.05.

The two charge control methods most often used are the following: (1) the use of a voltage limit to terminate or taper the charge current, and (2) the use of a fixed c/d ratio to terminate charge.

The NASA method used most often to charge Ni-Cd batteries in LEO applications is to charge to a temperature-compensated voltage limit. The major advantage of this charging method is that it minimizes heat dissipation when the Ni-Cd batteries are recharged. Charging to a voltage limit and then allowing the current to taper off works well for Ni-Cd batteries. The current tapers off rapidly and allows the Ni-Cd cells to become adequately charged, while at the same time minimizing the heat dissipation.

Using a fixed c/d ratio to recharge batteries is more difficult to implement because of the variations in the duration of the sunlight and eclipse periods, as shown in Table 2-1. When the batteries are recharged at a constant current, the recharge time needs to be adjusted every cycle to keep the c/d ratio constant. A coulometer is needed to integrate the ampere-hours removed and to adjust the recharge time to keep the c/d ratio fixed. After the batteries are recharged to the fixed c/d ratio selected, they should be switched to trickle charge.

$Ni-H_2$ batteries were selected to replace the Ni-Cd batteries on the Hubble Space Telescope (HST) satellite to extend the battery lifetime. The Hubble Space Telescope was designed to operate with Ni-Cd batteries using temperature-compensated voltage limit charging. In order to be able to substitute $Ni-H_2$ batteries in the power system, the NASA Marshall Space Flight Center and Lockheed Missile and Space Company had to develop a database for selecting the temperature-compensated voltage limits for $Ni-H_2$ cells. They evaluated different charge control voltage limits in a thermal vacuum test program run at LMSC and used the results to select the temperature-compensated voltage limits to be used [2-2], [2-3]. Lockheed Missile and Space Company simulated as close as possible the actual operating conditions in space for the thermal interface between the battery and the spacecraft. The $Ni-H_2$ battery used in the test was the flight spare battery for the program.

The charge control method selected for the Hubble Space Telescope during normal operation is to charge the batteries to the K1-3 and K2-3 (level 3) voltage limits and then switch to the trickle charge rate of approximately C/100* [2-4]. Presented in Figure 2-2 are the K1 and K2 battery voltage limits as a function of temperature. The K1-3 setting, for example, has a battery voltage limit of 33.31 volts for 22 cells at 0°C, or a cell voltage limit of 1.514 volts/cell. The battery is not fully charged at this voltage limit but rather charged to about 83 to 85 percent of its full capacity. When using this limit and the C/100 trickle charge rate, the battery was thermally stable with repetitive cycling in the thermal vacuum test described above. The battery was recharged to the same voltage limit each cycle, and with trickle charge, the batteries' end-of-charge pressure (state-of-charge) gradually increased with each cycle, asymmetrically approaching a steady-state condition at 90 to 100 percent state-of-charge.

During hardware safemode operation, the HST batteries are charged to the same K1-3 and K2-3 voltage limits with the current tapering off at the temperature-compensated voltage limit instead of being switched to the C/100 trickle charge rate. This method of charging was also shown to be thermally stable in the thermal vacuum tests at LMSC, but more heat was dissipated within the battery.

Unlike the Ni-Cd batteries, in which the current tapers rapidly to a low rate once the voltage limit is reached, the $Ni-H_2$ batteries do not perform this way in the taper mode. The current does not drop off as sharply for the $Ni-H_2$ cells once they have reached the voltage limit, and in the taper mode there is more of a chance that the battery will overheat and become thermally unstable. This is the reason the HST batteries are switched to trickle charge at C/100 once the battery reaches the voltage limit. With this switch to trickle mode, the heat dissipation is minimized.

* C is the rated capacity of the battery.

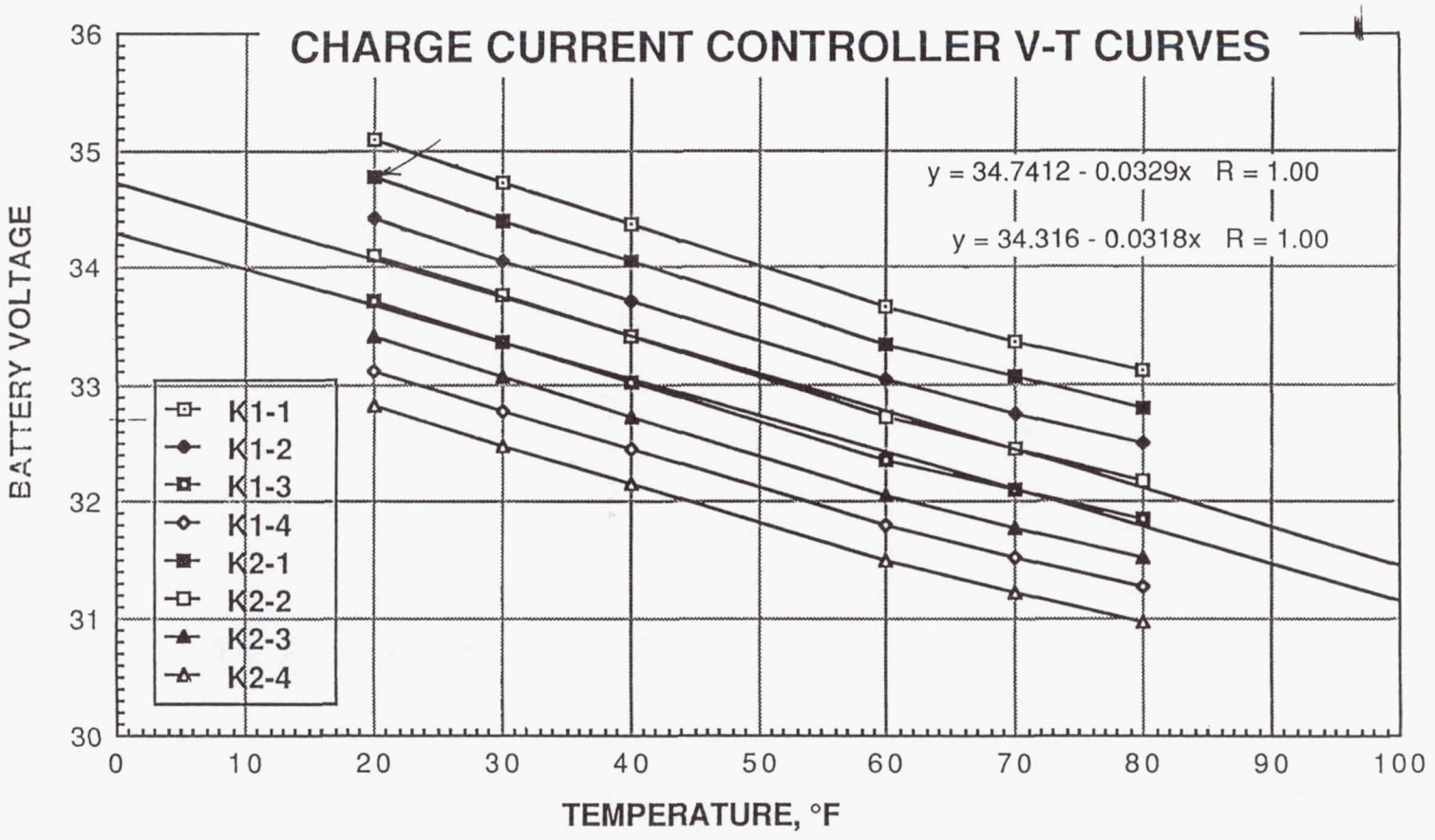

Figure 2-2. Charge current controller V-T curves.

2.1.3 Thermal Design

For LEO applications the major thermal requirement is to minimize heat dissipation. Design considerations for Ni-H_2 batteries are as follows:

1. The best overall watt-hour efficiency one can achieve with a Ni-H_2 battery is about 85 percent with the c/d ratio = 1.0. The remaining 15 percent of the energy is dissipated as heat. The watt-hour efficiency can be determined from the difference in voltage on charge and discharge; the ratio of the average discharge voltage to the average charge voltage is about 0.85.

2. It is essential to minimize the heat dissipated during recharging of the battery to control the temperature and extend cycle lifetime.

3. A battery cannot be fully charged without dissipating heat, but it can be charged to about 85 percent of full capacity (85 percent state-of-charge) with a minimum amount of heat dissipation. This can be achieved with a c/d ratio of about 1.03. This 85 percent state-of-charge is not to be confused with the 85 percent overall watt-hour efficiency (Consideration No. 1 above).

4. The battery should be thermally stable with repetitive cycling. In addition, the voltage, pressure, and capacity of the battery should become stable with cycling. The pressure provides a good indication of the state-of-charge.

5. The recommended temperature range of operation is -5 to 25°C. It is recommended that the battery be charged at 0°C to 10°C. Ampere-hour charge efficiency is higher at lower temperatures.

2.1.4 Hubble Space Telescope (HST) Program

LMSC ran two extensive thermal vacuum tests to verify the thermal performance of the battery under normal and worst-case conditions. LMSC also developed a thermal model that accurately duplicated the results of the thermal vacuum test. An essential input to this model was the average heat dissipated by the battery for any given charging mode. The heat dissipation data were provided by MSFC based on laboratory test data [2-3]. Hubble Space Telescope flight hardware Ni-H_2 cells and batteries were tested at the MFSC battery laboratory. These tests simulated the actual operating conditions of interest and the average heat dissipated per cycle was measured.

LMSC developed a model of the thermal interface between the battery and the spacecraft and the surrounding boundary conditions. This thermal model was modified to match the actual temperature data from the flight hardware in the

thermal vacuum test. The result is an excellent model of the thermal interface between the battery, the spacecraft, and the surrounding boundary conditions.

Using the average heat dissipation data and the thermal model, one can predict, quite accurately, the temperature performance of the battery. It was necessary to obtain the heat dissipation data experimentally. Perhaps in the future a sufficient database will be available to provide the average heat dissipation values for different operating conditions without resorting to experimental measurements.

2.2.0 GEO APPLICATIONS

2.2.1 Battery Requirements

The second battery application is the geosynchronous satellite, or communications satellite application. Synchronous satellites orbit the earth once a day around the equator and thus remain stationary in their location with respect to the earth.

As the earth moves through its ecliptic rotation each year, it crosses the vernal equinox on approximately March 21 and the autumnal equinox on approximately September 23. On these days the declination of the Sun is 0°. This declination varies throughout the year from +23.5° to -23.5°. GEO satellites go through eclipse periods each day around the vernal and autumnal equinox seasons. An eclipse occurs when the satellite is in the shadow of the earth. The eclipse season lasts for about 45 days. The longest eclipse period (72 minutes) occurs in the middle of the eclipse season on March 21 and September 23, when the declination of the Sun is at or near 0°. Table 2-2 shows the duration of the shadow in minutes during each eclipse period for the Spring 1991 eclipse season of a geosynchronous-orbit satellite at a longitude of 341.5° east. Battery DOD calculations generally use a 72-minute eclipse, rather than the 70-minute eclipse shown in Table 2-2, to allow for partial shadows (penumbra) as the spacecraft enters and leaves the eclipse period.

Communications satellites are required to operate continuously without interruption, which includes operation during eclipse seasons. The batteries supply power to the spacecraft during the eclipse periods and are recharged during the sunlight portion of each eclipse day. The longest eclipse period is 70 to 72 minutes. The remaining 22 hours and 48 to 50 minutes of the eclipse day are available to recharge the battery. During the summer and winter solstice periods (135 days each) between eclipse seasons, the batteries are kept on trickle charge (fully charged). Typical trickle charge rates vary from C/60 to C/120.

Table 2-2.
Duration of Each Eclipse Period for Spring 1991 Eclipse Season
(Spacecraft 506 INTELSAT V)

Enter Shadow					Leave Shadow					Dur.of Shadow
Yr	Mon	Day	Hr	Min	Yr	Mon	Day	Hr	Min	Min
91	2	27	1	19	91	2	27	1	39	20
91	2	28	1	15	91	2	28	1	43	28
91	3	1	1	12	91	3	1	1	45	33
91	3	2	1	9	91	3	2	1	48	39
91	3	3	1	7	91	3	3	1	50	43
91	3	4	1	5	91	3	4	1	51	46
91	3	5	1	3	91	3	5	1	53	50
91	3	6	1	1	91	3	6	1	54	53
91	3	7	0	59	91	3	7	1	55	56
91	3	8	0	58	91	3	8	1	56	58
91	3	9	0	57	91	3	9	1	56	59
91	3	10	0	56	91	3	10	1	57	61
91	3	11	0	55	91	3	11	1	58	63
91	3	12	0	54	91	3	12	1	58	64
91	3	13	0	53	91	3	13	1	58	65
91	3	14	0	52	91	3	14	1	59	67
91	3	15	0	51	91	3	15	1	59	68
91	3	16	0	51	91	3	16	1	59	69
91	3	17	0	50	91	3	17	1	59	69
91	3	18	0	50	91	3	18	1	59	70
91	3	19	0	49	91	3	19	1	59	70
91	3	20	0	49	91	3	20	1	59	70
91	3	21	0	49	91	3	21	1	58	70
91	3	22	0	48	91	3	22	1	58	70
91	3	23	0	48	91	3	23	1	57	69
91	3	24	0	48	91	3	24	1	57	69
91	3	25	0	48	91	3	25	1	56	68
91	3	26	0	48	91	3	26	1	56	68
91	3	27	0	49	91	3	27	1	55	66
91	3	28	0	49	91	3	28	1	54	65
91	3	29	0	49	91	3	29	1	53	64
91	3	30	0	50	91	3	30	1	52	62
91	3	31	0	50	91	3	31	1	51	61
91	4	1	0	51	91	4	1	1	50	59
91	4	2	0	52	91	4	2	1	49	57
91	4	3	0	52	91	4	3	1	47	55
91	4	4	0	53	91	4	4	1	46	53
91	4	5	0	55	91	4	5	1	44	49
91	4	6	0	56	91	4	6	1	42	46
91	4	7	0	58	91	4	7	1	40	42
91	4	8	0	59	91	4	8	1	38	39
91	4	9	1	2	91	4	9	1	35	33
91	4	10	1	5	91	4	10	1	32	27
91	4	11	1	8	91	4	11	1	27	19

Lifetime in Orbit and Depth-Of-Discharge

Lifetime in-orbit and battery mass are the significant factors for GEO applications. Communications satellites are now being designed and operated with 15 to 20 years of lifetime expectancy at 70 to 75 percent DOD. Ni-H_2 batteries are now being used for the majority of the GEO satellites to achieve these performance goals. The DOD should probably not exceed 80 percent as a practical limit for GEO applications, because some allowance is needed for performance degradation with time and because the batteries cannot be charged to 100 percent state-of-charge in the middle of the eclipse season (discussed under the Eclipse Operation section below).

2.2.2 Charge Control

A major requirement of GEO applications is to fully charge the batteries during the eclipse season. In the middle of the eclipse season the battery is discharged to 70 or 80 percent of its beginning-of-life rated capacity. At the end of life, after 15 years of operation, the battery still must meet the same initial load requirements.

This requirement to fully charge the battery is different for GEO and LEO applications. For most LEO applications the depth-of-discharge is lower, typically 35 to 40 percent DOD, and the emphasis is to minimize overcharge and heat dissipation. To accomplish this, the battery is only charged to about 85 percent of its full state of charge. It requires too much excess energy (heat dissipation) to fully charge the battery. This lower state of charge is quite acceptable at these lower depths of discharge.

The recommended charge method for GEO satellites is to recharge the battery at a fixed c/d ratio, returning 105 to 115 percent of the capacity removed on discharge at a high charge rate of C/10 to C/25. The batteries are then switched to a low trickle charge rate of C/60 to C/100 for the remainder of the 24-hour eclipse day to maintain the batteries at the full state of charge.

2.2.3 Thermal Design

Thermal design considerations for GEO applications:

1. During storage periods between eclipse seasons the battery temperature on trickle charge should be kept between -5.0 and 10°C. All of the energy put into the battery is dissipated as heat during trickle charge of the batteries between eclipse seasons. The trickle charge current multiplied by the battery voltage provides the rate of heat dissipated by the battery during the storage period. The battery spacecraft thermal interface must be designed to accommodate this rate of heat rejection while maintaining the battery temperature between -5.0 and 10°C.

2. The battery only goes through one charge/discharge cycle for each eclipse day. Thus, the thermal constraints are not nearly as severe as with the LEO application with 15 cycles per day.

3. During eclipse periods the temperature should be kept low for battery charging (0 to 10°C). Charging at these lower temperatures increases the charge efficiency and battery capacity. During overcharge the temperature will increase. The recommendation is to limit overcharge of this battery so that the temperature of the battery does not exceed 15°C.

4. To recharge INTELSAT V batteries, a c/d ratio of 1.15 is required at the C/25 rate. The battery is then switched to the C/63 to C/73 trickle rate. Average watt-hour efficiency is less than 74 percent.

5. During normal operation the temperature between cells within the battery should be limited to ± 5°C.

6. If bypass diodes are used, the worst-case condition occurs when one cell fails open. The discharge diode dissipates almost 10 times more heat than a normal cell. The spread in temperature between cells for this design case should be increased to 15°C.

2.2.4 INTELSAT V Program

The procedure for charge control during eclipse seasons, operation between eclipse seasons, and reconditioning used for the INTELSAT V Ni-H_2 batteries [2-5] are presented as an example for GEO operation.

Eclipse Operation

The method used for charging INTELSAT V batteries during an eclipse season is basically a coulometric charge control method. For each eclipse day, the time is calculated to return (at the high charge rate) 115 percent of the ampere-hour capacity removed on discharge. Ground commands are used to switch battery charging from the high rate to the trickle charge rate at the specified time. The high rate of charge is C/21 at beginning of life and C/25 at end of life. The trickle charge rate is C/63 at beginning of life and C/73 at end of life. The batteries are charged at a constant current from a string of solar cells operating on the constant current portion of the I–V curve. Solar cell degradation accounts for the change in the charge rates from beginning to end of life.

Storage Operation Between Eclipse Seasons

For the 135 days between eclipse seasons the batteries are kept on trickle charge at the C/96 rate at beginning of life and the C/110 rate at end of life.

The batteries are maintained in the fully charged condition on trickle charge between eclipse seasons. They remain fully charged as a safety precaution to provide power for any emergency operation that might occur. On several occasions the batteries have provided backup power as needed when the solar array unexpectedly went through a lunar eclipse.

Reconditioning

Each INTELSAT V spacecraft has two batteries; these batteries are reconditioned two weeks before each eclipse season. The batteries are reconditioned one at a time to keep one battery fully charged to provide power in case of an emergency. About two weeks are required to recondition both batteries, one week per battery. The procedure for reconditioning is as follows:

1. The 27-cell battery is discharged through a 50-ohm resistor.

2. A voltage scanning switch is used to scan individual cell voltages within the battery. The cell voltages are scanned once per minute. Cell voltages are monitored during the reconditioning discharge, and the discharge is terminated when the first cell in the battery reaches 0.5 volts.

3. The battery is recharged using the high rate until 115 percent of the ampere-hour capacity removed on discharge has been returned on charge (c/d = 1.15).

4. The battery is placed back on trickle charge until the beginning of the eclipse season at the C/96 rate.

The voltage profile during the Spring 93 reconditioning discharge is presented in Figure 2-3 for Cell 27 in Battery 1 on the 506 INTELSAT V spacecraft. From the voltage profile, one can observe in Figure 2-3 the second plateau, voltage plateau below 1.0 votls. Note that this is a negative (hydrogen) precharge cell. Positive precharge cells do not have this second plateau below 1.0 volts.

Figure 2-3 data points were taken once per hour. This figure provides a good presentation of the full reconditioning discharge, but lacks resolution at the end. An expanded plot of the voltage profile during the end of discharge, the second plateau, is presented in Figure 2-4. Data points for this figure were taken once per minute. Cell 27 was the first cell to reach 0.5 volts. Actually, Cell 27 reached 0.21 volts before the reconditioning discharge was terminated. The capacity discharge time, shown in the second plateau (approximately 5 hours) has remained constant throughout the life of the battery/cell to date [2-9].

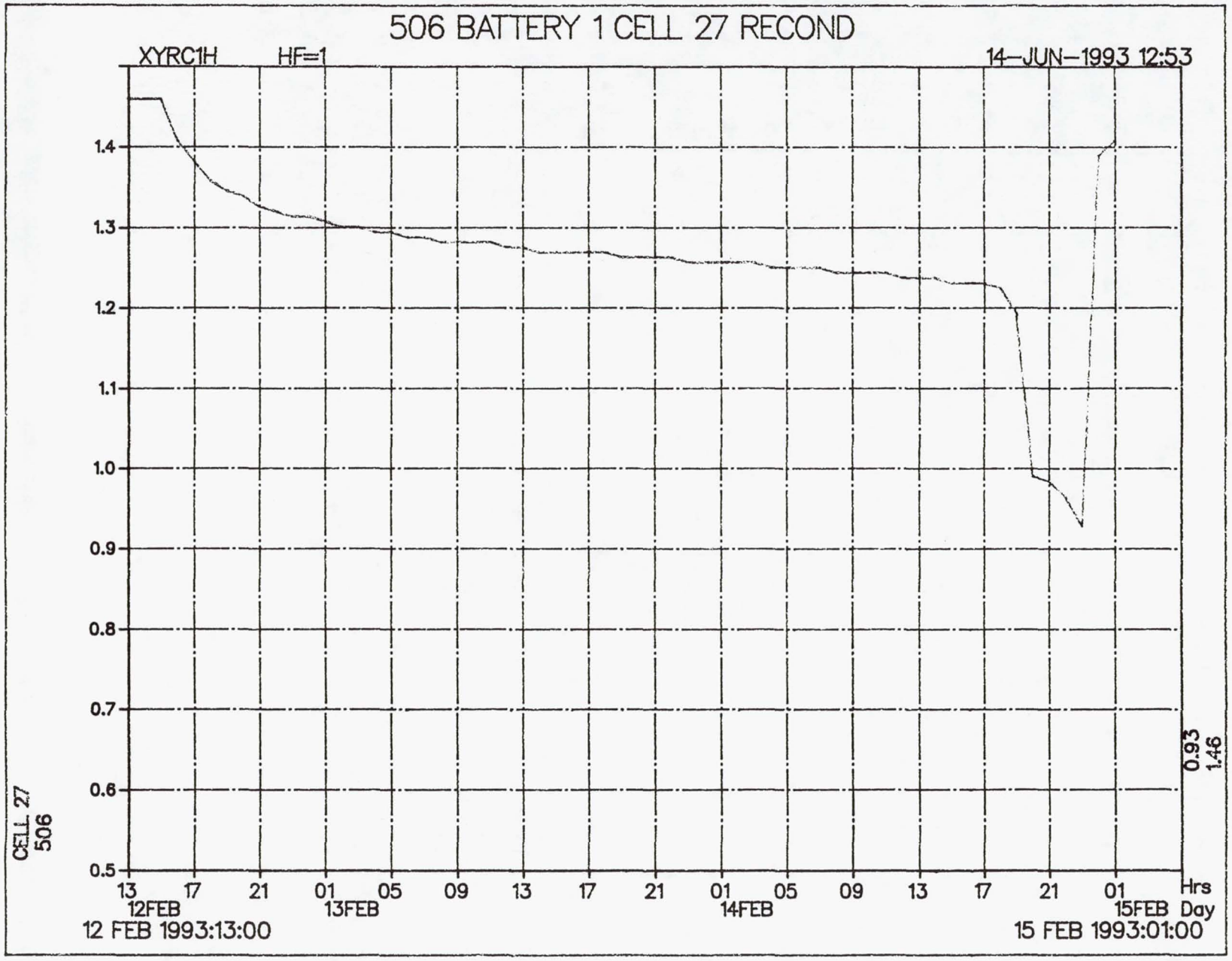

Figure 2-3. Reconditioning voltage profile Spring 93 INTELSAT V cell.

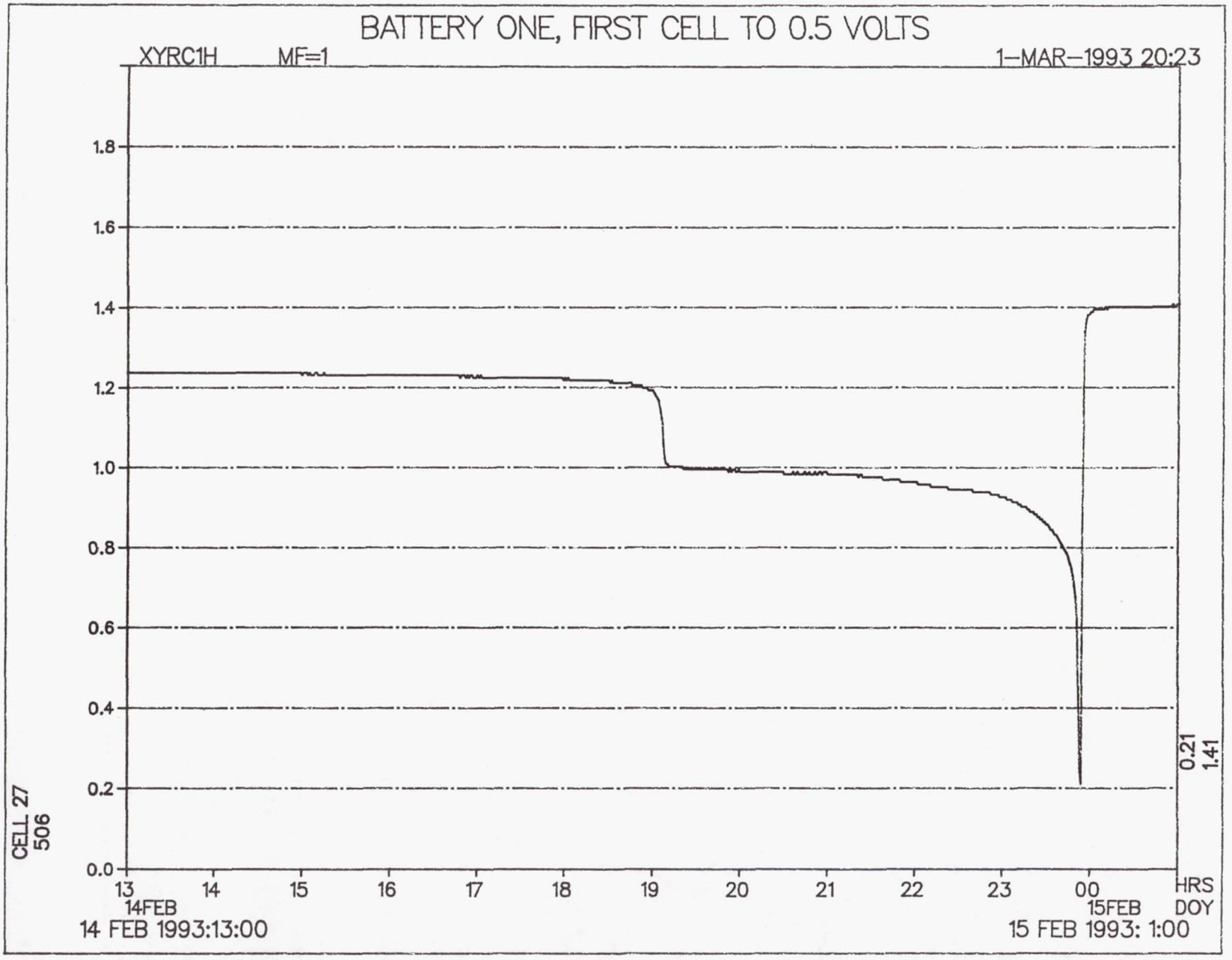

Figure 2-4. Second plateau portion of reconditioning discharge voltage profile Spring 93 INTELSAT V cell.

2.3.0 PRESSURE

The pressure in an Ni-H_2 cell can be used to:

- Determine state-of-charge of the Ni-H_2 cell/battery
- Charge control

During activation, the cell pressure is measured with a pressure gauge mounted on the fill tube. Once the cells are sealed the pressure is measured by mounting a strain-gauge bridge on the dome of the pressure vessel. The NTS-2 program was the first flight demonstration of the Ni-H_2 battery technology (see Chapter 3, Section 3.2.2). Strain-gauge bridges were mounted on two of the cells in the NTS-2 flight battery at COMSAT Laboratories.

A strain-gauge bridge mounted on the dome of an IPV cell has become the accepted method for measuring cell pressure in space. The basic approach is to use two active gauges mounted to the cell dome and two dummy gauges to provide temperature compensation.

A sketch of a Gates Aerospace Batteries (GAB) strain-gauge bridge circuit installation on the dome hemispherical portion of an Ni-H_2 cell is shown in Figure 2-5. GAB describes the strain-gauge as a Micro Measurements' Strain Gauge Part Number WK-06-250PD-350 [2-8]. The WK-series gauges have the wide temperature range and most extensive environmental capability of any general-purpose strain-gauge of the self-temperature-compensated type. The gauge is characterized as a dual-element pattern, fully encapsulated K alloy, equipped with integral, high-endurance beryllium-copper lead wires. The backing is a high-temperature epoxy-phenolic resin system enforced with glass fibers. Backing and adhesive life is projected as 5×10^5 hours (57 years) for typical LEO and GEO missions. The bridge circuit of this type with the WK-series Micro Measurements strain gauges is typical of the technology used to measure pressure of Ni-H_2 cells in space.

The two strain-gauge pairs form a typical four-component Whetstone Bridge Circuit with two active gauges hard-mounted (mounted to the pressure vessel dome) and two passive gauges soft-mounted (mounted to pods on the dome that are not stressed). The two passive gauges provide temperature compensation.

The strain-gauge resistance of the two active gauges changes as a function of the applied strain level. The strain is directly related to the surface stress in the pressure vessel dome INCONEL material, and surface stress is directly proportional to the internal pressure. The output of the bridge (calibration curve) is given as mV/psi for a given excitation voltage. For example, using the INTELSAT VII A cell L01-004, the calibration curve strain-gauge bridge output is 0.01 mV/psi with a 0 psi offset of 0.0 mV when the excitation voltage is 6.4 volts.

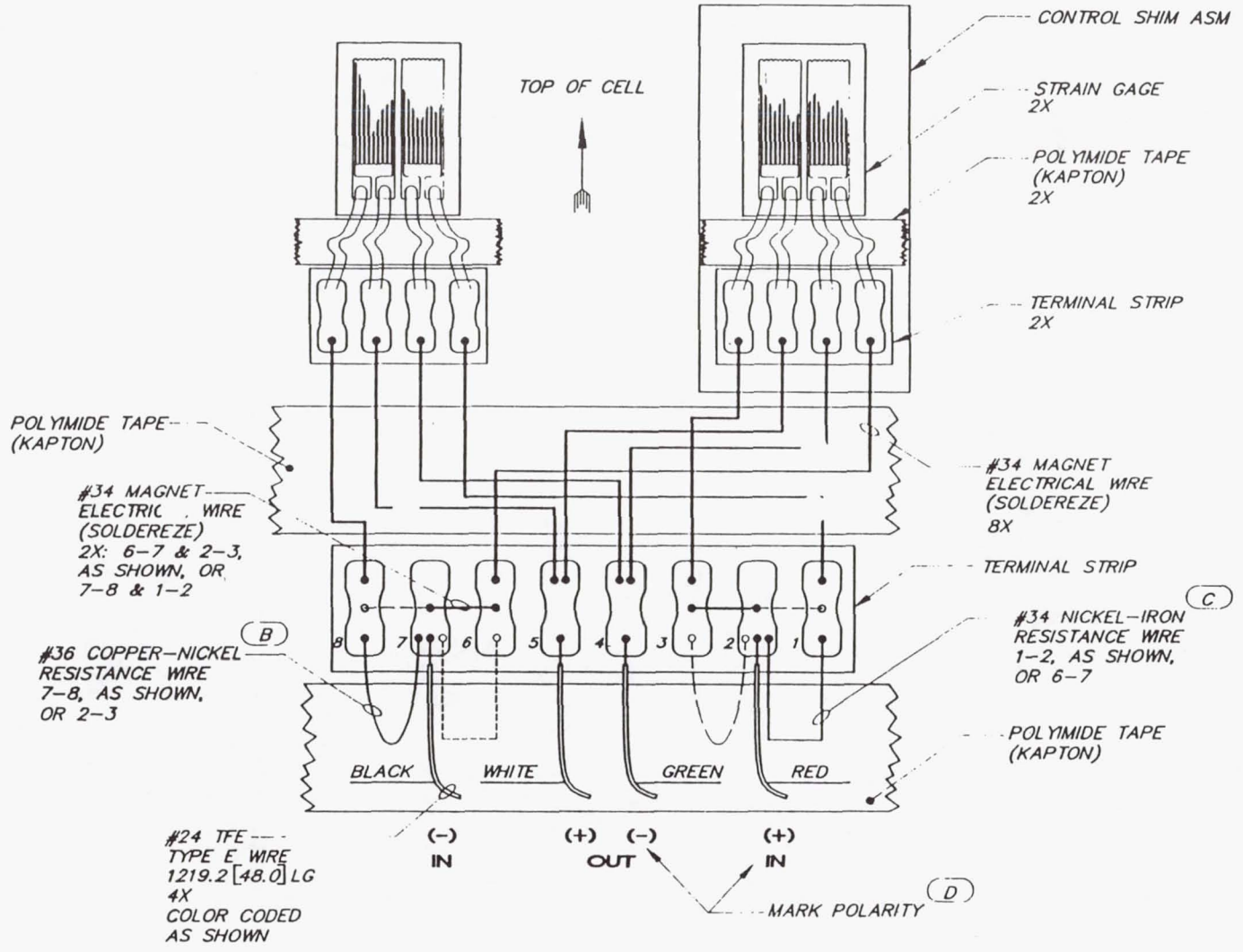

Figure 2-5. Typical strain gauge and installation.

In the "Reliability Study of the Ni-H_2 Strain-Gauge" [2-8], the fatigue analysis of the strain-gauge shows the gauge usage and the environment to be well below even the manufacturer's points of concern.

2.3.1 Capacity (State-of-Charge) Determined by Pressure

On charge, hydrogen gas is generated at the negative hydrogen electrode. At the positive electrode, $Ni(OH)_2$ is charged to NiOOH up to the onset of oxygen gas evolution. The pressure profiles on charge and discharge of an INTELSAT VII A cell are shown in Figure 2-6*. The derivative of the pressure with respect to time, dp/dt, gives the instantaneous ampere-hour charge efficiency for the cell during the charging cycle (see Figure 2-7). When the rate-of-charge of pressure with time is constant, all of the charging current is going into hydrogen evolution. At the onset of oxygen evolution, the dp/dt value (charge efficiency) starts to drop off. Once the cell is fully charged and all of the charging current is going into oxygen evolution, the dp/dt value (rate-of- charge of pressure with time) drops to zero (see Figure 2-7). The overall charge efficiency can be obtained by integrating the area under the curves over the charging period and dividing this area by the charging period. As one would expect, the charge efficiency drops off as the temperature increases.

Pressure Constant at 0°C

The charge/discharge pressure profiles from Figure 2-6 were normalized to 0°C, using the perfect gas law to correct the pressure for temperature changes. The normalized pressure profiles are shown in Figure 2-8.

From Figure 2-8, the slope on discharge was calculated. The slope ($\Delta p/\Delta C$) is defined as the pressure constant P_c at 0°C.

$$\text{Slope } (P_c) = -5.467 \text{ psi/Ah}$$

Capacity Determined from Pressure

To determine capacity from pressure, correct the pressure to 0°C using the perfect gas law. Then, divide the pressure by the pressure constant at 0°C to obtain capacity.

$$C \text{ (capacity)} = \frac{P - P_o}{P_c}$$

P_o = End-of-discharge pressure (normally set to zero at the beginning of life).

---

* A detailed description of the performance characterization of these I–VII A cells is presented in Chapter 5, Section 5.1.0.

		CHARGE		DISCHARGE	
	Temp.	Slope	Intercept	Slope	Intercept
———	0°C	63.49	54	-5.716	815
—·—·—	-10°C	60.78	52	-5.48	841
—··—·—	-20°C	58.25	50	-5.251	833
—·—·—	10°C	66.3	61	-6.161	794
— —	20°C	68.7	61	-6.438	734
— —	30°C	70.36	60	-6.656	608

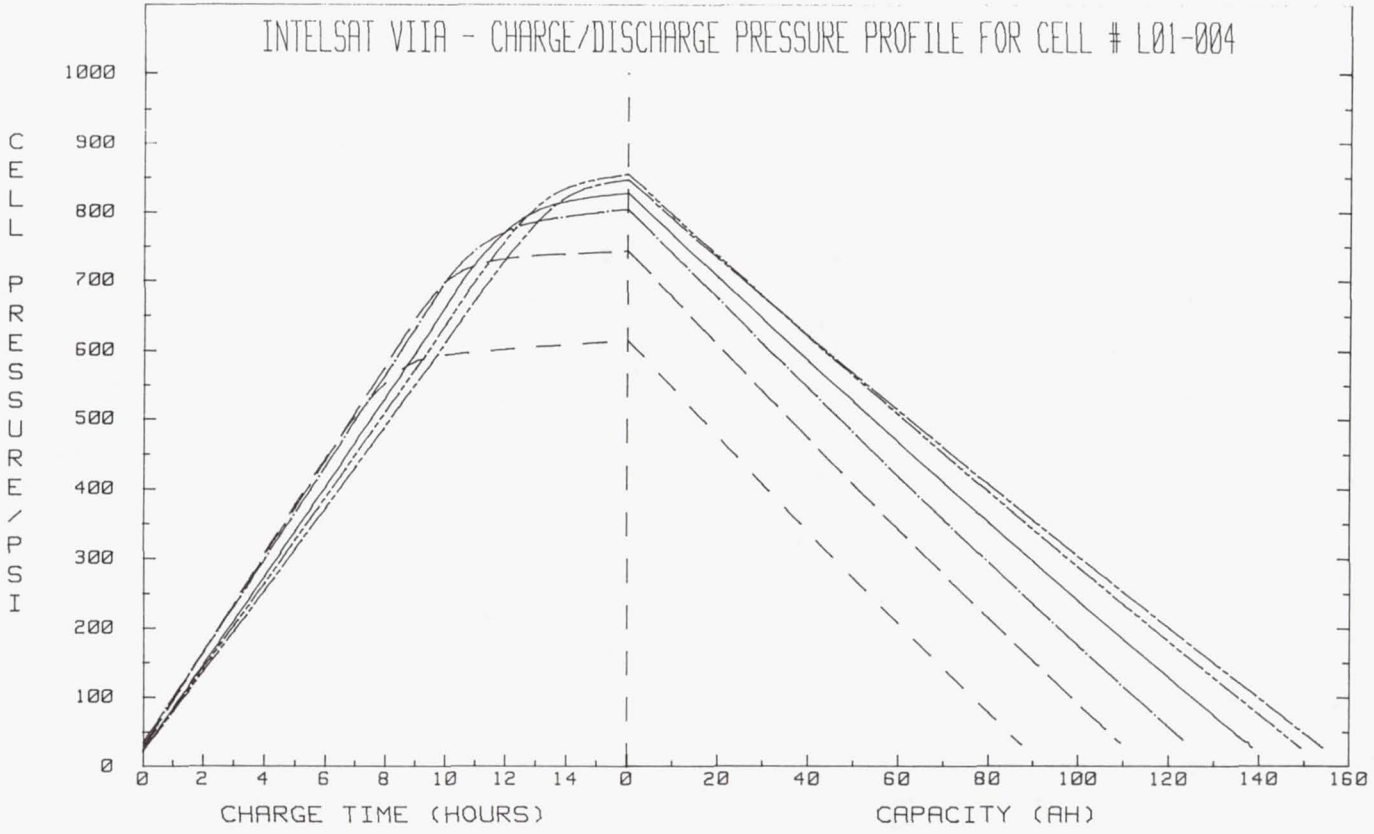

Figure 2-6. INTELSAT VII A charge/discharge pressure profile for cell L01-004.

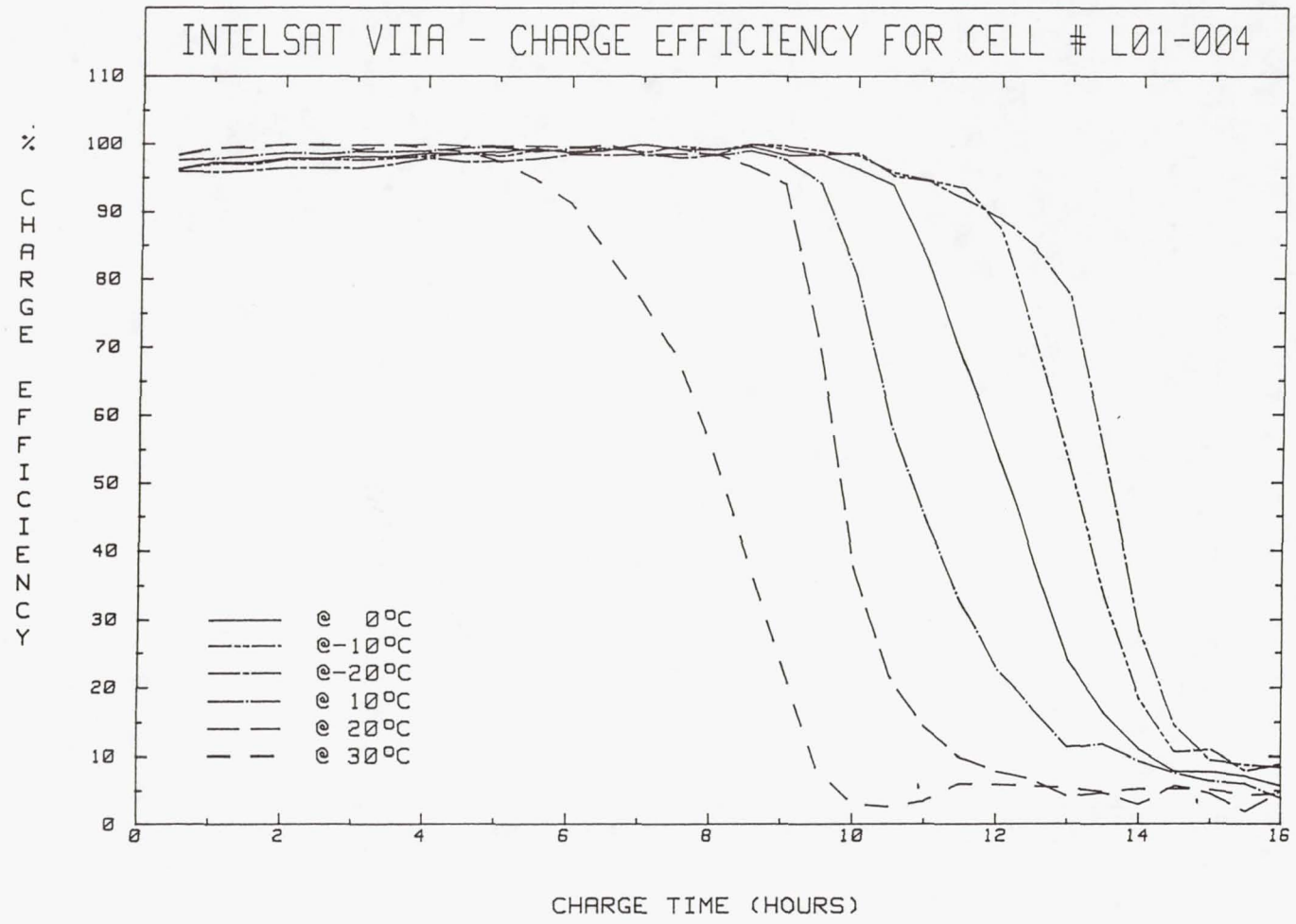

Figure 2-7. INTELSAT VII A charge efficiency for cell L01-004.

		CHARGE		DISCHARGE	
	Temp.	Slope	Intercept	Slope	Intercept
———	0°C	63.8	20	-5.467	779
— — — —	-10°C	63.54	21	-5.443	835
— — — —	-20°C	63.34	22	-5.415	858
— — — —	10°C	64.09	31	-5.65	727
— —	20°C	63.88	26	-5.698	649
— —	30°C	62.74	24	-5.734	523

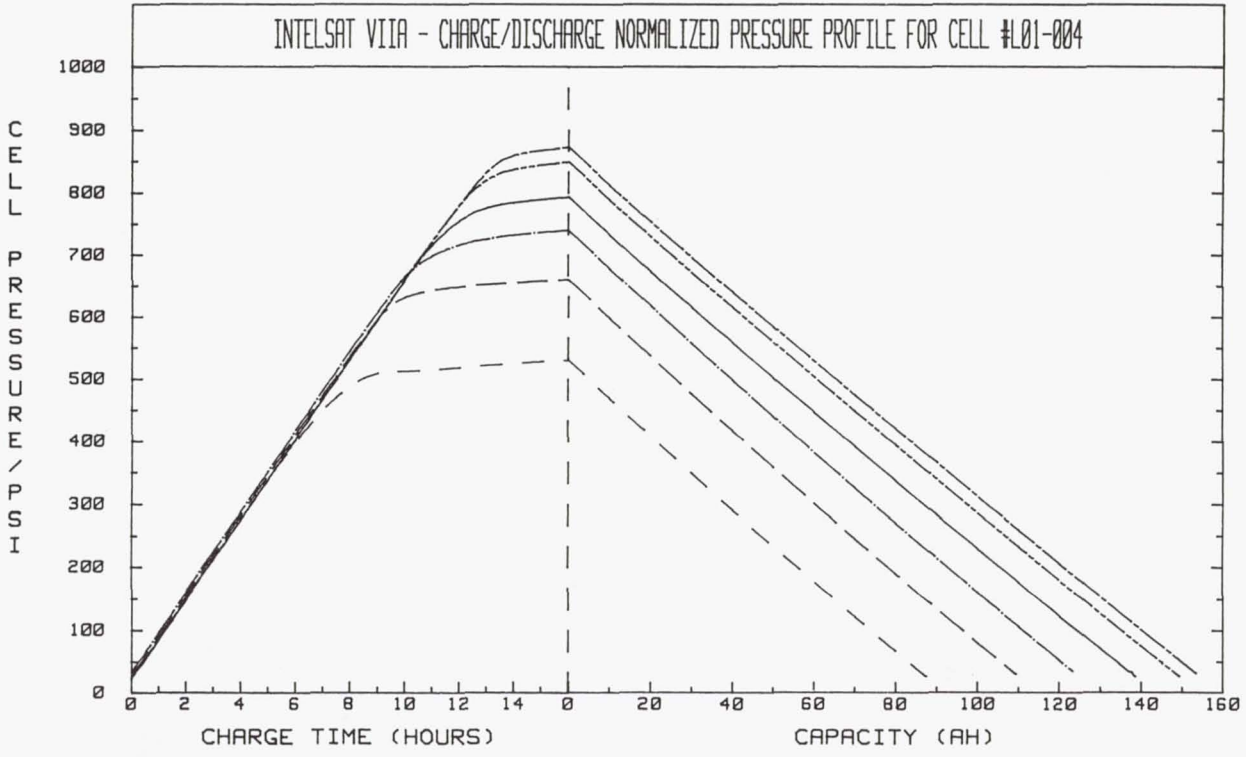

Figure 2-8. INTELSAT VII A charge/discharge normalized pressure profile for cell L01-004.

For example, in Figure 2-8, the end-of-charge pressure is 779 psi at 0°C and the end-of-discharge pressure is 20 psi at 0°C:

$$C \text{ (capacity)} = \frac{779 - 20}{5.467} = 138.8 \text{ Ah}$$

Measured Capacity to 0.0 V (at 0°C)	138.6 Ah
Capacity Determined from Pressure	138.8 Ah

Pressure Change with Lifetime in Orbit

A pressure increase in the end-of-charge pressure with lifetime in orbit has been observed for cells in a number of different programs, including INTELSAT V, INTELSAT VI, and HST.

There are several reasons why the EOC pressure will increase:

- The capacity increases
- The EOD (end-of-discharge) pressure increases (oxidation, corrosion within the cell)
- Drift in the strain-gauge bridge electronics

Note that there should not be any change in the pressure constant with time.

Ten years of pressure performance data are presented for the INTELSAT V Ni-H_2 batteries/cells in orbit in Chapter 5, Section 5.3.4. In summary,

- There is no drift in the strain-gauge bridge electronics.
- There is no evidence of oxidation corrosion within the cells; no change in the EOD pressure at the end of each reconditioning cycle has occurred over the 10 years of operation.
- The EOC pressure increased during the first few years of operation and then systematically leveled off. The increase in EOC pressure is consistent with the measured increase in capacity.

The same conclusions were reached for the HST Ni-H_2 battery/cells. There is no drift in the strain-gauge bridge electronics and no evidence of oxidation or corrosion within the cell. The pressure increase that has been observed with cycling is related to a capacity increase.

For the INTELSAT VI batteries, there was a substantial increase in EOC pressure and capacity during the first year of operation, approximately a 20 percent increase in capacity and pressure. After 1 to 2 years in orbit, the EOC pressure, EOD

pressure, and capacity appear to have stabilized. However, laboratory life tests at COMSAT Laboratories (5 years of real-time tests to date) show that the EOD pressure for INTELSAT VI batteries/cells is increasing at a rate of about 10 to 20 psi/year [2-6]. Destructive physical analysis (DPA) indicates that the EOD pressure increase is related to corrosion of the plaque in positive electrodes [2-6]. This I–VI plaque was not wet oxidized prior to impregnation.

2.3.2 Charge Control with Pressure

As described in the previous section (Section 2.3.1), the EOC pressure has been observed to increase with operational lifetime for both LEO and GEO satellite programs. This is the reason it is <u>not</u> recommended to use an absolute value for EOC pressure to charge batteries. Charging to a fixed pressure limit would either 1) undercharge the battery, or 2) lead to thermal runaway.

However, a very effective way for charge control with pressure would be to use the rate-of-charge of pressure with time dP/dt to control the EOC. As noted from Figure 2-7, a dP/dt value could be selected to effectively control the overcharge. This method for charge control was used at Sandia National Laboratories for charge control of terrestrial Ni-H_2 batteries, where the objective was to minimize overcharge to obtain a high overall watt-hour efficiency [2-7].

I suspect the reason that pressure, or rather dP/dt, has not been used to date for charge control of Ni-H_2 batteries in orbit is lack of a sufficient database to justify using this method. Secondly, there was a concern about the strain-gauge bridge drifting with time. There seems to be a sufficient database of in-orbit pressure performance data measured by a strain-gauge bridge circuit to justify use of the dP/dt method for charge control.

2.4.0 THERMAL VACUUM TEST

A thermal vacuum test is recommended to verify battery thermal design for the worst-case operating conditions for both LEO and GEO applications. One should use a qualification or flight spare Ni-H_2 battery and, where possible, flight hardware to simulate as close as possible the actual interfaces between the battery, deep space, and the spacecraft. As many of the worst-case design conditions as possible should be verified, including the following:

- Battery temperature and temperature gradient between cells under normal and worst case conditions.

- Battery temperature and temperature gradient between cells with one cell open circuited for those battery designs with bypass diodes.

2.5.0 GEO AND LEO SATELLITE PROGRAMS

GEO and LEO satellite programs are listed in Tables 2-3 and 2-4 to show the extent of the use of Ni-H_2 batteries for space applications.

Table 2-3. Flight Programs, GEO Satellites with Ni-H_2 Batteries

Satellite	Cell Mfr	Capacity Ah (rated)	DOD % rated capacity
INTELSAT V (FACC*/INTELSAT)	EPI	30 Ah	56% 6 satellites
	EPI	30 Ah	72% 2 satellites
G-STAR (RCA/GTE)	EPI	30 Ah	60% 4 satellites
SPACENET (RCA/Southern Pacific)	EPI	40 Ah	60% 3 satellites
ACS-1 (RCA‡/American Satellite Corp.)	EPI	35 Ah	65% 1 satellite
SATCOM K (RCA‡ /GE Americom)	EPI	50 Ah	65% 2 satellites
OLYMPUS (BAe/ESA)	EPI	35 Ah	60% 1 satellite
ITALSAT (FACC/Selenia)	EPI	30 Ah	65% 1 satellite
EUTELSAT II (Aerospatiale)	EPI	58 Ah	74% 5 satellites
TV-SAT II (AEG-Telefunken)	EPI	30 Ah	—
Astro 1A (GE Astro/SES Luxenburg)	EPI	50 Ah	70% 1 satellite
Astro 1B (GE Astro/SES Luxenburg)	EPI	50 Ah	65% 1 satellite
ANIK-E (GE Astro/Telesat-Canada)	EPI	50 Ah	70% 2 satellites
TELECOM 2 (MATRA)	EPI	83 Ah	75% 3 satellites
INTELSAT VI (HAC/INTELSAT)	HAC	44 Ah	60% 5 satellites
PANAMSAT (GE Astro/Panamsat Corp.)	EPI	35 Ah	60% 1 satellite
ASC II (GE Astro/American Satellite Corp.)	EPI	40 Ah	60% 1 satellite
AURORA (GE Astro/GE Americom)	EPI	40 Ah	60% 1 satellite
SUPERBIRD (SSL/Australia)	GEP	83 Ah	75% 2 satellites
Awaiting Launch			
INTELSAT K (GE Astro/INTELSAT)	EPI	50 Ah	65% 1 satellite
INTELSAT VII (SSL/INTELSAT)	GEP	85 Ah	70% 5 satellites
Satcom C3/C4 (GE Astro/GE Americom)	EPI	50 Ah	55% 2 satellites
Telstar 4 (GE Astro/AT&T)	EPI	50 Ah	70% 3 satellites
Inmarsat 3 (GE Astro/Inmarsat)	EPI	50 Ah	65% 4 satellites

*now Space Systems Loral (SSL)

‡Now GE Astro

Table 2-4.
Flight Programs, LEO Satellites with Ni-H_2 Batteries

Satellite	Cell Mfr	Capacity Ah (rated)	DOD % rated capacity
Hubble Space Telescope (HST)	EPI	88 Ah	8% 1 satellite
Space Station Freedom (SSF)	GEP	81 Ah	35% 1 station

2.6.0 REFERENCES

[2-1] R. J. Hass and A. K. Chawathe, "Space Station Nickel-Hydrogen Cell Design And Development," *Proc.*, Vol. 3, 23rd Intersociety Energy Conversion Engineering Conference August 1990, pp. 573–576.

[2-2] D. E. Nawrocki, J. D. Armantrout et al., "The Hubble Space Telescope Nickel-Hydrogen Battery Design," *Proc.*, Vol. 3, 25th Intersociety Energy Conversion Engineering Conference, Reno, Nevada, August 12–17, 1990, pp 1–6..

[2-3] J. E. Lowery, J. R. Lanier Jr., C. I. Hall, and T. H. Whitt, "Ongoing Nickel-Hydrogen Energy Storage Device Testing At George C. Marshall Space Flight Center," *Proc.*, 25 Intersociety Energy Conversion Engineering Conference, Reno, Nevada, August 12–17, 1990, pp. 28–32.

[2-4] J. C. Brewer, T. H. Whitt, and J. R. Lanier, Jr., "Hubble Space Telescope Nickel-Hydrogen Batteries Testing and Flight Performance," *Proc.* 26th Intersociety Energy Conversion Engineering Conference, 1991, pp. 257–261.

[2-5] D. Cooper and A. Dunnet, INTELSAT, private communications on the charge control on INTELSAT V nickel-hydrogen batteries in orbit.

[2-6] M. Earl, COMSAT Laboratories, private communications.

[2-7] D. M. Bush, Sandia National Laboratories, "Evaluation of Terrestrial Nickel-Hydrogen Cells and Batteries," SAND 88-0435, May 1988.

[2-8] G. C. Klein and D. E. Rash, "Reliability Study of the Ni-H_2 Strain Gauge," The 1992 NASA Aerospace Battery Workshop, NASA Conference Publication 3192, p. 553.

[2-9] D. Cooper, INTELSAT, private communications.

CHAPTER 3
NICKEL-HYDROGEN BATTERY DESIGN

3.1.0 GENERAL

In the preliminary design phase of a satellite, the power requirements and energy storage requirements are specified. The maximum depth-of-discharge (DOD) may also be specified. The ranges of values specified for the DOD for Ni-H_2 batteries for geosynchronous satellite (GEO) applications and low earth orbit (LEO) applications are given below:

GEO	10 to 20 years in orbit	50–80% DOD
LEO	3 to 7 years in orbit	20–40% DOD

Generally, two or more batteries are used per spacecraft to meet the energy storage requirements. The major advantage for using multiple batteries is reliability. If one battery fails, the other battery or batteries can maintain all or at least some portion of the spacecraft loads.

The battery designer must (1) specify the capacity and number of IPV cells to be used in each battery to meet the energy storage requirements, (2) design a multicell battery with these cells that can be integrated into the spacecraft and can meet the thermal and mechanical requirements of the mission as well as the energy storage requirements, and (3) design the charge/discharge control system for managing the battery in orbit.

Given the size and capacity of the Ni-H_2 cells, the number of cells per battery, and the number of batteries per spacecraft, one can begin to design the spacecraft battery. The disciplines involved in designing the battery include

- structural/mechanical design
- thermal design
- electrical design
- reliability.

It is essential for these different disciplines to interact with one another to achieve a battery design that will meet mission requirements.

Presented in this chapter are a number of different GEO and LEO battery designs that demonstrate the disciplines involved in designing these batteries. The mechanical, thermal, and electrical designs are presented in some detail. For GEO applications, both body-stabilized (INTELSAT V) and spin-stabilized (INTELSAT VI) satellite battery systems are presented. The EUTELSAT II Ni-H_2 battery is presented

to give an example of a GEO battery design made with second-generation Ni-H_2 cells as described in Chapter 1. LEO designs described include the Hubble Space Telescope and the Space Station Freedom Ni-H_2 battery systems.

A summary is presented at the end of the chapter to highlight the salient design features of the different batteries and to provide data on the specific energy and DOD for the different battery designs.

3.2.0 GEO BATTERY DESIGNS

3.2.1 TRW Battery Development Program

The TRW battery design and fabrication program pioneered the development of the Ni-H_2 battery technology for GEO applications. This work was performed in the 1975 time period under INTELSAT/COMSAT support. The objective of this program was to develop a Ni-H_2 battery design using the NTS-2 35-Ah cells described in Chapter 1.

A 10-cell Ni-H_2 battery was designed, fabricated, and tested by TRW [3-1]. Each of the cells in this battery was girth supported by an electrically insulated mounting bracket (see Figure 3-1). The cell mounting bracket assemblies were attached to a honeycomb mounting panel with cutouts and threaded inserts. Heat transfer was by radiation directly from the vessel walls and from the mounting panel to a secondary radiator. The secondary radiator was a north- or south-facing panel that radiated directly to space (indirect radiator design).

Electrical Design

For the electrical design, TRW concluded the following:

1. A fixed c/d recharge ratio (as described in Chapter 2, Section 2.2.2, "Charge Control for GEO Applications") would be an effective charge control method for maintaining the nickel/hydrogen battery energy balance for synchronous orbit duty cycles.

2. Cell pressure was not recommended for charge control of the batteries because not enough was known about the pressure performance of Ni-H_2 cells over long periods of operation.

3. Nickel/hydrogen batteries required protection electronics (bypass diodes) to prevent loss of a battery resulting from an open-circuited cell.

4. Protection against overdischarge with bypass electronics was not required for Ni-H_2 cells with hydrogen precharge.

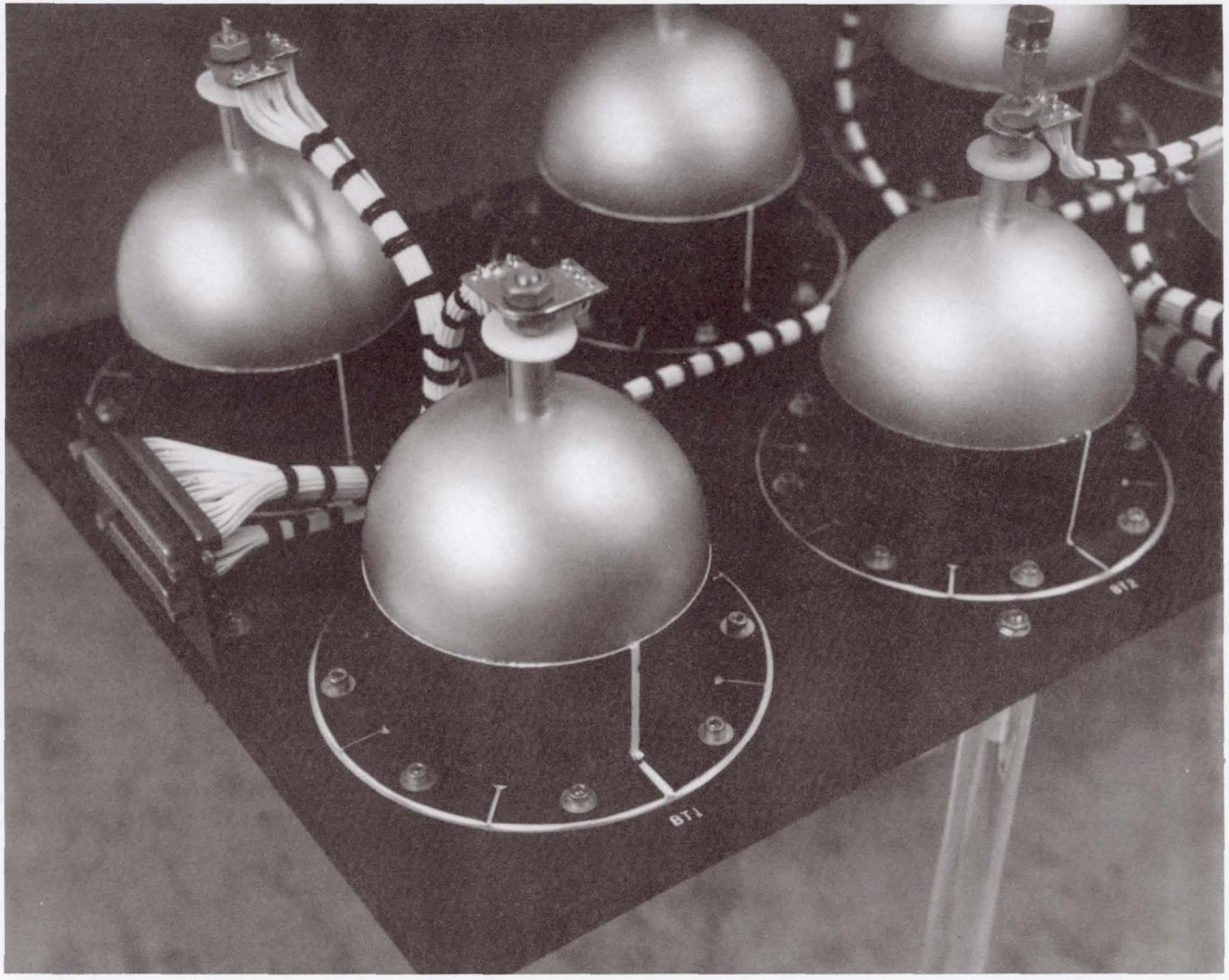

Figure 3-1. TRW battery with cells supported by an electrically insulated mounting bracket.

Ni-H_2 Bypass Circuit. Electronic bypass circuitry serves to bypass an open-circuited cell during charge or discharge without interfering with the operation of the other cells. The bypass circuit designed for the TRW battery is shown in Figure 3-2. Protection in the forward (charge) direction is provided by three silicon diodes in series, while protection in the reverse (discharge) direction is provided by one Schottky barrier diode.

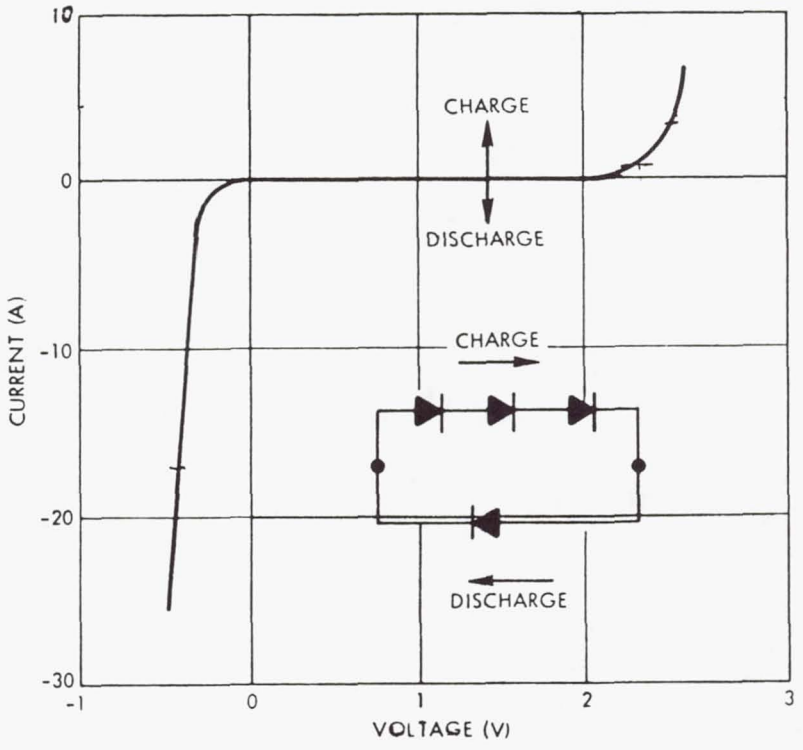

Figure 3-2. Ni-H_2 cell bypass circuit.

Mechanical Design

Each of the cells in the 10-cell battery was supported around the circumference of the pressure vessel with an insulated mounting bracket. These cell mounting bracket assemblies were attached to the honeycomb panel with cutouts and threaded inserts (Figure 3-1).

The cell mounting bracket had two functions: support the cell on the platform under launch loads and transfer the heat generated in the cell to the mounting plate. TRW concluded that the critical strength requirement was the ability of the bond to sustain the shear stress which develops when the pressure vessel expands under pressure. A two-part flexible silicone rubber adhesive system was used that cures uniformly over the large required area of contact and has a minimum bond thickness of 0.254 mm. This design concept for using a silicon

rubber adhesive to attach an aluminum mounting bracket to the cylindrical pressure vessel of a cell is still used today.

Thermal Design

The thermal design of the battery system was based on a 24-hour synchronous orbit with a maximum discharge period of 1.2 hours. A body-stabilized spacecraft was assumed with a north- or south-facing surface available for the battery system.

A fundamental consideration in battery design is the means of heat dissipation from the cells when mounted in the spacecraft. Radiation to space is the primary means of maintaining battery cell temperature within desired limits. TRW determined that it was easier to maintain the battery within a reasonably small temperature range with indirect radiation for their battery design. Heat dissipated within the cells is conducted radially to the pressure vessel walls, through the silicon rubber adhesive to the aluminum mounting bracket, and down the mounting bracket to the mounting panel. Heat transfer to space was by radiation from the battery pressure vessel walls and mounting panel to a secondary radiator. The secondary radiator was a north- or south-facing panel that radiated directly to space. Figure 3-1 shows how the cells are spread out over a large area for this indirect radiator design.

3.2.2 NTS-2

The U.S. Navy's Navigation Technology Satellite-2 (NTS-2), launched on June 23, 1977, was the first flight demonstration of the Ni-H_2 battery technology. The Naval Research Laboratory (NRL) chose to use the Ni-H_2 battery as the operational energy storage system to demonstrate the feasibility of this new technology in space [3-2]. The NTS-2 satellite operated in a 12-hour orbit at 20,183 km, 63° inclination, with two 30-day eclipse seasons per year. The battery cycled 60 times during each eclipse season, twice per day. During the longest eclipse of 0.94 hours, the DOD was 60 percent. The normal satellite load during eclipse periods was 325 watts.

Although the NTS-2 was in an inclined orbit with two eclipses per day and a 12-hour orbit instead of a 24-hour GEO orbit, the thermal, mechanical, and charge management design requirements were very similar to those for a GEO satellite battery. The design features of the NTS-2 battery provided the background for today's GEO technology.

Battery Design

The NTS-2 battery consisted of fourteen 35-Ah cells contained in two 7-cell assemblies; the battery assemblies are shown in Figure 3-3. Each cell was held in place by a cylindrical aluminum sleeve (0.787 mm thick) bolted to the magnesium-

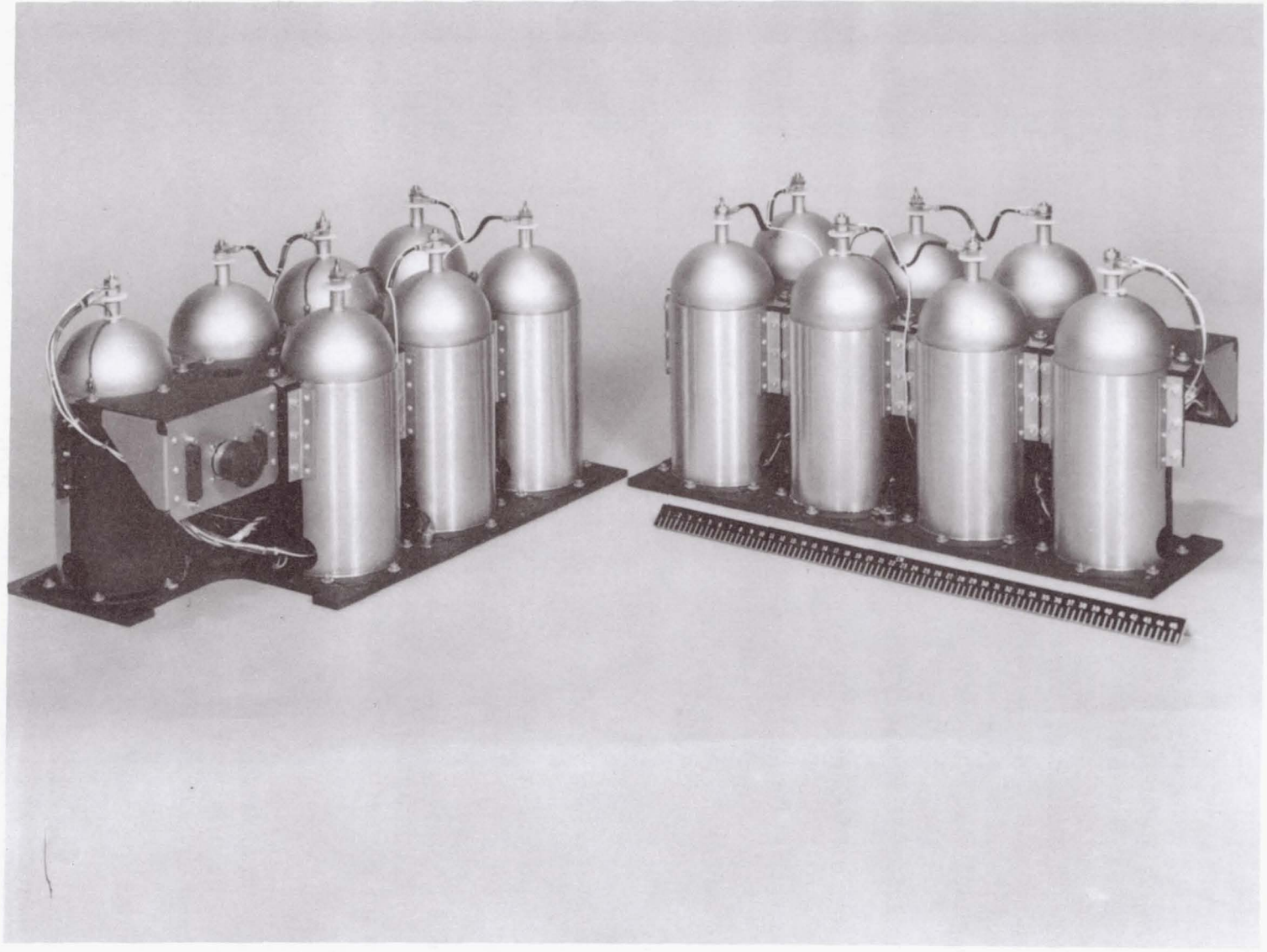

Figure 3-3. NTS-2 nickel-hydrogen battery.

thorium baseplate. Each sleeve was split lengthwise; the cell was clamped between the two half cylinders and electrically insulated from them by a thin (0.4-mm) layer of RTV silicon rubber and fiberglass. In addition to serving as an insulator, this layer also absorbs the pressure vessel expansion and contraction during cycling, thereby virtually eliminating stresses in the aluminum sleeve [3-3].

The NTS-2 design used direct radiation to space for temperature control of the battery. The two battery assemblies were mounted on two of the three rectangular surfaces of the satellite used to continuously view deep space [3-4]. The bottom of the baseplate radiated directly into space. The inner surface of the sleeve, as well as the cell dome inside it, was painted black to increase the emissivity and hence maintain temperature uniformity. The exposed cell dome was gold plated to minimize thermal radiation between the battery and other satellite components.

NTS-2 Ni-H_2 Cells

Salient features of the NTS-2 35-Ah Ni-H_2 cells were described in Chapter 1, Section 1.6.2, "NTS-2 Cell Design."

Mechanical Design

Aluminum Sleeve. The aluminum sleeves had two functions: support the cells on the baseplate under launch loads and conduct the heat generated within the cell to the baseplate. The critical strength requirement was the ability of the bond to sustain the shear stress between the cell and the sleeve that develops as a result of pressure vessel expansion as the cell is charged and cell pressure increases. A flexible silicone rubber adhesive was used that cures uniformly over the large required area of contact. NTS-2 used a bond thickness of 0.4 mm.

The conductivities, thickness, and interfaces of the assembly materials were examined closely to provide mechanical integrity and maintain temperature excursions within the specified range. The baseplate is a magnesium alloy 6.36 mm thick with a high lateral heat conduction to control cell-to-cell temperature gradients. This material was selected for its high thermal conductivity per unit weight. The sleeves were machined from 6061 aluminum heavy wall pipe, which was chosen for its conductivity and availability [3-2].

Thermal Design

Design objectives were to maintain the temperature between 0°C and 24°C during the longest eclipse day and between 0°C and 5°C between eclipse seasons. Temperature gradients between cells were not to exceed 2.5°C. COMSAT Laboratories provided detailed thermal characteristics of the battery cells [3-3] and the direct radiator design with aluminum sleeves.

Radiator Area. Each of the two Ni-H_2 battery 7-cell modules was mounted on a separate rectangular surface that continuously viewed deep space. The aluminum sleeves conducted heat from the cells to the baseplate, which in turn radiated the heat directly into space. The heat rejection capability of the radiator was dependent on the effective sink temperature that the radiator sees. The effective sink temperature is a convenient way to characterize the radiator thermal environment. It is calculated by summing all external heat inputs to the radiator and converting them into a corresponding radiation boundary temperature. For a body-stabilized satellite in synchronous orbit or the gravity-gradient stabilized NTS-2 satellite in an inclined orbit, the sink temperature will vary between -65°C and -273°C for a north- or south-facing panel with second surface mirrors. The minimum sink temperature depends on the radiator view to the appendages, such as the solar array. A conservative value of -65°C was used for the NTS-2 program. The batteries were mounted on a panel facing deep space, and the radiating surface of this panel was painted white.

For GEO satellites, the radiator area is sized to dissipate the heat generated by the battery when it is operating in the trickle-charge mode. The worst-case condition for heat dissipation under normal operation is when the batteries are continuously trickle charged on storage between eclipse seasons. All of the electrical energy put into the battery on trickle charge is dissipated as heat. For the NTS-2 satellite, the battery radiators were sized to maintain the battery at 0° to 5°C and to dissipate the heat generated by the battery during trickle charge operation, which was about 13 W for the battery at the C/60 rate. The baseplate area for one 7-cell NTS-2 battery was 998 cm^2, or 142.6 cm^2 per cell.

Each battery assembly had thermostatically controlled heaters to maintain a minimum temperature of -5°C if the satellite should shed loads or if the trickle charge should be interrupted and heat generated fell below expected values.

Electrical Design

Key features of the electrical design are the following:

1. The NTS-2 nickel/hydrogen batteries did not use bypass protection electronics for individual cells to protect against an open-circuited cell in the battery.

2. Protection against overdischarge with bypass electronics was not used.

3. Battery temperature was used for charge control during operation in the eclipse season.

4. On discharge, a boost regulator was used to control the bus voltage to 27 V, ±1 V.

5. The energy storage requirement for the battery was 612 Wh.

6. Pressure was monitored with strain gauges mounted on the dome of the pressure vessel of four cells.

Bypass Electronics. Bypass electronics were not used to protect against an open-circuited cell in the string of 14 series-connected cells in the battery. A backup Ni-Cd battery was available if the Ni-H_2 battery failed. With the three-year mission requirement, a high probability of success existed with a single battery. Hence, the Ni-H_2 battery was used as the prime energy source with Ni-Cd as an alternative [3-2].

Several other arguments exist against using bypass electronics. The diodes add about 5 percent to the weight of the battery system, and they add complexity to the electrical wiring.

The use of bypass electronics becomes a reliability argument between the probability of a Ni-H_2 cell failing open-circuited and the failure rates of diodes, including the added complexity of the wiring and mounting hardware.

Overdischarge of Cells. One of the reported advantages of the Ni-H_2 batteries is the capability for overcharge and overdischarge of individual cells without affecting battery performance, i.e., individual cells with hydrogen precharge can be overdischarged without damage to the cells. The NTS-2 battery inadvertently demonstrated the capability for overdischarge: when the satellite was first launched, the battery was fully discharged 3 or 4 times before the satellite was stabilized with no adverse effect upon battery performance. Reference 3-4 states in the conclusion, "The fear of overdischarge, so long a concern of nickel cadmium battery users, is alleviated with the nickel-hydrogen system."

Charge Control. Battery temperature is used for charge control of the battery [3-2], [3-6]. To explain how this works, refer to the mid-eclipse season orbital temperature profiles shown in Figure 3-4. During the eclipse period (first hour of the orbit), the battery temperature rises sharply due to the exothermic discharge reaction. On discharge, the heat dissipated by the cells exceeds the radiator capability, which results in a rise in temperature. Following this discharge, the battery is fully recharged at a constant current of 3.5 amperes (C/10 rate). The charging reaction is endothermic and cools the battery, until it approaches the fully charged condition. On overcharge the battery becomes exothermic again, increasing its temperature at a rapid rate. When the battery temperature reaches 18°C, the battery charging current is automatically switched from the C/10 rate to a C/60 rate. In addition to using the set point of 18°C, the rate of change of temperature with time must be positive to avoid switching during the endothermic portion of the recharge period when the battery is still cooling down.

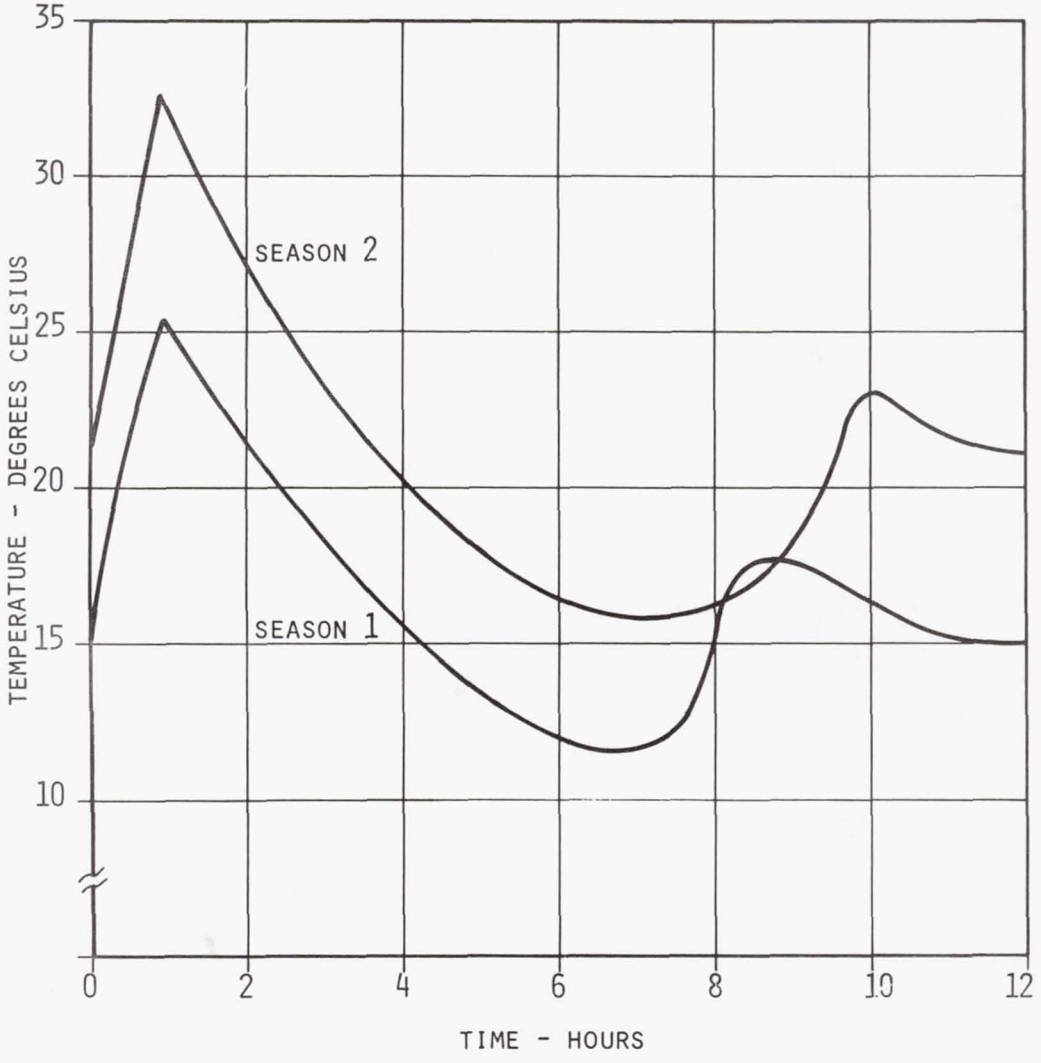

Figure 3-4. Ni-H_2 battery mid eclipse season orbital temperature profiles.

Discharge Control. The electrical power system bus voltage was designed to operate at 27 V, ± 1 V, regulated. The 14-cell, 17.5-V Ni-H_2 battery provides power to the bus through a high-efficiency (87 percent) boost regulator.

Energy Storage Requirements. For the longest eclipse day of 0.94 hours, the energy storage requirement for the battery was 612 Wh to meet the bus load requirement of 325 W at 57.4 percent DOD* with 87 percent efficiency of the boost regulator, as demonstrated in the following equation:

$$\frac{\text{Load (W)} \times \text{Discharge Time (h)}}{\text{DOD} \times \text{Eff Regulator}} = \text{Stored Energy (Wh)}$$

$$\frac{325\ \text{W} \times 0.94\ \text{h}}{0.574 \times 0.87} = 612\ \text{Wh}$$

$$\text{No. Cells (No)} \times \text{Capacity (Ah)} \times \text{Avg. Discharge Voltage (V)} = \text{Stored Energy (Wh)}$$

$$14\ \text{Cells} \times \frac{35\text{Ah} \times 1.25\ \text{V}}{\text{Cell}} = 612\ \text{Wh}$$

Pressure Data. Four of the cells have strain-gauge bridges mounted on their domes. The bridge has two active and two dummy legs. The dummy legs provide temperature compensation and are mounted on a coupon that was attached to the cell with RTV in the same region as the active gauges. The active gauges were bonded to the pressure vessel domes prior to the assembly of the cell stack into the pressure vessel, which allowed the bond to be cured at the required temperature. The strain-gauge bridge output is directly proportional to the cell pressure.

Telemetry Data. The following parameters were available through spacecraft telemetry:

- battery voltage
- individual cell voltages
- cell internal pressure, two cells per assembly
- four temperatures per assembly
- battery current.

The battery data were stored on board the spacecraft every 102 seconds for retrieval by ground command.

* DOD is based on rated capacity

Weight and Energy Density

A weight breakdown for the NTS-2 battery is presented in Table 3-1. The specific energy is 36.5 Wh/kg for the battery. The specific energy could be significantly improved by reducing the hardware weight, specifically the aluminum sleeves and baseplate weight. The overweight design of the thermal and mechanical support structure was understandable considering that it was the first flight experiment and the objective was to demonstrate Ni-H_2 battery technology rather than optimize the structure.

Table 3-1 provides a summary of the volume, mass, specific energy, and energy density [3-7].

Table 3-1. NTS-2 Battery

Nameplate Capacity (rated)	35 Ah
Measured Capacity at 10°C	43 Ah
Battery Assembly	
length	48.26 cm
width	24.13 cm
height	25.40 cm
Volume of Assembly	29,579 cm^3
Weight of Assembly	10.20 kg
Weight of Cell	1.028 kg
Weight of 14 Cells	14.39 kg
Weight of Battery	20.40 kg
Weight of Cells/Weight of Battery	70%
Stored Energy of Battery[1] (at 10°C)	752 Wh
Stored Energy Per Assembly	376 Wh
Number of Batteries	1 Ni-H_2 battery
DOD (percent of rated capacity)	57.4%
Specific Energy[3] (at 10°C)	36.5 Wh/kg
Energy Density (at 10°C)	0.0127 Wh/cm^3

[1]Stored energy of battery (at 10°C) is based on measured capacity of 43 Ah
[2]DOD is based on rated capacity
[3]Specific energy is based on measured capacity

Note that in the above table, as is standard practice in the battery industry, DOD is based on rated capacity, and specific energy and energy density are based on measured capacity at 10°C.

3.2.3 INTELSAT V Ni-H_2 Batteries

A total of eight INTELSAT V satellites were successfully launched with Ni-H_2 batteries between 1983 and 1987. The INTELSAT V geosynchronous communication satellites were designed and built by Ford Aerospace Communications Corporation (FACC)* [3-8]. The first five satellites F-1 through F-5 used Ni-Cd batteries for their energy storage subsystem. Starting with F-6, the remaining eight satellites in the INTELSAT V series used Ni-H_2 batteries. Two 27-cell, 30-Ah Ni-H_2 batteries shown in Figure 3-5 provide the electrical energy during launch, transfer orbit, and solar eclipses. The batteries are also on-line during sunlight operation to supplement the solar arrays in supplying power for load transients whenever the spacecraft bus voltage drops below a certain set voltage. Six of these satellites, F-6, F-7, F-8, F-10, F-11, and F-12, have on-station loads of approximately 480 watts per battery (56 percent DOD), and two of these satellites, F-13 and F-15, have on-station loads of 567 watts per battery (67 percent DOD) during the 1.2-hour eclipse period.

INTELSAT V Ni-H_2 Cells

Salient features of the 30-Ah INTELSAT V cells were described in Chapter 1, Section 1.7.0, "INTELSAT V Cell Design."

Mechanical Design

Aluminum Sleeves. The basic feature of the mechanical design was the support of each cell in a cylindrical aluminum mounting sleeve shown in Figure 3-6a. A flexible RTV silicon rubber sheet, 0.37 mm thick, was wrapped around the cell, and the aluminum sleeves (0.787 mm thick) were clamped down onto the rubber sheet with clamping screws. Twenty-seven of these cells with sleeves were attached together at the top and base of the sleeves into a closed packed hexagonal arrangement as shown in Figure 3-5. A baseplate, shown in Figure 3-6b, was riveted to the bottom of the sleeves. There were 27 cells per battery.

The aluminum sleeves serve two functions: support the cells and conduct the heat generated within the cell to the baseplate. They were fabricated from a high-strength aluminum alloy using an investment casting process. The sleeves were cast with mounting feet and brackets that, after heat treatment, required machining to their final dimensions.

---

* Now Space Systems/Loral

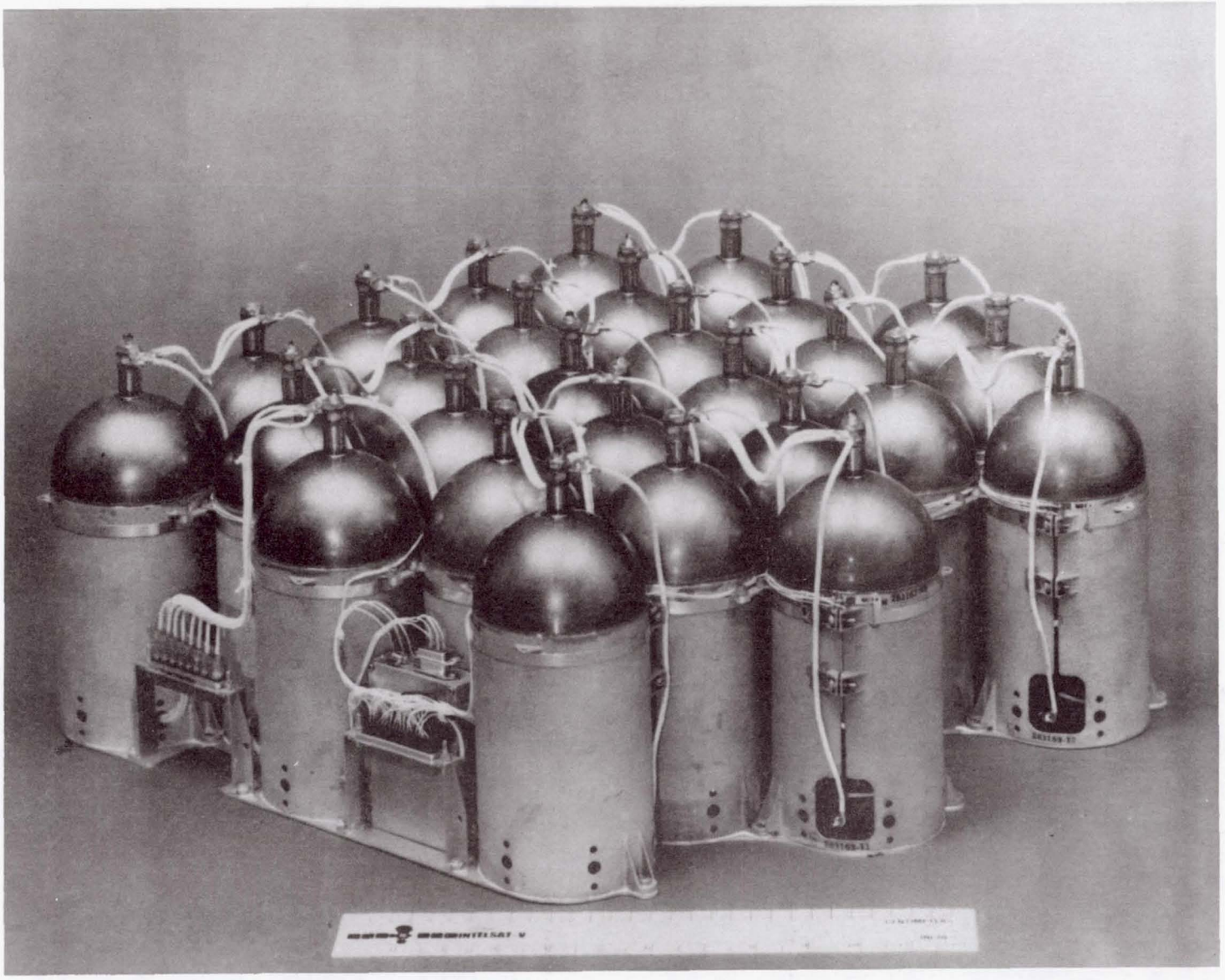

Figure 3-5. INTELSAT V nickel-hydrogen battery.

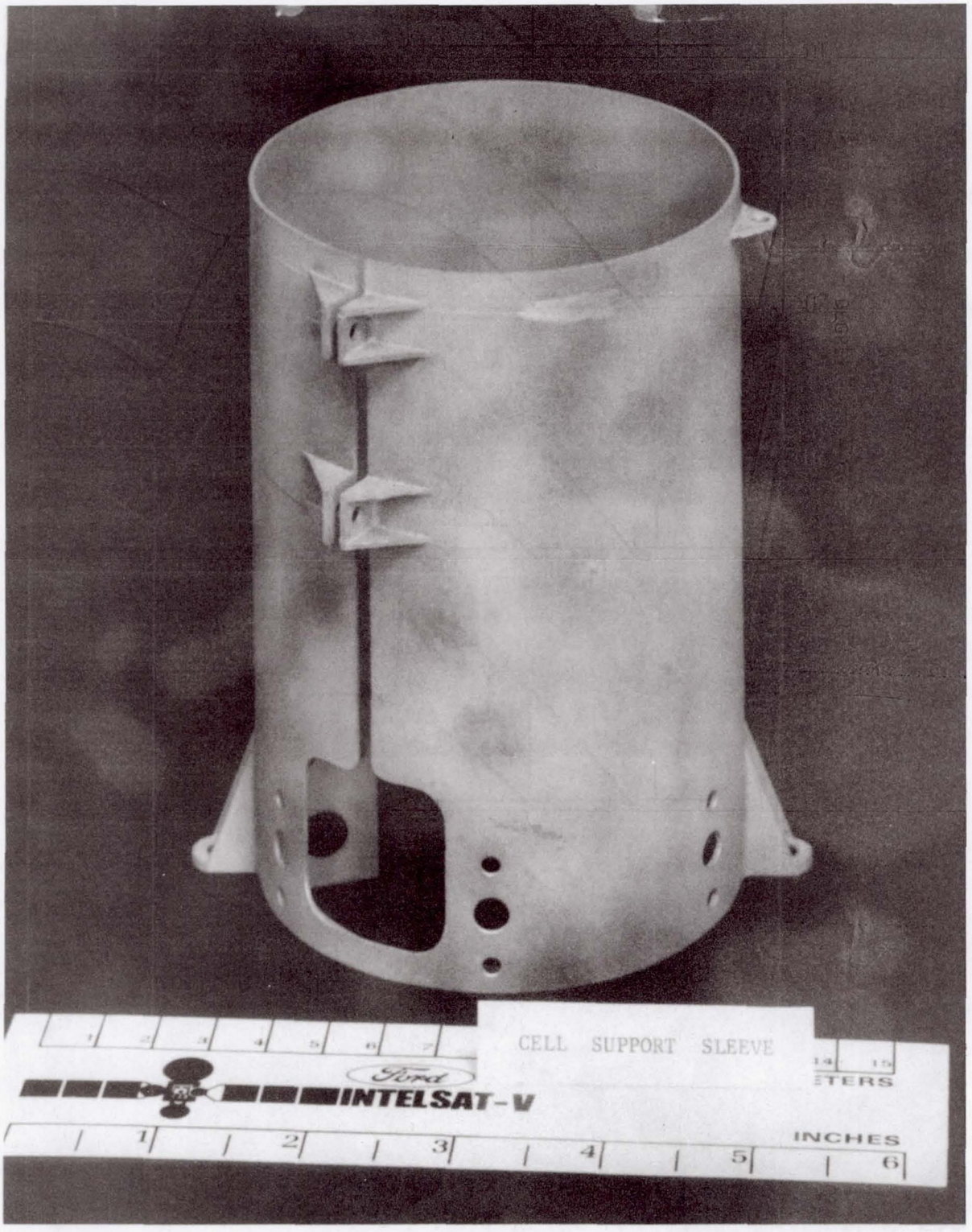

Figure 3-6a. Cell support sleeve.

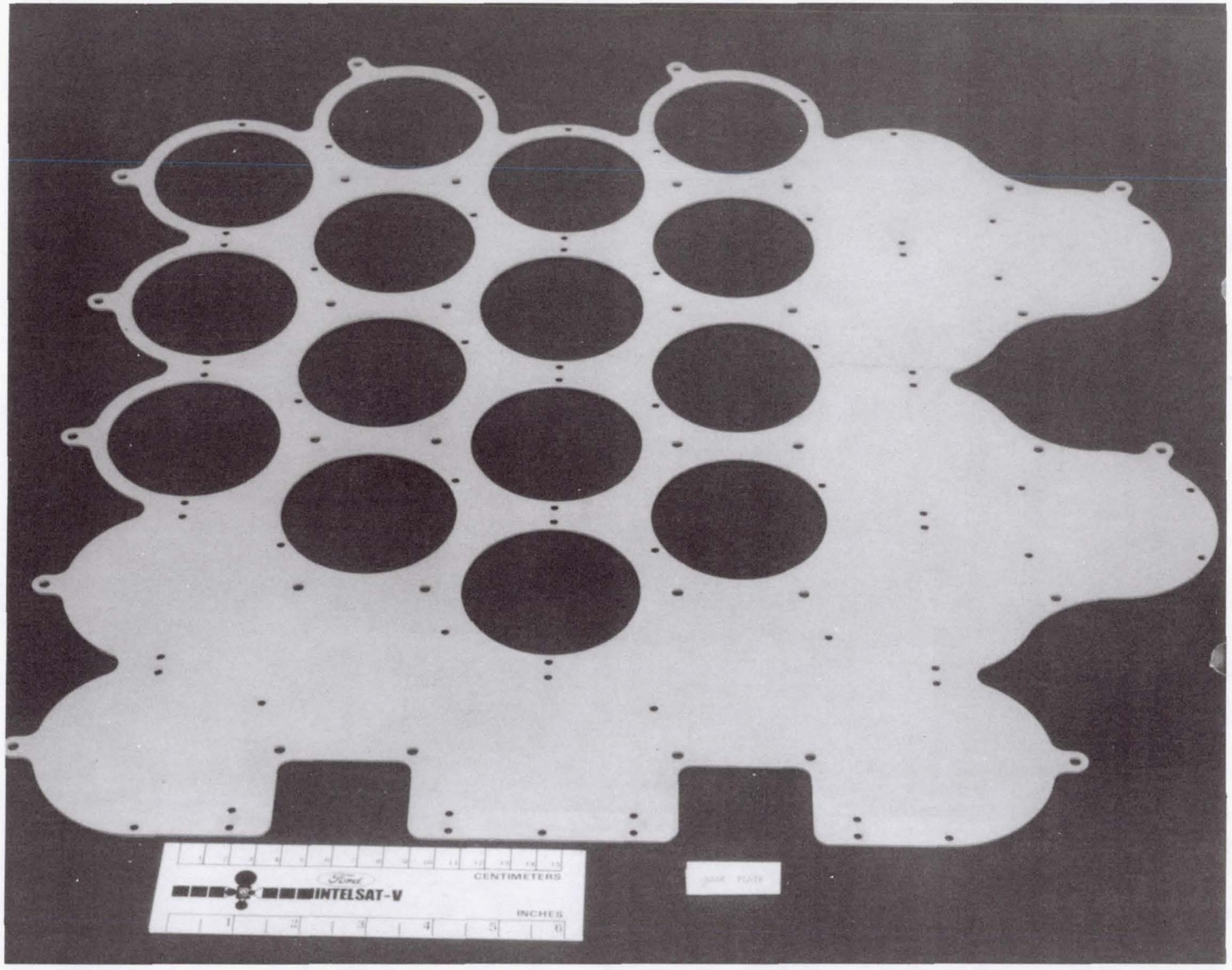

Figure 3-6b. Baseplate.

Thermal Design

The thermal design goals were to maintain the temperature between 2°C and 15°C during the eclipse season. During equinox periods between eclipse seasons the batteries were to be maintained between 2°C and 10°C.

Radiator. The Ni-H_2 batteries were designed to be interchangeable with the Ni-Cd batteries for the INTELSAT V satellites [3-8]. The north- or south-facing mounting panels had optical solar reflectors (OSR) of the same size for either type of battery. The radiator area was 1,580 cm^2 per battery, or 58 cm^2 per cell for the Ni-H_2 battery. The area or footprint of the Ni-H_2 battery was greater than the radiator area cutout. The aluminum sleeves, with the cells, were mounted to an aluminum baseplate. In the region over the radiator area, holes were cut in the baseplate to match the inside diameter of the flange on the aluminum sleeves (see Figures 3-6a and 3-6b). For the remainder of the cells not positioned over the radiator, heat is conducted from the base of the cells through the aluminum baseplate to the radiator. The baseplate thermal gradient was predicted to be 3.1°C under worst-case conditions.

The battery heat transfer paths are shown in Figure 3-7. Heat dissipated from within the cells and from the heaters located on the cell sleeves is conducted down the cast aluminum sleeves to the baseplate, through the north-south mounting panel to the radiator OSRs. The OSRs are optically coated glass mirrors. A thermal blanket is placed over the OSRs to control the area of the radiator, as shown in Figure 3-7.

Again, the radiator area is sized to dissipate the heat generated by the battery when operated in the trickle-charge mode. The OSR is capable of dissipating heat generated during continuous trickle charge at the C/63 rate, keeping the battery temperature below 10°C.

An important feature of the thermal design is the low-emittance treatment of the battery surface, which radiatively decouples the battery from other spacecraft components. A low-emittance lightweight shield is mounted over the exposed battery cell domes to provide an emittance of less than 0.1. The sides of the battery are wrapped with aluminized mylar.

In addition to the passive means of thermal control described above, charge control is used to limit the high temperature, and heaters are used to control the low temperature of the batteries. During eclipse operation, when the battery is fully recharged at the high rate, the charge control switches to the trickle charge rate to reduce thermal dissipation. At the low battery temperatures during solstice periods, the passive battery thermal control is augmented by 1-W heaters on each cell. The heaters are activated at +2°C and deactivated at +5°C. While on the heaters the battery temperature oscillates between 2° and 5°C. Thermistors and heater control electronics are used to automatically control the heaters.

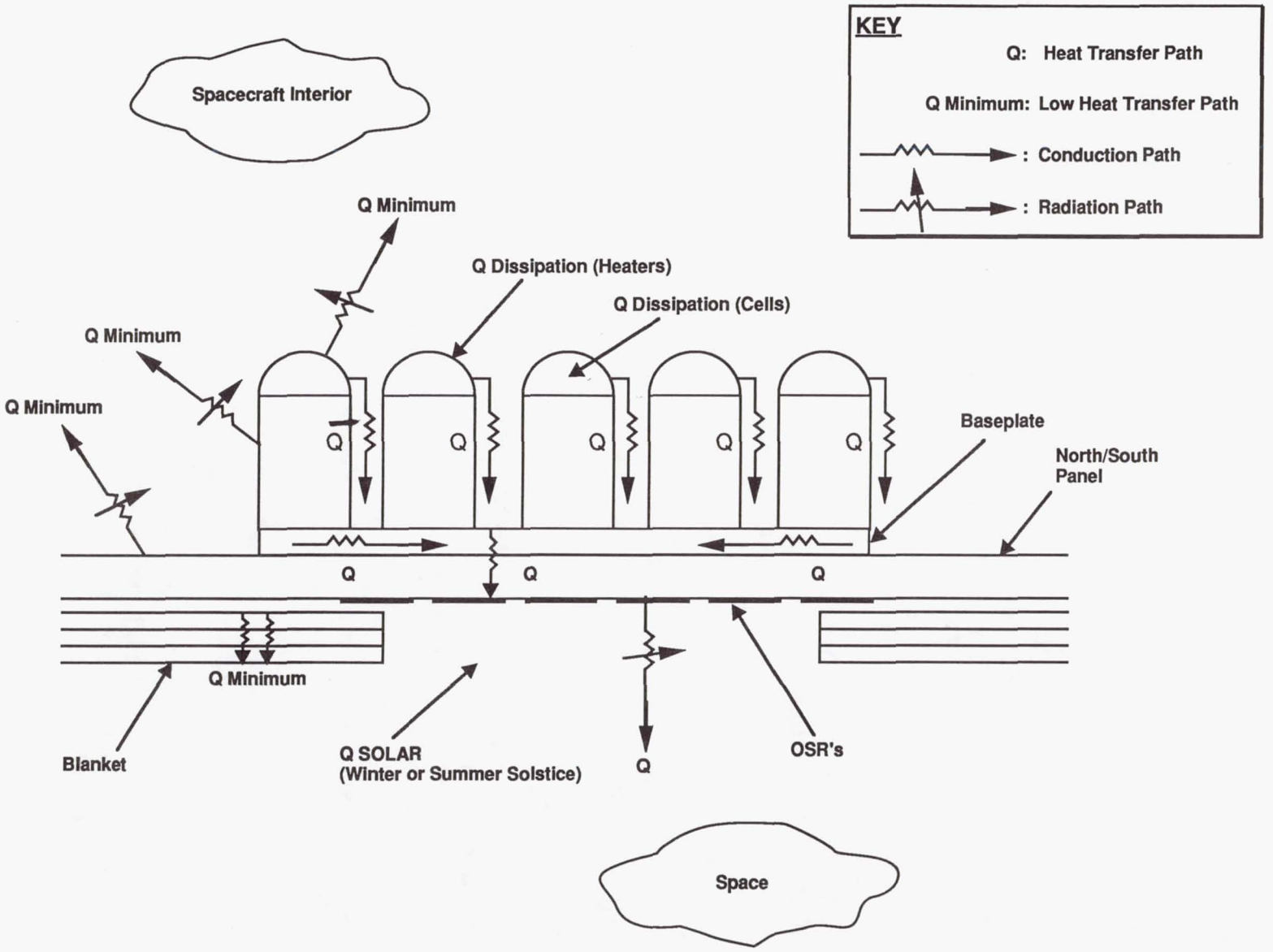

Figure 3-7. Battery heat transfer paths.

Electrical Design

Features of the electrical design are the following:

1. Bypass diodes are used to protect against an open-circuit cell.
2. A 50-ohm resistor is switched across the battery for reconditioning.
3. A fixed c/d ratio is used for charge control of the battery: c/d = 1.15 at C/21 rate (high rate) switched to C/63 trickle rate.
4. Each battery sees a constant power load on discharge.
5. Pressure is monitored with a strain-gauge bridge mounted on the dome of the pressure vessel of one cell per battery.
6. Individual cell voltages are monitored.

Reconditioning. The batteries are reconditioned prior to each eclipse season. A 50-ohm resistor is switched across the battery by ground command. The reconditioning discharge is discontinued when the first cell in the battery reaches 0.5 volts. The batteries are recharged at the high rate, returning 115 percent of the ampere-hour capacity removed on discharge. The batteries are reconditioned one battery at a time, so at least one battery will always be in the fully charged condition.

Charge Control. The batteries are discharged during the eclipse periods and recharged during sunlight operation. A c/d ratio of 1.15 is used for the INTELSAT V batteries. At the beginning of life (BOL), the batteries are recharged at a C/21 rate and then switched to the C/63 trickle charge rate by ground command. Corresponding end-of-life rates are C/25 for the high rate and C/73 for the trickle-charge rate.

All of the charge control switching functions are initiated by ground command. The ampere-hours removed during discharge are calculated by integrating the discharge current. The recharge time is calculated to return at the high charge rate 115 percent of the ampere-hours removed. At the appropriate time a ground command is initiated to switch to the trickle rate. The c/d ratio of 1.15 is required to fully recharge these batteries at the C/21 to C/25 rate. Trickle charge maintains the batteries in the fully charged condition.

Load. The first six INTELSAT V spacecraft with Ni-H_2 batteries (F-6, F-7, F-8, F-10, F-11, and F-12) have a constant power load of 480 W. The DOD for these batteries is 56 percent DOD on the longest eclipse day. For the last two spacecraft, satellites F-13

and F-15, the constant power load was increased to 567 W. The DOD for these batteries is 67 percent DOD on the longest eclipse day.

$$DOD = \frac{480\ W \times 1.2\ hr}{27\ cells \times 30\ Ah \times 1.25\ V} \times 100\% = 56.8\%$$

$$DOD = \frac{567\ W \times 1.2\ hr}{27\ cells \times 30\ Ah \times 1.25\ V} \times 100\% = 67\%$$

Traveling wave tubes (TWTs) account for over 80 percent of the spacecraft load; most of the rest is housekeeping. The TWTs are powered by a switching regulator (constant power regulator). Therefore, the batteries see a constant power load on discharge. As the battery voltage decreases, the current increases to keep the power constant.

Bypass Diodes. The bypass diode circuit is similar to the one previously shown in Figure 3-2. Protection in the forward (charge) direction is provided by three silicon diodes in series, while protection in the reverse (discharge) direction is provided by one Schottky barrier diode. The diodes are mounted at the base of the aluminum sleeve on the inside of the cylinder near the baseplate. Their proximity to the baseplate improves heat dissipation into space.

Pressure. One of the cells in each battery is instrumented with a strain-gauge bridge circuit. The voltage output from the bridge circuit is amplified to a value similar to a battery cell voltage for telemetry. This voltage output from the strain-gauge bridge circuit is directly proportional to the cell pressure.

The bridge consists of four strain gauges. Two are active and bonded directly to the pressure vessel; the other two are bonded to a small piece of INCONEL alloy 718 mounted onto a silicon rubber pad on the vessel. The properties and thickness of the rubber pad are selected so that the gauges are exposed to the vessel temperature but not to the stress in the wall. These dummy gauges provide temperature compensation for the active gauges.

The pressure is a direct indication of the state-of-charge of the battery for all eight of the INTELSAT V batteries. The strain gauge performance has been very stable throughout their lifetime. See Section 5.3.4 in Chapter 5 on pressure data in orbit for more information.

Weight and Energy Density

Table 3-2 includes a summary of the volume, mass, specific energy, and energy density for the INTELSAT V batteries. It also includes a summary for the Superbird and INTELSAT VII Ni-H_2 batteries.

Table 3-2. INTELSAT V, Superbird, and INTELSAT VII Ni-H_2 Batteries

	INTELSAT V	Superbird*		INTELSAT VII*	
Nameplate Capacity	30 Ah	83 Ah		85.5 Ah	
Measured Capacity at 10°C	36 Ah	91.5 Ah		97.0 Ah	
Battery	27 cells	15 cells	12 cells	15 cells	12 cells
length	51.8 cm	51.0 cm	51.0 cm	51.0 cm	51.0 cm
width	52.1 cm	51.0 cm	37.8 cm	51.0 cm	37.8 cm
height	22.2 cm	30.4 cm	30.4 cm	30.4 cm	30.4 cm
Volume of Battery	59,913 cm^3	79,070 cm^3	58,605 cm^3	79,070 cm^3	58,605 cm^3
Weight of One Cell	890 kg	1.867 kg		1.867 kg	
Weight of 27 Cells	24.03 kg	50.41 kg		50.41 kg	
Weight of Battery	30.12 kg	63.9 kg		66.7 kg	62.1 kg**
Weight of Cells/Weight of Battery	80%	79%		75.6%	81.1%**
Energy of Battery 10°C	1215 Wh	3088 Wh		3273 Wh	
Specific Energy	40 Wh/kg	48.3 Wh/kg		49.1 Wh/kg	52.7 Wh/kg
DOD (of rated capacity)					
F6, F7, F8, F10, F11, F12	56%	75%		70%	
F13 and F15	67%				
Energy Density	.020 Wh/cm^3	.022 Wh/cm^3		.024Wh/cm^3	

*Data on Superbird and INTELSAT VII provided by Anthony Z. Applewhite, Space Systems/Loral
**Lightweight INTELSAT VII Battery

The specific energy and energy density were determined using the measured capacities at 10°C.

Superbird Ni-H_2 Batteries

The Ni-H_2 batteries built by Space Systems/Loral for the Australian GEO communications satellites and INTELSAT VII satellites are an advanced version of the INTELSAT V batteries.

The Ni-H_2 cells, built by GEP for Superbird and rated 83 Ah, are described in Section 1.9.4 of Chapter 1. This cell has a high specific energy of 61.26 Wh/kg, as shown in Table 1-6. For the INTELSAT VII programs, the cells (exact same design) were rated at 85.5 Ah. The measured capacity for these INTELSAT VII cells is 97.0 Ah, providing a specific energy of 63.9 Wh/kg.

The Superbird battery is shown in Figure 3-8. Each cell is supported in a cylindrical aluminum mounting sleeve similar to the INTELSAT V design. A

flexible RTV reinforced silicon rubber sheet was wrapped around each cell, and the aluminum sleeves were clamped around the rubber sheet with clamping screws. The aluminum sleeves are machined from a block of aluminum to their final dimensions with mounting feet and bracket supports. The cells are spread apart more than for the INTELSAT V design to provide a larger radiator area for the larger capacity battery (more heat dissipation). Brackets are used to interconnect the aluminum sleeves, as shown in Figure 3-8. The 27-cell battery is made up of two modules, one 15-cell module and one 12-cell module (Figure 3-8). The exact same design is used for the INTELSAT VII batteries, except that the INTELSAT VII has bypass diodes. Superbird does not have bypass diodes. These diodes add 2.8 kg to the weight of the battery, as shown in Table 3-2.

The Superbird and INTELSAT VII batteries have the highest gravimetric energy density of all the batteries designed and built to date for GEO applications. A summary of the volume, mass, specific energy, and energy density are presented in Table 3-2 along with the INTELSAT V battery. The lightweight INTELSAT VII battery uses proprietary graphite/epoxy cell sleeves to replace the machined aluminum sleeves. Properties of these graphite/epoxy sleeves are lighter weight, improved conductivity (heat transfer), and improved mechanical strength. As shown in Table 3-2, the projected weight reduction is 4.6 kg for this lightweight INTELSAT VII battery with the graphite/epoxy sleeves [3-25].

3.2.4 The GSTAR and Spacenet Nickel-Hydrogen Batteries

RCA Astro-Electronics* was the prime contractor and manufacturer for the GSTAR and Spacenet satellite systems. The GSTAR program was for GTE Satellite Corporation (GSAT), and the Spacenet program was for GTE Spacenet [3-9]. Two Spacenet satellites were launched in 1984, one GSTAR was launched in 1985, and the second GSTAR was launched in 1986.

Both battery types share the same structural design that provides for a lightweight, high-strength, low-volume package. The basic COMSAT cell design was used, similar to the INTELSAT V cells. The GSTAR and Spacenet batteries use 30-ampere-hour and 40-ampere-hour nameplate capacity cells, respectively [3-9].

The electrical power subsystem of the GSTAR spacecraft provides for a three-parallel-battery operation, and the Spacenet design provides for two parallel-operation batteries. Each battery contains 22 Ni-H_2 cells packaged in two 11-cell battery modules.

* Now GE Astro-Space Division

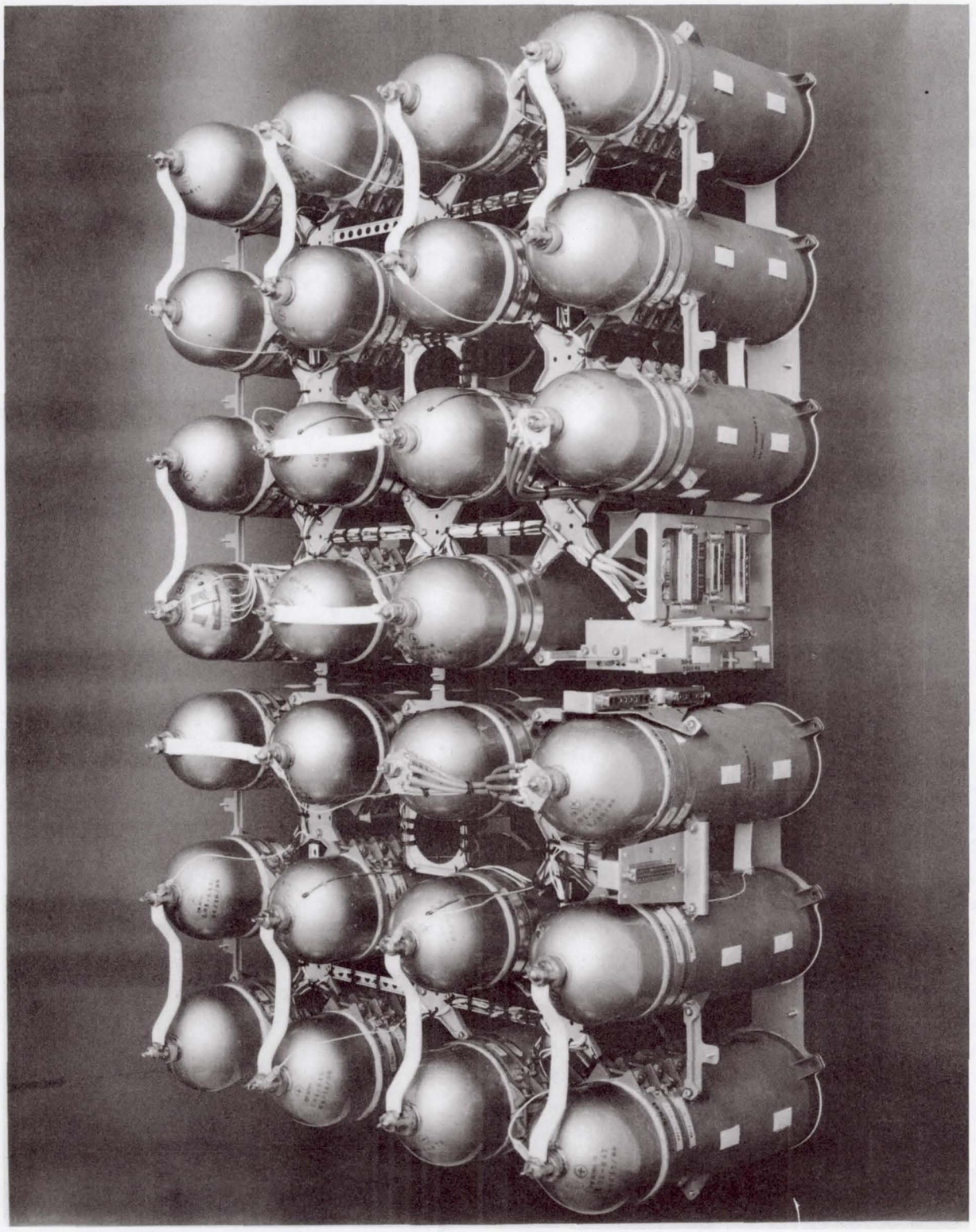

Figure 3-8. Superbird 83-Ah nickel-hydrogen battery.

Mechanical Design

The Spacenet battery module is described in Reference 3-9. Housing of the cells is provided by insulated titanium sleeves (rings) that are 5/8 inch wide. These rings are positioned to support the cells at each end of the cell's cylindrical straight portion. A dual-element flexible heater (primary and backup) was directly fastened to the cell in the area between the two sleeves. These heater strips are of sufficient length to almost cover the entire cylindrical region of the cell. These support sleeve/cells are interconnected to form the battery module mechanical structure. The support sleeves contain multiple tabs with threaded holes; they are connected by means of screws to the magnesium baseplate, magnesium side plates, magnesium top plate, and to each other, respectively, with the cell-tab to cell-tab interconnects. For each of these sleeve-tab to sleeve-tab connections, a small triangular flat titanium plate is used to accommodate multi-cell tolerance buildup. The bottom row of battery modules contains six cells, and the top row contains five cells. Two 11-cell modules constitute one 22-cell battery.

Thermal Design

The complete battery module package is painted black during the finishing operation to accommodate the indirect thermal radiator design as described in Reference 3-10. The terminology "indirect radiator design" is used here to mean that the battery radiates to the interior of the spacecraft, which, in turn, radiates to space. This same thermal design concept was used by TRW as described in Section 3.2.1, "TRW Battery Development Program."

The indirect radiator design described in Reference 3-10 was developed using the 30-Ah cells. Three cells were painted black (emissivity = 0.85) and placed in a triangular-shaped fiberglass test stand that minimized conduction between cells and to the baseplate. The data from both steady state and transient vacuum tests showed that the temperatures measured on the surface of the cells were always within 4.5°C of each other. That is, the local temperatures along the cell walls do not deviate significantly from the maximum temperature recorded at the center of the cell. By using a high-emissivity coating and a second surface radiator plate, the cells can be kept within narrow temperature limits. This indirect radiator design provides the packaging design engineer with an alternative to cell mounting with aluminum sleeves, where the heat is conducted from the cell to the baseplate and radiated directly into space.

An RCA study showed that this indirect radiator design would result in a weight savings; the weight would be 94.5 percent of the aluminum sleeve direct radiator design used on INTELSAT V.

Electrical Design

Features of the electrical design are the following:

1. Pressure is monitored with a temperature-compensated strain-gauge bridge mounted on the dome of one cell in each module.

2. Eleven sets of redundant individual cell reconditioning resistors and reconditioning relays are mounted on the baseplate of each module.

3. Individual cell bypass diodes are directly mounted to the baseplate module on the Spacenet batteries. (This is a two-battery system; if one of the batteries failed, the other battery could not support the full mission load requirements).

   Bypass diodes are not used for the GSTAR batteries. (This is a three-battery system, and if one battery failed the other two batteries could support the full mission load requirements.)

4. The GSTAR power system has individual cell voltage monitoring capability.

5. A fixed c/d ratio is used for charge control of the batteries.

Weight and Energy Density

Table 3-3 is a summary of the volume, mass, specific energy, and energy density.

Table 3-3. GSTAR and Spacenet

	GSTAR	Spacenet
Nameplate Capacity	30 Ah	40 Ah
Measured Capacity 10°C	35.4 Ah	48.3 Ah
Battery Module length/height/width	58.49 cm/19.68 cm/22.86 cm	58.49 cm/19.68 cm/26.67 cm
Volume of Module	26,268 cm^3	30,714 cm^3
Weight of Cell	0.89 kg	1.13 kg
Weight of 11 Cells	9.79 kg	12.43 kg
Weight of Module	12.50 kg	16.31 kg
Wt of Cells/Wt of Batt	78%	76%
Energy per Module 10°C	487 Wh	664 Wh
Energy per Battery	974 Wh	1,328 Wh
Number of Batteries	3 batteries	2 batteries
Number of Cells/Battery	22 cells	22 cells
DOD (of rated capacity)	60%	60%
Specific Energy*	38.96 Wh/kg	41.16 Wh/kg
Energy Density	0.0185 Wh/cm^3	0.0216 Wh/cm^3

*The specific energy includes the mass of the cells and mounting hardware plus the reconditioning resistors, relays, and bypass diodes.

3.2.5 INTELSAT VI Nickel-Hydrogen Batteries

The five INTELSAT VI geosynchronous communications satellites were designed and built by Hughes Aircraft Company, Space and Communications Group. The first of these five satellites was launched in October 1989. Two 32-cell, 44-Ah Ni-H_2 batteries provide electrical energy during launch, transfer orbit, and solar eclipses. The batteries are on-line during sunlight operation to supplement the solar arrays in supplying power for fault clearing or load transients whenever the spacecraft bus voltage drops below the discharge controller setpoint. The batteries are sized to accommodate the on-station load of 990 W maximum per battery for 1.2 hours with one cell failed and a 70 percent maximum end-of-life DOD [3-11], [3-12].

INTELSAT VI Ni-H_2 Cells

Salient features of the 44-Ah INTELSAT VI cells were described in Section 1.8.0, "Air Force Ni-H_2 Cell Design." The INTELSAT VI cells are exactly the same in design as the Air Force baseline 50-Ah cell. HAC derated the 50-Ah cell to a 44-Ah cell rated capacity for the INTELSAT VI program.

Mechanical Design

Figure 3-9 shows one of four identical quadrants that constitute the two batteries. Each 32-cell battery set comprises two battery packs. Each pack consists of a quadrant of a circular shelf with 16 cells mounted in the cell hole cutouts on each of the quadrants as shown. Two extra mounting holes are provided on each quadrant to allow for an increase in the number of cells per battery to 36. The shelf is made of a 2-inch-thick aluminum honeycomb panel.

Cells are mounted on the panel using a three-piece aluminum collar and flange arrangement (see Figure 3-10). The cell thermal mounting flange is attached to the cell using a frozen epoxy film adhesive which bonds the cylindrical portion of the pressure vessel to the inside surface of the cylindrical portion of the thermal flange. The film adhesive has a controlled maximum thickness and contains a loose weave fiberglass cloth carrier with a thickness greater than the minimum bond line requirement. The thermal flange consists of a circular aluminum collar which covers the entire stack length and has a "T" section in the middle for mounting to the panel and conducting heat to the panel.

Prior to installing the cells on the panel, a thermal end cap is installed on each end of the cell. The thermal cap is bonded onto the shoulder end of the thermal flange with silicon-oxide RTV adhesive and secured in place with a wrap of electrical conductive adhesive aluminum tape, which also provides a positive electrical static ground path between the thermal flange and the end cap.

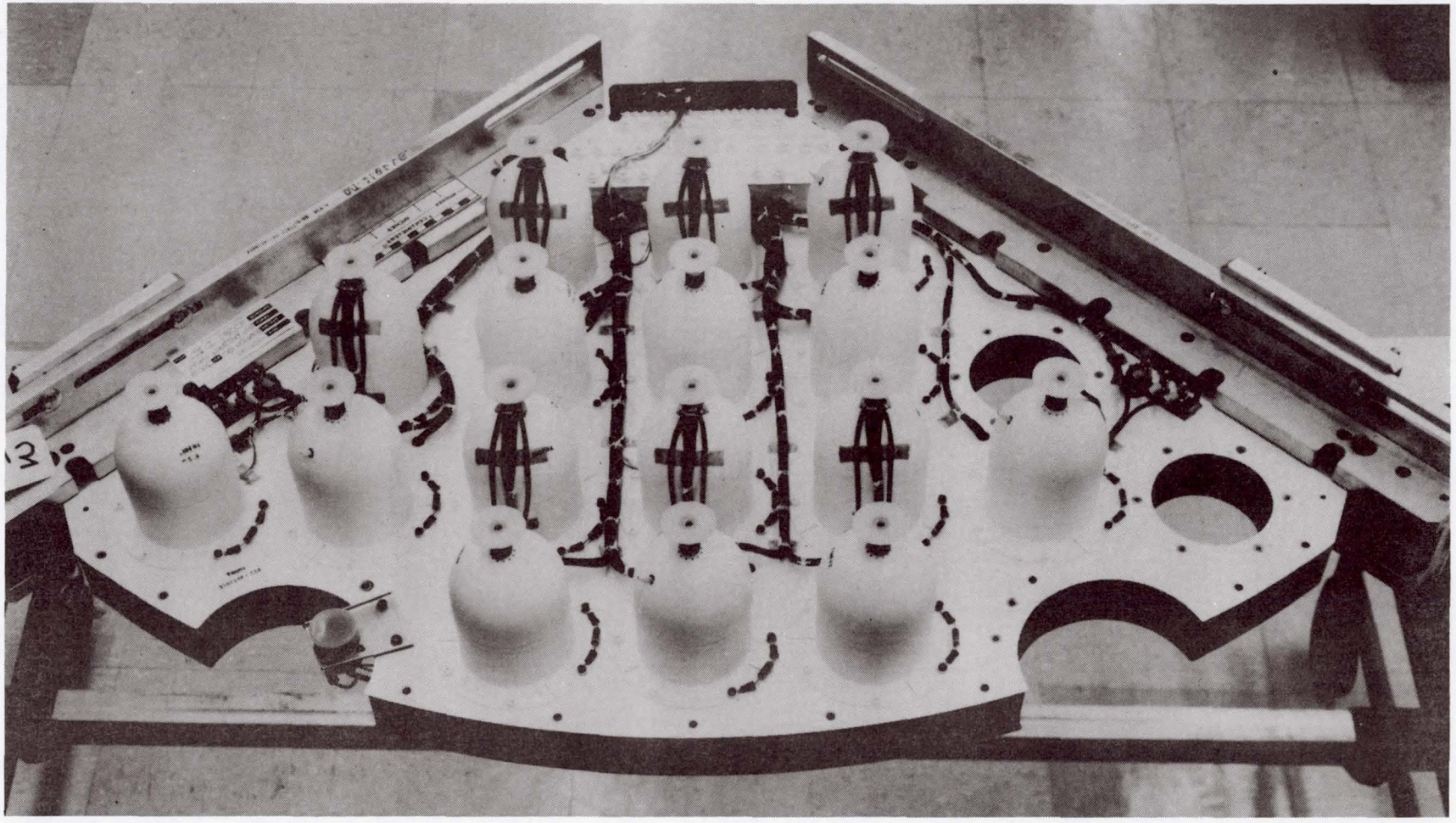

Figure 3-9. One quadrant of INTELSAT VI nickel-hydrogen batteries.

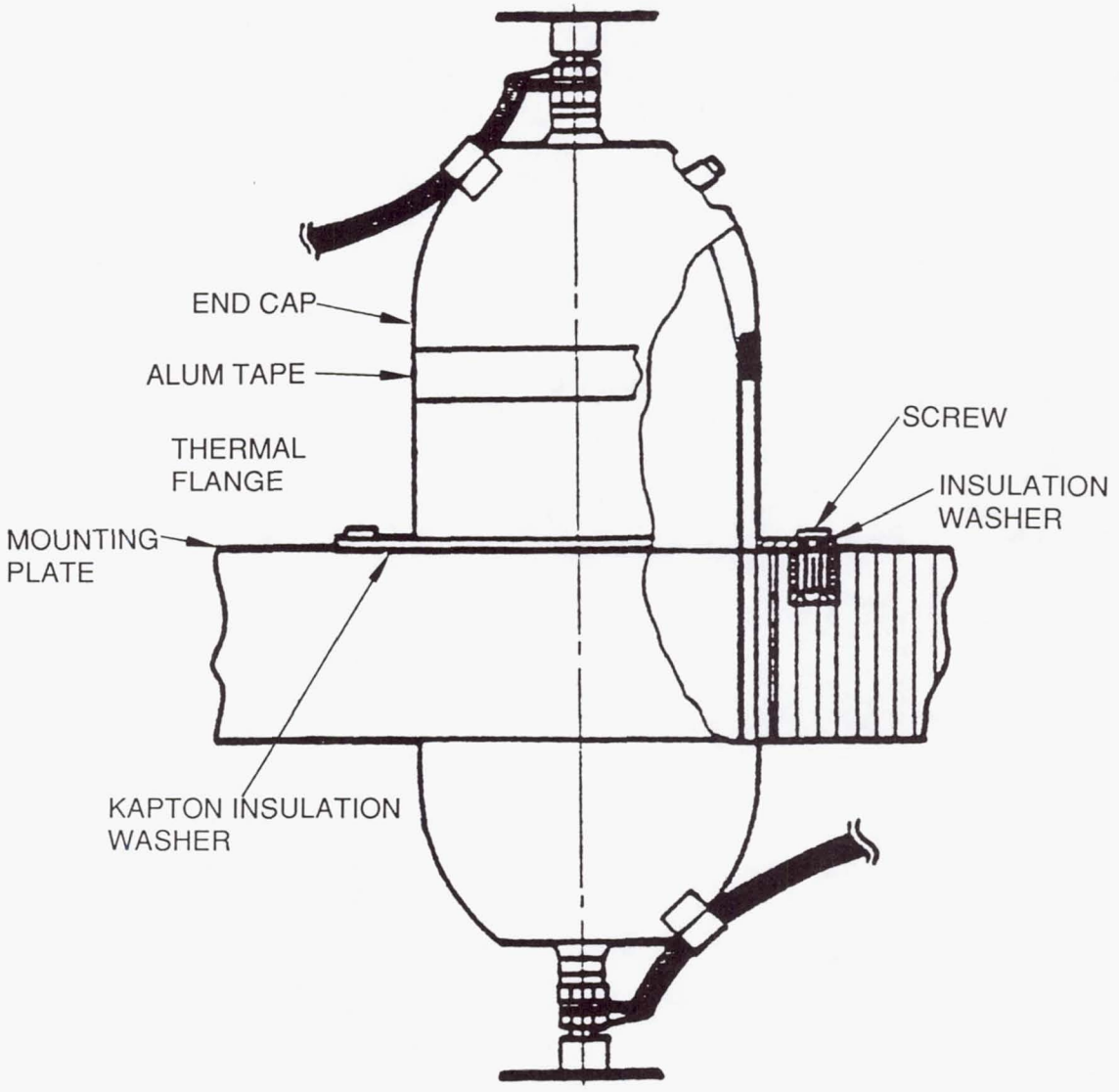

Figure 3-10. Battery cell installation.

A Kapton insulation washer is used on the battery mounting panel to provide redundant insulation between the cell and ground (Figure 3-10). Epoxy fiberglass shoulder washers are used to keep the cell mounting screw from shorting the cell flange to ground. After the cell is mounted to the panel, a resistor with a resistance value of 10,000 ohms is mounted on top of the cell flange for a static electricity ground.

The selection of the three-piece aluminum collar and flange assembly was described in a previous study [3-13]. (The nickel-hydrogen battery cell assembly described in Reference 3-13 was for a different program, but the three-piece aluminum collar and flange arrangement used for INTELSAT VI is similar in design.)

Thermal Design

The INTELSAT VI is a spin-stabilized satellite, cylindrical in shape, 6.4 m high, and 4.0 m in diameter in the stowed condition. A deployable cylindrical solar panel increases the height to 11.8 m. The solar panels are the radiating surfaces for the satellite.

Battery temperature is controlled passively by heat radiation to space from the battery cell end caps, the cell mounting flanges, and the battery mounting panel. The thickness of end caps, thermal flange, and mounting panel facesheets are sized to achieve an average battery temperature between 0° and 10°C in orbit. Design goals are to maintain the battery temperature between 0° and 15°C.

The entire aft side of the battery pack is painted white to achieve the desired thermal properties for radiation purposes (Figure 3-9). The forward side is facing the interior of the spacecraft and is thermally isolated with its shiny aluminum surface from the internal spacecraft components.

Cell components aid in overall thermal management. The separator bridges the 0.040-in. gap from the cell stack to the cell wall and provides the primary thermal path to the thermal flange. Heat is conducted from the thermal flange to the white domes and to the battery shelf.

In addition to the passive temperature control described, charge control is used to minimize heat dissipated on overcharge. The batteries are recharged at the "medium" C/13 rate using a fixed c/d ratio of 1.05 and then switched to trickle charge at a C/55 rate.

During transfer orbit, battery heaters are used to keep the battery temperature above -7°C. Two temperature sensors mounted on the battery turn the heaters on and off automatically. Once the spacecraft is in geostationary orbit, the heater electronic command is permanently turned off.

Electrical Design

Features of the electrical design are as follows:

1. Bypass diodes are used to protect against an open-circuited cell.

2. A 43.2-ohm resistor is switched across the battery for reconditioning (two 86.4-ohm resistors in parallel).

3. A fixed c/d ratio is used for charge control of the battery: c/d = 1.05 at the C/13 rate, switched to C/55 trickle rate.

4. Pressure is monitored with temperature compensated strain-gauge bridges mounted on the domes of five cells per quadrant.

5. Individual cell voltages are provided through telemetry data.

6. During discharge, each battery sees a constant power load of 990 W.

Reconditioning. The batteries are reconditioned prior to each eclipse season. The batteries are discharged through a 43.2-ohm resistor until the first cell reaches 1.0 V. The batteries are recharged at the high rate, returning 100 percent of the capacity removed during discharge. The batteries are reconditioned one battery at a time, so at least one battery is always fully charged.

Charge Control. The batteries are recharged at a C/13 rate to a fixed c/d ratio of 1.05 and then switched to trickle charge at a C/55 rate.

All of the charge current switching functions are initiated by ground command. The ampere-hours removed during discharge are calculated by integrating the discharge current with time. The recharge time is calculated to return at the high charge rate 105 percent of the ampere-hours removed on discharge. At the appropriate time, a ground command is initiated to switch to the trickle rate.

Terminal Design. The terminal stud has an external thread for attaching the battery intercell wiring (Figure 3-11). Copper nuts are used on the high-conductivity nickel 201 terminal stud to prevent the development of high-resistance surface oxides. A beryllium copper spring washer is used to maintain the preload in the terminal connection along with the copper top nut. The battery cells are connected electrically with redundant AWG 10-gauge copper wire. All connecting wires are soldered to the copper lug prior to the tightening of the top nut [3-12], [3-14].

The cells are alternately installed with either the positive or negative terminal ends on the aft battery pack face in accordance with the cell's position in the series string. This is done to facilitate the interconnections between cells.

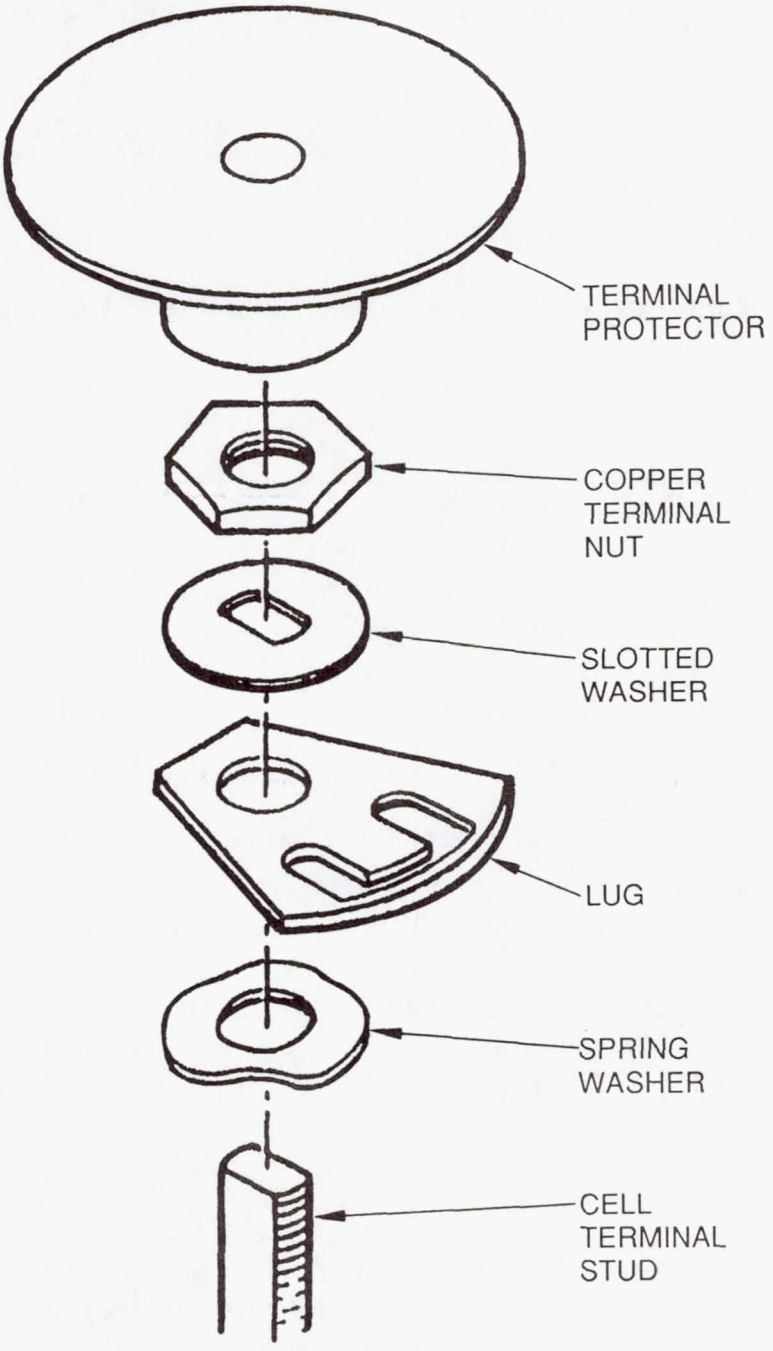

Figure 3-11. Battery cell terminal assembly arrangement.

The terminal protector, shown in Figure 3-11, has been replaced with shrink tubing to cover the terminal stud [3-26].

Load. The batteries are sized to accommodate an on-station load of 990 W maximum per battery for 1.2 hr, with one cell failed shorted and a 70-percent DOD at end of life.

$$\frac{44 \text{ Ah} \times 1.25 \text{ V/cell} \times 31 \text{ cells} \times 0.70}{1.2 \text{ hr}} = 994 \text{ W}$$

Weight and Energy Density

Table 3-4 provides a summary of the volume, mass, specific energy, and energy density.

Table 3-4. INTELSAT VI Batteries

Nameplate Capacity	44 Ah
Number of Cells per Battery	32 cells
Measured Capacity at 10°C	59 Ah*
Battery Shelf Assembly	1.6 m dia.
Height of Cells	26.9 cm
Volume of Battery	540,582 cm^3
Weight of Battery	66.3 kg
Weight of Cells	51.68 kg
Weight of Cells/Weight of Battery	77.9%
Average Cell Voltage (EOL)	1.25 V
Energy per Battery at 10°C	2,303 Wh
Specific Energy	34.7 Wh/kg
DOD (of rated capacity)	70%
Energy Density	0.00426 Wh/cm^3

* Reference 3-15 (initial capacity of INTELSAT VI cells at 10°C)

3.2.6 EUTELSAT II Ni-H_2 Batteries

The EUTELSAT II Ni-H_2 battery is designed to provide electrical energy for prelaunch, launch, transfer orbit, and geosynchronous orbit operations during solar eclipse periods and to meet peak load demands. The first of two flight sets of batteries was delivered in February 1990 and launched in August 1990 [3-16]. These EUTELSAT II batteries were designed and built by Eagle-Picher, Inc., (EPI) for Aerospatiale. The Ni-H_2 cells used are the second-generation cells as described in Chapter 1, Section 1.9.0, "Ni-H_2 Cells for the 1990s."

Ni-H_2 Cells

Salient features of the 58-Ah EUTELSAT II cells are as follows:

1. Back-to-back positive electrode stack design with the COMSAT configuration for electrode stack components and EPI dual-electrode stacks (tandem stack design).

2. INCONEL 718 pressure vessel with plastic compression seals.

3. Dry sinter plaque, electrochemically impregnated positive electrodes (aqueous process).

4. Asbestos separator material.

5. Platinum black negative electrodes with Teflon backing.

6. Electrolyte concentration of 31 percent KOH fully discharged.

7. Cell dimensions: diameter of 8.89 cm, length of 25.35 cm to end of terminals. Weight of each cell: 1.384 kg.

Mechanical Design

The battery cells are mechanically restrained by clamping them in a precision machined and anodized cast aluminum sleeve. The sleeves are in turn rigidly mounted to the anodized support plate using rivets through the foot of the sleeve and baseplate [3-16].

The domes on the top and bottom of the cells are painted black. The top dome is coated with Solathane 113 over the black paint to provide an added layer of insulation for the top dome. CHO-THERM, an insulating material, in sheet form (0.381 mm thick) is wrapped around the cylindrical section of the cell. The CHO-THERM overlaps the painted region with the Solathane coating to provide a double layer of insulation between the INCONEL pressure vessel wall and the aluminum sleeve. The aluminum sleeves clamp the cells, securing the wrap of CHO-THERM in place. This CHO-THERM cell/sleeve interface serves to both electrically isolate the cell from the battery structure and enhance thermal conduction [3-16]. RTV 142 is used to seal the CHO-THERM/cell/sleeve interfaces at the foot of the sleeve prior to riveting and between the top of adjacent sleeves to promote structural and thermal integrity along with added electrical/corrosion protection. Twenty-seven cells connected in series constitute one battery (Figure 3-12).

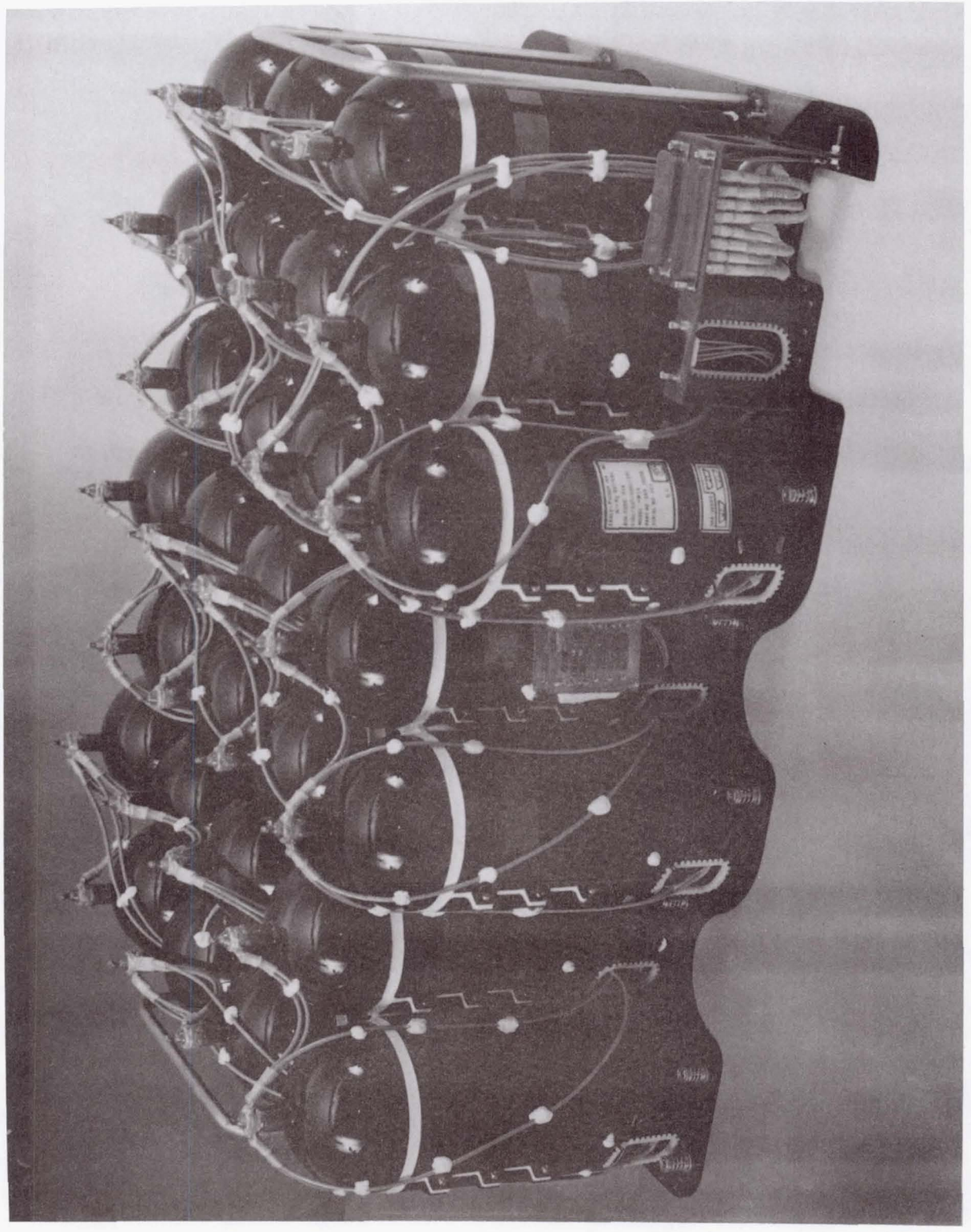

Figure 3-12. EUTELSAT II nickel-hydrogen battery.

Thermal Design

The thermal design for EUTELSAT II is basically the same concept as the INTELSAT V thermal design. Heat generated in the cell stack is conducted radially through the CHO-THERM layer to the aluminum sleeve, down the aluminum sleeve to the baseplate, and from the baseplate to the backside of the OSRs which radiate into space (direct radiation design).

In addition to the passive means of thermal control described above, charge control is used to limit the temperature at the high end, and heaters are used to control the temperature at the low end. For the heaters, 27 redundant heaters are mounted to the individual sleeves. These heaters are capable of dissipating a total of 40 watts per battery. Thermistors are located on the top domes of three cells to monitor the temperature of the battery.

Electrical Design

Features of the electrical design are as follows:

1. Bypass diodes used to protect against an open-circuited cell.

2. Strain-gauge electronics to monitor the pressure.

3. Individual cell voltage monitoring.

Bypass Diodes. The diodes are mounted at the bottom of the aluminum sleeve in brackets designed to rigidly support these devices. This cavity region below the cells and just above the support plate provides a protected location for the diodes and a short conductive path for heat flow to the radiator.

Protection in the forward (charge) direction is provided by three silicon diodes in series, while protection in the reverse (discharge) direction is provided by one silicon diode.

Strain-Gauge Electronics. Two cells in each battery are instrumented with a temperature-compensated strain-gauge bridge circuit. The bridge circuit is powered from the battery. The output from the bridge circuit is amplified to provide a 0- to 5-V signal output for the telemetry interface.

Weight and Energy Density

Table 3-5 provides a summary of the volume, mass, specific energy, and energy density.

Table 3-5. EUTELSAT II Battery

Nameplate Capacity	58 Ah
Measured Capacity 10°C	70 Ah
Battery	
length	60 cm
width	45 cm
height	27 cm
Volume of Battery	72,900 cm^3
Weight of Cell	1.385 kg
Weight of 27 Cells	37.39 kg
Weight of Batteries	48.60 kg
Weight of Cells/Weight of Battery	76.9%
Energy of Battery 10°C	2,363 Wh
Specific Energy (meas. cap.)	48.6 Wh/kg
DOD (of rated capacity)	74%
Energy Density	0.0324 Wh/cm^3

3.3.0 LEO BATTERY DESIGNS

As described above, there are a number of GEO satellites in orbit with nickel-hydrogen batteries as the energy storage subsystem. Performance of these different battery systems in orbit, along with the expertise gained in the fabrication of these batteries, is providing a valuable database for this technology.

For LEO applications, the in-orbit database is small at present; it is limited to the Hubble Space Telescope program. New programs, such as Space Station Freedom, need to rely on ground test data to verify their design approach, particularly for performance data.

The need for an LEO database was pointed out in Reference 3-17 by M. J. Milden and C. C. Badcock in 1984. They formulated a test program to be conducted at the Naval Weapons Support Center at Crane, Indiana. This program is needed to establish a large database for life/reliability predictions of Ni-H_2 cells in LEO applications. As mentioned in the above Reference 3-17, the ultimate database is, of course, flight data.

3.3.1 Air Force Nickel-Hydrogen Battery Space Experiment

The Space Experiment Program involved the design, development, manufacture, qualification, and flight test of a 21-cell, 50-Ah Ni-H_2 battery [3-18]. The purpose of the Space Experiment was to evaluate the performance characteristics of the Ni-H_2 battery system in an LEO space environment. This battery was launched as an experiment on an Air Force satellite in 1977. Over a seven-month flight period the battery was successfully subjected to a multiple cycle test regime. Eagle-Picher Industries was the prime contractor for this experimental battery.

Cell Design

Salient features of the Air Force 50-Ah experimental cells are as follows:

1. Pineapple-slice configuration with back-to-back positive electrode stack design [3-18].

2. Polysulfone core design with the tabs brought out through the center of the core.

3. INCONEL-625 pressure vessel with both the positive and negative terminals at one end of the pressure vessel, "rabbit ear terminals" with separate fill tube. Nylon Ziegler compression seals.

4. Electrochemically impregnated positive nickel-oxide electrodes (aqueous process). The nickel plaque was made using the wet slurry process.

5. EPI reconstituted fuel-cell-grade asbestos separator material.

6. Platinum black negative electrodes with Teflon backing.

7. Electrolyte concentration—38 percent KOH fully discharged.

8. Weight per cell: 1,890 g.

Mechanical Design

Because of a very short program time schedule and the major program objective of evaluating Ni-H_2 system performance characteristics, the design philosophy made maximum use of established and proven Ni-Cd battery space technology. The battery case design (one-piece casting) and cell assembly technique was influenced by EPI's Ni-Cd battery design. This philosophy permitted timely and successful program completion, but did not allow optimization of the battery design with respect to weight or energy density.

A view of the battery is shown in Figure 3-13. The 21 Ni-H_2 cells were housed in an investment cast aluminum housing using aluminum A-356-T61 alloy.

Thermal Design

The design goal was to operate the battery between 4.5° and 10°C. The low temperature limit was maintained by use of two 10-W redundant integral heaters, which could be powered by either the host vehicle or the battery itself. A passive cooling technique was utilized which featured a nonadjustable 5-W dissipation window. A charge voltage cutoff was selected to achieve 90 percent state-of-charge and to minimize heat dissipation on overcharge.

Electrical Design

Key features of the electrical design were the following:

1. A temperature-compensated voltage limit was used for charge control.

2. The pressure was monitored using a strain-gauge bridge mounted on the dome of the cell. Cell pressure proved to be an accurate indicator of the state-of-charge of the battery. There was good correlation between the voltage cutoff at 90 percent SOC and the measured cell pressure between 490 and 500 psig.

Weight and Energy Density

Table 3-6 presents a summary of the volume, mass, specific energy, and energy density values.

Table 3-6. Air Force Experimental Battery

Nameplate Capacity	50 Ah
Measured Capacity (20°C)	55 Ah
Battery Dimensions	64.64 x 43.89 x 26.82 cm
Battery Volume	76,102 cm^3
Battery Weight	50 kg
Cell Weight	1.89 kg
Weight of 21 Cells	39.7 kg
Weight of Cells/Weight of Battery	79%
Energy of Battery (10°C)	1,444 kW
Specific Energy	28.87 Wh/kg
Energy Density	0.0182 Wh/cm^3

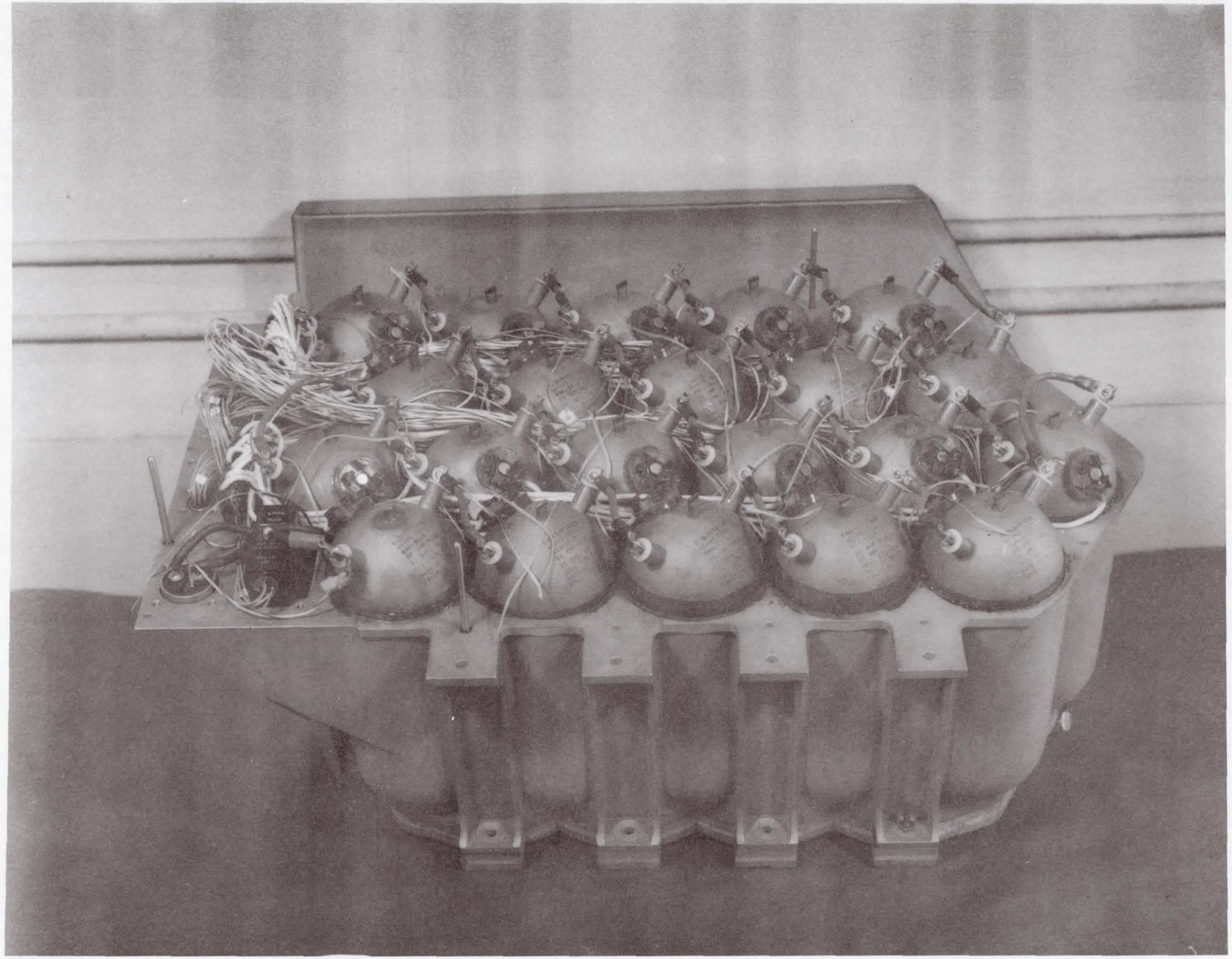

Figure 3-13. Air Force nickel-hydrogen battery space experiment.

There was no fixed DOD. A variable load bank provided four different loads for discharging the battery. Shallow DOD cycles (7 percent) were accumulated during periods in which the battery was used to supply power to the actual spacecraft bus.

3.3.2 Hubble Space Telescope

The Hubble Space Telescope (HST) was launched on April 24, 1990. The HST Ni-H_2 battery modules were designed by Lockheed Missiles & Space Company (LMSC) and manufactured by Eagle-Picher Industries (EPI) for Marshall Space Flight Center (MSFC). These Ni-H_2 battery modules replace the Ni-Cd batteries originally selected for this mission [3-19]. The requirements for longer lifetime and higher capacity resulted in the selection of the Ni-H_2 batteries instead of Ni-Cd batteries.

The HST operates in a 300-nautical-mile low-earth orbit. The orbit period is 96 minutes, approximately 35 minutes in eclipse and 61 minutes in sunlight. The total HST load ranges between 1,900 and 2,100 watts. The DOD ranges between 5 to 8 percent [3-20], as shown in Figure 3-14.

Cell Design

The HST 88-Ah Ni-H_2 cell design features were discussed in Chapter 1, Section 1.9.3, "Hubble Space Telescope Ni-H_2 Cell."

A polysulfone endplate with a polysulfone retaining nut and Belleville washers were used to keep the electrode stack at the required preload. Both positive and negative electrode tabs exit the same end of the electrode stack, allowing for both terminals to be located on the same end of the pressure vessel (Figure 3-15). This rabbit ear design feature allowed the Ni-H_2 battery module to fit into the limited space available in the designated battery equipment bay. The positive and negative terminals are each positioned 45° from the longitudinal axis. The seals are nylon Ziegler compression seals with the terminal bosses electron beam welded to the dome.

A unique feature of this design is the 0.040-inch-thick INCONEL pressure vessel. The maximum cell operating pressure is 1,200 psi. The pressure vessel is designed for a 4/1 safety factor. Burst pressure for this cell is over 4,800 psi.

The cells were activated with 27 percent KOH electrolyte in the charged state to promote long cyclic lifetime in orbit (31 percent KOH discharged).

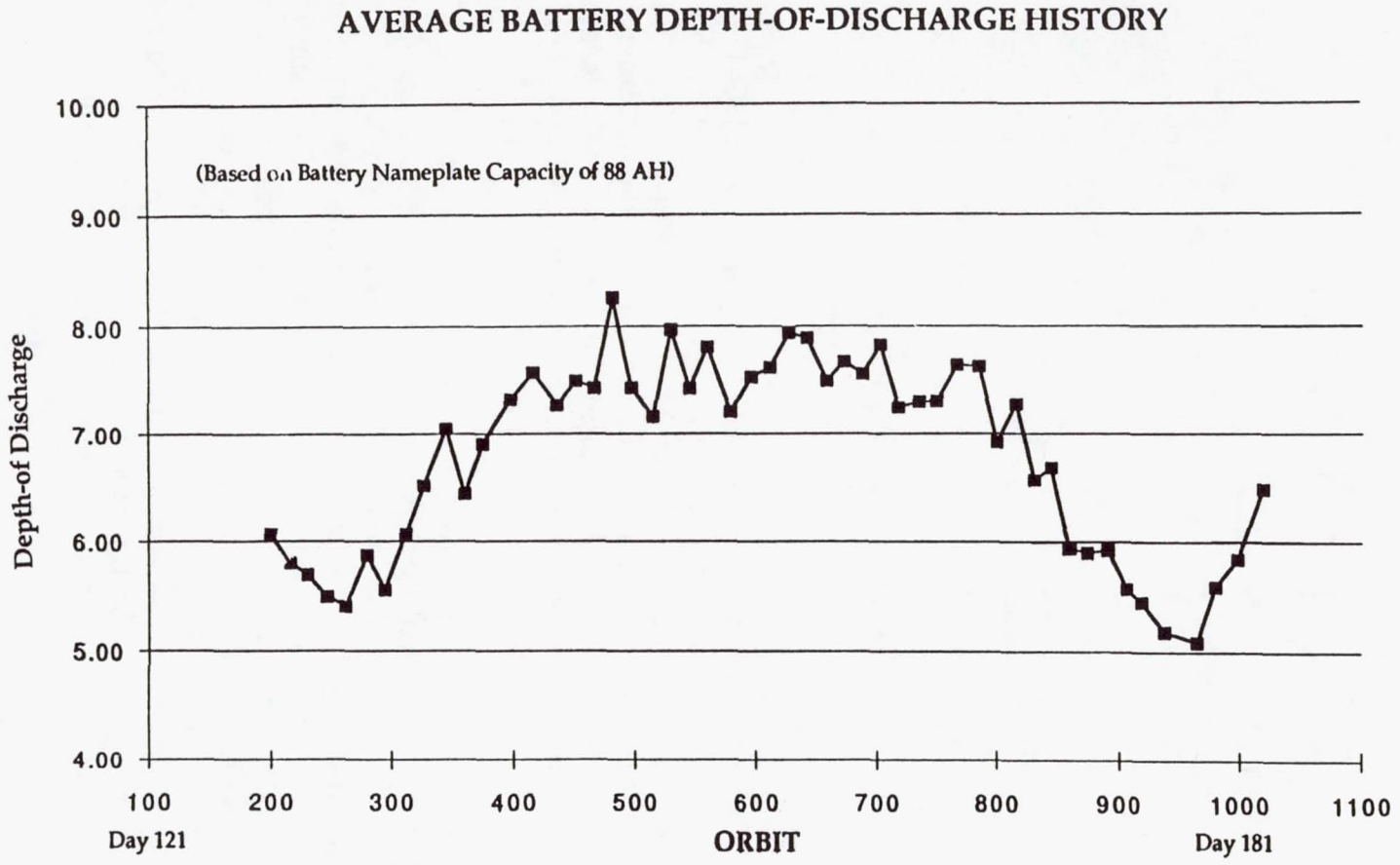

Figure 3-14. HST nickel-hydrogen battery depth of discharge.

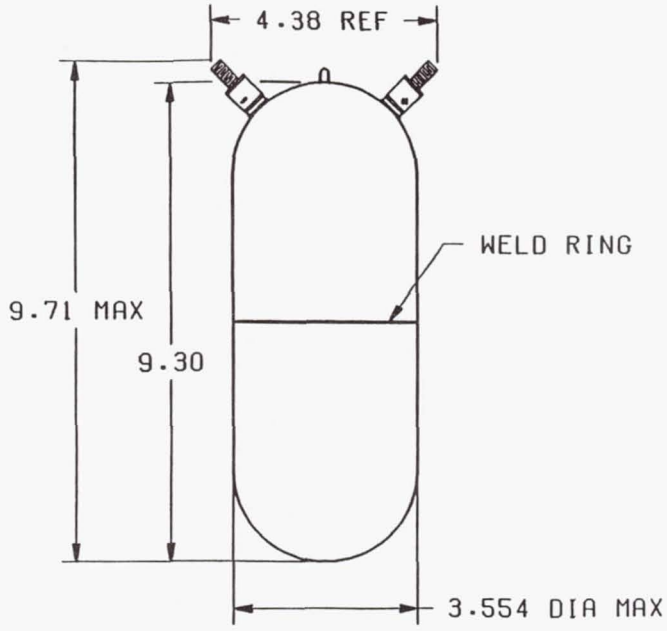

Figure 3-15. HST cell envelope.

Mechanical Design

Each cell is wrapped with a silicone-coated fiberglass cloth (CHO-THERM) for electrical insulation and then clamped with a cast aluminum sleeve. These sleeve/cell assemblies are fastened to a battery baseplate that is fabricated from a 0.125-inch aluminum base material. A support tube with the same diameter as each sleeve/cell assembly is attached to the baseplate. This support tube is located in the middle of the battery and provides support for the top cover of the module (Figure 3-16).

Module Design. As seen in Figure 3-16, three batteries are housed in an aluminum enclosure and mounted to a half-inch aluminum baseplate to form the battery module [3-19]. The battery connector brackets are fastened to the module connecting plate as shown. A three-sided enclosure assembly surrounds the rest of the three batteries. A cover encloses the top of the batteries and is bolted to the support tubes to provide overall structural integrity. The inside surfaces of the cover and enclosure are lined with polyamide foam for electrical short protection. Two bright yellow handles are fastened to the cover for astronaut handling of the modules in orbit. The module baseplate has 14 astronaut ORU latches to facilitate mounting. This 460- to 470-pound unit can be replaced in orbit by disconnecting three power and three telemetry wing-tabbed connectors and disengaging the 14 ORU latches.

Thermal Design

Design objectives were to maintain the temperature of the batteries with the primary heater elements.

Dual element heater strips are bounded at the inside bottom of each of the aluminum sleeves. The primary heater elements are switched on when the temperature of the battery drops below 0°C, and they are switched off when the temperature exceeds 2°C. The secondary heater elements switch on at -4°C. The design objective was to have the primary heater elements control the battery temperature and to use the secondary heater elements if the temperature of the battery dropped below -4°C [3-20].

As described above, the cast aluminum sleeve/cell assemblies were fastened to the aluminum baseplate module. The modules were mounted onto an anti-sun facing surface that viewed deep space. The radiator area was slightly oversized to dissipate the heat generated by the battery and the heat generated by the heaters on a 30- to 50-percent duty cycle. The reflector surface, a flexible optical solar reflector (FOSR), was more flexible and easier to apply than the optical solar reflector OSR, but the FOSR reflector properties are not quite as good as the OSR reflector properties.

The heat dissipated by the battery on charge is limited by the temperature compensated voltage limit used for charge control to limit the charging current (refer to Chapter 2, Sections 2.1.2 and 2.1.3). The HST was launched with the temperature-compensated voltage limits for the batteries set at the K1-3 and K2-3 levels (see Figure 3-17). The temperature-compensated voltage limit is used to minimize ampere-hour overcharge. The batteries were recharged to 83 to 85 percent state-of-charge at the beginning of life. During normal operation, the batteries are switched to a low trickle-charge rate once they reach the voltage limit. With the voltage limits of K1-3 and K2-3 and with the trickle-charge, the batteries/cells state-of-charge gradually increased with cycling, asymmetrically approaching 100 percent state-of-charge. During safemode operation the batteries remain on the voltage limit during overcharge and the current tapers off. During overcharge, all of the energy is dissipated as heat and, since the taper charge current is higher than the trickle charge current, more heat is being dissipated by the battery in safemode.

During the first 181 days of operation the battery temperature performance was as follows [3-21]:

- Normal operation temperature range of -1.5°C to 3.0°C
- Safemode (hardware charging) maximum temperature of 5.5°C
- Batteries operating on primary heater
- Secondary heaters not being used.

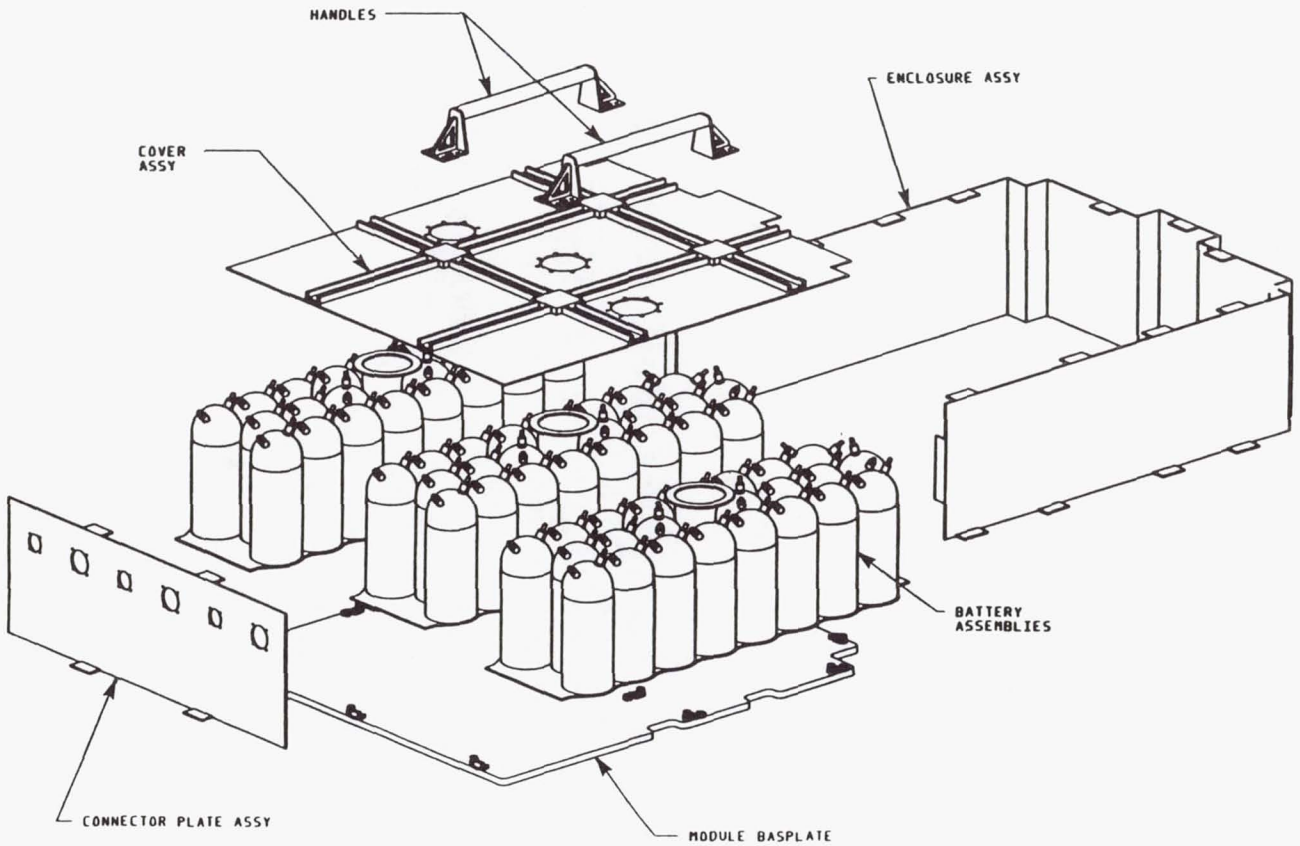

Figure 3-16. HST nickel-hydrogen battery module assembly.

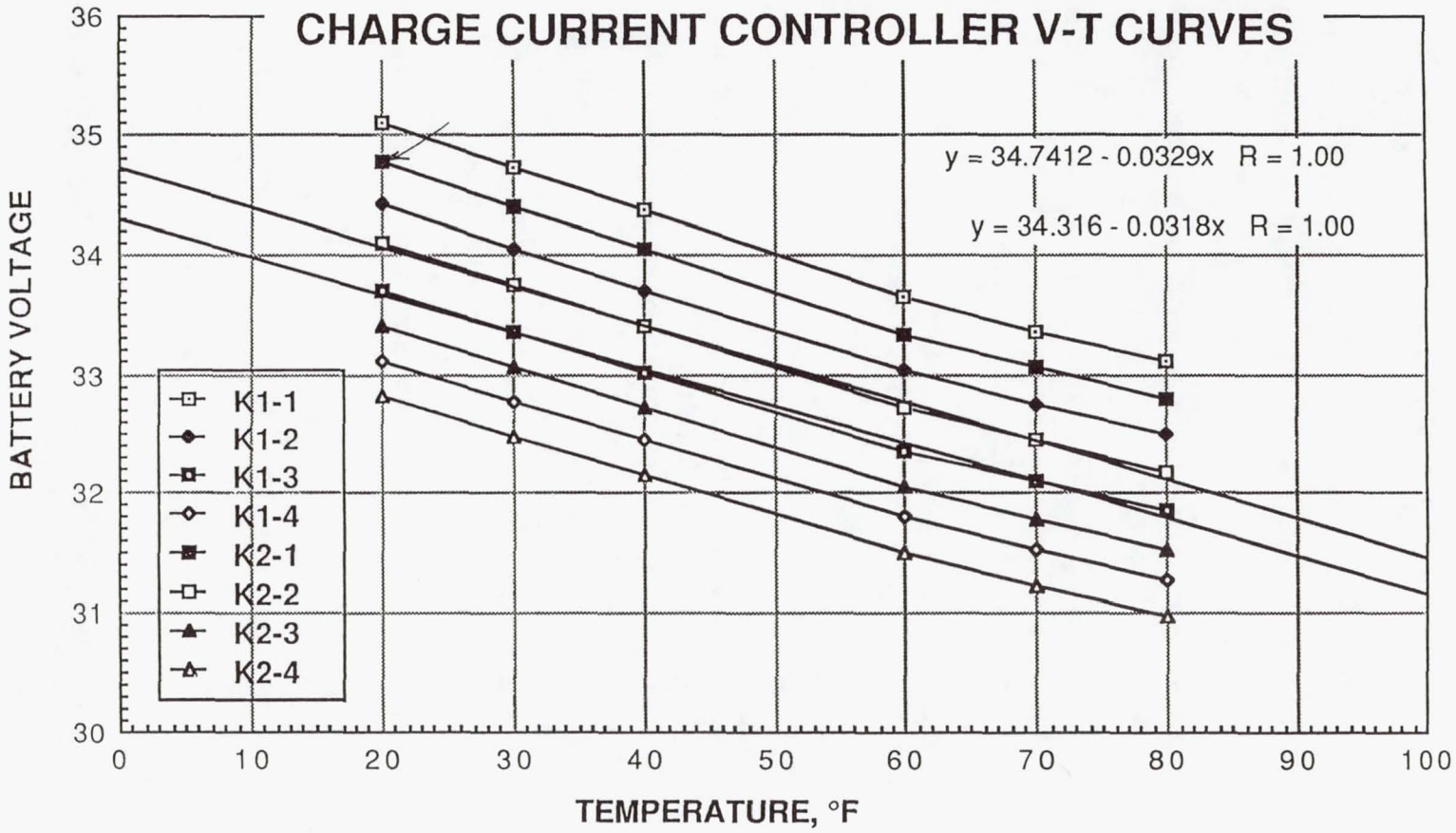

Figure 3-17. HST charge current controller V-T curves.

Electrical Design

Key features for the electrical design are as follows:

1. Bypass diodes not used.

2. A temperature-compensated voltage limit used for charge control of the battery.

3. Pressure monitored using a strain-gauge bridge mounted on the dome of the pressure vessel.

Bypass Diodes. Bypass diodes are not used with the HST; six batteries share the load on board the satellite. If one of these batteries should fail (due to an open-circuited cell) the remaining five batteries could share the load without a significant increase in the DOD (an increase from 8 to 10 percent DOD). Even two batteries could fail without major concern, and in time the battery module would be replaced by the astronauts. The disadvantages of the bypass diodes are that they add a considerable amount of weight and complexity to the system, which would more than offset any advantages they could offer.

Temperature-Compensated Voltage Limit Charge Control. Four different temperature-compensated voltage limits can be selected for both the K1 and K2 relays, resulting in eight charge-cutoff voltage levels for charge control of the battery (Figure 3-17) [3-20]. On charge under normal operation, when the battery voltage reaches the voltage limits set, the current is switched in two steps from the high rate C/8.8 (approximately 10 amperes) to a C/100 trickle rate. The voltage levels are set to maintain the battery at or about 85 percent state of charge while at the same time minimizing the heat dissipation or overcharge of the battery. The HST was launched using the K1-3 and K2-3 voltage levels. The K2-3 level (1.5 V/cell at 0°C) K2 relay switched the charge current from 10 A to 6.66 A and the K1-3 level (1.512 V/cell at 0°C) K1 relay switched the charge current from 6.66 A to the trickle rate of <1.2 A.

Two temperature-compensating charge control thermistors were bonded to the top of the cell vessels located in the middle of each battery. Two additional charge control thermistors were used for backup. If the battery begins to heat up, these thermistors would terminate the charge to prevent a thermal runaway condition.

Pressure. Each battery has two cell-pressure monitors. A strain-gauge bridge circuit is mounted on the dome of the cells. There are two active and two temperature-compensating dummy legs of each bridge circuit. The output from the strain-gauge bridge is amplified to generate a 1- to 5-V DC output, which corresponds to a cell pressure of 300 to 1,500 psi.

During the launch operation the pressure monitors provided the state-of-charge or capacity of the batteries at the launch site. Once in orbit, the pressure monitors were used to determine capacity, state-of-charge. A reconditioning conditioning cycle of two batteries in orbit verified the pressure data correlation with battery capacity [3-20].

Weight and Energy Density

As an ORU, the nickel/hydrogen module unit weight is 460 to 470 pounds. There are three 22-cell batteries per module. The batteries are rated at 88 ampere-hours. The actual measured capacity for the HST cells is 96 Ah at 10°C. The 96 Ah was measured under laboratory conditions where the batteries are fully discharged and recharged at a C/10 rate for 10 hours at 10°C followed by C/23 for 14 hours. Under actual operating conditions in orbit with the temperature-compensated voltage limit, the batteries reach a state-of-charge that is about 85 percent of the fully charged state. Using this V-T charge procedure, the actual EOC capacity in orbit is approximately 81.6 Ah (96 Ah x 0.85 = 81.6 Ah).

Table 3-7 presents a summary of the volume, mass, specific energy, and energy density:

Table 3-7. HST Battery

Nameplate Capacity (rated)	88 Ah
Measured Capacity (10°C)	96 Ah
Weight per Module	209 kg
Energy per Module (10°C)	7920 Wh
Specific Energy*	37.89 Wh/kg
DOD (of rated capacity)	8%

*Specific energy is based on measured capacity at 10°C.

3.3.3 Space Station Freedom Nickel-Hydrogen Battery System

The photovoltaic (PV) power subsystem for Space Station Freedom will use Ni-H_2 batteries for energy storage to support eclipse and contingency operations. These batteries will be designed for a 6.5-year design life expectancy and are configured as ORUs, permitting replacement of worn-out batteries over the anticipated 30-year station life [3-22].

The basic space station load requirement is 75 kW, which converts to a requirement of 90 kW of DC power from the battery to allow for downstream conversion and distribution losses (83.3 percent). Battery peak power of 130 kW is required for one 7.5-minute period during eclipse and one 7.5-minute period during sunlight. In support of infrequent contingency situations, the batteries must provide a minimum of 10 kW of load power during a full orbit following a worst-

case eclipse. Normal (DOD) depth-of-discharge for the battery is 35 percent with a design life of 38,000 cycles, and the maximum contingency (DOD) is 80 percent [3-23].

Energy Storage Requirement

$$\frac{\text{Load (W)} \times \text{Discharge Time (h)}}{\text{DOD} \times \text{Eff Regulator}} = \text{Energy Storage}$$

$$\frac{75\ \text{kW} \times (36/60)\ \text{h}}{0.35 \times 0.833} = 154\ \text{kWh}$$

To meet this energy storage requirement and also to provide for support of infrequent contingency situations, the baseline energy storage system design consists of 24 batteries. Each battery comprises 76 cells packaged in two 38-cell assemblies (Figures 3-18 and 3-19). The capacity of the cells is 81 Ah.

Cell Design

The cell configuration and component design features represent the integration of technology developed by Gates Energy Products and Space Systems/Loral. These were the cell design features as reported in Reference 3-24.

The Space Station 81-Ah Ni-H_2 cell design features are as follows:

1. Pineapple-slice configuration with recirculating positive electrode design, dual-stack.
2. Polysulfone core design.
3. INCONEL 718 pressure vessel, 3.5-inch diameter. Maximum BOL operating pressure of 900 psia with a 3/1 safety factor.
4. Electrochemically impregnated positive nickel-oxide electrodes, aqueous process. (The porosity of the nickel plaque is 81 percent and the loading of the positive electrode is 1.55 g/cc void.)
5. Zircar separator material with wall wick.
6. Platinum black negative electrode with Teflon backing.
7. Electrolyte concentration between 26 percent and 31 percent KOH being evaluated.
8. Cell assembly weight and length limited to 2.15 kg and 34.3 cm.

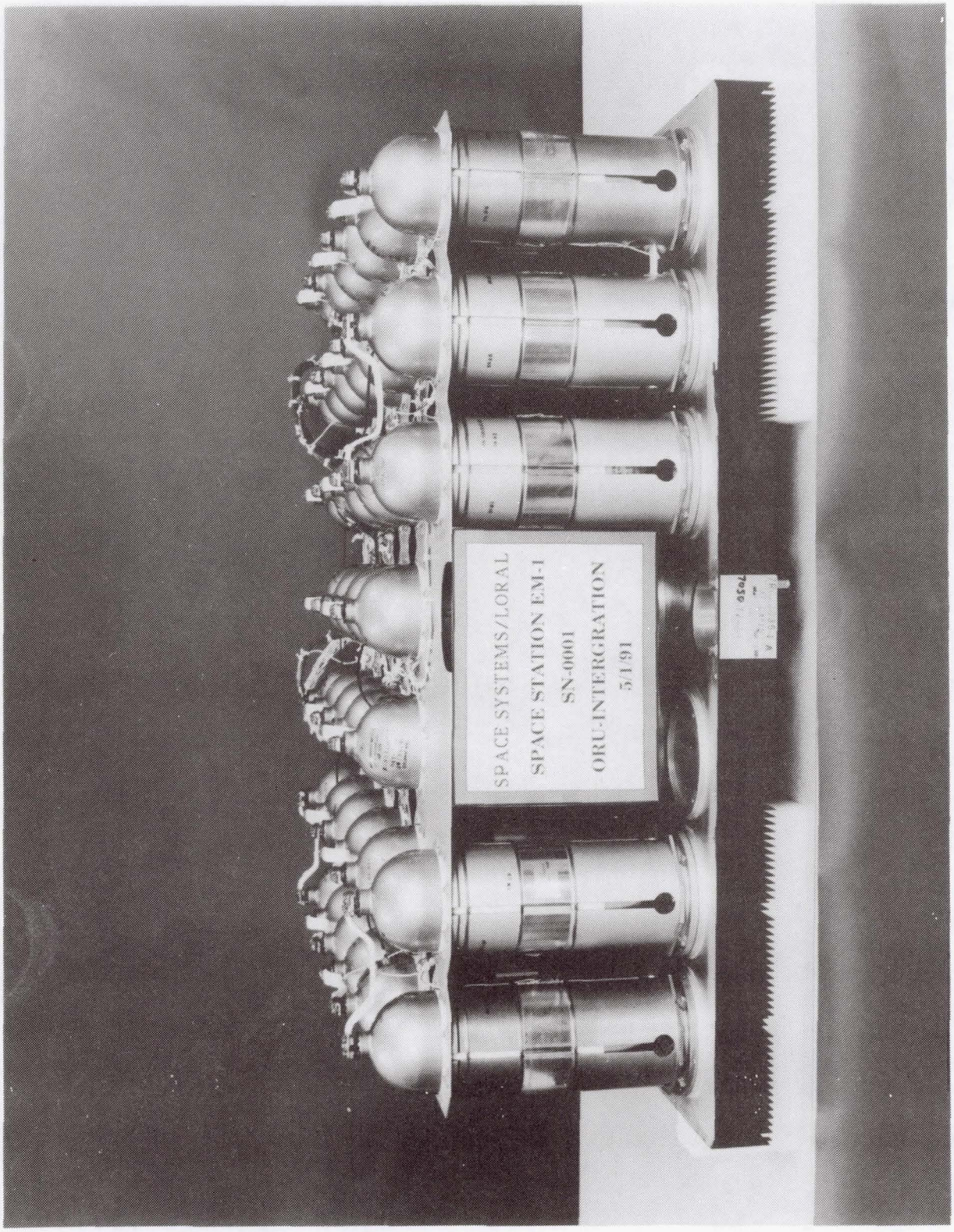

Figure 3-18. SSF nickel-hydrogen cells.

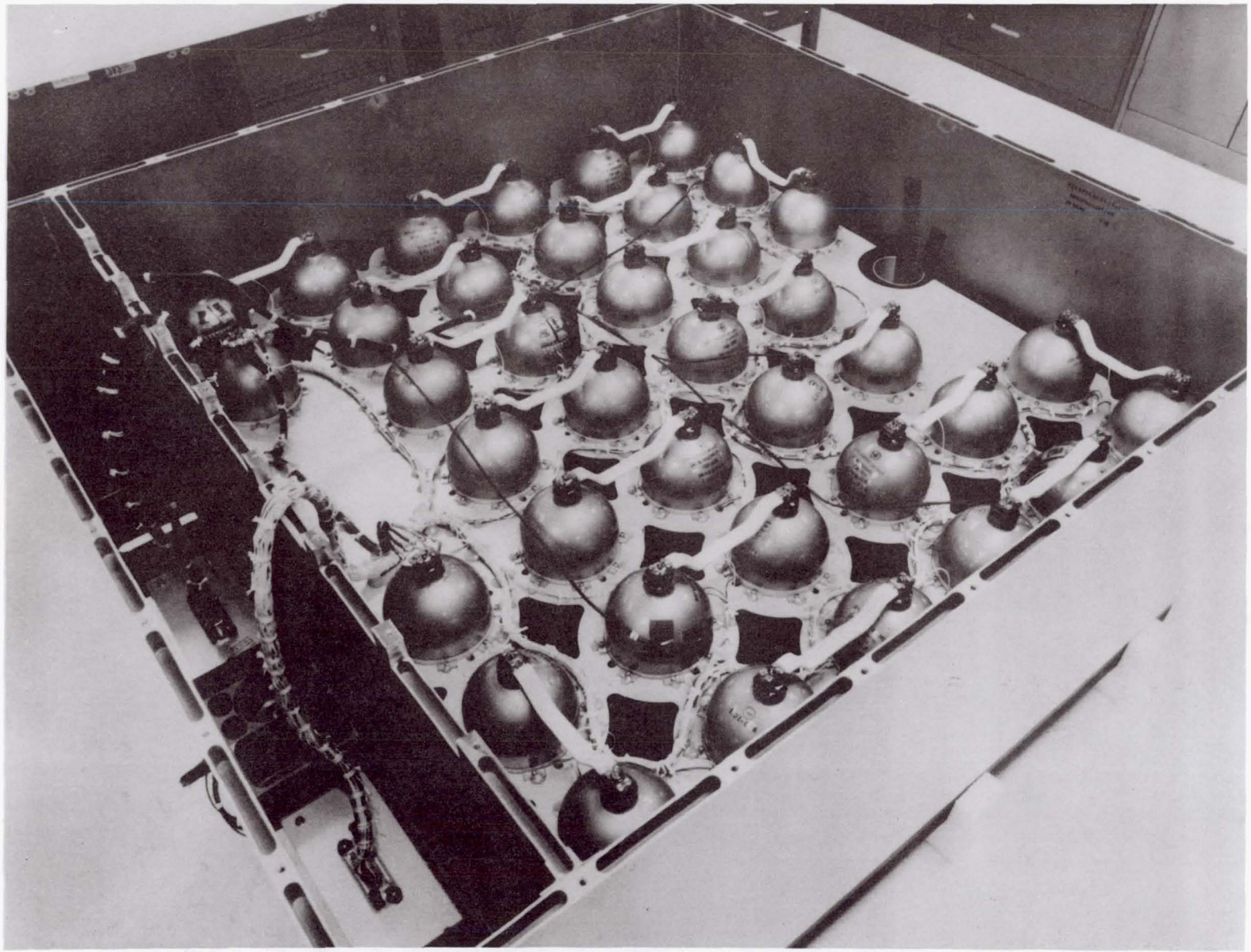

Figure 3-19. SSF 38-cell assembly.

Mechanical and Thermal Design

The Space Station Freedom battery assembly (ORU) will incorporate thirty-eight 81-Ah cells into a 7 x 6 cell matrix (less 4 cells). The cells are installed in thermally optimized sleeves attached to a baseplate. Heat is transferred by conduction from the baseplate of the battery to the active thermal control system of Space Station Freedom. The battery assembly with the enclosure is designed for orbital replacement. A shipset (also called a module) of batteries will consist of six batteries, each consisting of two series connected battery assemblies (ORUs) of 38 cells each. Space Station Freedom will utilize four modules of batteries.

The battery assembly (ORU), shown in Figure 3-20, contains a 7 x 6 rectangular matrix of cells/sleeve subassemblies on a baseplate 86.10 x 78.48 cm. These subassemblies are structurally interconnected with lightweight brace structures.

The battery assembly mounts structurally to a finned baseplate in the ORU enclosure. The enclosure is mounted to a mated finned plate by a locating and attachment mechanism compatible with robotic or EVA tools. This single action installation of an ORU also mates electrical connectors and establishes the radiative thermal coupling between the battery and the thermal control system.

The thermal control objective is to maintain 5°C, ± 5°C, at the midpoint of the cell stack during normal operation and 0°C to 20°C during off-normal operation. A heater/load circuit with relays in each battery assembly supports off-line battery discharge operations and heating in low dissipation modes.

Electrical Design

Key features of the electrical design are as follows:

1. Pressure monitored using a temperature-compensated strain-gauge bridge mounted on the dome of a pressure vessel.

2. Individual cell voltage monitoring.

3. Thermistors are used for backup charge control.

4. A fixed c/d ratio is used for charge control. This processor-based charge management technique provides the capability to impose an end-of-charge current taper profile and trickle charge.

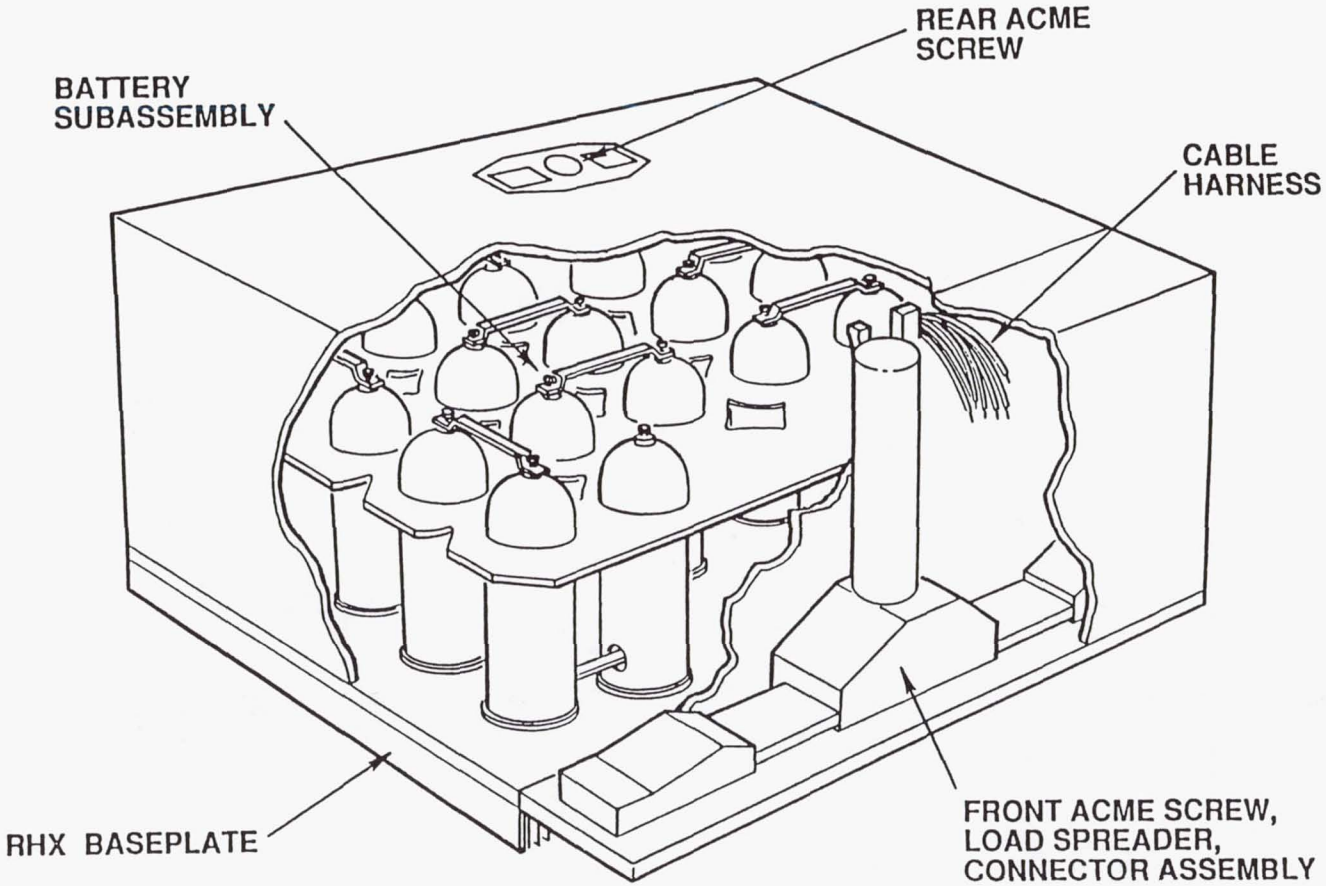

Figure 3-20. SSF battery ORU.

Weight and Energy Density

The Ni-H_2 battery ORU performance projections are presented in Table 3-8. The mass is 172.9 kg, the measured capacity is 89 Ah, and the dimensions are 91.44 x 101.6 x 44.45 cm.

Table 3-8. Space Station Freedom Battery

Number of Cells/Assembly	38 cells
Rated Capacity	81 Ah
Measured Capacity 10°C	89 Ah
Stored Energy/Assembly	4,227 Wh
Weight/Assembly	172.9 kg
Weight of 38 Cells	82.4 kg
Weight of Cells/Weight of Assembly	47%
Specific Energy	24.4 Wh/kg
DOD (of rated capacity)	35%
Volume of Assembly	413,028 cm^3
Energy Density	0.010 Wh/cm^3

3.4.0 SUMMARY

A summary of all the battery systems presented in this chapter follows.

3.4.1 GEO Applications

NTS-2 (Launch 1977)

Application:	inclined-orbit satellite, 3-year design life
Capacity:	35-Ah cells, 14 cells/battery
No. Batteries:	2
Cell Support:	machined aluminum sleeves
Insulation:	RTV silicon rubber and fiberglass (0.254 mm)
Baseplate:	magnesium thorium
Charge Control:	battery temperature charge control
Protection:	no bypass diodes
Reconditioning:	none
Radiator:	anti-sun side, white paint; direct radiator design
Specific Energy:	36.5 Wh/kg
DOD:	60%

INTELSAT V (Launch 1983–1987, eight satellites)

Application:	GEO satellite, 7-year design life
Capacity:	30-Ah cells, 27 cells/battery
No. Batteries:	2 batteries/spacecraft
Cell Support:	cast aluminum sleeves
Insulation:	flexible RTV silicon rubber sheet (0.254 mm)
Baseplate:	aluminum with cutouts
Charge Control:	fixed c/d ratio by ground command
Protection:	bypass diodes
Reconditioning:	fixed resistor across battery prior to each eclipse season
Radiator:	north/south panel with OSRs; direct ratiator design
Specific Energy:	40.0 Wh/kg
DOD:	56% (6 satellites) 67% (2 satellites)

Superbird (launch 1988)

Application:	GEO satellite, 10-year design life
Capacity:	83-Ah cells, 27 cells/battery
No. Batteries:	2 batteries/spacecraft
Cell Support:	machined aluminum sleeve
Insulation:	flexible reinforced RTV silicon sheet (0.254 mm)
Baseplate:	Honeycomb panel N/S panel opposite OSR
Charge Control:	fixed c/d ratio by ground command
Protection:	no bypass diodes
Reconditioning:	fixed resistor across battery prior to eclipse season
Radiator:	north/south panel with OSRs; direct radiator design
Specific Energy:	48.3 Wh/kg
DOD:	75%

INTELSAT VII (launch 1993)

Application:	GEO satellite, 10-year design life
Capacity:	85.5-Ah cells, 27 cells/battery
No. Batteries:	2 batteries/spacecraft
Cell Support:	machined aluminum sleeves *graphite/epoxy sleeves
Insulation:	flexible reinforced RTV silicon sheet (0.254 mm)
Baseplate:	Honeycomb panel N/S panel opposite OSRs
Charge Control:	fixed c/d ratio by ground command
Protection:	bypass diodes
Reconditioning:	fixed resistor across battery prior to each eclipse season
Radiator:	north/south panel with OSRs; direct radiator design

Specific Energy:	49.1 Wh/kg
	*52.7 Wh/kg
DOD	70%

*Lightweight INTELSAT VII design with graphite/epoxy composite sleeves

Spacenet (Launch 1984, two satellites)

Application:	GEO satellite, 7-year design life
Capacity:	40-Ah cells, 22 cells/battery
No. Batteries:	2 batteries/spacecraft
Cell Support:	titanium rings support the cell at each end
Baseplate:	magnesium
Charge Control:	fixed c/d ratio by ground command
Protection:	bypass diodes
Reconditioning:	resistor across each cell prior to each eclipse season
Radiator:	indirect radiator design
Specific Energy:	41.16 Wh/kg
DOD:	60%

GSTAR (Launched 1985–1986, two satellites)

Application:	GEO satellite, 7-year design life
Capacity:	30-Ah cells, 22 cells/battery
No. Batteries:	3 batteries/spacecraft
Cell Support:	titanium rings support the cells at each end
Baseplate:	magnesium
Charge Control:	fixed c/d ratio by ground command
Protection:	No bypass diodes
Radiator:	indirect radiator design
Specific Energy:	38.96 Wh/kg
DOD:	60%

INTELSAT VI (Launched 1989–1991, five satellites)

Application:	GEO satellite, 10-year design life
Capacity:	44-Ah cells, 32 cells/battery
No. Batteries:	2 batteries/spacecraft
Cell Support:	three-piece aluminum collar and flange assembly
Insulation:	frozen epoxy film adhesive with fiberglass
Baseplate:	aluminum honeycomb panel
Charge Control:	fixed c/d ratio by ground command
Protection:	bypass diodes

Reconditioning:	resistor across battery prior to each eclipse season
Radiator:	direct radiation to space from the battery cell end caps, mounting flanges, and mounting panel
Specific Energy:	34.7 Wh/kg
DOD:	70%

EUTELSAT II (Launch schedule 1990–1991, five satellites)

Application:	GEO satellite, 10-year design life
Capacity:	58-Ah cells, 27 cell per battery
No. Batteries	2 batteries/spacecraft
Cell Support:	cast aluminum sleeves
Insulation:	CHO-THERM (0.254 mm thickness)
Baseplate:	aluminum
Charge Control:	fixed c/d ratio
Protection:	bypass diodes
Reconditioning:	fixed resistor across battery prior to each eclipse season
Radiator:	direct radiator design
Specific Energy:	48.6 Wh/kg
DOD:	74%

3.4.2 LEO Applications

Air Force Ni-H_2 Battery Experiment (Launched 1977)

Application:	LEO satellite, short design life
Capacity:	50-Ah cells, 21 cells/battery
Cell Support:	cells contained in cast aluminum housing
Charge Control:	temperature-compensated voltage limit
Protection:	no bypass diodes
Specific Energy:	28.87 Wh/kg
DOD:	7%

Hubble Space Telescope (Launch 1990)

Application:	LEO satellite, 5- to 7-year design life
Capacity:	88-Ah cells, 22 cells/battery
No. Batteries:	6 batteries/spacecraft
Cell Support:	cast aluminum sleeve
Insulation:	silicon-coated fiberglass cloth (0.254 mm)
Baseplate:	machined aluminum baseplate
Charge control:	temperature-compensated voltage limit
Protection:	no bypass diodes

Radiator:	anti-sun panel, surface view deep space, "flexible" optical solar reflector (FOSR)
Specific Energy:	37.89 Wh/kg
DOD:	8%

Space Station Freedom (Launch date mid- to late 1990s)

Application:	LEO satellite, 6.5-year design life
Capacity:	81-Ah cells, 76 cells/battery
No. Batteries:	24 batteries/spacecraft
Cell Support:	machined aluminum sleeves
Baseplate:	aluminum
Charge Control:	fixed c/d ratio used for charge control
Protection:	no bypass diodes
Radiator:	radiative heat exchange between ORU baseplate and thermal control system
Specific Energy:	24.4 Wh/kg
DOD:	35%

3.5.0 REFERENCES

[3-1] R. E. Patterson, W. Luft, and J. D. Dunlop, "Development Of Spacecraft Power Systems Using Nickel-Hydrogen Battery Cells," 6th Communications Satellite Systems Conference, Montreal, Canada, 1976.

[3-2] F. Betz, J. Stockel, and A. Gaudet, "Nickel-Hydrogen Storage Battery For Use On Navigation Technology Satellite 2," *Proc.*, 11th Intersociety Energy Conversion Engineering Conference, September 12–17, 1976, Vol. 1, pp. 510-516.

[3-3] G. Van Ommering and J. F. Stockel, "Characteristics of Nickel-Hydrogen Flight Cells," *Proc.*, Power Sources Symposium, Atlantic City, N.J., June 21–24 1976, pp. 124–128.

[3-4] F. E. Betz, J. D. Dunlop, and J. F. Stockel, "The First Year In Orbit For The NTS-2 Nickel Hydrogen Battery," *Proc.*, 13th Intersociety Energy Conversion Engineering Conference, San Diego, Calif., August 20–25, 1978, Vol. 1, pp. 67–73.

[3-5] J. D. Dunlop, G. Van Ommering, and M. W. Earl, "Ni-H_2 Battery Flight Experiment," *Power Sources 6*, (edited by D. H. Collins) London: Academic Press, 1977, pp 231–247.

[3-6] J. F. Stockel, J. D. Dunlop, and F. Betz, "NTS-2 Nickel Hydrogen Battery Performance," 7th Communications Satellite Systems Conference, San Diego, Calif., April 1978, pp. 66–71.

[3-7] J. D. Dunlop and J. F. Stockel, "Status Of COMSAT/INTELSAT Nickel-Hydrogen Battery Technology," *Proc.*, 15th Intersociety Energy Conversion Engineering Conference, Seattle, WA, August 18–22, 1980, p. 1878.

[3-8] G. van Ommering, C. W. Koehler, and D. C. Briggs, "Nickel-Hydrogen Batteries For INTELSAT V," *Proc.*, 15th Intersociety Energy Conversion Engineering Conference, Seattle, WA, August 18–22, 1980, p. 1885.

[3-9] S. J. Gaston, "The GSTAR and Spacenet Nickel-Hydrogen Batteries For Geosynchronous Orbit Applications," *Proc.*, 19th Intersociety Energy Conversion Engineering Conference. San Francisco, CA, August 19–24, 1984, p. 257.

[3-10] R. S. Ritter, "Thermal Radiation Characteristics of a 30-Ah Battery Ni-H_2 Cell," *Proc.*, 17th Intersociety Energy Conversion Engineering Conference, 1982, p. 63.

[3-11] R. D. Parker, J. H. Hayden, W. O. Neel, and H. W. Wick Jr., "INTELSAT VI Spacecraft Power System," *Proc.*, 19th Intersociety Energy Conversion Engineering Conference, 1984, p. 448.

[3-12] D. W. Wong, J. Herrin, and S. J. Stadnick, "INTELSAT VI Nickel-Hydrogen Battery," *Proc.*, 21st Intersociety Energy Conversion Engineering Conference, August 25–29, 1986, Vol. 3, pp. 1541–1546.

[3-13] E. Alder, S. Stadnick, and H. Rogers, "Nickel Hydrogen Battery Advanced Development Program Status Report," *Proc.*, 15th Intersociety Energy Conversion Engineering Conference, August 18–22, 1980, Vol. 3 pp. 1891–1896.

[3-14] S. J. Stadnick, "Nickel Hydrogen Battery For A Spacecraft Power Subsystem," *Proc.*, Intersociety Energy Conversion Engineering Conference, August 18–22, 1980, Vol. 3 pp. 1897–1900.

[3-15] H. Vaidyanathan, "Effects Of Design Variables On the Cycling Characteristics of Ni-H_2 Cells," *Proc.*, 24th Intersociety Energy Conversion Engineering Conference, August 6–11, 1989, Vol. 3, pp. 1405–1409.

[3-16] P. Duff, "EUTELSAT II Nickel-Hydrogen Storage Battery System Design and Performance," 25th IECEC, Aug 1990, Vol. 6, p. 79.

[3-17] M. J. Milden and C. C. Badcock, "Overview Of Nickel-Hydrogen For Space Satellites," *Proc.*, 19th Intersociety Energy Conversion Engineering Conference, August 19–28, 1984, Vol. 1, pp. 191–195.

[3-18] L. E. Miller, "Air Force Nickel-Hydrogen Battery Space Experiment," *Proc.*, 14th Intersociety Energy Conversion Engineering Conference, August 5–10, 1979, Vol. 2, pp. 1301–1304.

[3-19] D. E. Nawrocki, J. D. Armantrout et al., "The Hubble Space Telescope Nickel-Hydrogen Battery Design," *Proc.*, 25th Intersociety Energy Conversion Engineering Conference, Reno, Nevada, August 12–17, 1990.

[3-20] J. C. Brewer, T. H. Whitt, and J. P. Lanier, Jr., "Hubble Space Telescope Nickel-Hydrogen Batteries Testing and Flight Performance," 26th Intersociety Energy Conservation Engineering Conference, 1991, pp. 257–261.

[3-21] J. L. Colbourn Jr. "HST Power System Performance Status," presentation NASA/GSFC, July 18, 1990.

[3-22] R. J Hass, A. K. Chawathe, and G. van Ommering, "Space Station Battery System Design and Development," *Proc.*, 23rd Intersociety Energy Conversion Engineering Conference, July 31–August 5, 1988, Vol. 3, pp. 577–582.

[3-23] C. Koehler, Space Systems/Loral; private communications in Nov. 1990.

[3-24] R. J. Hass and A. K. Chawathe, "Space Station Nickel-Hydrogen Cell Design and Development," *Proc.*, 23rd Intersociety Energy Conversion Engineering Conference, July 31–August 5, 1988, Vol. 3 pp. 573–576.

[3-25] A.Z. Applewhite, Space Systems/Loral, private communications.

[3-26] D.W. Wong, HAC, private communications.

CHAPTER 4
ADVANCED BATTERY DESIGN CONCEPTS

The common pressure vessel (CPV) Ni-H_2 battery and the bipolar Ni-H_2 battery are two advanced battery design concepts currently being investigated to improve the gravimetric and volumetric energy densities as compared to the IPV cell/battery Ni-H_2 technology. Presented in this chapter are the R&D activities for CPV and bipolar batteries. In addition, R&D activities are presented for larger-diameter (4.5-in. diameter) IPV cells. The flight-ready 4.5-in. diameter INTELSAT VII A 125-Ah cells are described at the end of this chapter.

4.1.0 COMMON PRESSURE VESSEL Ni-H_2 BATTERIES

Conceptually, a CPV Ni-H_2 battery consists of a number of individual cells connected together in series and contained within one common pressure vessel [4-1]. For the IPV cell, each individual Ni-H_2 cell is contained within its own pressure vessel.

Potential advantages for CPV Ni-H_2 batteries include a significant increase in volumetric energy density (a decrease in volume), a decrease in manufacturing cost, a reduction in the complexity associated with the wiring and interconnection of IPV cells, and, to a lesser extent, an increase in specific energy (gravimetric energy density).

Early developmental work on CPV Ni-H_2 technology [4-2] identified important design requirements for CPV multicell batteries:

1. No electrolyte bridging.
2. Independent electrolyte management for each individual cell.
3. Independent oxygen management for each individual cell.
4. Good heat dissipation.
5. Mechanically sound and practical interconnection.
6. Maximum commonalty of components and hardware with state-of-the-art IPV technology.

4.1.1 Terrestrial CPV Ni-H_2 Battery

The lightweight aerospace CPV batteries described in the next two sections (4.1.2 and 4.1.3) evolved from a multi-kilowatt terrestrial CPV Ni-H_2 battery that was developed for Sandia National Laboratories [4-3], [4-4]. The terrestrial battery employed prismatic cells connected in series within a common pressure vessel (see Figure 4-1). Each individual cell had rectangular electrodes and was contained within its own polypropylene cell case. The electrolyte was also contained within the plastic

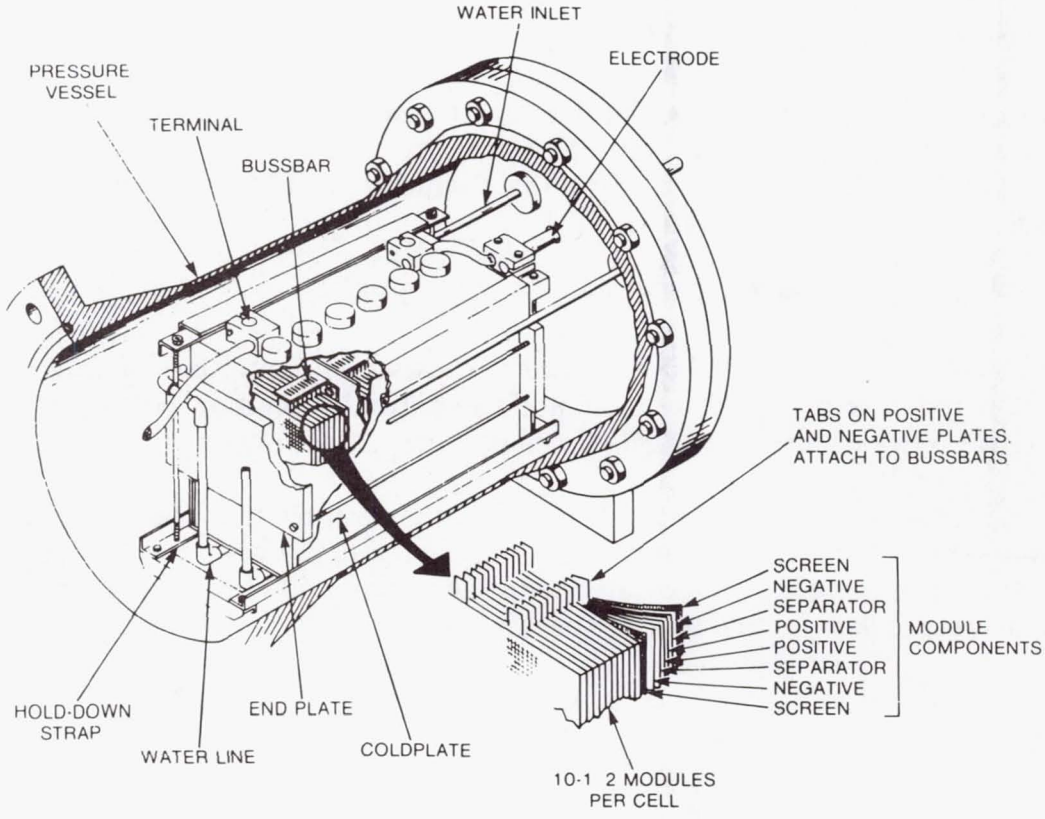

Figure 4-1. Terrestrial CPV Ni-H_2 battery.

cases so that it could not bridge from cell to cell. A gas port was provided to allow hydrogen gas to vent into and out of the cell. Certain features of the terrestrial battery were undesirable for aerospace use. It was heavy and required active cooling. New design and fabrication procedures were developed for the aerospace CPV battery, including a lightweight cylindrical pressure vessel. The geometry of the cells was changed to a cylindrical configuration to accommodate heat removal by conduction to the pressure vessel wall.

4.1.2 Ten-Inch Diameter, 24-Ah CPV Ni-H_2 Battery

A lightweight CPV Ni-H_2 battery was designed and developed jointly by COMSAT and Johnson Controls, Inc. [4-5], [4-6]. A prototype 26-cell, 24-Ah CPV battery (see Figure 4-2) was fabricated and tested to demonstrate the feasibility of this lightweight design for LEO applications. This battery comprised two 13-cell half-stacks

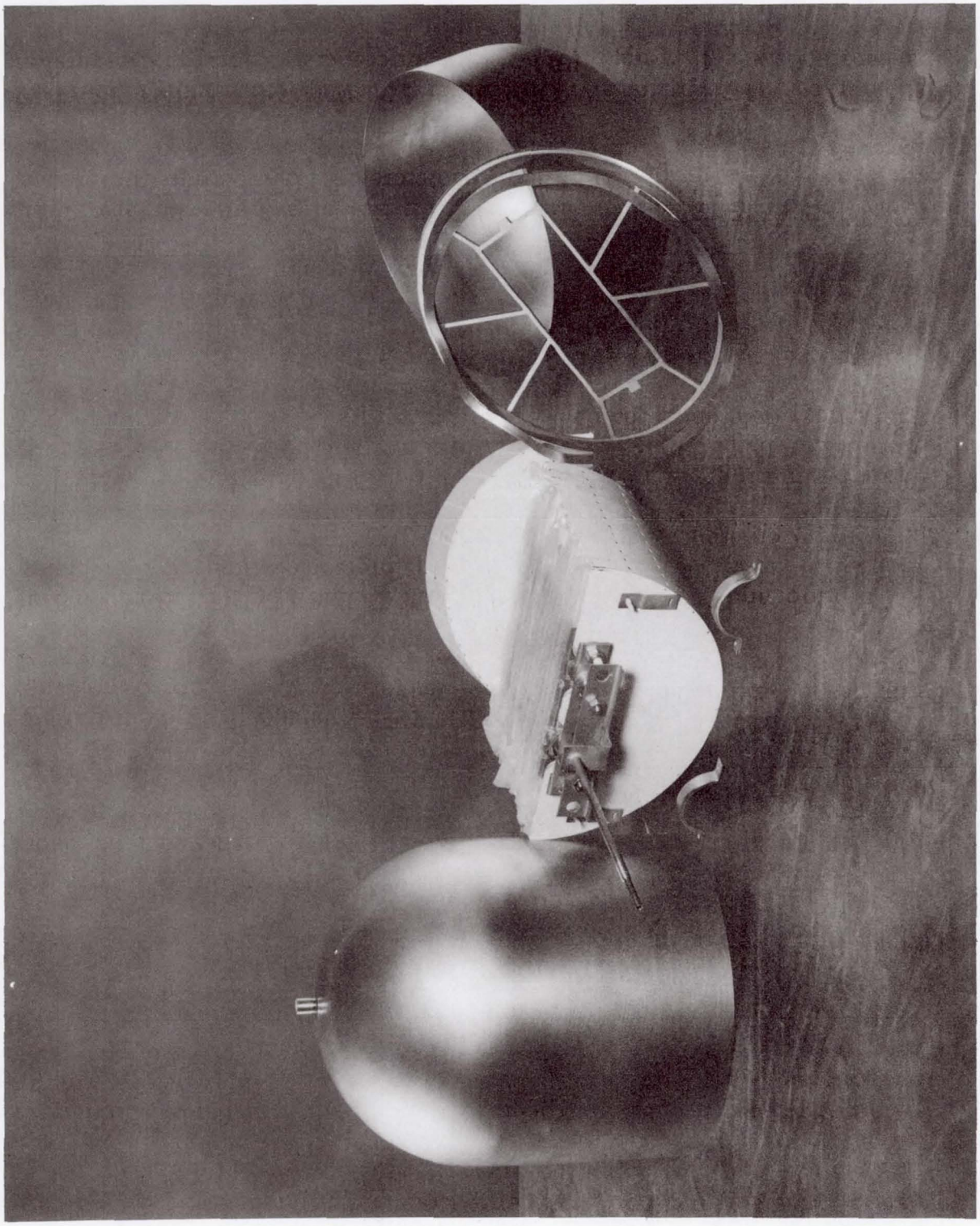

Figure 4-2. CPV battery compounds (2-cell battery).

connected in series within the single common pressure vessel to provide a nominal 32-volt battery.

Cell Design

The 10-inch aerospace design used a semicircular cell with a double tab design to enhance current distribution, as shown in Figure 4-3. The basic cell module comprised a back-to-back positive electrode configuration, two asbestos separators, and two negative electrodes. The module also contained an absorber material between the positive electrodes to provide an electrolyte reservoir. The modules were held together by two hydrogen gas-diffusion screens heat sealed around the periphery of the electrodes. Three of these modules were connected together in parallel to provide the desired 24-Ah cell capacity. The entire cell assembly was placed inside a multilayer synthetic polymer containment package that confined the electrolyte for the individual cell. Each cell was provided with a gas-diffusion membrane to allow for hydrogen gas exchange between the cell and the common gas storage volume.

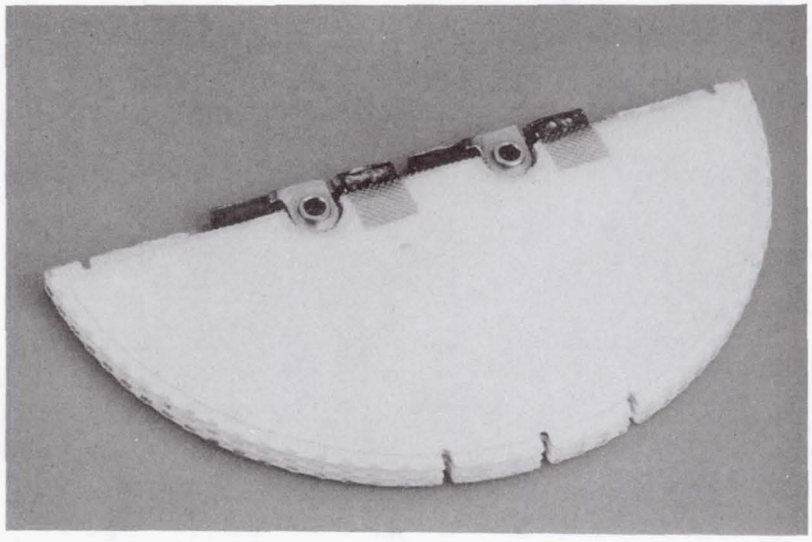

Figure 4-3. Ten-inch diameter semicircular cell.

The CPV cell design features are as follows:

1. Back-to-back positive electrode stack design.

2. Electrochemically impregnated positive electrodes (aqueous process), 26 mils thick, wet slurry nickel plaque.

3. Asbestos separator material.

4. Platinum on carbon negative electrodes with Teflon backing.

5. Absorber material reservoir between back-to-back positive electrodes.

6. Module design for cell stack with each module held together with hydrogen gas diffusion screens.

7. Electrolyte concentration 31 percent fully discharged.

Thermal Design

The thermal requirements were twofold: to maintain the gradient of electrode-to-pressure-vessel-wall temperature at less than 10°C and to maintain the maximum temperature difference between any two battery cells at less than 2°C. These design requirements were associated with the need to preclude water vapor transfer between cells and condensation of water on the vessel wall. To meet these requirements, a method for heat transfer was selected that used thermally conductive fins between the battery cells. Heat generated within the cell stack was conducted axially to the thermal fin, which then radially conducted the heat to the vessel wall. The fins were rigidly attached to another thermally conductive cylinder that made physical contact with the vessel wall. This continuous, integral structure provided a cavity housing for the battery cells that mechanically contained the individual cell structures and defined and controlled cell thickness. This structure also connected the cells mechanically and provided support for both the battery and cell-to-cell interconnects. Figure 4-3 shows the CPV battery components: the two half-cylinder thermal fin assemblies with battery cells installed, the two pressure vessel shells, and the weld ring and washers.

Vessel Design

The CPV pressure vessel design used INCONEL alloy 718 material for the shells, feedthrough bosses, and weld ring and Ziegler plastic compression terminal seals. The design and materials used drew heavily on prior work performed for the IPV technology; however, some changes were made. The weld ring was cut using a water jet and machined to match the vessel shells. Laser welding was used for the feedthroughs and girth weld, a change from the electron-beam welding used for the IPV cells. Electron-beam welding is done in a vacuum and laser welding is done at atmospheric pressure. This change was necessary because the CPV battery cells were activated with electrolyte and conditioned prior to final vessel welding.

Prototype CPV Battery

A prototype CPV battery was fabricated and tested. This battery was designed for LEO applications at 60 percent DOD. The 26-cell, 24-Ah battery had a diameter of 10 inches. The maximum operating pressure was 450 psig. For comparison, the prototype CPV battery is shown in Figure 4-4 along with an INTELSAT V 30 Ah Ni-H_2 battery with 27 IPV cells.

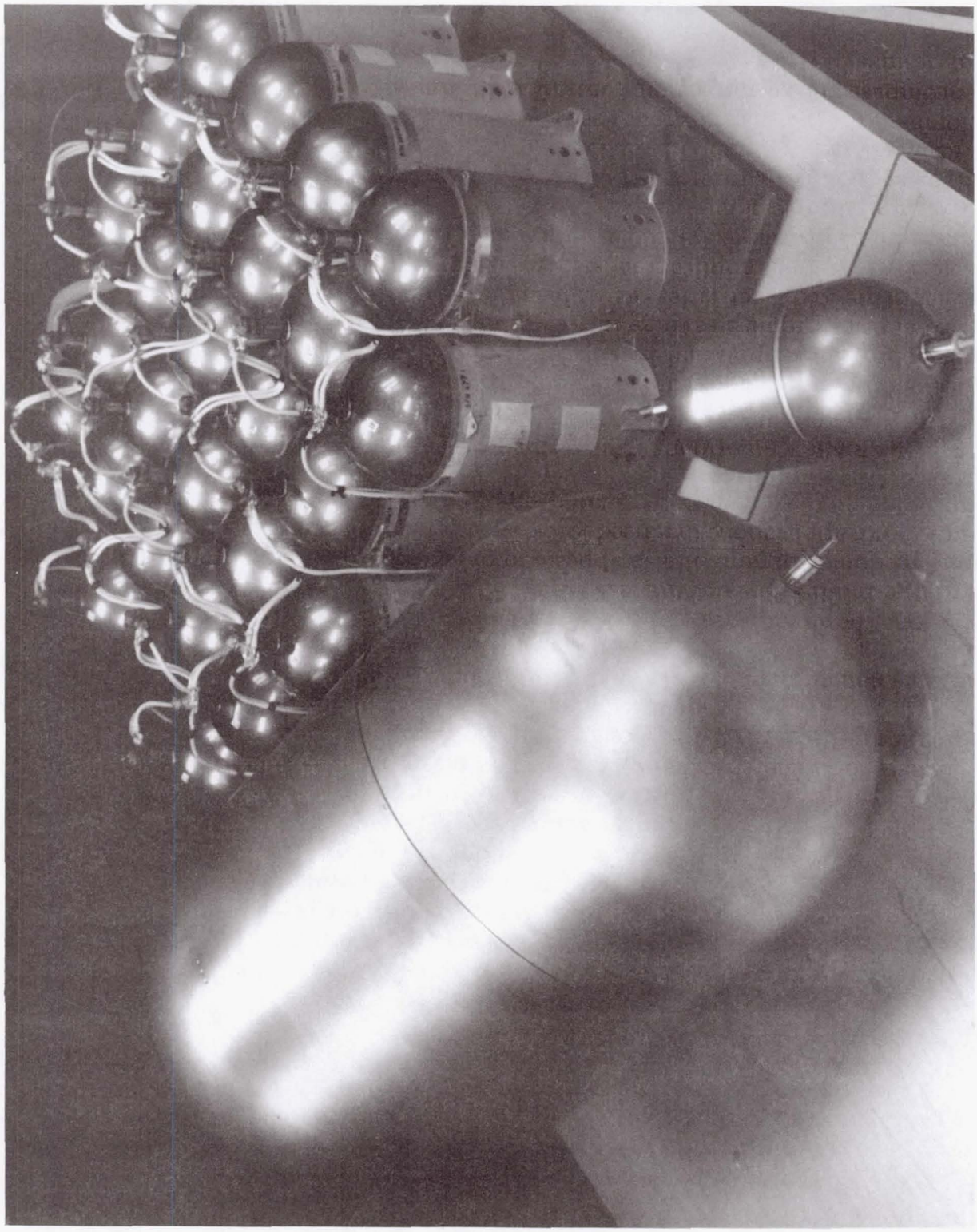

Figure 4-4. CPV nickel-hydrogen battery with INTELSAT V battery.

The 24-Ah CPV battery design features are as follows:

1. Diameter of 10 inches.
2. Capacity of 24 Ah.
3. Average discharge voltage of 32.5 V, 26 cells in series.
4. Maximum operating pressure of 450 psia.
5. Aluminum fins, LEO design, to meet thermal requirements.
6. Designed for up to 60 percent DOD in LEO applications.

Performance

Voltage performance for the CPV battery was quite good, with a mid-discharge voltage of 32.5 volts, or 1.25 volts per cell measured at the C/2 (12-A) discharge rate at 10°C (Figure 4-5). The battery was cycled, simulating an LEO application, discharged for 35 minutes at 16.5 A (44 percent DOD) and charged for 55 minutes at 11 A, which returned 105 percent of the capacity removed on discharge. End-of-charge and end-of-discharge voltages were stable through 6,000 LEO cycles at 44 percent DOD (Figure 4-6) The EOD voltage decreased from 31 volts initially to 29.8 volts at 6,000 cycles. After 6,400 cycles, rapid voltage degradation to failure occurred (less than 1.0 V/cell) at 7,400 cycles.

Subsequent destructive physical analyses (DPA) showed extensive electrolyte leakage. This leakage occurred primarily from the gas vent membranes and cell terminal compression seals and secondarily from electrolyte fill port heat seals and cell case edge heat seals. The resulting drying out of the positives and separators is believed to have caused the voltage decline and failure of the battery. All cell components, including the negative electrodes, were in excellent physical condition. No pinholes or other signs of popping were observed on the negative electrodes, and no signs of blistering or other physical degradation were observed on the positives [4-5], [4-6].

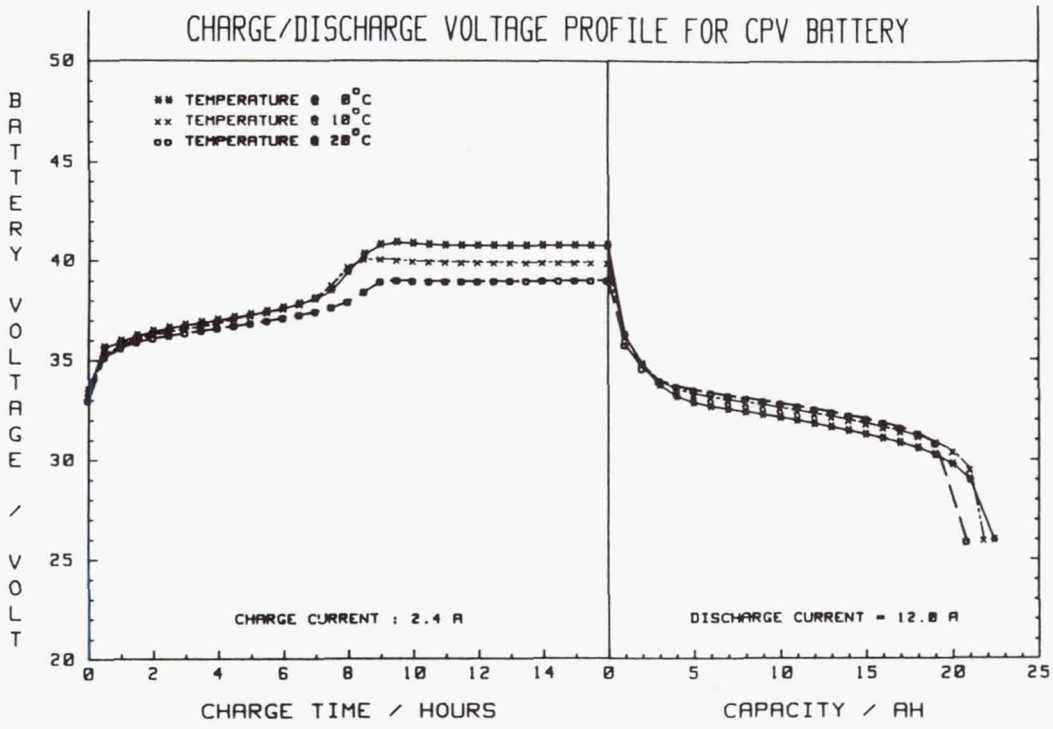

Figure 4-5. Voltage profiles for 10-inch diameter CPV battery.

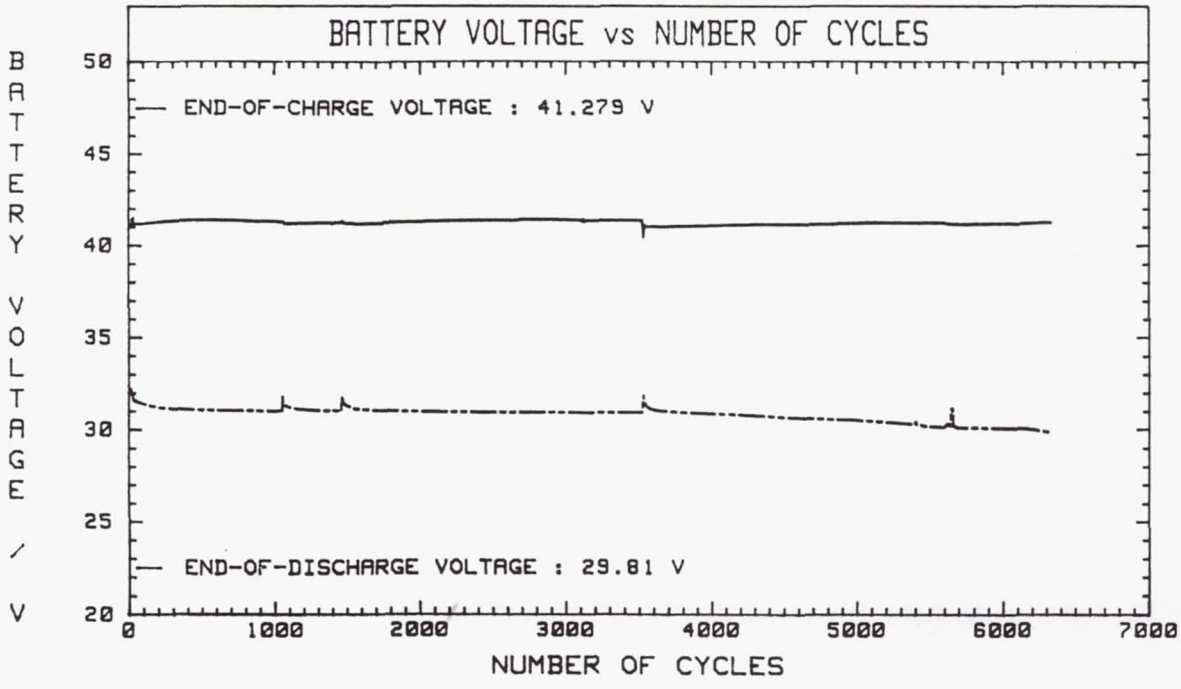

Figure 4-6. EOC and EOD CPV battery voltages during LEO cycle test.

4.1.3 Loose Heat Fin Five-Inch CPV Design

A new loose heat fin design was developed to facilitate insertion of the cells into the battery [4-7], [4-25]. The cell design was also modified by providing a double thin-walled polymeric container with a staggered vent pathway to further enhance the electrolyte management reliability. A five-inch diameter pressure vessel was used to contain the cylindrical cells. A circular cell with its loose heat fin is shown in Figure 4-7(a). The cells and heat fins are assembled into a stack using a special alignment fixture. The 10-cell stack, shown in Figure 4-7(b), has a 9.6-Ah capacity, is 9.7 inches long, and weighs 3 kg. The specific energy is 40 Wh/kg, which is quite good for a 9.6 Ah battery.

4.1.4 An Ni-H_2 CPV Battery Spacecraft Experiment

The Naval Research Laboratory (NRL) and Johnson Controls, Inc. (JCI) have joined together in a cooperative effort to use a JCI common pressure vessel (CPV) Ni-H_2 battery in a flight program [4-26], [4-27].

JCI is providing two 22-cell CPV batteries, one qualification battery and one flight battery. These batteries are made using the "Loose Heat Fin Five-Inch CPV Design" described in Section 4.1.3 above. NRL is responsible for integrating the battery into the spacecraft, launching the spacecraft, and providing battery performance data from the flight experiment. The interest of the experiment is to "space qualify" this CPV battery design.

4.1.5 Advantages of CPV Battery Technology

Presented below are the advantages of the CPV battery technology as compared to the IPV cell/battery technology.

1. Significantly higher volumetric energy density.

2. Reduced complexity.

3. Improved structural integrity.

4. Improved thermal control for LEO applications through a reduction in temperature gradients between the electrode stack and pressure vessel wall and a reduction in temperature gradients between cells.

5. Improved cycle life for LEO applications due to the improved thermal control.

6. Availability of lightweight, lower-capacity Ni-H_2 batteries down to 6-Ah in size. With the present IPV cell technology, the lower limit in capacity is about 20 Ah. It becomes impractical to build IPV cells below this capacity because their specific

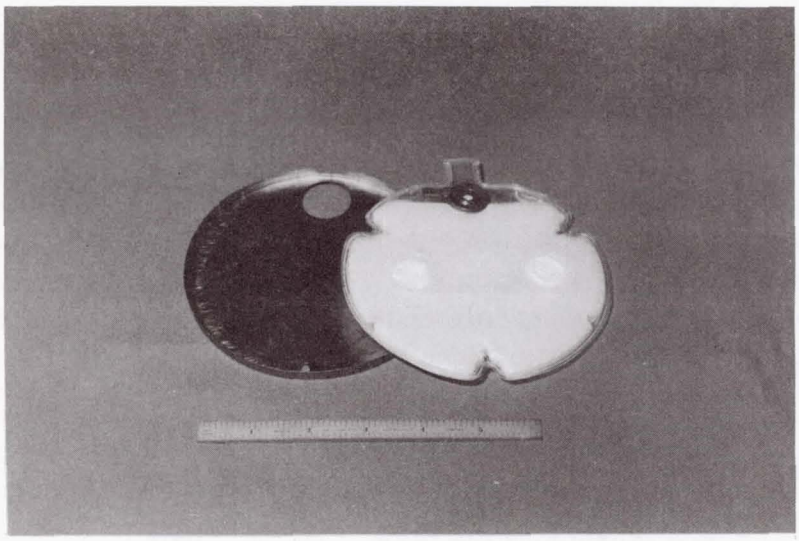

a

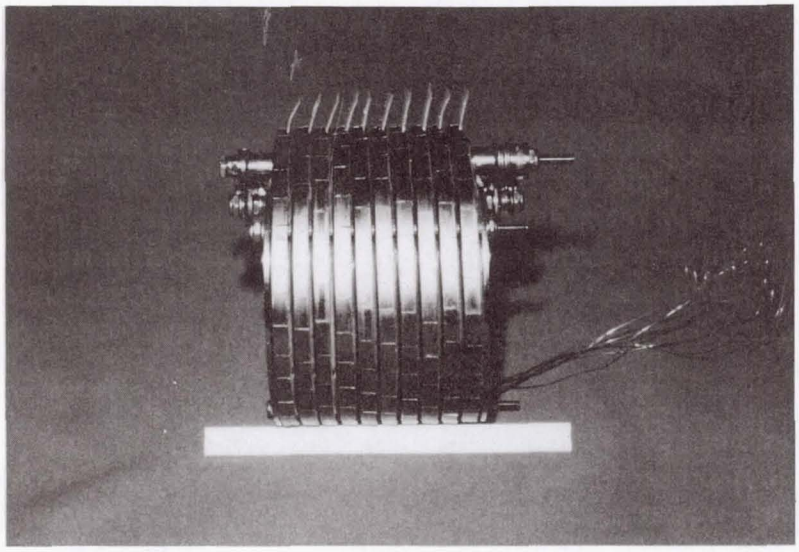

b

Figure 4-7. (a) Five-inch diameter circular cell and loose heat fin; (b) five-inch diameter 10-cell stack.

energy and energy density drop off very rapidly. This is not the case for CPV batteries.

7. Reduction in cost.

Conclusion. The advantages of the CPV nickel-hydrogen battery make it a candidate for use in large multi-kilowatt hour LEO energy storage applications, such as the Space Station Freedom Program. It also appeals to the other end of the spectrum: the small, 100- to 400-Wh applications that need low-cost, lightweight batteries [4-8].

4.2.0 BIPOLAR NICKEL-HYDROGEN BATTERIES

The NASA Lewis Research Center (NASA LeRC) has been actively engaged in the development of bipolar Ni-H_2 batteries [4-9 to 4-23]. Studies have shown that the bipolar batteries promise savings in weight and volume, compared to IPV and CPV batteries. The R&D activities have been directed toward large energy storage requirements for LEO applications as well as development of low-capacity units for small satellites. The large systems incorporate active cooling within the battery stack, which enables the use of high-capacity cells. Both actively and passively cooled bipolar Ni-H_2 batteries ranging from 1 to 40 Ah and 12 to 60 V have been designed, fabricated, and tested at NASA LeRC. NASA LeRC has also sponsored bipolar battery development through a contract at Space Systems/Loral. Bipolar development at Loral has encompassed batteries ranging from 3 to 75 Ah, 6 to 12 V. Passively and actively cooled designs have been investigated.

4.2.1 NASA Lewis 6.5-Ah Bipolar Battery

Battery component and design features for the 10-cell 6.5-Ah battery constructed in 1983 follow [4-14].

Component Design Features. (See Figure 4-8).

Nickel Electrode. The nickel electrodes were electrochemically impregnated to a loading of 1.6 grams/cm^3 of void volume. The plaque was dry sinter with nickel screen.

Hydrogen Electrode. The hydrogen electrode was a catalyzed porous screen, non-Teflon-backed fuel-cell electrode. The back of the electrode had no Teflon layer to allow current conduction normal to the face plane through the gas access screen to the adjacent bipolar plate.

Separator. The separator material was beater-treated asbestos (BTA). BTA is a reconstituted blend of asbestos sheets with a 5-percent latex binder.

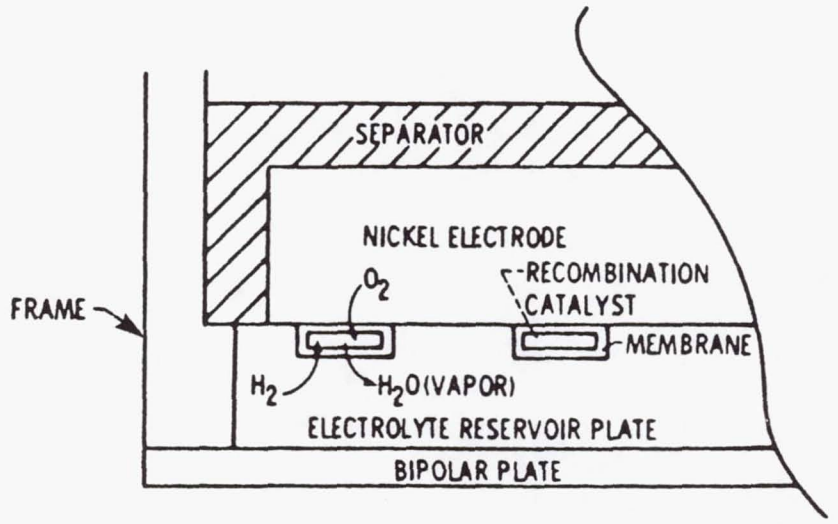

Graphic representation of oxygen - hydrogen recombination.

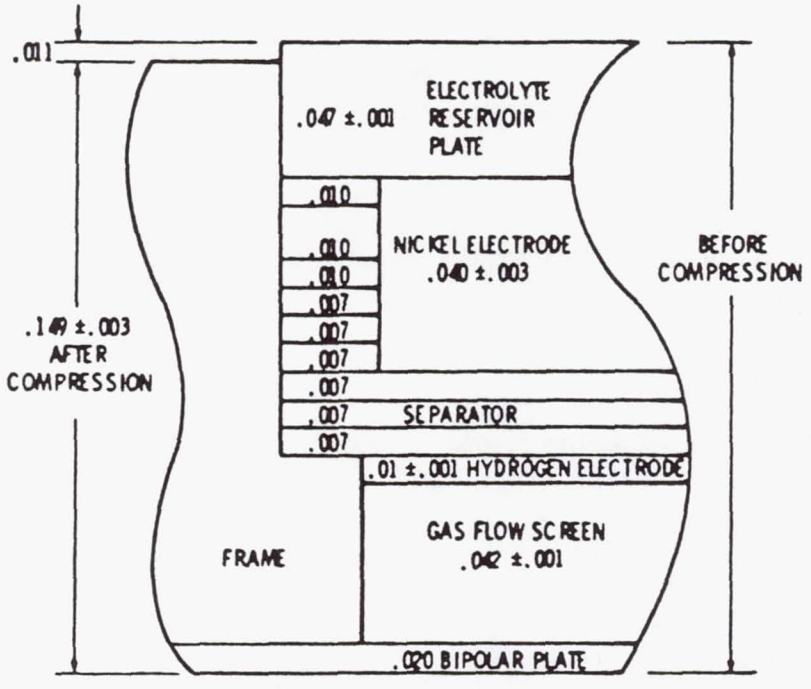

Cell cross section with dimensions of components, in.

Figure 4-8. Component design features for bipolar Ni-H_2 batteries.

Electrolyte Reservoir Plate. The electrolyte reservoir plate (ERP) was a foam nickel structure with a 90-percent porosity. Each plate was compressed from 0.25 cm to 0.125 cm, then cut with a rule die to make four slots to house the recombination strips. The average pore diameter was 0.025 cm, allowing the passage of hydrogen and oxygen gas through the ERP to the recombination sites. The water vapor formed at the recombination sites during the end of charge condensed on the nickel foam and was freely wicked out by the separator and nickel electrode.

Gas Flow Screen. A screen of expanded nickel was placed behind the hydrogen electrode to facilitate the ingress and egress of hydrogen gas. As with the ERP, an electrically conductive path must exist between the hydrogen electrode and adjacent bipolar plate. Gas channels were provided in the cell housing that aligned with the gas screen.

Cell Housing. Injection-molded polysulfone frames were used to contain the cell components and electrolyte. The inner frame ledge provided a means of sealing the separator around the nickel electrode, thus eliminating passing evolved oxygen to the hydrogen electrode. Hydrogen gas was channeled to the hydrogen electrode via slots connecting the inner frame to two manifolds. These slots were in line with the gas flow screen (expanded nickel). Similar slots and manifolding were provided on the other side of the frame to supply hydrogen gas to the recombination sites. These slots were aligned with the electrolyte reservoir plate.

Bipolar Plate. The bipolar plates were 0.050-cm nickel sheets and were sandwiched between each cell, which was enclosed between two bipolar plates. A neoprene gasket was fit into a recess in the frame and sealed against the bipolar plate, retaining the electrolyte within each cell. External current connections were made to the bipolar terminal plates on each end. The interior bipolar plates conducted current from the positive electrode of one cell to the negative electrode of the next, resulting in no intercell electrical connectors being needed. The bipolar plate was also used for heat rejection. Each plate extended beyond the frame on two opposite sides to form a set of cooling fins.

Electrolyte Activation. The method of electrolyte activation was to introduce electrolyte as each cell was assembled. The nickel electrodes were vacuum filled and drained, with an average take up of 9.3 ml. The ERP received 50 percent by weight (11 ml) and the separator 150 percent by weight (15 ml). These values were obtained from electrolyte retention tests performed on the separator and ERP. The hydrogen electrode was not vacuum filled because the required electrolyte interface would be provided from contact with the separator.

Test Data

Capacity Measurements. The capacity for each of the 10 cells was periodically measured to 1.0 volts at a C/4 discharge rate. A 30-percent loss in capacity was noted in all cells

after 3,900 LEO cycles. Initial capacity was 8.0 Ah for these cells, and the final capacity was approximately 5.6 Ah, as can be seen in Table 4-1 below. These cell were cycled at 70 to 80 percent DOD, which is a fairly severe test regime.

Table 4-1 [4-14]. Discharge Capacities to 1.0 Volts (at the C/4 rate of 1.9 A)

Cycle No.		CELL NUMBER									
		1	2	3	4	5	6	7	8	9	10
16	A*	7.8	8.0	8.0	8.0	8.0	8.0	8.0	8.0	8.0	8.0
2363	B**	5.7	5.7	5.7	5.8	5.9	5.7	5.7	5.9	5.6	5.7
2364	B	6.7	6.7	6.3	6.4	6.7	6.7	7.0	6.9	7.0	7.0
3350	C***	6.5	6.3	6.3	6.5	6.5	5.9	5.8	6.4	6.5	6.5
3862	C	5.9	5.8	5.7	5.8	5.9	5.2	5.6	5.7	5.9	5.9
3900	C	5.6	5.5	5.4	5.5	5.6	5.0	5.2	5.3	5.6	5.6

*A Charge: 9.1 Ah
**B Charge: 8 Ah, 4 A for 2 hours
***C Charge: normal LEO cycle interruption

Shorted Cell. Following a 72-hour self-discharge test after 4,075 LEO cycles, cells 6, 7, and 10 had zero volts. Cell 10 was removed, and analysis showed evidence of high compression; the impression of the gas screen could be readily seen in the hydrogen electrode and separator. An obvious shorting of the nickel and hydrogen electrodes through the separator had occurred.

4.2.2 75-Ah Bipolar Nickel-Hydrogen Battery

Ford Aerospace Corporation* and Whittaker-Yardney Power Systems** designed, built, and tested several actively cooled, 10-cell, Ni-H_2 batteries under the sponsorship of NASA LeRC [4-21], [4-22]. Two 12.5-Ah and two 75-Ah batteries have been tested. The 75-Ah batteries were constructed principally to assess the performance of the large-scale cell components in the bipolar stacking arrangement to demonstrate active cooling and to test several new design features. The cell design concept is similar to the NASA LeRC cell design described in Section 4.2.1 above. Oxygen gas generated on overcharge recombined with hydrogen gas at recombination strips located in the electrolyte

* Space Systems/Loral
** Yardney Technical Products

reservoir plate behind the positive electrode. (Oxygen recombination does not occur at the hydrogen electrode).

Cell Components

The cell component stacking sequence was as follows:

1. Bipolar conducting plate.
2. Nickel coarse mesh gas screen.
3. Nickel fine mesh gas screen.
4. Whittaker-Yardney fuel-cell hydrogen electrode.
5. Two layers of beater-treated asbestos separator.
6. Nickel positive plate.
7. Nickel felt electrolyte reservoir plate (ERP).
8. Platinum recombination strips.

Each of the cell components was separately activated with electrolyte prior to battery assembly, in accordance with the procedure developed at NASA LeRC. This procedure was used to minimize intercell electrolyte bridging that can arise when conventional activation methods are used.

The positive plates were 80 mils thick and loaded to 1.7 grams of active material/cm^3 of void volume.

Performance During Initial Characterization Tests

Capacity. The capacity measured to 10 volts (1 volt/cell) showed a significant drop as the discharge rate increased, as can be seen in Table 4-2 below from Reference 4-21. This rate dependence was somewhat unexpected, because the flooded positive plate tests conducted at Whittaker-Yardney Power Systems showed little change in the capacity of the positive plates at discharge rates from about C/4 to well over 2C rates.

EOD Pressure. The EOD pressures shown in Table 4-2 indicate that much of the hydrogen gas in the pressure vessel was not utilized at the higher discharge rates to 10.0 volts. Better utilization was obtained when the discharge was continued to 7.0 volts (0.7 volts per cell). These high EOD pressure data at high discharge rates were consistent with the reduced capacity data at high discharge rates.

EOC Voltage. The EOC voltage (16.2 volts at C/2 charge rate) was high. Conventional IPV nickel-hydrogen cells typically exhibit EOC voltages of about 1.50 to 1.54 volts at 10°C and C/2 charge rates, compared to the average EOC cell voltage of 1.62 volts for the bipolar battery at a C/2 charge rate.

Table 4-2 [4-21]. Bipolar Battery Characterization Tests Prior to LEO Cycling, Summary of Average Values

CHARGE RATE	--------C/2----------			
DISCHARGE RATE	C/4	C/2	C	2C
BOL Temperature (C)	10.8	10.7	10.7	10.1
EOC Battery Voltage (V)	16.3	16.2	16.1	16.3
EOC Pressure (PSI)	240.4	227.5	242.6	240.4
EOC Temperature (C)	16.3	14.1	15.6	16.2
EOD Pressure to 10 V (PSI)	97.8	103.8	122.0	193.1
EOD Pressure to 7 V (PSI)	78.8	89.6	105.8	112.1
EOD Temperature to 10 V (C)	13.1	13.6	17.5	16.4
EOD Temperature to 7 V (C)	14.3	14.8	18.6	16.6
Capacity to 10 V (Ah)	75.7	67.1	63.8	24.5
Capacity to 7 V (Ah)	86.2	74.4	72.5	46.3

Summary. This bipolar battery exhibits high internal impedance (polarization) characteristics that cause the performance to be highly dependent on charge and discharge rates. High-rate capabilities need to be improved, and several aspects of the present design require further study [4-21].

LEO Cycle Data

LEO cycling of the bipolar battery was initiated after the characterization cycles described. The battery was cycled at 40 percent DOD with a C/D ratio varying between 1.025 and 1.10. Performance data up through cycle 13,000 were reported in Reference 4-23. Testing of this battery was terminated following 15,000 40-percent DOD LEO cycles. Destructive physical analysis is being performed.

Voltage Performance. The overall battery performance remained essentially stable throughout the battery life. The charge and discharge voltages of the 40 percent DOD LEO cycling indicate that there was a slight degradation in battery performance over the 15,000 cycles. However, it appears that Cell 10's performance is the primary

influence in the decline. Poor electrolyte distribution or electrolyte starvation may be responsible for the poor cell performance of the weakest cell in the battery.

Capacity. The LEO charge/discharge cycling was interrupted periodically for capacity measurements. The battery capacity was measured to 10 and 7 volts, or until the first cell reached 0.5 volts. The battery capacity decreased from 75 Ah to approximately 60 Ah over the first 2000 LEO cycles, then remained essentially constant until cycle 10,000. After cycle 2000, the battery capacity drop to approximately 50 Ah was the result of low capacity in Cell 10. Cell 10 had 10-Ah less capacity than the next lowest cell.

4.2.3 Potential Advantages of Bipolar Battery Technology

1. Significantly higher volumetric energy density.

2. Improved structural integrity.

3. Actively cooled designs offer improved thermal control for LEO applications with a reduction in temperature gradients within the electrode stack and between the electrode stack and the pressure vessel wall.

4. Improved cycle life for LEO applications due to improved thermal control.

5. Availability of lightweight, lower-capacity Ni-H_2 batteries down to 6-Ah size.

6. Higher peak power performance, high rate of discharge for short durations of time (pulse power).

4.2.4 Status of Bipolar Nickel-Hydrogen Battery Technology

Advances have been made in the development of the bipolar nickel-hydrogen battery technology. Two different bipolar battery designs have exhibited 15,000 40-percent DOD LEO cycles, demonstrating the potential for extended cycle life for bipolar battery designs. However, additional development work is needed to make this technology useful for aerospace applications. The high impedance and voltage degradation problems are under investigation by LeRC and its contractors.

Bipolar battery designs are also being investigated for low-capacity applications [4-23]. Three- to five-inch diameter designs are being investigated for use in small satellite applications.

4.3.0 4.5-INCH IPV Ni-H_2 CELLS

The 8.89-cm (3.5-in.) diameter Ni-H_2 cell has an upper limit in capacity of about 100 Ah. Larger diameter IPV cells are being developed to increase the cell capacity to

meet requirements for larger storage Ni-H_2 batteries. Presented in this section are R&D activities for 11.43-cm (4.5-in.) diameter Ni-H_2 cells.

For LEO applications, heat transfer radially from within the cell stack to the pressure vessel wall is more of a problem with these 4.5-in. diameter IPV cells as compared with the 3.5-in. diameter cells. Both of the 4.5-in. diameter NASA cell designs presented use the catalytic wall wick described in Chapter 1, Section 1.11.0, "NASA R&D Programs."

4.3.1 NASA Lewis Advanced Design (125-Ah Experimental Cell)

Six NASA Advanced Design 125-Ah cells were built by EPI to NASA LeRC specifications. Three cells have the catalyzed wall wick, the serrated (BTA) asbestos separators, and the KOH concentration of 26 percent discharged. The other three cells have the EPI MANTECH design with asbestos separators, 38 percent KOH concentration discharged, and without the catalyzed wall wick. These cells are used as control cells. A picture of one of these experimental cells is shown in Figure 4-9.

NASA Advanced Cell Design Summary

1. Back-to-back cell stack design.

2. Pineapple-slice configuration with polysulfone core, EPI MANTECH design.

3. INCONEL 718 pressure vessel with nylon Ziegler compression seals. Electron beam girth welding of the pressure shells to an INCONEL 718 weld ring.

4. Positive electrodes—dry powder, alcoholic impregnation process.

5. Separator material—serrated BTA (asbestos) separators extended to contact wall wick.

6. Zirconium-oxide wall wick with catalyst sites.

7. Negative electrode—Teflon-bonded platinum, black with Teflon (Gortex) backing and photochemically etched grid.

8. KOH electrolyte concentration—26 percent discharged.

9. Cell dimensions: 11.8-cm diameter, 30.4-cm length terminal to terminal, and 23.3 cm length dome to dome.

10. Weight of cell—3.924 kg.

11. Measured capacity at 10°C—162 Ah.

Figure 4-9. 125-Ah nickel-hydrogen cell.

12. Specific energy (10°C)—51.6 Wh/kg.

Performance data are presented in Chapter 5, Section 5.4.3, "NASA-Sponsored Ni-H_2 LEO Life Tests."

4.3.2 220-Ah Nickel-Hydrogen Cells

Space Systems/Loral and Whittaker-Yardney teamed together to design and fabricate 220-Ah Ni-H_2 cells. One of these cells is shown in Figure 4-10. The objective of this program was to design, manufacture, test, and evaluate an IPV cell of 4.5-in. diameter and capacity commensurate with the upper limits of hydroforming deep cylindrical domed pressure vessels [4-24].

Cell Design Summary

1. Back-to-back positive electrode design, dual electrode stack.
2. Pineapple-slice configuration with polysulfone core.
3. INCONEL 718 pressure vessel, 4.5 inches in diameter.
4. Wall wick with catalyst sites.
5. Teflon axial compression seals.
6. Dual-layer asbestos-Zircar separator.
7. Platinum black negative electrode with Teflon backing.
8. EB welding of the terminal seal bosses on the centerline of each dome and EB welding of the girth weld.

Catalyst Wall Wick

The separators extend to the wall wick on the inside of the pressure vessel wall, providing a return path for the water formed at the catalyst sites. This cell design features the use of catalyst sites on the wall wick to induce oxygen recombination at the vessel wall as illustrated in Figure 4-11. By guiding the oxygen to recombine with hydrogen at the pressure vessel wall during overcharge, the localized heat generated during recombination is dissipated at the wall, eliminating large temperature gradients between the electrode stack and the pressure vessel wall.

Figure 4-10. 220-Ah nickel-hydrogen cell.

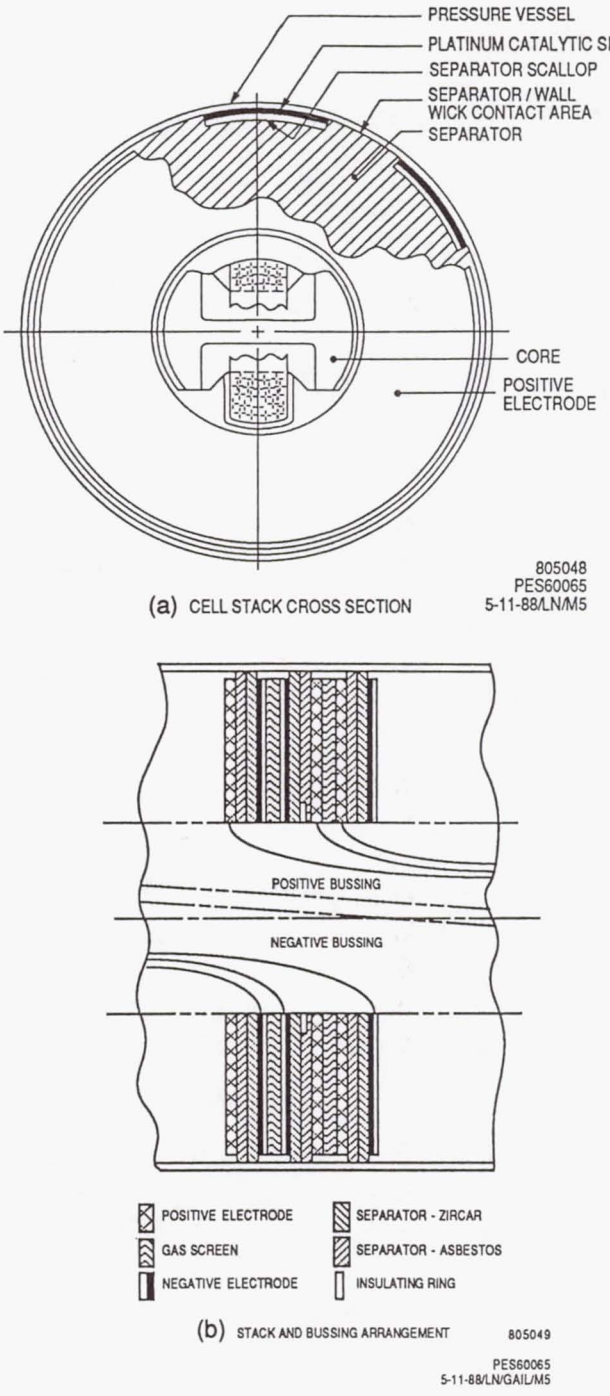

Figure 4-11. 220-Ah cell (cross-sectional view).

Physical Characteristics

Nameplate capacity	220 Ah
Diameter	4.5 inches
Length	18.5 inches
Weight	6,687 grams
Measured capacity	275 Ah
Specific energy (actual)	51.4 Wh/kg
Positive electrodes	104
Negative electrodes	104
Maximum operating temperature	1250 psi
Safety factor	3:1

4.3.3 INTELSAT VII A 120-Ah Cell

A 4.5-inch diameter 120-Ah Ni-H_2 cell was used by Space Systems/Loral for the 27-cell battery on the INTELSAT VII A program. These cells were manufactured by Gates Energy Products (GEP). The larger 4.5-inch diameter 120-Ah cells replace the 3.5-inch diameter 83-Ah cells used for the INTELSAT VII batteries, described in Chapter 1, Section 1.9.4.

The larger 4.5-inch diameter cell was used to increase the rated capacity to the 120 Ah necessary for the I–VII A battery. Other than the pressure vessel, the cell design features for the VII A cell are similar to the cell design features for the I–VII cells.

Pressure Vessel. The pressure vessel has both the terminals mounted on one end of the dome, as shown in Figure 4-12. Also shown are the cell dimensions and teh strain-gauges mounted on the dome [4-28]. The pressure vessel comprises three INCONEL 718 sections, two hydroformed domes, and one seam-welded cylindrical section, all of uniform thickness. TIG welding is used at the two girth welds joining the pressure vessel and weld rings.

Dual Weld Ring Supported Single Stack Design. A single electrode stack is supported between fixed endplates and weld rings. The dual weld rings support the single electrode stack in a floating core, as described in Reference 1-39 in Chapter 1.

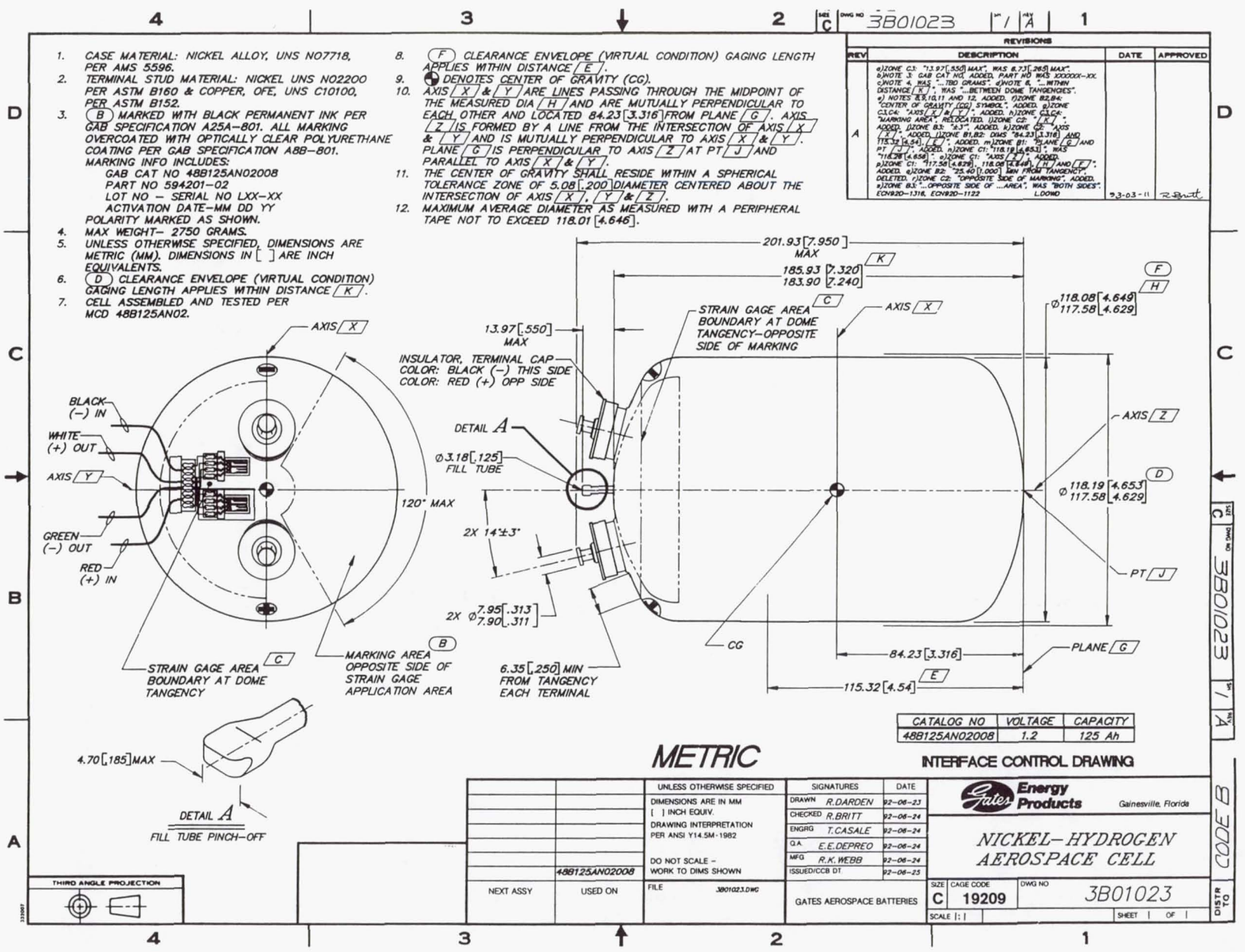

Figure 4-12. Outline of INTELSAT VII A cell.

INTELSAT VII A Cell Design Summary

1. Back-to-back electrode stack design, single electrode stack.

2. Pineapple-slice configuration with center core design.

3. INCONEL 718 pressure vessel with both terminals located at one end of the pressure vessel. The terminals are inverted with the seals on the inside. Ceramic-to-metal seals. TIG welding at the two girth welds.

4. Wall wick, plasma-sprayed zirconium oxide.

5. Endplates, INCONEL 718.

6. Positive electrodes—dry powder plaque, aqueous electrochemical impregnation process; 38 electrodes per cell.

7. Separator material—two layers of ZYK-15 knit Zircar.

8. Negative electrodes—platinum black negative electrodes (loading of 3.5 mg/cm^2 nominal) with Teflon (Gortex) backing with photochemically etched substrate; 38 electrodes per cell.

9. KOH electrolyte concentration—31 percent KOH discharged.

10. Positive precharge.

11. Cell dimensions: 11.819-cm diameter; 20.193-cm bottom of dome to top of terminal (rabbit-ear design), 18.593 cm dome-to-dome.

12. Weight of each cell—2750 g nominal.

13. Measured capacity at 10°C—125 Ah.

14. Specific energy at 10°C—56.82 Wh/kg.

Electrical characterization test results for six of these I–VII A cells are presented in Chapter 5, Section 5.1.0, "Performance Characteristics of Ni-H_2 Cells."

4.4.0 REFERENCES

[4-1] D. Warnock, U.S. Patent 2975210 (1976)

[4-2] G. L. Holleck, "Common Pressure Vessel Nickel-Hydrogen Battery Design," *Proc.*, 15th Intersociety Energy Conversion Engineering Conference, August 18–27, 1980, Vol. 3, pp. 1908–1911.

[4-3] D. M. Bush, "Evaluation of Terrestrial Nickel-Hydrogen Cells and Batteries," SAND88-0435, May 1988.

[4-4] J. Dunlop and W. Gentry, "Design and Development of Multi-Kilowatt-Hour Hydrogen/Nickel-Oxide Battery," Sandia National Laboratories, Contract Report No. SAND 87-7061, January 1987.

[4-5] M Earl, J. Dunlop, R. Beauchamp, J. Sindorf, and K. Jones, "Design and Development of an Aerospace CPV Ni-H_2 Battery," *Proc.*, 24th Intersociety Energy Conversion Engineering Conference, August 1989, Vol. 3, pp. 1395–1400.

[4-6] J. Zagrodnik and K. Jones, "Development of Common Pressure Vessel Nickel-Hydrogen Batteries," 25th Intersociety Energy Conversion Engineering Conference, August 1990.

[4-7] J. P. Zagrodnik and K. R. Jones, "Multiple Cell Common Pressure Vessel Nickel-Hydrogen Battery," SERT Conference, April 1991.

[4-8] J. Dunlop and R. Beauchamp, "Making Space Nickel-Hydrogen Batteries Lighter and Less Expensive," AIAA/DARPA Meeting on Lightweight Satellite Systems, Monterey, CA, August 1987, NTIS No. N88-13530.

[4-9] R. L. Cataldo, J. J. Smithrick, 17th Intersociety Energy Conversion Engineering Conference, 1982, p. 780.

[4-10] E. Adler, F. Perez, 18th Intersociety Energy Conversion Engineering Conference, Vol. 4, 1983, p. 1568.

[4-11] E. Adler, F. Perez, "Advanced Nickel-Hydrogen Cell Configuration Study," Final Report, Contract NAS3-22249, Spetember 1983.

[4-12] R. L. Cataldo, 20th Intersociety Energy Conversion Engineering Conference, Vol. 4, 1983, p. 1561.

[4-13] M. A. Manzo, L. J. Gonzalez-Sanabria, J. S. Herzau, L. J. Scaglione, 19th Intersociety Energy Conversion Engineering Conference, Vol. 2, 1984.

[4-14] R. L. Cataldo, 20th Intersociety Energy Conversion Engineering Conference, Vol. 1, 1985, p. 1346.

[4-15] R. L. Cataldo, 19th Intersociety Energy Conversion Engineering Conference, Vol. 2, 1984.

[4-16] R. L. Cataldo, 21st Intersociety Energy Conversion Engineering Conference, Vol. 3, 1986, p. 1547.

[4-17] R. L. Cataldo, et al., 22nd Intersociety Energy Conversion Engineering Conference, Vol. 2, 1987, p. 873.

[4-18] M. A. Manzo, et al., 22nd Intersociety Energy Conversion Engineering Conference, Vol. 2, 1987, p. 864.

[4-19] M. A. Manzo, 33rd International Power Sources Symposium, 1988.

[4-20] R. L. Cataldo, "Life Cycle Test Results of a Bipolar Nickel-Hydrogen Battery," *Proc.*, 20th Intersociety Energy Conversion Engineering Conference, August 1985, Vol. 1, pp. 1.346–1.351.

[4-21] S. Lenhart, C. Koehler, and A. Applewhite, "LEO Life Test on a 75-Ah Bipolar Nickel-Hydrogen Battery," *Proc.*, 23rd Intersociety Energy Conversion Engineering Conference, August 1988, Vol. 2, pp. 379–384.

[4-22] M. A. Manzo, S. J. Lenhart, A. M. Hall, 24th Intersociety Energy Conversion Engineering Conference, 1989.

[4-23] H. E. Damon, M. A. Manzo, R. Change, E. Cruz, "74-Ah and 10 Boilerplate Bipolar Ni-H_2 Battery Designs and Test Results," 27th IECEC, 1992.

[4-24] G. L. Hartjen and A. Z. Applewhite, "Storage and Testing of 220-Ah Nickel-Hydrogen Battery Cells in Low Earth Orbit," *Proc.* 23rd IECEC, Denver, Colorado, p. 363.

[4-25] J. P. Zagrodnik and K. R. Jones, "Nickel-Hydrogen Multicell Common Pressure Vessel Battery Development Update," *Proc.* 27 IECEC, Aug. 1992, p. 2–93.

[4-26] J. C. Garner, "A Nickel-Hydrogen Common Pressure Vessel Space Flight Experiment," *Proc.* 27 IECEC, Aug. 1992, p. 6–115.

[4-27] R. G. Skalitzky, "Common Pressure Vessel Ni-H_2 Battery Experiment Electronics," *Proc.* 27 IECEC, Aug. 1992, p. 1–85.

[4-28] T. J. Cassale, Gates Energy Products, Inc., private communications

CHAPTER 5
PERFORMANCE DATA FOR Ni-H_2 CELLS AND BATTERIES

In this chapter, performance characteristics of Ni-H_2 cells are discussed first, and then performance data are presented for both LEO and GEO applications.

5.1.0 PERFORMANCE CHARACTERISTICS OF NI-H_2 CELLS

Performance data presented are:

- Reconditioning charge/discharge voltage profiles
- Peak voltage on charge vs temperature
- End-of-charge voltage vs temperature
- Mid-discharge voltage vs temperature
- Capacity vs temperature
- Pressure profiles on charge/discharge
- Charge efficiency
- Specific energy
- Low-temperature limits
- Summary/comparison of different cell designs.

Performance data are presented for the I–VII A cells only, but in the summary, data are presented to compare I–V, I–VI, I–VII, and I–VIII A cell designs. The INTELSAT VII A electrical characterization test sequence is presented in Table 5-1.

Table 5-1. INTELSAT VII A Electrical Characterization Test Sequence

1.	Charge at 6.0 hours at 10°C Discharge: 60A to 0.1 V
2.	Charge at 12A for 16 hours at 10°C Discharge: 60A to 0.1 V
3.	Repeat Step 2
4.	Repeat Step 2 at 10°C
5.	Repeat Step 2 at 0°C for 2 cycles
6.	Repeat Step 2 at -10°C for 2 cycles

7. Repeat Step 2 at -30°C for 2 cycles

8. Charge at 12A for 16 hours at -20°C
   Trickle charge at 1.2A for 4 hours
   Discharge: 60A to 0.1A

9. Repeat Step 2 at 10°C for 2 cycles

10. Repeat Step 2 at 20°C for 2 cycles

11. Repeat Step 2 at 30°C for 2 cycles

12. Repeat Step 2 at 10°C for 2 cycles

13. Charge at 12A for 16 hours at 10°C
    Open circuit stand for 144 hours
    Discharge: 60A to 0.1V

14. Charge at 12A for 16 hours at 10°C
    Raise temperature to 20°C and
    Open circuits for 144 hours

15. Charge at 12A for 16 hours at 10°C
    Raise temperature to 30°C and open-circuit cells for 144 hours
    Discharge: 60A to 0.1V at 30C

5.1.1 Reconditioning

Six INTELSAT VII A 120-Ah cells were used for electrical characterizations [5-1]. A 48-hour reconditioning cycle at 10°C was used to reactivate the cells after storage. The cells were charged at 6A (C/20 rate) for 48 hours and discharged at 60 A (C/2 rate) to 0.0 volts. Reconditioning charge/discharge voltage profiles for the six cells are shown in Figure 5-1; note how well matched the six cells are both in terms of charge/discharge voltage and capacity.

5.1.2 Charge Voltage

Reconditioning was followed by capacity measurements at 10°C, 0°C, -10°C, -30°C, 10°C, 20°C, and 30°C. Two cycles were run at each temperature. The cells were charged at a 12A (C/10 rate) for 16 hours and then discharged at 60A (C/2 rate) to 0.1 V. Capacity data for each cell is presented in Figure 5-2. Figure 5-3 shows graphically the peak voltage that was measured during the charge portion of the capacity tests for each of the six cells as a function of temperature.

	Ichg	Idisc	TEMP	MID-DCHV (TO 0.1V)	CAPACITY(Ah) (TO 0.1V)	ENERGY(Wh) (TO 0.1V)	MID-DCHV (TO 1.0V)	CAPACITY(Ah) (TO 1.0V)	ENERGY(Wh) (TO 1.0V)
———	6.0A	60A	10°C	1.246	131.70	163.45	1.246	130.50	162.60
—-—-—	6.0A	60A	10°C	1.246	130.10	161.60	1.247	129.00	160.72
—-—-	6.0A	60A	10°C	1.246	130.60	162.16	1.247	129.40	161.26
—-—-	6.0A	60A	10°C	1.246	128.00	158.88	1.247	127.00	158.22
— —	6.0A	60A	10°C	1.246	126.90	157.37	1.246	125.90	156.67
— —	6.0A	60A	10°C	1.245	130.00	161.08	1.245	128.70	160.13

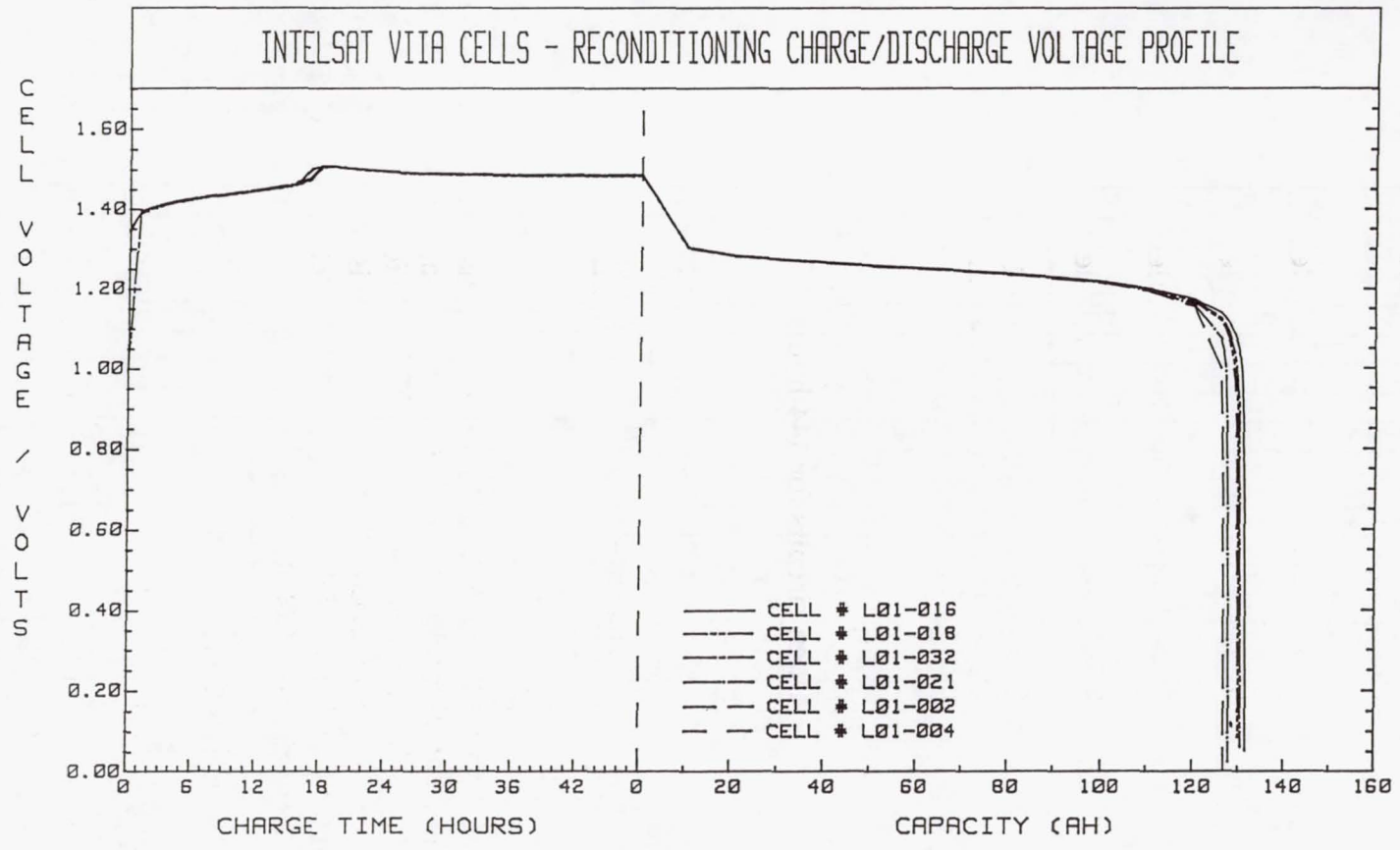

Figure 5-1. INTELSAT VII A cells—reconditioning charge/discharge voltage profile.

		CELL # L01-016			CELL # L01-018			CELL # L01-032			CELL # L01-021			CELL # L01-002			CELL # L01-004			
Cyc	Temp.	1.0 Volt	0.7 Volt	0.1 Volt	1.0 Volt	0.7 Volt	0.1 Volt	1.0 Volt	0.7 Volt	0.1 Volt	1.0 Volt	0.7 Volt	0.1 Volt	1.0 Volt	0.7 Volt	0.1 Volt	1.0 Volt	0.7 Volt	0.1 Volt	Rem
1	10°C	130.5	131.4	132.3	129.0	129.9	132.8	129.4	130.3	131.8	127.0	127.7	129.6	125.9	126.6	128.3	128.8	129.6	130.0	1
2	10°C	126.9	126.6	127.6	124.7	125.5	126.9	125.2	126.0	127.3	122.7	123.3	125.3	122.0	122.6	124.0	124.4	125.2	125.7	2
3	0°C	138.5	140.6	141.0	138.0	139.1	140.6	137.8	138.9	140.4	135.0	135.8	137.3	133.8	134.6	137.3	136.8	137.9	138.4	2
4	0°C	139.3	140.2	141.6	138.6	139.6	140.0	138.4	139.4	139.8	135.9	136.8	137.7	134.5	135.2	135.6	137.1	138.1	138.6	2
5	-10°C	147.7	149.4	149.9	146.8	148.6	149.1	145.7	147.5	148.1	143.9	145.5	145.9	142.0	143.4	143.8	145.3	147.0	147.5	2
6	-10°C	149.4	151.2	151.7	148.4	150.3	150.8	147.2	149.1	149.6	145.6	147.3	147.8	143.6	145.0	145.1	147.0	148.8	149.3	2
7	-20°C	150.4	154.4	155.1	149.7	153.7	154.4	147.7	152.0	152.8	146.5	150.3	150.9	144.5	147.7	148.3	148.2	152.0	152.7	2
8	-20°C	151.4	155.8	156.5	150.9	155.2	156.0	148.7	153.3	154.1	147.6	151.8	152.4	145.6	149.0	149.6	149.3	153.4	154.1	2
9	-30°C	117.2	154.3	156.0	122.3	153.3	155.5	133.9	148.0	152.3	136.7	149.6	151.6	133.6	146.0	148.1	134.8	146.6	149.2	2
10	-30°C	120.0	153.3	155.0	121.9	151.2	154.2	133.5	146.7	150.6	132.5	147.9	150.3	130.9	144.8	147.2	132.5	143.3	147.1	2
11	-20°C							145.0	149.0	151.7				136.7	145.0	147.5	139.5	145.0	148.8	3
12	10°C	124.8	126.5	127.2	124.6	126.2	127.0	125.8	127.8	128.5	121.9	123.3	123.9	122.6	124.2	124.8	121.8	123.9	124.8	2
13	10°C	124.6	126.2	126.8	124.7	126.3	127.0	123.1	125.0	125.8	121.6	122.9	123.4	119.4	120.8	121.4	120.3	122.4	123.2	2
14	20°C	109.4	110.9	111.4	109.3	110.8	111.4	108.5	110.3	111.0	106.9	108.0	108.5	105.3	106.5	107.1	106.6	108.5	109.2	2
15	20°C	109.4	111.0	111.6	109.4	111.1	111.8	108.5	110.4	111.1	106.6	107.8	108.4	105.0	106.3	106.8	106.5	108.5	109.3	2
16	30°C	92.7	94.2	94.7	94.3	96.1	96.7	93.3	95.1	95.8	87.6	88.5	88.9	85.1	86.2	86.7	88.3	90.2	90.9	2
17	30°C	89.5	91.6	92.2	92.1	94.5	95.2	90.8	93.3	94.0	82.8	84.0	84.5	80.0	81.3	81.9	84.3	86.7	87.4	2
18	10°C	130.8	132.5	133.0	131.6	133.3	133.9	130.0	132.2	133.0	126.5	127.9	128.4	123.7	125.3	125.8	127.7	129.6	130.4	2
19	10°C	124.2	125.8	126.3	125.0	126.6	127.1	123.7	125.6	126.3	120.1	121.4	121.9	117.6	119.0	119.6	120.8	122.7	123.4	2
20	10°C	120.7	104.6	105.1	103.4	104.3	105.7	102.0	104.3	105.0	99.8	101.4	101.8	97.7	99.6	100.1	99.8	101.9	102.6	4
21	10°C	74.1	75.4	75.7	74.4	75.7	76.1	74.0	75.6	76.0	72.1	72.9	73.2	70.4	71.4	71.8	72.6	74.1	74.6	5
22	10°C	71.1	72.5	72.8	69.6	71.0	71.4	69.6	71.3	71.7				69.2	70.5	70.8	70.0	71.7	72.1	6

1 - Charge for 48 hours, Discharge to 0.1V

2 - Charge for 16 hours , Discharge to 0.1V

3 - Charge for 16 hours, Trickle @ 1.2A for 4 hours, Discharge to 0.1V

4 - Charge for 16 hours @ 10°C, open circuit for 144 hours @ 10°C, discharge to 0.1V @ 10°C

5 - Charge for 16 hours @ 10°C, open circuit for 144 hours @ 20°C, discharge to 0.1V @ 20°C

6 - Charge for 16 hours @ 10°C, open circuit for 144 hours @ 30°C, discharge to 0.1V @ 30°C

Figure 5-2. INTELSAT VII capacity measurement (Ah).

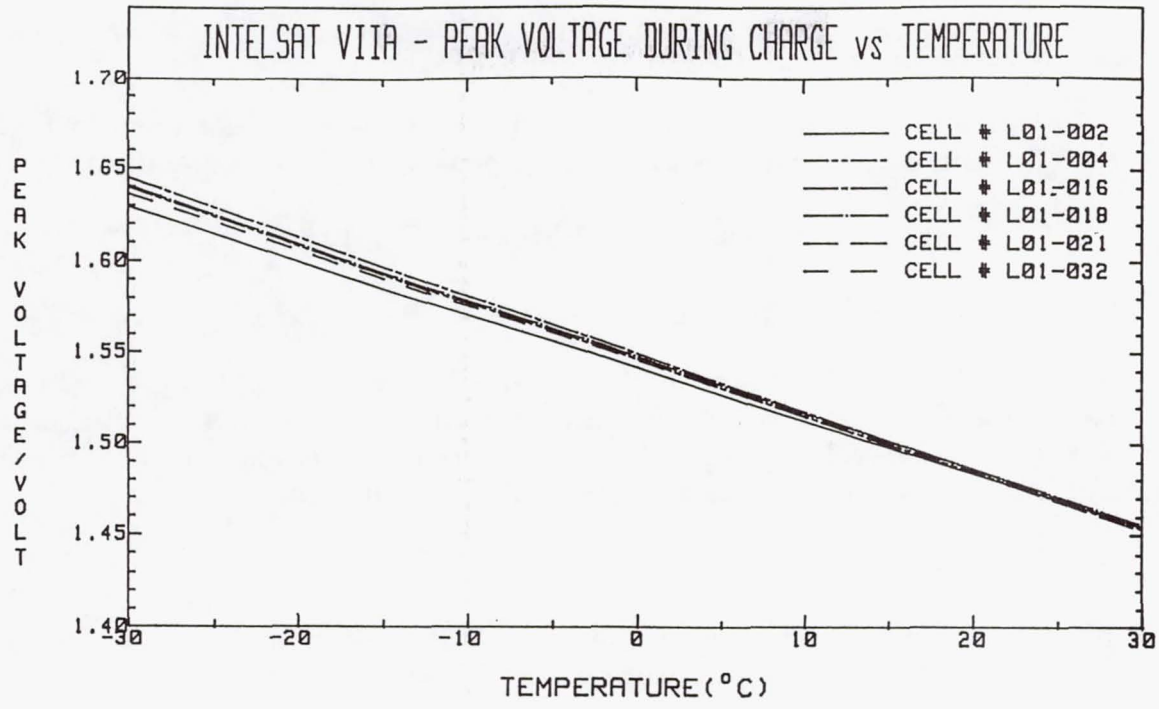

Figure 5-3. INTELSAT VII A—peak voltage during charge vs temperature.

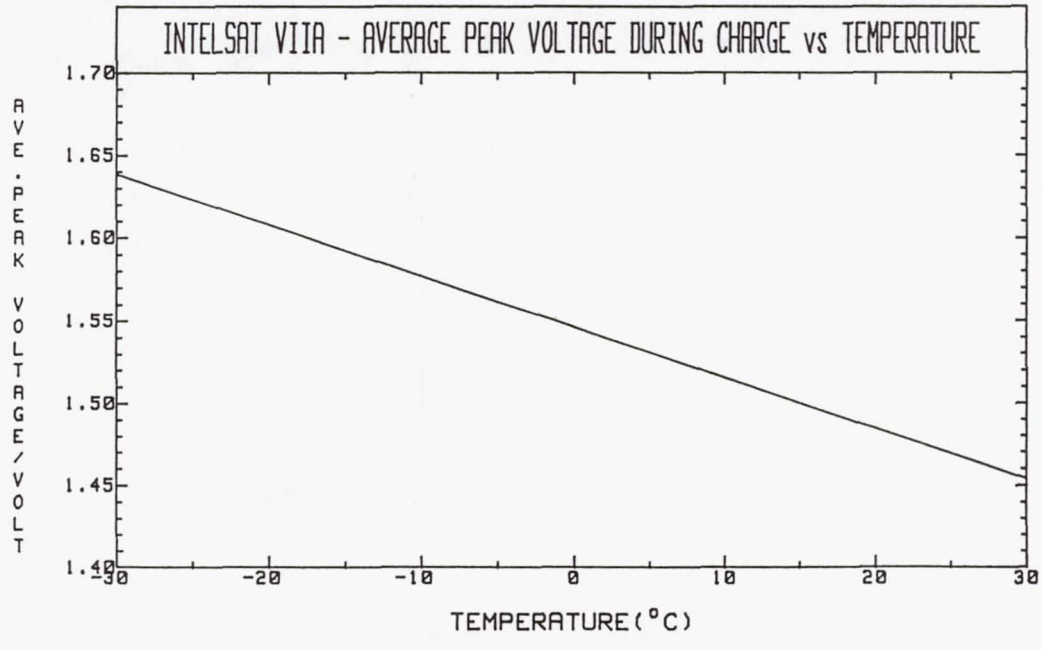

Figure 5-4. INTELSAT VII A—average peak voltage during charge vs temperature.

Average Peak Voltage

The average peak voltage during charge vs temperature is shown in Figure 5-4. The following equation relates the average peak voltage to temperature.

$$\text{Average peak voltage (V)} = 1.5462 - 3.075 \times 10^{-3} \times T\ (°C)$$

Average End-of-Charge Voltage (EOCV)

Figure 5-5 shows graphically the end-of-charge voltage (EOCV) that was measured at the EOC for each capacity test for each of the six cells as a function of temperature. The six-cell average EOCV vs temperature is shown in Figure 5-6. The following equation relates the average EOCV to temperature.

$$\text{EOCV (V)} = 1.5195 - 3.503 \times 10^{-3} \times T\ (°C)$$

Note that the peak voltage is higher than the EOCV. The voltage peaks and then rolls over as the cell stack heats up during the 16-hour charge. Peak voltage occurs after about 12 hours of charging.

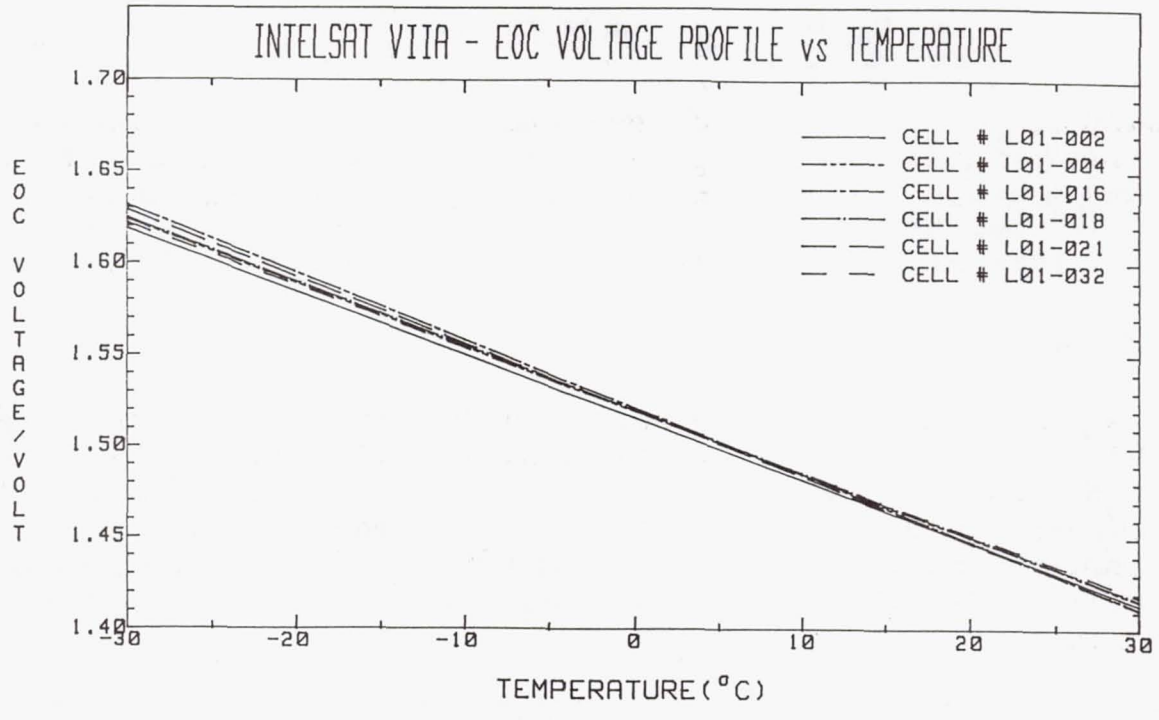

Figure 5-5. INTELSAT VII A—EOC voltage profile vs temperature.

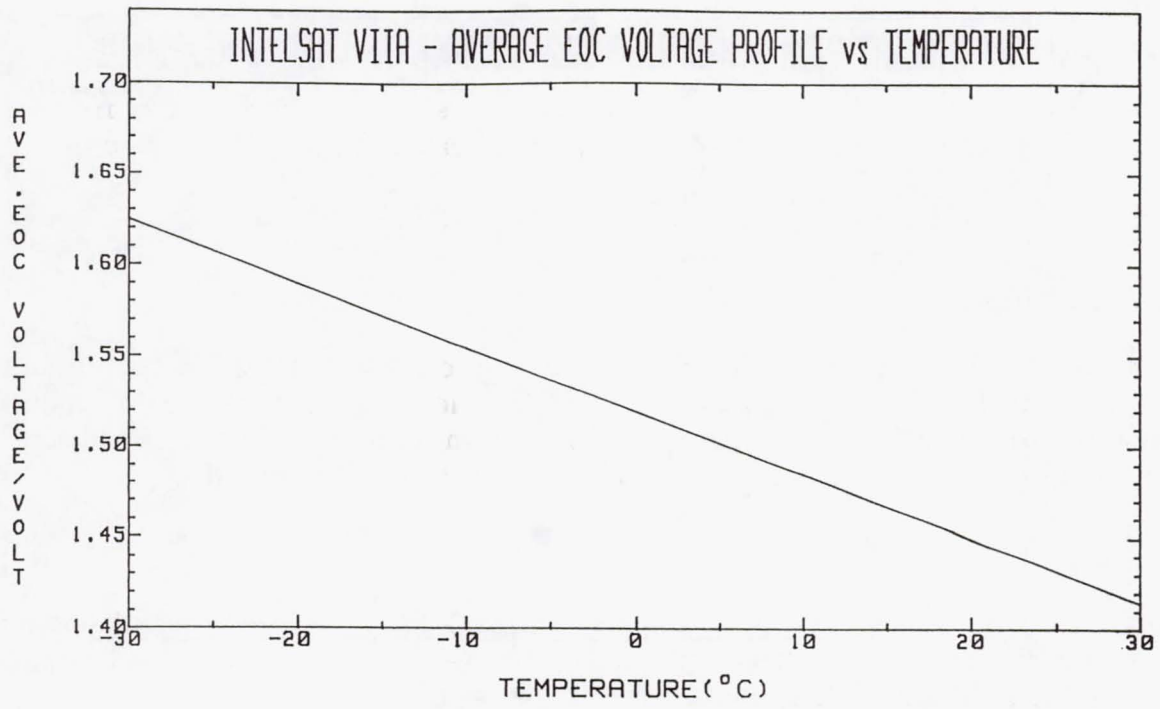

Figure 5-6. INTELSAT VII A—average EOC voltage profile vs temperature.

5.1.3 Mid-Discharge Voltage

Figure 5-7 shows graphically the mid-discharge voltage that was measured during discharge in the capacity test for each of the six cells as a function of temperature. This is the mid-discharge voltage to 1.0 volts at the C/2 rate (60A). The average mid-discharge voltage vs temperature is shown in Figure 5-8. The following equation relates the average mid-discharge voltage to temperature.

$$\text{Average Mid-Discharge Voltage (V)} = 1.2377 + 1.025 \times 10^{-3} \times T\ (°C)$$

5.1.4 Capacity

Figure 5-2 presents the measured capacity for each cell to 1.0 volts, 0.7 volts, and 0.1 volts. Voltage and temperature profiles of cell L01-004 are shown in Figure 5-9 for the capacity measurements at different temperatures. Figure 5-10 shows the capacity that was measured to 1.0 volts for each of the six cells as a function of temperature. The six-cell average capacity as a function of temperature is shown in Figure 5-11. The following equation relates the average capacity to 1.0 V to temperature.

$$\text{Capacity (C)} = 137.26 - 1.1572 \times T\ (°C) - 2.3786 \times 10^{-2} \times T^2\ (°C) + 2.1628 \times 10^{-4} \times T^3\ (°C)$$

The capacity for the I-VII A cells peaks at approximately -20°C.

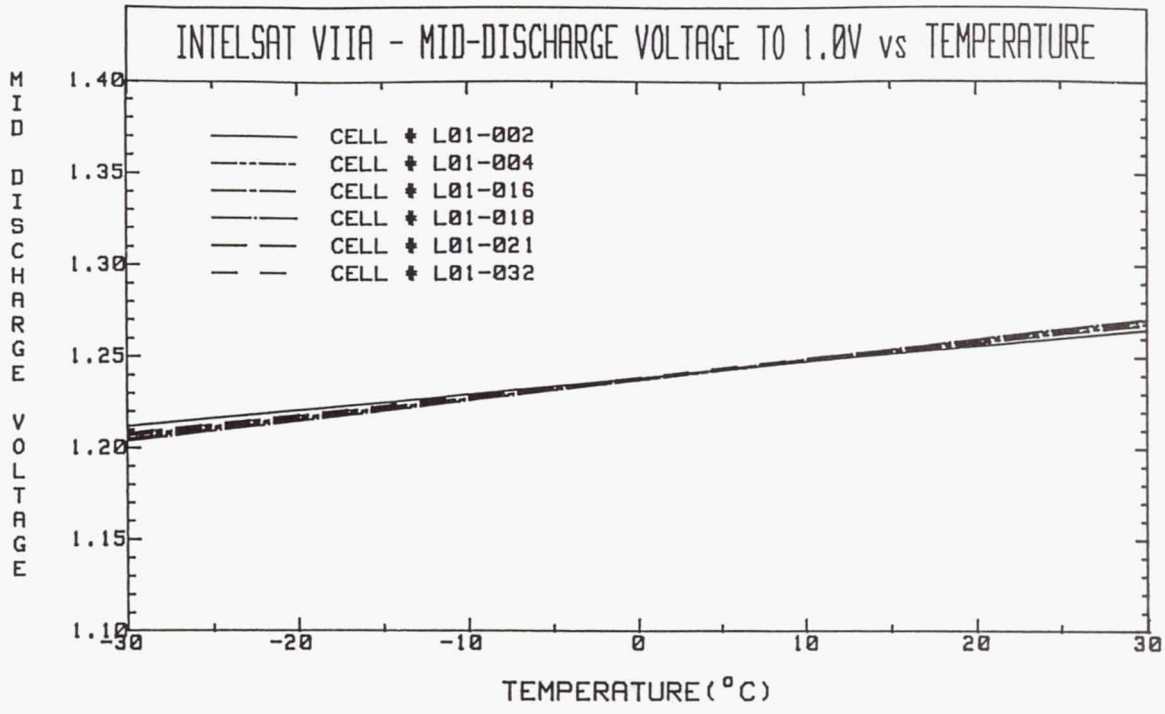

Figure 5-7. INTELSAT VII A—Mid-discharge voltage to 1.0 V vs temperature.

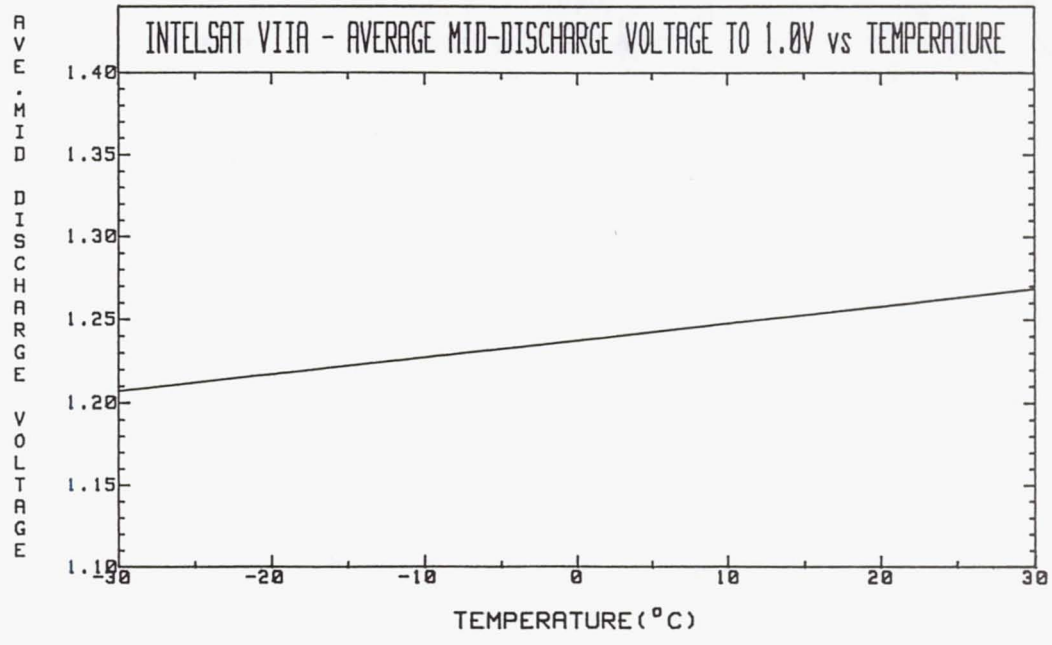

Figure 5-8. INTELSAT VII A—average mid-discharge voltage to 1.0 V vs temperature.

	TEMP	MID-DCHV (TO 0.1V)	CAP.(Ah) (TO 0.1V)	ENERGY(Wh) (TO 0.1V)	MID-DCHV (TO 1.0V)	CAP.(Ah) (TO 1.0V)	ENERGY(Wh) (TO 1.0V)
———	0°C	1.241	138.60	171.13	1.242	137.10	170.05
—·—·—	-10°C	1.230	149.30	182.60	1.232	147.00	180.81
—··—·—	-20°C	1.211	154.15	185.25	1.214	149.32	181.27
—·—·—	10°C	1.248	123.22	151.96	1.249	120.33	149.81
— —	20°C	1.261	109.34	135.54	1.262	106.51	133.46
— —	30°C	1.263	87.44	107.99	1.265	84.30	105.68

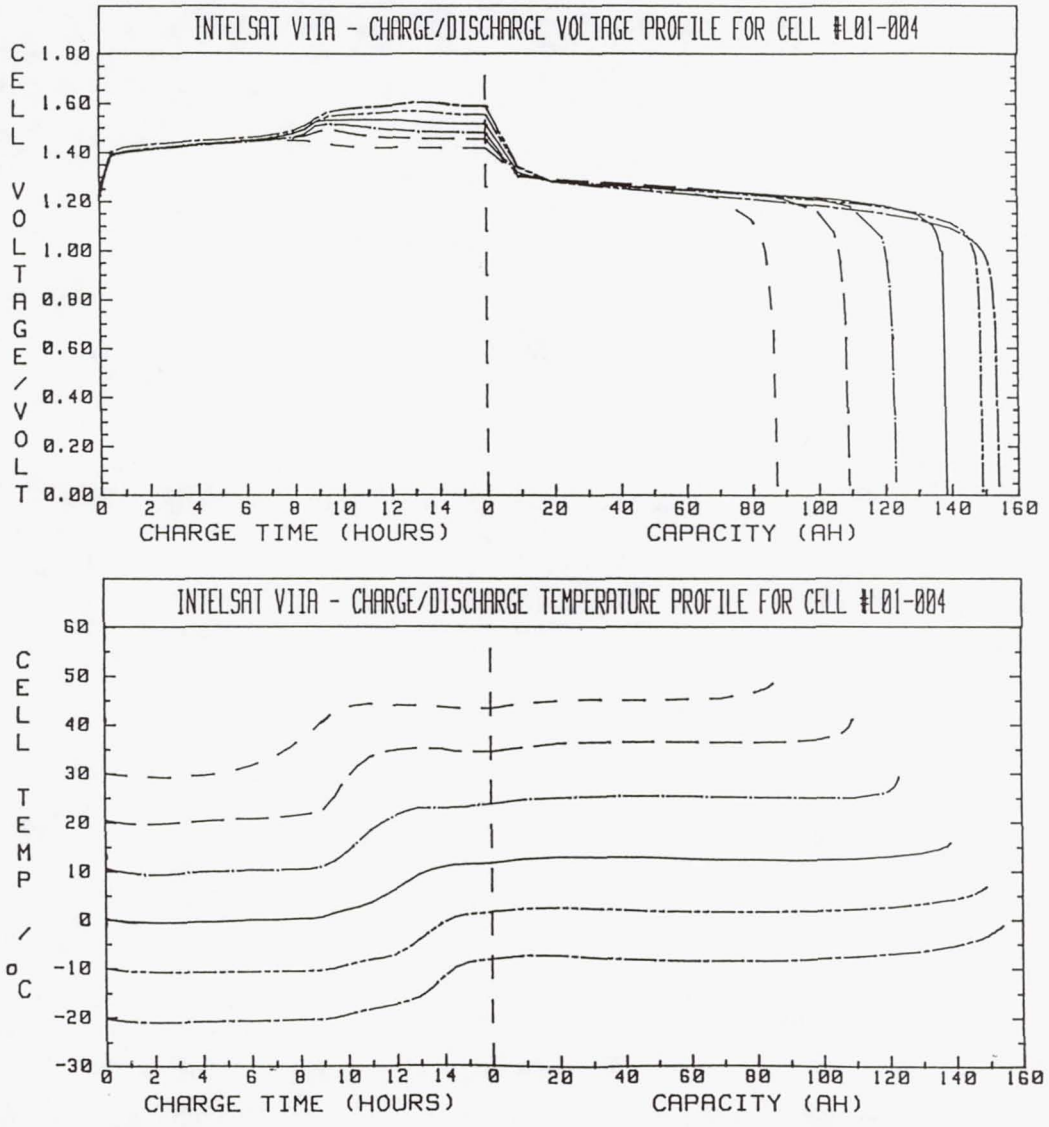

Figure 5-9. INTELSAT VII A charge/discharge voltage and temperature profile for cell L01-004.

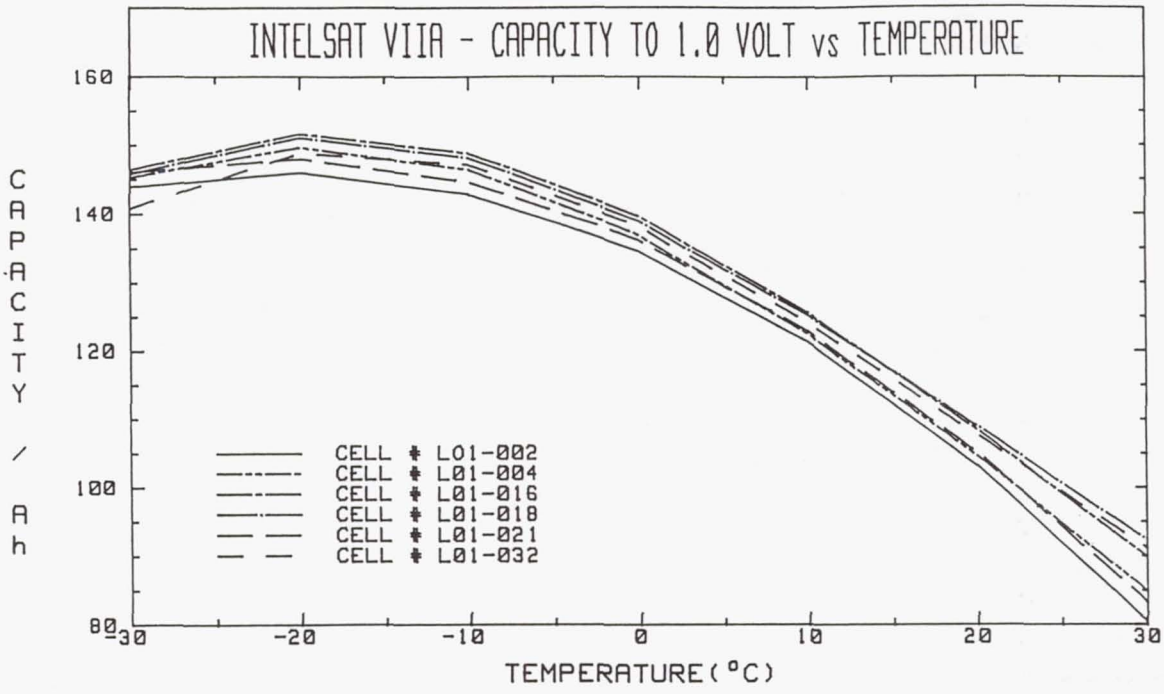

Figure 5-10. INTELSAT VII A—capacity to 1.0 V vs temperature.

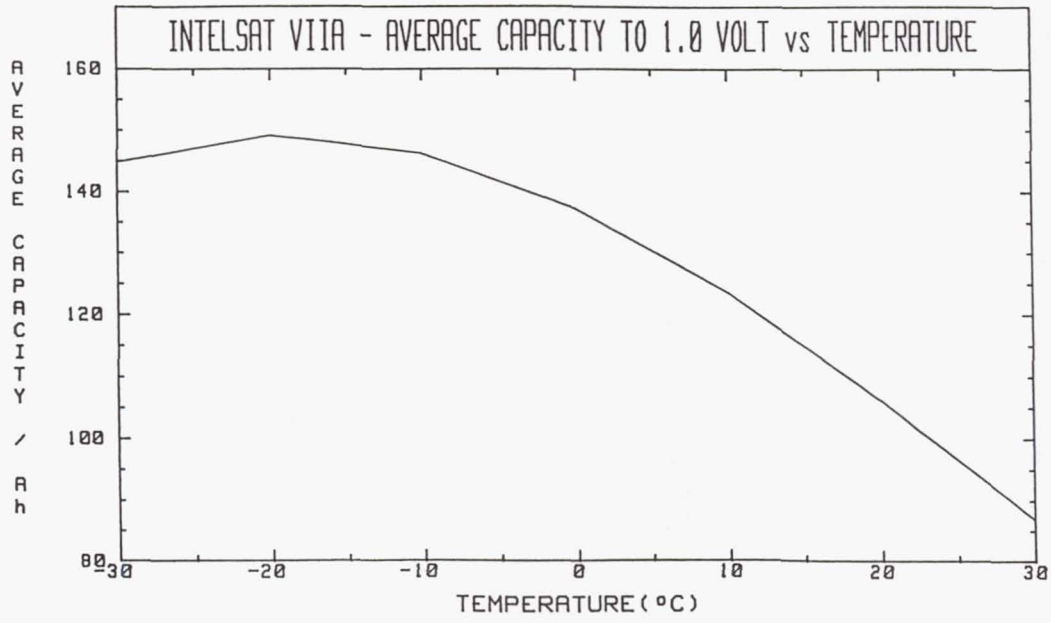

Figure 5-11. INTELSAT VII A—average capacity to 1.0 V vs temperature.

5.1.5 Specific Energy

Electrical energy (to 1.0 V) for each cell was calculated during capacity measurements. Figure 5-12 shows graphically the energy to 1.0 volts for all six cells as a function of temperature. The six-cell average energy as a function of temperature is shown in Figure 5-13. The following equation relates the cell energy to temperature.

$$\text{Energy} = 170.21 - 1.3222 \times T\,(°C) - 3.2850 \times 10^{-2} \times T^2\,(°C) + 3.0150 \times 10^{-4} \times T^3\,(°C)$$

The specific energy is determined by dividing the cell energy by the cell weight. At -20°C the specific energy is 68.15 Wh/kg, the maximum.

5.1.6 Pressure

The pressure profiles for the charge and discharge segments of the capacity measurements at different temperatures were generated from the strain-gauge bridge outputs for cell L01-004 (see Figure 5-14). These data were normalized to 0°C (using the perfect gas law). The resultant charge/discharge segments are shown in Figure 5-15. Note that the slopes (rate-of-change-of-pressure) on charge and discharge are almost identical; when the pressure data were normalized to 0.0°C. The variation in the slopes with temperature shown in Figure 5-14 occurred because of the gas law effect of pressure with temperature. The actual cell temperature during the charge and discharge cycle as shown in Figure 5-9 was used to normalize the pressure to 0°C.

$$pv = NRT$$

5.1.7 Charge Efficiency

The instantaneous charge efficiency is determined by taking the derivative of the pressure with time. A linear pressure rise during charge represents 100 percent charge efficiency. As the pressure rise starts to drop off (onset of oxygen evolution at the positive electrode), the instantaneous charge efficiency drops off. Charge efficiency profiles were generated for cell L01-004 by taking the derivative of the strain-gauge bridge output as a function of time. Charge efficiency profiles were generated at each of the different temperatures shown (see Figure 5-16). For example, at 30°C, the efficiency drops off after 5 hours of charging and drops to zero after about 10 hours of charging. For lower temperatures, the charge efficiency does not drop off until further into the charge; the charge efficiency improves at lower temperatures. One can calculate the overall charge efficiency by integrating the area under the curve over the 16-hour charge period.

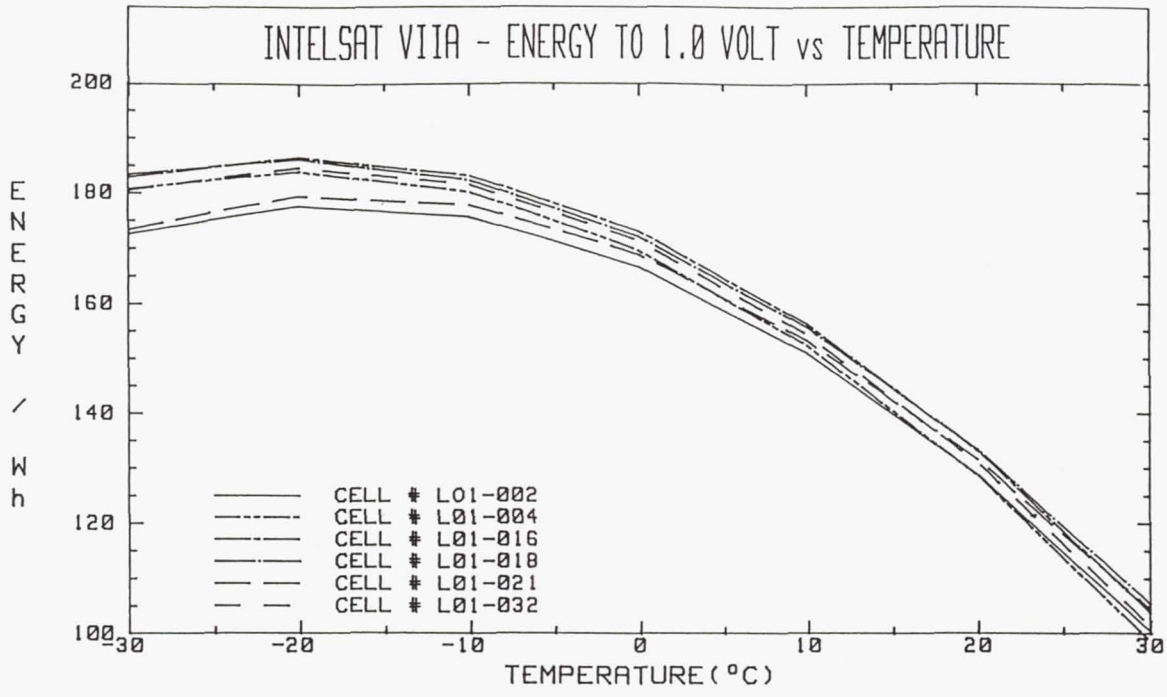

Figure 5-12. INTELSAT VII A—energy to 1.0 V vs temperature.

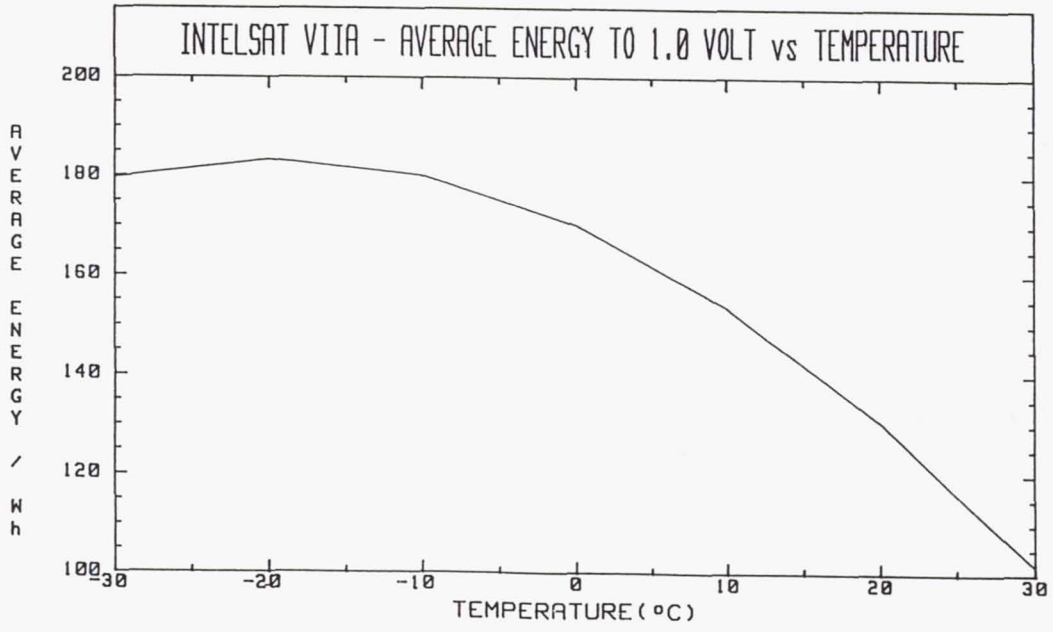

Figure 5-13. INTELSAT VII A—average energy to 1.0 V vs temperature.

		CHARGE		DISCHARGE	
	Temp.	Slope	Intercept	Slope	Intercept
———	0°C	63.49	54	-5.716	815
—·—·—	-10°C	60.78	52	-5.48	841
—··—·—	-20°C	58.25	50	-5.251	833
——·——	10°C	66.3	61	-6.161	794
— —	20°C	68.7	61	-6.438	734
— —	30°C	70.36	60	-6.656	608

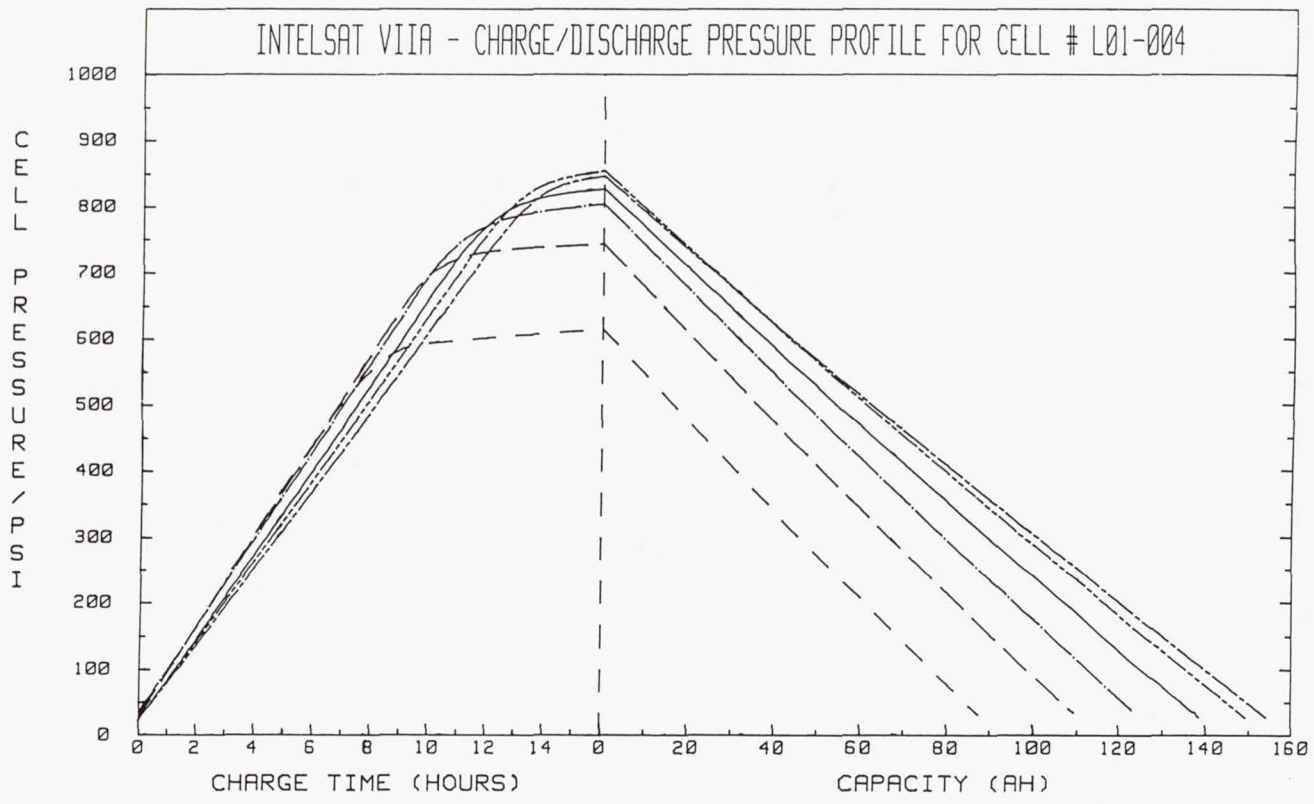

Figure 5-14. INTELSAT VII A—charge/discharge pressure profile for cell L01-004.

		CHARGE		DISCHARGE	
	Temp.	Slope	Intercept	Slope	Intercept
———	0°C	63.53	54	-5.467	779
—·—·—	-10°C	63.28	54	-5.443	835
—·—·—	-20°C	63.04	54	-5.415	858
—·—·—	10°C	63.91	59	-5.65	727
— —	20°C	63.84	57	-5.698	649
— —	30°C	63.29	55	-5.734	523

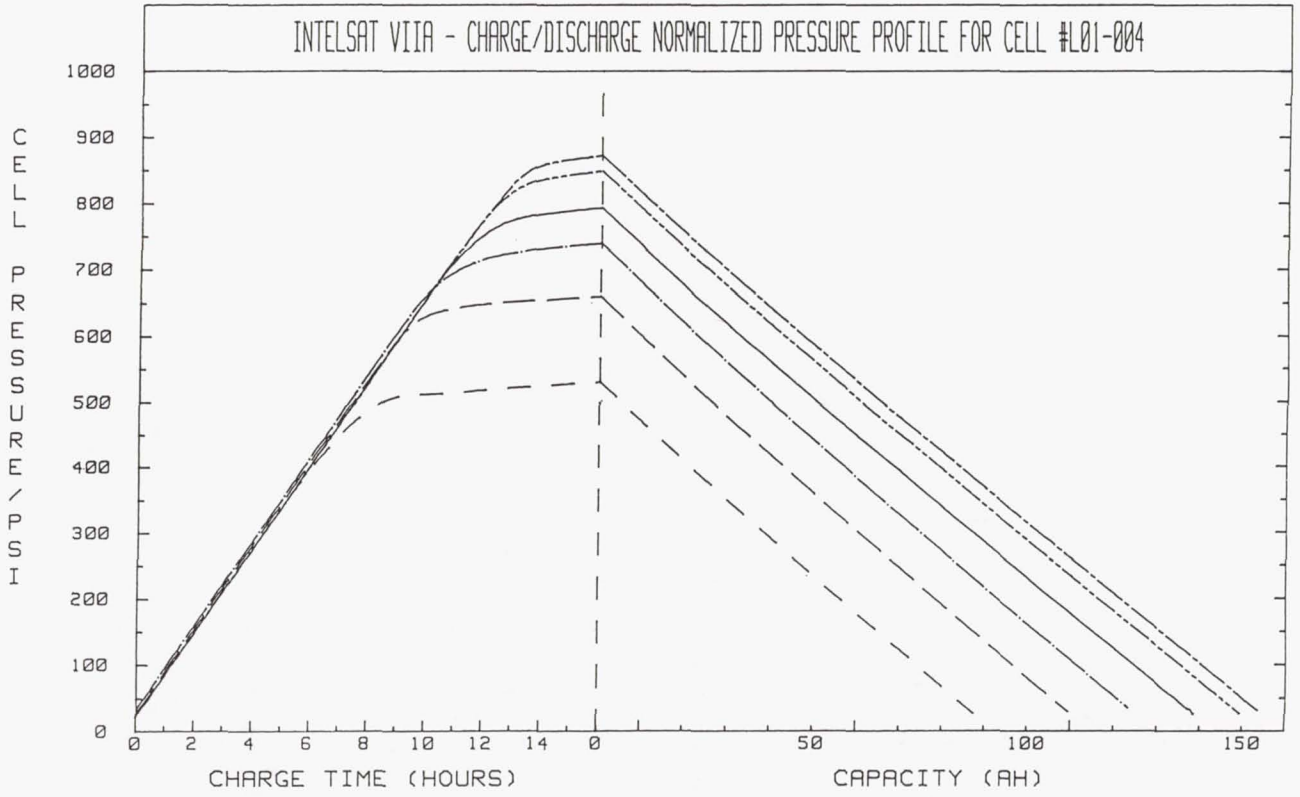

Figure 5-15. INTELSAT VII A—charge/discharge normalized pressure profile for cell L01-004.

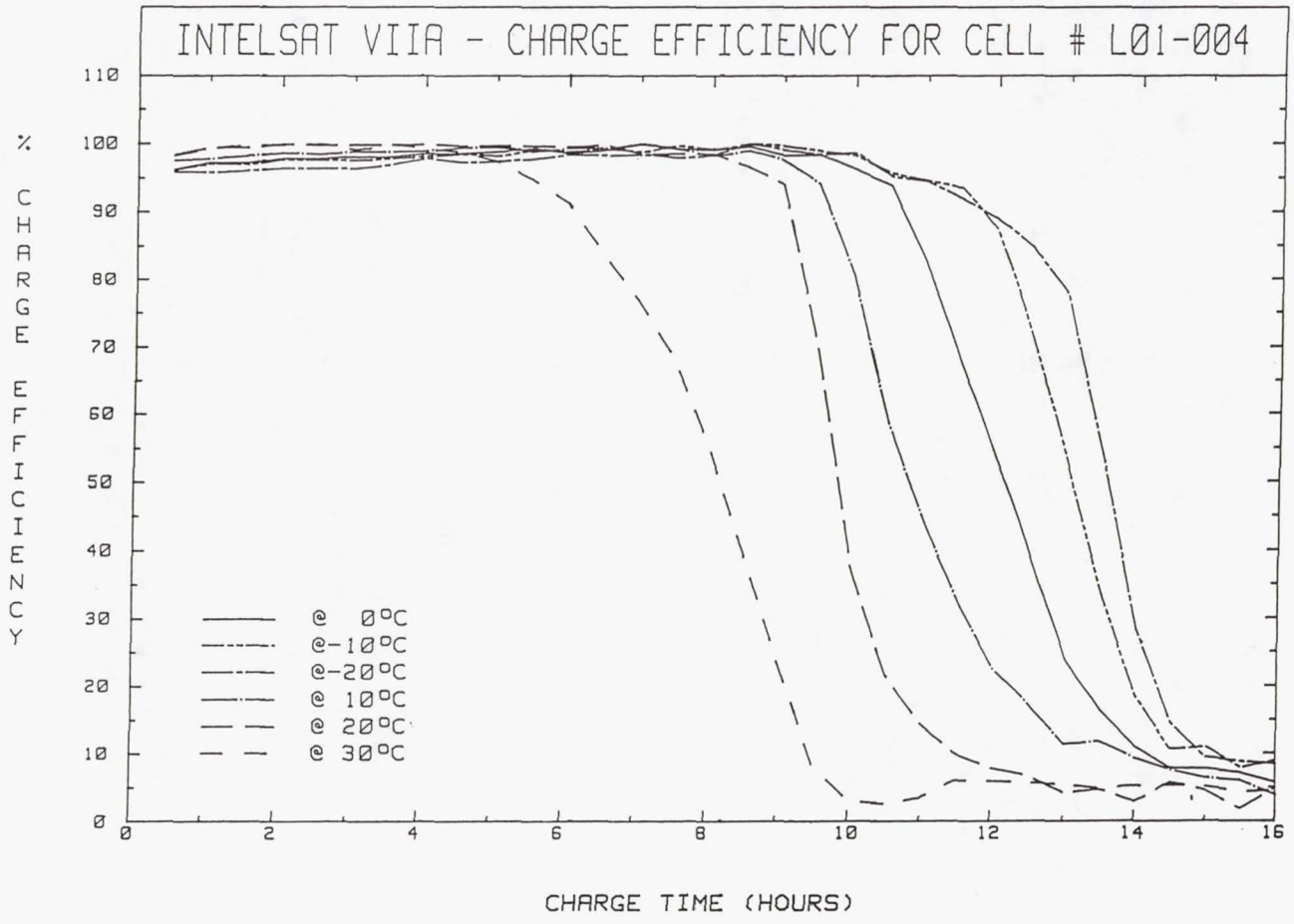

Figure 5-16. INTELSAT VII A—charge efficiency for cell L01-004.

Referring back to Figure 5-9 one can observe the temperature rise much sooner for cells at 30°C; the temperature starts rising after 6 hours charge time, as compared, for example, with cells at -10 or -20°C, where the temperature does not start rising until after 10 hours of charging. The heat produced by oxygen reduction causes the temperature increase.

5.1.8 Low-Temperature Limits

Low-temperature capacity measurements were used to define the limits of these I–VII A cells' performance. As previously mentioned, the cells were charged at a C/10 rate for 16 hours and then discharged at a C/2 rate to 0.1 volts. The discharge voltage profile at -30°C is shown in Figure 5-17. Note the initial drop in voltage on discharge, resulting from localized freezing of the electrolyte. After a few minutes on discharge, the heat produced by polarization warmed the cells sufficiently for voltage recovery.

A modified charge/discharge cycle was used to more closely simulate GEO operation. Cells were charged at a C/10 rate for 16 hours, followed by a C/100 rate trickle charge for 4 hours and then discharged at a C/2 rate to 0.1 volts. The discharge voltage profile at -20°C is shown in Figure 5-18. On discharge, three cells dropped to 0.1 volts in a few minutes, and the remaining three cells dropped below 1.0 volts. The heat produced by polarization warmed these cells sufficiently for the voltage to recover, and the discharge was completed with no loss in capacity to 0.1 volts.

As described in Chapter 1, the freezing point of the electrolyte decreases with increasing KOH concentration to a eutectic point at -66°C at 31 W/% KOH. At 20 W/% KOH the freezing point increases to about -25°C. These I–VII A cells had 31 percent KOH discharged and approximately 28 percent KOH charged.

From the discharge data shown in Figure 5-17 and 5-18 above, it appears that localized concentrations of electrolyte are below 20 W/% KOH in the separator at the positive electrode interface during overcharge. The electrode is freezing in these localized regions, causing the high impedance on discharge.

With trickle charging, there is considerably less heat generated during overcharge, which explains the results obtained at -20°C (Figure 5-17). This trickle charge mode more closely simulates GEO operation during eclipse periods.

Based on these results, it is not recommended to operate Ni-H_2 cells with 31 W/% KOH discharged below -10°C (some margin of safety is needed).

Note that cells with higher electrolyte concentrations (38 W/% KOH discharged) have a lower temperature limit of -20°C.

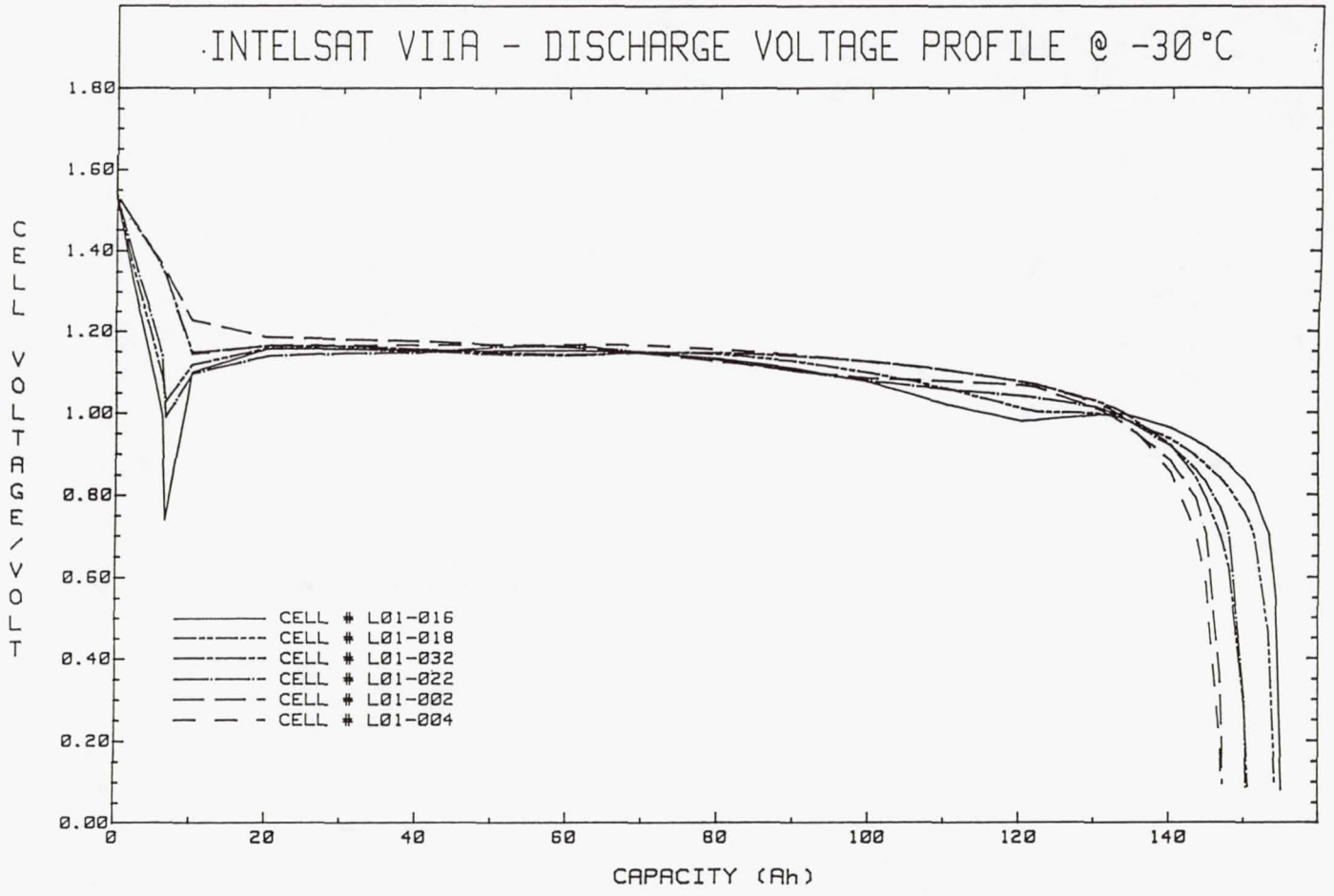

Figure 5-17. INTELSAT VII A—discharge voltage profile at –30°C.

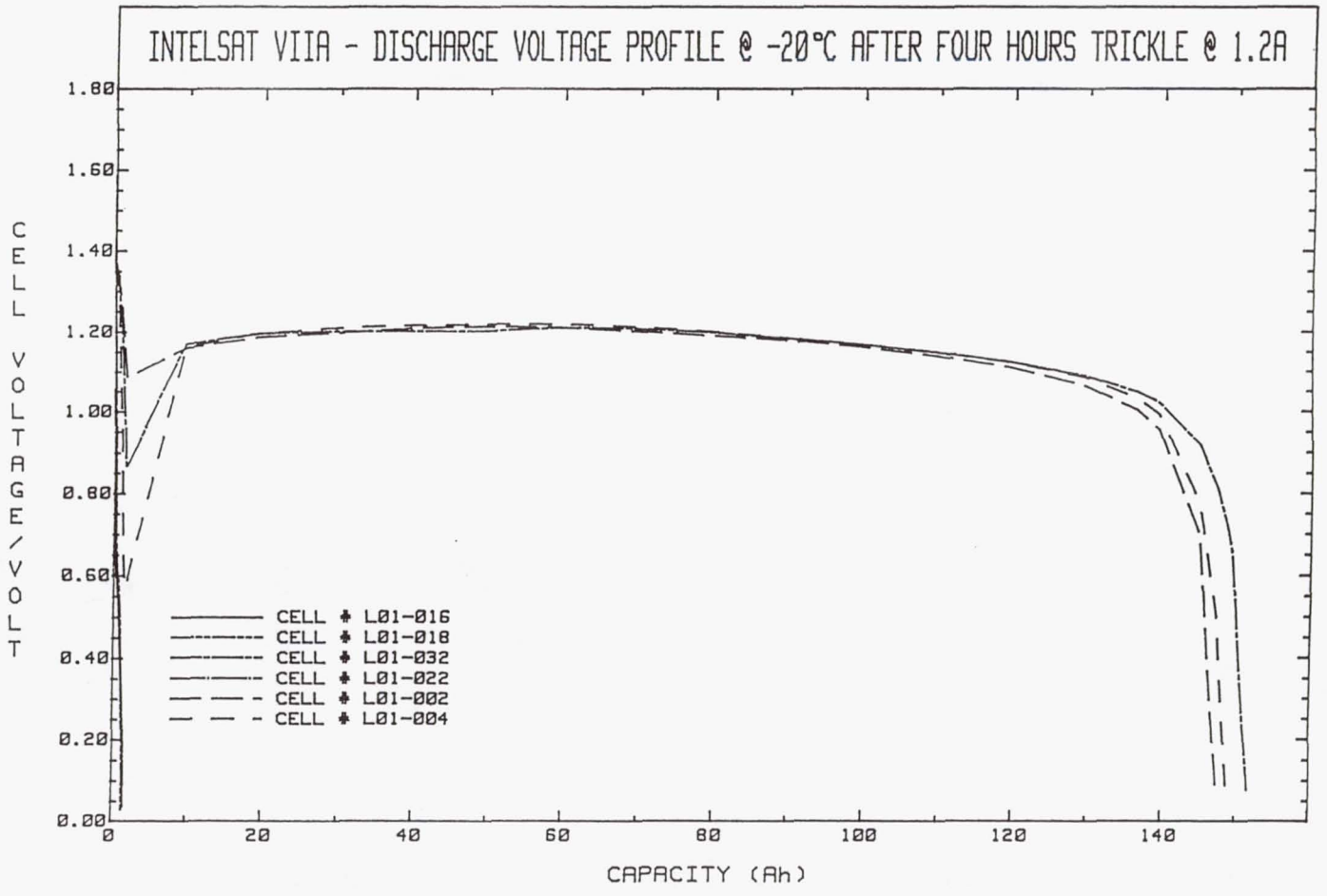

Figure 5-18. INTELSAT VII A—discharge voltage profile at –20°C after 4 hours trickle charge at 1.2 A.

5.1.9 Summary

COMSAT Laboratories performed the same electrical characterization tests for Ni-H_2 cells from the INTELSAT V, I–VI, I–VII, and I–VIII A programs [5-1]. Each of these INTELSAT programs used a different cell design. These different designs are described in Chapter 1 for the I–V, I–VI, and I–VII cell designs and Chapter 4 for the I–VII A cell design. Table 5-2 below is a comparison of design features.

Table 5-2. Cell Design Features

Design Features	I–V	I–VI	I–VII	I–VII A
Stack Design	back-to-back single-stack	recirculating single-stack	back-to-back single-stack	back-to-back single-stack
Plate Configuration	bus bar	pineapple slice	pineapple slice	pineapple slice
Separator	asbestos	Zircar/Zircar	Zircar/Zircar	Zircar/Zircar
Positive Electrode	slurry aqueous	dry powder alcohol	slurry aqueous	slurry aqueous
Electrode Concentration (discharged)	38%	31%	31%	31%
Precharge	negative	positive	positive	positive
Wall wick	none	ZrO	ZrO	ZrO
Cell Diameter	3.5 in.	3.5 in.	3.5 in.	4.5 in.

As described in Chapter 1, the I–V cell represents the COMSAT/INTELSAT cell design, and the I–VI cell represents the HAC/Air Force cell design. The I–VII and I–VII A cells represent "Second Generation" Ni-H_2 cell designs that combine the best features of both the COMSAT and Air Force designs as discussed in Chapter 1.

Peak Charging Voltage

The following equations relate the peak charging voltage to temperature for each of the different cell designs.

I–V	$V = 1.541 - 3.6 \times 10^{-3} T$ (°C)
I–VI	$V = 1.539 - 2.9 \times 10^{-3} T$
I–VII	$V = 1.543 - 2.7 \times 10^{-3} T$
I–VII A	$V = 1.546 - 3.1 \times 10^{-3} T$

Note that the peak charging voltages are very similar, independent of design variables, stack design, electrolyte concentration, separator type, etc. At 0°C, the difference between all four cell designs is only 7 mV (1.539 to 1.546 V).

End-of-Charge Voltage

The following equations relate the end-of-charge voltage to temperature for each of the different cell designs.

I–V	$V = 1.533 - 3.5 \times 10^{-3} T$ (°C)
I–VI	$V = 1.529 - 3.0 \times 10^{-3} T$
I–VII	$V = 1.523 - 3.3 \times 10^{-3} T$
I–VII A	$V = 1.519 - 3.5 \times 10^{-3} T$

Again, the end-of-charge voltages are similar for each of the different cell designs. At 0°C, the end-of-charge voltage varies from 1.519 V to 1.533 V (a difference of 34 mV).

The voltage variation with temperature (V/T curve) is similar for each of the different designs; the slope varies from -3.0×10^{-3} to -3.5×10^{-3} for the end-of-charge voltage. If a voltage limit is used for charge control, the slope of the V/T curve should fit these data (slope between -3.0×10^{-3} to -3.5×10^{-3}).

$$\frac{\Delta V}{\Delta T} = -3.0 \times 10^{-3} \quad (3 \text{ mV/°C})$$

The author recommends using the slope for the V/T curves used for charge control in LEO applications as described in Section 2.2.2.

Mid-Discharge Voltage

The following equations relate the mid-discharge voltage to the temperature for each of the four different cell designs.

I–V	$V = 1.221 + 1.511 \times 10^{-3} T$ (°C)
I–VI	$V = 1.256 + 6.80 \times 10^{-4} T$
I–VII	$V = 1.249 + 8.11 \times 10^{-4} T$
I–VII A	$V = 1.238 + 1.03 \times 10^{-3} T$

The mid-discharge voltage for the I–V cell is lower than I–VI, I–VII, and I–VII A cells. Design features of the I–V cells causing the lower mid-discharge voltage are a higher KOH electrolyte concentration and the use of asbestos separator material. The other cells have two layers of Zircar separators and, with the Zircar separators, there is more electrolyte and lower internal impedance.

Capacity and Voltage as a Function of Electrolyte Concentration

The effects of electrolyte concentration on capacity were determined experimentally using the HAC/Air Force 50-Ah Ni-H_2 cells as described in Chapter 1, Section 1.8.3. Cells were activated with different levels of electrolyte

concentration: 25, 31, and 38 W/% concentration of KOH. Figure 5-19 presents the average discharge voltage and the cell capacity as shown, as a function of electrolyte concentration. The capacity increases significantly with increasing electrolyte concentration, but the average discharge voltage decreases as the electrolyte concentration increases.

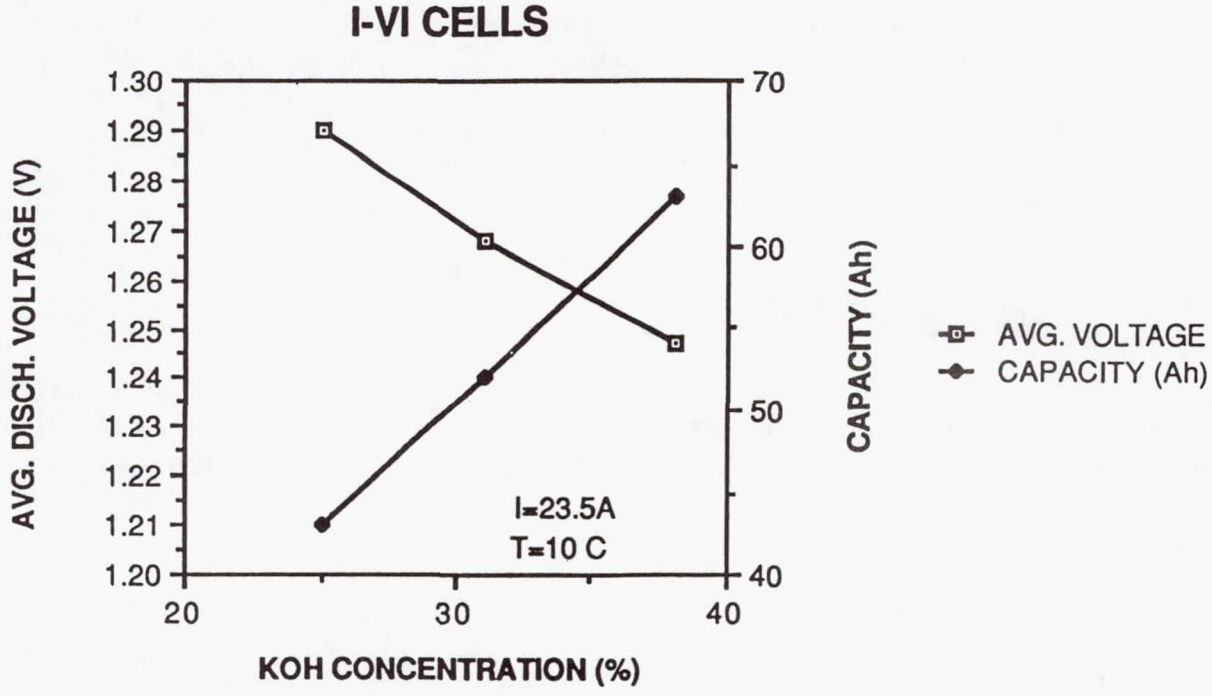

Figure 5-19. Capacity and voltage vs KOH concentration for I–VI cells.

Capacity as a Function of Temperature

The following equations relate the capacity measured to temperature.

I–V	$C = 40.05 - 0.11\ T\ (°C) - 1.05 \times 10^{-2}\ T^2\ (°C) - 1.90 \times 10^{-4}\ T^3\ (°C)$
I–VI	$C = 64.56 - 0.58\ T\ (°C) - 3.58 \times 10^{-3}\ T^2\ (°C) - 4.60 \times 10^{-5}\ T^3\ (°C)$
I–VII	$C = 100.70 - 0.81\ T\ (°C) - 8.37 \times 10^{-3}\ T^2\ (°C) + 1.29 \times 10^{-4}\ T^3\ (°C)$
I–VII A	$C = 137.26 - 1.16\ T\ (°C) - 2.38 \times 10^{-2}\ T^2\ (°C) + 2.16 \times 10^{-4}\ T^3\ (°C)$

Maximum cell capacity occurs at -20°C for I–VI, I–VII, and VII A and at -10°C for I–V.

Specific Energy

Presented below are the specific energies for each of the four cell designs. The specific energies are given at 30°C and at -20°C (-10°C for I–V) where the maximum capacity was measured.

Cell Type	Specific Energy (Wh/kg)		
I–V	33.3 at 30°C	55.9 at 0°C	58.8 at -10°C
I–VI	33.7 at 30°C	54.8 at 0°C	58.0 at -20°C
I–VII	49.12 at 30°C	66.9 at 0°C	74.0 at -20°C
I–VII A	40.9 at 30°C	63.7 at 0°C	68.1 at -20°C

There is a significant drop-off in the specific energy (capacity) at higher temperatures. The specific energy at 0°C is useful because this is closer to the recommended operating temperature in orbit.

5.2.0 SELF-DISCHARGE CHARACTERISTICS OF AIR FORCE 50-AH NI-H_2 CELLS

The rate of self discharge for Ni-H_2 cells is of concern for both GEO and LEO applications. The self-discharge rates are higher for Ni-H_2 cells than for Ni-Cd cells. For launch site planning, it is important to determine what the capacity fading, or battery capacity, will be after open circuit stand time prior to launch and after the transfer orbit period.

Charge retention after 72 hours of open-circuit stand at 10°C is one of the standard acceptance tests for Ni-H_2 cells. Typically, the cells retain greater than 85 percent of their initial capacity after this 72-hour open circuit stand at 10°C.

The self discharge rate as a function of temperature was determined experimentally for HAC/Air Force 50-Ah cells, used in the INTELSAT VI program [5-2]. HAC derated these cells to 44 Ah (nameplate capacity) for the INTELSAT VI program.

Test Results. HAC/Air Force 50-Ah cells (INTELSAT VI cells) were used to measure self-discharge on open-circuit stand at three temperatures: 10°C, 20°C, and 30°C. The data obtained at each temperature were fitted to an equation of the form

$$\ln (C) = \ln (C_O) - Kt$$

where

C = capacity remaining to 1 volt
K = slope or rate
t = open-circuit time
C_O = initial capacity

Figure 5-20 shows the self-discharge characteristics at 10°C, 20°C, and 30°C. The equations that best fit these data are

$$\ln (C) = \ln (90.66) - 0.00131t \quad \text{Temp} = 10°C \quad (1)$$
$$\ln (C) = \ln (92.02) - 0.00290t \quad \text{Temp} = 20°C \quad (2)$$
$$\ln (C) = \ln (89.32) - 0.00651t \quad \text{Temp} = 30°C \quad (3)$$

C is the percent capacity remaining.

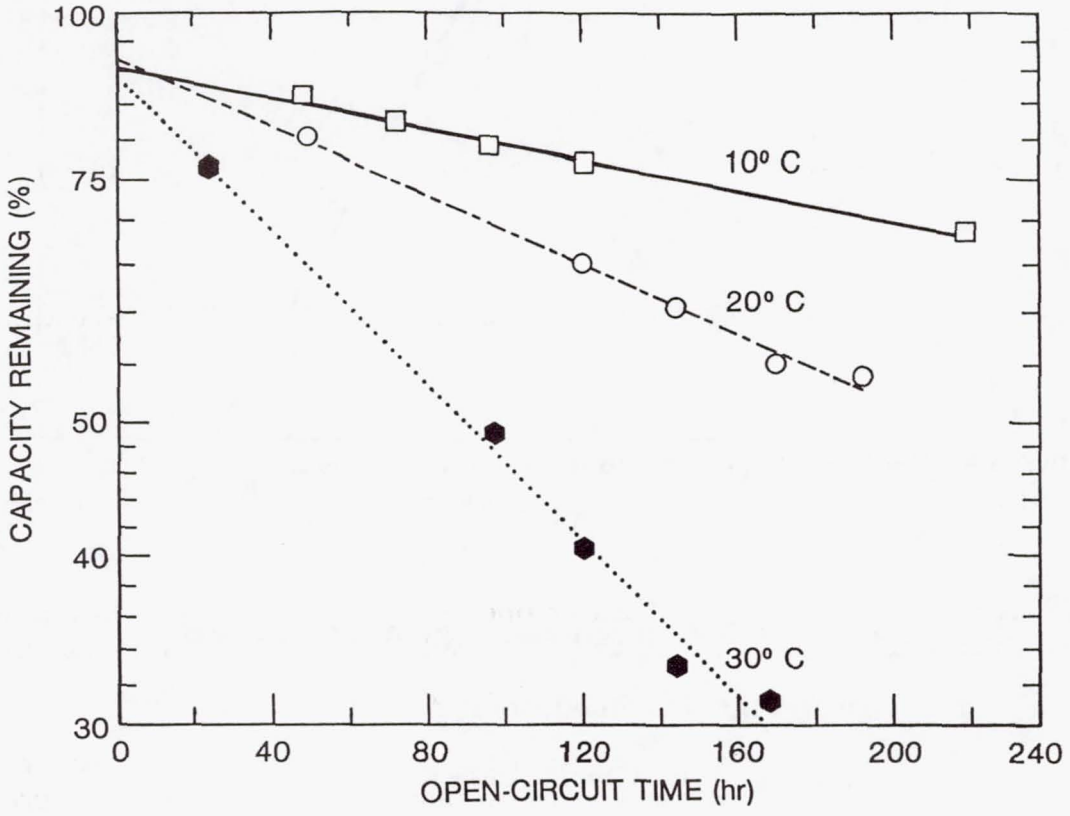

Figure 5-20. Self-discharge characteristics Ni-H_2 cells.

Figure 5-21 shows the Arrhenius plot for these three temperatures. The slope of the straight line regression fit to these three data points indicates an activation energy of 13.6 kcal/mole [5-2].

In the characterization tests described in Section 5.1.0 above, self-discharge tests were performed at 10°C, 20°C, and 30°C for I–V and I–VII A cells [5-1]. The cells were charged at a C/10 rate for 16 hours and left on open-circuit stand for 144 hours. Pressure profiles for the self-discharge test of I–VII A cell L01-004 are presented in Figure 5-22 and 5-23.

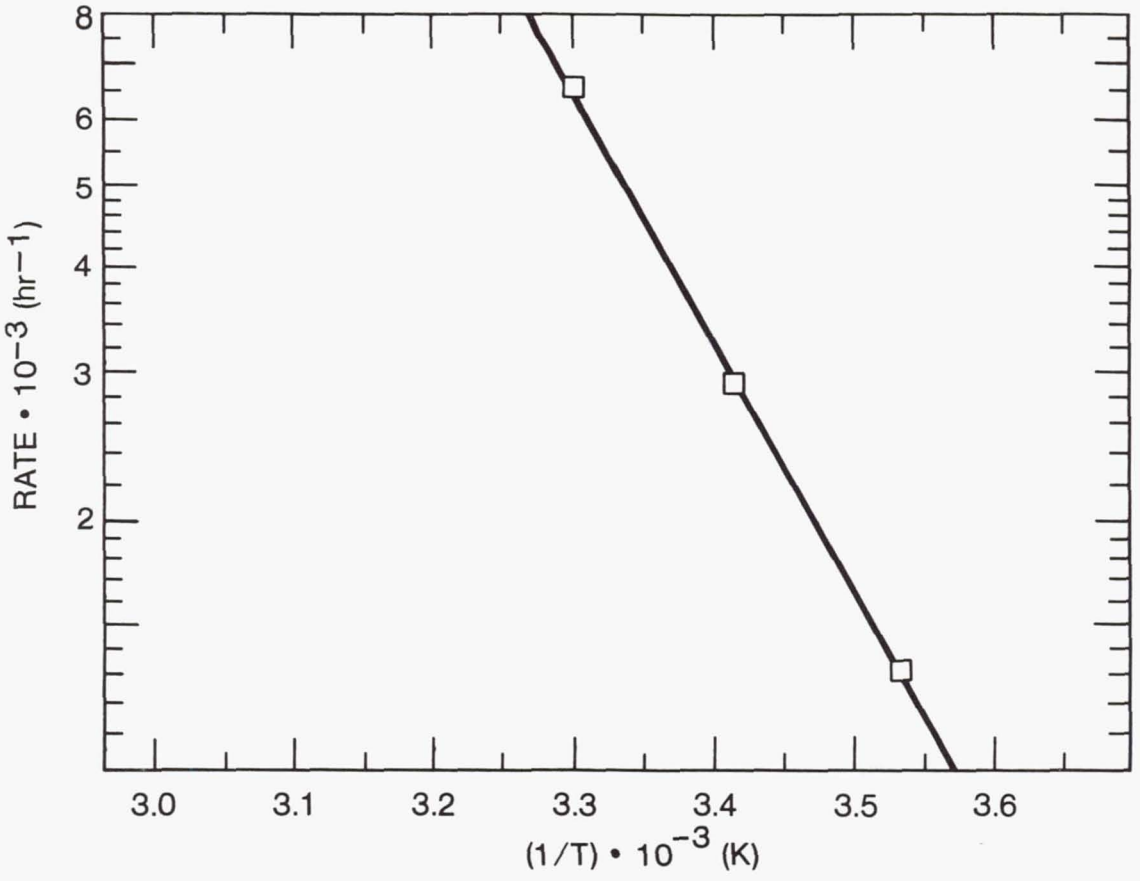

Figure 5-21. Rate of self-discharge vs temperature.

These data were also fitted to an equation of the form:

$$\ln (C) = \ln (C_o) - Kt$$

The equations that best fit the data are:

INTELSAT V

$\ln (C) = \ln (90.257) - 0.00127t$ Temp = 10°C
$\ln (C) = \ln (91.974) - 0.00198t$ Temp = 20°C
$\ln (C) = \ln (92.084) - 0.00313t$ Temp = 30°C

INTELSAT VII A

$\ln (C) = \ln (86.487) - 0.00104t$ Temp = 10°C
$\ln (C) = \ln (88.293) - 0.00191t$ Temp = 20°C
$\ln (C) = \ln (89.999) - 0.00329t$ Temp = 30°C

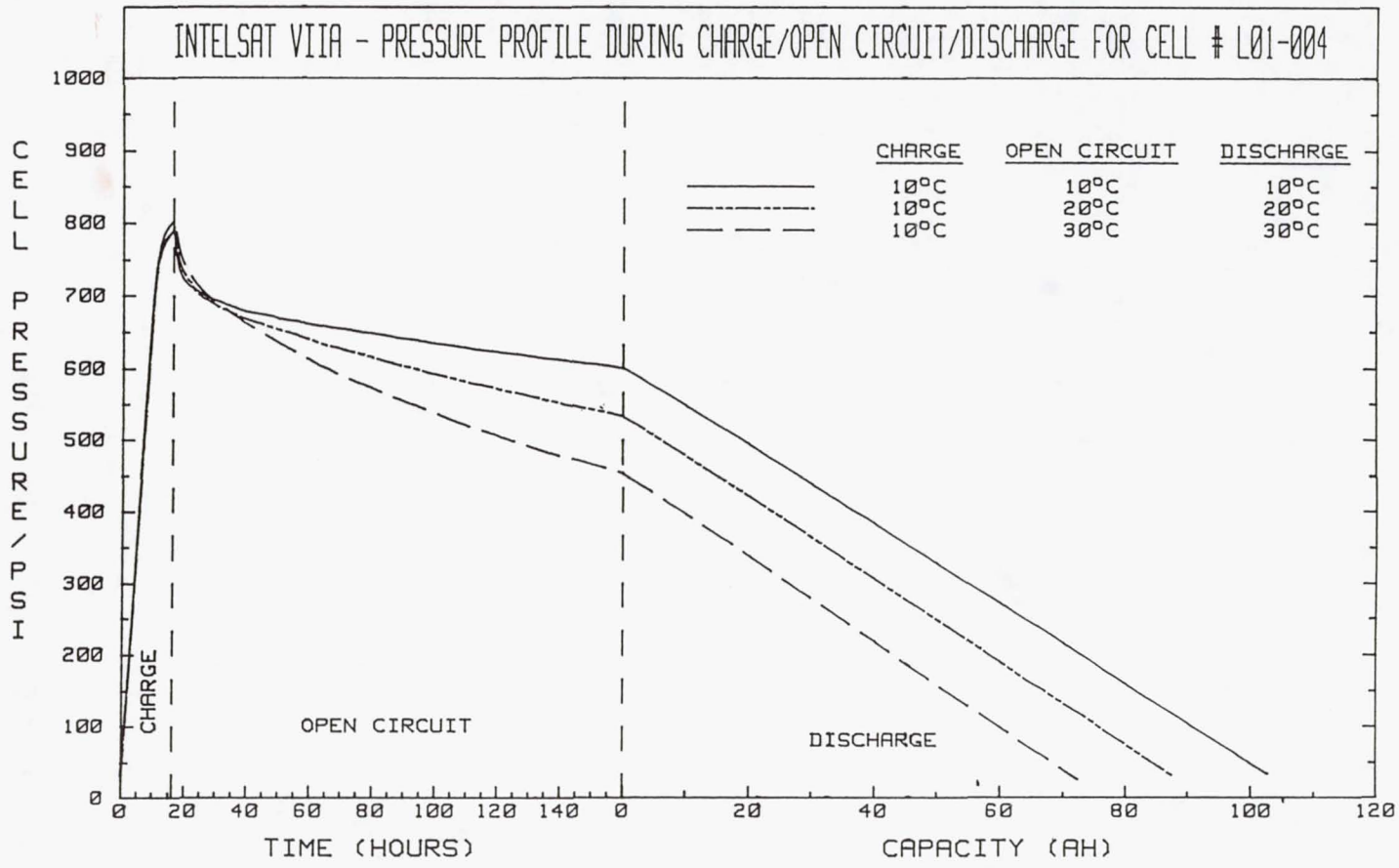

Figure 5-22. INTELSAT VII A—pressure profile during charge/open circuit/ discharge for cell L01-004.

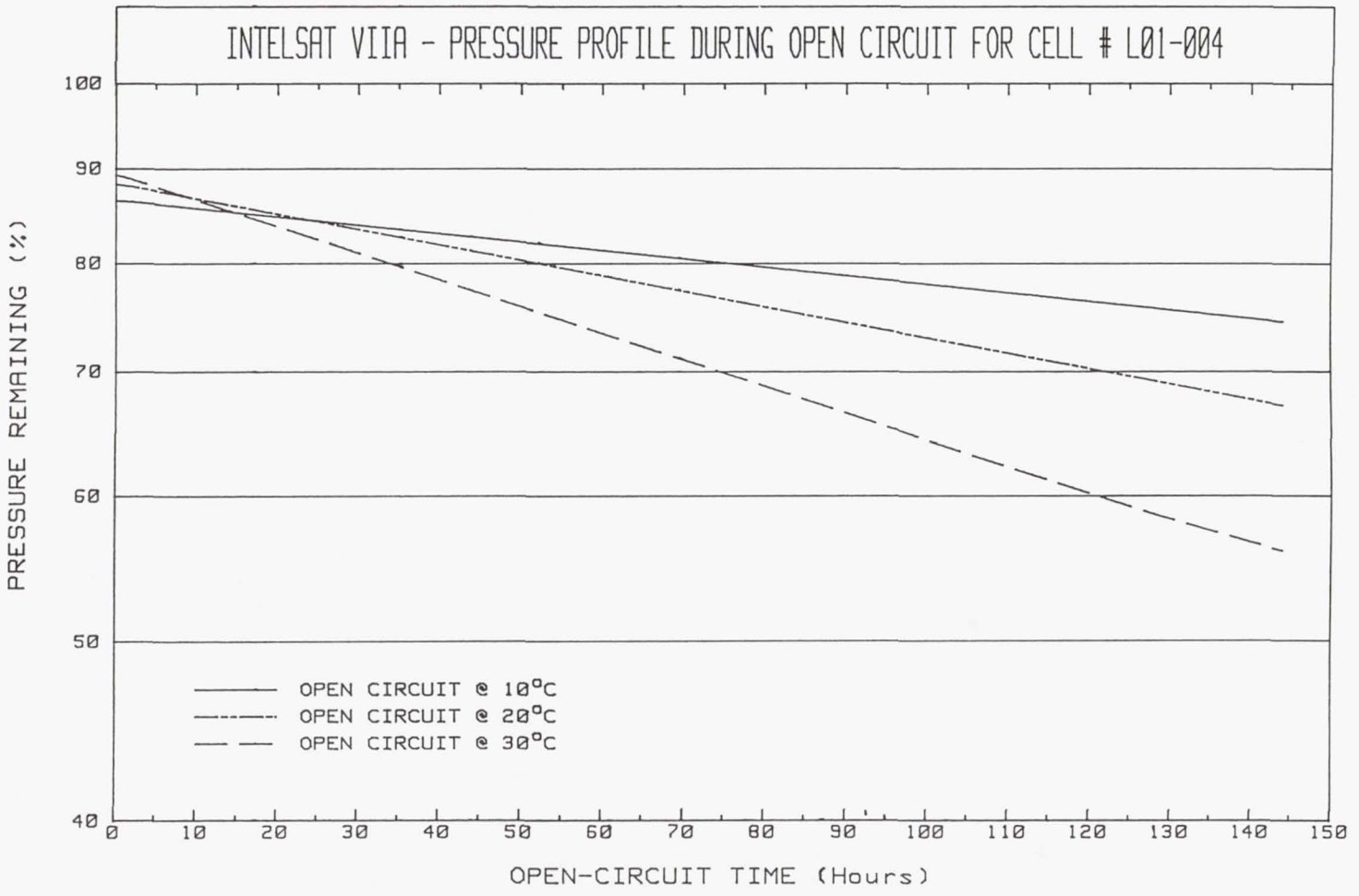

Figure 5-23. INTELSAT VII A—pressure profile during open circuit for cell L01-004.

The slopes (rate of self discharge) for the I–V, I–VI, and I–VII A are quite similar at 10°C. At the higher temperatures of 20°C and 30°C, there is some difference between the slopes reported in Reference 5-1 to the slopes reported in Reference 5-2.

A more rigorous treatment of self-discharge is presented in Reference 5-3. A mathematical model is used to characterize the self-discharge of a nickel oxyhydroxide (NiOOH) electrode in a hydrogen environment. This model includes diffusion of dissolved hydrogen in an electrolyte film which covers a flooded electrode, electrochemical oxidation of hydrogen, reduction of nickel oxyhydroxide, and changes of surface area and of porosity of the electrode during the self-discharge process. The predictions of the model are consistent qualitatively with experimental results reported here and in the literature. These include linear relationships between the logarithm of hydrogen pressure and time and between the logarithm of the capacity remaining and time.

5.3.0 GEO SATELLITES

As described in Chapter 2, geosynchronous-earth-orbit (GEO) satellites orbit the earth once every 24 hours in the equatorial plane and thus remain stationary in their location with respect to the earth. GEO satellites go through two 45-day eclipse seasons per year around the vernal equinox and the autumnal equinox. The satellites pass through eclipse periods each day during the equinox seasons. An eclipse occurs when the satellite is in the shadow of the earth. The longest eclipse period is 72 minutes, and it occurs in the middle of the eclipse season, March 21 (vernal equinox) for the spring season and September 23 (autumnal equinox) for the fall season.

The batteries are cycled once a day during the eclipse seasons; they are discharged while supplying power to the load during the eclipse periods and are recharged during the sunlight period of the eclipse day (45 cycles per eclipse season, or just 90 cycles per year). During the 138 days between eclipse seasons, the batteries are maintained fully charged on a trickle charge.

Future GEO satellites may support additional loads such as battery-powered electric propulsion. For this application the batteries will supply power to the thrusters once a day between eclipse seasons. The batteries would typically be cycled daily for approximately 2 hours to 60 percent depth-of-discharge (DOD). Four satellites (three experimental and one commercial) are scheduled to be launched in the 1992 to 1995 time frame with battery-powered electric propulsion for North-South stationkeeping. The TELSTAR satellite, scheduled to be launched in 1993, is a commercial communications satellite using an RRC-Arcjet. The other three satellites, Eureka, ETS-6, and Artemis, are experimental satellites using ion propulsion.

Performance data are presented for the Ni-H_2 batteries on board the INTELSAT V satellites [5-4]. The INTELSAT V F-6 GEO satellite launched in 1983 was the first GEO satellite to use Ni-H_2 batteries. Since then, a number of additional GEO satellites have been launched with Ni-H_2 batteries, including seven more of the INTELSAT V satellites (see Chapter 2, Table 2-3). The Ni-H_2 batteries on these INTELSAT V satellites have completed up to eight years in-orbit through 1991 with no cell failures. It is still too soon to know what the operational lifetime of these Ni-H_2 batteries will be.

5.3.1 Description of INTELSAT V Batteries

Two 27-cell, 30-Ah Ni-H_2 batteries provide the electrical energy during launch, transfer orbit, and solar eclipses. The batteries are also on-line during sunlight operation to supplement the solar arrays in supplying power for load transients whenever the spacecraft bus voltage drops below a certain set voltage. The F-6, F-7, F-8, F-10, F-11, and F-12 spacecraft batteries on-station load is approximately 480 watts per battery (56 percent DOD), and the F-13 and F-15 batteries on-station load is approximately 567 watts per battery (67 percent DOD).

The INTELSAT V cells described in Chapter 1, Section 1.7.0 were manufactured by EPI. The batteries were described in Chapter 3, Section 3.2.3.

In-Orbit Operation

Charge Control. A coulometric charge control method is used to recharge the INTELSAT V Ni-H_2 batteries. For each eclipse day, the time is calculated to return at the high rate 115 percent of the ampere-hour capacity removed on discharge. Ground commands are used to switch battery charging from the high rate to the trickle-charge rate at the specified time. The high rate of charge is C/21 at the beginning of life and C/25 at the end of life. The trickle charge rate is C/63 at the beginning of life and C/73 at the end of life.

Discharge Control. During eclipse periods, the battery is connected directly to the spacecraft bus through redundant discharge diodes. The purpose of the diodes is to block reverse current from the bus back through the battery. The bus is unregulated; the bus voltage drops off as the battery is discharged.

The battery sees a constant power load on discharge, because traveling wave tubes (TWTs) account for most of the spacecraft load, and each of these TWTs has an individual switching regulator to regulate its voltage. These TWTs appear as a constant power load to the battery; as the battery voltage decreases on discharge the battery current increases correspondingly to keep the product of the voltage and the current constant.

Solstice Operation. Between eclipse seasons (138 days) the batteries are maintained fully charged on trickle charge. The trickle-charge rate used to maintain the batteries fully charged is C/96 at the beginning of life and C/110 at the end of life.

Telemetry Data

There are two batteries on each of the INTELSAT V spacecraft. The telemetry data for each battery are

- Battery voltage
- Battery charge current
- Battery discharge current
- Individual cell voltages
- Battery temperature, at two locations for each battery
- Cell pressure, one cell in each battery, with a strain-gauge bridge circuit mounted on the pressure vessel dome.

F-7 Spacecraft

The F-7 spacecraft, battery 2, experienced a problem after two years in orbit. The pressure vessel of cell number 5 shorted through the RTV silicon rubber insulation sheet to the aluminum sleeve connected to ground. This cell is the fifth cell in the series string of 27 cells in the battery. The short created a leakage path (an electrolyte bridge) from the electrode stack to the pressure vessel wall to ground. This short to ground provided a leakage path that continuously drains all of the four cells in series below the fifth cell.

Most of the F-7 spacecraft loads on this battery were either turned off or were shifted to battery 1 and special handling of the F-7 spacecraft is required. Performance data for the F-7 battery are not presented because of these problems. Performance data for the other 14 batteries on the remaining seven INTELSAT V spacecraft are presented below.

5.3.2 Voltage Performance in Orbit (INTELSAT V Batteries)

In-orbit performance of the batteries is normally judged by the minimum end-of-discharge voltage observed during an eclipse season. The battery specification requires that the battery meet the minimum voltage requirement of 28.6 V with one cell failed shorted or 28.0 V with one cell failed open. With one cell failed open there is a 0.6 V drop due to the bypass circuitry. The individual cell minimum voltage requirement is 1.10 V/cell average for the remaining 26 cells. The minimum battery voltage requirement of 28.0 V corresponds to a bus voltage of 27.0 V. There is a 1.0-V drop between the battery voltage and the bus voltage due to the diodes and wiring harness IR losses. Below 26 V the traveling wave tubes (TWTs) are out of specification and below 23.5 V on the bus TWTs will trip off.

The minimum battery voltages and corresponding average load currents for each eclipse season are presented in Table 5-3. Also presented are the minimum cell voltage and the average cell voltage per battery for each eclipse season [5-4].

Table 5-3. Minimum Battery and Cell Voltage per Eclipse Season

S/C	Season	Batt 1	Batt 2	Batt 1	Batt 2	Batt 1		Batt 2	
		Current (Amps)		Voltage (Volts)		Cell Voltage Avg.	Min	Cell Voltage Avg.	Min.
F-6	F83	16.8	11.5	31.4	32.8	1.16	1.16	1.21	1.22
	S84	12.9	11.2	32.2	33.0	1.19	1.19	1.22	1.22
	F84	14.4	10.8	31.6	32.6	1.17	1.17	1.21	1.21
	S85	16.2	11.3	31.0	32.6	1.15	1.14	1.21	1.20
	F85	16.8	10.9	30.8	32.6	1.14	1.10	1.21	1.20
	S86	16.9	11.7	30.8	32.4	1.14	1.09	1.20	1.20
	F86	13.0	14.5	32.2	32.2	1.19	1.16	1.19	1.16
	S87	12.6	15.5	32.0	31.8	1.18	1.04	1.18	1.14
	F87	12.6	15.4	32.0	31.8	1.18	1.05	1.18	1.14
	S88	12.7	15.6	31.6	31.8	1.17	0.98	1.18	1.13
	F88	12.8	14.8	32.2	32.0	1.19	1.09	1.18	1.14
	S89	12.5	14.8	32.0	32.4	1.18	1.02	1.20	1.16
	F89	12.7	14.2	32.2	32.2	1.19	1.12	1.19	1.15
	S90	13.7	14.2	32.2	32.2	1.19	1.08	1.19	1.15
	F90	13.9	13.5	32.0	32.4	1.18	1.16	1.20	1.19
	S91	13.8	14.5	32.0	32.0	1.18	1.14	1.18	1.17
	F91	11.8	14.5	32.6	32.0	1.21	1.18	1.18	1.16
F-8	S84	13.2	15.8	32.0	32.4	1.18	1.18	1.20	1.20
	F84	13.2	12.9	32.0	32.4	1.18	1.18	1.20	1.20
	S85	13.0	13.0	31.8	32.2	1.18	1.18	1.19	1.19
	F85	10.9	13.2	32.8	32.2	1.22	1.22	1.19	1.17
	S86	13.4	13.5	31.8	31.8	1.18	1.17	1.18	1.15
	F86	13.2	12.8	31.8	31.8	1.18	1.18	1.18	1.07
	S87	13.3	12.8	31.8	31.8	1.18	1.17	1.18	1.05
	F87	14.4	12.6	31.4	31.6	1.16	1.16	1.17	0.98
	S88	13.7	13.0	31.6	32.0	1.17	1.15	1.18	1.13
	F88	15.1	13.3	31.4	31.8	1.16	1.16	1.18	1.04
	S89	14.1	14.3	31.6	32.0	1.17	1.16	1.18	1.13
	F89	14.9	13.4	31.4	32.2	1.16	1.15	1.19	1.17
	S90	14.8	13.3	31.4	32.2	1.16	1.16	1.19	1.19
	F90	13.7	13.6	32.0	32.0	1.18	1.18	1.18	1.18
	S91	13.5	15.1	31.8	31.6	1.18	1.17	1.17	1.17
	F91	14.3	14.3	31.4	31.8	1.16	1.16	1.18	1.16

Table 5-3. Minimum Battery and Cell Voltage per Eclipse Season (Continued)

F-10	S85	15.0	13.0	32.8	33.0	1.22	1.22	1.22	1.22
	F85	14.0	14.9	32.2	31.8	1.19	1.19	1.19	1.18
	S86	13.8	15.2	32.2	31.6	1.19	1.19	1.19	1.17
	F86	14.1	14.9	32.0	31.6	1.18	1.17	1.17	1.16
	S87	14.1	14.8	31.8	31.4	1.18	1.15	1.16	1.13
	F87	14.3	15.1	31.6	31.2	1.17	1.12	1.16	1.13
	S88	14.7	15.2	31.8	31.0	1.18	1.13	1.15	1.10
	F88	15.0	14.9	31.6	31.8	1.17	1.10	1.18	1.17
	S89	14.5	14.6	32.0	31.4	1.18	1.16	1.16	1.11
	F89	14.8	14.4	31.6	31.8	1.17	1.13	1.18	1.18
	S90	14.6	14.4	32.0	31.6	1.18	1.18	1.17	1.13
	F90	14.4	14.1	31.8	32.0	1.18	1.18	1.18	1.18
	S91	14.4	14.0	31.8	31.8	1.18	1.18	1.18	1.18
	F91	14.3	14.1	31.6	31.6	1.17	1.17	1.17	1.17
F-11	F85	13.7	14.1	32.2	32.4	1.19	1.19	1.19	1.20
	S86	13.9	14.5	32.0	32.2	1.18	1.18	1.18	1.19
	F86	13.9	14.6	31.8	32.2	1.18	1.18	1.19	1.19
	S87	14.0	14.6	31.8	32.0	1.18	1.17	1.18	1.16
	F87	14.5	14.8	31.4	32.0	1.16	1.12	1.18	1.17
	S88	14.7	15.8	31.6	31.6	1.17	1.13	1.17	1.14
	F88	14.3	15.9	31.8	31.6	1.18	1.15	1.17	1.16
	S89	14.6	15.7	31.8	31.6	1.18	1.18	1.17	1.13
	F89	14.5	15.6	31.6	31.8	1.17	1.14	1.18	1.18
	S90	14.1	15.8	32.0	31.4	1.18	1.18	1.18	1.15
	F90	14.1	15.1	32.0	32.0	1.18	1.18	1.18	1.18
	S91	14.1	14.6	32.0	32.0	1.18	1.18	1.18	1.18
	F91	14.2	14.6	31.8	31.8	1.18	1.18	1.18	1.17
F-12	F85	14.1	12.9	32.6	32.8	1.21	1.20	1.22	1.22
	S86	15.3	14.2	31.8	32.2	1.18	1.18	1.19	1.19
	F86	15.7	14.3	31.4	32.0	1.16	1.16	1.18	1.18
	S87	15.6	13.5	31.4	32.2	1.16	1.16	1.19	1.19
	F87	15.8	13.9	31.2	32.2	1.16	1.16	1.19	1.19
	S88	16.0	14.0	31.2	32.0	1.16	1.16	1.18	1.18
	F88	15.8	13.9	31.2	32.0	1.16	1.15	1.18	1.18
	S89	15.7	13.5	31.2	32.0	1.16	1.16	1.18	1.18
	F89	12.9	13.7	32.4	31.8	1.20	1.20	1.18	1.18
	S90	12.8	14.9	32.4	31.4	1.20	1.19	1.16	1.15
	F90	13.6	14.7	32.0	31.8	1.18	1.18	1.18	1.18
	S91	13.7	14.7	32.0	31.6	1.18	1.18	1.17	1.17
	F91	13.7	14.5	31.8	31.6	1.18	1.18	1.17	1.16

Table 5-3. Minimum Battery and Cell Voltage per Eclipse Season (Continued)

F-13	F88	16.6	14.6	31.4	32.2	1.16	1.16	1.19	1.19
	S89	16.8	15.2	31.0	31.8	1.15	1.14	1.18	1.18
	F89	16.5	14.1	31.0	32.2	1.15	1.14	1.19	1.19
	S90	16.7	15.0	31.2	31.8	1.16	1.14	1.18	1.16
	F90	16.9	15.0	31.2	31.8	1.16	1.15	1.18	1.17
	S91	16.7	14.9	31.2	31.8	1.16	1.14	1.18	1.17
	F91	16.0	14.8	31.4	31.8	1.16	1.14	1.18	1.16
F-15	S89	18.3	16.7	31.0	31.8	1.15	1.15	1.18	1.18
	F89	18.0	15.8	31.0	31.8	1.15	1.15	1.18	1.18
	S90	16.8	15.0	31.2	31.8	1.16	1.16	1.18	1.13
	F90	16.8	15.8	31.2	31.8	1.16	1.16	1.18	1.16
	S91	17.0	15.7	31.2	31.6	1.16	1.16	1.17	1.12
	F91	16.9	15.8	31.0	31.8	1.15	1.15	1.18	1.15

A summary of the average battery loads and minimum end-of-discharge voltages are presented for the Fall 1990 eclipse season in Table 5-4.

Table 5-4. Fall 1990 Eclipse Season Battery Loads and Minimum Voltages for 1990 Fall Eclipse Season

	DOD (%)		Current (Amps)		Voltage (Volts)		Cell Voltage Avg.	Min	Cell Voltage Avg.	Min.
S/C	**Batt 1**	**Batt 2**	**Batt 1**	**Batt 2**	**Batt 1**	**Batt 2**	**Batt 1**		**Batt 2**	
F-6	55.8	53.1	14.2	13.5	32.0	32.4	1.20	1.16	1.20	1.19
F-8	54.0	54.4	13.7	13.8	32.0	32.0	1.20	1.18	1.20	1.18
F-10	56.9	55.7	14.4	14.3	31.8	32.0	1.19	1.18	1.20	1.18
F-11	55.3	60.0	14.1	15.4	32.0	32.0	1.20	1.18	1.20	1.19
F-12	53.5	58.0	13.6	14.8	32.0	31.8	1.20	1.18	1.18	1.18
F-13	67.0	59.0	16.9	15.0	31.2	31.8	1.17	1.15	1.19	1.17
F-15	67.0	62.3	16.9	15.8	31.2	31.8	1.17	1.16	1.18	1.16

Summary of Voltage Performance

- A number of individual cells within these batteries had low end-of-discharge voltages. Changes have been made in the operational procedures to recover (increase) the end-of-discharge voltage performance of these cells (see next section, "Low Voltage Cells").

- As of Fall 1990, the eclipse season minimum end-of-discharge battery voltages are well above the required 28.6 V minimum for all 14 INTELSAT V batteries (see Table 5-4).

- Based on these data it is certain that, under the present operating conditions, these batteries will last well beyond the 7-year design life at 56 percent DOD.

- It is difficult to predict the lifetime because these Ni-H_2 batteries are now showing very little if any voltage loss after seven years in orbit. The expectation is that these batteries will last for 15 to 25 years.

- The spacecraft loads are divided between the two batteries, and these loads are reconfigured periodically to accommodate communications demands. An attempt is made to match the loads between the two batteries as closely as possible.

- The minimum EOD voltage range was 31.2 V—32.4 V for all 14 batteries during the Fall 1990 eclipse season (see Table 5-4).

Low-Voltage Cells

In Table 5-3, the minimum battery voltages are presented for each eclipse season along with the minimum cell voltage within each of the batteries. The minimum cell voltage within each battery is compared to the average cell voltage per battery. When the minimum and average cell voltage are the same or very close (within 20 mv), the cell voltages at the end of discharge are considered to be well matched. However, when a significant difference exists between the average cell voltages and the minimum cell voltage (40 mv or more), one or more of the cells have dropped out and become low-voltage cells. Observe the data in Table 5-3 for F-6 battery 1; this battery has a low voltage cell that started dropping out after just two years in orbit, and by the S88 eclipse season, the minimum end-of-discharge voltage of this cell was down to 0.98 volts (170 mV below average).

The voltage loss was investigated at COMSAT Laboratories, and it was determined that water loss from the electrode stack was causing the cell impedance to increase. As part of this investigation, an in-orbit voltage recovery procedure was implemented starting in the fall of 1988 [5-5]. This recovery procedure was effective in returning water back to the electrode stack in the defective cells, resulting in a voltage recovery for those cells on discharge. The driving mechanism for the water loss was the continuous trickle charge of the batteries during storage. The trickle charge rate was reduced from C/63 to C/96 during solstice storage between eclipse seasons. The combination of using the recovery procedure and reducing the trickle charge rate has been effective in improving battery voltage performance. For example, all of the INTELSAT V battery cells were well matched at their minimum end-of-discharge voltages during the Fall 1990 eclipse season (maximum deviation

is ±20 mV between cells within the same battery; see Table 5-4). The one exception is cell 22 in battery 1 on the F-6 spacecraft. This cell is still 40 mV low in voltage, but it has been recovering steadily each eclipse season.

5.3.3 Reconditioning Capacity in Orbit

The batteries are reconditioned prior to each eclipse season. A 50-ohm resistor is switched across the battery by ground command. The reconditioning discharge is discontinued when the first cell in the battery reaches 0.5 V. The batteries are recharged at the high rate, returning 110 percent of the ampere-hour capacity removed on discharge.

Capacity

The reconditioning capacity is calculated by using the average discharge current of 0.68 amperes multiplied by the hours on discharge. This method assumes that, during the reconditioning discharge, the average battery discharge voltage is 34.0 volts, or 1.26 volts/cell.

Reconditioning capacities for the INTELSAT V Ni-H_2 batteries are presented in Table 5-5.

Table 5-5. Reconditioning Capacity for Each Eclipse Season

Season	F-6		F-8		F-10		F-11		F-12		F-13		F-15	
Battery	#1	#2	#1	#2	#1	#2	#1	#2	#1	#2	#1	#2	#1	#2
						(CAPACITY)								
F83	35.7	38.1												
S84	36.3*	35.4												
F84	40.0*	37.7	36.2	36.1										
S85	35.8	37.6	33.5	36.7										
F85	38.4	37.5	37.2*	35.8	34.3*	33.9*	33.3	31.8						
S86	33.7	37.9	34.2	37.0	36.9	34.4	41.2*	35.2	35.4	34.7				
F86	38.8	37.6	38.2	38.2	40.8*	38.8	42.3*	39.1	39.6*	37.1				
S87	35.3	38.3*	35.1	39.0	40.5	38.8	43.3	40.6*	41.1	37.9				
F87	37.6	37.2	38.6	39.0	39.6	39.9	41.9	39.9	39.6	36.0				
S88	35.2	38.8	36.9	39.8	40.5	40.1	42.9	37.3	40.9	37.5				
F88	38.8	37.8	38.4	41.3	40.0	40.5	41.7	38.7	40.5	39.1	42.6	37.3		
S89	36.9	36.9	37.9	39.8	38.6	41.4	43.7	39.7	40.8	38.4	43.3	42.2		
F89	40.1	40.2	39.8	41.7	41.0	41.1	43.1	39.6	40.4	38.4	43.5	42.0	40.7	40.0
S90	38.1	38.6	37.9	42.0	40.9	41.5	43.1	41.3	41.4	38.6	42.9	41.8	40.6	40.2
F90	39.9	36.0	42.0	40.4	40.9	41.5	42.7	40.1	39.3	38.1	42.5	41.2	39.7	40.6
S91	36.5	39.5	37.7	40.3	42.0	40.7	43.3	40.7	41.3	39.0	44.7	38.4	40.3	41.3
F91	40.8	39.0	41.8	39.2	38.8	40.5	40.7	41.0	38.6	40.0	43.4	40.9	38.7	38.3

*Electro-Thermal Thruster (ETT) firing plus reconditioning

Pre-Launch Battery Capacity

The "standard" 10°C capacity of the batteries, measured prior to the shipment of the batteries to the launch site, is presented for comparison with the reconditioning capacity in orbit. For the "standard" 10°C capacity measurements, the batteries were charged at the C/10 rate for 16 hours and then discharged at a C/2 rate (15 amperes) to 1.0 volts. The measured 10°C capacity is presented in Table 5-6 [5-4].

Table 5-6. 10°C Prelaunch Capacity of INTELSAT V Ni-H_2 Batteries

S/C	Launch Date	Battery	Cell Lot	Measured Capacity (Ah)
F-6	19 May 83	1	6	37.2
		2	6	36.7
F-7	19 Oct 83	1	11	38.1
		2	11	38.2
F-8	5 Mar 84	1	10	36.0
		2	10	36.3
F-10	22 Mar 85	1	18	34.9
		2	15	31.8
F-11	30 Jun 85	1	17	33.1
		2	18	34.2
F-12	28 Sep 85	1	21	35.1
		2	21	34.3
F-13	17 May 88	1	23	36.7
		2	23	35.1
F-15	27 Jan 89	1	24A	38.8
		2	13, 17, 18, 23	37.4

Summary of Capacity Data

- The initial 10°C capacity of the INTELSAT V batteries was between 36 and 38 Ah when they were first assembled. (Capacity measured by C/10 charge for 16 hours and C/2 discharge to 1.0 V/cell average.) The initial reconditioning capacity was typically about 2 Ah higher, between 38 and 40 Ah. The reconditioning capacity is higher because of the lower rate of discharge, approximately a C/50 rate.

- The batteries on F-10, F-11, and F-12 had low pre-launch capacity, as well as low capacity at the beginning of life in orbit (Tables 5-5 and 5-6). After one or two eclipse seasons in orbit the capacity recovered (increased by 6 to 7 ampere hours) and stabilized. This in-orbit capacity recovery is shown for F-10, F-11, and F-12 batteries in Figures 5-24, 5-25, and 5-26.

- The low pre-launch capacity for F-10, F-11, and F-12 batteries resulted from capacity fading during room temperature storage of the batteries (discharged open-circuit stand at room temperature).

- Pre-launch capacity fading was recovered in orbit by normal eclipse cycling and trickle charge between eclipse seasons.

- The batteries on F-6 and F-8 increased in capacity by 2 to 4 ampere-hours with lifetime in orbit (see Figures 5-27 and 5-28). These F-6 and F-8 batteries had higher pre-launch capacity (less capacity fading) than the F-10, F-11, and F-12 batteries. The storage time was shorter for the F-6 and F-8 batteries.

- The batteries on F-13 and F-15 had high capacity at the beginning of life in orbit. No prelaunch capacity fading occurred for these batteries. They had a different storage procedure, as described in the next section.

- In-orbit capacity for all of the batteries in F91 ranged from 38.3 to 43.4 Ah (see Table 5-5).

Battery Storage

- The pre-launch capacity and the initial capacity in orbit are dependent on the storage and handling of the batteries.

- Prior to 1985, INTELSAT V Ni-H_2 batteries were stored discharged and open-circuited at room temperature. As seen by the pre-launch capacity measurements for the F-10, F-11, and F-12 batteries, capacity fading of 5 to 6 Ah occurred with this storage method (see Table 5-6). Fortunately, the loss in capacity was recovered during the normal in-orbit operation of the batteries in one or two eclipse seasons.

- Since 1985, the batteries have been stored on trickle charge (C/63 rate) at 10°C. The F-13 and F-15 batteries benefited from this new storage mode, as seen by the pre-launch capacity and the initial capacity in orbit (Table 5-5 and 5-6).

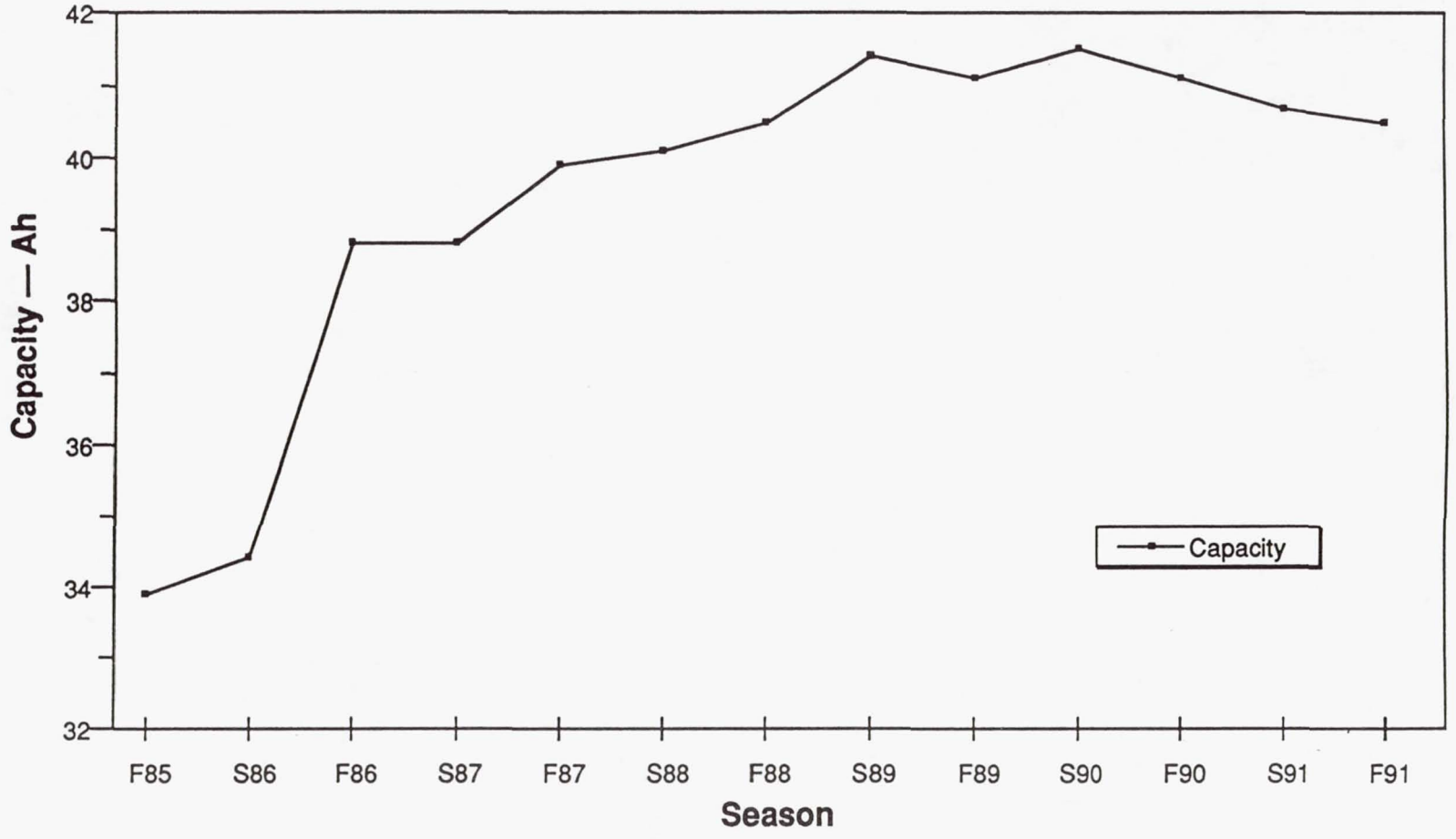

Figure 5-24. Capacity vs eclipse season INTELSAT V F-10 battery 2.

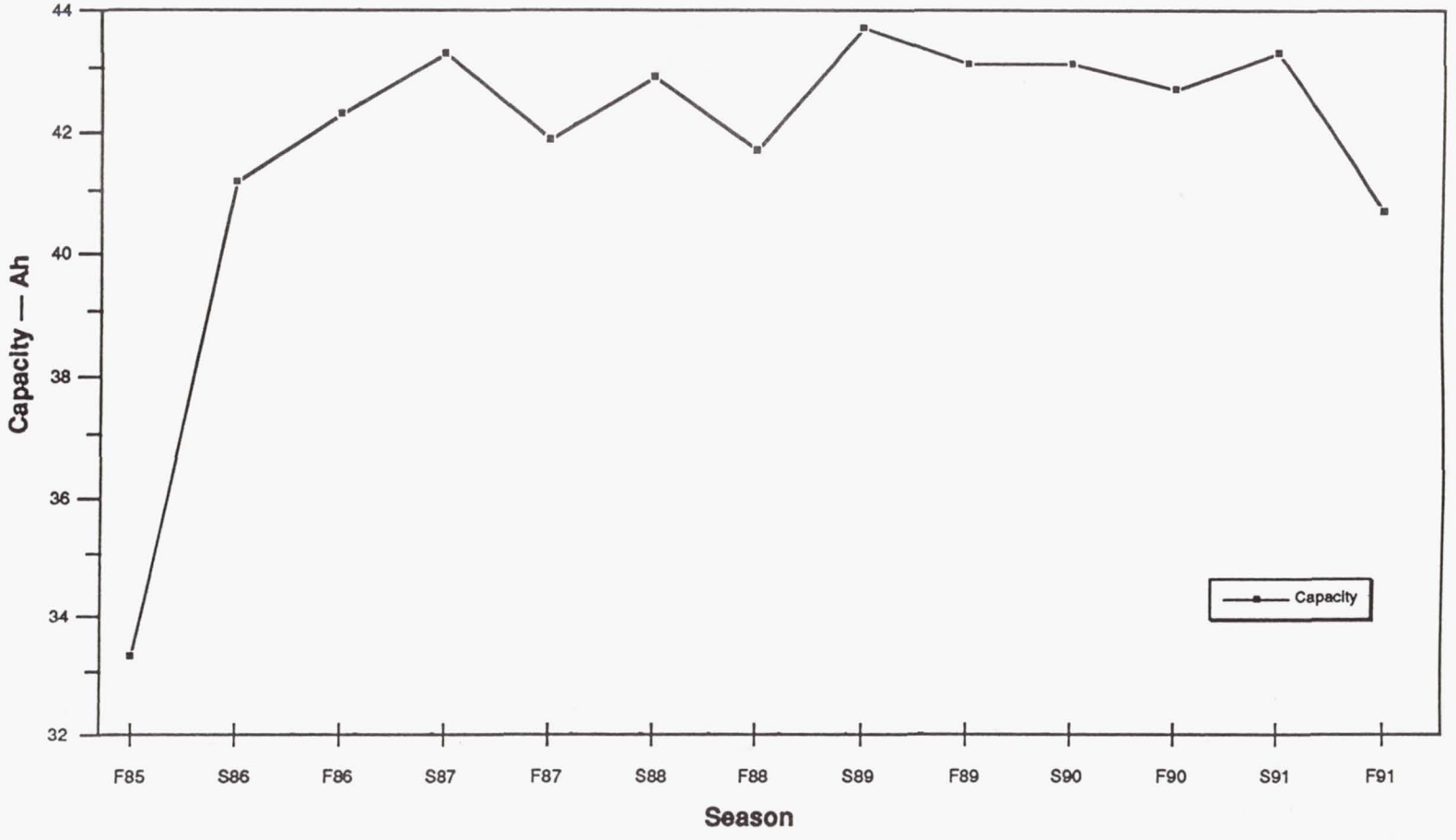

Figure 5-25. Capacity vs eclipse season INTELSAT V F-11 battery 1.

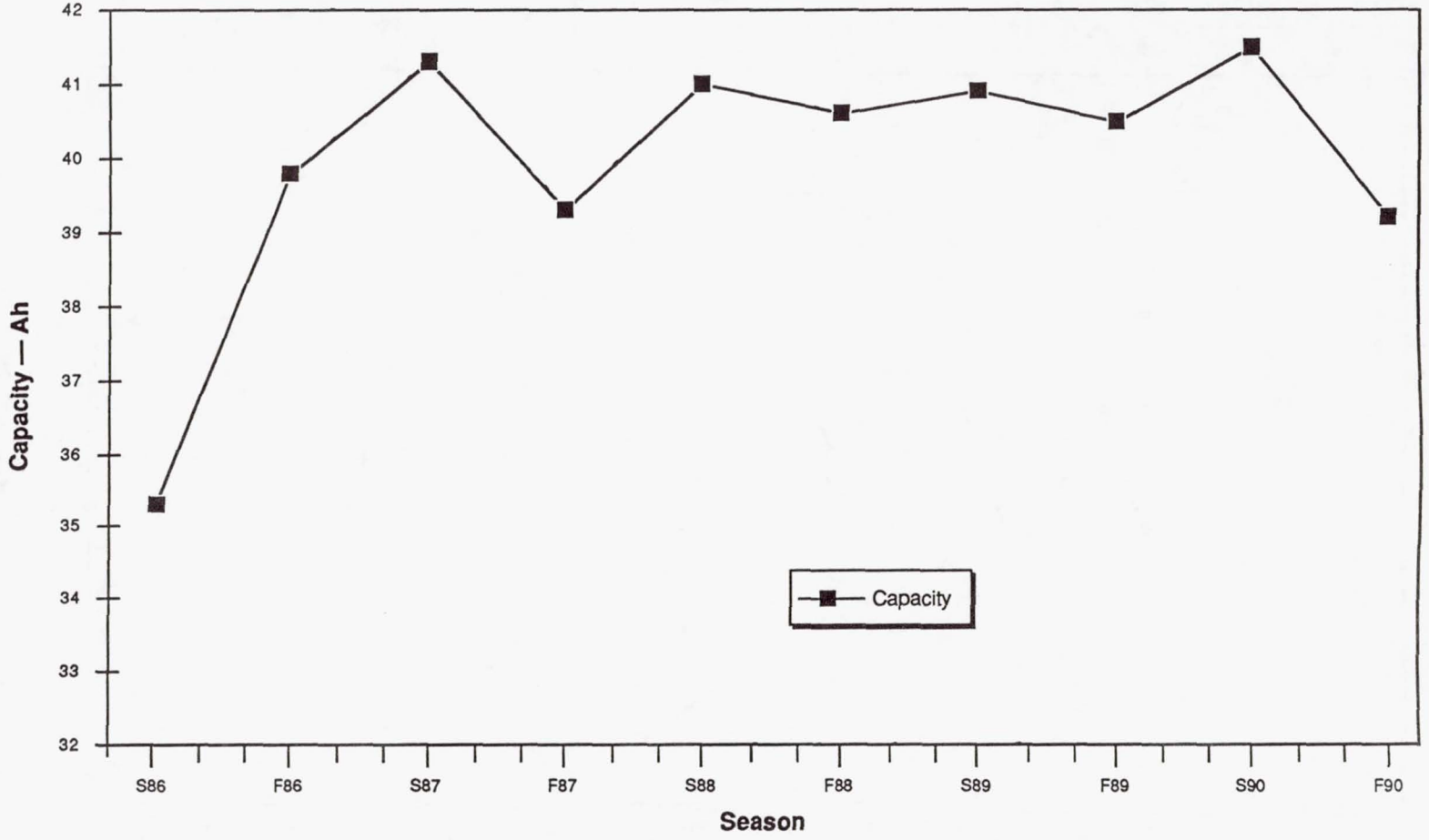

Figure 5-26. Capacity vs eclipse season INTELSAT V F-12 battery 1.

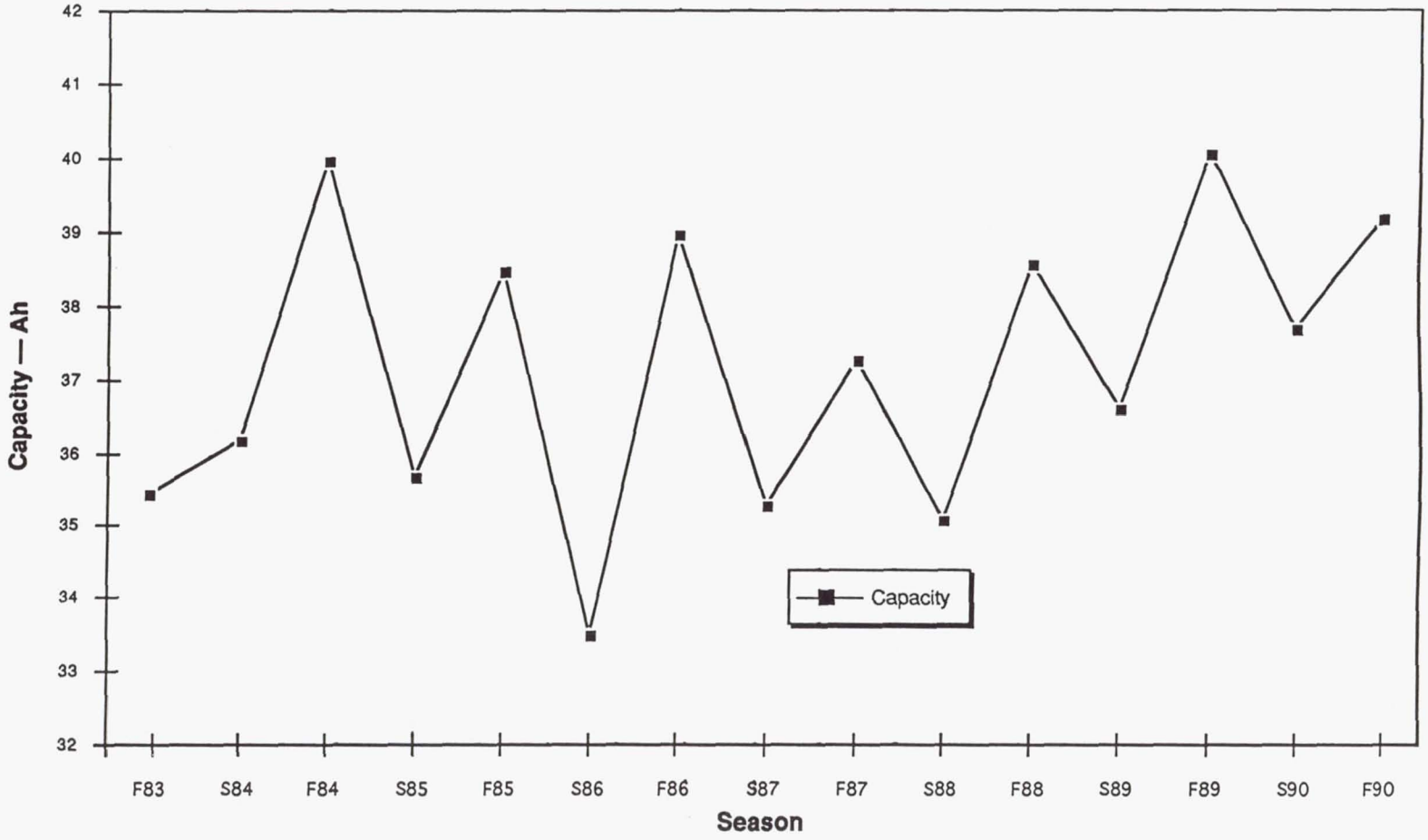

Figure 5-27. Capacity vs eclipse season INTELSAT V F-6 battery 1.

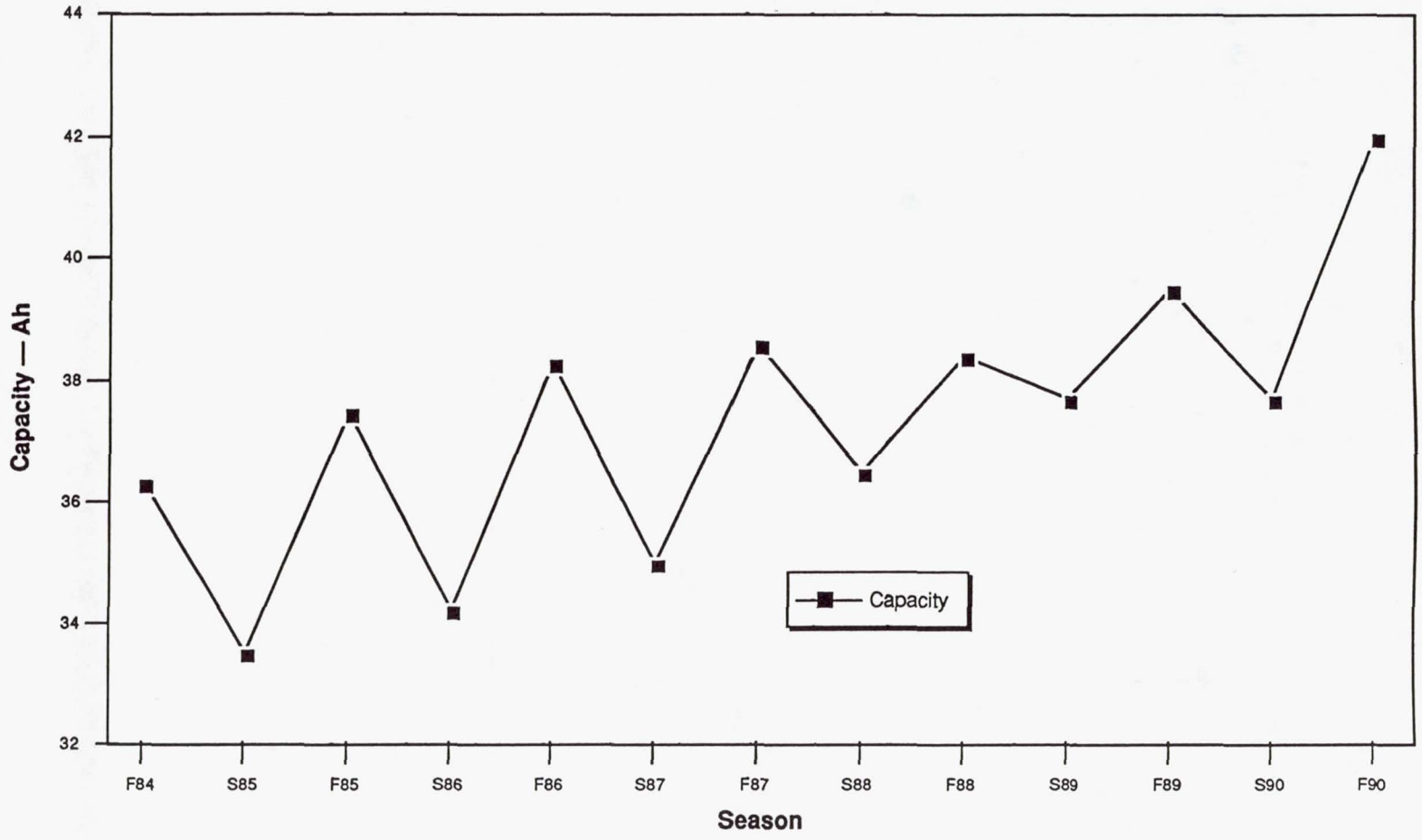

Figure 5-28. Capacity vs eclipse season INTELSAT V F-8 battery 1.

5.3.4 Pressure Data

Historical Database

The INTELSAT database was accessed to obtain plots of the pressure and temperature vs time for each reconditioning of the INTELSAT V Ni-H_2 batteries over their operational lifetime. Figure 5-29 is one of these plots of pressure and temperature vs time for the Fall 1984 reconditioning of F-6 battery 2. The F-6 battery 2 reconditioning pressure data are representative of all the INTELSAT V batteries. The F-6 data were selected because this spacecraft has been in orbit for the longest period of time.

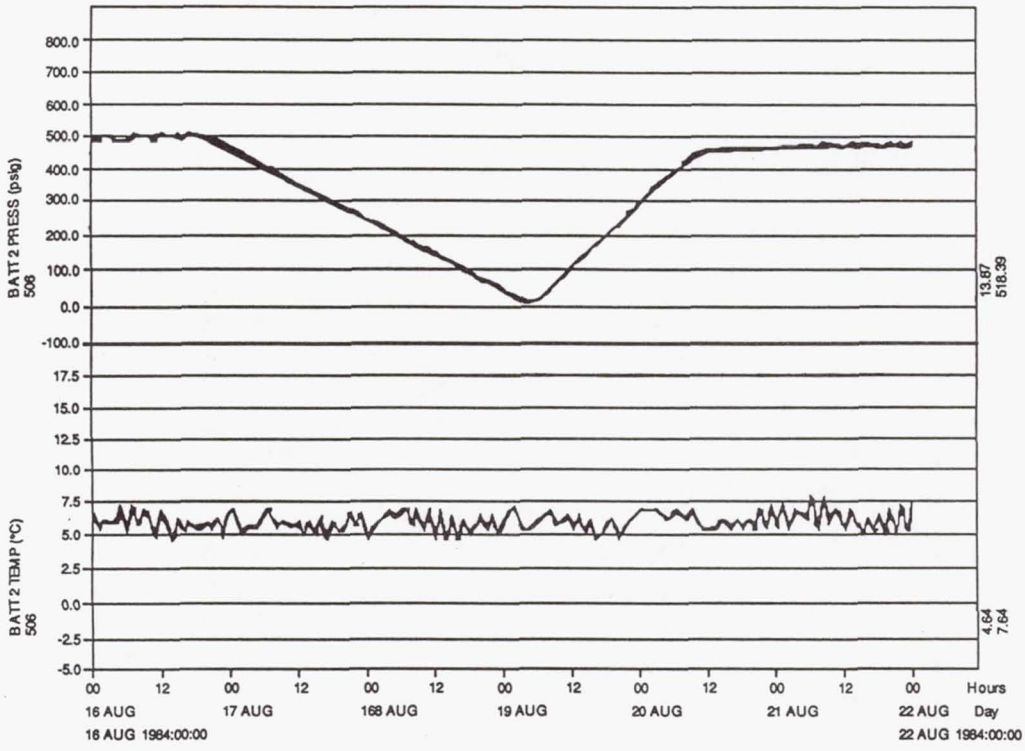

Figure 5-29. Cell pressure during Fall 1984 reconditioning INTELSAT V F-6 battery 2.

The temperature during the reconditioning discharge is between 5° and 7.5°C. The battery heaters are switching on and off to control temperature. This temperature is the same from season to season or from year to year; therefore, any changes in the strain-gauge pressure data from year to year during reconditioning are not affected by temperature compensation.

Reconditioning Capacity vs Delta Pressure

Reconditioning capacity and pressure data for F-6, battery 2 for each eclipse season are presented in Table 5-7. The EOC pressure is the pressure at the start of the reconditioning discharge and the EOD pressure is the pressure at the end of the reconditioning discharge. The pressure constant is the ratio of ΔP/measured capacity [5-4].

Table 5-7. Reconditioning Capacity and Pressure Data INTELSAT V F-6 Battery 2

Eclipse Season	Measured Capacity (Ah)	EOC Pressure Max (psi)	EOD Pressure Min (psi)	ΔP (psi)	Pressure Constant ΔP/Meas. Cap. (psi/Ah)
F83	38.1	no pressure data in database			
S84	35.4	no pressure data in database			
F84	37.7	516.39	13.87	502.62	13.33
S85	37.6	518.49	17.90	500.59	13.31
F85	37.5	515.14	17.23	497.9	13.27
S86	37.9	519.34	15.32	504.02	13.29
F86	37.6	519.73	22.03	497.70	13.23
S87	38.3	519.34	13.87	505.47	13.19
F87	37.2	519.73	22.03	497.7	13.37
S88	38.3	525.78	16.20	509.58	13.30
F88	37.8	521.86	17.90	503.96	13.33
S89	36.9	526.91	18.67	508.24	13.77
F89	40.2	534.22	-0.57	534.79	13.30
S90	38.6				
F90	36.0	530.87	38.04	492.83	13.68
S91	39.5	546.52	17.23	529.29	13.39
F91	39.0	545.30	17.90	527.40	13.52
					avg: 13.37

These EOC and EOD pressure data are presented graphically in Figure 5-30 for INTELSAT V F-6 battery 2. This figure also contains the straight-line regression fits to these data points. The slopes for these equations represent the pressure rise per eclipse season. The minimum end-of-discharge pressure increase is almost negligible; from the regression fit, the pressure increase is 0.45 psi/season, or 0.90 psi/year.

The EOC pressure measured at the end of trickle charge (the beginning of reconditioning discharge) increases for the first few years in orbit. This EOC pressure increase is a result of the capacity increase with time. Since the EOD pressure is almost constant, the increase in EOC pressure corresponds to an increase in the delta pressure, which is directly proportional to the increase in capacity (Table 5-7).

Reconditioning End-of-Discharge Pressure

The beginning-of-life and Fall 1990 reconditioning end of discharge (EOD) pressure data are presented for all of the INTELSAT V batteries in Table 5-8. Also presented are the slopes from a regression fit to these EOD pressure data [5-4].

Table 5-8. Reconditioning EOD Pressure Data

Batteries	Eclipse Season	1st Season EODP	Fall 1990 EODP	Slope psi/season
F-6 Bat 1	F84	-5.9*	2.3	0.37
F-6 Bat 2	F84	13.9*	38.0	0.45
F-8 Bat 1	F84	16.5	32.9	-0.03
F-8 Bat 2	F84	27.3	59.6	0.59
F-10 Bat 1	F85	23.4	29.8	0.05
F-10 Bat 2	F85	66.0	38.8	-2.08
F-11 Bat 1	F85	114.0	50.8	2.24
F-11 Bat 2	F85	81.1	15.3	-1.76
F-12 Bat 1	F86	13.7	52.5	4.08
F-12 Bat 2	F86	17.2	28.2	1.73
F-13 Bat 1	F88	20.0	31.3	3.10
F-13 Bat 2	F88	13.0	19.4	2.30
F-15 Bat 1	F89	24.0	36.1	
F-15 Bat 2	F89	21.0	17.1	
	Avg.	**31.7**	**32.3**	**0.89**

*No pressure data existed in the historical database for the F-6 spacecraft batteries during the first two eclipse seasons.

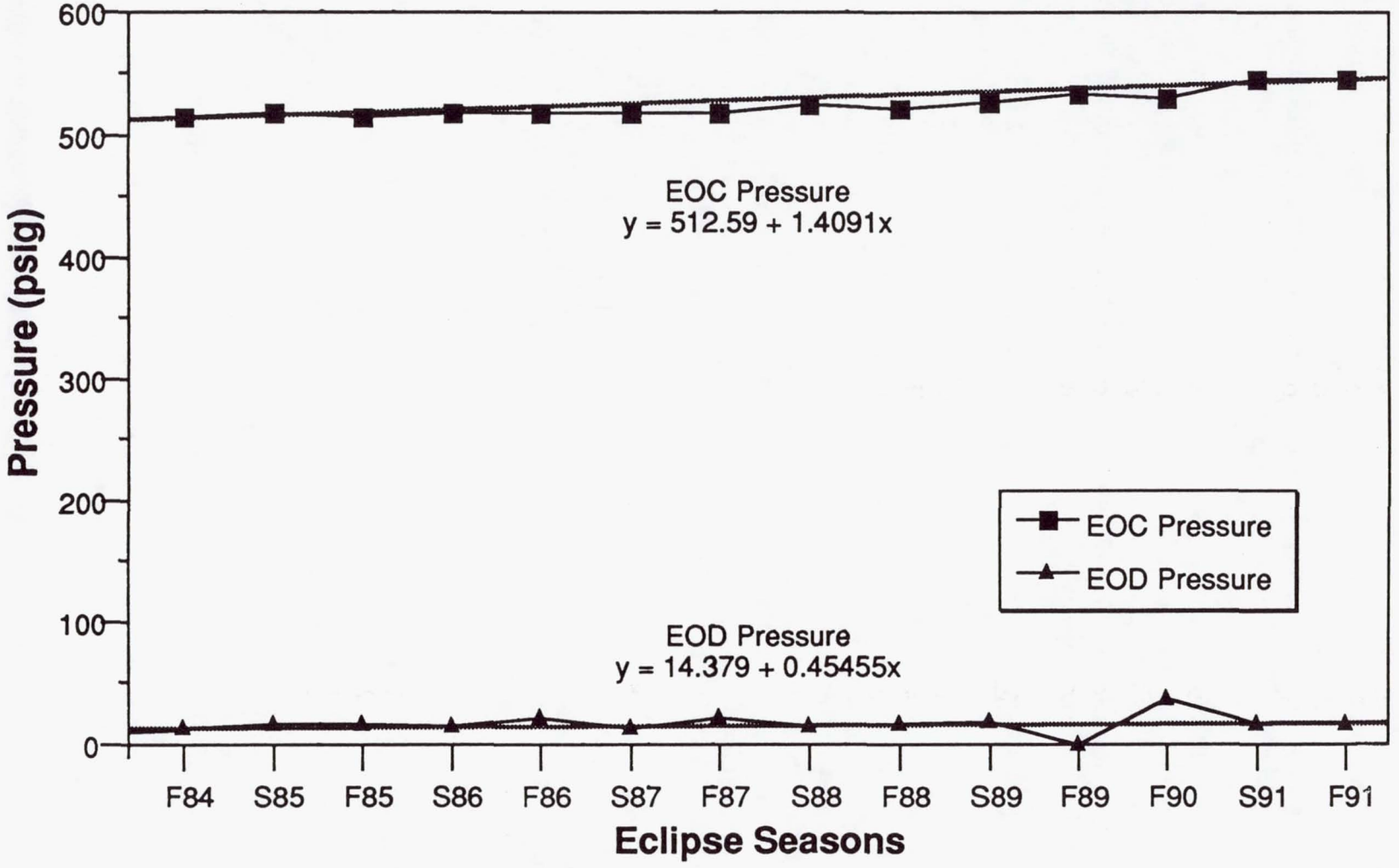

Figure 5-30. Reconditioning pressure data vs eclipse seasons INTELSAT V F-6 battery 2.

Reconditioning EOD Pressure Data Summary

- The strain-gauge bridge circuit provides useful pressure data.

- No significant change has occurred in the reconditioning EOD pressure with time for these INTELSAT V batteries. Actually, the regression fit for all of the cells shows a slight pressure increase with time; the average slope for pressure increase with time is 0.89 psi/eclipse season, or 1.78 psi/year, from Table 5-8 above.

- The average EOD pressure in Fall 1990 is almost the same as the EOD pressure at the beginning of life in orbit (see Table 5-8).

- The significance of these data is that no oxidation, or corrosion, occurs within these cells. Any oxidation of the cell components would result in a pressure increase at the end of reconditioning discharge.

- The beginning-of-life EOD pressure is high on three batteries: F-10 battery 2 and F-11 batteries 1 and 2 (114 psig for F-11 battery 1). This high EOD pressure is an indication that the batteries, or at least some of the cells in these batteries, could not be fully discharged. These same batteries exhibited poor initial capacity (33.3 Ah for F-11 battery 1). However, after one eclipse season in orbit the EOD pressure decreased to 23 psi, and the capacity increased back to 41.2 Ah for F-11 battery 1, which is typical of the recovery seen for the other two batteries.

- The beginning-of-life high EOD pressure and low capacity is attributed to capacity fading during room temperature storage of these batteries prior to launch. (For more information on capacity fading refer to Chapter 8). Fortunately, this capacity fading is recovered after one or two eclipse seasons in orbit.

5.4.0 LEO APPLICATIONS TEST DATA

The most demanding requirement for low-earth-orbit (LEO) applications is the number of times the battery must be cycled without failure. For example, the Space Telescope is an LEO satellite, orbiting 300 nautical miles above the earth with a constant orbital period of 96 minutes. The satellite is in the sunlight for approximately 61 minutes and in the earth's shadow approximately 35 minutes. The actual duration of the eclipse periods vary daily over a range from 27 to 36 minutes as discussed in Chapter 2, Table 2-1. Programs such as the Hubble Space Telescope and the Space Station Freedom require at least five to seven years of operation in orbit:

15	cycles/day
5,475	cycles/year
27,375	cycles/5 years
38,325	cycles/7 years.

The battery provides power for the spacecraft load during eclipse periods, and it is recharged during the sunlight periods.

Extensive ground testing is being conducted to determine the cycle lifetime to failure of Ni-H_2 cells under different LEO operating conditions. A review of the ground testing and test results are presented below.

5.4.1 Nickel Hydrogen Cell Testing at Martin Marietta

The major objective of the Martin Marietta test program was to determine if IPV Ni-H_2 cells could support 20,000 LEO cycles at 40 percent DOD at a temperature of 10°C [5-6].

Eighty-two Ni-H_2 cells with a nameplate capacity rating of 50 ampere-hours were initially procured. Testing was initiated in 1985. Since then an additional twenty-four 50-Ah cells and twenty-one 100-Ah cells have been added to the test program, totaling 127 cells. Four separate vendors were selected for cell procurement: Eagle-Picher (Joplin), Eagle-Picher (Colorado Springs), Yardney Technical Products, and Gates Energy Products.

Cells on test include the following:

50-Ah Air Force design
100-Ah Air Force design
50-Ah COMSAT design
50-Ah YEC MANTECH design

All groups were tested using a 90-minute LEO cycle, with a 55 minute charge and a 35 minute discharge. A fixed C/D ratio of 1.03 to 1.10 was used, depending on test temperature. The recharge ratio was minimized to prolong cell life.

The design variables for the cells are presented in Table 5-10.

Test Results

A failure is defined as the inability of a cell to support an end-of-discharge voltage of 1.0 volts.

Table 5-11 shows the status of the Ni-H_2 cells on test at Martin Marietta as of April 1993 [5-6].

Table 5-9. Martin Marietta Ni-H_2 Test

Mfg.	Cell (Ah)	Size (in.)	DOD %	Temp (°C)	# Cells	Pkg	Electr. Design	KOH %	Sep.	Pos. Plate Proc.	Impreg. Proc.
EP-J	50	3.5	40	10	16	IPV	Recirc.	31	Zircar	Dry Sinter	Aqueous
EP-J	50	3.5	40	20	8	IPV	Recirc.	31	Zircar	Dry Sinter	Aqueous
EP-J	50	3.5	60	10	8	IPV	Recirc.	31	Zircar	Dry Sinter	Aqueous
EP-J	50	3.5	60	20	4	IPV	Recirc.	31	Zircar	Dry Sinter	Aqueous
Gates	50	3.5	40	10	16	IPV	Recirc.	31	Zircar	Dry Sinter	Aqueous
Gates	50	3.5	40	20	8	IPV	Recirc.	31	Zircar	Dry Sinter	Aqueous
Gates	50	3.5	60	10	8	IPV	Recirc.	31	Zircar	Dry Sinter	Aqueous
Gates	50	3.5	60	20	4	IPV	Recirc.	31	Zircar	Dry Sinter	Aqueous
Yardney	50	3.5	40	10	6	IPV	Recirc.	31	Abs/Zirc	Slurry	Aqueous
Yardney	50	3.5	60	10	9	IPV	Recirc.	26	Abs/Zirc	Slurry	Aqueous
Yardney	50	3.5	60	10	9	IPV	Recirc.	31	Abs/Zirc	Slurry	Aqueous
EP-J	50	3.5	40	10	4	IPV	B/B	38	Asbestos	Dry Sinter	Aqueous
EP-J	100	4.5	40	10	8	IPV	B/B	31	Zircar	Dry Sinter	Aqueous
EP-CS	100	4.5	40	10	4	IPV	Recirc.	31	Zircar	Dry Sinter	Alcohol
Gates	100	4.5	40	10	5	IPV	Recirc.	31	Zircar	Dry Sinter	Aqueous
Yardney	100	4.5	40	10	4	IPV	Recirc.	31	Zircar	Slurry	Aqueous

Table 5-10. LEO Test Data from Martin Marietta

Mfg.	Rated Cap (Ah)	Temp (C)	DOD (%)	No. Cells orig.	No. Cells remain.	Cycles Completed
Group 1						
EP/Joplin	50	10	40	16	3	31,535
Gates (GE)	50	10	40	16	16	33,314
EP/Joplin	50	20	40	8	0	24,309
Gates (GE)	50	20	40	8	3*	32,888
EP/Joplin	50	10	60	8	0	9,499
Gates (GE)	50	10	60	8	0	10,232
EP/Joplin	50	20	60	4	0	5,304
Gates (GE)	50	20	60	4	0	9,013
Group 2						
Yardney (YEC)	50	10	40	6	0	22,318
Yardney (YEC)	50	10	60	9	1	11,018
Yardney (YEC)**	50	10	60	9	0	8,210
Group 3						
EPI/Joplin	50	10	40	4	0	14,691
Group 4						
EP/Joplin	100	10	40	8	8	30,338
Gates (GE)	100	10	40	5	5	30,460
EP/CS	100	10	40	4	4	26,369
Yardney (YEC)	100	10	40	4	0	25,545

* Cell case arced by test personnel ** Activated with 26 percent KOH

Cell Design Variables

All of the 24 cells in Group 1 failed at 60 percent DOD after the number of cycles shown in Table 5-11. The cells typically fail at about 10,000 cycles. Group 1 cells were made using the Air Force recirculating design with Zircar separators and wall wicks as shown in Table 5-10.

All of the 18 Yardney Group 2 cells except one failed at 60 percent DOD, as shown in Table 5-11. One cell is still working after 11,000 cycles. These cells are also made with the recirculating design, but the separators consist of one layer of asbestos and one layer of Zircar.

At 40 percent DOD at 20°C, most of the Group 1 cells failed prior to completing 30,000 cycles. However, for the Gates (GE) cells at 10°C and 40 percent DOD, all 16 cells are still running after 33,000 cycles.

Group 2 cells have the dual separators, one layer of asbestos, and one layer of Zircar. All of these cells but one have failed at 60 percent DOD. One cell stands out and is still running after 11,000 cycles. All of the remaining 24 cells have failed, including the 9 cells with 26 percent KOH and the 6 cells at 40 percent DOD.

Group 3 cells, at 40 percent DOD, failed at about 14,000 cycles. These cells were the COMSAT design, with asbestos separators and no wall wick.

The Group 4 cells, the 100-Ah cells, are all still performing, with the exception of the Yardney cells with the asbestos/Zircar separators. All of the Yardney cells failed after 25,000 cycles. All of the other 100-Ah cells are still running.

Failure Mode

Destructive physical analyses (DPA) were performed on failed cells to determine the failure mechanisms [5-7]. A summary of results follows.

1. Four 50-Ah cells failed early in the 10°C test at 60 percent DOD. These cells failed after completing 511 to 4,032 cycles. These cells were tested in a horizontal position that allowed free electrolyte to pool in the downward portion of the cell stack. Examination of the stack revealed signs of extreme heat, fused and scorched gas screens, absence of separator material, and pin holes in the negative plates. It was hypothesized that excess electrolyte pooled in the downward area of the cell stack assembly, causing localized recombination and "popping." Separators, gas screens, and plates were also damaged, ultimately causing plate-to-plate shorts [5-6]. The remaining cells on test were reoriented to a vertical testing position following these failures. Since then, no further failures have resulted from this mechanism.

2. A more typical failure for the Group 1 50-Ah cells is characterized by the gradual, long-term degradation of cell performance. Both the voltage and capacity were observed to degrade. The majority of the Group 1 50-Ah cells that failed exhibited this capacity and voltage degradation. Analyses of positive plates from these failed cells showed expansion of the plates. Typically the plates had expanded to .040 to .045 inches from an original thickness of approximately .030 inches (50 percent expansion). The active material appeared to have expanded out of the substrate; it was very soft in consistency, and was easily removed from the substrate with a spatula. The actual cause of failure appeared to be due to the active material extruding from the substrate and rendering itself useless. In the more extreme cases of positive plate expansion, the active material had expanded into the gas screen and through the separator material, causing a soft internal short. These Air Force cells had positive plates with plaque made by the dry sinter process with aqueous impregnation of active material.

3. The Group 3 COMSAT 50-Ah cells showed similar voltage and capacity degradation to failure as the above-mentioned Air Force 50-Ah cells. However, analysis of the positive plates showed virtually no positive plate expansion. The surface of the positive plates was solid and did not show the deterioration seen on the dry sinter plates. These COMSAT cells had positive plates with plaque made by the wet slurry process with aqueous impregnation of active material.

   These COMSAT cells did not have a wall wick to return electrolyte lost by entrainment, or to return water lost by evaporation and condensation.

Summary and Conclusions

1. These data show that the LEO cycle lifetime at 40 percent DOD and 10°C was greater for the Gates recirculating (Air Force) design cells with Zircar separators and wall wicks than for the back-to-back (COMSAT) design cells with asbestos separator material and no wall wicks.

2. A postulated failure mode for the COMSAT design cells is that the cells dried out at the separator electrolyte interface, increasing the internal impedance and causing voltage and capacity to degrade with cycling. The most probable mechanism for drying out of the separator is evaporation of water from the electrode stack and condensation of water at the pressure vessel wall. With no wall wick, there is no return path for the water to the electrode stack.

   The COMSAT cells were designed for GEO applications; the electrolyte concentration in the cells was 38 percent KOH discharged, compared to 31 percent KOH discharged for the Group 1 Gates cells.

3. One should note that EP/Joplin often specifies the KOH concentration in the fully charged state, and Gates specifies the KOH in the fully discharged state. If so, 31 percent charged is equivalent to 38 percent discharged. This difference in KOH concentration between Gates and EP/Joplin could explain the difference in performance for the Lot 1 Gates and EPI cells. Lower electrolyte concentration improves cycle lifetime.

4. The Gates cells with the recirculating design and Zircar separators (2 layers) and wall wick with 31 percent KOH are the best performing cells.

5. The Yardney cells with one layer of asbestos and one layer of Zircar did not perform well enough to justify the combination (choice) of separator materials over two layers of Zircar.

5.4.2 Air Force LEO Testing At Crane

The Air Force (Aerospace Corporation) is sponsoring the Naval Weapons Support Center at Crane, Indiana, to test Ni-H_2 cells. Included in these tests are Ni-H_2 cells from three different Aerospace manufacturers: Gates Energy Products; Eagle-Picher, Inc.; and Yardney Technical Products. The Air Force has set several goals for this LEO life-test program [5-8].

- 30,000 LEO cycles at 40 percent DOD at different operating temperatures from -5°C to 10°C.

- 20,000 LEO cycles at 60 percent DOD at different operating temperatures from -5°C to 10°C.

All of these cells are manufactured to the Air Force recirculating design, with Zircar separators and wall wicks.

Test Program

All of the cells are being tested under conditions simulating real-time LEO operation for a 90-minute orbital period, 60 minutes in the sunlight on charge and 30 minutes in the eclipse on discharge. For each test the C/D ratio is periodically checked and adjusted by varying the charge rate. (The discharge rate or DOD is fixed). The C/D ratio is adjusted to minimize overcharge. For all test groups, the C/D ratio was adjusted to between 1.01 and 1.04. Even slightly excessive overcharge (two or three percent more overcharge) can reduce cell life [5-8].

A failure is defined as the inability of a cell to support an end-of-discharge voltage of 1.0 V.

Test Results

The status of the cells on test are summarized in Table 5-12 [5-9].

Table 5-11. Ni-H_2 LEO Life Test at Crane (March 1, 1993)

Manufacturer	Capacity (Ah)*	Diameter (cm)	Temp (°C)	DOD (%)	Cycles complete	No. Cells (orig.)	(remain)
Gates	50	8.89	-5	53	24,000	10	10
Gates	50	8.89	10	54	24,500	10	10
Hughes	50	8.89	-5	50	31,100	10	10
Hughes	50	8.89	10	49	24,500	10	10
Yardney	50	8.89	-5	41	31,100	10	10
Yardney	50	8.89	10	41	33,800	10	10
Yardney	50	8.89	10	25	19,500	5	5
Eagle-Picher (CS)	90	11.43	10	40	24,000	8	8
Hughes	90	11.43	10	40	23,800	5	5
Gates	90	11.43	10	40	24,000	8	8
Eagle-Picher (CS)	150 Ah	11.43	10	25	16,500	5	5
Gates	150 Ah	11.43	10	25	17,500	5	5
Others							
Eagle-Picher (CS)	150	11.43	10			Storage Test	5
Gates	150	11.43	10			Storage Test	5
Yardney	110	11.43	10	40	5,200	9	9
Eagle-Picher (J)	50	8.89	10	40 (pulse test cells)	6,000	15	15
Eagle-Picher (J)	50	8.89	10	40	12,900	7	7
Removed From Test (failed)							
Gates	50	8.89	10	60	5,000	10	0
Hughes	50	8.89	10	74	22,914	10	10
Yardney	50	8.89	10	60	5,000	10	0
Eagle-Picher (J)	50	8.89	10	60	13,000	2	0

* Capacity is the nameplate (rated) capacity by manufacturer

5.4.3 NASA-Sponsored Advanced Ni-H_2 Cell Technology LEO Life Test

As part of the NASA Aerospace Flight Battery Systems Program, the Electrochemical Technology Branch of the NASA Lewis Research Center is sponsoring the Naval Surface Weopons Center at Crane, Indiana, to perform testing to verify advanced Ni-H_2 cell design component developments.

One advanced design technology is the use of 26 percent KOH electrolyte concentration. Two three-cell groups of HAC/Air Force 48-Ah Ni-H2 cells were tested to evaluate the effects of electrolyte concentration. One group was activated with 31 percent KOH. The two cell groups were placed in the same series string and tested under typical LEO regime at 10°C and 80 percent DOD. The three cells with 31 percent KOH failed after 3,729; 4,165; and 11,356 cycles. The cells with 26 percent KOH failed at 15,314; 19,500; and 23,700 cycles. As discussed in Section 1.13.2, additional tests with cells from other manufacturers are now in progress.

The use of a catalyzed wall wick is also being evaulated in tests being run at Crane. Six 125-Ah cells incorporating serrated separators and 26 percent KOH were built by Eagle Picher. Three cells also featured the use of a catalyzed wall wick. The cells are being cycled at 60 percent DOD and 10°C. All three cells without the catalyst on the wall have failed (Cycle 9,588; 13,900; and 20,575). The cells with the catalyst on the wall have accumulated more than 21,500 cycles with no failures. The voltage performance of the cells with the catalyst on the wall has been more stable throughout the test. A description of these cells is presented in Chapter 4, Section 4.3.1.

Additional design and technology features under investigation in similar tests at Crane involve cell stacking (back-to-back vs recirculating), nickel electrode impregnation process (aqueous vs alcoholic), and separator evaluations.

5.5.0 MATHEMATICAL MODEL OF THE BEHAVIOR OF A NICKEL-HYDROGEN CELL ON CHARGE, DISCHARGE, AND OPEN-CIRCUIT STAND

The U.S. Central Intelligence Agency's Office of Research and Development is sponsoring a program for the mathematical modeling of the behavior of an NiOOH/H_2 cell on charge, discharge, and open circuit stand [5-10]. The objectives of this program are:

- Develop a realistic model for the behavior of an NiOOH/H_2 cell.
- Gain a better understanding of reaction mechanisms and transport processes in the cell during operation.
- Predict the optimum design parameters for specific applications or optimum operating conditions for given cells.

The model [5-11] includes diffusion and migration in the electrolyte phase as well as proton diffusion and ohmic drop across the solid active material in the porous nickel electrode. It also takes into account oxygen evolution and hydrogen oxidation on the nickel electrode and oxygen reduction at the hydrogen electrode in addition to the main reactions of a Ni-H_2 cell. It can be used to predict the concentration of the electrolyte and dissolved hydrogen inthe electrolyte phase, the composition of the active material in the nickel electrode, and the potentials in the electrolyte phase and in the solid active material within the nickel electrode as a function of position and time. It can also be used to predict the partial pressure of hydrogen and oxygen, and the cell voltage as a function of time during charge, dischargem and open circuit.

To demonstrate, Figure 5-31 shows the model's theoretical predictions as compared to the voltage profile of an experimental Ni-H_2 cell during charge, open-circuit stand, and discharge. The model gives an excellent fit during the open-circuit stand period and during the discharge [5-10].

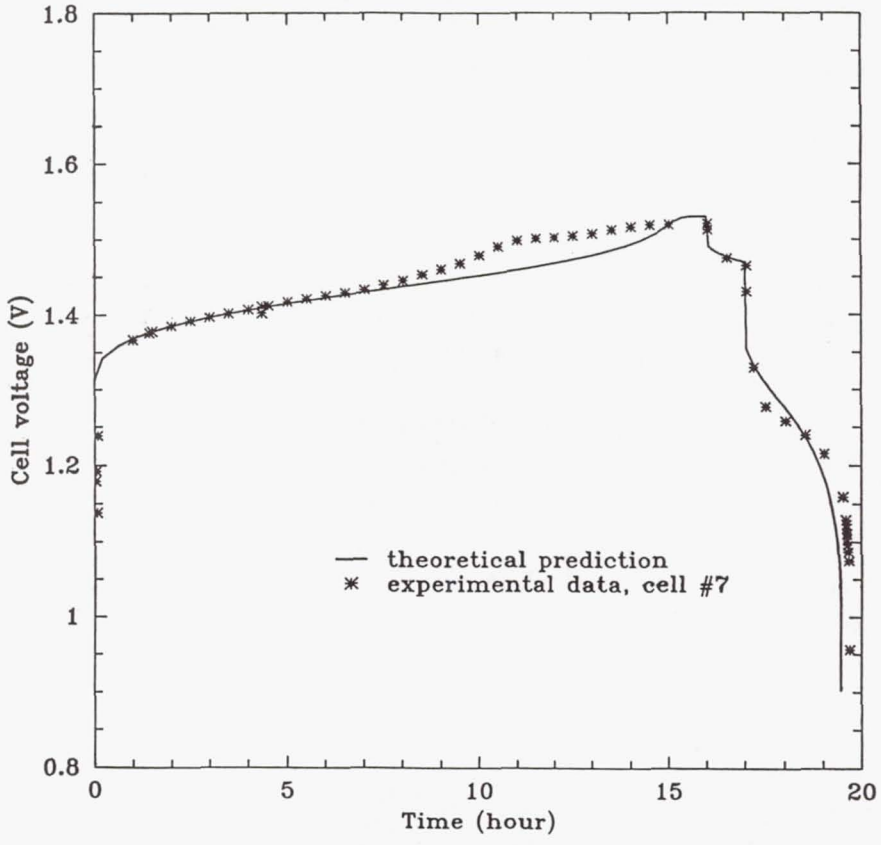

Figure 5-31. Comparison of theoretical prediction and experimental data for the behavior of a NiOOH/H_2 cell during charge, open-circuit, and discharge.

5.6.0 REFERENCES

[5-1] Private communications with M. Earl, COMSAT Laboratories; work performed for INTELSAT Contract Note SSTD/93-130, "INTELSAT VII A Ni-H_2 Cell Evaluation," March 17, 1993.

[5-2] J. F. Stockel, "Self-Discharge Performance and Effects of Electrolyte Concentration on Capacity of Nickel-Hydrogen (Ni/H_2) Cells," 20th Intersociety Energy Conversion Engineering Conference, August 25–29, 1986. Volume 1, p. 1.171.

[5-3] Z. Mao and R. E. White, "A Mathematical Model of the Self-Discharge of a Ni-H_2 Battery," *Journal of the Electrochemical Society*, Submitted December 1990, Revised May 1991.

[5-4] J. Dunlop, A. Dunnet, and D. Cooper, "Performance of INTELSAT V Batteries In Orbit (1983–1991)," 27th Intersociety Engineering Conversion Engineering Conference, San Diego, California, August 3–7, 1992.

[5-5] M. Earl, T. Burke, and A. Dunnet, "Method for Rejuvination of Ni-H_2 Battery Cells," 27th IECEC, San Diego, California, August 1992.

[5-6] Gerald W. Byers, "Nickel-Hydrogen Low Earth Orbit Testing at Martin Marietta Space Center," 25th Intersociety Energy Conversion Engineering Conference August 12–17, 1990. Reno Nevada, Volume 6 p. 65.

[5-7] K. H. Fuhr, "Failure Analysis of 3.5 Inch, 50 Ampere-Hour, Nickel-Hydrogen Cells Undergoing Low-Earth-Orbit Testing," 22nd Intersociety Engineering Conversion Engineering Conference, p. 889.

[5-8] S. W. Donley, C. A. Hill, A. Minichiello, P. J. Dalton, R. L. Haag, and S. W. Hall, "Nickel-Hydrogen Cell Low Earth Orbit Life Test at NWSC/Crane," 24th Intersociety Energy Conversion Engineering Conference, August 6–11, 1989. Volume 3 p. 1417.

[5-9] Michelle Manzo, private communications.

[5-10] J. Stockel, private communications, U.S. Central Intelligence Agency, Office of Research and Development.

[5-11] Z. Mao and R. E. White, "Mathematical Modeling of the Behavior of a NiOOH/H_2 Cell on Charge, Discharge, and Open Circuit," Spring Meeting of the Electrochemical Society, May 16–21, 1993, Abstract No. 97, pp. 145–146.

CHAPTER 6
STORAGE AND HANDLING

6.1.0 GENERAL

Storage and handling of Ni-H_2 cells and batteries must cover a number of different stages in the cell/battery lifetime, including:

1. Storage of the cells after manufacture and before assembly into batteries.
2. Storage of the batteries after assembly and prior to launch. This storage period may be up to 5 years.
3. Storage of the cells/batteries during shipment.
4. Storage of the batteries at the launch site.
5. Storage of the batteries in orbit.

Capacity fading during storage (loss of capacity to 1.0 volts) is the major concern with Ni-H_2 cells and batteries for each of the five different storage stages described above.

Section 6.2.0 describes storage methods that have been used throughout the industry to store Ni-H_2 cells and batteries for long periods of time. The application of these storage methods to the different stages of the cell/battery lifetime are discussed in Section 6.3.0 through 6.7.0. Should capacity fading occur during any stage of the cell/battery lifetime, capacity recovery procedures are described in Section 6.8.0, which can be used to recover capacity. These storage methods and their effects on capacity, along with the capacity recovery procedures, were presented and discussed at the Nickel-Hydrogen Storage Workshop on April 11, 1991 [6-1] and the 1992 NASA Aerospace Battery Workshop [6-2].

The effect of cell design variables on capacity fading are presented in Section 6.9.0. A mechanism for capacity fading (loss of capacity with no second plateau) is presented in Section 6.10.0. The effects of different storage conditions on capacity fading are presented in Section 6.11.0.

Storage conditions that lead to a low voltage second plateau are discussed in Reference 6-3 (see Appendix A). A mechanism for the capacity loss is formulated. The use of minimal hydrogen precharge is recommended to avoid the formation of oxygen gas in the discharged cell. At low potentials (that of a discharged Ni precharged cell), the platinum catalyst accepts the potential of an oxygen electrode.

At this potential, the Pt catalyst will undergo oxidation and dissolve platinum metal from the negative into a soluble material which can diffuse throughout the cell.

6.2.0 METHODS USED FOR STORAGE OF Ni-H_2 CELLS/BATTERIES

6.2.1 Storage at -20°C

In this storage method, cells are stored at the low temperature of -20°C with the cells discharged and on open circuit stand. The cells are fully discharged to 1 V per cell and a 1-ohm resistor is placed across the cells for at least 16 hours. These cells are then put into cold storage at -20°C on open-circuit stand.

This method of storage can be used for any duration of time from several days or weeks up to years. It has been used for storage of the INTELSAT V and VI Ni-H_2 cells for over two years with no measurable loss in capacity [6-4].

This cold storage method is the same procedure used by the aerospace community for long-term storage of Ni-Cd cells and batteries, with the exception that NASA stores Ni-Cd cells shorted rather than open circuited.

6.2.2 Trickle Charge

The trickle charge storage method stores batteries at a temperature of 0 to 10°C and a trickle charge rate of C/60 to C/120. The cells/batteries are fully charged and then maintained in the fully charged condition by trickle charging the cells. The cells should be kept below room temperature, preferably between 0 and 10°C.

The trickle charge method is the in-orbit method used on GEO communication satellites for storage of Ni-H_2 batteries between eclipse seasons.

6.2.3 Storage at 0°C

In this method, cells are stored at a low temperature of 0°C, with the cells discharged and on an open circuit stand. This procedure is the same as the low-temperature storage procedure described in Section 6.2.1 except that the cells are stored at 0°C instead of -20°C.

This procedure can be used to store cells for six months to one year. Beyond one year of storage, capacity fading has been observed for hydrogen precharge cells [6-4]. Positive precharge cells maintain capacity in this storage mode.

6.2.4 Periodic Recharge at Room Temperature

In this method, the cells and batteries are placed fully charged on an open-circuit stand, and they are recharged at a C/10 rate every 7 days to a pressure limit of 70 percent state of charge. Several variations of this storage method exist, such as recharging the cell or battery every 14 days using a voltage limit, pressure limit, or a fixed recharge time (such as 6 hours to recharge at a C/10 rate) to terminate the recharge.

The periodic recharge every 7 days to a pressure limit (estimated at 70 percent state of charge) has been used successfully for the INTELSAT VI flight batteries for storage periods up to 2 years [6-4], [6-5]. No capacity fading occurred with this method.

A major advantage of this storage method is that the battery can be stored at room temperature with no capacity fading. The periodic recharge every 14 days also worked well using a C/10 charge rate for 6 hours [6-5],[6-6].

6.2.5 Room Temperature with the Cells/Batteries Fully Discharged Open-Circuit Stand

Open-Circuit Stand discharge at room temperature is <u>not</u> recommended for long-term storage of cells. It is, of course, necessary that cells and/or batteries be left on open circuit or short circuit stand at room temperature for periods of time such as during handling, assembly, and shipment. If possible, it is recommended that cells not be left at room temperature on an open circuit stand for periods longer than 14 days. They should be recharged every 7 to 14 days as described above.

6.3.0 STAGE 1: STORAGE OF CELLS

Storage of Ni-H_2 cells between the time of manufacture and before assembly into batteries can vary for different programs, and ranges from a few weeks to over one year.

The preferred method is to fully discharge the cells and store them at -20°C discharged on open-circuit stand. This method of storage maintains capacity for any period of time from weeks up to several years.

If facilities are not available for storage at -20°C, then another option is low-temperature storage at 0°C. Again, the cells should be fully discharged and left on an open-circuit stand. This method of storage is useful for shorter periods of time, from several weeks up to six months for hydrogen precharge cells. Positive precharge cells do not show capacity fading at 0°C.

If the cells are to be stored at room temperature then they should be periodically recharged every 7 to 14 days. This method of storage maintains capacity for any period of time from weeks up to several years.

Trickle charging at 0 to 10°C with a C/60 to C/120 rate can also be used for long-term storage of cells.

Regardless of which of these storage methods is used, it is necessary to measure the capacity before and after storage to determine if any capacity fading has occurred during storage. After the cells are manufactured, they normally go through acceptance testing and possibly even vibrational and thermal vacuum testing before storage. Whatever the requirements, just prior to storage the capacity of the cells should be measured using the Standard Capacity Test described in Chapter 7. After storage, the capacity of the cells should be remeasured using the same Standard Capacity Test. If capacity fading has occurred during storage, one of the methods described in Section 6.8.0 of this chapter can be used to recover the capacity.

6.4.0 STAGE 2: STORAGE OF BATTERIES AFTER ASSEMBLY

Once the flight batteries are assembled, they are generally stored until they are shipped to the launch site for assembly into the spacecraft. For flight batteries the storage period can vary in time from a few months to several years. The longer storage periods result from program delays affecting launch schedules. A good example is the INTELSAT VI program. The launch was delayed for over two years after the batteries were activated [6-5]. Suffice to say it is important to make provisions for the long-term storage of batteries. The recommended methods for storing the batteries are similar to those for cells.

Trickle charge and periodic recharge are the preferred methods. The advantage of these methods is that the battery can be maintained for years with no measurable loss in capacity. On trickle charge, the batteries should be maintained at 0 to 10°C.

Batteries stored at room temperature should be maintained on open circuit stand and recharged every 7 to 14 days. This method maintains capacity for at least 2 years. With the periodic recharge to 70 percent state of charge, a minimum amount of heat is dissipated within the cell (no overcharge).

Low temperature storage at 0°C with the battery discharged and on open circuit is acceptable for short storage periods of up to six months. With this method of storage, it is very important to check for loss in capacity after storage.

6.5.0 STAGE 3: STORAGE OF CELLS/BATTERIES DURING SHIPMENT

6.5.1 Cells

$Ni-H_2$ cells should be fully discharged and shorted during shipment. The cells are shorted to avoid any possible arcing or current leakage paths. Each cell is wrapped separately with its own packaging material. Five to ten cells are packed within the same container. These containers are normally marked as fragile and shipped by air express to minimize the shipping time. During shipment the cells are at ambient temperature (0 to 30°C).

Cells are normally shipped from the manufacturer's facility to a NASA or aerospace company where the cells are fabricated into batteries or used for special testing. As soon as the cells are received they should be acceptance tested. A standard procedure such as the Standard Acceptance Test Procedure should be followed. It is also recommended that this same Standard Capacity Test be performed prior to shipment of the cells. These data should be used to determine if any capacity fading occurred as a result of shipment. If capacity loss did occur, one of the recovery procedures described in Section 6.8.0 of this text should be used.

6.5.2 Batteries

$Ni-H_2$ batteries should be shipped separately within their own special container, fully discharged and left on open circuit stand during shipment. The batteries should not be shorted unless each cell can be shorted individually. (Some batteries are designed with individual resistors, sometimes called pull-down resistors, which can be placed across each individual cell). In this case, the battery should be shipped fully discharged with the individual resistors across each cell.

The reason not to short down a battery with a single resistor across the battery terminals is that any mismatch in capacity within the cells will result in the lower capacity cells being driven into reversal. Cell reversal is not recommended, particularly for positive precharge cells. A special shipping container should be designed to protect the battery from damage during shipment. The batteries should be shipped air express to minimize shipping time.

6.6.0 STAGE 4: STORAGE OF BATTERIES AT THE LAUNCH SITE

If possible, batteries should be shped separately and installed at the launch site.

Prior to shipment, the capacity of the batteries should be checked using the Standard Capacity Test. This should include a calibration of the strain-gauge bridge for pressure/capacity gauge. Once the batteries are received at the launch site, storage and handling facilities become limited. During handling the batteries should

always be in the fully discharged state. Reconditioning resistors should be used across each cell if available; otherwise, the discharged battery should be placed on open-circuit stand.

During storage at the launch site, the batteries should be stored at ambient temperature and recharged every 7 to 14 days. The battery should be recharged to approximately 70 percent state of charge. This same storage procedure is recommended for storage of the battery in the bay area and after installation within the spacecraft. Recharging the battery every 7 days is recommended to keep the battery in a ready mode for the final full charge prior to launch. During recharge, temperature should be used as a backup control mode. Monitor the temperature and use a temperature limit as a backup to control charging. If the battery and/or spacecraft are heating up, the recharge time should be reduced as necessary. Use pressure to determine battery capacity at the launch site.

6.7.0 STAGE 5: STORAGE OF BATTERIES ON GEO SATELLITES

Ni-H_2 batteries on synchronous orbit communication satellites have design lifetimes of 10, 15, or even 20 years. The batteries are trickle charged during the storage period between eclipse seasons. Trickle charge rates are between C/60 and C/120 and the battery is kept fully charged at temperatures of 0 to 10°C. This storage method has been used successfully on a number of commercial communication satellites, starting with the INTELSAT V series in 1983 (see Chapter 5). The lower C/100 to C/120 rates are recommended to reduce heat dissipation within the cells. A more detailed discussion of charge control methods is presented in Chapter 2.

6.8.0 CAPACITY RECOVERY METHODS FOR Ni-H_2 CELLS/BATTERIES

6.8.1 Background

When Ni-H_2 cells are first manufactured, they go through acceptance testing. Part of this acceptance test procedure includes a Standard Capacity Test at 10°C. Cells manufactured from one lot should be well matched in capacity. Generally, matching of capacity is the first criterion used for selecting cells to constitute a battery.

When batteries are first assembled, the cells within the battery are well matched in capacity so that the capacity measured for the battery is only slightly less than the capacity measured for the cells used to make up the battery. Again, the Standard 10°C Capacity Test is used to measure the battery capacity at the beginning of life.

After the cells/batteries pass through one of their different lifetime stages as defined in Section 6.1.0, it is necessary to repeat the Standard 10°C Capacity Test to determine if a loss in capacity has occurred and, if so, to what extent. If a capacity

loss of greater than 10 percent of the initial capacity has occurred, one of the recovery methods described below is recommended.

Two methods are described in this text that are used for both storage and capacity recovery; they are trickle charge and periodic recharge.

6.8.2 Recovery Methods

Trickle Charge

As mentioned above, Ni-H_2 batteries at geosynchronous orbits are stored on trickle charge between eclipse seasons. This storage mode proves beneficial not only in maintaining capacity between eclipse seasons, but also in recovering capacity lost due to capacity fading that may have occurred prior to launching of the battery; see Chapter 5, Section 5.3.3, Reconditioning Capacity In Orbit.

Periodic Recharge

This method seems to work surprisingly well for cells/batteries on open circuit stand at room temperature. One option is to recharge at a C/10 rate to 70 percent state of charge every seven days using pressure to terminate the charge. The other option is to recharge the cells at a C/10 rate for 6 hours every 7 days. About 2 months are required to achieve capacity recovery with either method [6-4]. The Standard 10°C Capacity Test should be used to recheck capacity if possible.

Periodic recharge is the best method to use at the launch site for recovering capacity fading that resulted from shipping and handling. This method is also recommended for storage to keep the battery recharged before launch. Pressure can be used as an indication of the state of charge of the battery.

6.9.0 EFFECTS OF CELL DESIGN VARIABLES ON CAPACITY FADING

The capacity fading behavior on the storage of Ni-H_2 cells was studied as a function of cell design variables, as described in Reference 6-7. The major objectives of this investigation were to compare capacity fading behavior of alcoholic impregnated positive electrodes with aqueous impregnated positive electrodes in Ni-H_2 cells with both positive precharge and hydrogen precharge.

Cell design variables were the following:

1. Dry sinter plaque (D)
2. Wet slurry plaque (W)
3. Alcoholic impregnation process (Al)
4. Aqueous impregnation process (Aq)
5. 26 percent KOH concentration

6. 31 percent KOH concentration
7. Positive precharge, 0 psia hydrogen pressure
8. Hydrogen precharge, 100 psig hydrogen pressure.

Experimental Ni-H_2 boilerplate cells, containing four nickel electrodes in each cell, were used for this investigation. The electrode stacks were assembled using the recirculating design with two layers of Zircar separator.

Two methods of storage were investigated:

1. Trickle charge at 50 mA (approximately C/100) at 21°C.
2. Fully discharged, shorted, on stand at 30°C

6.9.1 Cells Stored on Trickle Charge

With continuous trickle charge charging there was very little change in the capacity of the cells after 229 days of storage. These results verify the use of the trickle charge method for storage of Ni-H_2 cells/batteries independent of the cell design variables.

6.9.2 Cells Stored Discharged Shorted at 30°C

Capacity Tests to Evaluate the Effects of Storage

Storage tests included an initial capacity test, storage of test cells for a given period of time, an interim capacity test after each time period, and a final capacity test at the end of the storage test. The storage time period was approximately 40 days, and there were typically four to five storage time periods per storage test.

Aqueous Impregnated Electrodes, Wet Slurry Plaque (W/Aq)

Cell design variables for this positive electrode include the following:

W/Aq/26%/0 psia	26 percent KOH and 0 psia hydrogen pressure
W/Aq/26%/100 psig	26 percent KOH and 100 psig hydrogen pressure
W/Aq/31%/0 psia	31 percent KOH and 0 psia hydrogen pressure
W/Aq/31%/100 psig	31 percent KOH and 100 psig hydrogen pressure

Capacity data at the end of each storage period is shown in Figure 6-1 for these four cells.

To summarize capacity fading with storage for these four cells (from Figure 6-1):

1. The initial capacity is higher for the cells with the higher KOH concentration, (5.0 to 5.5 Ah for 26% KOH vs. 5.75 to 6.5 Ah for 31% KOH).

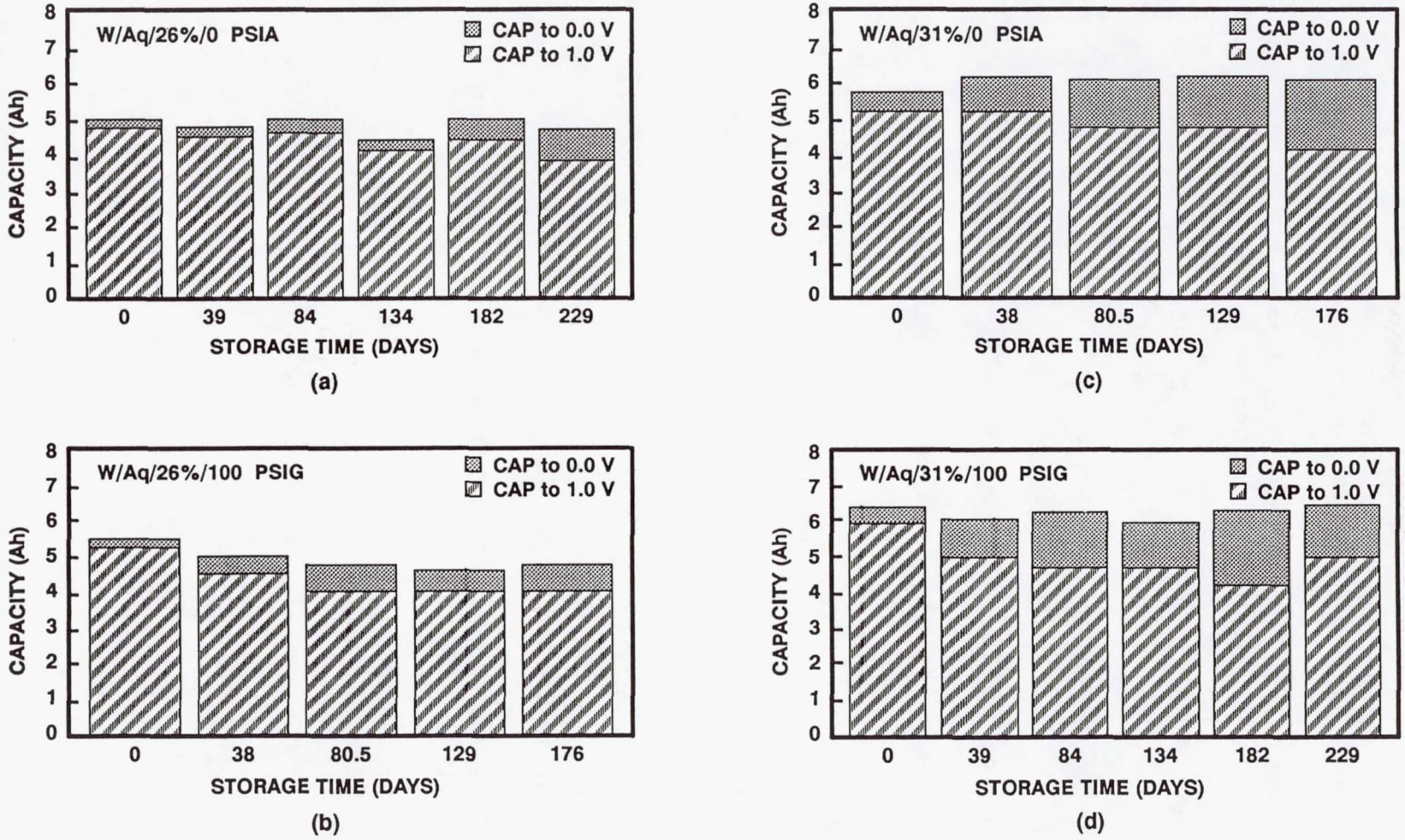

Figure 6-1. Capacity changes of "W/Aq" type electrodes with storage, discharge shorted at 30°C.

2. None of the four cells lost capacity to 0 volts during the four to five storage periods (no significant change in capacity).

3. The two cells at 31% KOH lost 25 to 35 percent of their capacity to 1.0 volt during the four storage periods. This loss in capacity shows up as capacity in the second plateau. The other two cells at 26% KOH lost less capacity, 10 to 15 percent of their initial capacity to 1.0 volt during the four storage periods. Again, this loss in capacity shows up as capacity in the second plateau.

4. Hydrogen pressure had no effect on capacity fading.

Aqueous Impregnated Electrodes, Dry Powder Plaque (D/Aq)

Cell design variables for this positive electrode include the following:

D/Aq/26%/0 psia	26 percent KOH and 0 psia hydrogen pressure
D/Aq/26%/100 psig	26 percent KOH and 100 psig hydrogen pressure
D/Aq/31%/0 psia	31 percent KOH and 0 psia hydrogen pressure

The fourth cell with design variables D/Aq/31%/100 psig, 31 percent KOH and 100 psig hydrogen pressure was left out of this test group.

Capacity data at the end of each storage period is shown in Figure 6-2 for these three cells.

To summarize capacity fading with storage for these three cells (from Figure 6-2):

1. Initial capacity is high and approximately the same for all three cells in this test, approximately 6 Ah.

2. No capacity fading was observed for the cell at 100 psig hydrogen pressure and 26 percent KOH electrolyte concentration.

3. Electrolyte concentration had no effect.

4. Hydrogen pressure had no effect.

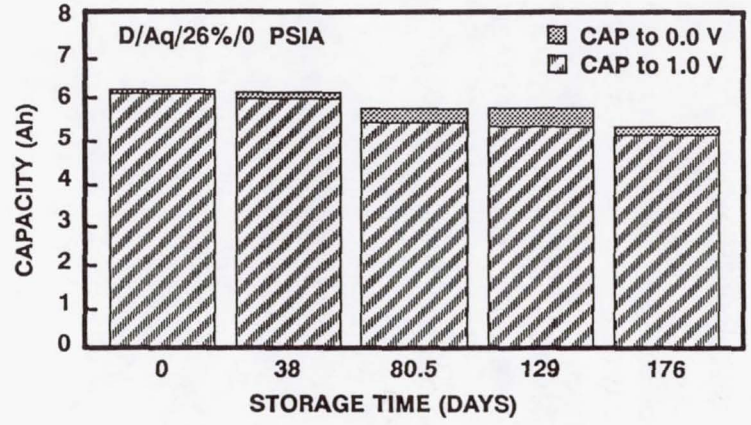

(a)

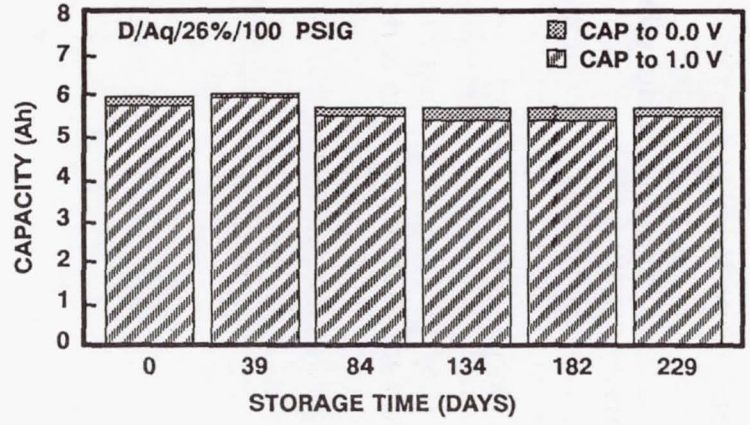

(b)

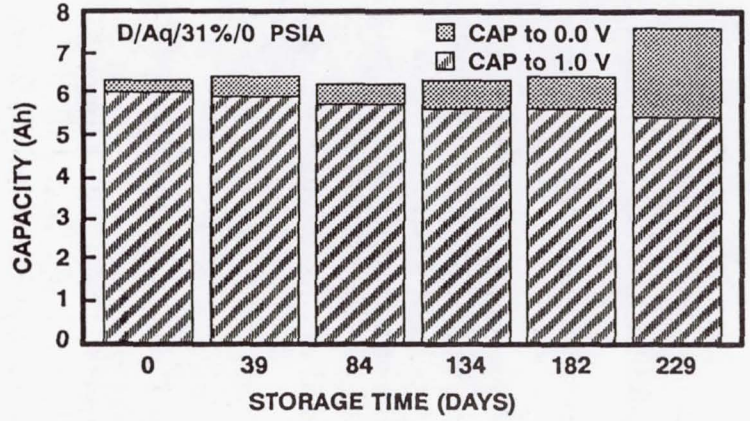

(c)

Figure 6-2. Capacity changes of "D/Aq" type electrodes with storage, discharge shorted at 30°C.

Alcoholic Impregnated Electrodes, Wet Slurry Plaque (W/Al)

Cell design variables for this positive electrode include the following:

W/Al/26%/0 psia	26 percent KOH and 0 psia hydrogen pressure
W/Al/26%/100 psig	26 percent KOH and 100 psig hydrogen pressure
W/Al/31%/0 psia	31 percent KOH and 0 psia hydrogen pressure
W/Al/31%/100 psig	31 percent KOH and 100 psig hydrogen pressure

Capacity data at the end of each storage period is shown in Figure 6-3 for these four cells.

To summarize capacity fading with storage for these four cells (from Figure 6-3):

1. Initial capacity is higher for cells with higher KOH concentrations.

2. A significant amount of capacity fading occurred for the two cells at 100 psig hydrogen pressure. The measured capacity to 0 volts decreased by over 50 percent after four to eight storage periods for the cell at 31 percent KOH and for the cell at 26 percent KOH. This capacity fading was observed for the capacity measured both to 1.0 volts and to 0.0 volts. There was no significant amount of capacity in the second plateau below 1.0 volts.

3. There was little or no capacity fading for cells stored at 0 psia to 0.0 volts.

4. Hydrogen pressure had a significant effect on capacity fading.

5. Electrolyte concentrations had very little effect on capacity fading.

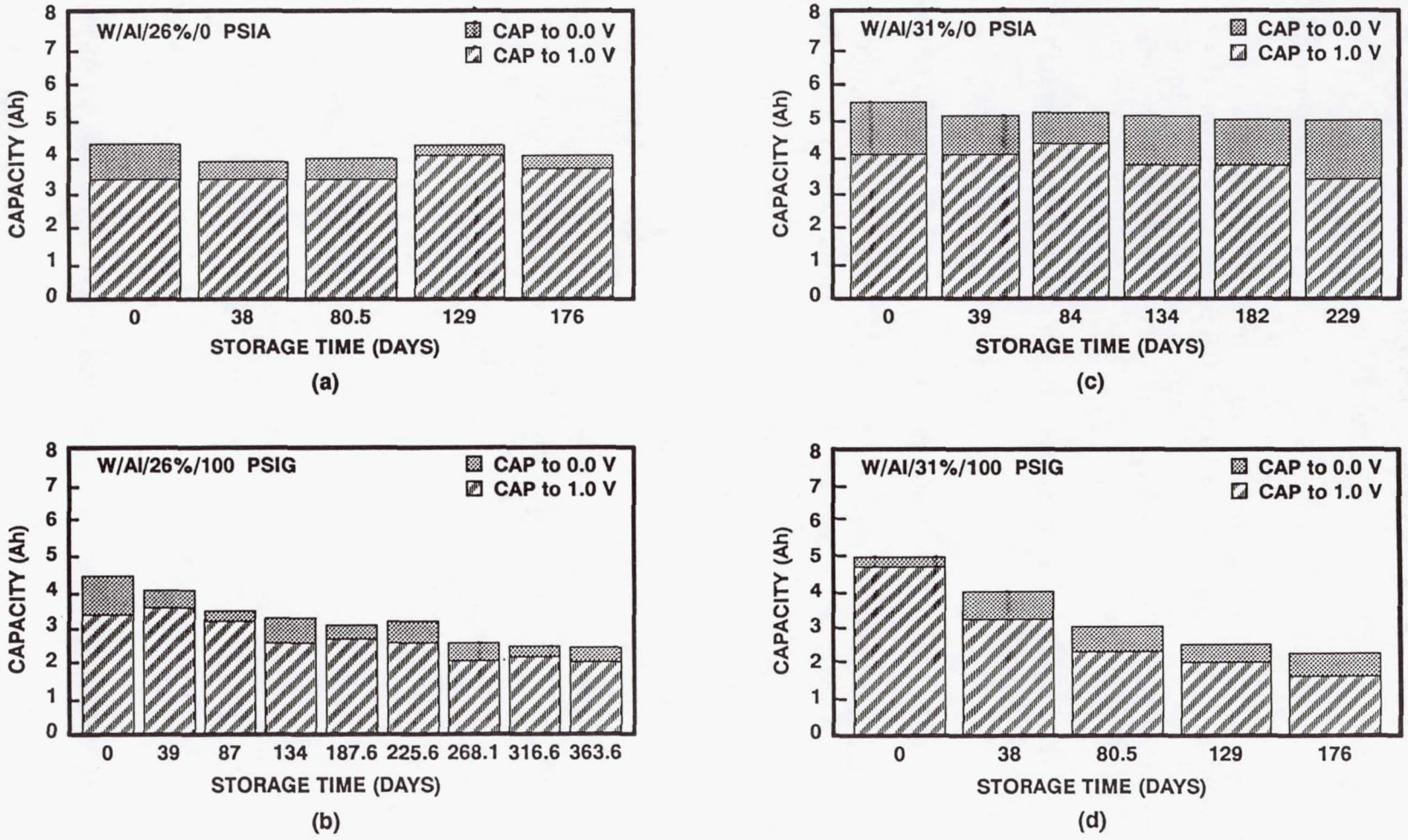

Figure 6-3. Capacity changes of "W/Al" type electrodes with storage, discharge shorted at 30°C.

Alcoholic Impregnated Electrodes, Dry Powder Plaque (D/Al)

Cell design variables for this positive electrode include the following:

D/Al/26%/0 psia	26 percent KOH and 0 psia hydrogen pressure
D/Al/26%100 psig	26 percent KOH and 100 psig hydrogen pressure
D/Al/31%/0 psia	31 percent KOH and 0 psia hydrogen pressure
D/Al/31%/100 psig	31 percent KOH and 100 psig hydrogen pressure

Capacity data at the end of each storage period is shown in Figure 6-4 for these four cells.

To summarize capacity fading with storage for these four cells (from Figure 6-4):

1. A significant amount of capacity fading occurred for cells at 100 psig. The measured capacity decreased by about 50 percent after four to five storage periods for both cells at 100 psig hydrogen pressure. There was very little capacity in the second plateau; all of the capacity fading that occurred was due to a loss of capacity to 1.0 volts.

2. At 0 psia hydrogen pressure, the measured capacity dropped off after the first storage period and then remained almost constant for the next 4 to 8 storage periods.

3. Hydrogen pressure has a significant effect on capacity fading.

4. Electrolyte concentration was not a factor.

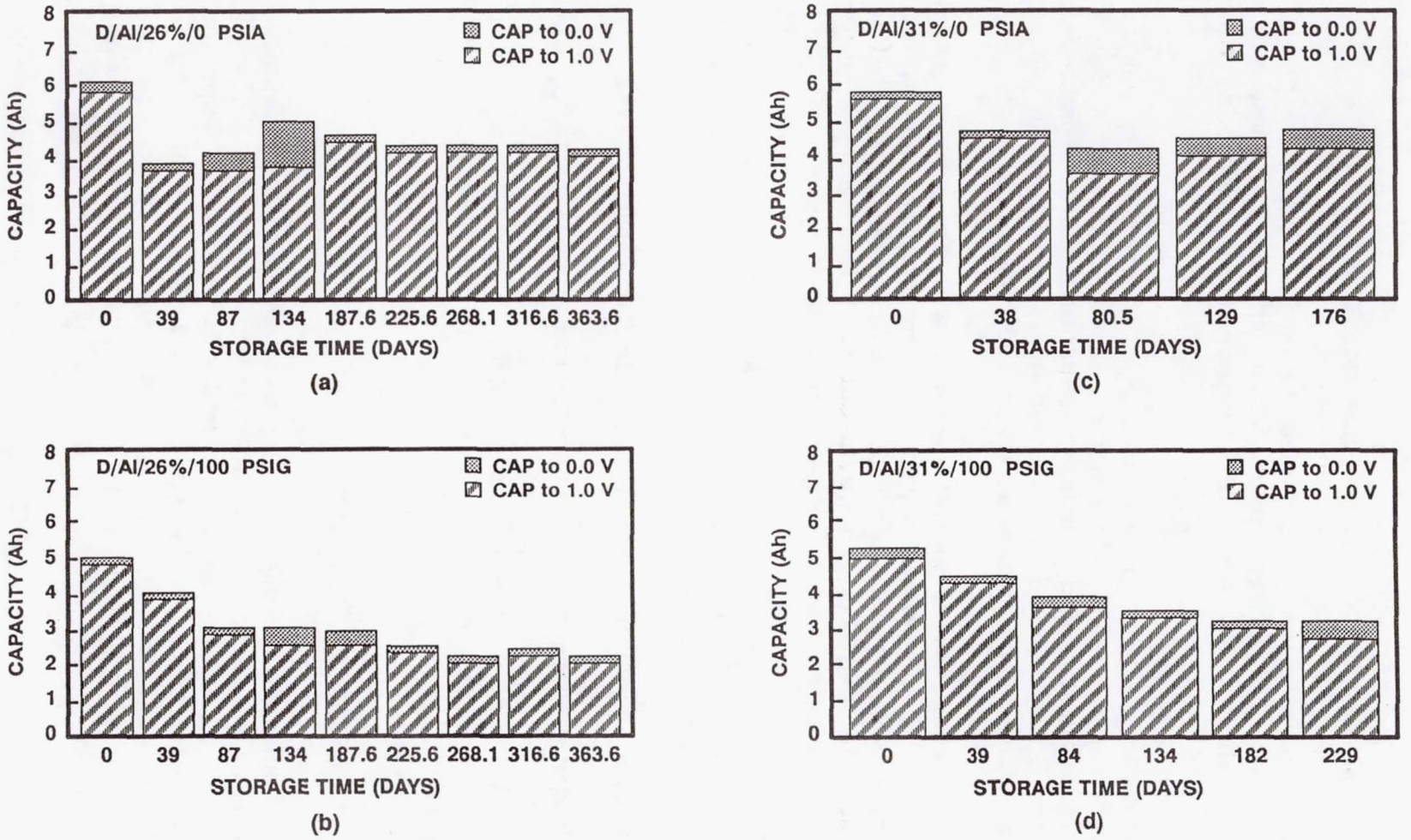

Figure 6-4. Capacity changes of "D/Al" type electrodes with storage, discharge shorted at 30°C.

6.9.3 Summary Of Results For Cells Stored Shorted At 30°C

1. Aqueous impregnated positive electrodes with dry powder plaque (D/Aq) showed very little if any capacity fading with storage. These cells also had high initial capacity. They were the best performing electrodes in the storage test.

2. Aqueous impregnated positive electrodes with wet slurry plaque (W/Aq) show no capacity fading with storage to 0.0 volts. There was a 25 to 35 percent loss in measured capacity to 1.0 volts that occurred during the four storage periods. This capacity fading showed up as an increase in capacity in the second plateau (capacity between 0 volts and 1.0 volts).

3. Alcoholic impregnated positive electrodes with dry powder and wet slurry plaque (D/Al and W/Al) showed significant capacity fading when stored at 100 psig hydrogen pressure for 182 days. The measured capacity to 1.0 volt decreased by 40 to 50 percent for the cells at 100 psig hydrogen pressure. There was no significant amount of capacity in the second plateau.

4. Alcoholic impregnated positive electrodes with dry powder and wet slurry plaque (D/Al and W/Al) showed very little if any capacity fading when stored at 0 psia hydrogen pressure.

5. Electrolyte concentration had very little effect on capacity fading.

6. Hydrogen pressure had a significant effect on capacity fading for alcoholic impregnated positive electrodes.

7. Hydrogen pressure had no effect on capacity fading for aqueous impregnated positive electrodes.

6.10.0 MECHANISM FOR CAPACITY FADING

A mechanism for capacity fading was postulated in Reference 6-7. This mechanism is based on results of destructive physical analysis (DPA) of alcoholic impregnated (dry powder) positive electrodes taken from the experimental cells described in Section 6.8.0 above. The positive electrodes were taken from boilerplate cell #8 (BP8). The cell design variables were dry power plaque, alcohol impregnation, 31 percent KOH, and 100 psig hydrogen pressure. These positive electrodes showed significant capacity fading during the storage test.

Energy dispersive x-ray (EDX) analyses were conducted to determine the distribution of cobalt-to-nickel atomic ratio of the active material between nickel

particles. The distribution in new electrodes was uniform across the active material layer with a concentration of between 11 and 12 percent. This is in agreement with the average value of 11.2 percent cobalt in the active material of electrodes from the alcoholic impregnation bath. In contrast, the cobalt concentration of an electrode from BP8 had a distribution showing a maximum in the middle of the mass of active material. The peak value is about 19 percent while it was as low as 7 percent at one point near the surface (Figure 6-5). These changes in the cobalt distribution suggest that cobalt had probably migrated from the surface of the nickel sinter toward the bulk of active material with the resulting capacity fading as reported by Zimmerman [6-8].

The capacity fading mechanism postulated is based on the observed cobalt segregation. As the cobalt concentration is depleted at the active material/nickel sinter interface, the active material is expected to be converted to a purer beta-phase than the active material located away from the interface where the cobalt concentration in higher. When the electrode is discharged the active material near the interface is expected to be discharged earlier than the active material located away from the interface, not only because of the proximity to the current collector, but also because beta-NiOOH discharges before gamma-NiOOH due to the higher discharge potential of beta-NiOOH. Fully discharged beta-$Ni(OH)_2$ is known as an insulator [6-9]. Therefore, an insulating layer will be formed at the interface during discharge long before the complete discharge of the active material. As more cobalt migrated out of the interface region it will become more and more difficult to discharge the electrode completely, causing capacity fading.

Although this proposed mechanism appears plausible, it does not explain all observations. This mechanism would explain the capacity fading observed for the alcoholic impregnated positive electrodes at the 100 psig hydrogen pressure. One would expect to see a loss in capacity to both 1.0 volt and 0 volts (no second plateau). One would also expect to see a higher end-of-discharge pressure which should account for most of the capacity loss. However, this mechanism does not explain the result for the aqueous impregnated electrodes. Cells with dry powder aqueous impregnated electrodes showed no capacity fading at either 0 psia or 100 psig. The cells with wet slurry aqueous impregnated showed no capacity loss to 0 volts, but they did develop a second plateau with long-term storage. A mechanism to explain the second plateau is presented in Reference 6-3 (Appendix A).

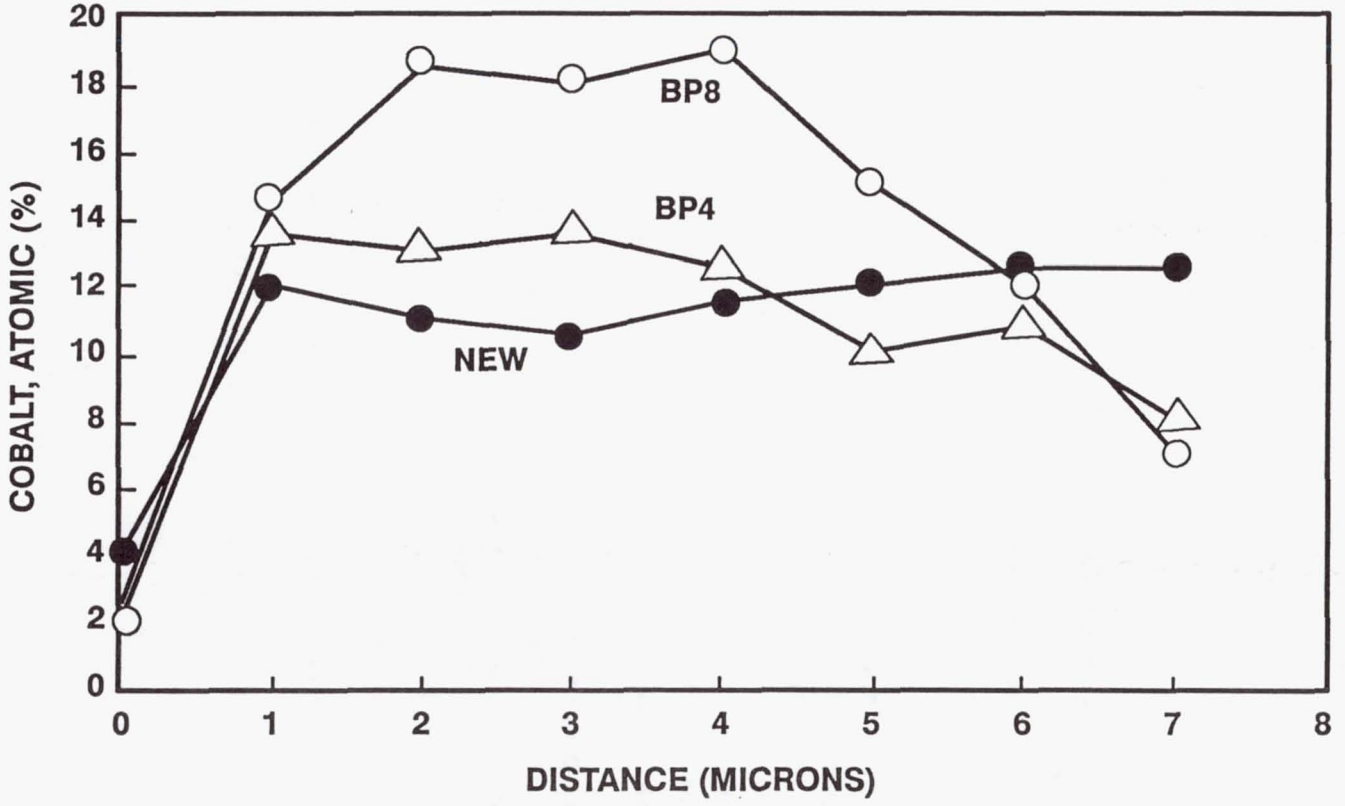

Figure 6-5. Microscopic distribution of cobalt in active material between two nickel particles which were About 10 μm apart for "D/Al" type positive electrodes. A new electrode compared with capacity-faded electrode from BP8.

6.11.0 INVESTIGATION OF STORAGE METHODS

Nickel-hydrogen cells from the INTELSAT VI program were used to evaluate the effects of prolonged storage under different storage conditions [6-4] and [6-6]. The cells are of the Air Force/HAC design, containing 40 sets of positive and negative electrodes, with two layers of Zircar separator material in a recirculating stack configuration. There are two types of precharge, positive precharge and negative precharge. The negative precharge cells have about 150 psig of hydrogen precharge remaining when the positive electrode is fully discharged. The positive precharge cells have 0 psia when the cells are fully discharged, with a small amount of positive capacity remaining in the second plateau.

The storage conditions used were the following:

1. 0°C open-circuit discharged
2. room temperature open-circuit discharged
3. periodic recharge at room temperature
4. trickle charge at room temperature
5. -20°C open-circuit discharged.

6.11.1 Cells Stored Open-Circuit Discharged at 0°C

Two negative-precharge cells and one positive-precharge cell were stored discharged open-circuit at 0°C, and their capacity with time in storage was measured (Figure 6-6). The hydrogen-precharge cells maintained their capacity for about 2 months, and then lost approximately 4 to 6 percent of their capacity in the next 12 months. Thereafter, these cells showed a significant decline in capacity (from 25 to 30 percent) after 650 days of storage. The positive-precharge cell maintained its capacity with a negligible loss in capacity of 1.7 percent over 650 days.

6.11.2 Cells Stored Open-Circuit Discharged at Room Temperature

Five cells were stored discharged open-circuit at room temperature, and their resulting capacity fading with days in storage is shown in Figure 6-7. (Cells with hydrogen-precharge are denoted by the letter N, and those with positive-precharge by the letter P). The hydrogen precharge cells lost as much as 47 percent of their capacity after just 94 to 165 days of storage. The positive precharge cells lost 25 to 42 percent of their capacity after 165 days of storage. The capacity loss seems to level off after 165 days of storage.

The capacity fading (loss of capacity measured to 1.0 volts) shows up as an increase in capacity in the second plateau (Figure 6-8) which shows a complete discharge of the cells to 0 volts after 94 days of storage. These cells were completely discharged to 0 volts at 23.5 Amperes.

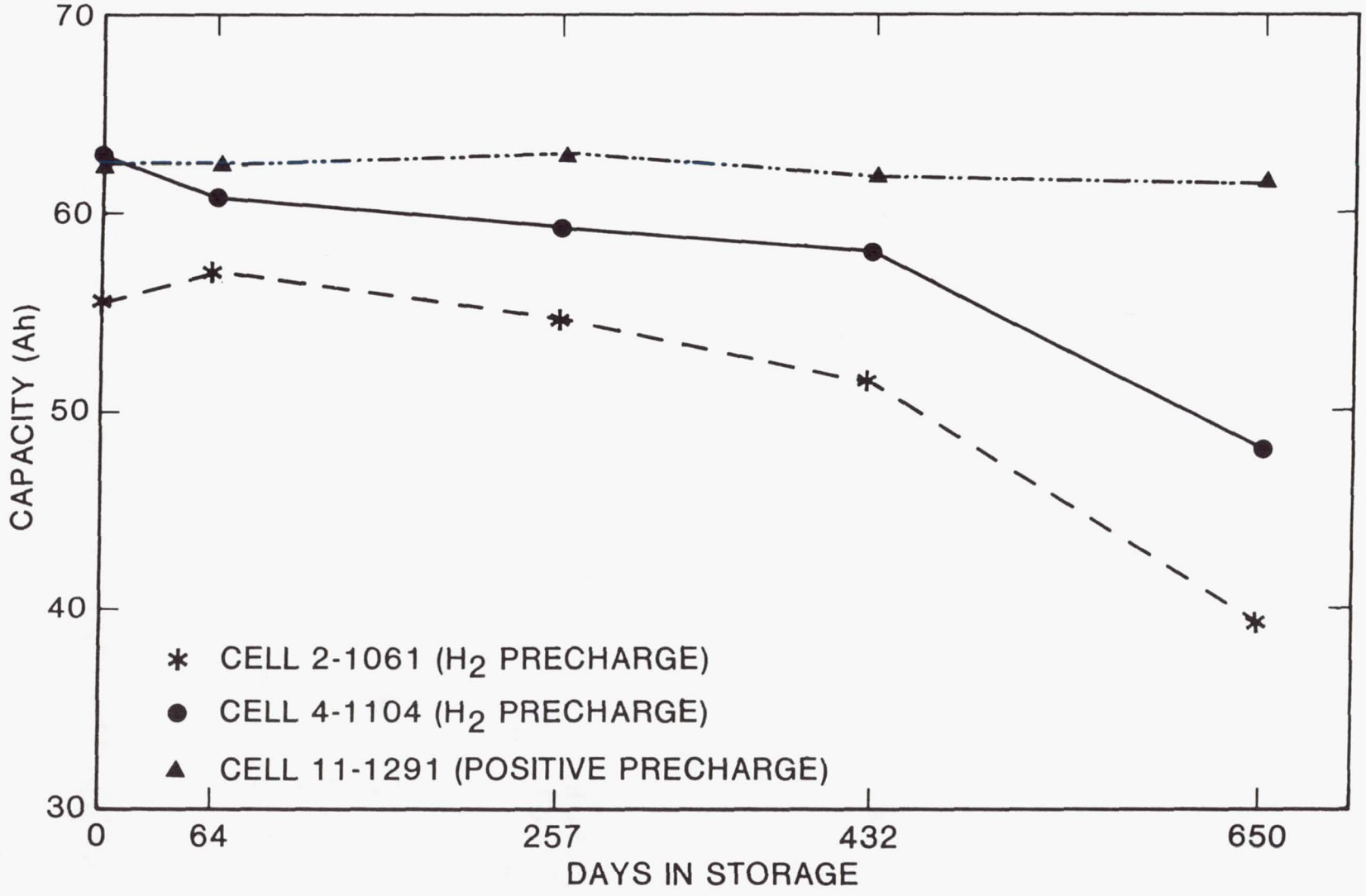

Figure 6-6. Capacity (to 1.0 V). Maintenance for cells stored at 0°C.

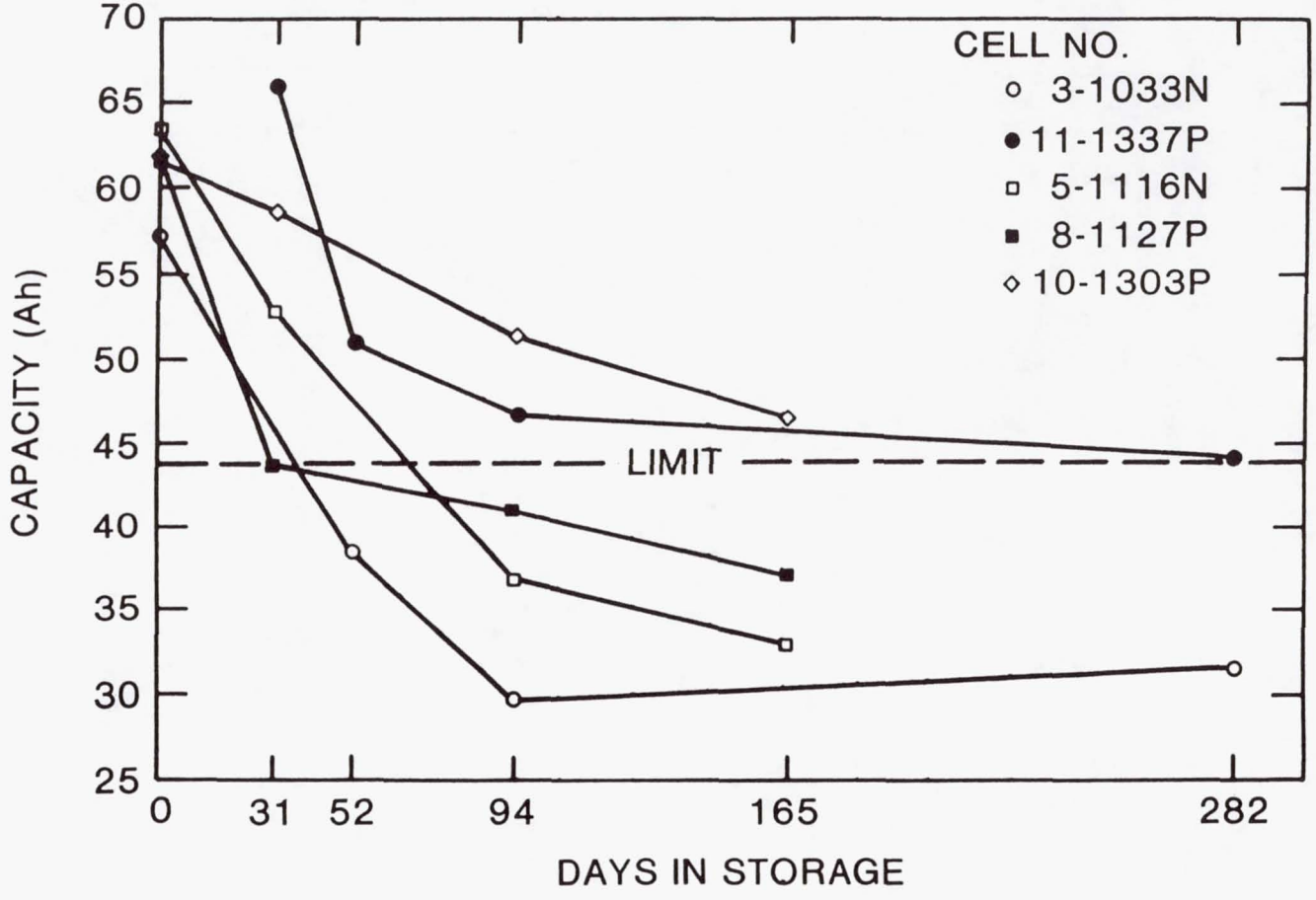

Figure 6-7. Capacity (to 1.0 V). Maintenance for cells stored at room temperature.

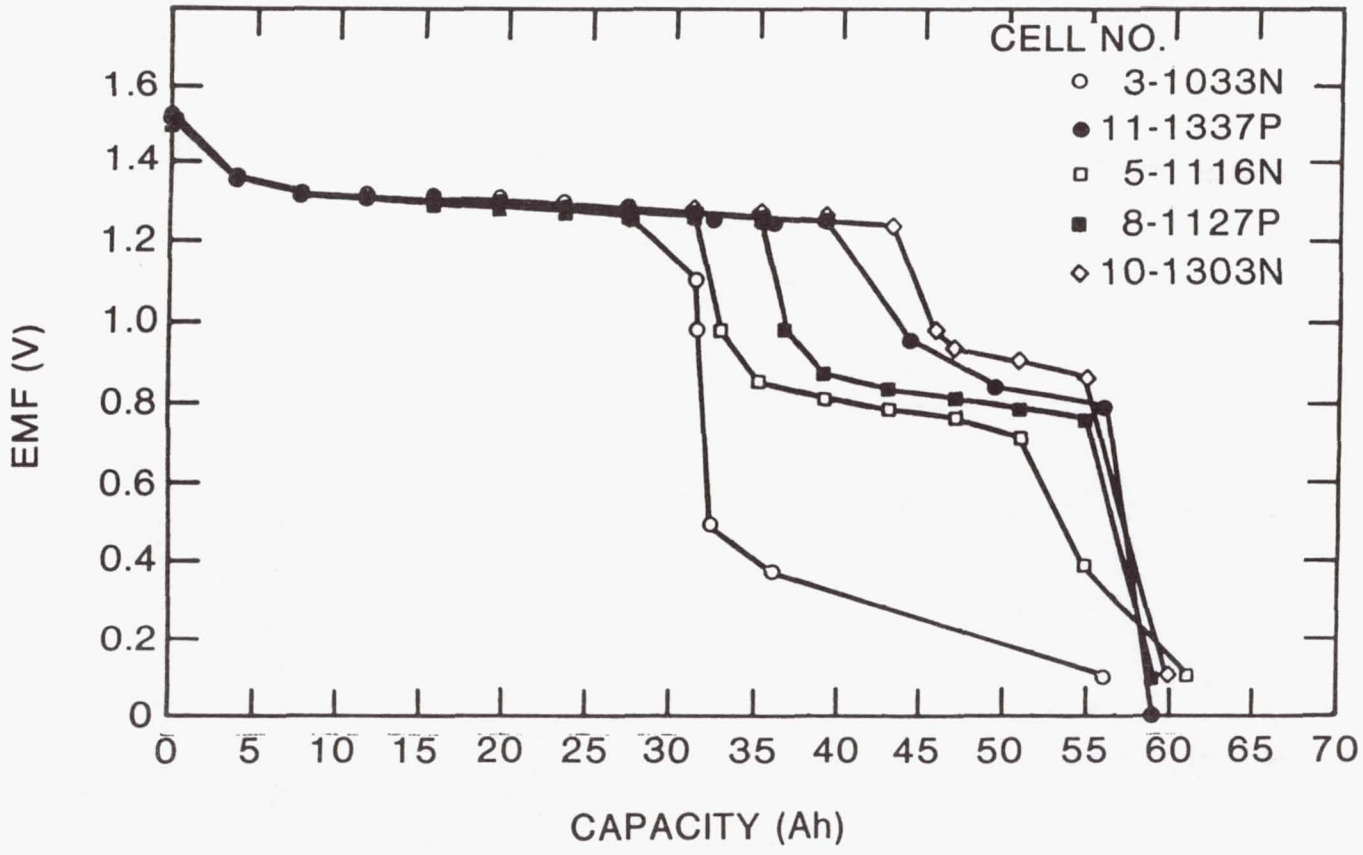

Figure 6-8. Discharge voltage profiles of cells stored at room temperature (second plateau).

6.11.3 Cells Stored with Periodic Recharge at Room Temperature

Three of the cells from the room temperature storage test above were removed after 165 days of storage and recharged periodically at room temperature. A fourth cell was removed from cold storage at -20°C and added to this test.

The four cells were recharged for 10 hours at 4.8 A every seven days, and the capacity was checked after six weeks and again after 12 weeks. Figure 6-9 shows the capacity recovery with top charging. The three cells with low capacity (capacity fading) showed remarkable recovery after 12 weeks of periodic recharging.

Figure 6-10 shows the discharge voltage profile for the four cells after periodic recharge for 12 weeks. Included in Figure 6-10 is the voltage profile for cell S/N 8-1127P before and after the periodic recharge for 12 weeks. Note that the second plateau has been almost completely eliminated by the periodic recharge.

6.11.4 Cells Stored on Trickle Charge at Room Temperature

One hydrogen-precharge cell and two positive-precharge cells were stored in the trickle charge mode. Their capacity during storage is shown in Figure 6-11. The cells were trickle charged at 0.65 A (which is a charge rate of approximately C/80). After 413 days on trickle charge at room temperature, the two positive-precharge cells both had a capacity of 59.2 Ah, and the hydrogen-precharge cell had a capacity of 57.2 Ah. Overall, these capacity values are excellent, and this trickle charge storage mode maintains capacity.

The voltage profiles of the cells during discharge did not show any anomalies, such as a second plateau.

Life test batteries show capacity recovery on trickle charge at lower temperatures of 5 to 10°C.

6.11.5 Cells Stored Discharged, Open-Circuited at -20°C

A group of four cells, three with hydrogen precharge and one with positive precharge, were stored discharged open-circuit at -20°C. Two of the cells gained capacity and the other two maintained their capacity after 112 and 270 days of storage (Table 6-1). These capacity data are excellent, indicating that this storage mode maintains and/or improves the capacity with long term storage.

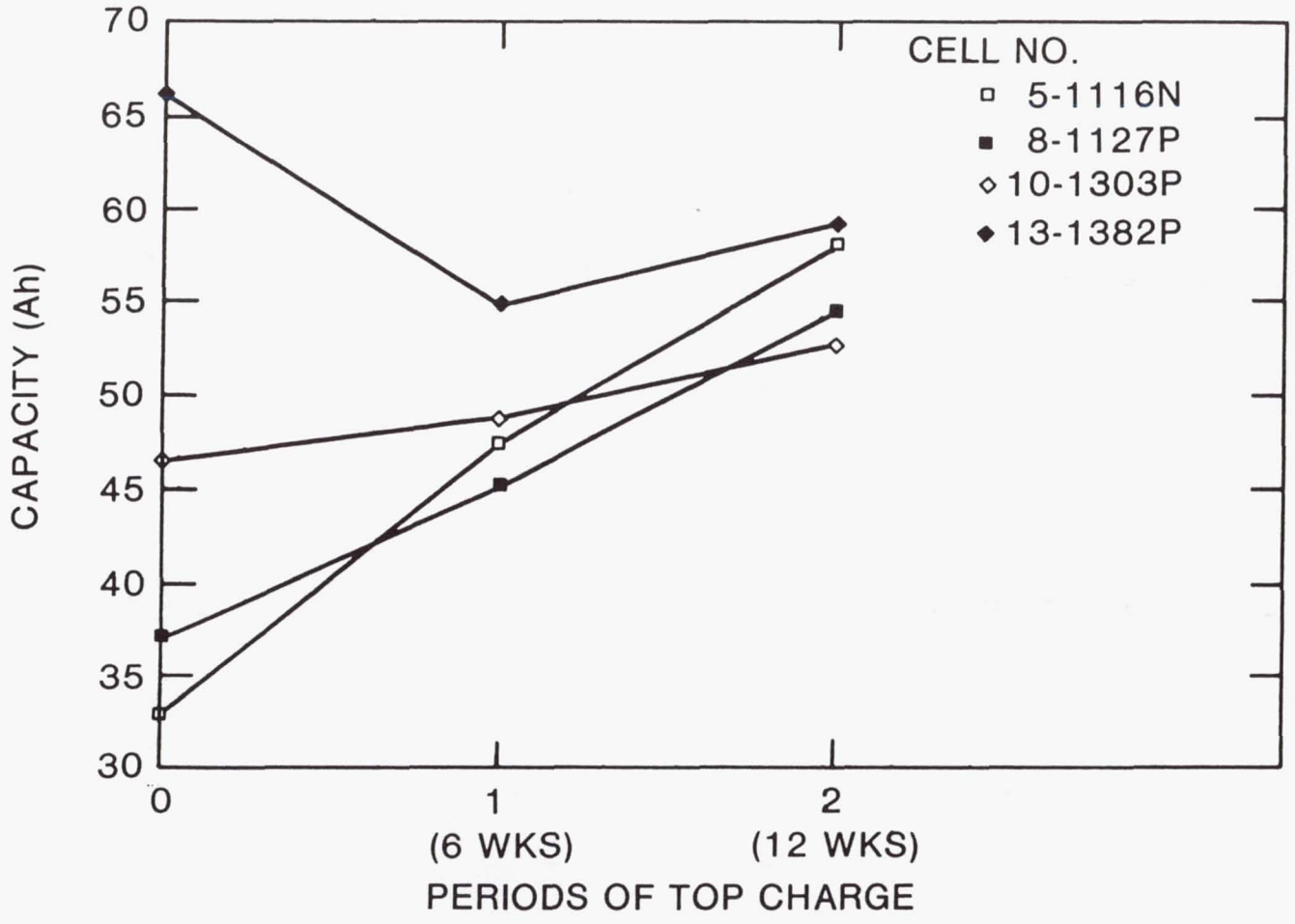

Figure 6-9. Capacity (to 1.0 V) recovery for cells stored charged open circuit stand with recharge every 7 days.

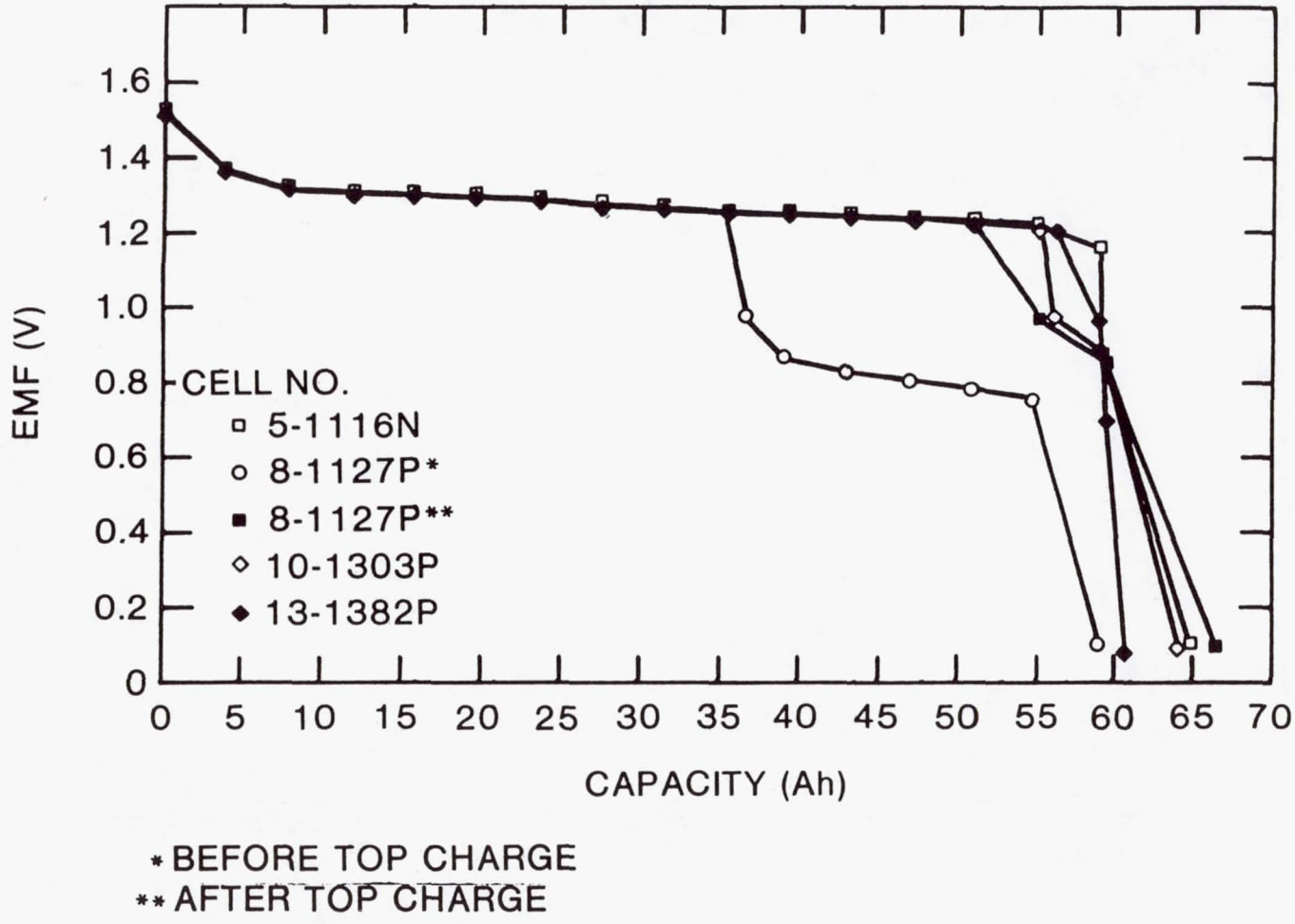

Figure 6-10. Discharge voltage profiles of cells after 12 weeks of periodic recharge *Before top charge **After top charge.

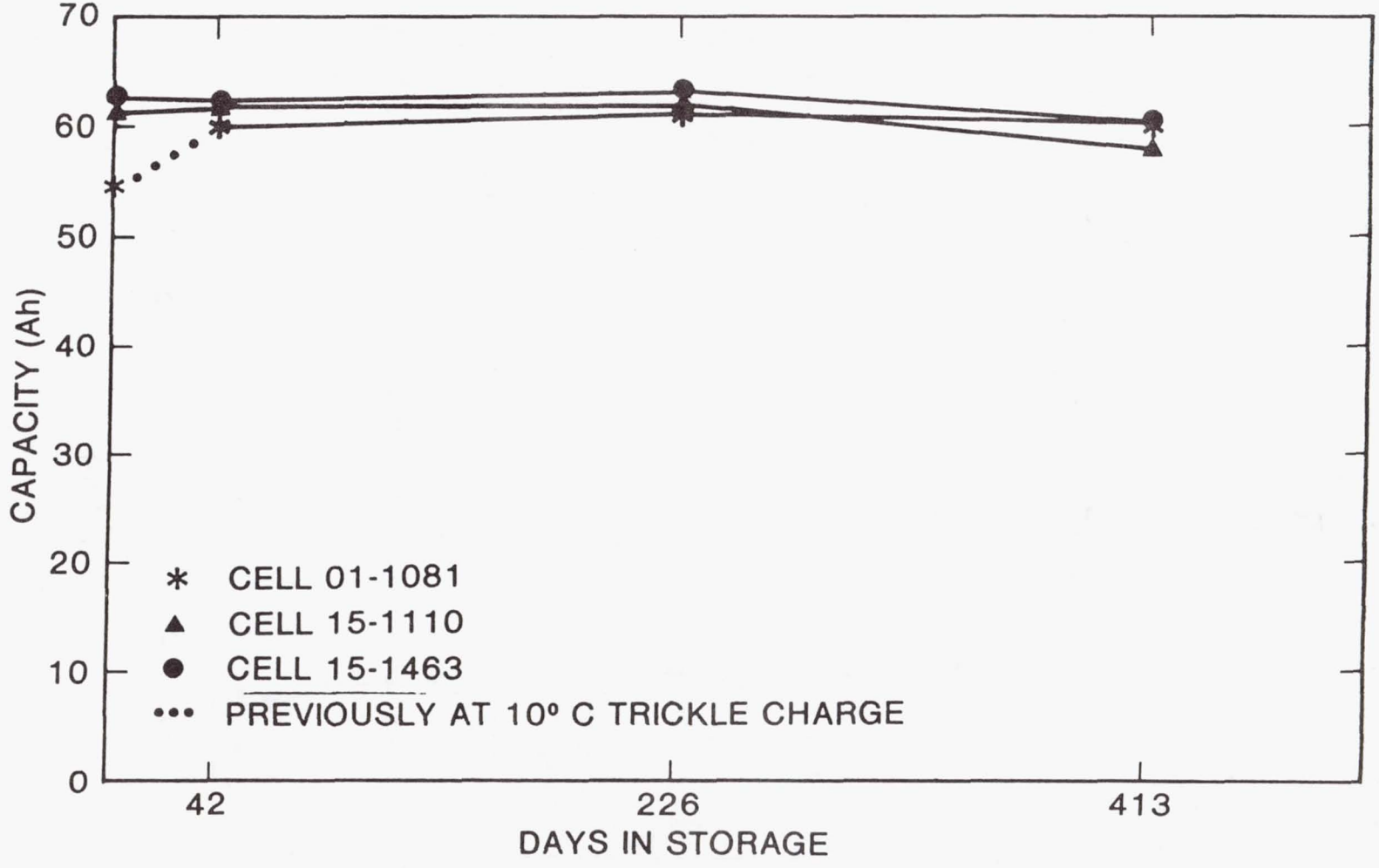

Figure 6-11. Variation in capacity (to 1.0V) for cells in the trickle charge storage mode.

Table 6-1. Storage Discharged Open-Circuit at -20 C

Cell No.	Initial Capacity Ah	Storage Period days	Final Capacity Ah
4-1104N	63.6	270	66.0
5-1116N	60.7	270	67.2
13-1382P	66.7	112	66.3
1-1081N	59.9	112	60.3

6.11.6 Summary

1. Positive precharge cells maintain their capacity stored discharged open-circuited at 0°C.

2. Hydrogen precharge cells maintain their capacity when stored at 0°C for a period of time up to one year, but thereafter show capacity fading.

3. Hydrogen-precharge cells show capacity fading when stored discharged open-circuit at room temperature. This loss in capacity (capacity fading) to 1.0 volts shows up as an increase in capacity in the second plateau.

4. Periodic recharge at room temperature can be used to maintain capacity for long periods of storage (up to two years). Periodic recharge can also be used to recover capacity for cells that have experienced capacity fading.

5. Low temperature storage of cells at -20°C can be used to maintain capacity for long periods of time.

6. Trickle charge storage can be used to maintain capacity for long periods of time.

6.12.0 REFERENCES

[6-1] Nickel-Hydrogen Storage Workshop, sponsored by the Office of Research and Development, U.S. Government, under direction of Joseph Stockel, April 11, 1991, Rosslyn, VA.

[6-2] The 1992 NASA Aerospace Battery Workshop, NASA Conference Publication 3192, November 15–19, 1992, "Nickel-Hydrogen Storage/Capacity Fade Session.".

[6-3] R.V. Whitely and A. Gibney, "Storage Considerations for Ni-H_2 Battery Cells," 1988 NASA/GSFC Battery Workshop, Greenbelt, Maryland, 3 Nov. 1988.

[6-4] H. Vaidyanathan, "Long-Term Storage of Nickel-Hydrogen Cells," *Journal of Power Sources*, 22 (1988) pp. 221–228.

[6-5] A. Dunnet, INTELSAT, private communications.

[6-6] H. Vaidyanathan and M. Earl, "Capacity and Pressure Variation of INTELSAT VI Nickel-Hydrogen Cells with Storage and Cycling," 23rd Intersociety Energy Conversion Engineering Conference, July 31–August 5, 1988, Denver, Colorado, Vol. 2, pp. 471–475.

[6-7] H. S. Lim and S.A. Verzwyvelt, "Effects of Electrode and Cell Design Variables on Capacity Fading of a Nickel-Hydrogen Cell on Storage," 25th Intersociety Energy Conversion Engineering Conference, Reno, NV, 1990, pp. 7–15.

[6-8] A. H. Zimmerman, Electrochemical Society Fall Meeting, Hollywood, FL, October 15–20, 1989.

[6-9] D. Tuomi, *Journal of the Electrochemical Society*, 112, Vol. 1 (1965).

CHAPTER 7
STANDARD TEST PROCEDURES

To establish reliability, or probability of the battery meeting mission requirements, one needs a database relevant to both the cell/battery design and the operational requirements. In general, when a cell manufacturer is required to perform a reliability study, he will include semi-relevant data to determine a probability figure. His results are questionable, simply because he does not have an adequate database from which to work. At the 1988 NASA Battery Workshop, the NASA Task Force Group Investigation of Standard Test Procedures, headed by Thomas Yi, recommended that cell/battery manufacturers maintain a log of all battery programs as a reference against which to judge performance expectations. Included in this log would be the following:

- Cell design
- Analyses data for electrode stack components analyzed
- Analyses data for cells analyzed
- Cell acceptance test data
- Battery acceptance test data
- Operational performance, lifetime, and documentation of any failures.

Standard test procedures are needed for acceptance testing of Ni-H_2 cells and batteries. In this chapter, procedures are proposed as a standard for the industry to provide a common base for comparison of Ni-H_2 cells and batteries throughout the industry. They are not meant to be all inclusive but rather to serve as a nucleus; each individual program would add additional test procedures to meet its specific requirements.

Standard procedures include the following:

Cell Acceptance Tests
Cell Selection Criteria
Battery Acceptance Tests
Electrochemical and Chemical Analysis of Cell Components

Electrochemical and chemical analyses for plaque, electrode stack components, and cells are also proposed as a standard for the industry to provide a common basis for comparing the electrode stack components used throughout the industry on different programs. These analyses data would also provide a measure for quality control of the production process by determining chemical composition and physical properties of the electrode stack components.

7.1.0 CELL ACCEPTANCE TESTS

7.1.1 Reconditioning of Cells (Cells Fully Discharged)

a. Set temperature to 10°C
b. Charge at a C/20 rate for 48 hours
c. Discharge at C/2 rate to 1.0 volts
d. Place a 1- ohm resistor across the cell for 24 hours
e. Recharge at a C/10 rate for 16 hours
f. Discharge at a C/2 rate to 1.0 volts
g. Place a 1-ohm resistor across the cell for 24 hours

7.1.2 Standard Capacity at 10°C

a. Set temperature to 10°C
b. Charge at a C/10 rate for 16 hours
c. Discharge at a C/2 rate to 1.0 volts (standard capacity)
d. Discharge at a C/10 rate to 0.0 volts
e. Place a 1-ohm resistor across the cell for at least 16 hours

7.1.3 Capacity at 0, 10, 20, and 30°C

a. Set temperature to 0°C
b. Charge at a C/10 rate for 16 hours
c. Discharge at a C/2 rate to 1.0 volts
d. Place a 1-ohm resistor across the cell for at least 16 hours
e. Repeat at 10, 20, and 30°C

7.1.4 Charge Retention

a. Set temperature to 10°C
b. Charge at a C/10 rate for 16 hours
c. Open circuit and let stand for 72 hours
d. Discharge at a C/2 rate to 1.0 volts and measure capacity

Capacity after a 72-hour stand should be greater than 85 percent of the full capacity at 10°C.

7.1.5 Open Circuit Voltage

a. Set temperature to 10°C
b. Discharge at a C/2 rate to 1.0 volts
c. Place a 1-ohm resistor across the cell for 16 hours
d. Charge the cell at a C/10 rate for 5 minutes
e. Open circuit and let stand for 16 hours

Voltage should remain above 1.0 volts after the 16-hour open-circuit stand period.

7.1.6 Cycle Test for GEO (Optional)—6 hour cycle

a. Set temperature to 10°C
b. Charge at a C/10 rate for 16 hours
c. Cycle 30 times continuously at 80 percent DOD
   - Discharge at a C/1.5 rate for 1.2 hours
   - Charge at a C/6.0 rate for 4.8 hours (C/D ratio = 1.05)
d. On the 30th cycle, discharge the cell to 1.0 V and measure capacity.

Record the end-of-charge and end-of-discharge voltages. The end-of-discharge voltage should stabilize after a few cycles and will provide information on cell impedance, voltage, charge efficiency, stability, and design.

7.1.7 Cycle Test for LEO (Optional)

a. Set temperature to 0°C
b. Charge at a C/10 rate for 16 hours
c. Cycle continuously 30 times at 40 percent DOD (Use 90-minute cycle, 30-minute discharge, and 60-minute charge time.)
   - Discharge at a 0.8C rate for 0.5 hours
   - Charge at a 0.5C rate to a voltage limit of 1.51 V, and then switch to a trickle charge of C/100. (Terminate charge after 1 hour for total charge time.)
d. On the 30th cycle, discharge the cell to 1.0 V and measure capacity.

An option for charging would be to use a fixed c/d ratio of 1.05. The actual method for charging should be determined by the program office to demonstrate in-orbit operation.

7.1.8 Pressure Proof-Test and Burst Pressure

Each cell pressure vessel should be proof-tested to a pressure of 1.5 times the maximum expected operating pressure. There should not be any measurable permanent deformation of the pressure vessel after this proof test.

Two cell pressure vessels from each program should be destructively tested to determine their burst pressure. A minimum ratio of 3/1 is recommended for the safety factor.

7.1.9 Radiographic Examination

Radiographs should be taken of each cell to inspect for workmanship, proper busing configuration, the integrity of the weld ring pressure vessel welds, popping damage, etc.

The new FEINFOCUS series FXS-160 (160 kV) permits X-ray image magnification up to a factor of 200, providing excellent resolution, contrast, and brilliance. System configurations are provided, with a capability for film documentation, a real-time TV chain, and a 5-axis robot system, which give the units versatility for use in quality assurance [7-1].

7.2.0 PURPOSE/OBJECTIVES OF CELL ACCEPTANCE TESTS

The objectives for the proposed cell acceptance tests are to provide the minimum basic data needed for cell performance to allow one to judge acceptability and to compare different cell production runs.

7.2.1 Standard Capacity

Standard capacity is needed as a basis for comparing capacity data throughout the battery community as well as within a given battery program. The standard capacity data can be used to show or determine how well the cells are matched in capacity within each production run (or runs) for a flight program. Matching cells by capacity is the most commonly used method for selecting cells to be used in a battery. The standard capacity could also be used to compare capacity per unit weight for cells with different design features. Note that the recommended procedure is to discharge the cell completely to 0.0 volts. The discharge rate below 1.0 volts is reduced to a C/10 rate to minimize the heat generated during discharge. It is important to determine the capacity below 1.0 volts (sometimes called capacity at the second plateau). A large amount (over 30 percent) of the cell capacity below 1.0 V at the beginning of life would indicate that the cell had been improperly stored or activated and that some type of capacity recovery procedure is required as identified in Chapter 6.0.

7.2.2 Capacity at 0, 10, 20, and 30°C

The capacity of the cells at 0 to 30°C covers the normal operating temperature range for most applications.

7.2.3 Charge Retention

The charged open circuit stand test provides a good check for any internal shorts within the cell. The capacity remaining after 72 hours open-circuit stand should be closely matched between cells of the same production run. If significant differences of more than a few ampere-hours exist, the cells in question should be

rechecked. Minimum requirement: the capacity remaining after 72 hours open-circuit stand should be greater than 85 percent of initial capacity.

7.2.4 Open-Circuit Voltage

The purpose of this test is to determine if any high-impedance shorts exist in the cell. The cell open-circuit voltage should remain above 1.0 volts.

7.2.5 Cycle Test (GEO)

The purpose of the 30-cycle GEO test is to ensure that the cells can be cycled to a deep depth-of-discharge and be recharged with a c/d ratio of 1.05 at the C/6 rate. The end-of-charge and end-of-discharge voltages should stabilize after a few cycles and stay relatively constant thereafter. The end-of-discharge voltage after the cell has stabilized gives a good indication of what one can expect in orbit at the beginning of life at deep depths of discharge.

7.2.6 Cycle Test (LEO)

The purpose of the 30-cycle LEO test is also to demonstrate that the cells can be high-rate cycled using the charge control method proposed for the program.

7.2.7 Proof-Test

The purpose of the proof test is to verify that each of the cell pressure vessels has been properly heat treated and that the cells are capable of operating at 1.5 times the maximum operating pressure. The burst test is done on two sample cells from each lot to verify the safety margin and burst pressure of the pressure vessels.

7.3.0 CELL SELECTION CRITERIA

The number of cells manufactured for each battery should be sufficient to allow for selection/rejection criteria of the program. For example, to build a 27-cell battery, at least 31 cells should be fabricated to allow for a rejection of up to 4 cells. Each flight battery should be made up of cells from one manufacturing lot.

The following are cell selection criteria:

- Visual inspection
- Radiographs
- Capacity (matching)
- Weight of cells/weight of electrolyte

7.3.1 Visual Inspection

After all acceptance testing is completed, the cells should be visually inspected for dents in the pressure vessel, continuity and appearance of the weld regions, and evidence of corrosion or poor workmanship. The most common reason for rejection has been dents in the pressure vessel. Any such dent is cause for rejection. Occasionally, cells are also rejected because the girth weld at the weld ring does not pass inspection. Typically, one or even two cells in a production lot are rejected by these visual inspections.

7.3.2 Radiographs

Radiographs produce a visual inspection of the electrode stack inside the cell. The radiographs can be used to examine the electrode stack components, tabs, welds, alignment, etc. They provide a useful tool for examination of failure mechanisms.

7.3.3 Cell Acceptance Tests (Charge Retention)

The charge retention test and the open circuit voltage test were designed to show high impedance shorts within the cell. For the charge retention test the capacity at the end of the 72-hr charged open-circuit stand should be about 85 percent of the measured capacity at 10°C. Data for all of the cells should be compared, and specific attention focused on any cells with low capacity. Any cell that stands out from the others by more than 5 percent of average capacity should be rejected.

7.3.4 Weight of Cells/Weight of Electrolyte

The weight of all the cells should be similar, particularly if the positive electrodes are matched in weight for each cell stack. The major weight variation between cells is usually caused by the variation in quantity of electrolyte. If any of the cells deviate from the average weight by more than plus or minus 5 percent, these cells should be rejected. A low quantity of electrolyte may result in a loss of capacity and poor voltage performance. Excess electrolyte indicates that the cell was not activated properly and internal damage may have occurred to the electrode stack due to popping.

7.3.5 Measured Capacity

The measured capacities should be reviewed at 0, 10, and 20°C. Cells from the same production lot should be matched in capacity to plus or minus 3 percent. Cells that do not meet the ±3 percent criteria should be rejected.

7.4.0 BATTERY ACCEPTANCE TESTS

7.4.1 Reconditioning

The method for reconditioning the battery depends somewhat on the battery design. There should be voltage sensing leads for measuring the voltage of each cell in the battery. One method for reconditioning uses a resistor across the entire battery. This resistor is typically sized to discharge the battery in 50 to 100 hours. The battery is discharged until the first cell in the battery reaches 0.5 volts. The objective is to fully discharge the battery without reversing individual cells.

The method below should be followed for reconditioning. This measured reconditioning capacity establishes a baseline to be compared with the reconditioning capacity measured in space.

a. Set the temperature to 10°C
b. Charge the battery at a C/20 rate for 48 hours
c. Discharge the battery with the reconditioning resistor across the battery
d. Terminate the discharge when the voltage of the first cell reaches 0.5 volts.

A second method is to place an individual resistor across each cell. The individual resistor is typically sized to fully discharge the cell in 25 to 50 hours.

The reconditioning should be done using the same procedure intended for use in space.

7.4.2 Standard Capacity

a. Set temperature to 10°C
b. Charge at a C/10 rate for 16 hours
c. Discharge at a C/2 rate until the first cell reaches 1.0 volts
d. Repeat the cycle a second time
e. Battery capacity should be at least 95 percent of average cell capacity at 10°C.

7.4.3 Charge Retention

a. Set the temperature to 10°C
b. Charge at a C/10 rate for 16 hours
c. Open the circuit and let stand for 72 hours
d. Discharge at a C/2 rate until the first cell reaches 1.0 volts
e. The capacity remaining should be a minimum of 85 percent of the initial capacity (capacity measured at 10°C).

7.4.4 The 30-Cycle Test GEO (Optional)

a. Set temperature to 10°C
b. Charge at a C/10 rate for 16 hours
c. Cycle 30 times continuously at 80 percent DOD
   - Discharge at a C/1.5 rate for 1.2 hours
   - Charge at a C/6.0 rate for 4.8 hours (c/d ratio = 1.05)

The end-of-charge and end-of-discharge voltages for the battery should be recorded, as should the battery temperatures and pressures at end of charge and end of discharge.

7.4.5 The 30-Cycle Burn-In Test LEO (Optional)

a. Set temperature to 0°C
b. Charge at a C/10 rate for 16 hours
c. Cycle 30 times continuously at 40 percent DOD (Use 90-minute cycle, 30-minute discharge, and 60-minute charge time.)
   - Discharge at a 0.8C rate for 30 minutes
   - Charge at a 0.5C rate to a voltage limit of 1.51 volts/cell and then switch to a trickle charge at a C/100 rate. (Terminate charge after 1 hour for the total charge time.)

An option for charging would be to use a fixed c/d ratio of 1.05. The actual voltage limits and charge control method should be selected by the program office.

7.5.0 PURPOSE/OBJECTIVES OF BATTERY ACCEPTANCE TESTS

The objectives for these battery acceptance tests are to provide the minimum performance data needed to judge the acceptability of a battery. These data also provide the basis for comparing batteries from different production runs.

7.6.0 ELECTROCHEMICAL AND CHEMICAL ANALYSES OF CELL COMPONENTS

Electrochemical and chemical analyses data for each production lot of cells for each program provides a method of verifying the manufacturing process control. Presented below are recommendations proposed as a standard for the industry.

The analyses could be done either by the cell manufacturer or by an independent laboratory, depending on the capability of either. The important point is that the analyses results should have credibility.

7.6.1 Sinter Plaque Analysis

Tensile Strength
Weight/Unit Area
Thickness
Porosity
Corrosion
SEM Analysis
Pore Size Distribution (Mercury Intrusion Pore Symmetry)

7.6.2 Positive Plate Analysis

Chemical Analysis
Flooded Capacity
Weight and Thickness
SEM Analysis
Pore Size Distribution (Mercury Intrusion Pore Symmetry)

7.6.3 Negative Plate Analysis

Loading Level of Platinum
Polarization Measurements
Weight and Thickness

7.6.4 Separator Analysis

Chemical Composition
Weight and Thickness
Pore Size Distribution (Mercury Intrusion Pore Symmetry)
Electrolyte Retention

7.7.0 MATERIAL ANALYSIS REPORT (SEM ANALYSIS)

A Materials Analysis Report of an SEM examination of an INTELSAT VI positive plate is provided as Appendix B to show examples of the following:

- SE images of positive plate surface after EDTA extraction of the active material Ni(OOH) from the nickel sinter.
- BSE images of a cross section of a positive plate showing nickel sinter, voids, active material, and girth wires.
- BSE profiles showing sinter, voids, active material, and fill factor from one surface to the other in the cross-sectional view.

7.8.0 REFERENCES

[7-1] Ben Harden, "X-Ray Test and Analysis," Lockheed Missiles and Space Company, Inc., Ni-H_2 Battery Working Group, 6–7 October, 1992.

CHAPTER 8
BATTERY PROCUREMENT

8.1.0 INTRODUCTION

There are presently three approaches for procuring Ni-H_2 batteries:

1. Procuring a battery to a battery specification.
2. Procuring cells to a cell specification and procuring batteries to a battery specification.
3. Procuring cells to a cell specification and fabricating the batteries in-house (spacecraft manufacturer) to a battery specification.

8.1.1 Procurement of a Battery to a Battery Specification

Most foreign entities procure Ni-H_2 batteries from a U.S. cell manufacturer. The U.S. Government has identified the Ni-H_2 cell technology as sensitive and has restricted any detailed design information from being provided to a foreign company. Due to this restriction, a foreign aerospace company cannot write a detailed cell specification. Therefore, batteries are procured to a battery specification and the cell specification remains internal with the cell manufacturer. In some instances, foreign entities procure the batteries from a U.S. aerospace company. The aerospace company in turn procures the cells to its specification and fabricates the battery to meet the customer's specifications.

8.1.2 Procuring Cells to Cell Specifications and Procuring Batteries to a Battery Specification

Some of the U.S. aerospace companies now have batteries fabricated for them rather than fabricating the batteries themselves. A good example is the Hubble Space Telescope (HST) program; the cells and batteries for the program were fabricated by Eagle-Picher Industries (EPI) to Lockheed Missiles and Space Company (LMSC) specifications for the NASA HST program. This approach is new for many U.S. aerospace companies, who in the past ordered cells to their own specifications and fabricated the batteries in house.

8.1.3 Procuring Cells to a Cell Specification and Fabricating the Battery In-House (Spacecraft Manufacturer)

The major advantage to this approach is that the spacecraft manufacturer controls all spacecraft interface design features for the battery: the thermal, mechanical, and electrical interfaces. For many applications this may be the overriding consideration, as the battery represents a major portion of the spacecraft

weight and volume. Thermal control, charge/discharge control (electrical interface), and mechanical design for the battery are so essential to the success of the mission that the design and fabrication of the battery by the spacecraft engineers is essential.

8.2.0 BATTERY SPECIFICATIONS

Procurement of a battery to a battery specification is the most straightforward method and leaves decisions about cell design to the battery or cell manufacturer; this is the way most large commercial batteries (lead-acid, for example) are made. If a standard aerospace cell design existed, this method should be the acceptable method to procure aerospace Ni-H_2 batteries.

8.2.1 Battery Procurement Specification

A battery procurement specification should include the following major sections:

- Scope
- Applicable Documents
- Spacecraft Interfaces
- Battery Performance Requirements
- Battery Assembly/Packaging Requirements
- Quality Assurance
- Cell Specification and Acceptance Criteria
- Battery Specification and Acceptance Criteria
- Storage and Delivery Requirements

8.2.2 Scope

This section describes the operational and environmental constraints for the battery.

- The spacecraft orbit, LEO or GEO, etc.
- Power requirements (energy requirements) for the battery
- Eclipse periods and number of eclipses per year
- Number of charge/discharge cycles per year
- Lifetime expectancy of the battery
- Maximum allowable depth-of-discharge
- Minimum allowable end-of-discharge voltage
- Launch environment, shock, and vibration
- Normal operating temperature range for the battery
- Maximum and minimum temperatures for the battery
- Power/energy requirements during pre-launch
- Launch and transfer orbit phases
- Peak power requirements.

The scope of the mission as it relates to the performance of the battery should be well defined so that the battery manufacturer is aware of these requirements. If the battery manufacturer has any concerns about meeting these requirements, he should identify them at the start of the program.

8.2.3 Applicable Documents

A list of applicable documents should be specified to be included as part of the battery procurement. Included in this list should be the following:

- Product assurance requirements
- Safety requirements
- Handling requirements
- Data management requirements.

8.2.4 Spacecraft Interfaces

This section describes how the battery interfaces with the spacecraft in terms of the electrical interface, the thermal interface, and the mechanical interface.

Electrical Interface

The interface between the battery and the spacecraft electrical bus should be described. Generally, a battery charge/discharge control unit is used to connect the batteries to the bus. The control unit can be operated either from an on-board computer or from ground commands issued through the telemetry command system.

Battery monitoring features are needed for both control and monitoring the health of the battery, and include the following.

- Battery voltage
- Individual cell voltages
- Battery current charge/discharge
- Temperature on the baseplate and several different cell locations within the battery
- Pressure monitoring of one or more strain-gauge bridges
- Status of the battery heater elements
- Status of the charge control relays
- Status of reconditioning resistors.

Where possible, the sensor devices used for each of the above monitoring features should be specified, along with the location of the devices within the battery. Sensor devices to be specified include the following:

- Strain-gauge bridge circuitry
- Current sensing resistor
- Thermistors
- Reconditioning resistors

Bypass diodes should be specified if they are to be used across each cell in the battery.

Mechanical Interface

The mechanical interface requirements for the battery should be described:

- Stiffness requirements, the minimum natural frequency in all axes
- Dynamic loads (qualification level/flight level)
- Static loads (qualification level/flight level)
- Detailed mechanical drawing requirements for the battery
- Mass requirements
- Center of gravity/moment of inertia
- Battery assembly procedures
- Mounting provisions
- Insulation requirements
- Battery handling requirements
- Protective cover.

Thermal Interfaces

The thermal interface between the battery and the spacecraft should be described, along with the thermal control system, and whether it is active or passive, etc. Typically, passive control systems have been used for Ni-H_2 batteries when heat is conducted away from each cell through an aluminum sleeve to the baseplate. This heat is then directly radiated to space from the battery radiator plate. The battery is generally thermally isolated from the rest of the spacecraft.

Temperature Requirements. The temperature requirements should be defined for the following conditions:

- Normal operating temperature range at beginning of life (BOL)
- Normal operating temperature range at end of life (EOL)
- Worst-case temperature range at EOL
- Long-term storage temperature (0°C or -20°C is recommended)
- Handling and transportation temperature range (-5°C to 25°C)
- Qualification testing temperature range
- Integration and test temperature range
- Maximum and minimum temperatures

- Transfer-orbit temperature range
- Maximum temperature gradient within the battery.

The thermal control of the battery should be such that cell wall temperatures are maintained within these limits throughout the life of the battery, provided that the thermal environment is no more severe than that defined.

Heaters should be specified for thermal control of the batteries to maintain temperatures above the lower operating limits.

The aluminum sleeves and baseplate must be adequately designed to maintain the temperature gradients between the cell sleeve and the baseplate within the maximum allowable range.

The battery manufacturer must provide heat dissipation data for normal operating conditions and for worst-case operating conditions as specified above. The battery manufacturer needs to provide charge and discharge voltage profiles for the beginning and end of life, or at least estimates of the average charge and discharge voltages for the temperature conditions specified above. These heat dissipation data are essential to the thermal design.

8.2.5 Battery Performance Requirements

The battery performance specification should include the following:

- Cycling requirements/lifetime requirements
- Energy storage requirements under normal operation
- Battery capacity (method for measuring capacity)
- Number of batteries required/spacecraft
- Peak power requirements under normal operation
- Transfer-orbit energy storage and peak power requirements
- Maximum depth-of-discharge (DOD) in ampere-hours
- Maximum DOD (worst-case conditions)
- Type of charge: constant current, voltage control, or other
- Type of discharge: constant current, constant power, or other
- Charge control method, percent overcharge, voltage limit, or other
- Trickle charge mode/operation during sunlight
- Reconditioning requirements
- Fault clearance requirements
- Minimum end-of-discharge voltage at BOL and EOL
- Reliability requirements.

8.2.6 Battery Assembly/Packaging Requirements

Some of the more general packaging requirements that need to be specified include the following:

- Number of cells/battery
- Configuration of cells (number of rows of cells, etc.)
- Battery cell bypass protection
- Strain-gauge bridge pressure sensors (number of cells monitored)
- Location of battery current monitor
- Location of battery heaters
- Location of thermistors
- Location of battery voltage monitor
- Individual cell voltage monitor wiring
- Redundant wiring for intercell connections (rating specified)
- Connector type and location

8.3.0 QUALITY ASSURANCE

The quality assurance section of a specification should define what is to be done to assure the quality of the battery and the cells as they are being manufactured. The cells and batteries are manufactured in accordance with Manufacturing Control Documents (MCDs). Accompanying these MCDs are the cell and battery Travelers. Any discrepancies are reported in Material Reports (MRs). These MRs become part of the cell or battery Travelers. Even if a battery is being procured to a battery specification, assurance of the quality of the cell is still required.

Quality assurance ensures that the cells and battery are manufactured the same way today as they were yesterday. Assurance that the manufacturer is following the MCDs and keeping accurate records using the cell travelers, along with the materials reports for documentation of discrepancies is desired. Assurance that the cell components used meet specifications and that each stage of the cell and battery assembly is adequately inspected.

With adequate quality assurance, one can expect to procure cells and batteries that will meet performance expectations. If possible, cell design changes should be avoided during flight hardware programs. There are a number of different ways to augment quality assurance at the cell level:

- Review of manufacturing control documents
- Inspection of manufacturing facilities/audit (NASA)
- Mandatory inspection points at cell level
- Mandatory inspection points at battery level
- Analysis of sample number electrode stack components

8.3.1 Mandatory Inspection Points at Cell Level (MIPs)

Cell Lot Definition (Wet Slurry Plaque)

To recommend mandatory inspection points at the cell level, it is first necessary to define a cell production lot. All cells used to make up one battery (one qualification battery, one engineering model battery, or one flight battery, etc.) should come from the same production lot of cells. The general definition for a production lot is that all of the cells are manufactured from the same plaque lot. Refer to the cell manufacturer for a definition of plaque lot. There is some variation between manufacturers, but in general, the concept is to have the plaque made at one time from the same blend of nickel powder, etc. More than one battery can be manufactured from cells produced from the same plaque lot as long as all the cells in each battery come from the same plaque lot.

The reason for this recommendation is that variations in cell performance can generally be traced to lot-to-lot variations in plaque properties. A single plaque lot is a very important concept for the quality assurance of a production lot of cells. Within a given plaque lot, the structure and physical properties of the plaque are very similar. Therefore, only a few samples need to be analyzed to characterize the entire plaque lot. The same concept applies to positive electrodes made from the same lot. Impregnation of positive electrodes (loading levels and uniformity) is dependent on the plaque properties. Analyses of a small number of positive electrodes are sufficient to characterize the entire production lot.

Finally, when cells are fabricated from one lot of plaque, the cells are well matched in terms of capacity and electrical performance. Again, the major variations are lot to lot and not within a given lot. Therefore, the analysis of one or two cells within a given lot is sufficient to characterize all cells in that lot.

Cell Lot Definition with Dry Powder Plaque

With dry powder plaque the lot definition changes. The plaques for all of the positive electrodes are basically made one plaque at a time. The criteria for a positive electrode lot definition is that the plaque is made continuously (no intervening production runs) and that this plaque is impregnated continuously with no intervening production runs. The criteria for a cell lot definition is that the cells are manufactured together at the same time.

From one lot of INCO nickel powder there are 35 drums of nickel powder per lot, and each drum contains 165 pounds of nickel powder. With dry powder plaque, even very large programs can be done with one lot of INCO powder. One lot of INCO nickel powder was used for the entire INTELSAT VI program (10 flight batteries plus flight spares). All of the plaque and positive electrodes were made at one time, and these positive electrodes were used to make all of the cells and batteries for the entire program, including qualification batteries, engineering model

batteries, life-test batteries, flight batteries, and spares. But the batteries were not all made at the same time; rather, the positive electrodes were stored in dry nitrogen and taken out of storage as required to make the batteries. For example, when it was time to make the F1 (flight one) batteries, a sufficient number of positive electrodes were removed from storage to make the two batteries needed for the F1 spacecraft. These cells used in the two batteries for the spacecraft were identified as one production lot.

MIPs. For each production lot of cells four MIPs are recommended.

MIP No. 1: Plaque Analysis

An adequate amount of plaque from each sinter lot should be set aside to perform the following analyses. It is recommended to use one plaque sample 11 x 11 inches or equivalent per sinter lot for anaylsis.

1. Analyze plaque samples for the following:

   - Weight and thickness (density)
   - Corrosion*
   - Strength (pull test)
   - Porosity
   - Pore size distribution

2. Review all of the plaque production manufacturing control documentation to ensure that the procedures are being followed.

3. Document the results of these analyses in the MIP 1 report. The plaque samples must pass this mandatory inspection prior to the impregnation step.

MIP No. 2: Positive and Negative Plate Inspection

The purpose of this MIP is to inspect all of the positive and negative electrodes (100 percent) and to review all of the manufacturing control documentation.

1. Inspection of Positive Plate

   a. Visually inspect for blisters, cracks, exposed grid, jagged edges, etc.
   b. Verify target loading level of active material
   c. Review weight and thickness data
   d. Review weight distribution data

* Standard Bell Labs corrosion test for plaque.

e. Review flooded capacity performance data
f. Review high-rate stress test* data.

High-rate stress test

- Charge at 10C rate for 12 minutes flooded in 31 percent KOH at 10°C (100 percent overcharge)
- Discharge at 10C rate for 6 minutes (100 percent DOD)
- Repeat for 200 cycles

A sample number of positive electrodes from each production lot are subjected to this high-rate stress test, known as the Bell Laboratories Stress Test [8-1]. This test was specifically developed for electrochemically impregnated electrodes to demonstrate that they could withstand this stressful high-rate cycling without blistering or expanding. The acceptance criteria is less than a 5-percent increase in thickness and no blisters. Conventional chemically impregnated aerospace positive electrodes will fall apart during this stress test.

2. Analysis of Positive Electrodes

Select five electrodes for analysis, then sort the remaining positive electrodes in the lot by weight. A review of the weight distribution is part of the mandatory inspection.

Analyses should be performed either by the cell manufacturer, an outside laboratory, or both. The following analyses should be performed:

- Weight and thickness measurements
- Flooded capacity
- Chemical analysis to determine composition and loading of active material
- High-rate cycle test for blisters and expansion (see MIP 2)
- SEM technique to determine distribution of active material, sinter, and voids from a cross section of the electrode and plaque corrosion.

Target compositions should be specified, and failure to meet specifications could be cause for rejection of a positive plate lot.

3. Inspection of Negative Plates

Visually inspect for the following:

a. Foreign material on platinum or Teflon surfaces
b. Exposed grid surface from Teflon peeling

c. Teflon separation from the grid structure
d. Holes through the electrode
e. Platinum on tab weld zone.

4. Analysis of Negative Electrode

   Select five negative electrodes at random from each cell lot for analysis.

   These analyses should also be performed either by the cell manufacturer, an outside contractor, or both. The following analyses should be performed:

   - Weight and thickness
   - Oxidation and reduction polarization measurements
   - Chemical analysis to determine the loading level of the platinum per unit area

   Target compositions should be specified, and failure to meet these specifications could be cause for rejection of the negative plates.

5. Review the cell traveler, which contains all data pertinent to the manufacturing of these electrodes. Discrepancies of any kind are documented in the materials reports attached to the cell traveler. The cell traveler, with attached materials reports, is reviewed for correctness and completeness up to the occurrence of the MIP 2.

6. Document the results in a MIP 2 report. There should be a plate buyoff (approval) of the MIP 2 report prior to moving on to assemble the positive and negative plates into electrode stacks.

MIP No. 3: Cell Stack Inspection

The purpose of this MIP is to inspect all of the electrode stacks before they are installed into the pressure vessels.

1. Inspect the cell stack for workmanship, handling damage, cleanliness, and compliance with the assembly drawings.

2. Review the cell traveler for correctness and completeness up to the occurrence of this MIP 3.

3. Document the results and findings in a MIP 3 report.

MIP No. 4: Cell Inspection After ATP

The purpose of this MIP is to inspect the cells after assembly and all of the acceptance testing is completed.

1. Inspect the cells for compliance with the assembly drawings, workmanship, handling damage, and cleanliness.

2. Review the cell traveler for correctness and completeness up to the occurrence of this MIP 4.

3. Review the cell acceptance test data to determine that the cells meet specifications.

4. Select cells for use in the battery. Selection/rejection criteria are based on the following:

   - Cracks, flaws, or dents detected in the pressure vessel or weld regions
   - Capacity data at 0, 10, and 20°C
   - Weight of the cells
   - Weight of the KOH added to the cells

5. Cell Destructive Physical Analysis (DPA)

   One cell from each lot should be selected for electrical and chemical analysis. These analyses should include the following.

   - Tear-down analysis, condition of electrode stack components and electrolyte distribution in cell
   - Weight and thickness of all the positive electrodes
   - Flooded capacity of average positive electrode
   - Polarization measurements of negative electrode

   These analyses are done to ensure the following:

   - The sample cell meets performance specifications
   - The cell was properly activated with no damage to the electrode stack
   - The electrolyte is properly distributed within the cell
   - The electrolyte concentration meets specifications.

6. Document the findings and results in a MIP 4 report.

8.3.2 Mandatory Inspection Points at the Battery Level

Three mandatory inspection points (MIPs) are recommended for each battery.

MIP No. 1: First Row of Cells

1. Inspect the battery after the first row of cells have been installed onto the baseplate. This inspection insures that the cells are assembled in compliance with the assembly drawings and that workmanship and cleanliness meet expectations.

2. Review the battery traveler for correctness and completeness up through this MIP 1.

3. Document results in the MIP 1 report.

MIP No. 2: Complete Battery Assembly

1. Inspect the battery after assembly is complete. This inspection is to ensure that the battery was assembled in compliance with the assembly drawings and that workmanship and cleanliness meet expectations.

2. Review the battery traveler for correctness and completeness through this MIP 2.

3. Documents the results and findings in the MIP 2 report.

MIP No. 3: After Completion of the Acceptance Test

1. Review all of the acceptance test data for compliance to the specifications.

2. Review vibration test results. Compare the battery performance data before and after the vibration test.

3. Review the thermal vacuum test result. Compare the battery performance data before and after the thermal vacuum test.

4. Document the findings and results in the MIP 3 report.

8.4.0 CELL SPECIFICATION AND ACCEPTANCE CRITERIA

Establishing the acceptance criteria at the cell level is an extremely important part of any specification and is the one part that is often very weak. This weakness

occurs because the cell manufacturer is concerned that stringent cell acceptance criteria may result in too many rejected cells and this may be too costly. Cell manufacturers strongly influence the acceptance criteria. Many specifications contain voluminous amounts of information on the mission requirements, etc., but have very little information on acceptance criteria. The result is that no meaningful criteria exists in the specification that can be used for acceptance or rejection of cells.

The cell specification should include, as a minimum, the following cell acceptance/rejection criteria:

- Quantity of electrolyte per cell (specify amount and range)
- Weight of cell (specify weight and range)
- Capacity (specify value and range) at 0, 10, and 20°C
- End-of-charge voltage at the above temperatures
- Self-discharge, capacity after 72-hour stand open circuit
- 30-cycle burn-in test; c/d ratio, temperature, end-of-discharge voltage, and capacity after 30 cycles.
- Pressure proof-test (1.5 times the maximum expected operating pressure)
- Burst pressure (3.0 times the maximum expected operating pressure)
- Leak test (with the specification that the hydrogen leak rate from a fully charged cell shall not exceed 10^{-6} cc/sec.)
- Radiographic examination for 100 percent of the cells for workmanship, absence of foreign material, weld integrity, etc.

8.5.0 BATTERY SPECIFICATION AND ACCEPTANCE CRITERIA

Wide variations may exist in the acceptance testing performed on different programs depending on mission requirements or program office objectives/ directives. The following is a recommended outline of a battery acceptance test plan.

8.5.1 Performance Criteria

- Measure capacity (specify value and range) at 0°C, 10°C, 20°C, and 30°C. Standard capacity measurements are recommended using a C/10 charge for 16 hours and a C/2 discharge to 1.0 volts.

- Calibrate the strain-gauge bridge circuit at 0°C, 10°C, 20°C, and 30°C, along with the capacity measurements above.

- Measure individual cell voltages on charge and discharge during the capacity measurements above.

- Conduct a 30-cycle burn-in test simulating mission requirements (specify c/d ratio, temperature, end-of-discharge voltage, end-of-charge voltage, and capacity after 30 cycles).

- Measure the self-discharge rate over 72 hours (specify the minimum capacity at the end of 72-hour stand at 10°C).

- Measure the insulation resistance (specify the minimum resistance between the battery case and the positive terminal, negative terminal, bypass diodes, heaters, etc., of each cell.

- Conduct a fault-clearance test (specify the requirements for fault clearance).

8.5.2 Vibration

Depending on the program, there may be engineering model batteries, qualification batteries, spacecraft integration batteries, and flight batteries. The program office should specify the level of vibration testing required for each battery in the program, including random vibration, sine level vibration, and acceleration testing. After completion of the vibration testing, some of the performance measurements above should be repeated to verify that the battery successfully passed the vibration testing. Tests to be repeated are the following:

- Capacity (standard) at 10°C. Compare with the initial capacity as measured above and specify acceptance criteria.

- Calibration of the strain-gauge bridge at 10°C.

- Self discharge rate over 72 hours. Specify acceptance criteria.

- Visual examination of components, wiring, etc.

- Insulation resistance.

8.5.3 Thermal Vacuum Testing

The program office should specify the requirements for the thermal vacuum testing for each of the batteries in the program. After completion of the thermal vacuum testing, some of the performance measurements above should be repeated to verify that the battery successfully passed the thermal vacuum testing. Tests to be repeated are the following:

- Capacity (standard) at 10°C. Specify acceptance criteria.

- Calibration of the strain-gauge bridge at 10°C.

- Self-discharge rate over 72 hours. Specify acceptance criteria.

- Visual inspection of components, wiring, bounding of strain-gauge bridges, etc.

- Insulation resistance.

8.6.0 STORAGE AND DELIVERY REQUIREMENTS

8.6.1 Short-Term Storage

It is not recommended to store the battery discharged or charged on open-circuit stand at room temperature for longer than 14 days. However, if the battery is kept at room temperature for longer periods of time, the battery should be reconditioned and the capacity checked at 10°C. If there has been a measurable loss in capacity, one of the recovery procedures recommended in Chapter 6 to restore the capacity can be used.

8.6.2 Long-Term Storage

For long-term storage of batteries up to three years, the following procedures are recommended in order of their preference.

1. Periodic Recharge. Store the battery fully charged on open-circuit stand at room temperature. Recharge the battery every seven days. Do not overcharge the battery.

2. Trickle charge the battery at C/100 to C/120 rate with temperature maintained between 0°C and 10°C.

3. Discharged -20°C, open-circuit stand. This method is ranked third because it is usually difficult to store the batteries at low temperature simply because of the size and complexity of the batteries. The battery may not be qualified for -20° operation.

8.6.3 Shipping

A special shipping container should be designed and built to house the battery. Batteries should be shipped by air express. The shipping container or battery can be instrumented to monitor shock and vibration during shipping, which may be important because it seems that if something is wrong with the battery on arrival the shipper is always blamed. The temperature of the battery should not exceed 30°C during shipping.

The cells should be completely discharged on open-circuit stand during shipping.

Battery storage and handling procedures are described in more detail in Chapter 6.

8.7.0 REFERENCES

[8-1] Dr. D. Maurer, Bell Laboratories, private communications.

CHAPTER 9
SAFETY

9.1.0 INTRODUCTION

The purpose of this chapter is to provide information for the safe handling, storage, assembly, and operation of Ni-H_2 flight cells and batteries. Potential cell and battery hazards are identified. Operational conditions that can create hazards are described. Controls to identify and eliminate these hazards are presented.

Good safety practices start with the Ni-H_2 cells and batteries themselves—their design, fabrication, quality control, etc.

9.1.1 Cell Design

The first safety issue is the cell design [9-1]. For the cell, most programs try to utilize flight-qualified cell designs that have already been used on other programs. The same is true for battery designs.

New design concepts are introduced to improve performance or increase reliability or both. Cells built to a new design must be qualified by NASA or others for use on their programs. In addition, a change in the pressure vessel design requires qualification of the new pressure vessel. A good example is the new pressure vessel design used by Lockheed on the Hubble Space Telescope program [9-2].

For manned space vehicles, there is a "Manned Space Vehicle Battery Safety Handbook" which describes all hazards associated with the use of batteries as well as acceptable controls for these hazards [9-3]. In the introduction of this handbook, it is suggested that contact be made with battery engineers in the Power Branch of Johnson Control Center as early as possible for guidance in the design of batteries for manned space programs.

9.1.2 Verification Procedures for Flight Cells

The next safety issue is to verify that cells are fabricated to meet design specifications, which can be accomplished with a number of different manufacturing process control checks: acceptance tests, manufacturer process control, mandatory inspection points, quality control, analysis of electrode stack components, destructive physical analysis (DPA) of cells, etc. These verification procedures were discussed in Chapters 7 and 8.

To provide information for the safe handling and operation of Ni-H_2 flight cells and batteries, the potential cell and battery safety hazards are identified. The cell

and battery faults that could cause one or more of these hazardous conditions are identified, including operational faults that could also cause hazardous conditions. Operating procedures are recommended that will help identify and eliminate fault conditions leading to safety hazards.

9.2.0 CELL/BATTERY HAZARDS

A list of the potential cell and battery safety hazards are identified below.

9.2.1 Safety Hazards

- Hydrogen gas leak from pressure vessel
- High pressure rupture of pressure vessel
- Explosive mixture of hydrogen and oxygen in cells
- Electrolyte expulsion from cell.

Identified below are the cell and battery faults that could cause one or more of these safety hazards.

9.2.2 Cell and Battery Faults

- Short from cell pressure vessel case to ground
- Soft short internal to the cell
- Hydrogen gas leak from the pressure vessel.

Identified below are the operational faults that could cause one or more of the above safety hazards.

9.2.3 Operational Faults

- Cell reversal
- External short across battery or cells
- High temperature operation (over 30°C)
- Excessive overcharge
- Low temperature operation (below -25°C).

9.3.0 DISCUSSION OF HAZARDS

9.3.1 Hydrogen Gas Leak From Pressure Vessel

Hydrogen gas leakage from the cell into the surrounding environment can be hazardous. The hydrogen gas will either disperse into the atmosphere, burn, or, if the concentration is high enough, ignite.

Hydrogen gas will rise rapidly and, with adequate venting, disperse into the atmosphere. However, it could be trapped at the ceiling in a room lacking proper ventilation. Ventilation and dispersion of the hydrogen into the atmosphere is the most probable result of a gas leak.

Control 9.1: Provide adequate venting in areas with batteries

Control 9.2 : Install a hydrogen gas detector at the ceiling of the battery area.

Control 9.3 : Do not smoke in battery areas.

9.3.2 High-Pressure Rupture of Pressure Vessel

Ni-H_2 cells are designed to operate at high pressures when fully charged. The Hubble Space Telescope (HST) cells are designed to operate at 1000 psi fully charged. These cells have a 4/1 safety factor between the cell-burst pressure and the maximum operating pressure. All of the cells are proof-tested to 1.5 times the maximum operating pressure for verification and safety.

Fracture mechanical analysis of the HST pressure vessel showed that the maximum size flaw or crack-like defect that could exist after proof-testing would not grow to critical size in four complete lifetimes [9-2].

INTELSAT V cells were pressure cycled with hydrogen gas between 0 and 600 psi. It required over 250,000 pressure cycles to cause a failure in the pressure vessel. The failure was a leak caused by crack propagation in the region of the weld at the electrical feedthrough [9-4]. These experimental results were substantiated by fracture mechanics analysis of this INCONEL 718 pressure vessel by TRW which showed that crack propagation to failure will result in a leak before a burst for the 0 to 600 psi pressure range of operation [9-5].

Control 9.4: Proof test all Ni-H_2 cells to 1.5 times the maximum operating pressure.

Control 9.5: Burst test at least two cells from each production lot of INCONEL 718 pressure vessels. At the least, a 2/1 safety factor is required between the burst pressure and the maximum operating pressure. The recommended value is at least a 3/1 ratio between the burst pressure and the maximum operating pressure.

9.3.3 Explosive Mixture of Hydrogen and Oxygen in Cells

Localized concentrations of hydrogen with oxygen within a cell have resulted in mini explosions, referred to as "popping" because of the popping noise heard when one of these mini explosions occur. These mini explosions were common

during the activation of the cells. (Activation includes expulsion of excess electrolyte, creation of proper gas channels, and elimination of trapped oxygen bubbles.) Cell design changes and modifications to the activation procedures have, for the most part, eliminated or minimized the damage of these mini explosions. Some problems with popping during activation are still being reported for cells with high end-of-charge pressure (800 psig or greater).

Ni-H_2 cells and batteries perform well, without popping, over a wide range of operating conditions once they have been activated. In fact, one of the major advantages of these batteries is their ability to sustain high rates of charge and discharge over wide temperature ranges. However, it is still important to operate the battery within the range of operating conditions specified.

The cell/battery manufacturer should specify the range of conditions acceptable for handling and operating the batteries.

Control 9.6: Ensure that the cells and batteries are maintained within the range of handling and operating conditions specified by the manufacturer.

9.3.3 Electrolyte Leakage or Expulsion From Cells

Leakage of the potassium hydroxide electrolyte is similar to a gas leak; if there were an electrolyte leak there would be a gas leak. A white encrustation on a seal or on the case is an indicator of an electrolyte leak. Again, the test should be halted, the battery removed, and the cells that exhibited a leak replaced.

Control 9.7: Perform a 100 percent inspection of the terminals and the weld regions on all cells to look for indications of electrolyte leakage.

Control 9.8: Use a hydrogen leak detector to inspect each cell within the battery during battery acceptance testing and final checkout of the battery prior to launch.

9.4.0 CELL AND BATTERY FAULTS

Following is a discussion of cell and battery faults that cause battery failures and can also lead to safety hazards.

9.4.1 Short From a Cell Pressure Vessel Case to Ground

A typical battery will have 27 to 28 individual cells connected in series to make up the battery. Each cell is housed within an aluminum sleeve. A layer of insulating material is wrapped around the INCONEL 718 pressure vessel to insulate the pressure vessel from the aluminum sleeve. These aluminum sleeves are often connected to ground in the battery design. If there is a short between the pressure vessel and the aluminum sleeve through the insulating material (which occurred

on one battery cell in the INTELSAT V-F7 spacecraft), then the leakage current is limited only by the impedance of the corrosive leakage path from the electrode stack to the INCONEL 718 pressure vessel wall. Because of this problem, most aerospace battery designs now insulate the aluminum sleeves from ground to avoid this failure mode.

Control 9.9: Inspect the battery pack for any possible leakage paths to ground.

9.4.2 Soft Shorts Internal to the Cell

The most common failure observed for Ni-Cd aerospace cells was loss of capacity due to internal shorts within a cell. This type of failure may also become the most common failure for Ni-H_2 cells.

Control 9.10: Monitor the individual cell voltages within a battery to determine if there are any low-voltage (low-capacity) cells.

9.4.3 Hydrogen Gas Leak From Pressure Vessel

A hydrogen gas leak from the pressure vessel has not been a failure mode for Ni-H_2 cells. If there were a leak problem it would be evident by a drop in pressure and loss of capacity. A very low leak rate would require time—days, weeks, or even years, but eventually it will show up as a loss in capacity.

If hydrogen gas does leak from a cell, that cell becomes negatively limited on discharge. The other normal cells within the battery will drive the negative limited cell into reversal on discharge. In reversal, oxygen will be generated at the negative electrode. On recharge the oxygen will be consumed (reduced) first, and then hydrogen will be generated at the negative electrode. The cell will probably continue to work this way until the electrode stack dried out and the cell shorted or open circuited.

Control 9.11: Monitor the individual cell voltages within a battery to determine if there are any mismatched cells. Remove mismatched cells from battery.

9.5.0 OPERATIONAL FAULTS

Following is a discussion of operational faults that cause battery failures and can also lead to safety hazards.

9.5.1 External Short Across Battery or Cells

External shorts are potentially one of the most dangerous hazards of handling Ni-H_2 batteries. If shorted, a charged battery will discharge at extremely high rates. It can cause arcing across switches, meltdown of a shorting relay, arcing between the case of a pressure vessel and a ground wire, etc. In addition to the damage the battery can do to external load components and equipment, a short or low impedance load will cause excessive heating of the battery itself., which will damage the electrode stack components and possibly cause a leak at the seal.

Control 9.12: Store cells and batteries discharged on an open-circuit stand.

Control 9.13: Provide a protective cover for the battery.

Control 9.14: Handle the batteries only when discharged.

Control 9.15: Install the batteries when discharged, if possible.

Control 9.16: Batteries should go through a capacity check just prior to installation on the spacecraft.

9.5.2 High-Temperature Operation (over 30°C)

Normal operating temperature of a battery in orbit should be in the range of -5 to 15°C. During handling of the battery, the temperature should not exceed 30°C. Extended operation or exposing a battery to temperatures in excess of 30°C results in permanent loss of capacity.

Control 9.17: Monitor the temperature of the battery continuously during handling and operation of the battery. Do not allow the temperature to exceed 30°C at any time.

9.5.3 Excessive Overcharge

When a battery is overcharged, all of the excess energy is dissipated as heat. Excessive overcharge results in a temperature rise of the battery and a possible thermal runaway condition. When a battery is being cycled in LEO or GEO applications in a ground test or in orbit, a certain amount of overcharge is required to fully recharge the battery. Under normal operating conditions, the battery temperature is maintained between -5 to 15°C. However, if the battery is excessively overcharged the temperature will rise rapidly.

If a power system design should fail in such a way as to allow the battery to be excessively overcharged, it could cause damage to the cells and a potentially

hazardous condition for the environment. The cells would heat up, internally damaging the positive and negative electrodes and melting the plastic gas diffusion screens. The plastic compression seals may leak, venting hydrogen gas into the atmosphere.

Control 9.18: Install thermocouples at several different locations within the battery on the aluminum sleeves and baseplate to monitor the temperature. Use a temperature limit on the battery to set off a warning alarm to shut down the power system charging the batteries. This would serve as a backup to the primary charge control system in case of a malfunction.

9.5.4 Low-Temperature Operation (below -25°C)

During storage or handling, the battery should not be operated below -25°C. "Liquidus curves for the system KOH-K_2CO_3-H_20 from 25 to -60°C" are presented in Reference 9-6. They show that for the electrolyte used in Ni-H_2 cells, which is typically between 26 and 38 percent KOH, the freezing point would be between -30 to -40°C. To allow for a margin of safety, the low temperature limit is set at -25°C. Cells with low electrolyte concentration (26 percent KOH or lower) should not be operated below -10°C. Freezing of the electrolyte has been reported at -15°C. One can postulate that electrolyte concentration gradients exist within the cell and that freezing is occurring in the region around the negative electrode during overcharge.

Control 9.19: Monitor the temperature of the battery and do not allow the temperature to go below -25°C at any time. Use heaters to control low temperatures.

9.6.0 GENERAL GUIDELINES FOR BATTERY HANDLING/OPERATION

The following general guidelines for battery handling and operation were provided by J. Miller and W. Shields from MSFC [9-7].

9.6.1 Batteries should not be charged or discharged in parallel. Some method of isolation must be provided to preclude a failure of one battery affecting other batteries in the system.

9.6.2 Batteries should be charged and all functions and cells checked out thoroughly prior to installation in a flight vehicle.**

9.6.3 Batteries should never have a "tap" on any portion of the string of cells in series that can cause unbalanced loading of portions of the battery.

9.6.4 Battery cells should never have their normal operating potential reversed. It is recommended that a positive method, such as a battery cell protection circuit, for precluding such a reversal be installed in all flight Ni-H_2 batteries.

9.6.5 Power system designs should preclude excessive overcharge of batteries. A recharge ratio monitor or limit to protect against excessive overcharge is recommended.

** The batteries may be installed into a flight vehicle in a discharged state if they can be adequately charged once they have been installed. It is easier and safer to install a battery in a discharged state. However, it may not be practical to charge the batteries once they have been installed in the flight vehicle. In that case the batteries must be installed in the charged state.

9.7.0 SUMMARY OF CONTROLS

Control 9.1: Provide adequate venting in areas with batteries

Control 9.2: Install a hydrogen gas detector at the ceiling of the battery area.

Control 9.3: Do not smoke in battery areas.

Control 9.4: Proof test all Ni-H_2 cells to 1.5 times the maximum operating pressure.

Control 9.5: Burst test at least two cells from each production lot of INCONEL 718 pressure vessels. At the least, a 2/1 safety factor is required between the maximum operating pressure and the burst pressure.

Control 9.6: Ensure that the cells and batteries are maintained within the range of handling and operating conditions specified by the manufacturer.

Control 9.7: Perform a 100 percent inspection of the terminals and the weld regions on all cells to look for indications of electrolyte leakage.

Control 9.8: Use a hydrogen leak detector to inspect each cell within the battery during battery acceptance testing and final checkout of the battery prior to launch.

Control 9.9: Inspect the battery pack for any possible leakage paths to ground.

Control 9.10: Monitor the individual cell voltages within a batteries to determine if there are any low-voltage (low-capacity) cells.

Control 9.11: Monitor the individual cell voltages within a batteries to determine if there are any mismatched cells. (Check for hydrogen leak.)

Control 9.12: Store cells and batteries discharged on an open-circuit stand.

Control 9.13: Provide a protective cover for the battery.

Control 9.14: Handle the batteries only when discharged.

Control 9.15: Install the batteries when discharged, if possible. If it is necessary to install the battery when charged, start operation with a low-rate trickle charge if possible.

Control 9.16: Batteries should go through a capacity check just prior to installation on the spacecraft.

Control 9.17: Monitor the temperature of the battery continuously during handling and operation of the battery. Do not allow the temperature to exceed 30°C at any time.

Control 9.18: Install thermocouples at several different locations within the battery on the aluminum sleeves and baseplate to monitor the temperature. Use a temperature limit on the battery to set off a warning alarm to shut down the power system charging the batteries. This would serve as a backup to the primary charge control system in case of a malfunction.

Control 9.19: Monitor the temperature of the battery and do not allow the temperature to go below -25°C at any time. Use heaters to control the low temperature limit for the batteries/cells.

9.8.0 HST SYSTEM SAFETY BASELINE REQUIREMENTS FOR THE Ni-H_2 BATTERY

The following safety information was provided by David E. Nawrocki from LMSC [9-8].

The safety requirements that were imposed on the Ni-H_2 batteries from JSC and KSC were as follows. The basic JSC Safety document for STS payloads is NHB 1700.7A. The following paragraphs are applicable to the Ni-H_2 battery design:

- Para 201.2 Critical Hazards
- Para 202.2 Catastrophic Hazards
- Para 208.4 Pressure Systems
- Para 209.1a Hazardous Materials

These requirements cover the inherent hazards resulting from the pressure vessel design and the use of potassium hydroxide and hydrogen. Refer to the individual paragraphs for the specific criteria. It should be noted that all new programs are using NHB 1700.7B.

Materials and Design Requirements also addressed safety-related design criteria. Cells were designed to the structural requirements of MSFC-HDBK-505. Cells were built with a burst factor of four times the maximum expected operating pressure.

JSC 07700 requirements describe the loading conditions which must be met. Battery module factors of safety design were specified as 1.25 Yield and 2.0 Ultimate for all mission phases.

Fracture control implementation is based on the requirements specified in MIL-STD-1522A. Materials usage is in accordance with MSFC-SPEC-522A. This requirement regulates the use of hazardous and flammable materials.

EVA concerns are based on NSTS 07700 Vol. XIV (JSC 10615). This document covers all the EVA concerns for Orbital Replacement Units (ORUs) remove-and-replace operations. For example, some design concerns that are addressed are the following: connector spacing, sharp edges and corner criteria, protrusions and fastener criteria, EVA handling aid design, electrical connector protection and isolation, connector design, crew load factors/limits, etc.

The KSC basic requirements document is KHB 1700.7A. This document covers all aspects of safe payload handling at KSC. Because the Ni-H_2 battery must be serviced at KSC, it requires its own ground support equipment (GSE). The GSE is covered under the design and safety requirements specified in KHB 1700.7A. Paragraphs 4.1.3 and 4.3.9 are applicable.

The same safety concerns are still relevant: cell pressure over-pressurization, leakage or rupture, contact with corrosive electrolyte (potassium hydroxide). Again, the design requirements are the following: MSFC-HDBK-505, cell burst factor of three times the maximum expected operating pressure, and cell design loads based on JSC 07700 requirements. Module factors of safety design are 1.25 Yield and 2.0 Ultimate for all mission phases.

Cells are designed to the requirements of MIL-STD-1522A and fracture control is implemented per MIL-HDBK-1453. Materials are chosen in agreement with MSFC-SPEC-522A.

Ground operations/battery conditioning is controlled by a vehicle battery service console (VBSC). The KHB 1700.7A requirements are explicit for GSE. This type of GSE not only interfaces with a flight item, but also interfaces with KSC facilities and personnel. GSE handling is covered by this requirement, and proper certification is described.

Proof loads and proof and pressure testing are specified in KHB 1700.7A. These are the safety verification methods that are implemented to verify that the design requirements have been met. Other quality tests include burst tests, non-

destructive evaluation (NDE) on each pressure vessel (cell case), and x-ray or dye penetrant inspection. Material usage is reviewed by MSFC Material Application and Evaluation Board (MAEB). For M&R, these requirements were also covered by MSFC-STD-126.

9.9.0 REFERENCES

[9-1] G. Halpert, S. Subbarao, and J. J. Rowlette, "The NASA Aerospace Battery Safety Handbook," JPL Publication 86-14, July 15, 1986.

[9-2] "Hubble Space Telescope Nickel Hydrogen Battery Fracture Control Report," Contract NAS 8-32697, Modification 593, #6332, LMSC/F228318B, November 15, 1989.

[9-3] "Manned Space Vehicle Battery Safety Handbook," NASA Lyndon B. Johnson Space Center, JSC-20793, September 1985.

[9-4] P. Schrantz, B. Allen, COMSAT Laboratories, private communications.

[9-5] R. Patterson, V. Mikol, and A. Koplin, "Nickel Hydrogen Battery Development Final Report," Report Number 76-8215-6-013, May 17, 1976.

[9-6] S. U. Falk and A. J. Salkind, "Alkaline Storage Batteries," Section 8.2: Properties of Potassium Hydroxide Solution, Copyright 1969 by John Wiley & Sons, Inc., Library of Congress Catalog No. 77-82980.

[9-7] J. Miller and W. Shields, "Recommendations for the Battery Systems Handbook," Nov. 1989, NASA Marshall Space Flight Center.

[9-8] D. E. Nawrocki, LMSC, private communications.

APPENDIX A

Storage Considerations for Nickel-Hydrogen Cells

Storage Considerations for Ni-H_2 Battery Cells

NASA/GSFC Battery Workshop, 3 Nov. 1988
Goddard Space Flight Center, Greenbelt, Maryland 20771

Whitely, Chemistry Department, Pacific University, Forest Grove, OR
Gibney, O/62-12, Lockheed Missiles and Space Co., Sunnyvale, CA

Introduction

The principle concern with the long-term storage of nickel-hydrogen battery cells is the development of a low-voltage plateau in the discharge profile of the cell (Figure 1). While the total capacity of a cell might remain essentially unchanged despite long periods of storage, the formation of this secondary plateau constitutes a decrease in the discharge voltage of some of the cells' capacity. While this lower voltage is below the voltage requirements of a particular power system, that portion of the capacity is no longer considered useful capacity, and therefore, there is a loss in useful capacity.

In order to understand this loss in useful capacity, the problem was characterized as fully as possible: the nature of the secondary plateau, the storage conditions which affect the development of the secondary plateau, the cell designs which make cells less likely to show losses in useful capacity after storage, and charging/discharging regimes which lead to recovery of some useful capacity losses were all delineated (Table 1). The strategy was, then, to formulate a mechanism for the capacity loss which would be consistent with all these characteristics. Only with the correct mechanism in hand would it be possible to propose measures (storage, design, cycling) which would mitigate the loss of useful capacity after long-term cell storage.

Discussion

The nature of this secondary plateau and its causes and effects (Tables 1 and 2) are consistent with the formation of a higher resistance barrier between the current-carrying sinter and the active material of the positive electrode. The nickel sinter intrinsically develops a thin barrier of NiO which inhibits electron transfer, and it is this barrier which protects the sinter from spontaneous oxidation by the Ni(III) and Ni(IV) hydroxides which are generated on cell charging. Without this barrier, the sinter would eventually become the bivalent nickel hydroxide by way of:

$$Ni^0 + 2\,NiOOH + 2\,H_2O \rightarrow 3\,Ni(OH)_2$$

and/or

$$Ni^0 + NiO_2 + 2\,H_2O \rightarrow 2\,Ni(OH)_2$$

The barriers of resistive metals can be thought of as energy barriers, as illustrated in Figure 2. Although the electrons in metallic nickel are at a constant higher energy

than those in the NiOOH and NiO_2, there is minimal electron transfer, and therefore minimal oxidation of the sinter, because the electrons in the metallic nickel are unable to overcome the small energy barrier of the intrinsic oxide film. On the other hand, electrons in the platinum negative electrode are at a sufficiently high energy to surmount this barrier when the platinum is exposed to H_2 gas; that is, when the cell contains any pressure of hydrogen.

It should be noted at this point that some of the other proposed mechanisms for the development of a secondary plateau after long-term storage are not entirely consistent with the characteristics delineated in Table 1. For example, a recent explanation suggests that CoOOH (or $Co(OH)_3$) is reduced by the hydrogen gas in a Ni-H_2 cell and that this leads to differential solubilities of the nickel and cobalt hydroxides. It is proposed that there is a migration of Co from the active material matrix. Certainly, such a mechanism would profoundly affect the charge and discharge profile of a cell stored for long periods. But the secondary plateau is found in Ni-Cd cells despite the absence of hydrogen, and it is found in Ni-H_2 cells with a positive precharge. Such cells have a residual oxidizing environment, and reduction of Co(III) in the active material would be highly unlikely. Even Ni-H_2 cells with a modest hydrogen precharge show residual Ni(III) in their positive electrodes after several years of storage in the shorted condition. In the presence of Ni(III), the reduction of Co(III) to bivalent Co is unlikely.

The NiO film on the nickel sinter is not the only energy barrier between the metallic nickel and the active material: the active material itself can provide considerable electrical resistance (a high energy barrier). The height of this barrier is indeterminate because the electrical resistance of the active material barrier is largely a function of its thickness, structure, and the oxidation state of the Ni within the structure. The fully discharged positive electrode contains mostly bivalent nickel hydroxide. There is the brucite form, usually referred to as b-$Ni(OH)_2$, and there is the loosely hydrated form, a-$Ni(OH)_2$, which can contain 0.5 to 0.7 molecules of H_2O per Ni atom. This alpha form is a much more open structure as its intercalated water molecules hold the Ni-O planes 0.8 nm apart. This is also a much more electrically conductive material than the b-$Ni(OH)_2$, which contains as little as one H_2O molecule per 20 Ni atoms and has an interlaminar spacing of only 0.46 nm.

So, although a higher energy barrier might be expected of the b-$Ni(OH)_2$ than of the a-$Ni(OH)_2$ active material, other considerations determine the exact barrier heights. It is evident that the b-$Ni(OH)_2$ barrier can become insurmountable to even those electrons from the charged negative electrode. The conclusion is drawn from the destructive physical analyses of cells which have been short-circuited for years: the apparent oxidation state of the nickel in the active material is always found to exceed +2, indicating the presence of at least some trivalent nickel. The analyses typically show about 5 percent NiOOH in the active material and it has been observed that the discharged active material is b-$Ni(OH)_2$. For the most part, however, the active material is accessible for discharge, and this is largely at about the same energy or voltage. Highly resistive regions do not compromise all of the

capacity because the positive electrodes behave much like a network of innumerable parallel resistors (Figure 3). The high resistance paths are simple bypassed until all of the active material in low resistance regions is discharged. Only then is the more isolated material discharged.

The highly resistive nature of the b-$Ni(OH)_2$ is due, only in part, to the lack of water in its interlaminar regions. As this bivalent hydroxide ripens, its structure becomes more and more regular (ordered), and it is the highly ordered form of b-$Ni(OH)_2$ which shows such poor electrical conductivity. Water is not the only defect in the structure which can enhance the electrical conductivity of the material, even traces of higher oxidation state material like NiOOH can have a profound effect. And so, while it might seem desirable to achieve total reduction of the higher oxidation state nickel when discharging a cell, it is preferable to leave traces of the Ni(III) and Ni(IV) within the active material matrix to act as defects as the b-$Ni(OH)_2$ ripens over time. Fortunately, leaving some undischarged material is unavoidable as discussed earlier.

Charged positive electrodes have been found to contain a-NiOOH, b-NiOOH, g-NiOOH, and some form of tetravalent Ni, which, for simplicity, will be described here as NiO_2. The b-NiOOH and g-NiOOH are the important charging products. It is generally accepted that the beta structure is more conductive than the gamma structure, but the key issue is the structures themselves. On charging of the cell b-$Ni(OH)_2$ is smoothly oxidized to b-NiOOH with only minor changes to the crystal structure. The interlaminar distance opens slightly, from 0.46 nm to 0.48 nm. g-NiOOH on the other hand is a product of charging a-$Ni(OH)_2$ or of prolonged overcharging of b-NiOOH, and this, as with the a-$Ni(OH)_2$, is a much more open structure. Cell dimensions indicating an interlaminar spacing of 2.1 nm have been reported. The separation of the Ni-O planes in this structure is attributed to the incorporation of K^+ ions which are drawn into the structure during charging and expelled during discharging.

Because the g-NiOOH is a poorer conductor than the b-NiOOH, the g-NiOOH material discharges at a lower voltage and is therefore a less desirable product of cell charging. However, it is the precursor to a-$Ni(OH)_2$, and in that respect it is more desirable to form g-NiOOH on cell charging. By forming g-NiOOH through extended overcharging, a-$Ni(OH)_2$ will be formed on subsequent discharge, and this more conductive form of discharged material will provide a lower energy barrier between the active material and the nickel sinter. This is why some capacity lost to the low-voltage discharge can be recovered through severe overcharging of the cell: any active material which has not been isolated by highly resistive b-$Ni(OH)_2$ is charged, first to b-NiOOH, and then to g-NiOOH. This opens the structure of the active material, allowing H_2O and K^+ between the layers of Ni and O atoms. On discharge, a significant amount of a-$Ni(OH)_2$ is formed in the pores of the sinter. Repeated cycling (overcharging and overdischarging) slowly works H_2O into the structure of the active material. This is not likely to be an efficient process, and so total recovery of capacity is not expected. When the b-$Ni(OH)_2$ becomes highly

ordered (dehydrated) after prolonged storage, it is not easily re-hydrated and therefore remains highly resistive.

The hypothesis that the loss of useful capacity is a dehydration process is consistent with most of the factors delineated in Table 1. Dehydration of either form of $Ni(OH)_2$ is thermodynamically favorable, and so the discharged active material has a natural tendency to lose water and become less conductive. But dehydration is a slow process and can be virtually eliminated at very low temperatures (cf. Table 2). Dehydration could readily occur in cells with no H_2 precharge as is the case in Ni-Cd and negative-limited Ni-H_2 cells, and some low-voltage discharge plateau has been observed in both of these cell designs (Table 2). Recovery of capacity by overcharge and trickle charge is not surprising when these reactions at the positive electrode are examined (Table 3). The trickle charge reaction is the same as the overcharge reaction: both consume hydroxide ions, but more importantly, both generate H_2O within the active material, and this is the source for the "re-hydration" process. The final factor described in Table 1 is not obviously connected to dehydration of active material.

The sensitivity of capacity loss to the rigidity of the plaque is due to the significant changes in the volume of active material as a function of state-of-charge. Zimmerman and Effa have clearly demonstrated that the intrinsic volume of discharged material (b-$Ni(OH)_2$) is considerably larger in a fully discharged cell than in a partly charged cell (Figure 4). This implies that when a cell is fully discharged, the active material swells inside the pores of the nickel sinter, creating stresses within the positive electrode. These stresses can be relieved by expansion of the pores or by squeezing water from the $Ni(OH)_2$ structure to reduce its volume. Expansion of the pores is a function of the rigidity of the plaque, and for plaque with a high bend strength, this is less likely. This leaves only the dehydration option. Given that dehydration of Ni(II) hydroxides is already thermodynamically favorable, the stresses created by rigid plaque can only accelerate the process. And given that the highly conductive a-$Ni(OH)_2$ occupies much more volume than the less conductive b-$Ni(OH)_2$, more rigid plaque should favor formation of b-$Ni(OH)_2$.

Closely related to the issue of rigid plaque is loading levels: electrodes which are heavily loaded, like rigid plaque, are less able to expand to accommodate a-$Ni(OH)_2$ as the cell is discharged. And so, such electrodes are more likely to enhance the formation of the highly resistive, dehydrated b-$Ni(OH)_2$ which leads to the secondary voltage plateau. It has been pointed out that plaque contains large void volumes even after being heavily loaded, but it should also be pointed out that access to these voids is the issue. It is unlikely that any form of nickel hydroxide has any ductility to speak of, and therefore, as it expands, it is unlikely that it would flow into any available voids. Instead, it will create stresses within the electrode pores and spontaneously dehydrate.

The hypothesis that the loss of useful capacity is a dehydration process is not consistent with all of the factors delineated in Table 1. These inconsistencies are

explained when a more general description of the process is used. It is the highly ordered form of b-$Ni(OH)_2$ which is a poor conductor, and the presence of crystal defects, like H_2O, enhance its conductivity. Other defects, however, are possible and are vital to maintaining good conductivity within the active material. Either form of NiOOH serves this purpose well. Besides providing Ni^{3+} defects within the b-$Ni(OH)_2$ structure, neither form of NiOOH has much tendency to dehydrate as the two forms of $Ni(OH)_2$ and the g-NiOOH brings the K^+ ions, which further disrupt the highly regular structure of the b-$Ni(OH)_2$. The need for NiOOH within the discharged active material explains the observations that cells with a hydrogen precharge and cells stored in the shorted condition are more likely to develop a secondary plateau (Tables 1 and 2).

The NiOOH defects can be removed from the active material matrix by any or all of the reactions listed in Table 3 for self discharge at the nickel electrode. The first reaction listed does not require hydrogen; it is the mechanism for self discharge of Ni-Cd cells. If it occurs in a Ni-H_2 cell, it is evidently coupled to the self discharge reaction under "At the Platinum Electrode or on Any Ni^o Surface" (Table 3), because O_2 does not accumulate during Ni-H_2 cell self discharge. Nevertheless, in a discharged cell, the higher oxidation state nickel ions are spontaneously removed from the matrix by the electrolyte and by any hydrogen precharge, the greater the H_2 precharge, the more thoroughly the NiOOH can be removed from the matrix. Inasmuch as residual NiOOH is always found in Ni-H_2 cells, even those stored for long periods with a hydrogen precharge, it can be said that this reduction process is not absolutely complete.

The intrinsic nature of each electrode in a fully discharged cell is very much a function of the precharge on the cell (Tables 4A and 4B). With either cell design, the open circuit voltage of the positive electrode should lie at least 100 mV positive of the negative electrode (Table 5). This means that in either design, the positive electrode is inherently electron-deficient with respect to the negative electrode. When, however, the electrodes are shorted together <u>after full discharge</u>, the potential of each electrode to become artificially electron-rich (and the negative, artificially electron-poor). This electron-rich environment will enhance the reduction NiOOH defects in the active material. This is why cells stored shorted consistently show a greater proclivity for the secondary plateau (Table 2). On the other hand, when a cell is stored at open circuit after discharge, each electrode remains at its intrinsic rest potential and an artificially electron-rich (reducing) environment is not created within the positive electrode.

Purely in terms of mitigating the secondary voltage plateau, it is apparent that the negative limited cell (that with a positive precharge) is preferable. With its positive precharge, a higher concentration of NiOOH defects remain in the active material matrix after fully discharging the cell. But other storage issues should be considered. Because NiOOH can be reduced by H_2O to produce O_2, as described earlier, it should not be expected that a negative limited cell will retain its precharge as NiOOH. Rather, on prolonged storage, the positive precharge is probably inventoried as O_2

gas. The disadvantage of this is that the precharge is then no longer confined to the positive electrode; it is free to move throughout the cell. As the cell is recharged, H_2 will be generated at the negative electrode, and the $H_2 + O_2$ recombination to form H_2O will quickly follow. But prior to recharge, the liberated oxygen gas can be problematic. In an alkaline solution, as in the Ni-H_2 cell, oxygen can readily dissolve platinum metal from the negative electrode by:

$$Pt^o + O_2 + 4\ OH^- + 2\ H_2O \longrightarrow 2\ Pt(OH)_4^{2-}$$

Other platinum oxidation processes can be written, and all of them show that the platinum becomes a soluble material which can diffuse throughout the cell. Only the oxidized platinum which remains in contact with the negative electrode would be reduced back to Pt metal on charging the cell. When the negative limited cell is stored shorted, the oxidation of Pt from the negative can proceed without the need for the O_2 shuttle. In this case the electron deficiency created at the negative is enough to drive the oxidation reaction.

Conclusions

The loss of some capacity after prolonged storage of Ni-H_2 batteries and battery cells is unavoidable; it is simply a consequence of confining several elements, each existing in two or more oxidation states, to a single container for extended periods. Thermodynamically, the oxidation-reduction reactions are highly spontaneous as are the deleterious dehydration reactions which cause the active material to lose its conductivity. But the rates of these reactions, particularly below room temperature, become sufficiently slow to make capacity losses acceptably small. Other measures, besides low temperature storage, can further decrease the rate of capacity-draining reactions. The discharge prior to cell storage should be somewhat modest, i.e., it should not be so thorough as to drive both electrodes to the same voltage (a zero volt open circuit condition). The use of minimal hydrogen precharge and open-circuit storage of the cells also slow the reduction of NiOOH in the active material. With such relatively simple precautions, it should be possible to store Ni-H_2 batteries and battery cells for prolonged periods with virtually no capacity loss to a voltage plateau.

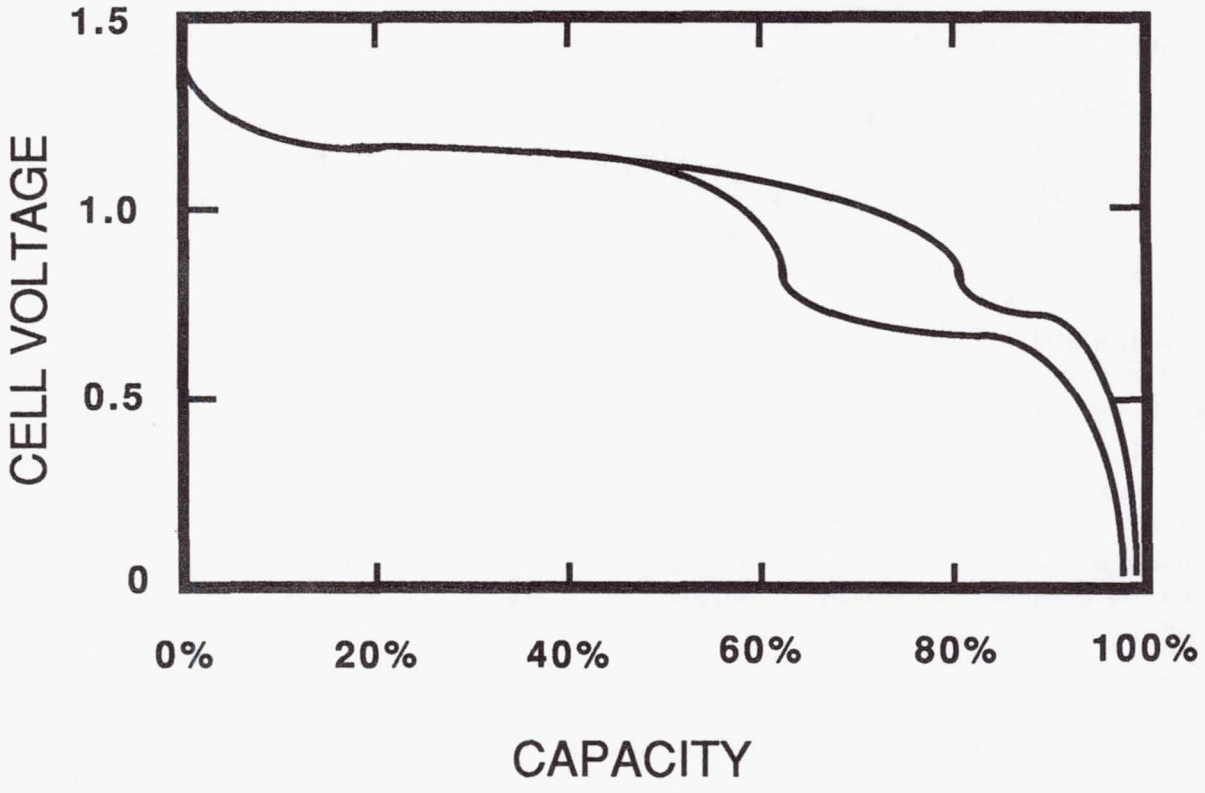

Figure 1 Two discharge profiles: one with a small secondary plateau and another with a significant secondary plateau.

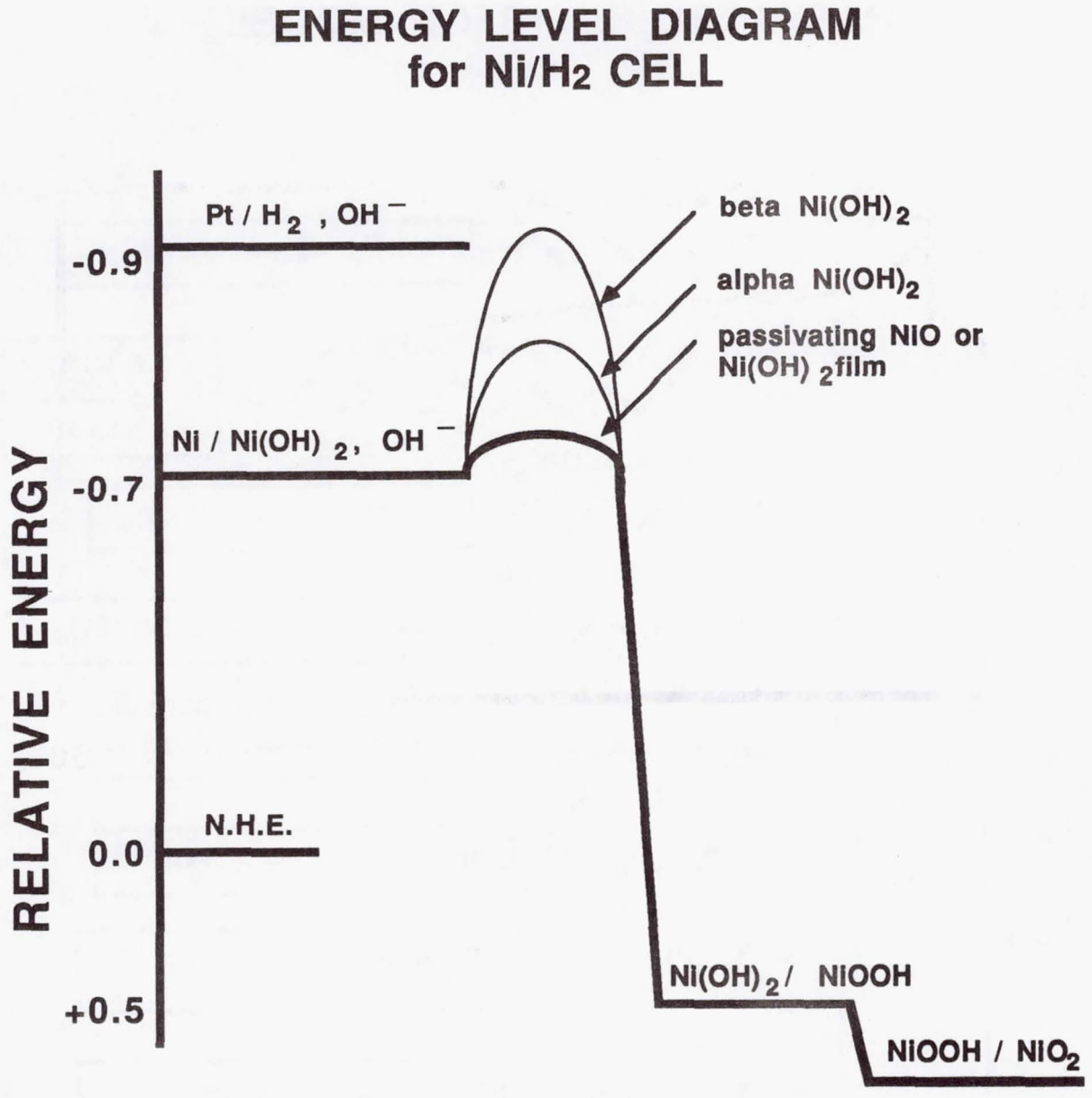

Figure 2. Relative energies of electrons in the various materials in the Nickel-Hydrogen cell electrodes. For a single electron the ordinate is expressed in electron volts; for one Coulomb, this axis would be in expressed Joules.

PARALLEL RESISTOR MODEL

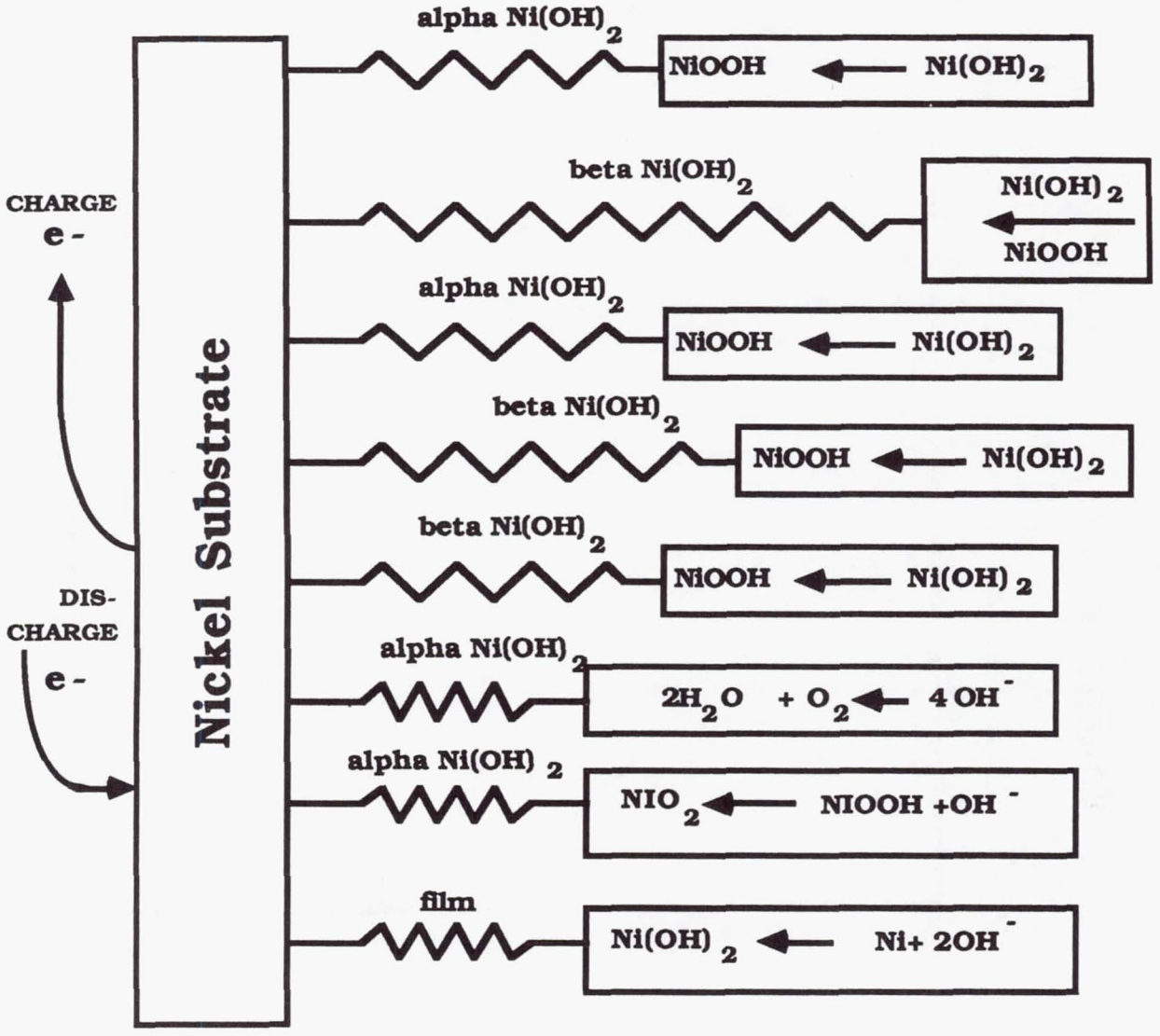

Figure 3. A parallel resistor model illustrating the many different resistive barriers between the nickel sinter and the active material. The boxes represent regions of active material, and the arrows within those boxes are in the direction of the charging reaction. The length of a particular resistor is an indication of its relative resistance.

From: A.H. Zimmerman and P.K. Effa, Nickel Hydroxide Active Material Densities, Aerospace Technical Memorandum SD-TR-88-02, Aerospace Corporation, El Segundo, CA 90245-4691.

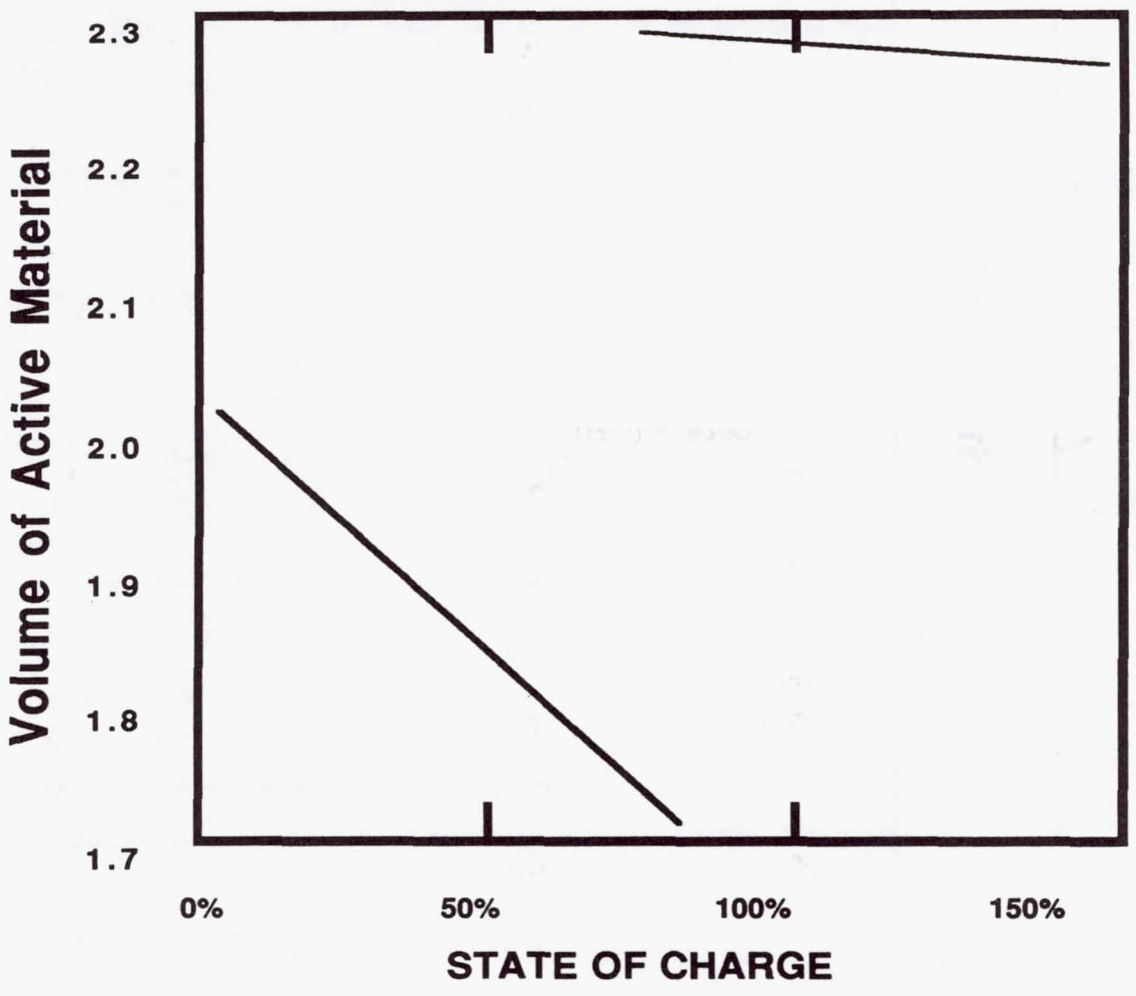

Figure 4 The volume of active material as a function of state of charge for a nickel electrode containing 10% cobalt hydroxide in the active material.

Table 1

CHARACTERISTICS of the SECONDARY VOLTAGE PLATEAU PROBLEM

It diminishes useful capacity (up to 30% loss).
The total capacity is essentially retained, but a significant portion is shifted to a discharge voltage of less than 0.9 V

It develops relatively slowly, even at room temperature.

The rate of development is clearly affected by temperature.
It is almost non-existent at O°C and below.

The severity of the problem depends upon cell precharge.
It is sensitive to the presence of H_2 pressure.

The plateau is more prominent in cells stored shorted.

It diminishes charge efficiency.
Cells with this plateau show premature oxygen evolution.

Capacity loss can be recovered with severe overcharging.

The problem is somewhat mitigated with trickle charge.

It seems to be sensitive to physical properties (rigidity) of the plaque.

Table 2

REFERENCE DATA

From: H. Vaidyanathan, Long-Term Storage of Nickel-Hydrogen Cells, COMSAT Laboratories, Clarksburg, MD 20871-9475

Five cells were fully discharged and stored open-circuit at room temperature. After 30 days, all five cells had retained at least 71% of initial capacity.

Fully discharged cells stored open circuit at 0°C retained more than 90% of initial capacity after 253 days in storage, and cells stored at -20°C showed 103% of initial capacity after similar storage period.

With -20°C, 0°C, and room temperature storage of fully discharged, open circuited cells, those with a negative precharge (residual H_2 pressure after discharge) always lost the greater fraction of initial capacity.

From:B. Vyas and M.P. Bernhardt, Effects of the Mode of Storage on the Capacity Fading of the Sintered Nickel Electrode, 1981 Goddard Battery Workshop.

Loss in Capacity for Ni-Cd Cells

STORAGE CONDITION	STORAGE TEMPERATURE		
	Room Temp.	60°C	80°C
Shorted	5	30	37
Open Circuit	2	6	17

Table 3

Reactions of Interest

Charge

At the Nickel Electrode

$$Ni(OH)_2 + OH^- \rightarrow NiOOH + H_2O + e^-$$

$$NiOOH + OH^- \rightarrow NiO_2 + H_2O + e^-$$

At the Platinum Electrode

$$2\,H_2O + 2e^- \rightarrow H_2 + 2\,OH^-$$

Overcharge

At the Nickel Electrode

$$4\,OH^- \rightarrow 2\,H_2O + O_2 + 4\,e^-$$

At the Platinum Electrode

$$2\,H_2O + 2e^- \rightarrow H_2 + 2\,OH^-$$

Self Discharge

At the Nickel Electrode

$$4\,NiOOH + 2\,H_2O \rightarrow 4\,Ni(OH)_2 + O_2$$

$$2\,NiOOH + H_2 \rightarrow 2\,Ni(OH)_2$$

$$NiO_2 + H_2 \rightarrow Ni(OH)_2$$

At the Platinum Electrode or on Any Ni^o Surface

$$2\,H_2 + O_2 \rightarrow 2\,H_2O$$

Table 4A

THE POSITIVE LIMITED CELL

-Will contain a residual pressure of hydrogen gas after full discharge. The negative electrode will, therefore, contain adsorbed hydrogen.

-Will contain no electrochemically available NiOOH in the active material (positive electrode) after full discharge.

-Non-electrochemically available NiOOH will continue to be reduced, either by H_2O or by H_2. The extent and rate of this reduction will depend largely on the amount of H_2 precharge.

Shorted for Storage

-Both electrodes will be driven to the same potential.

-This will enhance oxidation of the adsorbed layer of H_2 at the Pt (negative) electrode.

-Reduction of $Ni(OH)_2$ and $Co(OH)_2$ in the positive electrode will be enhanced.

-The artificially induced reducing environment in the nickel (positive) electrode will drive the reduction of NiOOH.

Open Circuit for Storage

-Each electrode is allowed to achieve its rest potential.

-Neither electrode drives the other.

Table 4B

THE NEGATIVE LIMITED CELL

-Will contain no residual hydrogen, not even adsorbed to the negative electrode.

-Will contain electrochemically available NiOOH in the positive electrodes.

-All remaining NiOOH will continue to be reduced, but by H_2O only.

-Oxygen gas could accumulate in the discharged cell.

Shorted for Storage

-Both electrodes will be driven to the same potential.

-The positive electrode will enhance oxidation at the negative electrode, and with no adsorbed H_2 to be oxidized:

$$2\ Pt + O_2 + 2\ H_2O + 4\ OH^- \longrightarrow 2\ Pt(OH)_4^{2-}$$

-The negative electrode will drive electrons into the positive electrode thereby accelerating the reduction of electrochemically available NiOOH.

Open Circuit for Storage

-Each electrode is allowed to achieve its rest potential.

-Neither electrode drives the other.

Table 5

ESTIMATES of ELECTRODE REST POTENTIALS
For Two Cell Designs

The positive limited cell:

The negative electrode is	Pt/ H_2, OH^-	E = -0.85 V *vs* N.H.E.
The positive electrode is	Ni/ $Ni(OH)_2$, OH^-	E = -0.73 V *vs* N.H.E.

The negative limited cell:

The negative electrode is	Pt/ $Pt(OH)_2$, OH^-	E = +0.15 V *vs* N.H.E.
The positive electrode is	Ni/ $Ni(OH)_2$, NiOOH	E = +0.47 V *vs* N.H.E.

Table 6

SUMMARY

.The active material in a fully discharged cell is a mixture of α-$Ni(OH)_2$, β-$Ni(OH)_2$, and higher oxidation state hydroxides of Ni, principally β-NiOOH.

-This material is an excellent electrical conductor and therefore is easily charged.

-The excellent conductivity is due to:

.The presence of α-$Ni(OH)_2$ because of its open lattice which holds H_2O molecules between Ni-O planes.
.The presence of Ni(III) and Ni(IV) hydroxides and oxides. These create defects in the β-$Ni(OH)_2$ lattice as it forms. Also, these hydroxides do not readily dehydrate.

-Over extended storage:
.The bivalent hydroxides dehydrate, and the oxyhydroxides are reduced.
.A highly ordered form of beta-$Ni(OH)_2$ slowly forms. This material is a poor electrical conductor.

-Dehydration is thermodynamically favorable and is accelerated by:
.Elevated temperature
.Compression of the active material by rigid plaque.

-Reduction of the oxyhydroxides is also thermodynamically favorable and is accelerated by:
.High pressure hydrogen (hydrogen precharge)
.Shorting the positive electrode to the negative electrode during storage

Table 7

RECOMMENDATIONS

-Use minimal negative precharge after cell activation.

-Store cells at low temperature (*ca.* 0°C).

-Store cells in open circuit condition after full discharge.

Table 8

ADDITIONAL REFERENCES

P.C. Milner and U.B. Thomas, *Advances in Electrochemistry and Electrochemical Engineering,* Interscience Publishers (1967), New York, C.W. Tobias (ed.), **5**, 1-86.

R.S. McEwen, "Crystallographic Studies on Nickel Hydroxide and the Higher Nickel Oxides," *J. Phys. Chem.*, 1782-1789, **75**, (1971).

R. Barnard, G.T. Crickmore, J.A. Lee, and F.L. Tye, "The Causes of Residual Capacity in Nickel Oxyhydroxide Electrodes," *J. Appl. Electrochem.*, **10**, 61-70, (1980).

D.H. Fritts, "The Mechanics of Electrochemically Coprecipitated Cobalt Hydroxide in Nickel Hydroxide Electrodes," *J. Electrochem. Soc.*, **129**, 118-122, (1982).

B. Mani and J.P. de Neufville, "Dehydration of Chemically and Electrochemically Impregnated (CI and EI) Nickel Hydroxide Electrodes, *J. Electrochem. Soc.*, **135**, 800-803, (1988).

APPENDIX B

SEM Analysis

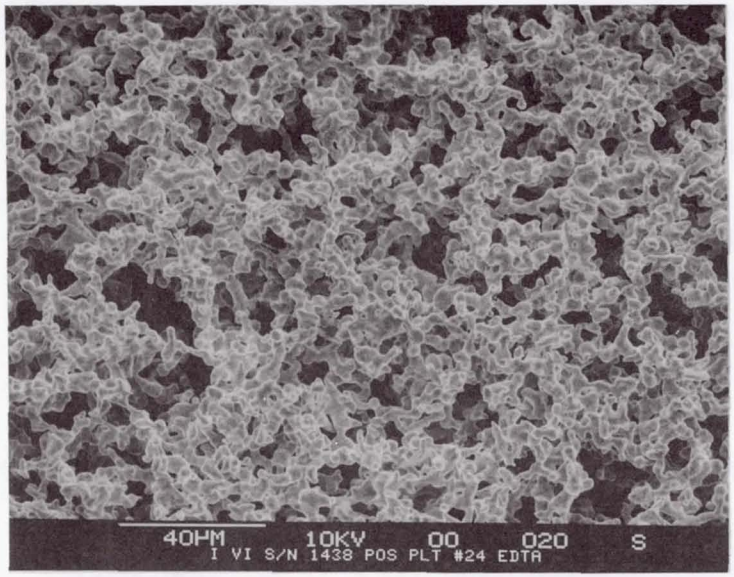

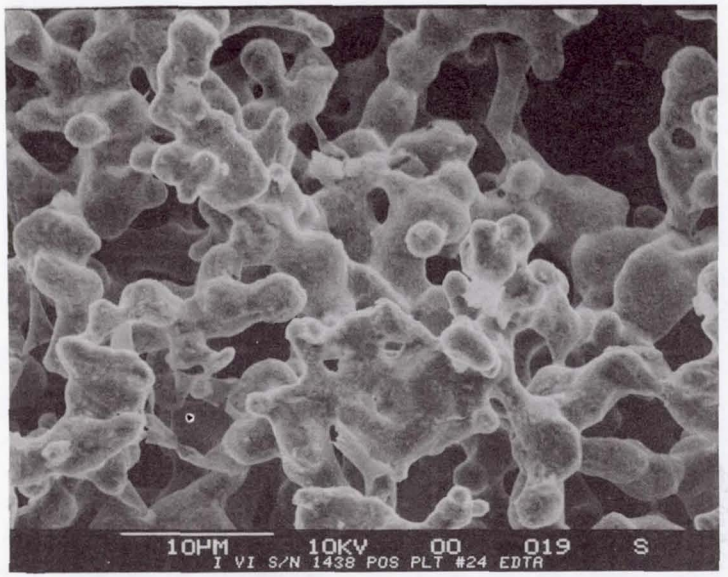

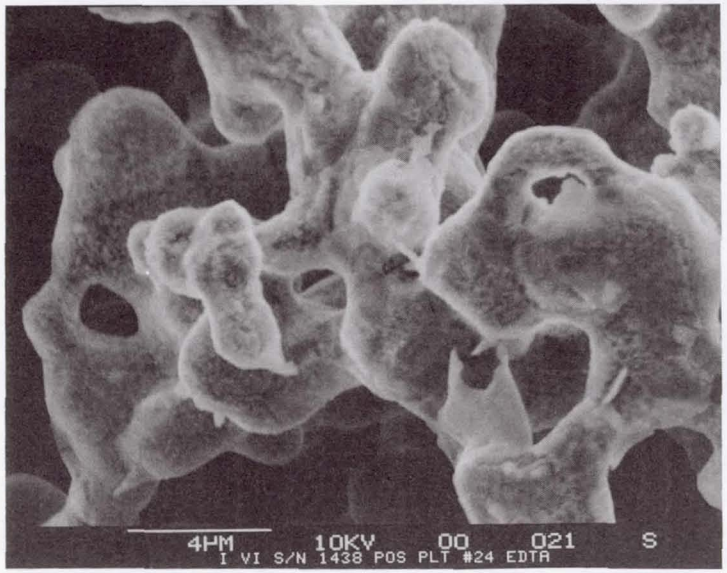

Figure 1. SE images of Intelsat VI positive plate #24 S/N 1438 after EDTA - area 1, side 1. 9 21211STA.

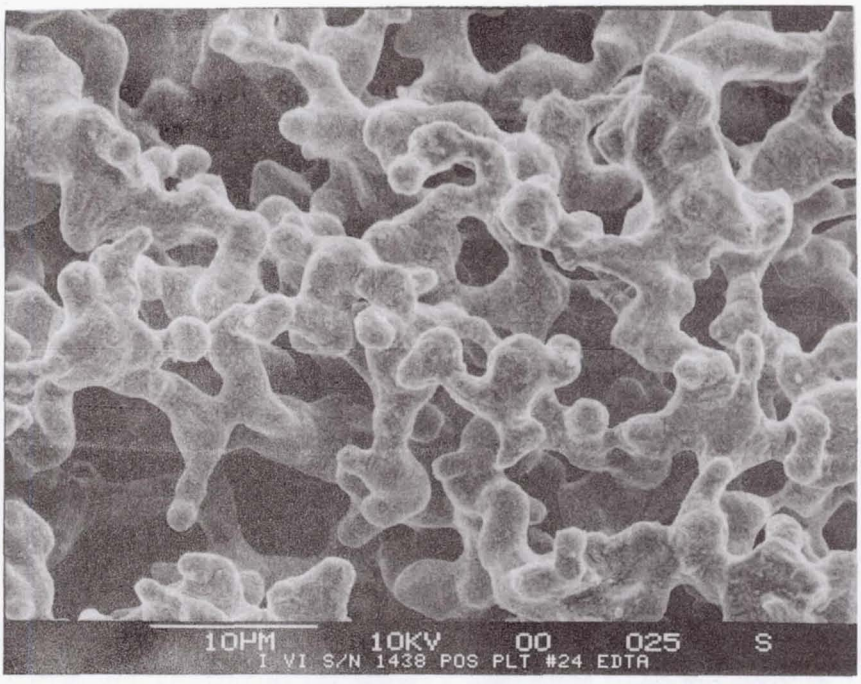

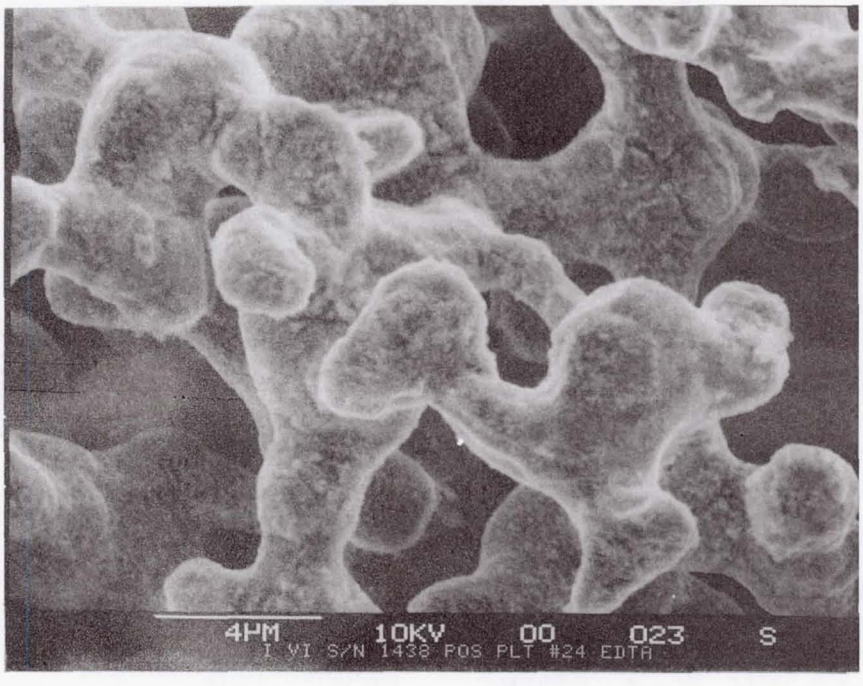

Figure 2. SE images of Intelsat VI positive plate #24 S/N 1438 after EDTA - area 2, side l. 9 21211STA.

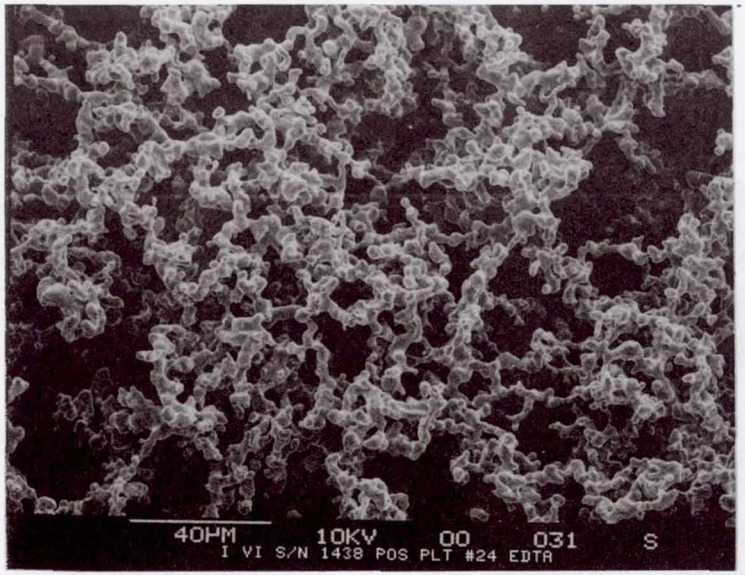

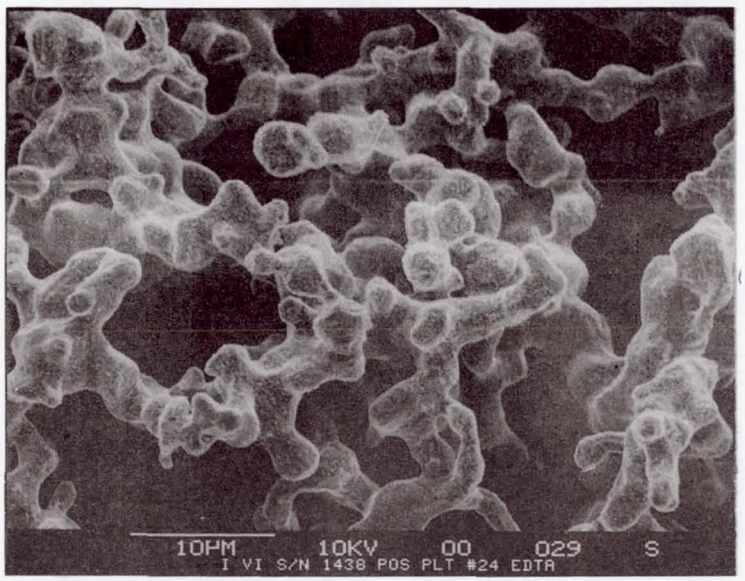

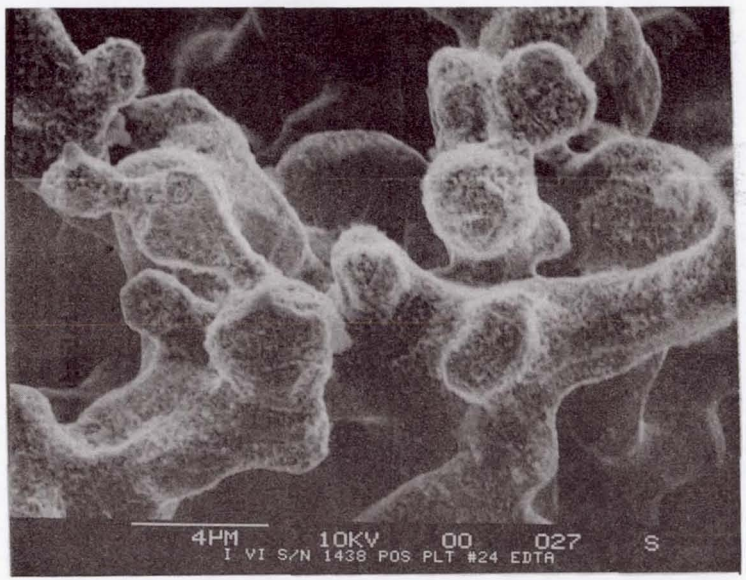

Figure 3. SE images of Intelsat VI positive plate #24 S/N 1438 after EDTA - area 1, side 2. 9 21211STA.

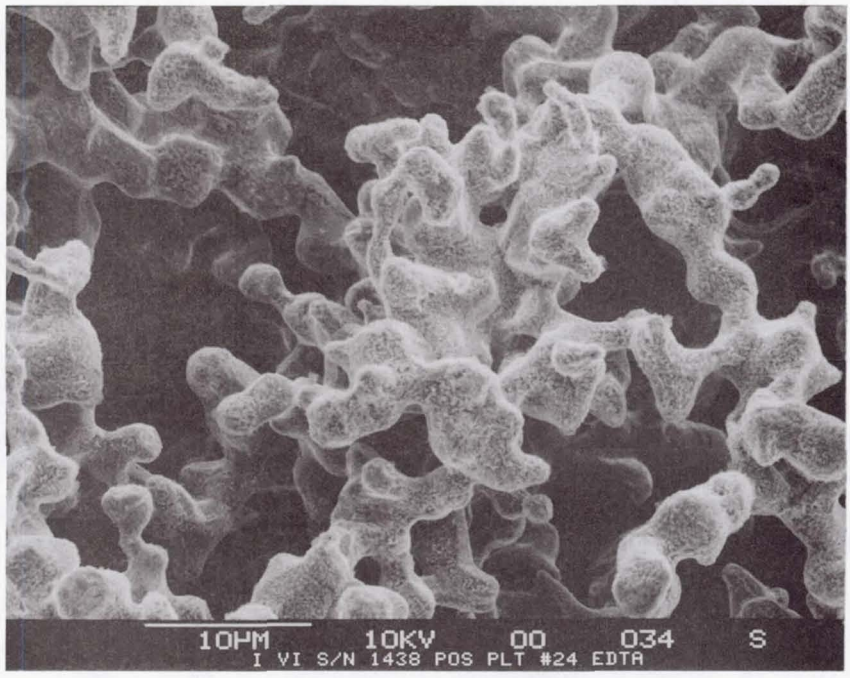

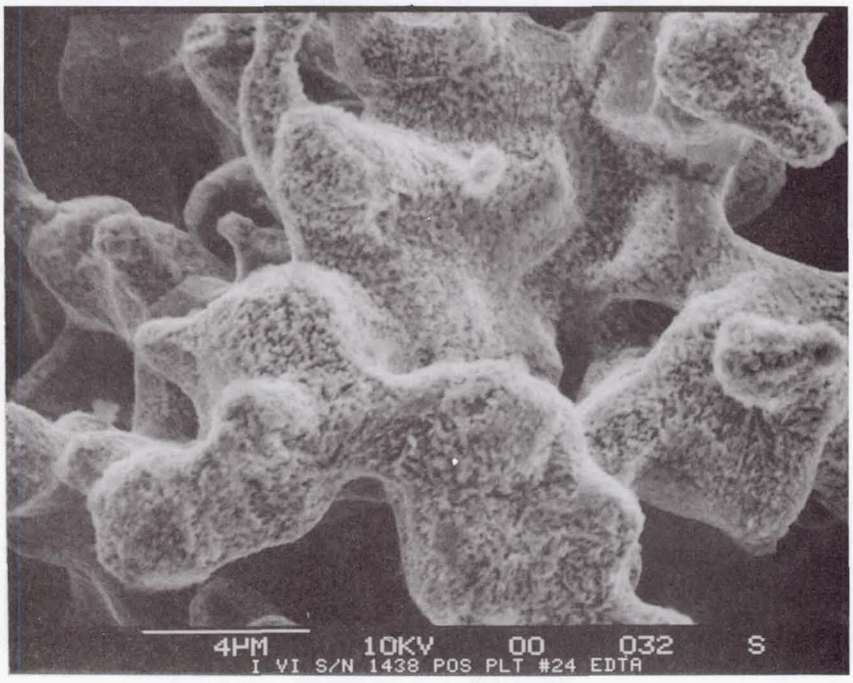

Figure. 4. SE images of Intelsat VI positive plate #24 S/N 1438 after EDTA - area 2, side 2. 9 21211STA.

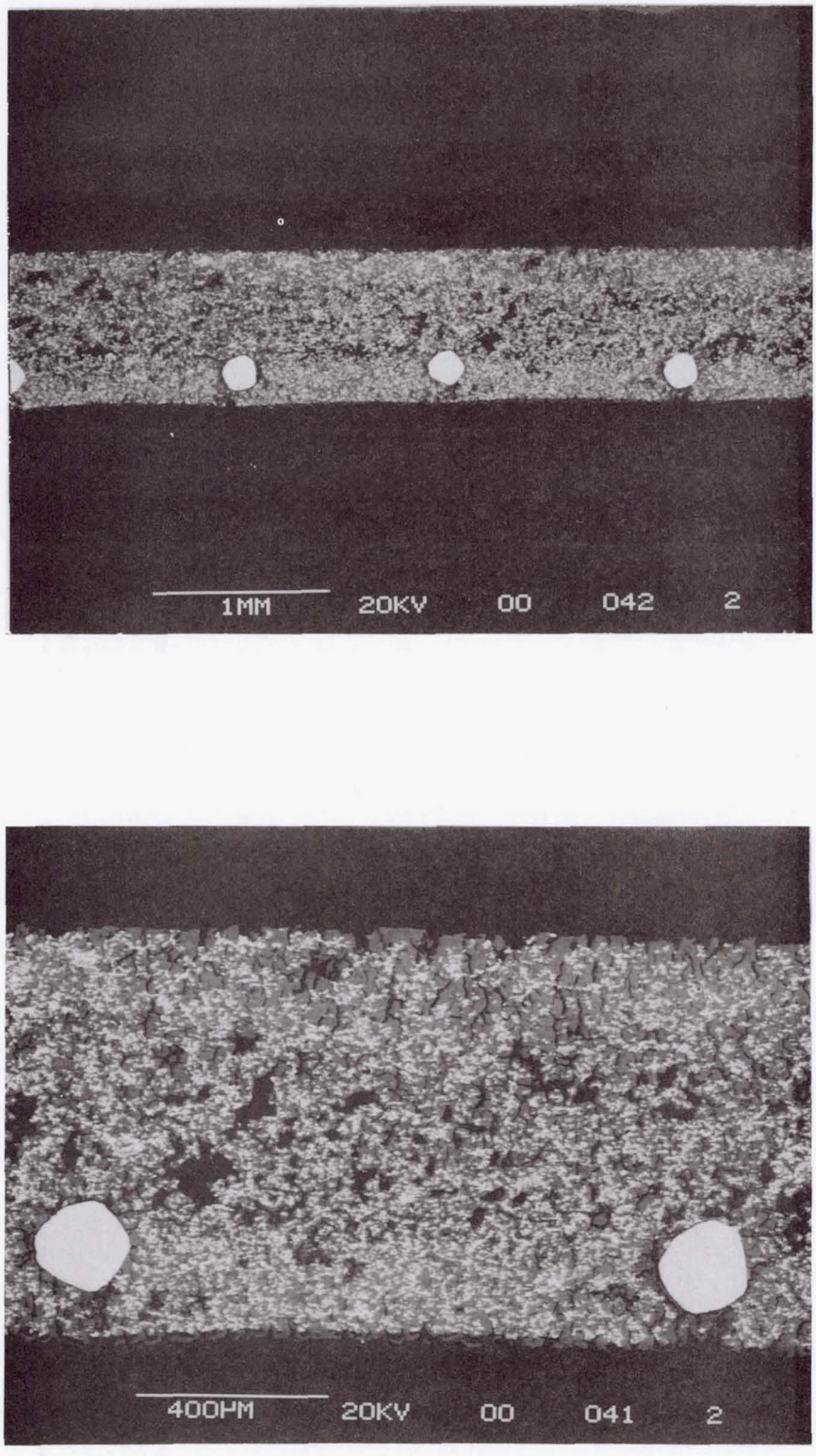

Figure. 5. BSE images of Intelsat VI positive plate #24 S/N 1438 (no EDTA).

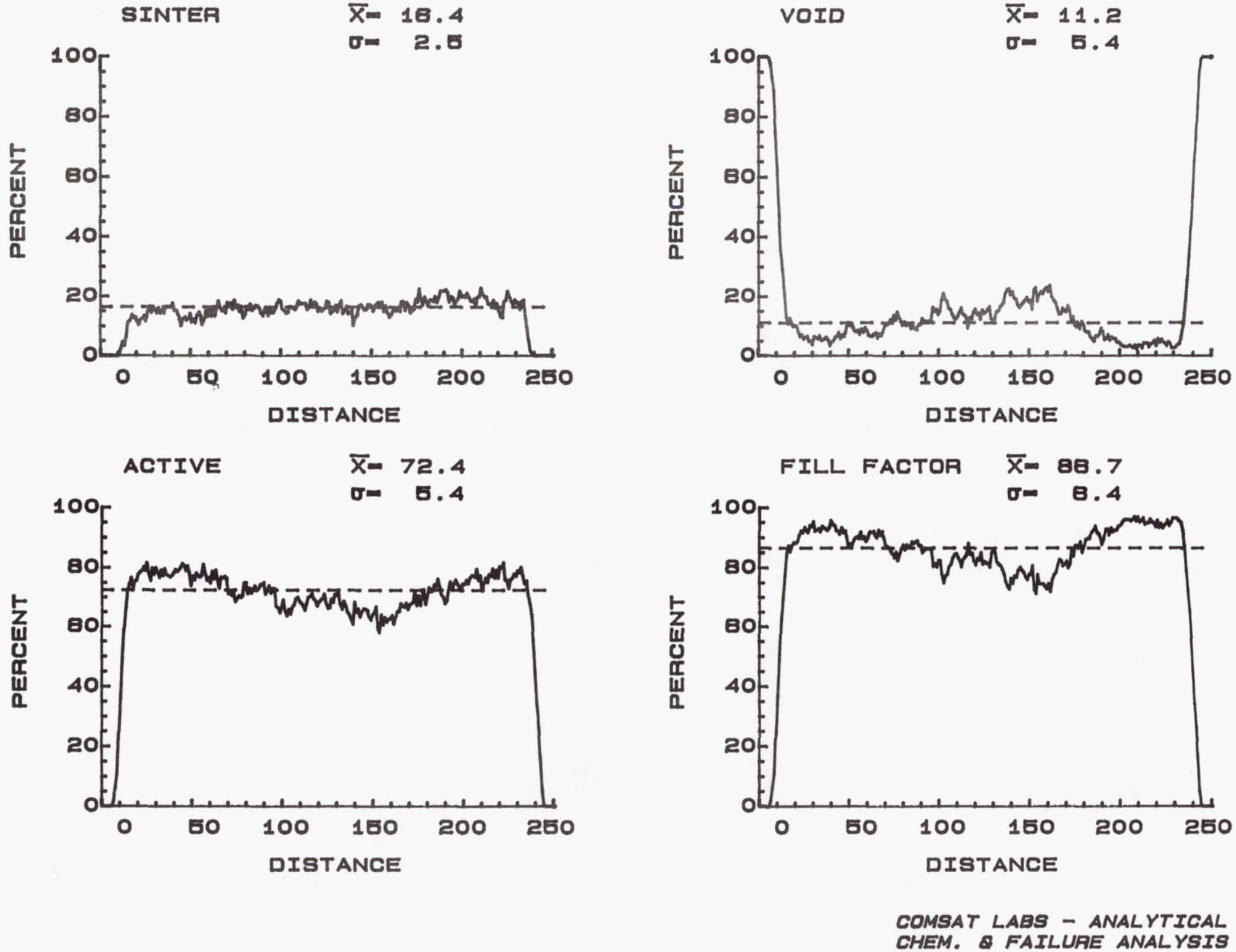

Figure. 6. BSE profiles of I VI PLT24 S/N 1438 - Composite of 3 areas.

REPORT DOCUMENTATION PAGE

Form Approved
OMB No. 0704-0188

1. AGENCY USE ONLY *(Leave blank)*	2. REPORT DATE	3. REPORT TYPE AND DATES COVERED
	September 1993	Reference Publication

4. TITLE AND SUBTITLE

NASA Handbook for Nickel-Hydrogen Batteries

5. FUNDING NUMBERS

730

6. AUTHOR(S)

James D. Dunlop, Gopalakrishna M. Rao, and Thomas Y. Yi

7. PERFORMING ORGANIZATION NAME(S) AND ADDRESS (ES)

Goddard Space Flight Center
Greenbelt, Maryland 20771

8. PEFORMING ORGANIZATION REPORT NUMBER

93B00106

9. SPONSORING / MONITORING ADGENCY NAME(S) AND ADDRESS (ES)

National Aeronautics and Space Administration
Washington, DC 20546-0001

10. SPONSORING / MONITORING ADGENCY REPORT NUMBER

NASA RP-1314

11. SUPPLEMENTARY NOTES

J. Dunlop, Consultant, Gaithersburg, Maryland; G. Rao and T. Yi, Goddard Space Flight Center, Greenbelt, Maryland

12a. DISTRIBUTION / AVAILABILITY STATMENT

Unclassified - Unlimited
Subject Category 20

12b. DISTRIBUTION CODE

13. ABSTRACT *(Maximum 200 words)*

Nickel-hydrogen (NiH2) batteries are finding more applications in the aerospace energy storage. Since 1983, NiH2 batteries have become the primary energy storage system used for Geosynchronous-Orbit (GEO) Satellites. The first NASA application for NiH2 batteries was the Low Earth Orbit (LEO) Hubble Space Telescope Satellite launched in 1990. The handbook was prepared as a reference book to aid in the application of this technology. That is, to aid in the cell and battery design, procurement, testing, and handling of NiH2 batteries. The design of individual pressure vessel NiH2 cells is covered in Chapter 1. LEO and GEO applications and their requirements are discussed in Chapter 2. The design of NiH2 batteries for both GEO and LEO applications is discussed in Chapter 3. Advanced design concepts such as the common pressure vessel and bipolar NiH2 batteries are described in Chapter 4. Performance data are presented in Chapter 5. Storage and handling of the NiH2 cells and batteries are discussed in Chapter 6. Standard test procedures are presented in Chapter 7. Cell and battery procurements are discussed in Chapter 8. Finally, safety procedures are discussed in Chapter 9.

14. SUBJECT TERMS	15. NUMBER OF PAGES
Nickel-Hydrogen, Batteries, Cells Aerospace, Common Pressure Nickel-hydrogen, Bi-polar Nickel-hydrogen, LEO, and GEO	370
	16. PRICE CODE

17. SECURITY CLASSIFICATION OF REPORT	18. SECURITY CLASSIFICATION OF THIS PAGE	19. SECURITY CLASSIFICATION OF ABSTRACT	20. LIMITATION OF ABSTRACT
Unclassified	Unclassified	Unclassified	UL

National Aeronautics and
Space Administration

Goddard Space Flight Center
Greenbelt, Maryland 20771

SPECIAL FOURTH-CLASS RATE
POSTAGE & FEES PAID
NASA
PERMIT No. G27